

1996

Paper No	Paper Title	Author Details	Company	Page
1.1	Comparison Test and Calibration of Coriolis Meters	John M Eide Stephen Gwaspari	Con-Tech A/S Con-Tech UK Ltd	3
1.2	Practical Application of Coriolis Meters for Offshore Tanker Loading from the Harding Field	V R Withers W Strang and G Allnutt	BP International Limited BP Exploration	30
1.3	North American Inter-Laboratory Flow Measurement Testing Program	J Bosio S Caldwell U Karnik E Bowls	Statoil CEESI NOVA Research & Tech Corp SWRI	45
1.4	Crude Oil and Condensate Expansion Co-efficients	R Third N Colyer	Rhomax Amerada Hess	69
1.5	Unpredicted Behaviour of Venturi Flowmeter in Gas at High Reynolds Numbers	A W Jamieson P A Johnson, J A Sattary and E S Spearman	Shell NEL	96
2.1	Sampling 3-Phase Fluids (Gas / Hydrocarbon Liquid/Water) for Quality Determination	Tom Welker	Welker Engineering Company	115
2.2	Production Evaluation and Testing of a High Viscosity / High Gas Volume Fraction Multiphase Meter	Bernie Tuss	Conoco Inc (Retired)	120
2.3	Assessment of Multiphase Flowmeter Performance	Tim Whitaker	NEL	134
2.4	The Importance of Calculating Resulting Permittivity and Conductivity in Mixtures of Two Liquids	Erling A. Hammer	University of Bergen	143
3.1	Review of Operation of Ultrasonic Time of Flight Meters	Terry Cousins	SGS Redwood Technical Services	151
3.2	Ultrasonic Metering on an Offshore Gas Platform	Phil Robbins	Arco British Limited	161
3.3	Operation of Multipath Ultrasonic Gas Flowmeters in Noisy Environments	Kjell-Eivid Froyso and Per Lunde Reidar Sakariassen Jens Grenstad Rune Norheim	Christian Michelsen Research Statoil, K-Lab Kongberg Offshore AS Fluenta AS	203
3.4	Practical Experience with Gas Ultrasonic Meters	K J Zanker W R Freund Jr	Daniel Industries UK Daniel Industries USA	221
3.5	Multipath Ultrasonic Flow Meter Performance	Terrence Grimely	South West Research Institute	231
3.6	Oil Flow Performance of Ultrasonic Meters	Gregor Brown	NEL	243

1996

Paper No	Paper Title	Author Details	Company	Page
3.7	Development of an In-Situ calibration Method for Multiphase Flow Meters Using a Radioactive Tracer Technique	T Sevel, N H Pedersen, C E Weinell and B Lind-Neilson	FORCE Institute	267
4.1	An Oil / Water / Gas Composition Meter Based on Multiple Energy Gamma Ray Absorption (MEGRA) Measurement	A M Scheers W Letton	Shell International E&P Daniel Industries Inc	277
4.2	Two Phase Effects on Single Phase Flowmeters	A Skea	NEL	290
4.3	Three-Phase Metering in Sumatra Using the StartCut Meter – An Example of Perfect Fit to a Specialized Niche	Jack Marrelli	Texaco EPTD	300
4.4	Current State of Development of the CSIRO Gamma-Ray Multiphase Flow Meter	G J Roach, J S Watt and W K Ellis	CSIRO Australia	308
5.1	The Density of Rich Natural Gas Mixtures	J Watson	NEL	321
5.2	Fluidic Pressure Pulse Transmitting Flowmeters for Remote Oil Flow Measurement	H Wang, S B M Beck, G H Priestman R F Boucher	University of Sheffiled University of Manchester	338
5.3	The Orifice Plate Discharge Co-efficient The Equation for ISO 5167-1	M J Reader-Harris and J A Sattary	NEL	371
5.4	Verification of Meter Performance and Well Allocation by Data Analysis	Frank Kemp	Statoil	394
5.5	Computation of Flow Through Bends	J A Sattary and M J Reader-Harris	NEL	413
	Focus Discussion Group A	Drew Cheshire	Fisher-Rosemount	444
	Focus Discussion Group	A Mazzoni Arstein Bringsvor	AGIP SPA Multi-Fluid International AS	452
	Focus Discussion Group C	D Irvine	British Gas plc	469
	Focus Discussion Group D	B H Torkildsen B V Hanssen	Framo Engineering AS	481
	Focus Discussion Group E	U Karnik	Novacor Research & Tech Corp	490
	Focus Discussion Group F	R Third	Rhomax	517
	Focus Discussion Group G	M Godfrey	Kelton Engineering	519

COMPARISON TEST AND CALIBRATION OF CORIOLIS METERS

John M. Eide, Con-Tech a/s
Stephen C. Gwaspari, Con-Tech UK Ltd

SUMMARY

Coriolis Mass Meters are just as accurate and linear as many Turbine Meters. They should be calibrated under the same conditions as they are to be operated at otherwise metering errors of up to 3% can be experienced. The meters zero stability are good and not influenced by increasing pressures or temperatures. They also show a small viscosity dependent effect on readings.

If a Coriolis Meter is operated at elevated pressures and temperatures, the density output option should be used with great care.

Verification with the manufacturer of the fluid density used when stating meter throughput or pressure drop versus flowrate is recommended

1.0 BACKGROUND

In 1992 Con-Tech was approached by Statoil a/s with a request for our interest to participate in an evaluation test of Coriolis Meters. The purpose of the testing was to evaluate the meters under simulated process conditions similar to those experienced offshore. Of particular interest was the region common to an allocation metering and test separator metering environment, those of high temperature and high pressure. As those test were not available at the that time, a purpose built calibration facility was required.

The resulting specifications for the calibration facility became as follows:

- Hydrocarbons to be used as calibration liquids
- Multiple storage tanks for various qualities of hydrocarbon liquids
- 0 - 400 m³ / hour as range of flowrates
- 0 - 95 barg pressure range
- 20 - 85 °C temperature range
- 3 parallel meter streams
- 2 by-pass type densitometers in parallel
- Multiple pressure and temperature transmitters
- Real time data acquisition and computations
- Resemblance to a offshore metering station was desired
- Due to the use of hydrocarbons all electrical equipment to be EEx

In summer 1994, following the completion of a 10 month test program, the calibration facility became commercially available for calibration of any liquid flow meters, volume or mass.

2.0 CALIBRATION SET-UP

The calibration loop consists of 3 parallel streams connected to an inlet and outlet header (Fig. 1). One stream is 6" pipe and 2 streams are 4" pipe. Each stream has a double block and bleed inlet valve and space for installing a Coriolis Mass Meter (CMM), Turbine Meter, Ultrasonic Meter, Positive Displacement Meter, or any other meter for liquid measurement.

Adjustable points for meter or pipe support, pressure taps before and after the meter under test, pressure and temperature transmitters, location for insertion densitometers and outlet flow control valve are installed. Dual Schlumberger Oil Densitometers, model 7835, are located downstream of the outlet header with one pressure and two temperature transmitters. Further downstream is the takeoff to the heat exchangers with a bypass flow control valve. Next comes a variable speed circulation pump before the liquid enters a Brooks Compact Prover. The tie-in for liquid filling and pressurisation is also upstream of the pump.

Signals from meters under test, densitometers, pressure and temperature transmitters are all connected to a Siemens Sicomp process machine (Fig. 2). This machine, with its installed calculation algorithms, is similar to machines used on offshore platforms for fiscal flow measurement. Temperatures and pressures on the Compact Prover are routed to its Computer, for display and printout.

The VDU presentation consists of, for every stream; temperature, pressure, volumetric flow rate, mass flow rate from a CMM, calculated mass flow rate from reference if a comparison test is ongoing, density, density meter temperature and pressure.

The process machine software also has a feature for data sampling and averaging, sampling time selectable by operator. Accumulated mass and volume, measured and calculated from reference, during the sampling period are also displayed.

All data collected during a sampling period can be transferred to our PC for presentation in engineering units. This data file is transferred to a calculation program, developed by Con-Tech, and any manually logged data is also entered here.

This calculation program converts Compact Prover volume, volume displaced during meter calibration and density to the conditions at the turbine meter. Hence the calculated accumulated mass or mass flowrate is at turbine meter conditions and this data is compared to the accumulated mass or mass flowrate from the CMM under test. The density output from the CMM is also compared to our reference densitometers, with this density calculated to Coriolis meter conditions.

As an extra verification of the density, an oil sample is drawn during a test and sent to an independent laboratory for density and also viscosity determination.

Coefficients for the oil's thermal expansion and compressibility are determined by varying temperature and pressure and then calculating density changes per °C and barg. This is done in the range where the calibration is performed.

3.0 CALIBRATION PROGRAM

The large calibration program, with 6 different CMM's, to be performed for Statoil a/s, was set up to be a 5 point calibration over the meters said range; or the range achieved with a maximum of 1,5 bar differential pressure over the meter and with the following pressure and temperature conditions:

20 °C, 60 °C 85 °C 10 barg, 70 barg 95 barg

Calibration liquids to be water, 3 crude oils with density range 0,83 to 0,89 kg/l and viscosity range 5 to 19 cSt, and naphtha with density 0,65 kg/l and viscosity 0,6 cSt.

In addition the following criteria's were to be adhered to:

- Calibration on every rate and condition should be repeated 3 times.
- Calibration data should be collected for at least 3 minutes.
- The master meter should be calibrated every time the conditions changed, with 5 runs of 5 passes on the Compact Prover, and a spread of the 5 runs to be better than 0,05%.
- Temperature stability during a test to be within $\pm 0,2$ °C.
- Zero flow to be recorded for every change in pressure/temperature, but not adjusted.
- Density and temperature readout from the CMM to be recorded and compared with reference.

This calibration matrix gave a total of 4050 data points to collect and a minimum of 33750 single calibrations of the master meters, 2" and 3" Brooks Parity High Resolution Turbine Meters.

Following discussions with Statoil a/s it was decided that the CMM's to be tested would be:

ABB Kent-Taylor	K-Flow K-2500	2"
Endress+Hauser	M-Point DQ 600	3"
Exac Corporation	Exac EX 3000 H	3"
Foxboro Company	Foxboro CFS 10	2"
Micro Motion Inc	Elite CMF 300 M	3"
Schlumberger	Massmaster 150	2"

Due to start-up delays it was decided to omit one of the crude oils from the test program. Also, due to various circumstances, three meters were not tested through the full program. (Table 1.)

The final calibration program became as follow: (meters in random order)

Table 1.

METER NO:	WATER		NAPHTHA		CRUDE OIL		CRUDE OIL	
	1 kg/l	1 cSt	0,65kg/l	0,6 cSt	0,84 kg/l	7 cSt	0,89kg/l	19 cSt
A								
B								
C								
D								
E								
F								

4.0 PROCEDURE

The various CMM's were installed and supported in strict accordance with the manufacturers recommendations. The CMM's flow computer were configured by vendor representatives and the complete installation were accepted by the vendor in writing.

The initial calibrations on each CMM were to be on water at 20 °C and 10 bar in order to compare this calibration with the factory calibration and thus have an indication of a healthy meter and calibration set-up.

By monitoring the pressure drop whilst increasing flow rate, the maximum flow rate was found, and the meter was calibrated on the 3 highest points. After some number crunching the data was compared with the reference and if they were within $\pm 0,2$ % of the factory calibration, the factory K-factor was not changed and the rest of the curve completed.

In order to compare the result from the CMM with the result from the reference a special calculation program was developed. Process data and flow data was averaged and accumulated during the sampling period by the Sicomp Process Machine. The sampling period was set to 3 minutes so that one pulse lost would have a influence in the final result of 0,002% or less. For the low rate on 2" meters the sampling time was 5 minutes.

The turbine meter was calibrated after any change in flowing conditions by using the Compact Prover. The procedure was 5 passes per run and 5 runs, with a repeatability better than 0,05%. The meter factor was corrected to turbine meter conditions, hence recalculating the prover volume also to turbine meter conditions.

This meter factor was entered into the Process Machine and the sampling period started. After completion the collected data was transferred to a data file and a new sampling period started. A third sampling period was also performed with the repeatability of CMM and reference monitored.

5.0 CALIBRATION RESULTS

5.1 General.

The detailed calibration results belong to our client but we are allowed to present results in a general manner. The results and comments are not connected to any particular manufacturer.

5.2 Pressure Drop

The pressure drop results obtained from various meters on various fluids are detailed in Table 2.

We experienced some problems in achieving the maximum flowrate at the maximum test programme pressure drop (1.5 bar). One manufacturer claimed they have used a liquid density of 1,5 kg/l in order to achieve the maximum mass flowrate.

Some of the results to note are:

- Meter C on water with a pressure drop of 0.8 bar at 140 tonnes per hour (tph). The manufacturers literature quotes 3.1 bar at 272 tph.
- Meter F on water with a pressure drop of 1.5 bar at 50 tph. The manufacturers literature quotes 0.7 bar at 42 tph.

- Meter D on water with a pressure drop of 1.5 bar at 40 tph
The manufacturers literature quotes 2.45 bar at 68 tph.

5.3 Temperature Reading

The coriolis mass meter temperature read out results compared to the reference temperature instrument are published in Table 3. Results from the coriolis meters ranged from 0 up to 2.5°C differences from the reference, the highest vaiances not considered as acceptable for fiscal or custody transfer purposes.

5.4 Density Reading

The coriolis mass meter density readings at various temperatures and pressure were noted on the various test fluids and compared to the reference density meters. The results are published in Tables 4 to 7.

All the meters tested showed either some pressure dependence, temperature dependence or a combination of both when the results were compared to the reference instruments. In general, the results over the test fluid parameter ranges do not conform to what is " normally " acceptable for custody transfer or fiscal metering standard instruments.

5.5 Coriolis Mass Meters

5.5.1 Meter Zero

When checking zero-flow the procedure was to close valves both upstream and downstream of the meter. All meters were zeroed at the initial water calibration and they did not require to be re-zeroed during the test, even at the highest pressure and temperature combination. The zero-flow indication varied between -0,2 to 0,5 ton/hour and the indication for most of the meters varied in an unsystematic way. For one of the meters we experienced a substantial increase in flow indication when the downstream butterfly valve was closed. This gave indication of sensitivity to frequency reflection and feedback.

Table 8. shows the zero error readings for a number of meters on a variety of fluids over the test pressure and temperature ranges.

5.5.2 Water Calibrations

The initial calibrations were performed on water at 20°C and 10 bars pressure.

Results from the initial water calibrations performed on all the meters are shown in Fig.3. As one can see, meter C and meter F stand out with very good linearity. Only meter D gave results which were positive relative to the reference.

After initial water calibration and consultation with the manufacturer, for one of the meters we changed the manufacturer supplied K-factor by 0,25% .

Next the test pressure was elevated to 95 bars whilst keeping the temperature at 20°C. The results are shown in Fig. 4. Meters B and E were not present for these tests.

Meter A took a drop of 0.5 % at the lowest rates whilst meter C kept the linearity but gave a further 0,75% under registration. The same applies to meter F with a good 1% drop in registration, however it kept its linearity.

Testing was then carried out on the water at 85 °C with 10 bar pressure, results are shown in Fig.5. Meter F still has very good linearity but 0,5% drop in reading. Meter D has improved its linearity and now has a 1% under registration. Meter A likes temperature better than pressure and meter C is now using the fiscal requirement for linearity, $\pm 0,25\%$, to its fullest extent.

The meters were then tested over a variety of temperatures and pressure on water. A typical set of results is shown in Fig. 6 which gives results for 5 of the meters on water at 60 °C and 95 bar. If this is your process conditions meter A stands out as the meter to use. Meter C and F are still linear but now 1 - 1,5% down in reading. Meter E also likes these conditions now around the zero line, up from -0,75% at the initial calibration.

Meter F at all water points is shown in Fig.7. This was the most linear meter we found on water. The meter is clearly temperature and pressure sensitive but this can easily be corrected for after a calibration.

5.5.3 Hydrocarbon Calibrations

The CMM's were tested using a variety of crude oils / hydrocarbons and pressure and temperature ranges as on water. The initial viscosity's at 20°C are shown in Table 1

Figs.8 and 13 show all the calibration points for meters F and A on the heavy crude oil. For meter F at elevated temperatures and pressures the excellent linearity has now gone. With meter A most of the points are within a 2% span however its temperature sensitivity on this liquid can be observed. This meter has good linearity if a 4:1 turn down can be accepted.

A comparison between 3 meters on heavy crude is shown in Fig.9. We can observe that meter A performance improves under high temperatures and pressures whilst meter F deteriorates.

A comparison of results for a mid range viscosity crude (0.84 kg/l, 7 cSt) at elevated temperature and pressure is shown in Fig.11. All meters show a significant shift in readings.

For one meter we experienced a 10 % under-registration at 70 bar, and it was claimed that the flow computer corrected for pressure effects. We also tested one other meter of this model with the outcome being similar results.

For the low end viscosity naphtha was used. No results for the high temperature / low pressure ranges were obtained as naphtha is not a single phase fluid in these regions. We observed that our pump cavitation did not end until we were above 50 bar pressure at 85°C.

Fig.10 shows a comparison of results for three meters on naphtha. Linearity has improved on some meters when compared to the heavy crude results, except at the lower flow rates.

In Fig.12 we have plotted all calibration results for meter A when calibrated on naphtha. All points, except 3, are within $\pm 0,5\%$ from the reference.

In general, from the results all meters show a small viscosity dependent effect.

5.5.4 Reference Turbine Meters

For information purposes the calibration results for the turbine meter references used during the CMM calibrations are presented

Fig.14 shows results from the calibration of the 3" turbine on water when meter A was calibrated. For most of the points we find a meter factor between 30,15 and 30,50 pulses per litre, which represents a span of 1,16%! The average meter linearity on 20 °C 10 bar calibrations was $\pm 0,38\%$ over 10:1 turndown. The average meter repeatability in the various points was 0,015%.

Fig.15 shows results from the calibration of the 2" turbine on water when meter D was calibrated. For all points, less one, we find a meter factor between 48.23 and 48.80 pulses per litre, which represents a span of 1,17%! The average meter linearity on 20 °C 10 bar calibrations was $\pm 0,23\%$ over 10:1 turndown. The average meter repeatability in the various points was 0,013%. We observed a shift in the meter factor leaving 20 °C but a similar shift in meter D performance was not observed.

Fig.16 plots the meter curves for the 3 hydrocarbon liquids. Sensitivity to viscosity can clearly be observed and also that we achieved better linearity calibrating on naphtha.

Finally fig.17 plots all calibration points for the 3" turbine on the heavy crude. This graph clearly displays the temperature sensitivity, i.e. liquid viscosity. The total range for all these meter factors are 2,35%.

6.0 CONCLUSIONS

All meters were sensitive to pressure and temperature increases. It can be concluded the Coriolis Mass Meter should be calibrated at process conditions in a test facility or the user should install connections and valves and have sufficient space so the meter can be calibrated in-situ.

All meters were, more or less, showing less than actual throughput. The problem is easy to correct during a calibration.

There is a small viscosity effect, the higher the viscosity the higher the error. A positive effect is that lower viscosity improved the meters linearity.

Meter zero was good and not influenced by increasing temperature and pressure.

All of the density outputs from the Coriolis Mass Meter's tested showed some dependence on either temperature or pressure or on both parameters. At elevated temperatures and pressure the density outputs should be used with care as they may not be suitable for custody transfer or fiscal purposes.

Potential users must clarify what conditions/liquids the manufacturer is using as his basis for throughput quotations.

In general the temperature output signals from the meters tested were not considered as suitable for use other than as indication instruments.

TABLE 2. CORIOLIS METER PRESSURE DROP vs FLOW RATE RESULTS

METER	FLUID	FLOW RATE Tonnes/hour	PRESSURE DROP Bar
A	WATER	130	1.0
A	NAPHTHA	92	1.1
A	MEDIUM CRUDE	107	1.5
A	HEAVY CRUDE	104	1.4
C	WATER	140	0.8
C	NAPHTHA	96	0.6
C	MEDIUM CRUDE	110	0.9
C	HEAVY CRUDE	108	0.9
D	WATER	42	1.5
F	WATER	50	1.5
F	NAPHTHA	52	1.5
F	MEDIUM CRUDE	45	1.5
F	HEAVY CRUDE	45	1.5

TABLE 3. CORIOLIS METER TEMPERATURE READ OUT DIFFERENCE FROM REFERENCE READING

METER	FLUID	TEMPERATURE DIFFERENCE °C
A	WATER	-0.2 to +0.2
A	NAPHTHA	-0.2 to -0.4
A	MEDIUM CRUDE	0.0 to -0.6
A	HEAVY CRUDE	0.0
C	WATER	0.0 to -1.5
C	NAPHTHA	-0.2 to -2.2
C	MEDIUM CRUDE	0.0 to -2.5
C	HEAVY CRUDE	-0.1 to -2.2
D	WATER	0.0 to -1.5
F	WATER	-0.2 to -1.0
F	NAPHTHA	-0.25 to -0.7
F	MEDIUM CRUDE	-0.2 to -1.0
F	HEAVY CRUDE	-0.2 to -0.7

TABLE 4. CORIOLIS METER DENSITY READINGS PERCENTAGE DIFFERENCE FROM REFERENCE

METER	FLUID	PRESS.Bars / TEMP °C	20	60	85
A	WATER	10	-0.1	+0.1	+0.4
"	"	70	+1.4	+1.3	+1.5
"	"	95	+1.8	+1.9	+1.9
"	NAPHTHA	10	0.0	+1.1	-
"	"	70	+1.0	+1.7	+2.8
"	"	95	+2.2	+2.5	+2.4
"	MEDIUM CRUDE	10	-0.1	+0.1	+0.5
"	"	70	+1.5	+1.4	+1.9
"	"	95	+2.0	+1.9	+2.4
"	HEAVY CRUDE	10	+0.2	+0.7	+0.1
"	"	70	+1.1	+0.9	+0.9
"	"	95	+1.9	+1.5	+1.5

TABLE 5. CORIOLIS METER DENSITY READINGS PERCENTAGE DIFFERENCE FROM REFERENCE

METER	FLUID	PRESS.Bars / TEMP °C	20	60	85
C	WATER	10	+0.1	-0.3	-0.1
"	"	70	-0.1	-0.3	-0.2
"	"	95	-0.1	-0.2	-0.4
"	NAPHTHA	10	+0.3	+0.9	-
"	"	70	+0.4	+0.8	+1.1
"	"	95	+0.2	+0.7	+1.2
"	MEDIUM CRUDE	10	-0.2	-0.4	-0.6
"	"	70	-0.1	-0.8	-0.7
"	"	95	-0.1	-1.1	-1.6
"	HEAVY CRUDE	10	-0.2	-0.8	-1.3
"	"	70	-0.3	-1.1	-1.3
"	"	95	-0.2	-1.2	-1.3

TABLE 6. CORIOLIS METER DENSITY READINGS PERCENTAGE DIFFERENCE FROM REFERENCE

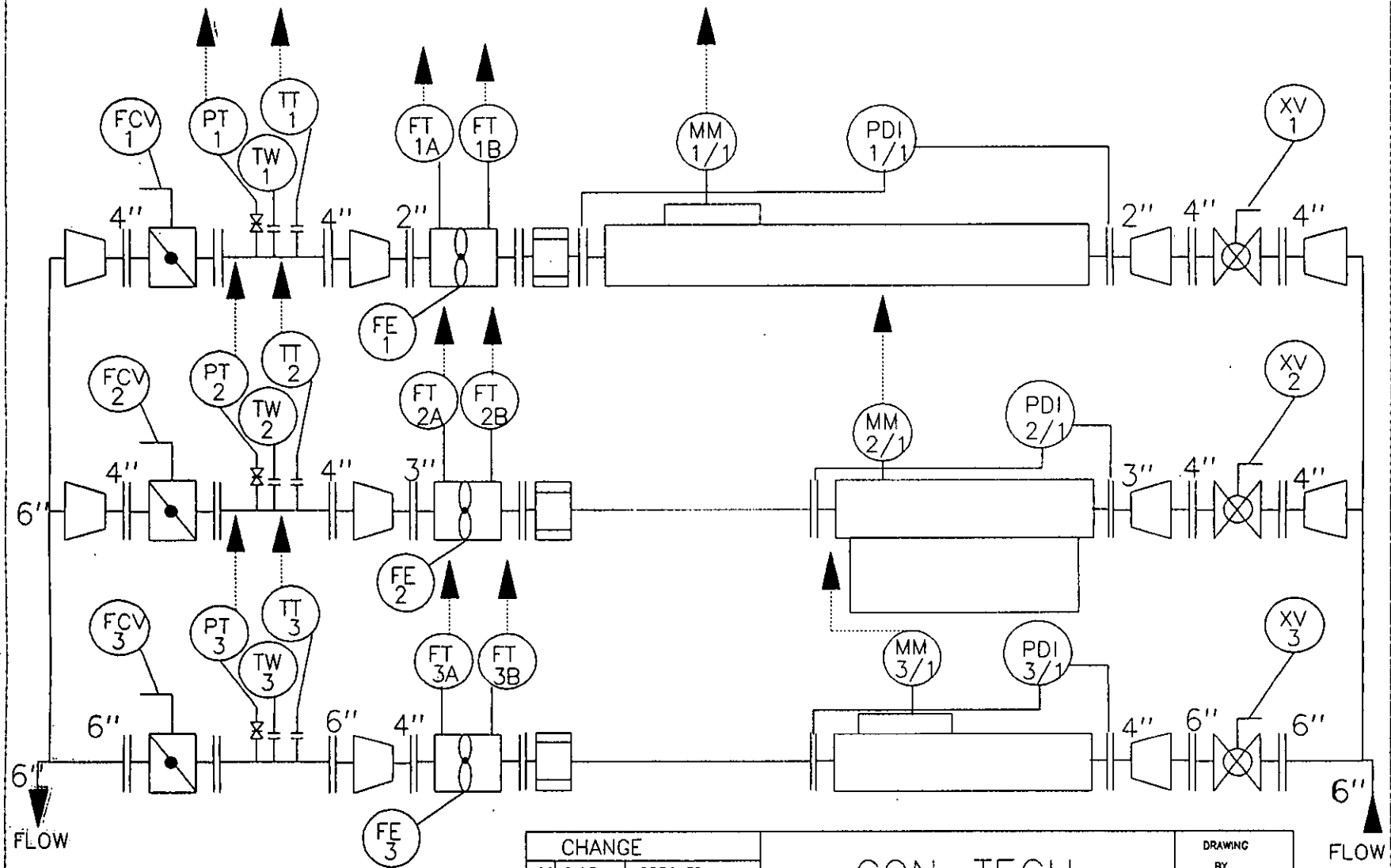
METER	FLUID	PRESS.Bars / TEMP °C	20	60	85
D	WATER	10	+0.1	-0.4	-0.9
"	"	70	-0.6	-1.3	-1.7
"	"	95	-0.7	-1.5	-2.0

TABLE 7. CORIOLIS METER DENSITY READINGS PERCENTAGE DIFFERENCE FROM REFERENCE

METER	FLUID	PRESS.Bars / TEMP °C	20	60	85
F	WATER	10	-0.1	-0.2	+0.1
"	"	70	-1.8	-1.7	-1.7
"	"	95	-2.4	-2.4	-2.3
"	NAPHTHA	10	+0.5	+1.4	-
"	"	70	+2.7	+3.1	+3.3
"	"	95	+3.5	+3.8	+4.3
"	MEDIUM CRUDE	10	-0.6	-1.7	-1.6
"	"	70	-2.5	-2.7	-2.6
"	"	95	-3.0	-3.6	-3.3
"	HEAVY CRUDE	10	-0.6	-1.3	-1.7
"	"	70	-2.2	-3.3	-3.5
"	"	95	-2.9	-4	-4.0

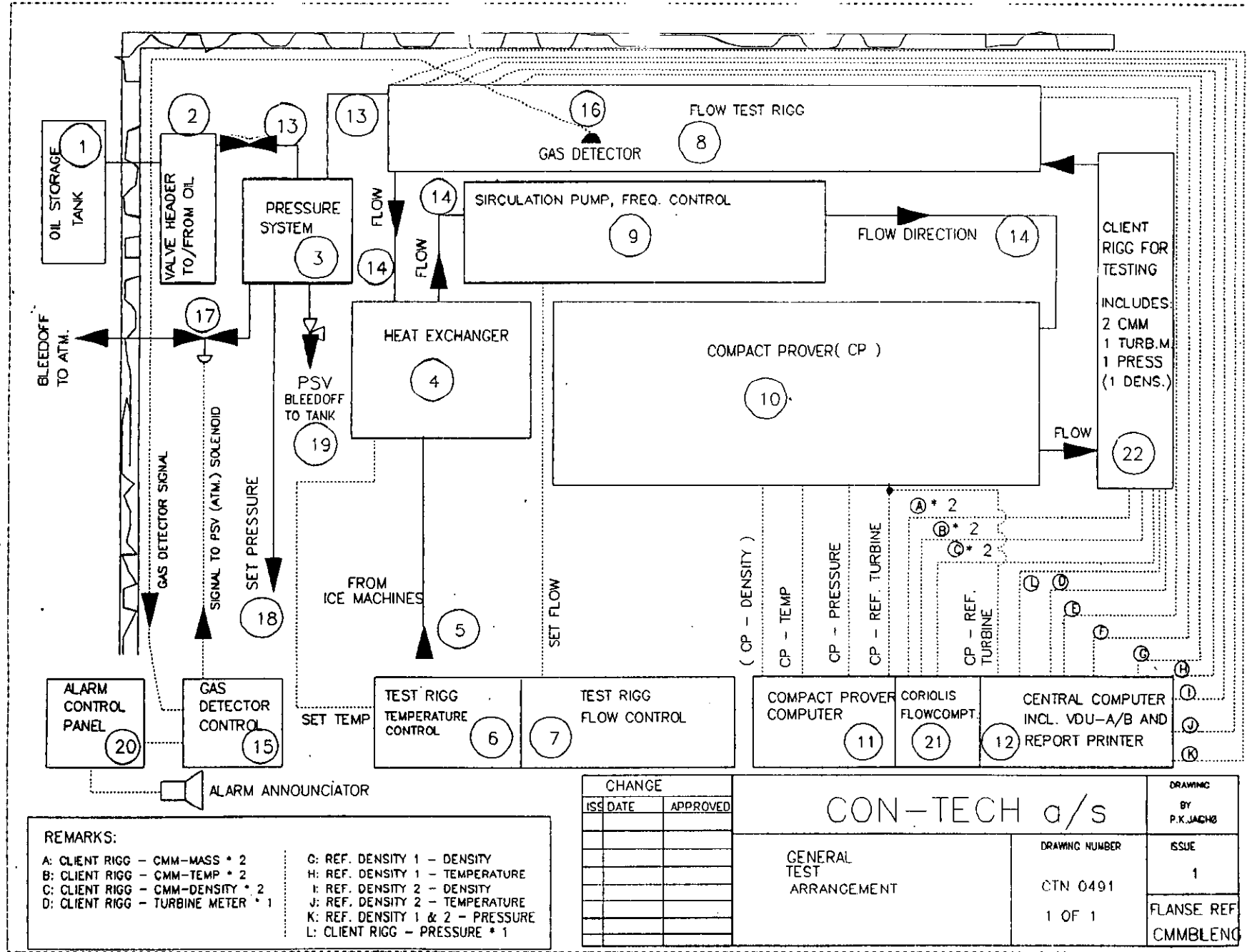
TABLE 8. CORIOLIS MASS METER ZERO ERROR RESULTS

METER	FLUID	ZERO ERROR Tonnes/hour
A	WATER	-0.7 to +0.2
A	NAPHTHA	+0.14 to +0.25
A	MEDIUM CRUDE	-0.2 to +1.0
A	HEAVY CRUDE	-0.1 to +0.54
C	WATER	0.0 to +0.20
C	NAPHTHA	0.0 to +0.26
C	MEDIUM CRUDE	0.0 to +0.24
C	HEAVY CRUDE	0.0 to +0.23
D	WATER	0.0 to +0.10
F	WATER	0.0 to +0.28
F	NAPHTHA	-0.06 to +0.24
F	MEDIUM CRUDE	-0.04 to -0.21
F	HEAVY CRUDE	0.0 to +0.30



CHANGE		CON-TECH a.s		DRAWING	
ISS DATE	APPROVED			BY	ISSUE
		TYPICAL ARRANGEMENT P & I DIAGRAM		DRAWING NUMBER	1
				CTN 1292	Flange ref.
				1 OF 3	CMMKJOR

Fig. 1



REMARKS:

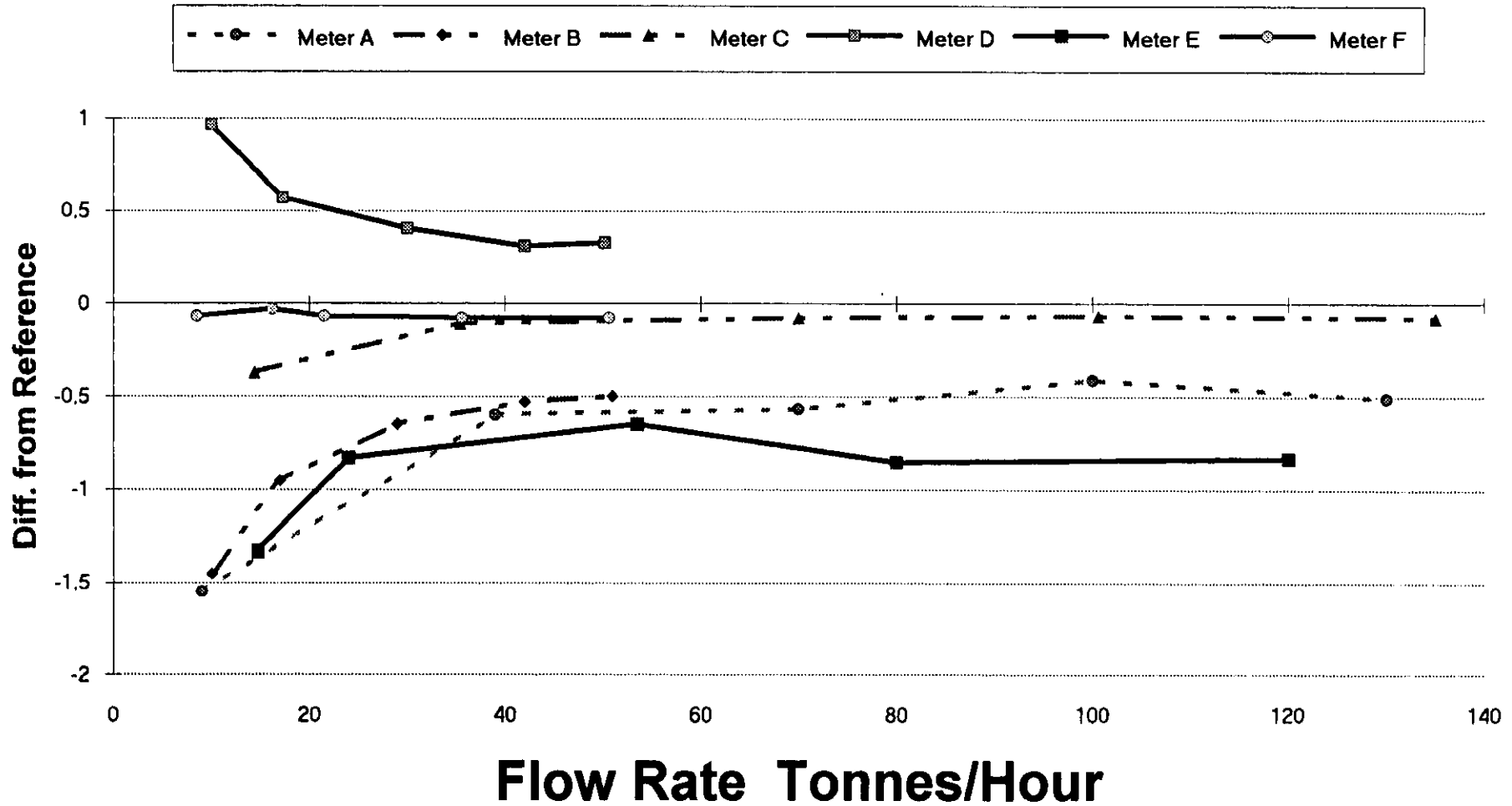
A: CLIENT RIGG - CMM-MASS * 2	G: REF. DENSITY 1 - DENSITY
B: CLIENT RIGG - CMM-TEMP * 2	H: REF. DENSITY 1 - TEMPERATURE
C: CLIENT RIGG - CMM-DENSITY * 2	I: REF. DENSITY 2 - DENSITY
D: CLIENT RIGG - TURBINE METER * 1	J: REF. DENSITY 2 - TEMPERATURE
	K: REF. DENSITY 1 & 2 - PRESSURE
	L: CLIENT RIGG - PRESSURE * 1

CHANGE	
ISS DATE	APPROVED

CON-TECH a/s		DRAWING BY P.K.JACHO
GENERAL TEST ARRANGEMENT	DRAWING NUMBER CTN 0491 1 OF 1	ISSUE 1 FLANSE REF CMMBLENG

FIG. 2

Initial Water Calibration



Water at 20 °C and 95 barg

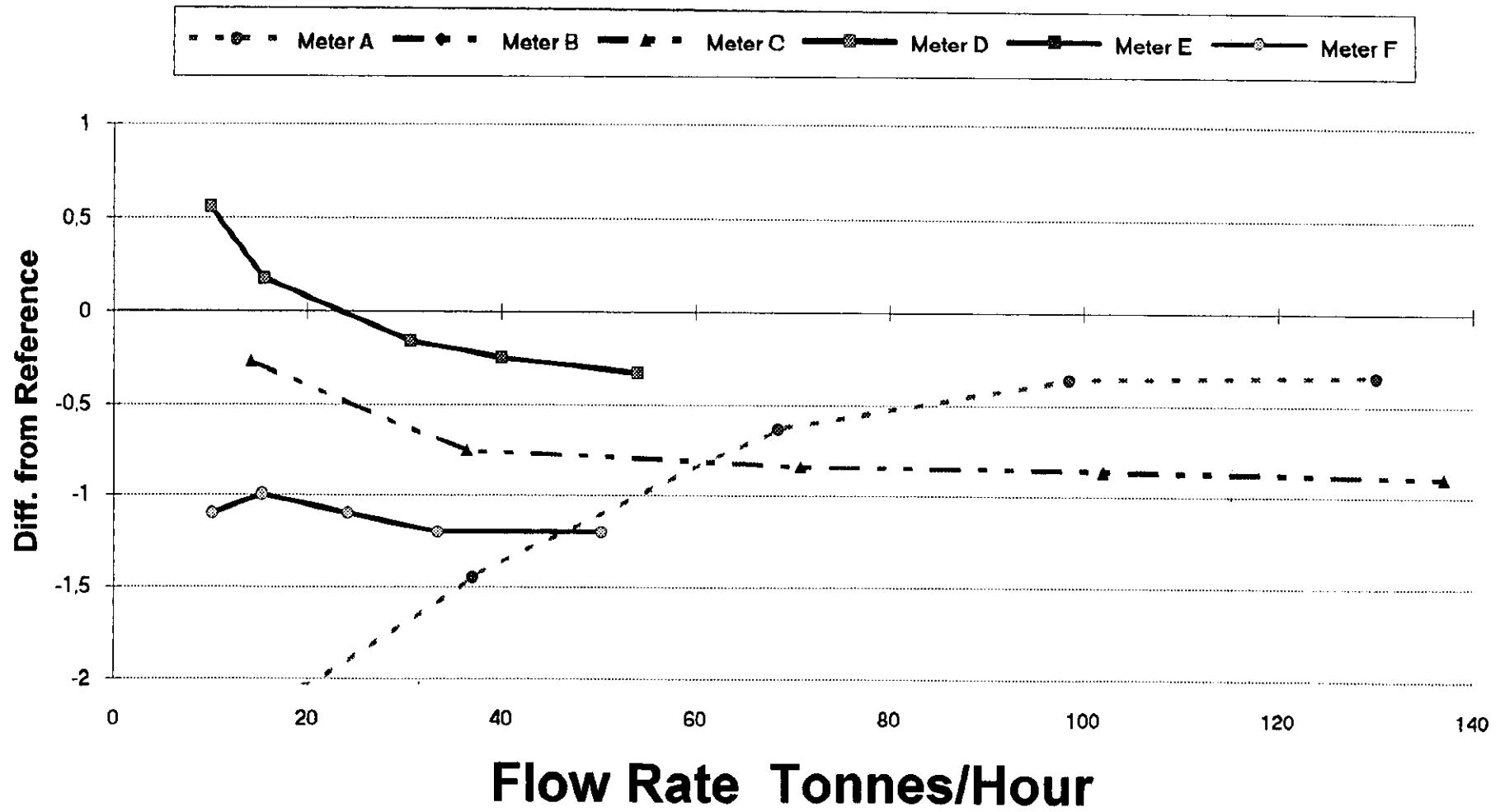


Fig. 4

Water at 85 °C and 10 barg

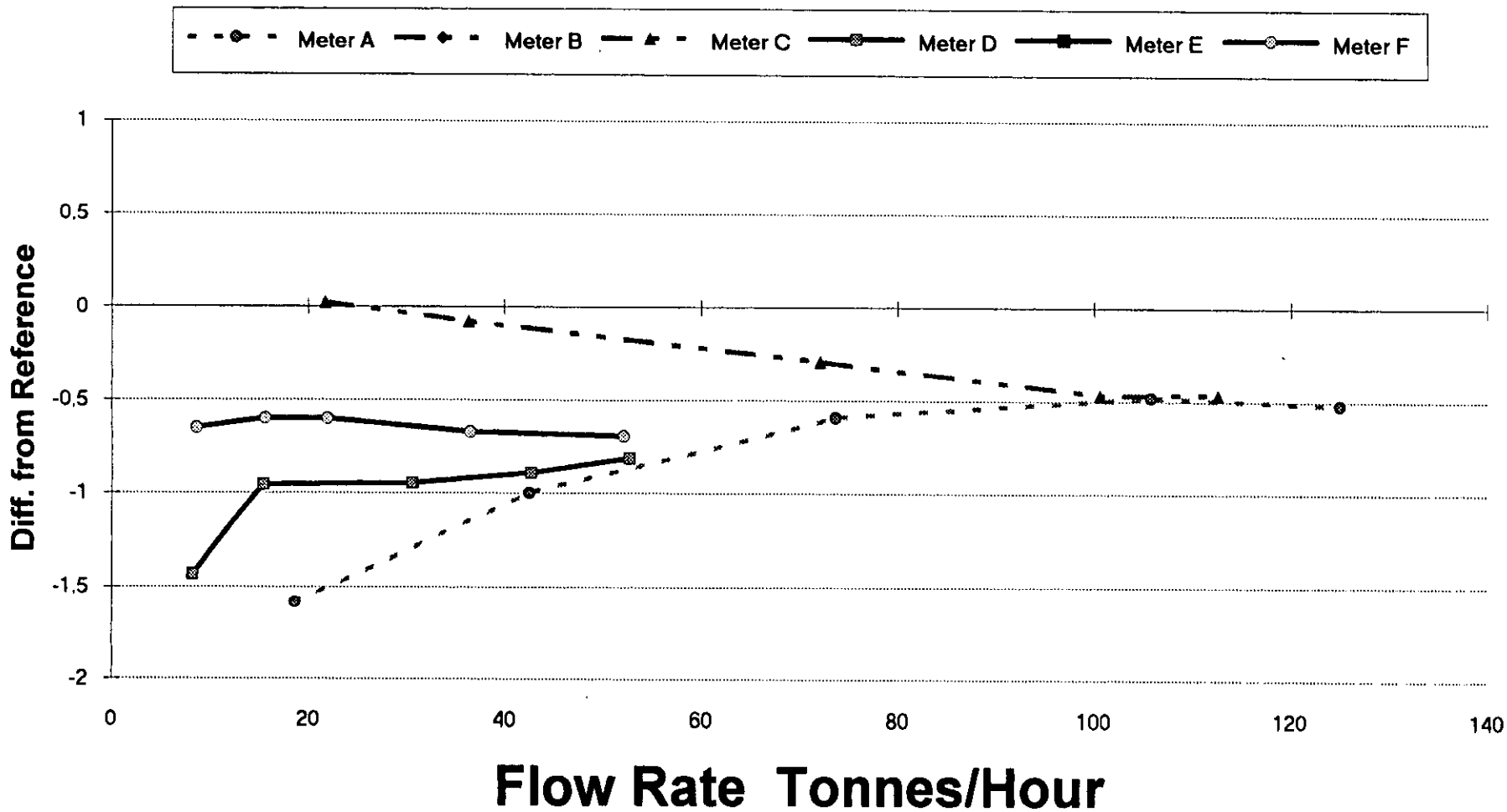


Fig. 5

Water at 60 °C and 95 barg

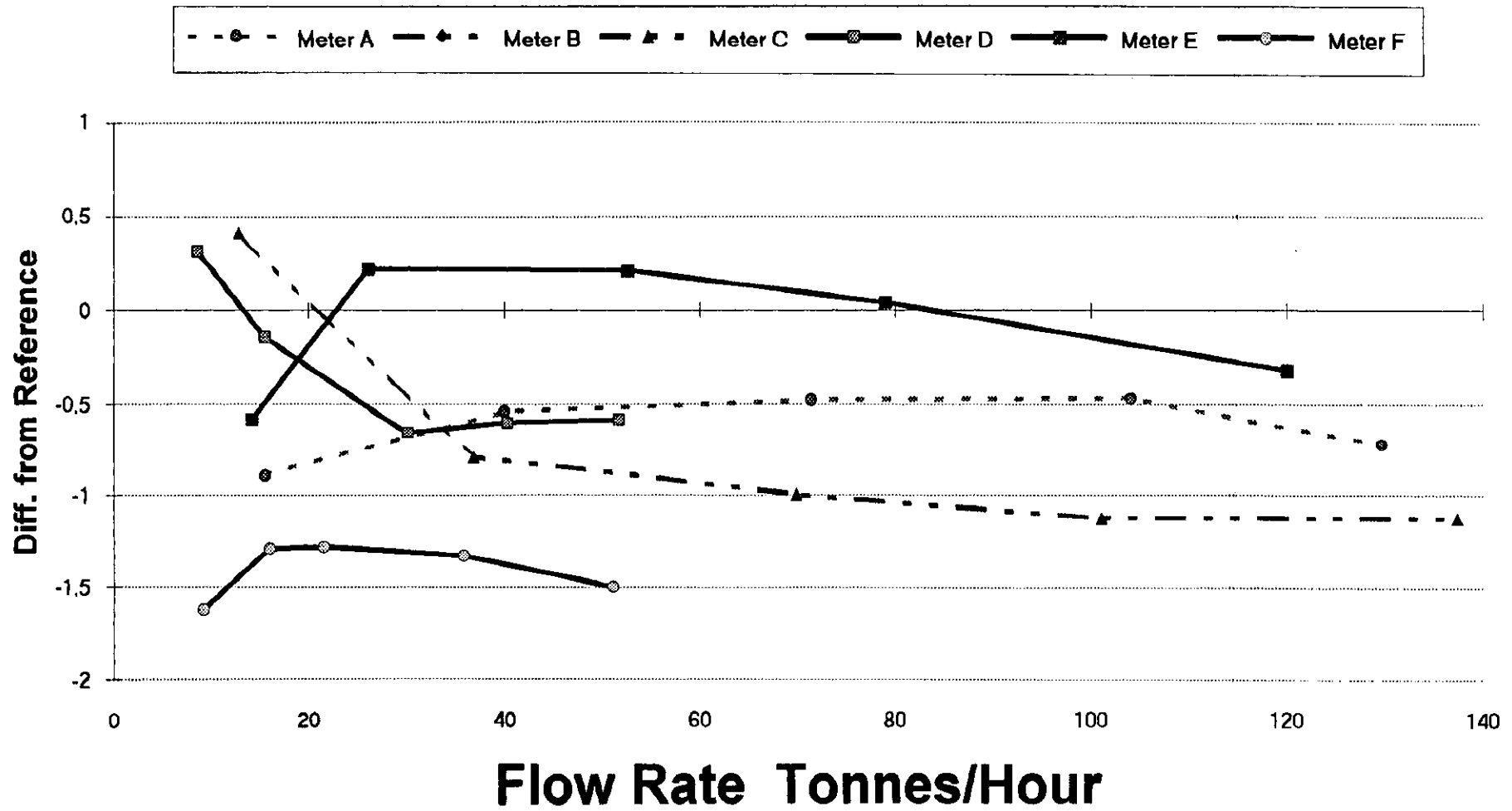


Fig. 6

Meter F at all Water Points

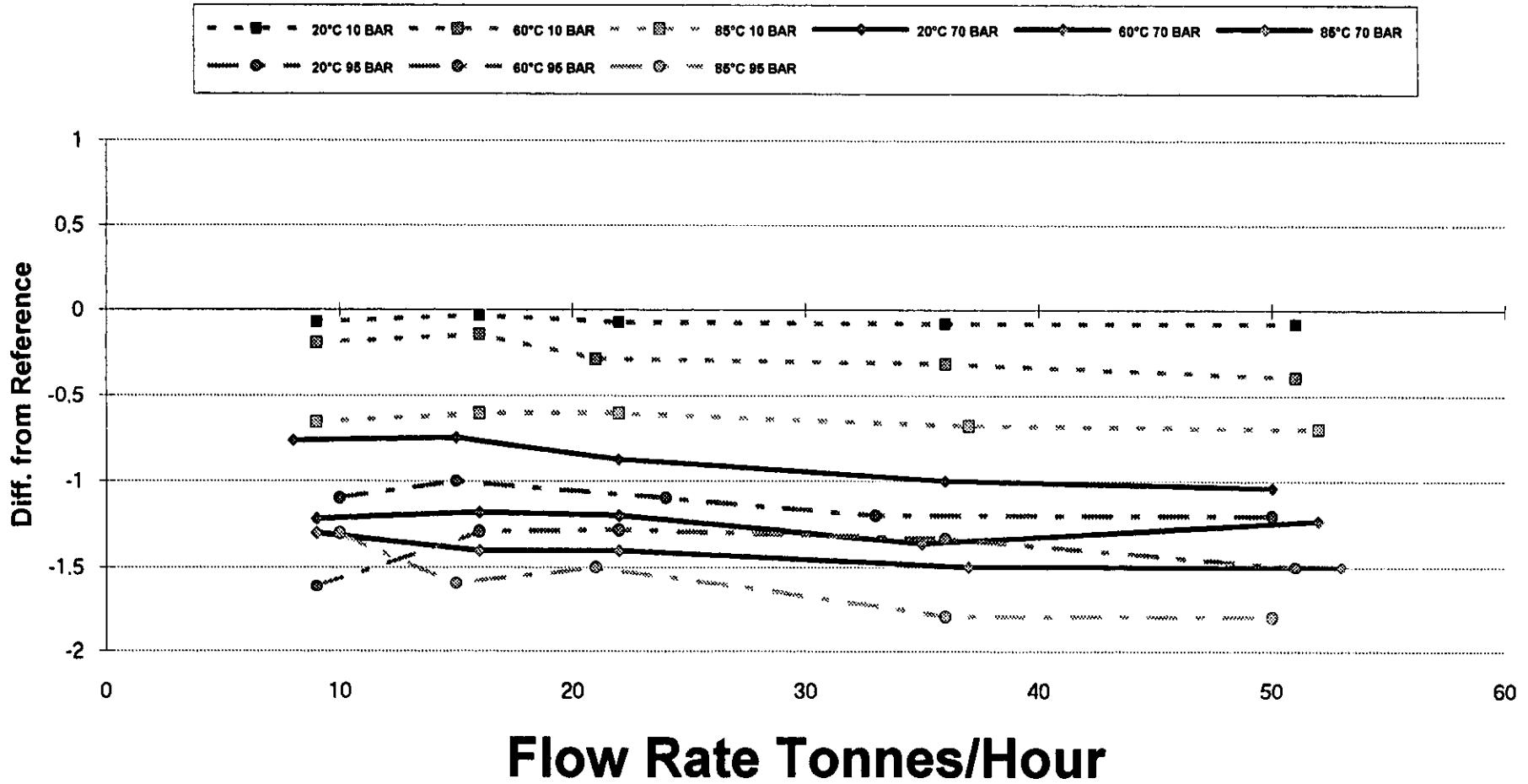


Fig. 7

Meter F Crude Oil 0,89 kg/l and 19 cSt 20°C

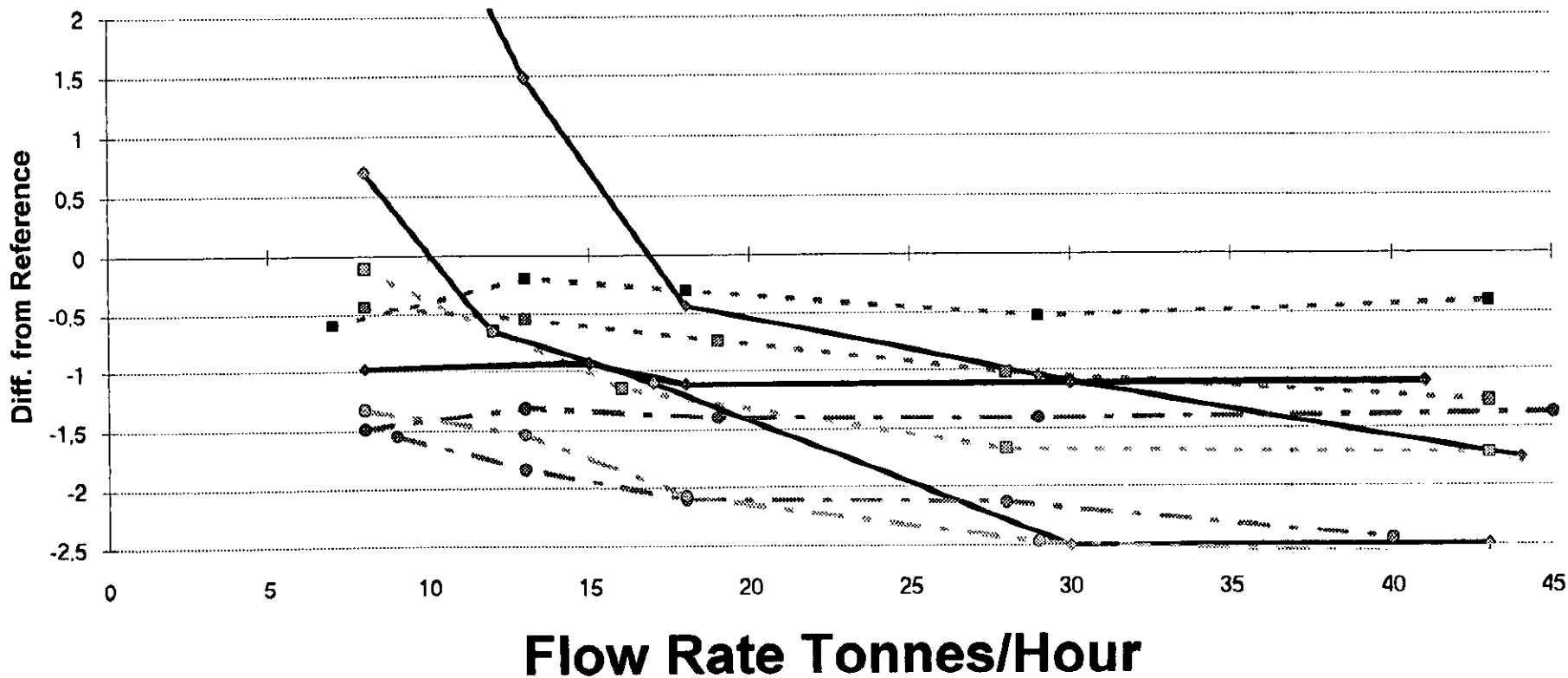
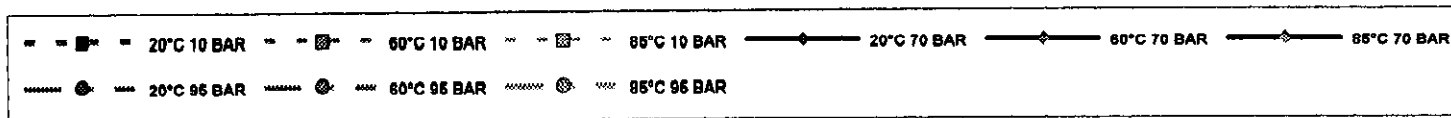


Fig. 8

Crude Oil 0,89 kg/l and 19cSt at 20/10 (°C/bar) and 60/70 (°C/bar)

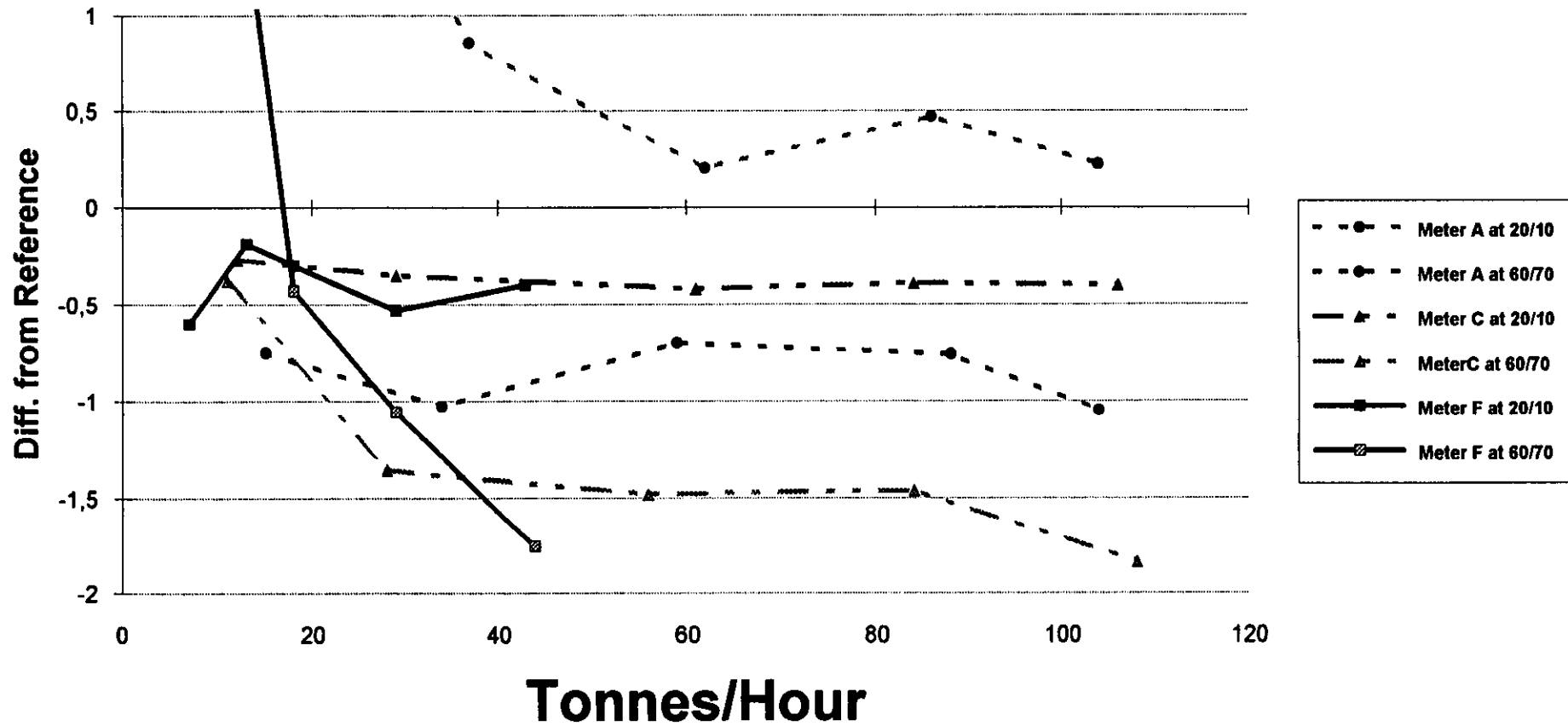


Fig. 9

Naphtha 0,65 kg/l and 0,6cSt at 20/10 (°C/bar) and 60/70 (°C/bar)

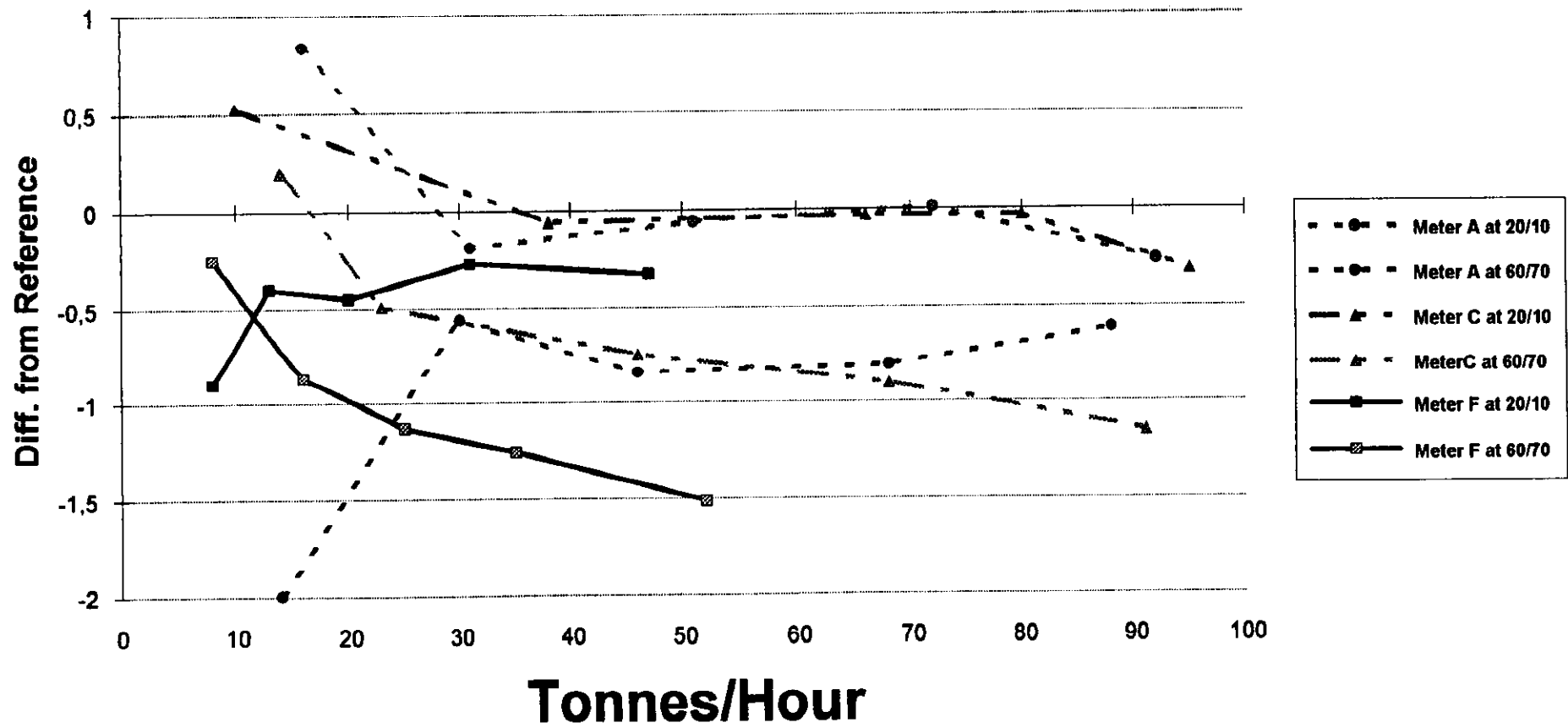


Fig. 10

Crude Oil 0,84 kg/l and 7cSt at 20/10 (°C/bar) and 60/70 (°C/bar)

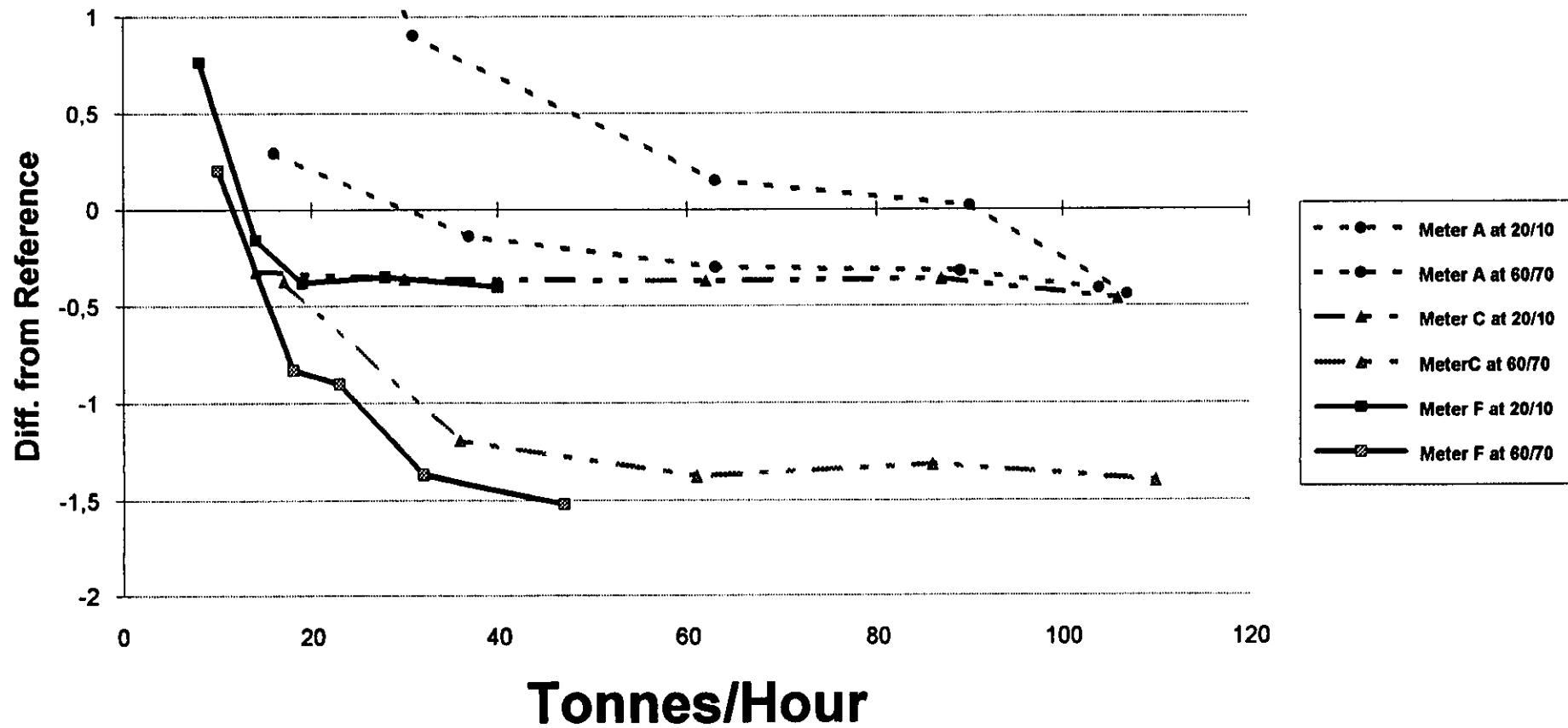


Fig. 11

Meter A at all Points Naptha

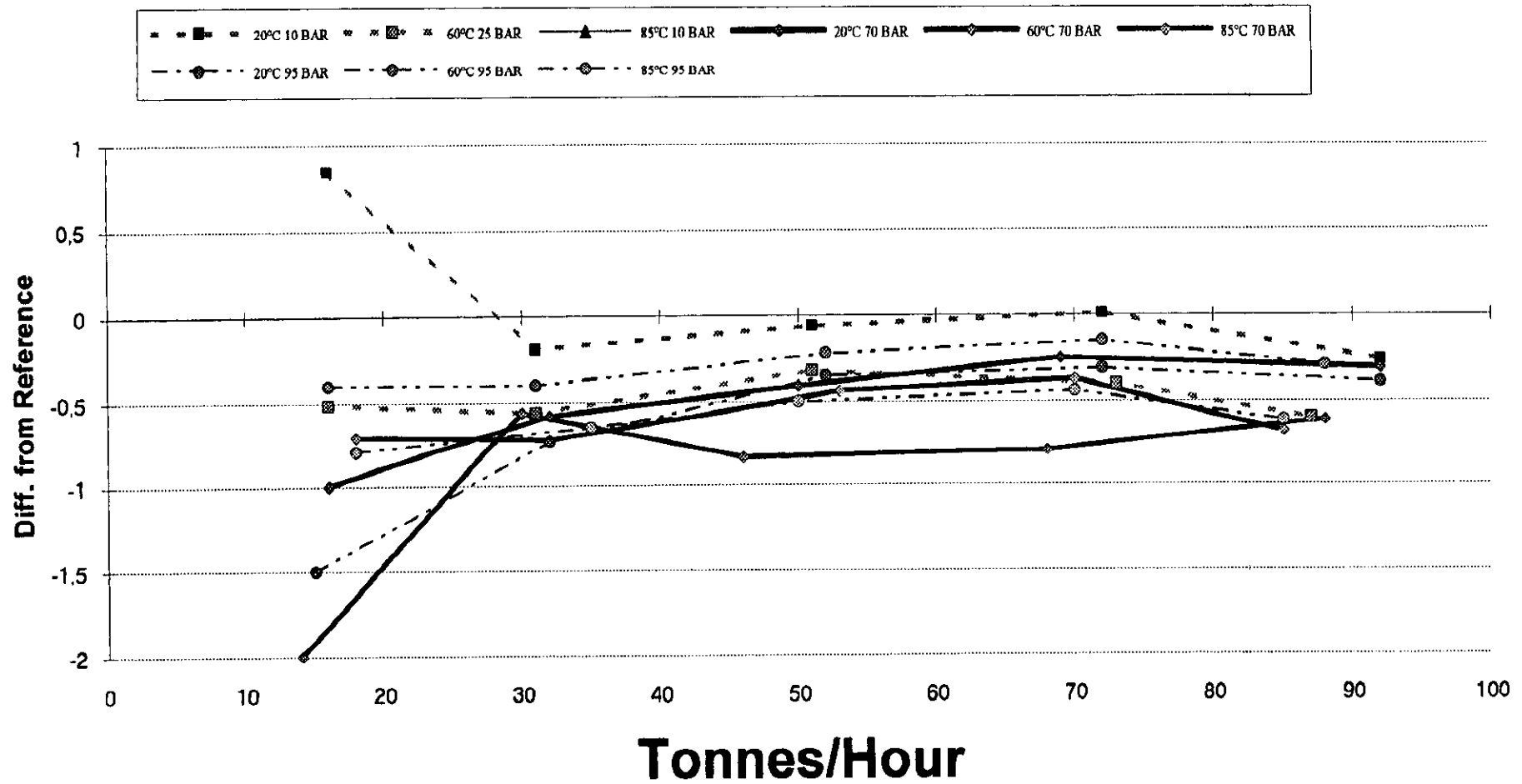


Fig. 12

Meter A at all Points Crude Oil (0,89/19)

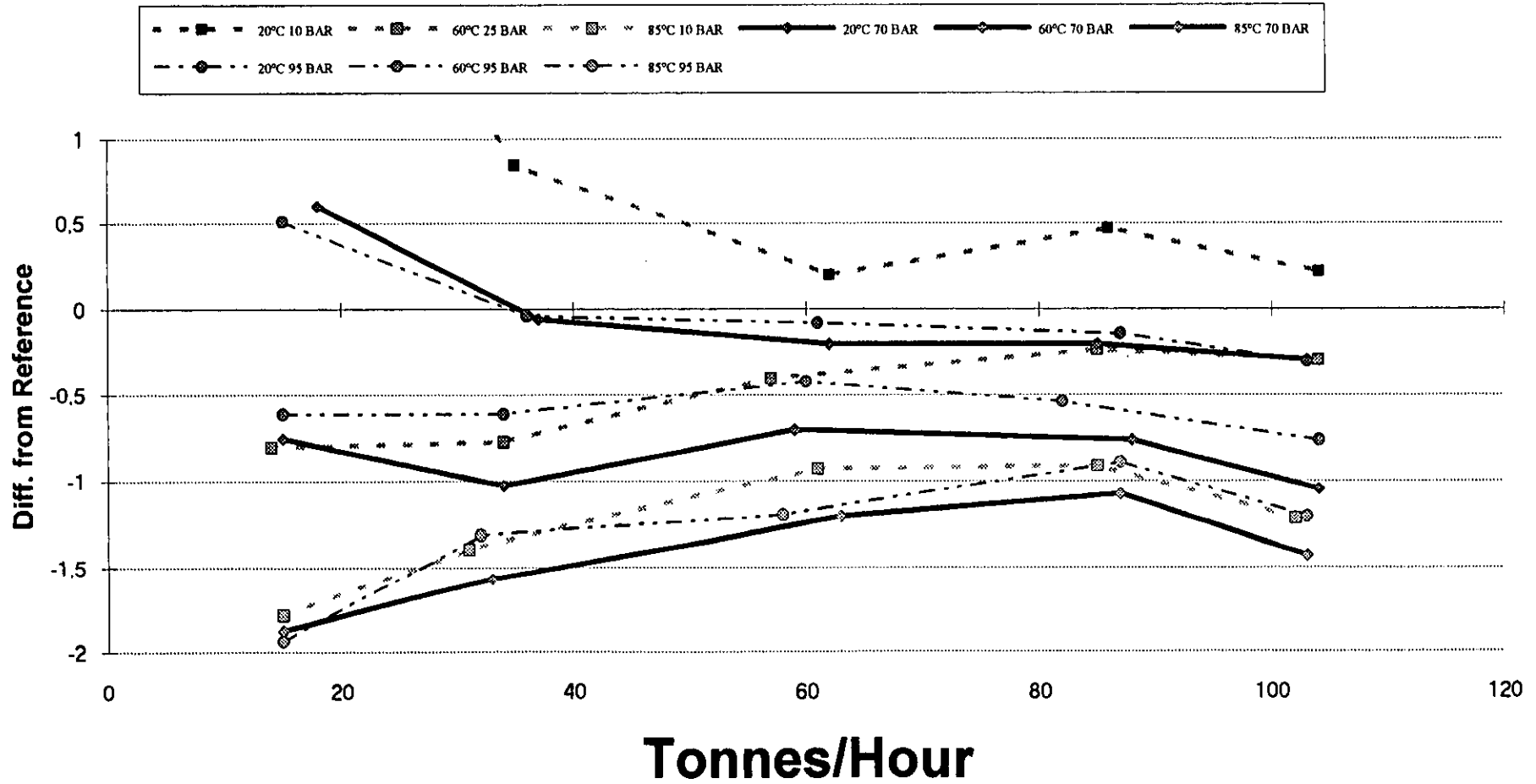


Fig. 13

Reference Turbin Meter 3" on Water

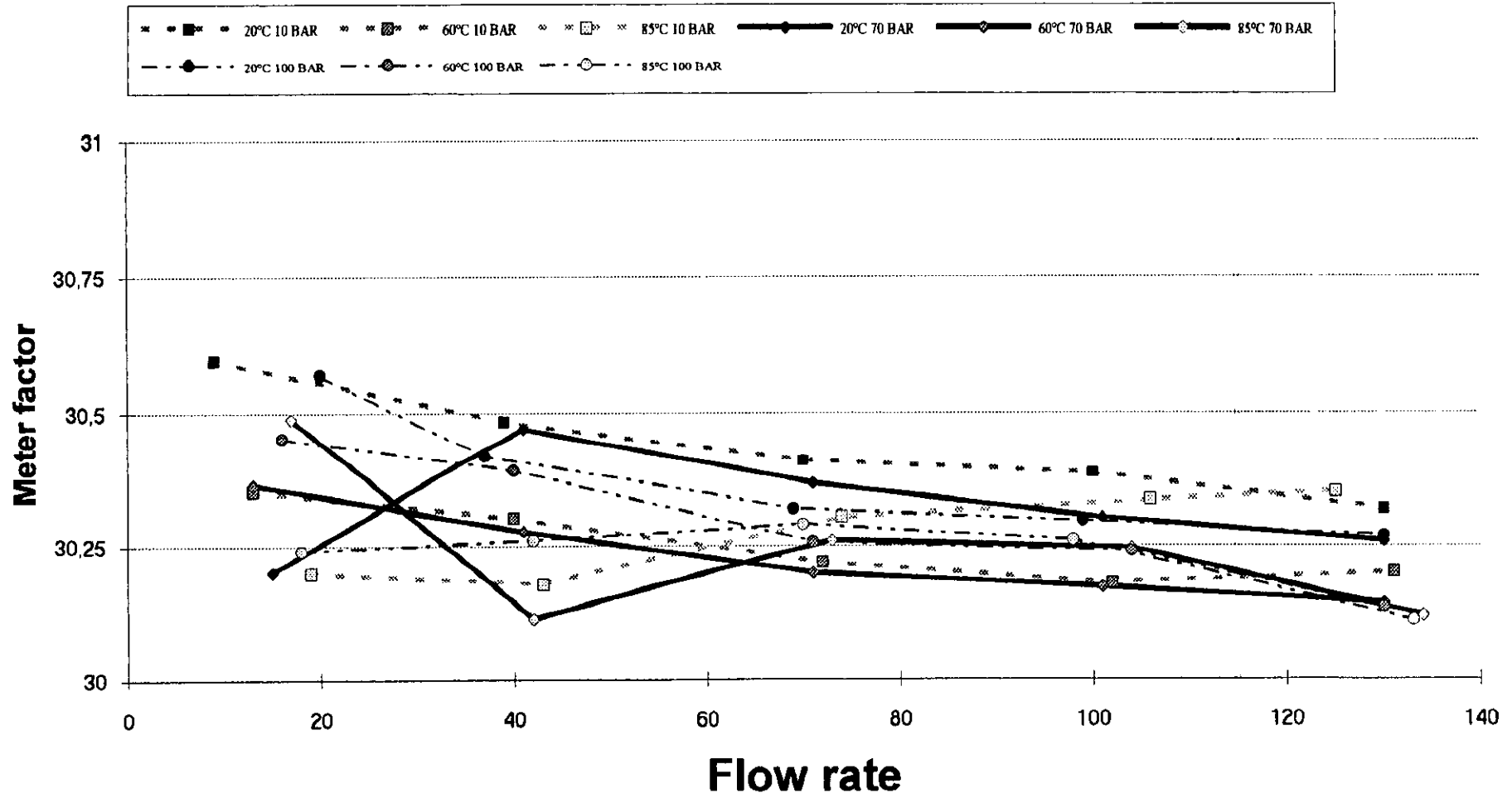


Fig. 14

Reference Turbin Meter 2" on Water

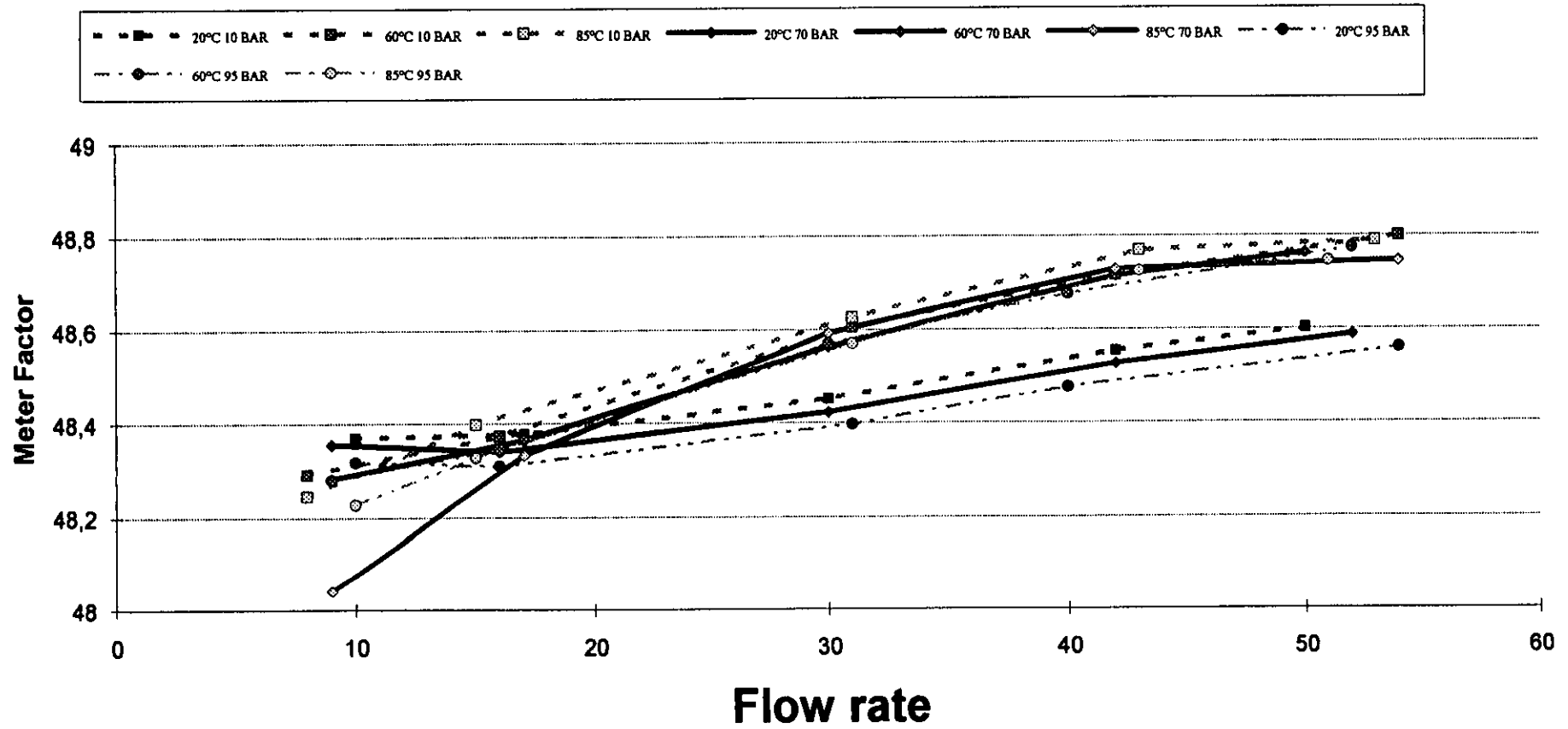


Fig. 15

Reference Turbin Meter 3" on Hydrocarbons

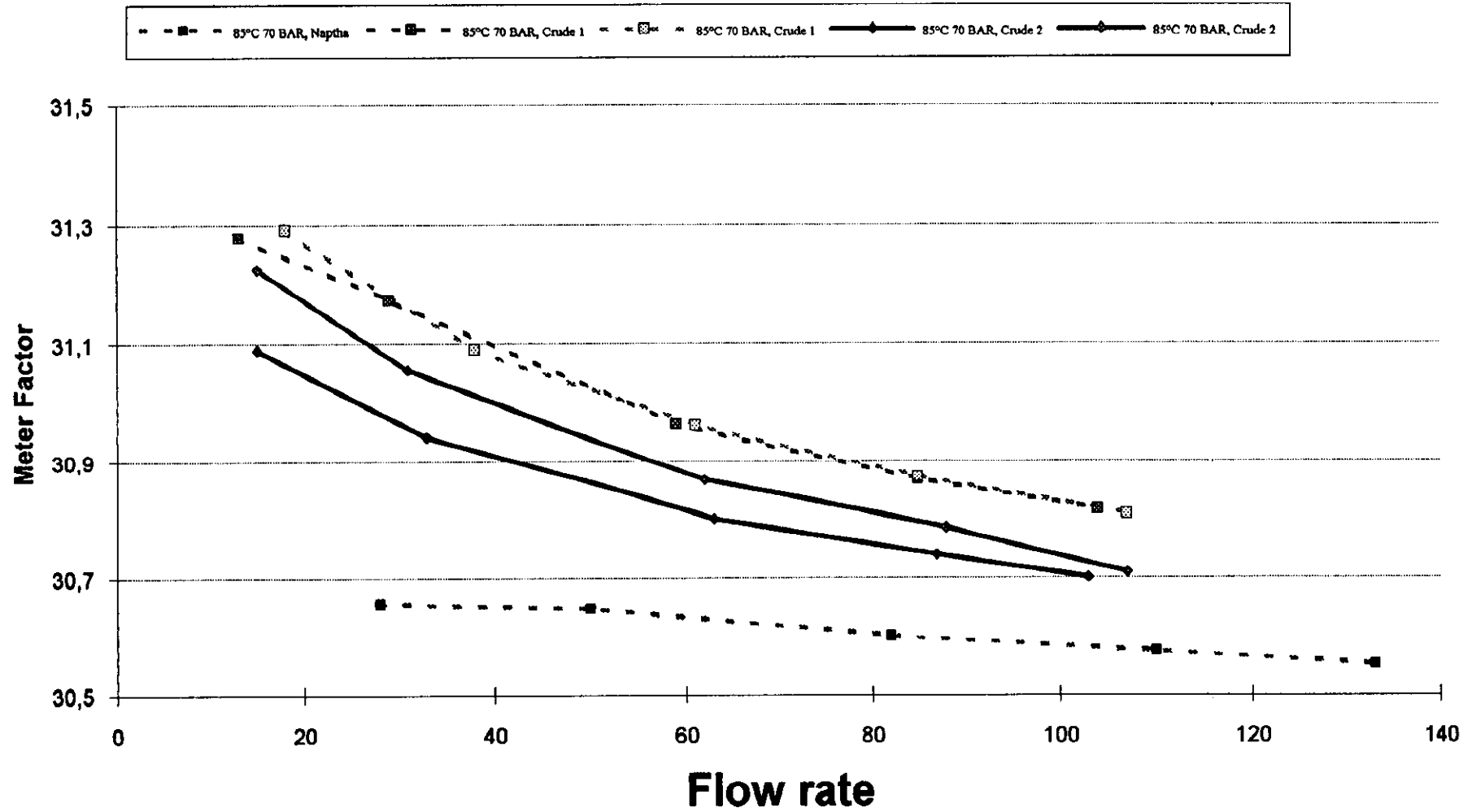


Fig. 16

Reference Turbin Meter 3" on Crude Oil

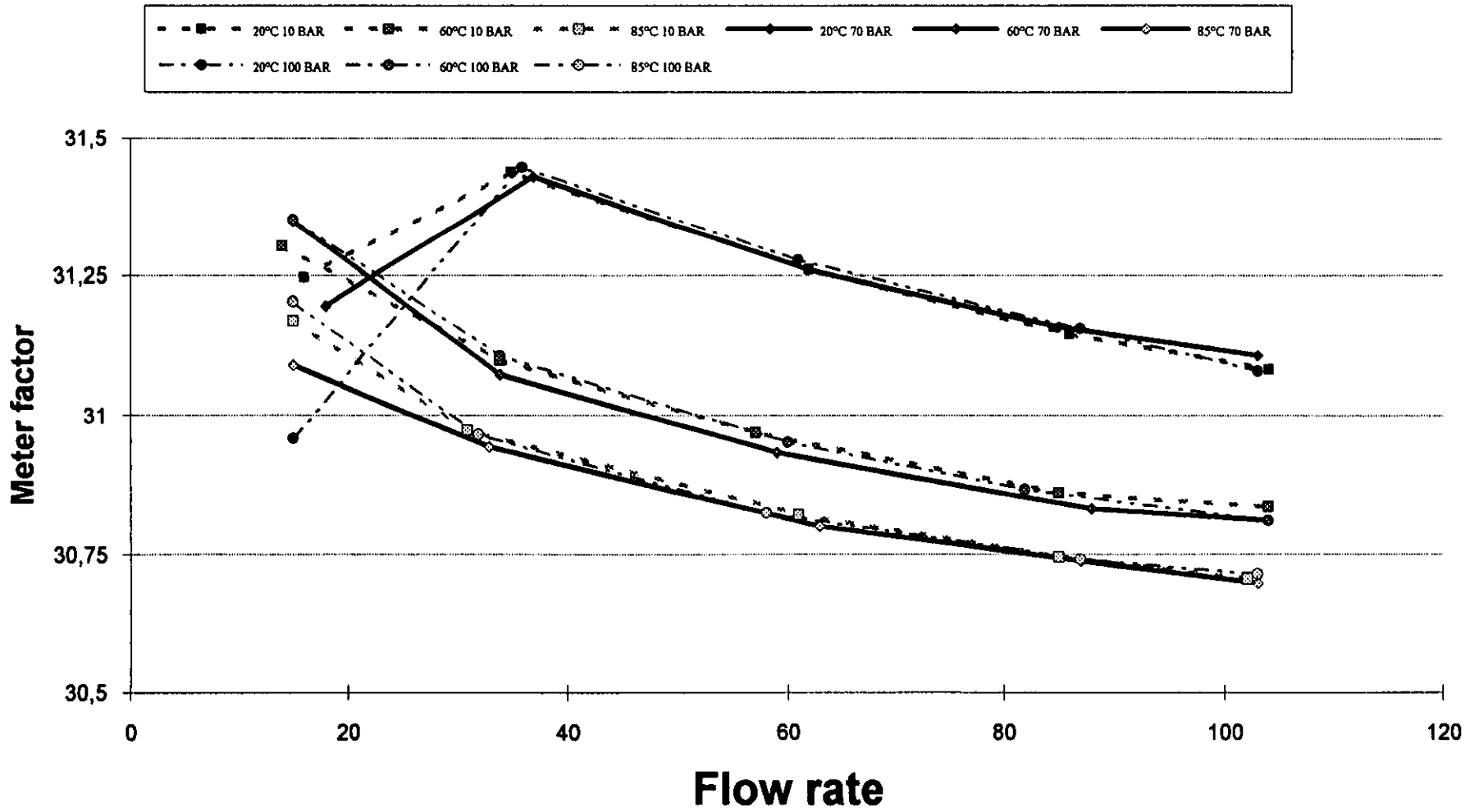


Fig. 17

PRACTICAL APPLICATION OF CORIOLIS METERS FOR OFFSHORE TANKER LOADING FROM THE HARDING FIELD

V. R. Withers - BP International, Research and Engineering

W. Strang - BP Exploration, Harding Development

G. Allnutt - BP Exploration, Harding Development

SUMMARY

The Harding Oil Field is a first application of Coriolis meters for the offshore measurement of 'oil won and saved' and tanker export. A meter skid comprising six inch Micro Motion D600 Coriolis meters and a 24 inch Rosemount Brooks compact prover has been manufactured, tested, installed and commissioned offshore. Coriolis meters were chosen because of the high viscosity of the Harding oil and operating cost savings from hoped for extended meter proving intervals up to 6 months.

The experience from the first three months of field operations and factory acceptance trials are presented in the paper. This shows successful performance of the Coriolis meter and compact prover combination in an offshore custody transfer environment. Stability of meter proving over the first three months is within a band of $\pm 0.2\%$, which bodes well for the anticipated reduction in frequency of proving. Comparisons between offshore proving on oil and factory calibration on water are within 0.4%, which gives support for the use of Coriolis meters without offshore proving.

1. BACKGROUND

The Harding Oil Field lies in UKCS licence block 9/23b in the Northern North Sea, approximately 320km Northeast of Aberdeen, 190km north of Forties and 35km south of Beryl. It is an Eocene reservoir and was discovered by Britoil (now owned by BP Exploration) in January 1988. The Partners are BP (Operator), Repsol and Ranger.

The Harding field was originally named Forth and changed in 1993 in memory of David Harding CBE former Chief Executive BP Exploration Europe. The field comprises several pools of oil. When initially examined for development, using conventional production platform technologies, it could not be made commercially viable. Radical new approaches were necessary.

The chosen solution for the Harding Development is a novel, large, purpose designed, heavy duty jack-up platform, providing fully integrated drilling, production and quarters (PDQ) facilities. It has been fabricated by Hyundai in Korea. It is fixed to a gravity base tank (GBT) foundation, designed and constructed by a Costain Taywood Joint Venture in London and Hunterston in Scotland. It also acts as storage for the separated crude oil and as a well template.

Oil temporarily stored in the concrete gravity base is exported via a short (2km) 24" pipeline and submerged turret loading (STL) system to shuttle tankers on a batched basis.

These facilities combined with the advantages made possible by significant advances in horizontal well technology turned Harding round from a being at best a marginal prospect into a viable enterprise.

2. METERING PHILOSOPHY AND DESIGN CONCEPT

2.1 Meter Selection

The Harding crude oil is heavy by North Sea standards. It is low in sulphur and wax content, but is particularly viscous at low temperature (600 to 1200 cP). With this high viscosity Harding crude cannot be measured using traditionally approved turbine meter methods. The viscosity was also too high for Faure Herman Heliflu turbine meters, often appropriate for more intermediate viscosity. So first thoughts were to use positive displacement (PD) meters. However these have moving parts, require regular proving, can generate high vibration and tend to require relatively high levels of maintenance.

Coriolis meters appeared to offer an obvious alternative. The mass flow measurement is claimed to be insensitive to viscosity variations and the meters have no rotating parts. They potentially have high inherent stability of calibration and low operating costs. This calibration stability of Coriolis meters offers the potential prize of significantly increased periods between calibration checks.

After careful review of the Coriolis meters on the market it was concluded that the Fisher Rosemount Micro Motion Coriolis mass flow meters met the requirements for the operational ranges of flow rate. Detailed analysis of the measurement and calibration uncertainty was conducted through close working between the BP Harding Development team, BP Research and Engineering, Jordan Kent Metering Systems (JKMS, the chosen skid supplier) and Fisher Rosemount. It was concluded that a viable solution was achievable using Coriolis meters.

2.2 Proving

Proving of mass meters in situ remains a problem because there is, as yet, no direct mass proving system available for an offshore application. The alternative is to prove against a volume prover with a closely associated on line density meter.

Use of alternative routine calibration methods to a conventional pipe prover were considered, with the emphasis being to minimise skid size, weight, and capital cost and to reduce maintenance costs. These alternatives included use of a reference meter with onshore calibration or transportable compact prover combined with reduced frequency of proving.

A Rosemount Brooks 24 inch compact prover in combination with Solartron Type 7835 density meters installed in a conventional fast sample loop were chosen for proving. A particular issue here was whether an acceptable repeatability of proving could be obtained with Coriolis meters and the short proving times (down to one second) that are inevitable with large

meters in conjunction with a compact prover. This was first substantiated by pre-purchase testing at Micro Motion facilities in the USA.

2.3 Uncertainty Calculations

Calculations showed that, using a compact prover with a Coriolis meter, an overall measurement uncertainty of $\pm 0.25\%$ on standard volume flow was possible. Mass flow uncertainty was slightly less at $\pm 0.23\%$, because there is less dependence on density measurement. The largest contribution to uncertainty was a generous allowance of $\pm 0.2\%$ to allow for possible shifts in calibration during the hoped for 6 monthly proving intervals. Tables 1 and 2 show more detail.

Given these uncertainties and the special case of high viscosity, the DTI (GOM) were happy to see Harding as a first application for metering crude oil 'won and saved' offshore using Coriolis meters. A requirement for all parties was that acceptable calibration methods and operating practices were developed to achieve the necessary performance.

2.4 Detail of Metering

The metering concept adopted was to use a single six inch D600 meter (named P) to measure the oil produced to the GBT storage (64,000 barrels per day, tested to 500 t/h) and six, similar meters (named T1 to T6), to measure the oil exported from the storage tank to the offshore shuttle tankers (400,000 barrels per day, tested to 500 t/h per meter). Volume is the primary measurement for tanker loading. The Coriolis meter internal density function and the separate density meter are used for conversion from mass to volume as measured and then to standard volume, using the normal temperature and pressure corrections for oil. The density part of the Coriolis meter is calibrated against the separate density meter which is also used for the mass proving.

Figure 1 shows the configuration of the meters and prover. The density loops are standard fast sample loops containing the Solartron 7835 density meter, flow proportional samplers and an MFI microwave water in oil analyser.

New issues, to be taken into account in applying the Coriolis meters, included dealing with the potential effects of external vibration, cross coupling vibration causing frequency shift of meters in adjacent streams, mechanical stress, meter orientation and support. The meters were oriented so that flow is vertically upward to avoid any trapped gas pockets in the 'U' bend of the instruments. They are solidly supported at the inlet and outlet and structurally bonded to the relatively large mass of the skid. This is to minimise cross-talk effects between streams and external stress influences. Effects due to external vibration were thought to be unlikely, but provision was made to mount the complete metering skids on anti-vibration mounts should it later become necessary. Field operation has so far not identified vibration as a problem.

2.5 Flow Computers

Flow computers are used in addition to the Coriolis meter field transmitters. This application required some extra functionality and then modification to standard flow computers. Details of the data flow are shown in Figure 2. Mass pulses were chosen as the primary data, because

these are necessary for accurate proving. To check the continuous integrity of these pulses, comparisons are made between mass totals and mass flow rates as derived from the pulses and as derived from interrogation of the transmitters via the serial data link. This link is also used to pass on any Coriolis alarm states. The flow computer also applies corrections to the raw readings, in particular for the effect of pressure on mass flow rate.

The control and computer panel for the metering skids was supplied by SpectraTek as part of the JKMS package. SpectraTek chose to use a modified version of their S500 stream computers with two S1000 supervisory computers to manage the skid operation and quantity reporting.

2.6 Determination of Water

MFI continuous analysers are installed to determine water content. It is hoped that, after a period of verification, these continuous measurements will be used in place of traditional sampling and analysis. The flow computers were also modified to perform continuous live calculations of dry oil quantities. This is not a critical application because Harding water content is expected to be low.

3. FACTORY ACCEPTANCE TESTING

All meters were tested on water as part of factory acceptance at JKMS over a flow range of 10:1 from 490 t/h for the D600 meters. The table below shows the nominal test points.

TEST FLOW RATES	
Percent of Design	6 inch D600 Meters
100%	490
60%	294
20%	98
10%	49
PRESSURE	1 to 5 barg
TEMPERATURE	15 to 30 °C

The results are shown in Figures 3 and 4. Four of the meters were within 0.1% of the factory calibration at all flow rates. Of the other three meters, two were within 0.2% of the factory calibration at all flow rates while the last one was only outside this limit at the 20% flow rate and below.

The differences between the individual tests for a meter at the higher flow rates indicate the separate effects of stability of calibration with time after manufacturer calibration, cross-talk effects from special combination tests and test errors (from water density, prover swept volume and manufacturer mass calibrations). Total variations between tests are within a spread of $\pm 0.1\%$. This raises hopes that extended calibration stability and proving intervals may be achievable.

For each separate test, the K-factors in a sequence of up to 30 separate passes were determined. The standard deviation for the separate passes is shown for the tanker meters and the production meter in the table below. At the maximum flow rate the pass time was only 1.8 seconds.

Stream	T1	T2	T3	T4	T5	T6	P	Average
Number of Tests	6	7	8	7	7	9	11	
Standard Deviation %	0.09%	0.05%	0.06%	0.07%	0.09%	0.08%	0.09%	0.08

This is equivalent to a 95% confidence limit on a single pass of approximately $\pm 0.16\%$. This is equivalent to a 95% confidence limit on the average of 10 passes of $\pm 0.05\%$ ($0.16 / \sqrt{10}$). This is acceptable repeatability performance and is marginally better than that inferred from the earlier trials performed by Micro Motion. The averages of two groups of 10 passes should then agree within a 95% confidence limit of $\pm 0.07\%$ ($0.05 * \sqrt{2}$). During the tests such grouped averages were compared and their differences were broadly in line with this.

The above has led to a modification of the traditional standard turbine meter proof repeatability criteria to one that is more suitable to Coriolis meters in conjunction with compact provers. A prove will be made up of two proof runs each of 10 passes which should give a 95% confidence on the over all mean of the 20 passes of $\pm 0.036\%$. Proof acceptability for repeatability is that the two runs (each of 10 passes) should not differ from their mean by more than $\pm 0.035\%$. This limit will have to be reassessed during continuous operation to match the performance as found then with crude oil.

Qualitative observations during testing confirmed the known effect of pressure on the D600 accuracy of about -0.07% per bar. This was allowed for in the test results.

4. OFFSHORE PRACTICAL EXPERIENCE

First production started in May 1996. The production and tanker export meters have been successfully proved and used since then. This paper covers experience up to 5 August 1996. Data are being gathered as a matter of routine and analysis of them is ongoing. The written conclusions must then be seen as first thoughts and potentially subject to change and substantiation. The intention is to provide any up to date, as appropriate, during the presentation at the Workshop in October 96.

4.1 Meter and Proving Performance to Date

The all important performance of the meters and prover together in the field are simply seen by time plots of all the prove K-factors in Figures 5 to 8. For the production meter, proves prior to number 21 had to be discounted because of data entry errors in the flow computers.

There is a clear message that the proves are within a $\pm 0.2\%$ band of the averages for each meter. This is confirmed with the calculated 95% confidence limits shown in Table 3. The conclusion is that the residual scatter, regardless of its source, is small. So in operational terms, proving need not be performed as frequently as was done during this commissioning phase. For the time being proving is being continued once per tanker loading and weekly for

the production meters. It can be seen that there is every hope that, given continued similar performance, proving frequencies can be further reduced.

The residual scatter is of limited interest to routine operations but it is of technical interest. There is some evidence of a drift with time (Figure 7 for meter T5 is the most pronounced). The flow curves Figures 9 and 10, show that it is impossible to distinguish between any true flow linearity effect or a time trend. The other meters showed less of any effect.

Temperature has always been above 25°C, so viscosity in excess of 100 cP has not yet been experienced. Operating temperature is in the range 30°C to 50°C. A correction for the effect of pressure on the Coriolis meter tube is continuously applied (0.072%/bar). Export meter pressures are in the range 16 to 25 barg, while production meter pressures are approximately 6 barg.

4.2 Repeatability of Compact Prover Runs

The acceptance criterion for a "good" prove is that the averages of two sets of 10 passes do not differ from their mean by more than 0.07%. This is a relaxation of the figure derived in the factory acceptance tests. Table 4 shows that the average repeatability for each meter was below this tolerance and that four of the seven meters never exceeded the limit. There is evidence that this tolerance could be reduced, particularly because conditions are likely to be more stable after commissioning. This is being reviewed as more data are gathered.

4.3 Absolute Comparisons Against Factory Tests on Water

From a commercial perspective, it is the meter performance as proved against the compact prover offshore on oil with the swept volume from the offshore water draw that is relevant. It is technically interesting to compare the offshore proved K-factors on oil with those from the skid factory acceptance trials and the original Rosemount Micro Motion factory calibration at Veenendaal (calibration K-factor = 36716 pulses/tonne). This is shown in the table below and graphically in Figure 11 (negative % means factory calibration K-factor higher).

Difference From Factory Calibration on Water							
Meter	T1	T2	T3	T4	T5	T6	P
FAT - Water	-0.04%	-0.07%	-0.05%	-0.04%	0.06%	0.06%	-0.16%
Field - Oil	-0.33%	-0.41%	-0.43%	-0.41%	-0.26%	-0.33%	-0.85%

These data are all corrected back to a common pressure of 0 barg using the Micro Motion supplied factor of 0.072%/bar (the K-factors quoted in Table 3 are referenced back to 29.6 barg and 6.5 barg for the tanker and production meters respectively). At 29.6 barg the K-factors are 2% lower without this correction. A 17% increase in this correction factor would be sufficient to reduce the average difference for the field results to zero. The uncertainty in this coefficient is unlikely to be much better than this. The larger difference for the production meter could be due to trace gas break-out immediately after separation, though this is far from proven. However there was also a larger deviation for this meter at the factory acceptance trials, so some installation effect is another possibility.

The important conclusion is that, for the more important export meters, the size of the difference from original factory calibration is only 0.4%. This gives substantiation to the use of Coriolis meters with factory calibration on water only and no offshore calibration on oil, provided an uncertainty of say 0.5% is acceptable. To substantiate a lower uncertainty, a satisfactory explanation for the residual difference is required. Possible effects to be considered are:

- Error in density measurement (calibration and temperature) - some effect here likely.
- Residual pressure or temperature effects on the Coriolis meter.
- Installation effects offshore (pipe stresses etc.).
- Effect of viscous oil rather than water on Coriolis meters.
- Effect of viscous oil rather than water on compact prover.
- Difference from reverse direction water draw with "downstream" prover.
- Error in water draw of compact prover (unlikely - factory/offshore agreement).

The relative merits of these possibilities, and indeed other suggestions should provoke much discussion.

5. CONCLUSIONS

It is too early to finalise conclusions on the all important offshore experience. To date this has shown successful performance of the Coriolis meter and compact prover combination in an offshore custody transfer environment. Stability of meter proving over the first three months of operations has shown all meter proving to be within a band of $\pm 0.2\%$, which bodes well for the anticipated reduction in frequency of proving. The intention is to increase proving intervals progressively up to once every six months as operating experience justifies this.

Comparisons between offshore proving on oil and factory calibration on water are within 0.4%, which gives support for the use of Coriolis meters without offshore proving.

In project terms, the adoption of Coriolis technology combined with working very closely with the skid supplier JKMS, the flow computer supplier SpectraTek and Fisher Rosemount has resulted in a significant reduction in capital costs. The expectation remains that significant savings are to be realised on Harding during operations, compared with the once per tanker loading proving and maintenance overheads associated with more conventional high accuracy metering methods.

Acknowledgements

The authors wish to thank the Harding team, in conjunction with SGS Redwood, for providing the experience and data upon which this paper was based.

MAIN SOURCES OF UNCERTAINTY	MEASUREMENT UNCERTAINTY	
	MASS %	VOLUME %
Swept Volume	0.05	0.05
Prover Density 0.5 kg/m ³	0.06	0.06
Liquid Temperature/Pressure Corrections		
Prover Densitometer 0.5 deg C	0.05	0.05
Prover	0.05	0.05
Meter		
Repeatability of prove with meter	0.04	0.04
Calculations	0.00	0.00
TOTAL K-Factor	0.11	0.11

Table 1 - Uncertainties - Proved K-Factor

MAIN SOURCES OF UNCERTAINTY	MEASUREMENT UNCERTAINTY	
	MASS %	VOLUME %
Prove (from above)	0.11	0.11
Allowable deviation between proves	0.20	0.20
Meter Densitometer - Header (Schlumberger)		
Including drift between cal. 0.5 kg/m ³		0.06
Liquid Temperature/Pressure Corrections		
Meter Densitometer 0.5 deg C		0.05
Meter (for standard volume) 0.5 deg C		0.05
Coriolis Meter Pressure Corr. 10% of corr.	0.04	0.04
Calculations	0.00	0.00
TOTAL	0.23	0.25

Table 2 - Uncertainties - Metering

K-Factor Stability over Time				
Meter	Average all proves p/t	Difference from Average all tanker %	Standard Deviation all proves %	95% Confidence Limit %
T1	35827	0.03%	0.09%	0.19%
T2	35796	-0.05%	0.07%	0.14%
T3	35792	-0.06%	0.08%	0.16%
T4	35798	-0.05%	0.07%	0.15%
T5	35850	0.10%	0.10%	0.21%
T6	35827	0.03%	0.09%	0.18%
P	36234	1.17%	0.06%	0.12%
Average	35815	< All Tanker		

Table 3 - Prove K-Factors to 5 August 96

Proof Repeatability - Two Sets of Ten Passes					
Meter	Maximum Difference from Mean (+/-)				
	Average	Max	Total Count	Number Greater Than:	
				0.070%	0.035%
T1	0.03%	0.10%	31	3	9
T2	0.02%	0.07%	26		5
T3	0.06%	0.40%	25	6	10
T4	0.03%	0.14%	26	3	9
T5	0.02%	0.05%	25		3
T6	0.02%	0.06%	26		4
P	0.02%	0.05%	66		6

Table 4 - Repeatability of Proves to 5 August 96

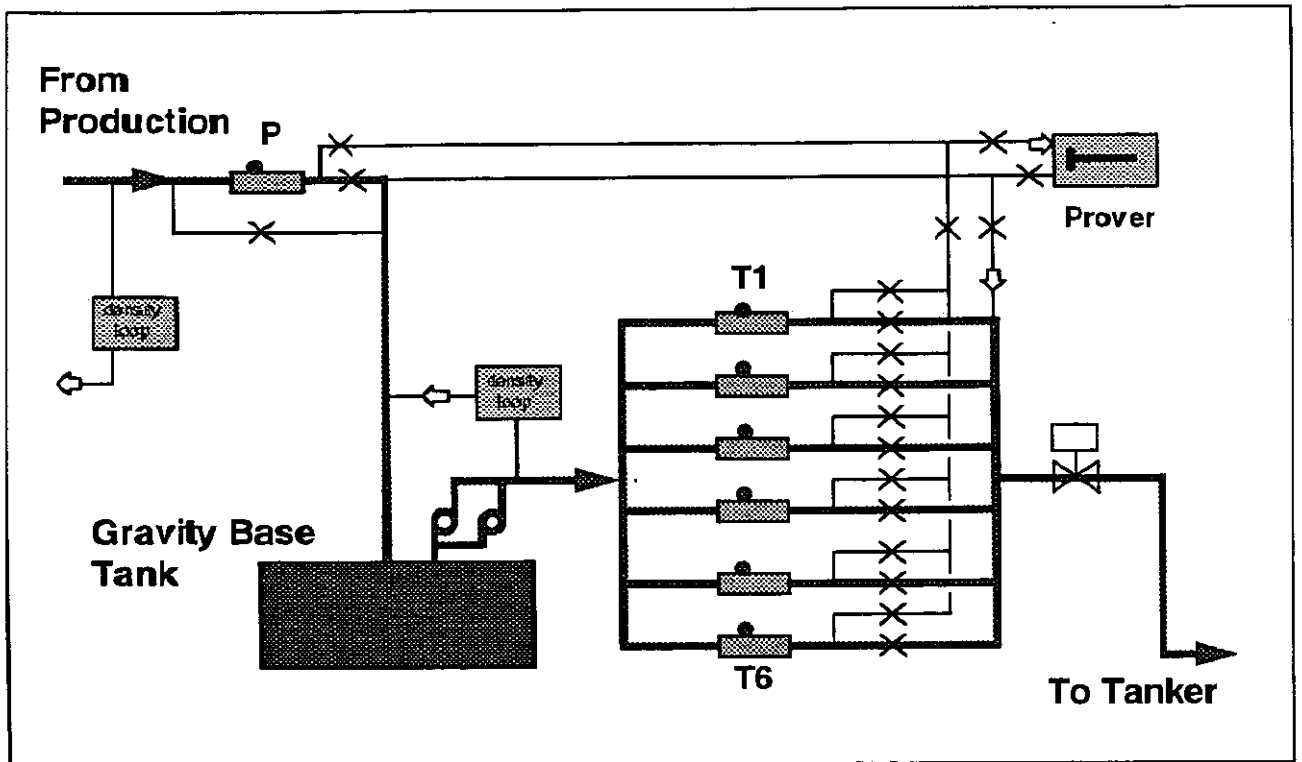


Figure 1 - Configuration of Meters and Prover

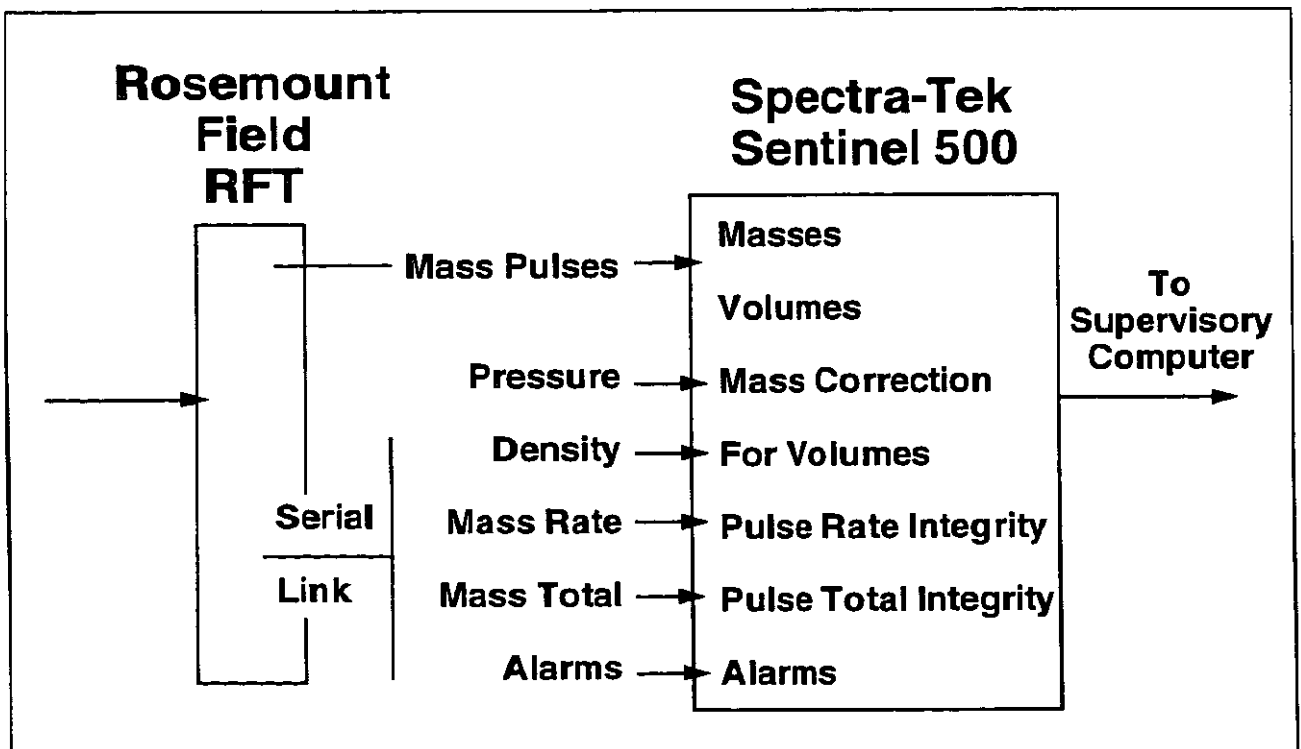


Figure 2 - Flow Computers and Data Flow

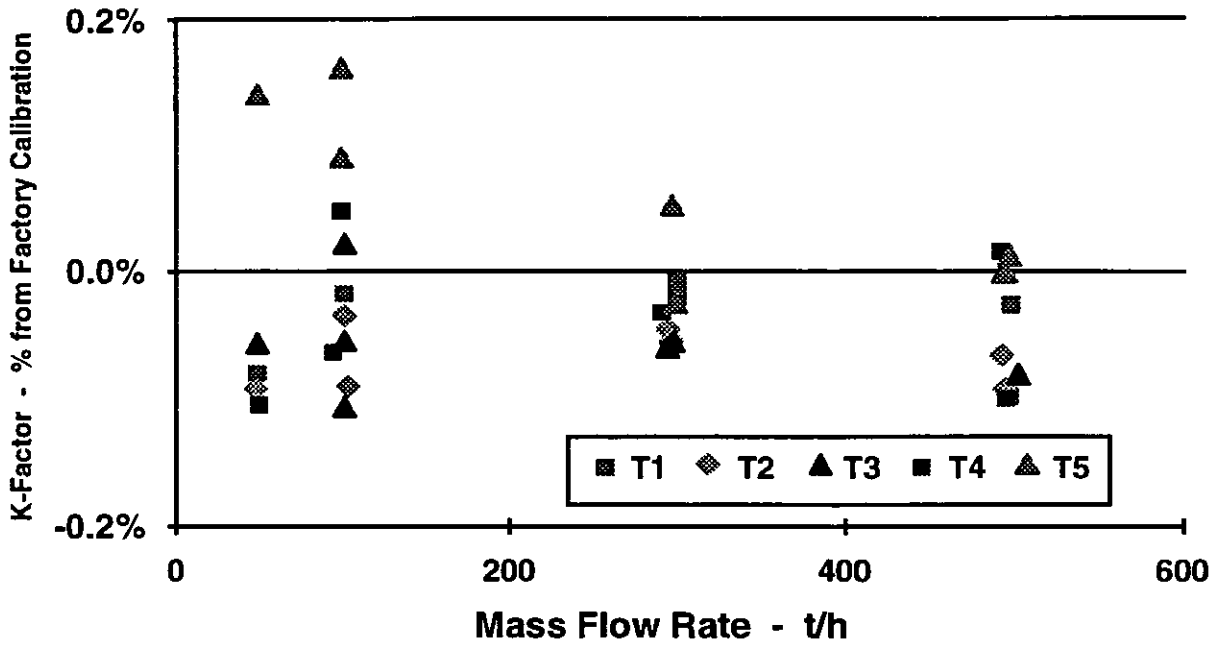


Figure 3 - Acceptance Tests on Water - Meters T1 to T5

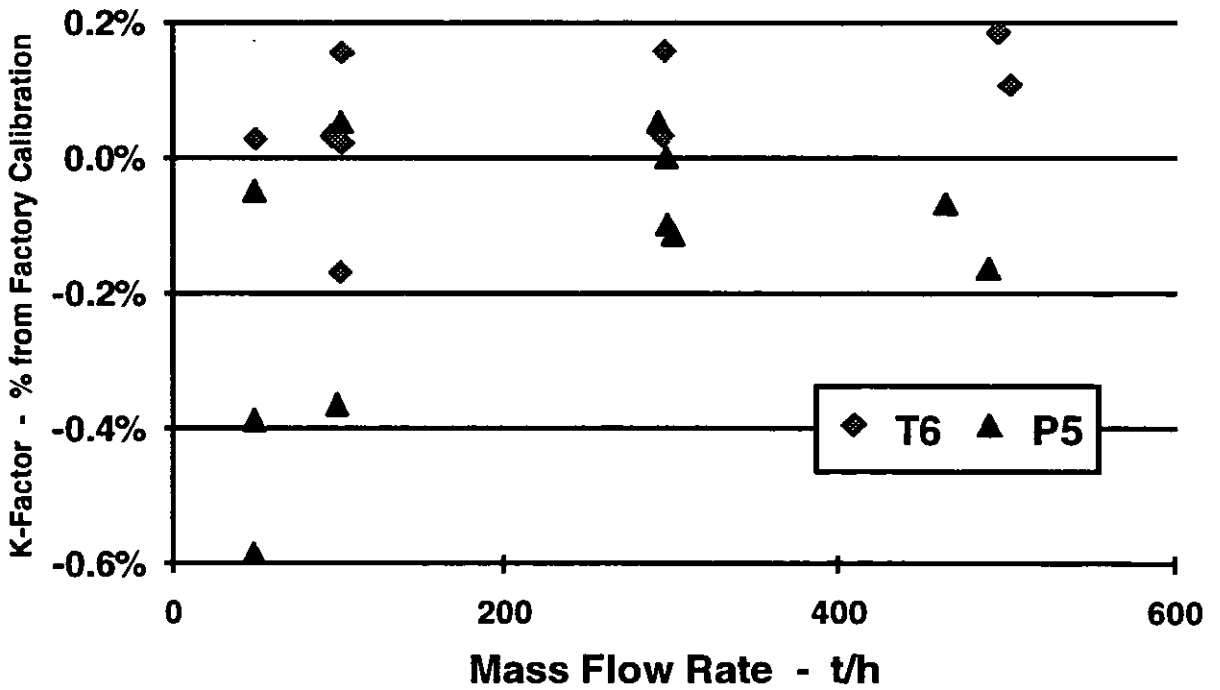


Figure 4 - Acceptance Tests on Water - Meters T6 and P

Control Chart - All Tanker Meters

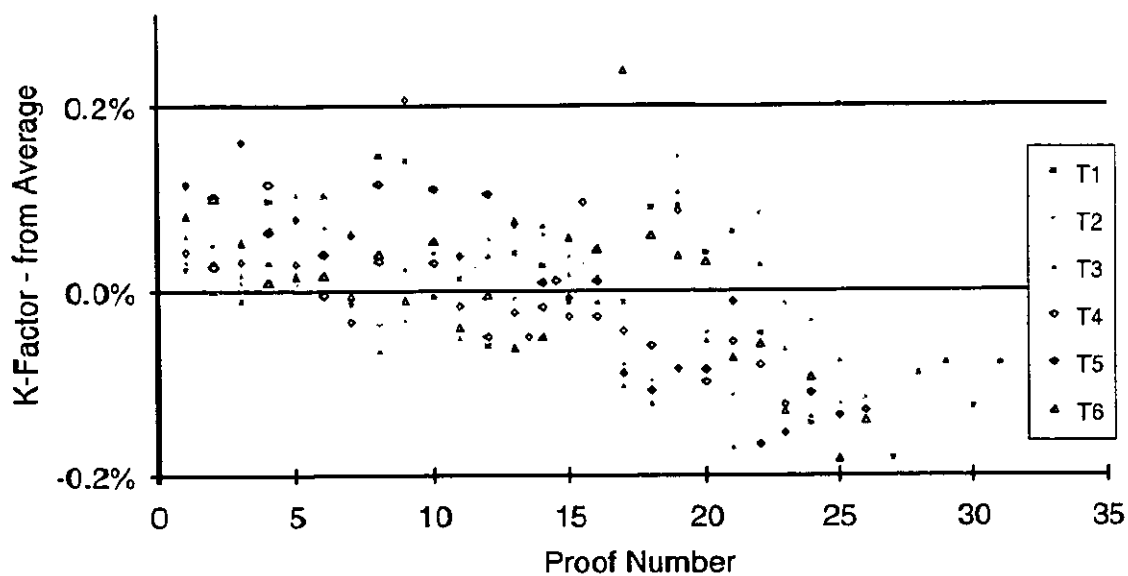


Figure 5 - Proves for All Tanker Meters (to 5 August 96)

Control Chart for Meter T2 - Typical

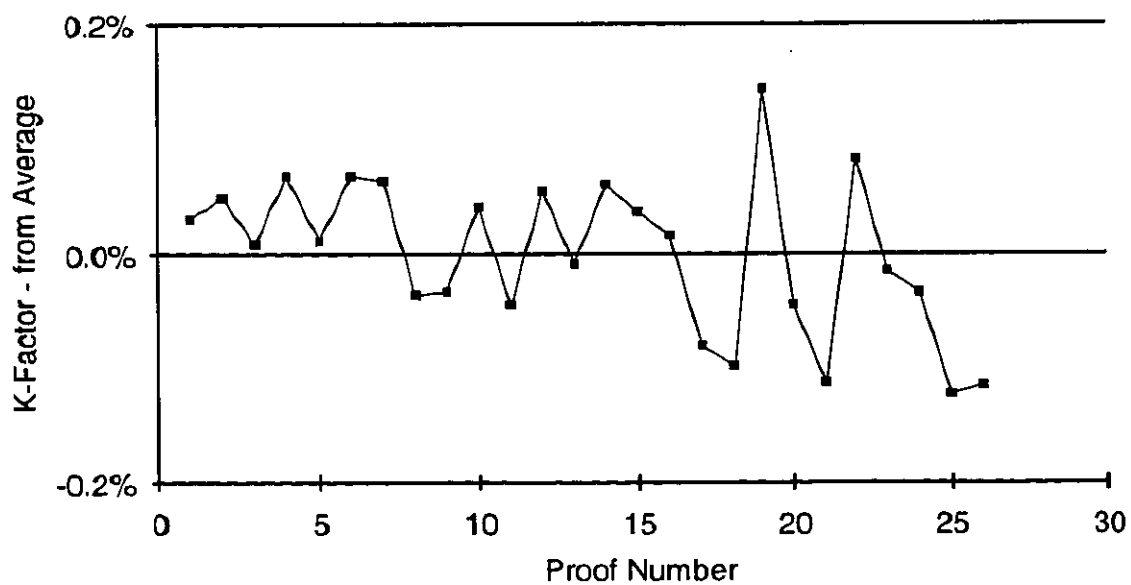


Figure 6 - Proves for Tanker Meter 2 (to 5 August 96)

Control Chart for Meter T5 - Possible Trend

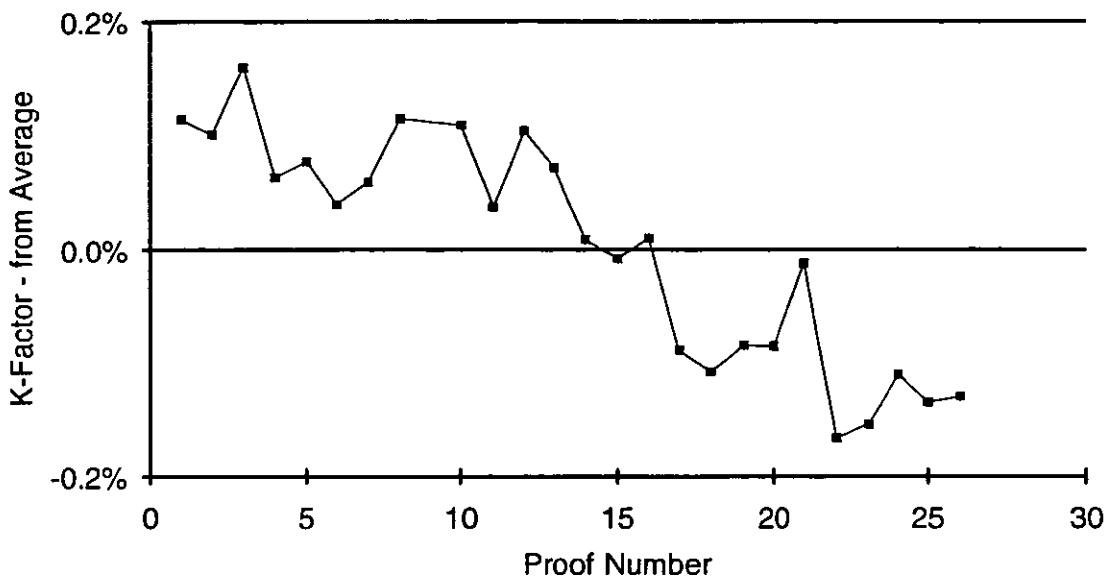
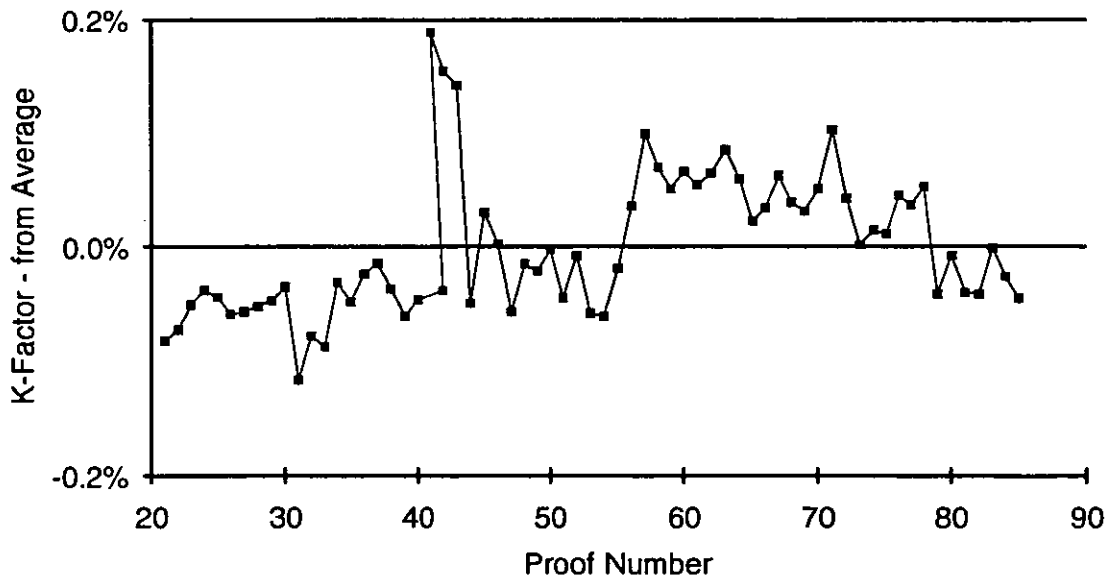


Figure 7 - Proves for Tanker Meter 5 (to 5 August 96)

Control Chart for Production Meter



Proves prior to number 21 had to be discounted because of data entry errors in the flow computers.

Figure 8 - Proves for Production Meter (to 5 August 96)

Flow Curve for Meter T5 - Possible Trend

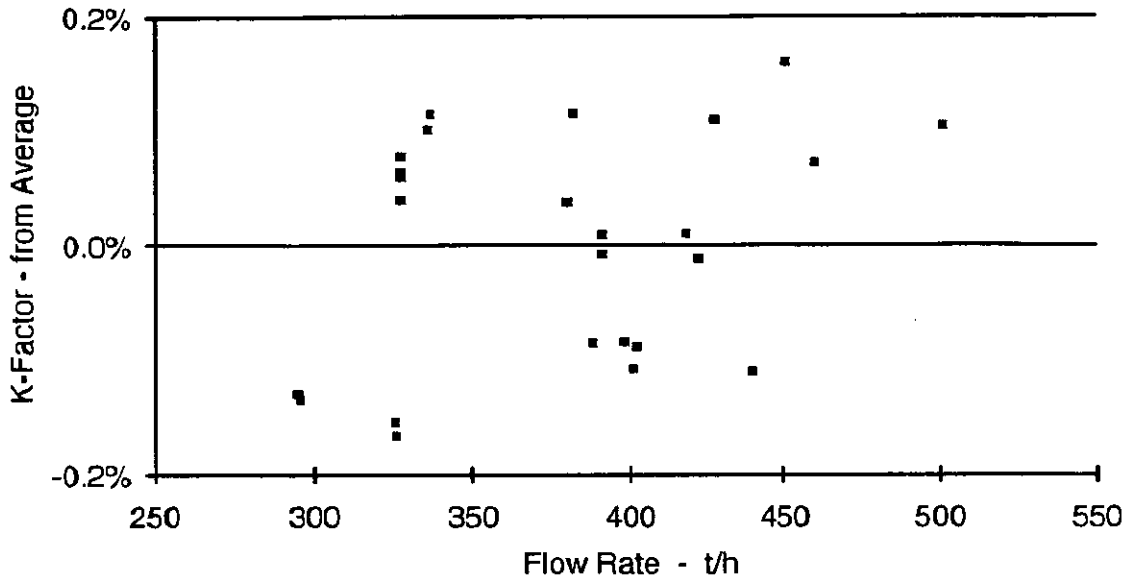


Figure 9 - Flow Curve for Tanker Meter 5

Flow Curve for Production Meter

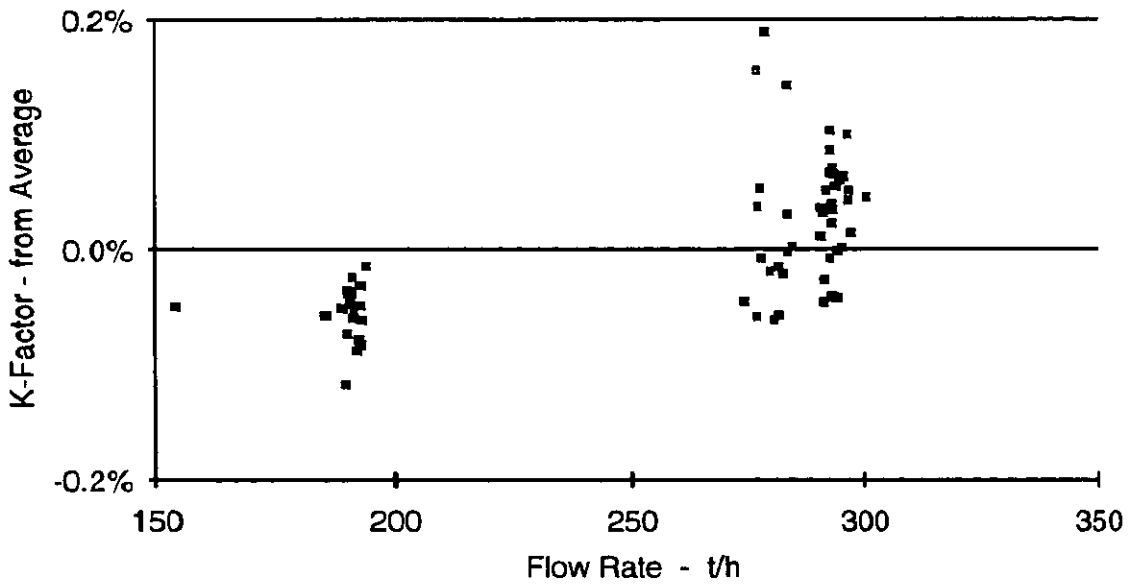


Figure 10 - Flow Curve for Production Meter

Absolute Comparison of All Results

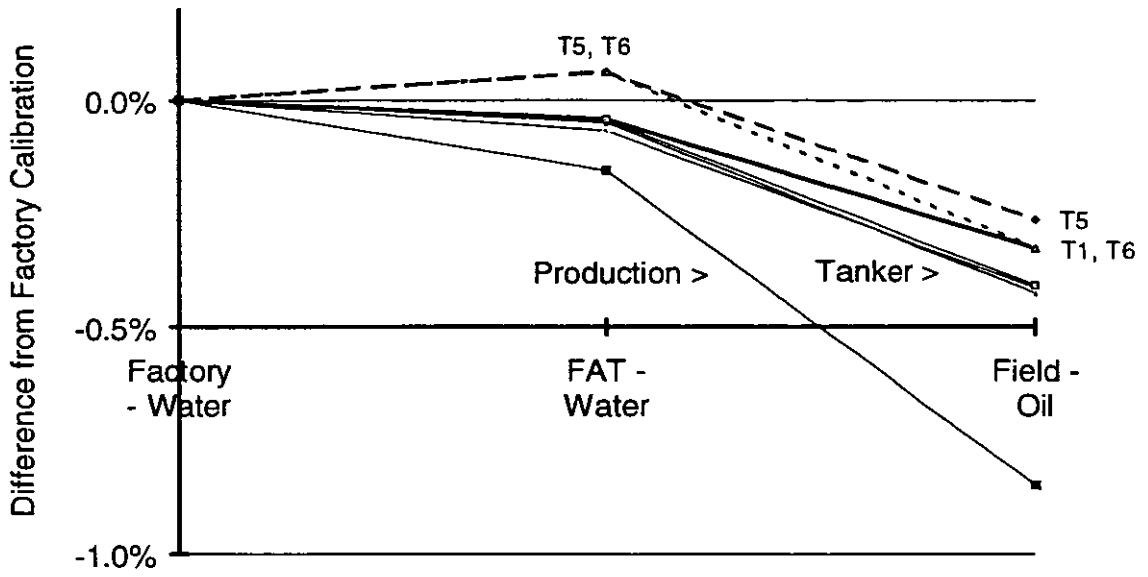


Figure 11 - Comparisons Back to Factory Calibration

NORTH AMERICAN INTER-LABORATORY FLOW MEASUREMENT TESTING PROGRAM

Umesh Karnik, NOVA Research & Technology Corporation, Calgary, CANADA.

Edgar B. Bowles, Jr., Southwest Research Institute, San Antonio, Texas, USA.

Jan Bosio, Statoil/Kärstø Metering & Technology Laboratory, Haugesund, NORWAY.

Steve Caldwell, Colorado Engineering Experiment Station Inc., Nunn, Colorado, USA.

ABSTRACT

An inter-laboratory flow measurement testing program has been established for the purpose of benchmarking individual North American facilities relative to each other and to other flow facilities in Europe. The North American laboratories involved are Colorado Engineering Experiment Station, Inc. (CEESI) in Nunn, Colorado, USA; the Gas Research Institute (GRI) Metering Research Facility (MRF) at Southwest Research Institute (SwRI) in San Antonio, Texas, U.S.A; and the NOVA Gas Dynamic Test Facility near Calgary, Alberta, Canada. Also, the Kärstø Metering & Technology Laboratory (K-Lab) in Haugesund, Norway, is directly participating in some of the North American round robin testing.

The initial inter-laboratory comparison tests involve two critical flow venturi nozzles: a NOVA nozzle (with a throat diameter of 10 mm) and a K-Lab nozzle (with a throat diameter of 23.3 mm). Tests have been conducted for a variety of compressible fluids using primary and secondary methods of flow reference. Results from both nozzles are presented for the three North American facilities and K-Lab. Test results, with the NOVA nozzle, from the National Engineering Laboratory (NEL) in Scotland are also included. Results for both nozzles indicate that, at a comparable Reynolds number, the facilities agree to within $\pm 0.2\%$. Results also suggest that the uncertainty in C^* may be negligible. Future North American inter-laboratory comparison plans include testing of the Groupe Européen de Recherches Gazières (GERG) G-650 tandem turbine meter transfer standard package and the EUROMET critical flow nozzle. The NOVA nozzle is also to be tested at Ruhrgas in Germany and at the Korean Research Institute of Standards and Science (KRISS) in Korea.

1.0 INTRODUCTION

In North America and elsewhere around the world, natural gas is more commonly being bought and sold as a commodity. The gas is typically bought and sold more than once between

the time it is produced at the wellhead and delivered to the end user. Because large amounts of gas are involved in these transactions and the financial stakes are high, a premium is placed on accurate measurement of the gas passing through each custody transfer point along the way. As an example, the NOVA transmission and distribution system (which is only one component of the gas transportation network in North America) transports approximately 1×10^{11} cubic meters (or 4 trillion cubic feet) of natural gas per year.¹ Thus, the cost associated with measurement uncertainties and errors in this one system can be quite significant, and increases proportionately with increased trade.

To ensure the highest level of flow meter performance, gas producers and transport companies either flow calibrate their meters (e.g., turbine and ultrasonic flow meters) or design and build their meters according to accepted industry standards (e.g., orifice meters). In the latter case, flow meter calibrations may still be necessary, particularly when custody transfer-disputes must be resolved. When flow calibrations are deemed appropriate, such tests are typically performed at facilities proven to have acceptable limits on measurement uncertainty and repeatability. At present, there are several flow calibration laboratories around the world that claim to meet these stringent performance requirements.

Mass and time can independently be measured very accurately and each can be referenced to an accepted standard. However, in the absence of a flow standard, one way of confirming that calibration laboratories can achieve acceptable measurement accuracy levels is to conduct inter-laboratory comparison tests. These inter-laboratory comparisons, or round-robin tests, involve the flow calibration of a single test artifact, such as a sonic nozzle, tandem turbine meters or other flow element, under similar test conditions at each facility. The results from the participating labs are then compared to ensure that the labs are in reasonably close agreement and that the customers of these facilities are provided with the best estimate of the true mass flow rate. Apart from providing the best estimate of the true mass flow rate, a round-robin test allows the facilities involved to identify and correct problems. Such tests must be repeated periodically so that the laboratories can preserve their measurement integrity.

Recently, several European flow calibration laboratories participated in a round-robin test of two twin-turbine meter packages conducted under the auspices of GERG (Technical monographic, 1993). This paper presents the results of similar tests performed at CEESI, the GRI MRF, NOVA and K-Lab involving two sonic nozzles. The participating North American labs are now also testing one of the GERG twin-turbine meter packages. There is also a possibility that in the near future, these same labs will test a sonic nozzle previously tested by the EUROMET consortium.

2.0 DESCRIPTION OF FACILITIES

A comparison of the facilities that have participated in the current inter-laboratory comparison is shown in Table 1. The facilities have a similar theme i.e. measure the mass flow rate as accurately as possible. For the measurement of mass, NOVA, GRI MRF and K-Lab use a weigh tank/scale manufactured by Wöhwa as the primary device. CEESI on the other hand uses a volumetric method to measure the mass. All facilities use high accuracy timers to evaluate the mass flow. Usually, the primary method is used in conjunction with a bank of sonic nozzles for flow stability. The nozzle bank used at GRIMRF and K-Lab is designed as a binary system. Nozzles with different throat diameters are used and can be choked in various combinations to obtain the chosen mass flow. The NOVA system is different in this regard. The nozzles in the nozzle bank are all identical and thus the flow rate can be increased in equal steps with the opening of each nozzle. CEESI does not have a bank of sonic nozzles, but uses a CEESI standard nozzle appropriate for the test. The facilities compare well with regards to calibration techniques and instrumentation for pressure, temperature, gas composition (CEESI uses air) and other parameters necessary for mass flow measurement.

The following sections provide a description of the individual facilities.

2.1 Colorado Engineering Experiment Station Inc.

A simplified operational schematic is contained in Figure 1. Air can flow out of one of two pressure vessels, they are identified as "calibration" and "supply". For the calibration vessel there is a known relationship between volume and pressure; at atmospheric pressure the volume is approximately 8.5 m^3 . The maximum pressure in the test section ranges between 7 and 70bar. The vessel is instrumented for the measurement of pressure and temperature (P_3 and T_3) hence the mass of air within the vessel can be determined. The supply vessel is a series of tanks with total volume of approximately 312 m^3 and maximum pressure capability of 170bar. The pressure vessel providing air flow to test section can be selected based on the position of a three way valve (V_2).

A pair of critical flow nozzles are installed in the test in series, one is the unit under test, the other is a CEESI standard used as a calibration check. The availability of a particular CEESI standard nozzle determines the installation details, the downstream unit must have the larger throat diameter of the two. A control valve (V_3) is located at the test section inlet to provide for flow control. Each nozzle is provided with pressure and temperature measurements (P_1 , T_1 , P_2 and T_2).

When the air expands as it flows through the system, the temperature will drop. If cool air flows through a warm pipe an air temperature measurement will be subjected to errors due to conductive and radiative heat transfer. To reduce such errors heat exchangers are installed downstream of each control valve, they are not shown in Figure 1. The heat exchangers are designed to maintain the air flow at ambient room temperature.

The mass flow is measured on the basis of measured pressure and temperature (P_3 & T_3) and knowing the volume of air in the calibration vessel. The uncorrected average mass flow rate is defined as the change of mass within the calibration vessel divided by the elapsed time. A small correction must be made to account for the air contained within the pipes and fittings that connect the calibration vessel and test section. The uncertainty in mass flow rate is estimated to be 0.1% at a 95% confidence level. Additional details regarding the operation and uncertainty of the present and a similar system are given by Arnberg and Britton (1971) and Kegel (1995).

The volume and maximum pressure of the calibration vessel limit the maximum flow rate to a value of approximately 4.0 kg/s. In order to obtain data at higher values of mass flow rate a CEESI nozzle is used as a calibration standard. The relationship between Re and C_d is determined based on the work of Smith and Matz (1962), Stratford (1964) and Arnberg, Britton and Seidl (1974). The uncertainty in the resulting mass flow rate is estimated to be 0.5% at a 95% confidence level (Kegel, 1994).

2.2 Gas Research Institute Metering Research Facility

The Gas Research Institute Metering Research Facility is operated by Southwest Research Institute and is located on the grounds of SwRI in San Antonio, Texas, U.S.A. The GRI MRF consists of three separate flow facilities: a High Pressure Loop (HPL), a Low Pressure Loop (LPL) and a Distribution Test Stand (DTS). All three flow facilities use either dry natural gas or nitrogen as the test medium. The HPL is the largest of the three flow systems and has the highest rated flow capacity and line pressure. The LPL is similar in configuration to the HPL, but is smaller in scale and operates at lower flow rates and line pressures. Both the HPL and LPL are closed-loop, continuous-flow facilities. The DTS is the smallest of the three flow systems at the MRF and is configured as a blowdown system. The inter-lab tests described herein were performed only in the HPL and LPL. The operating parameters for the HPL and LPL are included in Table 1.

Each MRF flow facility has a primary calibration system specifically sized for its range of operation. These primary mass flow standards are gravimetric systems. The HPL and LPL gravimetric systems both feature gyroscopic force balances that are believed to be the most

sensitive weighing systems available for this application. The capacity of the HPL weigh scale is 1,000 kilograms. The total uncertainty of the HPL scale is ± 0.021 kilogram or ± 0.0021 percent of full scale. The total estimated uncertainty in the measured mass flow rate for the HPL primary calibration system is ± 0.02 to $\pm 0.04\%$ at a 95% confidence level. The capacity of the LPL weigh scale is 155 kilograms. The total uncertainty of the LPL weigh scale is ± 0.010 kilogram or ± 0.006 percent of full scale. The total estimated uncertainty in the measured mass flow rate for the LPL primary calibration system is ± 0.01 to $\pm 0.04\%$ at a 95% confidence level. The weigh scales are calibrated using Class F mass standards traceable to the National Institute of Standards and Technology (NIST) of the United States.

As noted above, both the HPL and LPL are re-circulating flow loops. When a primary flow calibration is performed using either of these flow loops, gas flow from the re-circulating portion of the loop is diverted to the primary calibration system weigh tank. Gas is collected in the weigh tank during a precisely measured time interval. The weight of the gas collected is then accurately measured and the mass flow rate is determined. In order to maintain constant flow conditions in the test section of either the HPL or LPL during a primary calibration run, gas must be added to the re-circulating portion of the loop at the same rate that it is diverted to the weigh tank. Therefore, both the HPL and LPL are fitted with gas storage bottles that are used to supply makeup gas to the test loop at the same rate gas is diverted to the weigh tank. Special, fast-acting hydraulically-powered diverter valves in both the HPL and LPL are used to control the flow of gas to the weigh tank and from the makeup bottles. The weigh tank diverter valves have a switching time of 50 milliseconds. A schematic of the basic HPL primary calibration system is provided in Figure 2. The configuration of the LPL is similar to that of the HPL, although the weigh tank, piping, control valves, and flow elements are of smaller capacity.

The primary calibration systems in the three MRF flow facilities are used to routinely calibrate secondary or transfer flow calibration standards. For the HPL and LPL, the secondary standards consist of ASME/ANSI MFC-7M critical flow nozzles and industrial turbine meters. The estimated total uncertainty in sonic nozzles calibrated using the primary standards is less than $\pm 0.2\%$.

To determine test gas composition, the MRF has a fully-automated, laboratory-grade Hewlett-Packard Model 5890 Series II gas chromatograph (GC) that has been modified to perform an extended C_{10+} hydrocarbon analysis through capillary column separation and flame ionization detection (FID), in conjunction with packed column separation and thermal conductivity detection (TCD) of inorganic compounds. The packed columns are arranged to separate oxygen from nitrogen to allow for the verification of complete loop purges.

With regard to the measurement accuracy of the MRF GC, the precision limit for a high-quality methane sample was measured as ± 0.04 mole-percent (95 percent confidence). Gas density and gas properties are calculated using the composition data and the detail characterization method in American Gas Association Report No. 8 ("Development of Improved Capabilities for Computation of Gas Supercompressibility Factors and Other Properties," 1985).

The mass flow rate is determined from a combination of the mass collected in the weigh tank, the measured valve diversion time and corrections to account for mass storage in the interconnect piping between the nozzles and the weigh tank (Park, et al., 1995). The nozzle discharge coefficient is calculated from the ratio of the theoretical mass flow rate to that of the weigh tank system. The theoretical mass flow rate is based on the measured gas composition, plenum temperature and pressure, and is calculated by the SUPERZ program (Savidge, 1989) which incorporates A.G.A.-8 density calculations and additional thermodynamic equations of state to determine the critical flow at the nozzle throat.

Additional details about the MRF can be found in a GRI report by Johnson, et al. (1992) whereas information about MRF measurement uncertainties can be found in papers by Behring (1994) and Park, et al. (1995).

2.3 Kärstø Metering and Technology Laboratory

K-Lab, standing for Kärstø Metering & Technology Laboratory, is a test and calibration laboratory owned by Statoil, located in Norway, operating in natural gas in the pressure range 1 MPa to 15 MPa, in a closed loop mode, with a gravimetric primary calibration system installed on a by-pass to the test line, as shown on Figure 3. The primary calibration system is the basics in the traceability chain for calibrations at K-Lab. The facility is traceable to the *Bureau international des Poids & Mesures* (BIPM). K-Lab is accredited by the National Measurement service and has a quality system in accordance with EN-45001 and ISO/IEC Guide 25.

The primary calibration system, shown on Figure 4, consists of a 3" diverter valve with a closing time less than 30 ms enabling the gas to be filled into a 5.5 m³ spherical tank installed on a gyroscopic force balance. The amount of gas to be filled into the tank may vary between approximately 40 kg and 600 kg depending on the operating pressure with a corresponding filling time between 40 and 400 sec.

The discharge coefficient, C_d , of the sonic nozzle is calculated using the general equation from ISO-9300. The critical flow function, C^* , is computed from SONFLOW, a specially

developed software for calculation of thermodynamic and dynamic properties of natural gas (Weberg, 1988)

The calibrations took place at stagnation temperatures of approximately 37°C and in the pressure range, 2 MPa to 10 MPa, corresponding to Reynolds from 3×10^6 to 2×10^7 . The 2σ , on the discharge coefficient; C_d , is less than $\pm 0.2\%$.

2.4 NOVA Gas Dynamic Test Facility

The NOVA Gas Dynamic Test Facility has been described in several publications in the past (Studzinski et al, 1994 and Williamson et al. ,1995). A sketch of the layout of the test facility is shown in Figure 5. and details of the nozzle bank/gravimetric prover are shown in Figure 6. The facility test loop draws natural gas from the mainline by means of a Solar compressor. This gas, after flowing through the test loop, is then re-injected back into the mainline. Thus, the static pressure and temperature are governed by prevailing conditions in the mainline and there is no need for a cooling system to maintain temperature stability. The static pressure is typically around 6000 kPa and the total flow that can potentially be measured with the 24 sonic nozzles is around 23kg/s. However, with the current compressor, only 14 nozzles can be choked resulting in a capacity of around 13kg/s.

The NOVA meter prover consists of a bank of 24 identical (10mm throat diameter) sonic nozzles and a gravimetric component which includes a Wöhwa gyroscopic scale and a 3.2m^3 spherical pressure vessel. Gas flow from one nozzle is directed to the gravimetric component where the mass flow for that one nozzle is determined by measurement of mass and time. The total pipe mass flow is thus equal to the mass flow of the diversion nozzle multiplied by the number of choked nozzles. This process eliminates the effect of gas composition on the uncertainty of the discharge coefficient. This method is unique and differs from methods used in other facilities. The overall uncertainty, in mass flow, for such a mode of operation, as evaluated by Williamson et al. (1995) is between 0.13% and 0.16% depending on the number of nozzles being choked. This mode of operation is time-consuming and limits the number of tests that can be conducted on a given day.

The prover can also be operated by using the nozzle bank alone. For example, a historical discharge coefficient can be obtained for the diversion nozzle using the gravimetric component. Since all nozzles are manufactured to be identical, this can be assumed to be the discharge coefficient for all the nozzles. Thus, the total flow can be measured by knowing the number of nozzles being choked. This mode of operation allows more tests to be conducted in a given day. However, the uncertainty associated with such a procedure was rated to be 0.25%

assuming negligible uncertainty in C^* (see Williamson et al., 1995). Majority of the uncertainty is attributed assumption that all the nozzles are identical. The possible variations in the nozzle diameters and discharge coefficients have since been quantified and thus, the uncertainty in using the procedure of the nozzle bank alone is reduced to less than 0.2%.

The test facility is also equipped with a 102.26mm orifice meter located downstream of a 76D honed, unflanged section of pipe. This meter serves as a secondary method of calibration. Further, the facility includes an 202.7mm orifice meter run located in ideal flow conditions which can also be used as a secondary transfer standard.

Instrumentation includes smart pressure and temperature transmitters for measuring the static pressures, differential pressures and temperatures. The pressure transmitters ($\pm 0.1\%$ and better) are calibrated by means of a dead weight tester whereas the temperature transmitters ($\pm 0.1\text{deg.C}$) are calibrated with a dry block calibrator using a NIST traceable high precision platinum RTD as a reference. Gas composition was measured by using a Daniel gas chromatograph.

3.0 EXPERIMENTAL RESULTS

3.1 The NOVA Nozzle

The 10mm NOVA nozzle (shown in Figure 7) is a nozzle from the NOVA meter prover sonic nozzle bank. The design of this nozzle is unlike that described in conventional standards. There exists an intentional step change in the diameter at the throat. This step prevents the possibility of downstream disturbances propagating upstream through the boundary layer to the nozzle throat. Thus, the discharge coefficient curve for this nozzle may differ from those resulting from the use of conventional nozzle geometries.

At the NOVA facility, the NOVA nozzle was placed in the diversion slot of the nozzle bank and was calibrated with the weigh scale at a typical throat Reynolds Number of around 1×10^7 . This nozzle was calibrated in air by NEL and CEESI. The former using a primary standard and the latter using a primary and secondary standard. Calibrations by K-Lab were performed with natural gas using a primary standard. At the GRI MRF, calibrations were performed with nitrogen and natural gas in the LPL and with natural gas in the HPL with a primary standard as the reference.

Results of tests are shown in Table 2. and Figure 8. The results indicate that data from GRIMRF, K-Lab and NEL are in good agreement but differ from the 1994 CEESI/NOVA data by around 0.2% at a Reynolds number of 1×10^7 . Considering the time interval between the

calibrations, the nozzle was re-calibrated by CEESI and NOVA in September 1996. CEESI were able to obtain one primary calibration whereas NOVA obtained 6 calibration points. For the data collected in 1996, the agreement between all facilities is well within $\pm 0.1\%$. The 1994 calibrations fall within the $\pm 0.2\%$ bounds of the 1996 calibrations.

3.2 The K-LAB Nozzle

The K-Lab nozzle is a 23.293mm toroidal nozzle built in accordance with the requirements of ISO-9300 and is shown in Figure 9. Results of calibrating this nozzle are shown in Table 3. and Figure 10.

At the NOVA Facility, this nozzle was calibrated in location A, shown in Figure 5, downstream of the proving device. Since the design of the facility does not permit the choking of nozzles in series, a transfer standard is used in the calibration of the K-Lab nozzle. This secondary calibration was performed by using a 202.7mm orifice meter placed in ideal flow conditions using a β -ratio of 0.3132. The calibration of the orifice meter was performed on the same day as the calibration of the K-Lab nozzle. The meter factor for the orifice meter had a $2\sigma=0.05\%$. The resulting calibration of the nozzle (12 points) at a throat Reynolds number of around 24×10^6 is around $0.9972 \pm 0.1\%$. In the case of the other facilities the GRI MRF utilized the HPL using natural gas and K-Lab also performed the calibrations with natural gas. Both facilities used primary standards for the reference. CEESI performed the calibrations with air using primary and secondary standards.

It is clear from Table 3. and Figure 10 that the agreement between the facilities, at a Reynolds number of 24×10^6 , is excellent (within $\pm 0.1\%$). The entire curve is fitted with a 2nd order regression curve and except for a few outliers, all the data falls within $\pm 0.2\%$ of this curve. The K-Lab data are well represented by the "offset" curve from ISO 9300. The data are within the $\pm 0.5\%$ limits of ISO9300.

4.0 DISCUSSION AND CONCLUSIONS

For the NOVA nozzle, recent calibrations of the GRI MRF, K-Lab and NEL measured a discharge coefficient which is 0.2% greater than that measured in the 1994 calibrations by NOVA and CEESI at a throat Reynolds number of 1×10^7 . In general, inter-laboratory comparisons that agree to within $\pm 0.2\%$ are considered to be excellent. The GERG program (1993), for example, which consisted of several European laboratories, reported an agreement to within $\pm 0.25\%$.

The 0.2% difference in the case of the NOVA nozzle could possibly be explained by the observation that the calibrations of NOVA and CEESI were performed in 1994 and those of GRI MRF, NEL and K-Lab were performed in late 1995 and early 1996. Therefore, the NOVA nozzle was re-calibrated at the CEESI and NOVA facilities. Recalibration of the nozzle at the NOVA (6 points) and CEESI (1 point) facilities indicates that the nozzle discharge coefficient has indeed changed. The 1996 data for all facilities now agree to within $\pm 0.1\%$ of the mean value of the discharge coefficient.

The reasons for the change in discharge coefficient is unknown. Although there was some damage to the external diameter at the inlet, there was no significant damage on the inlet surface or the throat of the nozzle. In the case of the NOVA facility, calibrations on another identical nozzle over the past 2 years have resulted in data that are within $\pm 0.1\%$ of the mean. Thus, there does not appear to be a plausible reason for the shift in discharge coefficient. In any event, an agreement to within $\pm 0.2\%$ between facilities is excellent. This experience (variations with time interval) only emphasizes the need for frequent inter-laboratory calibrations.

The inter-laboratory agreement seen with measurements taken with nitrogen, air and natural gas as the fluids suggests that the uncertainty in C^* is not as severe as previously thought (Studzinski et al., 1988 and Erdal et al., 1992). This observation was also made by Williamson et al. (1995), but, it was thought to be pre-mature since data existed from only two facilities (NOVA and CEESI). However, with the present data in hand from several facilities using fluids such as air, nitrogen and natural gas and two different artifacts, this belief could in fact be a reality. One may be tempted to make a stronger statement that the uncertainty in C^* is negligible.

Conclusions from this program can be summarized as follows :

1. Within the stated measurement uncertainty and repeatability of the participating facilities, the agreement (within $\pm 0.2\%$ of the mean) between the facilities involved in the present tests is excellent.
2. The agreement between the facilities for various test fluids (air, natural gas and nitrogen) and two separate artifacts, suggests that the uncertainty in C^* is negligible.

It is recommended that this program be continued so that the quality of the facilities can be maintained and variances in measurements can be minimized. Future plans include the testing of the EUROMET nozzle and the 150mm GERG turbine meter transfer standard package at the three North American facilities and the testing of the NOVA nozzle by Ruhrgas (Germany) and KRISS (Korea).

5.0 ACKNOWLEDGMENTS

The authors would like to acknowledge the contributions of Tom Kegel in the preparation of the description of the CEESI facility. The support of NOVA Gas Transmission Limited and GRI and their permission to publish this document is also acknowledged.

6.0 REFERENCES

1. "Development of Improved Capabilities for Computation of Gas Supercompressibility Factors and Other Properties," A.G.A. Report No. 8, American Gas Association, Arlington, Virginia, USA, 1985.
2. "Natural Gas Critical Mass Flow Computations". Weberg, Trond, Thesis. The Norwegian Institute of Technology 1988. ISBN 82-7119-074-1
3. GERG Technical Monograph, 1993, "Intercomparison Exercise of High Pressure Test Facilities within GERG", also presented at the 3rd International Symposium on Fluid Flow Measurement, San Antonio.
4. Arnberg, B.T. and Britton, C.L., 1991, "Two Primary Methods of Proving Gas Flow Meters", Symposium on Flow : Its Measurement and Control in Science and Industry.
5. Arnberg, B.T., Britton, C.L. and Seidl, W.F., 1974, "Discharge Coefficient Correlations for Circular-Arc Venturi Flowmeters at Critical (Sonic) Flow", ASME Journal of Fluids Engineering.
6. Kegel, T., 1994, "Uncertainty Analysis of a Compressible Flowmeter Calibration Process", ASME Forum on Fluid Flow Measurement Uncertainty.
7. Kegel, T., 1995, "Uncertainty Analysis of a Volumetric Primary Standard for Compressible Flow Measurement", 3rd International Symposium on Fluid Flow Measurement, San Antonio.
8. Smith, R.E. and Matz, R.J., 1962, "A Theoretical Method of Determining Discharge Coefficients for Venturis Operating at Critical Flow Conditions", ASME Journal of Basic Engineering.
9. Stratford, B.S., 1964, "The Calculation of the Discharge Coefficient of Profiled Choked Nozzles and the Optimum Profile for Absolute Air Flow Measurement", Journal of the Royal Aeronautical Society.

10. Studzinski, W., Williamson, I.D., Jungowski, W., Botros, K.K., Sawchuk, B.D. and Strom, V. "Nova's Gravimetric Meter Prover and Sonic Nozzle Facility", CGA Gas Measurement School, Banff, Alberta (1994).
11. Williamson, I.D., Sawchuk, B.D. and Karnik, U. "The NOVA Meter Prover", 3rd International Symposium of Fluid Flow Measurement, San Antonio, USA (1995).
12. Studzinski, W., Weiss, M.H. and Botros, K.K. "Critical Flow Factor for Natural Gas", 2nd International Conference on Flow Measurement, London, U.K., 1988.
13. Erdal, A., Cabrol, J.F., Bosio, J., Thomassen, D. and Weberg, T. "Analysis of Calibration data from K-Lab for prediction of sonic nozzle discharge coefficients and critical flow functions" Proceedings of 11th International Conference on Offshore Mechanics and Arctic Engineering, Calgary, 1992, VolA. Part A, pp39-45.
14. Park, J.T., Behring II, K.A. and Grimley, T. A., 1995, "Uncertainty Estimates for the Gravimetric Primary Flow Standards of the MRF," Proceedings of the 3rd International Symposium on Fluid Flow Measurement, San Antonio.
15. Savidge, J., 1989, "SUPERZ Extended Thermodynamic Properties Computer Program," Gas Research Institute.
16. Johnson, J.E., Bowles, Jr., E.B., Buckingham, J.C., Harrell, P.J., McKee, R.J. and Sparks, C.R., 1992, "Metering Research Facility Design," Topical Report (July 1987-December 1990), Gas Research Institute Report No. GRI-91/0251, March 1992.
17. Behring II, K.A., 1994, "Application of Uncertainty Analysis in the GRI Metering Research Facility," American Society of Mechanical Engineers Winter Annual Meeting, Chicago, IL, November 6-11, 1994.

Facility	Primary Standard	Fluid	Operating Pressure kPa	Facility Flow Capacity Kg/s	Uncertainty in Mass Flow	Secondary Standards
NOVA	Gravimetric Wöhwa Scale	Natural Gas	≈6000	primary : 1 secondary : 23	primary:±0.16% secondary:±0.25%	Nozzles, Orifice, Turbin
GRIMRF LPL	Gravimetric Wöhwa Scale	Nitrogen Natural Gas	140 to 1450	primary : 1.9 secondary : 2.4	primary:±0.04% secondary:±0.2%	Nozzles, Orifice, Turbin
GRIMRF HPL	Gravimetric Wöhwa Scale	Nitrogen Natural Gas	1035 to 8275	primary : 29 secondary : 44	primary:±0.04% secondary:±0.2%	Nozzles, Orifice, Turbin
CEESI	Gravimetric and Volumetric	Air, other gases & gas mixtures	Atm. to 9500	primary : 8 secondary : 100	primary:±0.1% secondary:±0.5%	Sonic Nozzles
K-Lab	Gravimetric Wöhwa Scale	Nitrogen Natural Gas	2000 to 15000	0.2 to 78	±0.3%	Sonic Nozzles Turbine

Table 1. Comparison of Facilities

Facility	Throat Reynolds No.	C_d	Deviation from Regression	Date of Calibration	Fluid
NOVA	$\approx 10 \times 10^6$	0.9903	-0.21%	Jul-Nov '94	Natural Gas
	$\approx 10 \times 10^6$	0.9920	-0.04%	Sept. 1996	Natural Gas
CEESI (eqn.)	10×10^6	0.9902	-0.22%	April 1994	Air
	8.6×10^6	0.9919	-0.05%	Sept. 1996	Air
SwRI	$\approx 10 \times 10^6$	0.9925	0.01%	Sept. 1995	Natural Gas Nitrogen
NEL	$\approx 10 \times 10^6$	0.9920	-0.04%	March 1996	Air
K-Lab	$\approx 10 \times 10^6$	0.9926	0.02%	July 1996	Natural Gas
Regression Average	10×10^6	0.9924			

Table 2. Interfacility Comparisons of Calibrations of NOVA Nozzle

Facility	C_d	Deviation from Regression	Date of Calibration	Fluid
NOVA	0.9972	-0.01%	Jan. 1996	Natural Gas
CEESI	0.9982	0.09%	April 1996	Air
SwRI	0.9966	-0.06%	June 1996	Natural Gas Nitrogen
K-Lab	0.9970	-0.03%	Sept. 1996	Natural Gas
Regression Average	0.9973			

Table 3. Interfacility Comparisons of Calibrations of K-Lab Nozzle at a throat Reynolds Number of 24×10^6 .

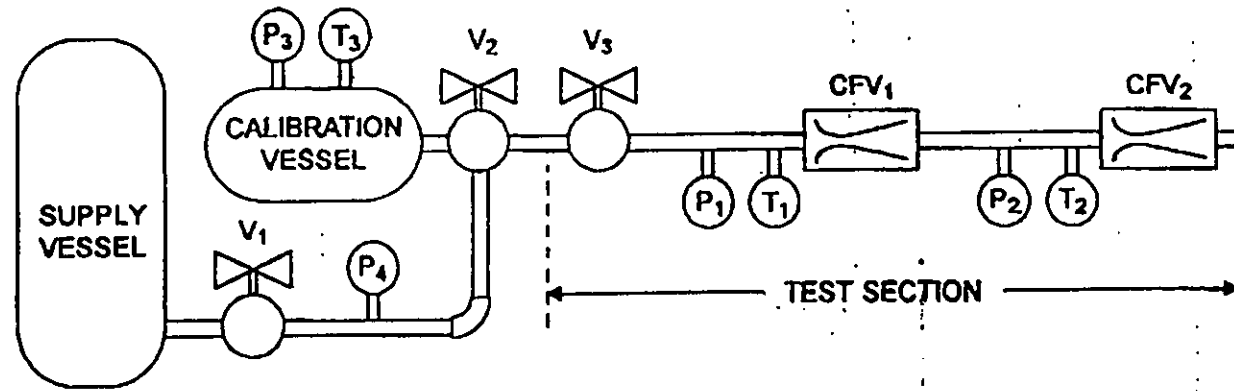


Figure 1. Operational Sketch for the CEESI Facility

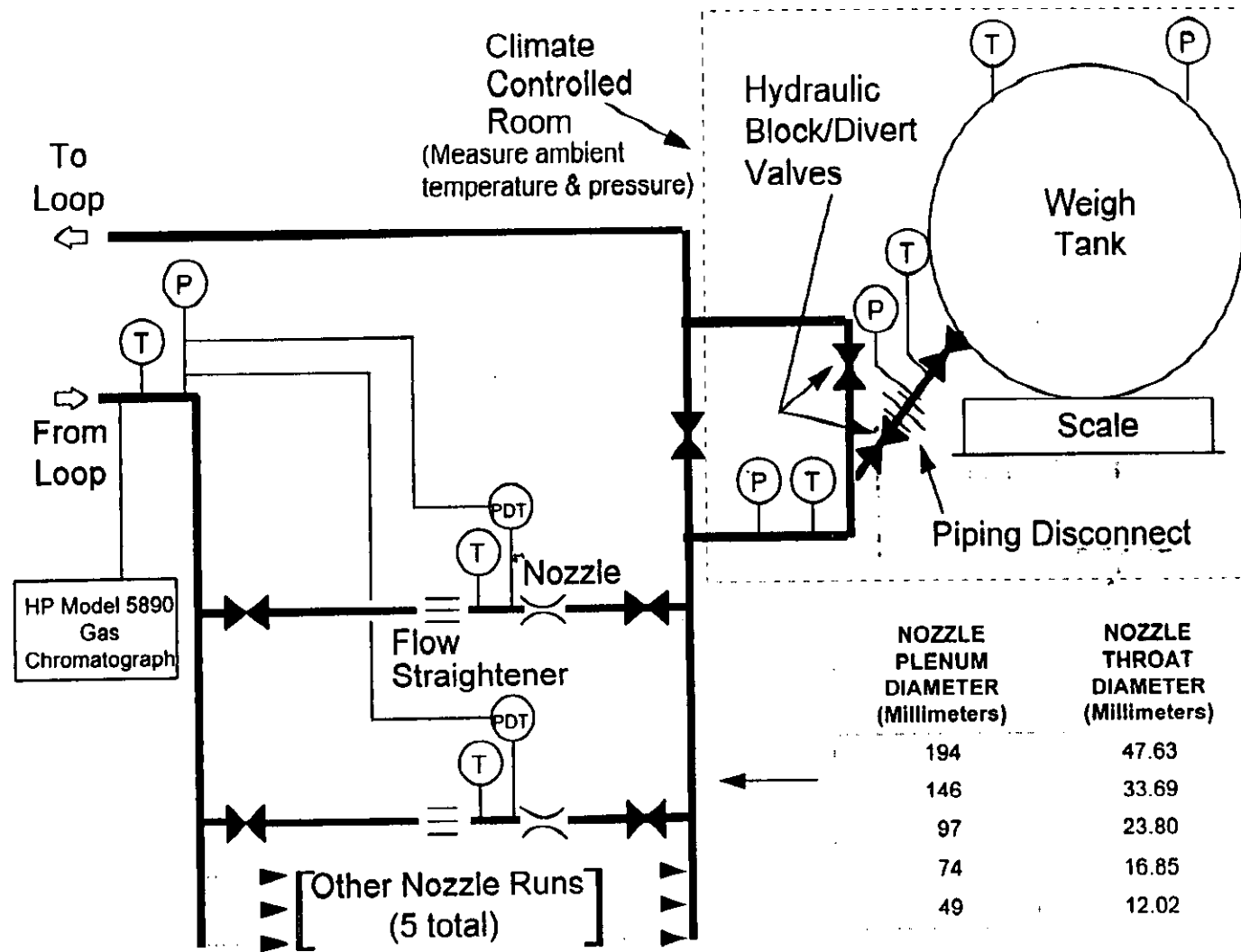


Figure 2. GRI Metering Research Facility Schematic of the High Pressure Loop (HPL) Weigh Tank System.

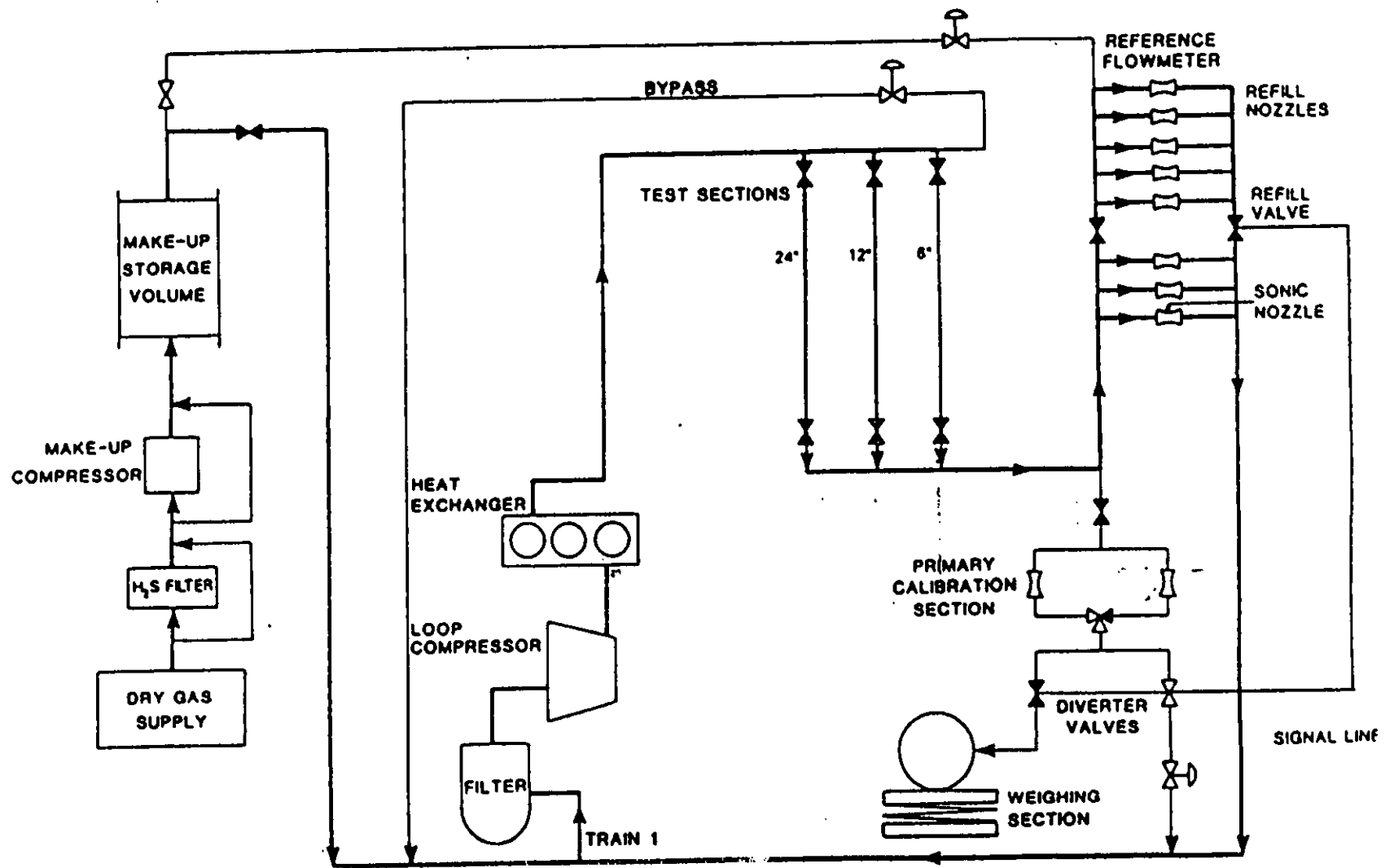


Figure 3. Schematic Layout of K-Lab Test Loop

PRIMARY CALIBRATION SECTION

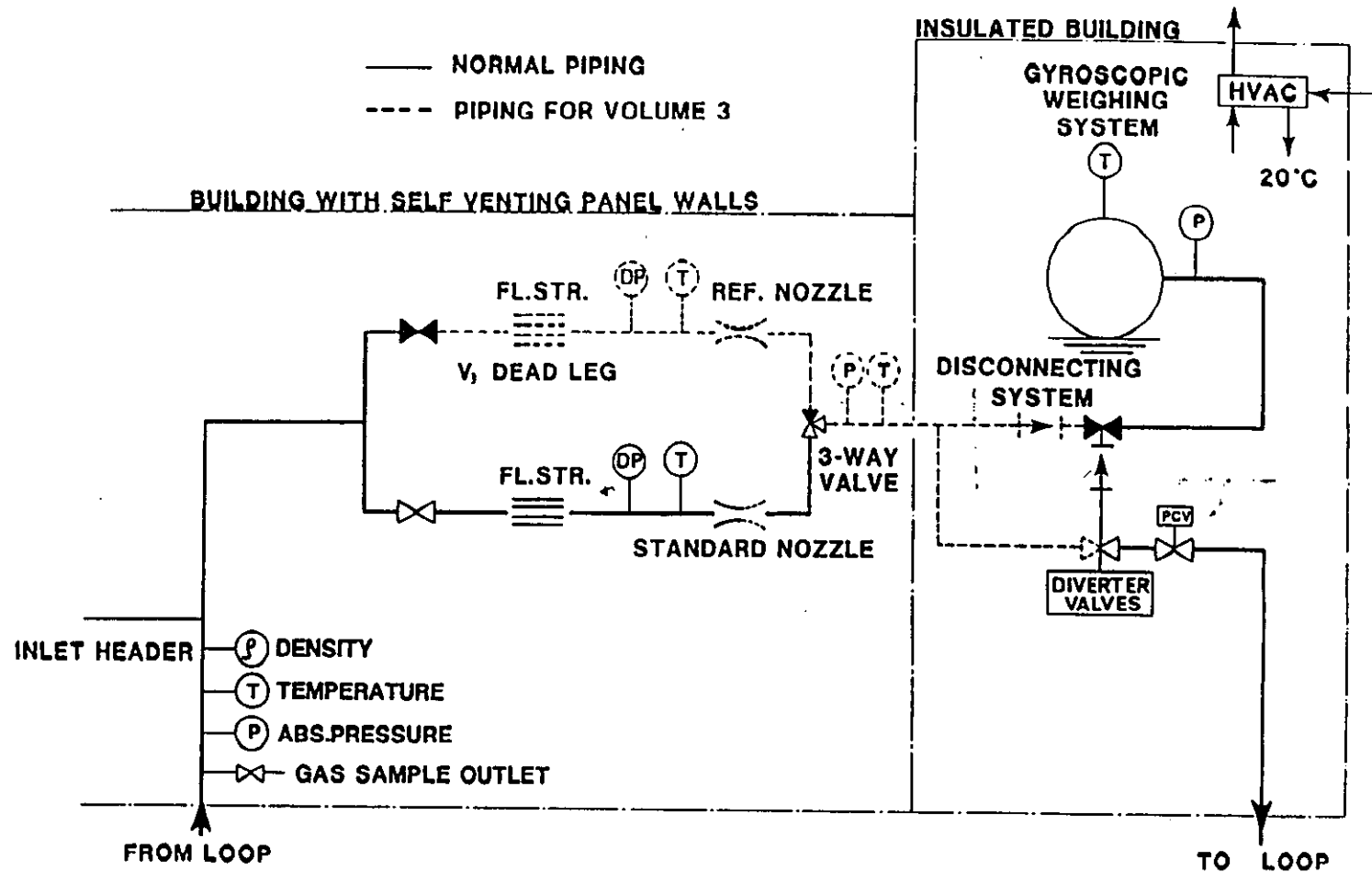


Figure 4. K-Lab Primary Calibration Section

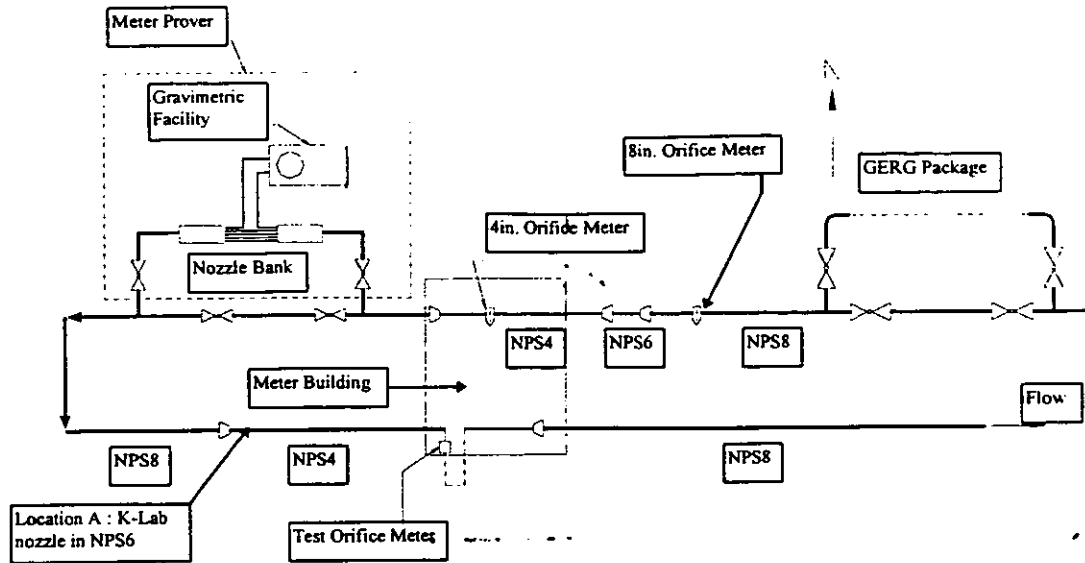


Figure 5. Schematic Layout of the Test Facility

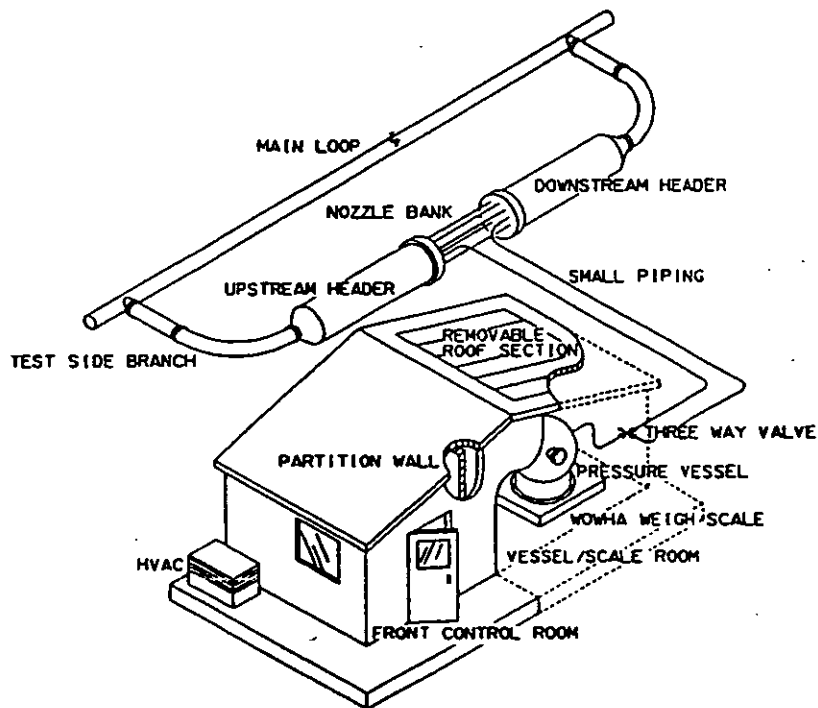


Figure 6. Components of the NOVA Meter Prover

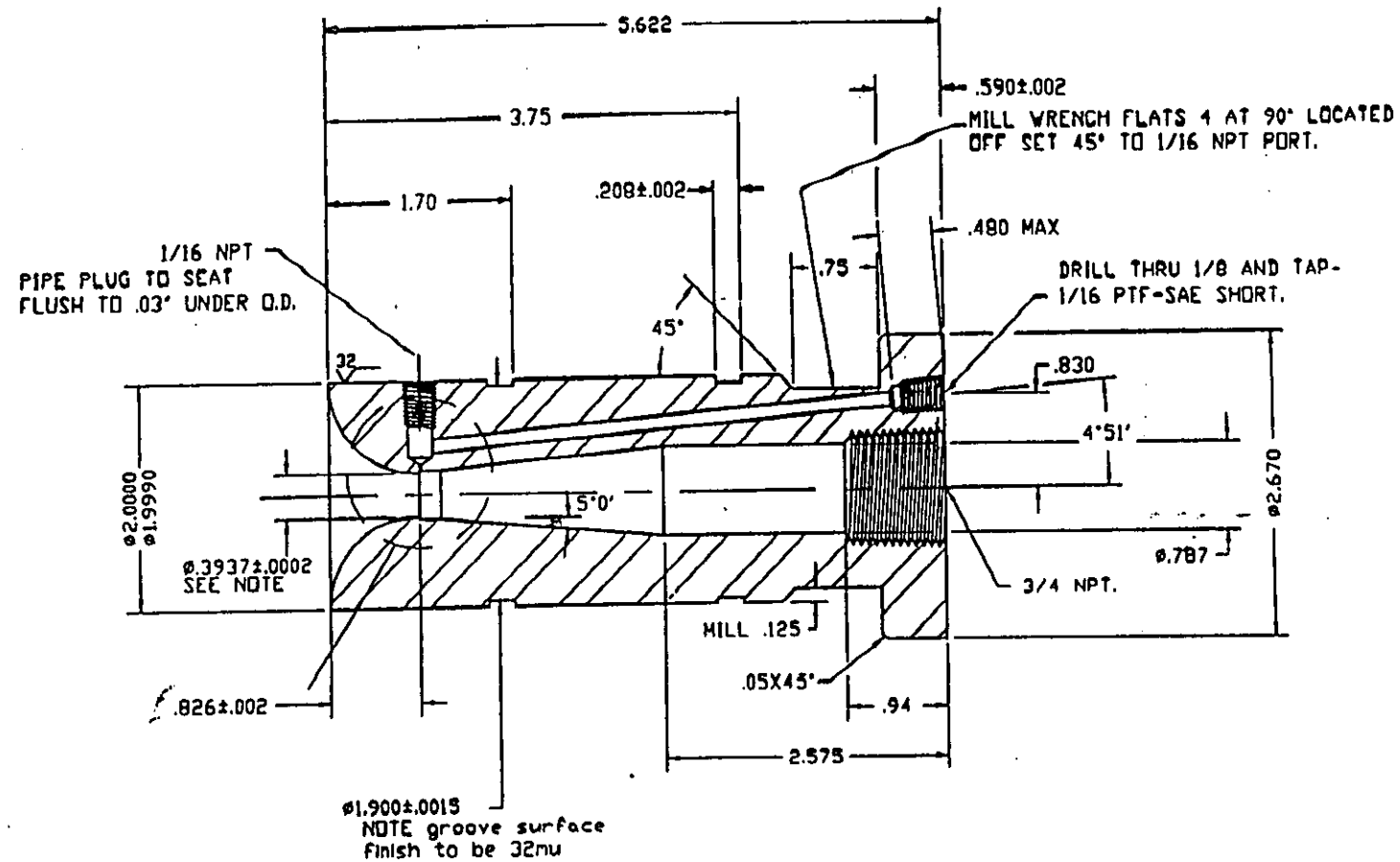


Figure 7. The NOVA Nozzle

Calibration of NOVA Nozzle

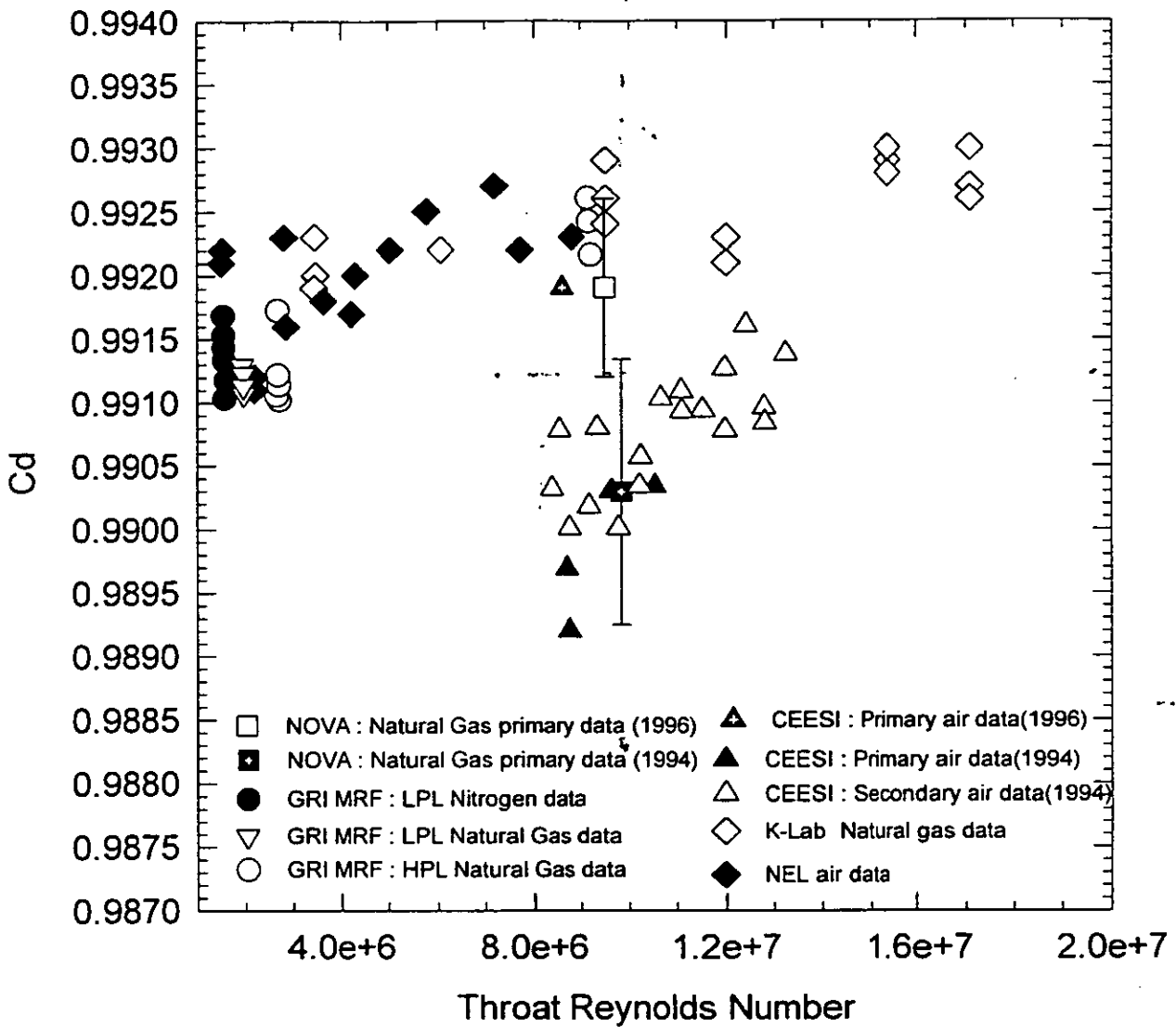


Figure 8. Calibration of NOVA Nozzle

Calibration of NOVA Nozzle

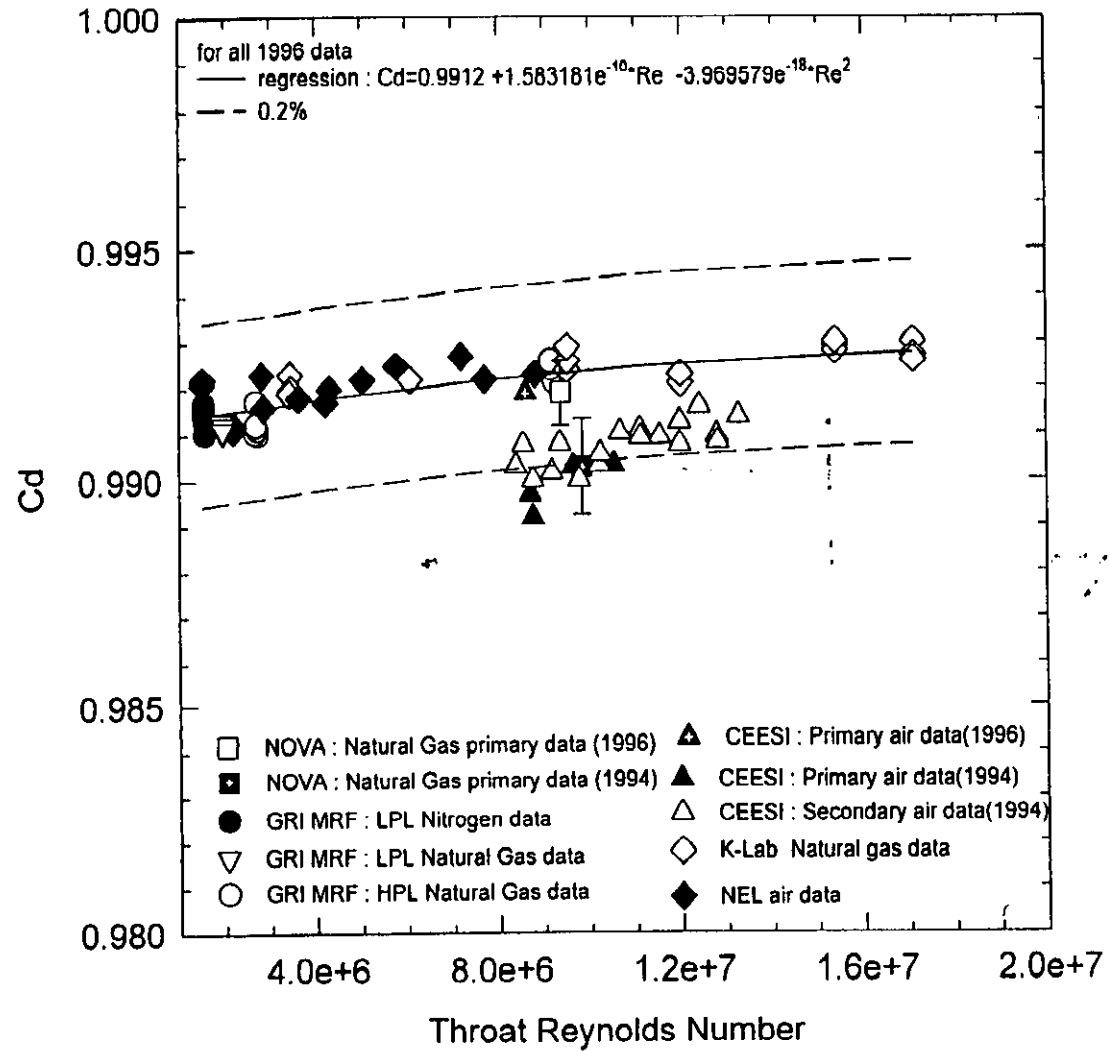


Figure 8. Calibration of NOVA Nozzle

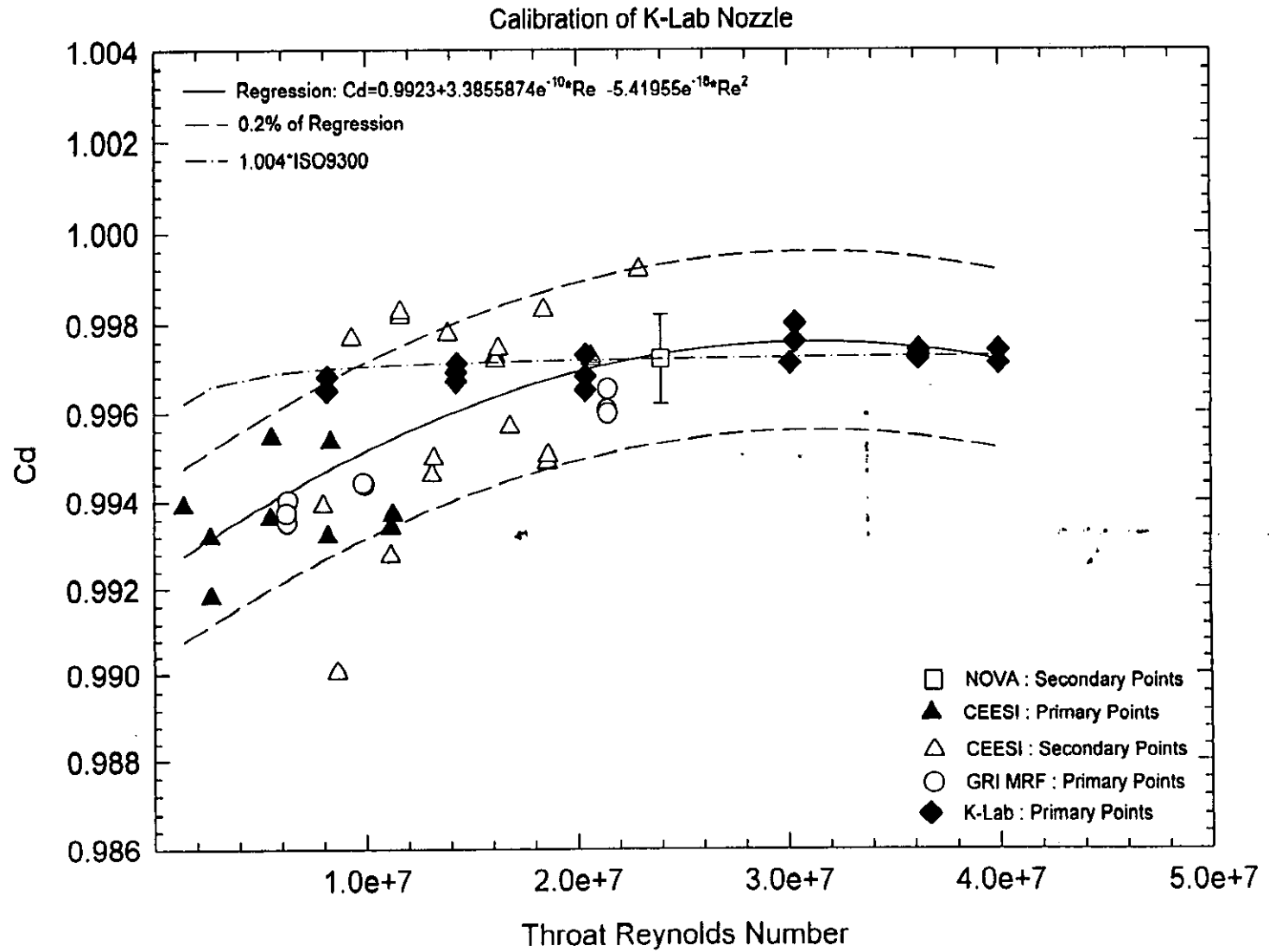


Figure 10. Calibration of K-Lab Nozzle

**CRUDE OIL
EXPANSION
COEFFICIENTS**

R Third

Rhomax Engineering

SUMMARY

THE CURRENT REGIME

THE STANDARDS

METER K-FACTOR CALCULATIONS

CHOICES AVAILABLE

EVALUATION OF CHOICES

AN ALTERNATIVE

CUSTOM COEFFICIENTS FOR SPIKED OR WET CRUDE

FIELD MEASUREMENTS OF DENSITY AND WATER CONTENT

THE DATABASE

THE EXPERIMENTAL CALCULATIONS

PRELIMINARY RESULTS

DISCUSSION OF RESULTS

SUMMARY

The need to account for the effects of temperature and pressure on the volume occupied by a mass of hydrocarbon liquid is a universal one in our industry.

The methods commonly used in the North Sea are summarised, and their inherent anomalies are listed.

The effects of applying the various different methods to the determination of liquid quantities are briefly evaluated.

Fairly gross changes in base density can be accommodated without very significant effect on meter K-factor.

Comparatively small changes in base density are likely to cause fairly meaningful changes in Standard Volume.

A method of gathering large amounts of field data directly from remote flow and quality measurement instruments is described, and techniques for using data thus gathered for further useful analysis is described.

Tentative volume coefficients based on such field measurement data, suitable for use with various different mixes of crude/water/condensate, are described.

Note that in the following text the term "expansion" is used as meaning "change in volume", which can be in both a positive or a negative direction.

THE CURRENT REGIME

THE STANDARDS

API 2540

CONCEPT OF VCF

To predict the volume likely to be occupied by a quantity of crude at a temperature of 15 °C, the concept of a Volume Correction Factor (VCF) is invoked.

If one knows the temperature at which the volume was measured, and the density of the crude at 15 °C, one can find a unique Volume Correction Factor appropriate to those conditions listed in a set of Tables.

Multiplying the measured volume of the crude by the VCF gives the notional likely volume at 15 °C :

$$V_{15} = V_m \times \text{VCF}$$

where,

V_{15} is the volume of the crude at 15 °C, m^3

V_m is the volume of the crude at meter temperature, m^3

Equally, if one knows the *density* of the liquid at 15 °C and the measurement temperature, one can predict the density of the crude at some other temperature.

Tables which allow these calculations are in the American Petroleum Institute (API) Manual of Petroleum Measurement Standards, Chapter 11.1, or in the separate (identical) Standard API 2540 (also adopted by other bodies and published by them, designated ANSI/ASTM D1250 or IP 200).

BASIS OF API 2540

The work upon which the Tables are based was done by the American National Bureau of Standards (now the National Institute for Standards and Technology) in 1976. The research included only two samples from the North Sea, one from each of the Forties and Auk fields.

One of the limitations of the research was that none of the samples was allowed to contain more than 0.38% of water.

A further limitation was that each sample was allowed to stabilise in an open container prior to its being tested. It is unclear from the original research paper just what proportion of the 'light ends' would thus have remained in solution for each sample.

What is explicit is that the original paper states that "tests would be discontinued when vapour pressure exceeded atmospheric pressure or when the sample under test approached a non-liquid state".

These limitations are further discussed below.

Cautionary Note : The term C_{dt} - Correction for the effect of Temperature on the Liquid - is used interchangeably with VCF. There is, however, a common alternative usage for VCF. In this alternative usage $\text{VCF} = C_{dt} \times C_{pt}$

where C_{pt} is the Correction for the effect of Pressure on the Liquid.

THE STANDARD - COMPUTER ROUTINES

The Standard resides not in the Tables, but in the specific implementation of the computer routine described in Volume X of API 2540. This routine is for the solution of an equation, and specifies the rounding or truncation of the numbers used, and the precision of exponentials, etc.

The equation is

$$VCF = \exp [\alpha_{15}\Delta t (1 + 0.8 \alpha_{15}\Delta t)]$$

where

α_{15} is the tangential thermal expansion coefficient of the crude at 15 °C, and

Δt is the difference between measurement temperature and 15 °C

The α_{15} value depends upon the density of the crude oil at 15 °C, as follows:

$$\alpha_{15} = K0 / \rho_{15}^2 + K1 / \rho_{15}$$

where K0 and K1 are constants applicable to the type of fluid, given in the Standard. For crude oils, K0 = 613.97226, and K1 = 0

ρ_{15} is the density of the crude oil at 15 °C, kg/m³.

The Tables which occupy the majority of API 2540 were derived using these routines.

UNCERTAINTY

The uncertainty of the VCF calculation is stated in API 2540 Volume X as follows:

Temperature of the crude (°F)	Uncertainty
100 (approx. 37.8 °C)	± 0.05 %
150 (approx. 65.6 °C)	± 0.15 %
200 (approx. 93.3 °C)	± 0.25 %
250 (approx. 121.1 °C)	± 0.35 %

API 11.2.1M

This is a further part of the American Petroleum Institute Manual of Petroleum Measurement Standards, and is concerned with the effect of pressure on hydrocarbon liquids.

For our crudes, the liquids involved are those whose density at 15 °C is in the range from 638 - 1074 kg/m³.

The Standard contains Tables of Liquid compressibility factors.

Unlike API 2540, the standard is the printed Tables, not the calculation routine which is also included in the document.

COMPRESSIBILITY FACTOR, F

Central to the Tables is the compressibility factor, F, which participates in the equation

$$V_e = V_m / [1 - F \times (P_m - P_e)]$$

where

V_e is the volume at equilibrium pressure (P_e), m³

V_m is the volume at the meter pressure (P_m).

The Standard uses density in kg/l, volume in m³, temperature in °C, and pressure in kPa.

The compressibility factor, F, is calculated from

$$F = \exp (A + BT + C/\rho + DT/\rho^2)$$

where

A, B, C, and D are constants, given in the Standard thus:

$$A = -1.62080$$

$$B = 0.00021592$$

$$C = 0.87096$$

$$D = 0.0042092$$

T is the meter temperature, °C,

ρ is the density of the liquid at 15°C, kg/l

BASIS OF THE API 11.2.1 TABLES

The Standard was derived from three separate research papers which describe work done on seven different crude oils, five gasolines and seven middle-distillate oils. All of these were lumped together in the calculation of the constants.

None of the crude oils was of North Sea origin. Those included had base density values from 825.2 to 890.9 kg/m³, and were investigated over a temperature range of 4.44 to 76.7 °C and 0 to 3503 kPa pressure for five of the samples, over a temperature range of 37.78 to 76.67 °C for the sixth and over a temperature range of 15.56 to 76.67 °C for the seventh. The experimental work included five measurement points for each of six of the crude oil samples, and four data points for the seventh sample.

From this very limited database, data was obtained by extrapolation for a temperature range of -30 to 90 over a temperature range of 37.78 to 76.67 °C, a density range of 600 - 1074 kg/m³, and a pressure range from 0 to 10300 kiloPascals.

The API Committee generating API 11.2.2 were aware of this shortcoming. To quote from the Standard "The data base is.....not large enough to cover the range of current commercial operations. When new data are available, they will be incorporated into an expanded standard". That was the case when the Standard was first published, and was still the case when the BS / ISO versions were published in 1991 / 1989.

HISTORIC USE OF 'DOWNER' EQUATION

Use of the API 11.2.1M tables (or equation) is comparatively new in the UK. A similar (*not identical*) function was previously performed by use of the "Downer" equation. This calculated a compressibility value for the crude, but took no account of the vapour pressure of the liquid.

The Downer equation was used to calculate a value, β , as follows:

$$\beta = \exp ([a + bT - (c+dT) \ln (\rho_{15} / 1000)] \times 10^{-5}$$

where

β is the secant compressibility of the liquid, bar^{-1}

a, b, c, and d are constants as follows

$$a = 1.38315$$

$$b = 0.00343804$$

$$c = 3.02909$$

$$d = 0.0161654$$

T is the measured temperature, °C

ρ_{15} is the density of the crude oil at 15 °C and 1.01325 bar a, kg/l.

β is, to all extents and purposes, the same as F.

This β value was then used to calculate the Correction for the effect of Pressure on the Liquid as follows

$$C_{pt} = 1/(1 - \beta P)$$

where

P is measured pressure, bar g

This correction was used to predict the notional volume the liquid would occupy at 15 °C and 0 bar g.

Calculation routines based upon use of the Downer equation (see IP Measurement Paper No 2 below) are incorporated into a great many flow computers in use in the UK, and are written into several pipeline agreements.

UNCERTAINTY IN COMPRESSIBILITY

Assessment of the uncertainty associated with the use of the API 11.2.1M Tables (and the equation) is not straightforward.

The maximum uncertainty of the compressibility factor, F , as predicted by the Tables, when compared with the actual compressibility factor for the same liquid, is stated as $\pm 6.5\%$.

The resulting uncertainty in *volume* is related to the measurement pressure, but may also be compounded by an extra uncertainty related to the effect of pressure on the compressibility. The point at which this pressure effect becomes significant is not clear. However, there is a hint that the 4902 kPa limit of the experimental data may be taken as the break point.

In considering the values for any installation metering at approximately 7000 kPa this extra uncertainty should be considered.

On the basis of a ρ_{15} value of 840 kg/m^3 , temperature of $46 \text{ }^\circ\text{C}$, and pressure of 70 bar, API 11.2.1M gives a compressibility factor value of $0.903\text{E-}6$.

The uncertainty is then estimated in line with the method suggested in API 11.2.1M as follows:

Basis A Uncertainty (no pressure effect)

$$0.903\text{E-}6 \times 6.5 \times 7000$$

$$\text{i.e., } \approx 0.04 \%$$

The Standard states that this value may be *doubled* for pressures over the break point, giving a possible value of approximately 0.08%.

IP PAPER NO 2

This is primarily a guide for users of the API 2540 Standard, but its valuable contribution to the industry is a detailed routine for the calculation of C_{dl} , C_{pl} and base density.

Using these combined conversion factors, the Paper No 2 routine allowed the calculation of the notional volume the crude would occupy at 15 °C and 0 bar g, approximately Metric Standard Conditions (stated in ISO 5024 as 15 °C temperature and 1.01325 bar a pressure), the "Standard Volume"

The overall calculation made possible by the Paper is as follows:

$$Q_{vs} = Q_{vg} \times C_{dl} \times C_{pl}$$

where

Q_{vs} is the Standard Volume, Sm^3 ,

Q_{vg} is the Gross Volume, m^3 , the measured volume.

The routine is based upon a series of nested iterations, which take as entry data the measured density, temperature and pressure.

The calculations use the API 2540 algorithms for the determination of C_{dl} , along with the "Downer" equation (currently being replaced by the API 11.2.1M routine), for the determination of C_{pl} .

It incorporates specific methods for the rounding and truncation of input data values, and specifies the precision of the polynomial series used for the exponential values within the calculation. In one form or another, the routine is built into many of the current flow computers in use in the UK, and is written into pipeline operating agreements.

BASIS OF MEASURED DENSITY

The attraction of the approach is that the calculation is firmly based upon current measurements, and closely follows changing process conditions. Any change in the water content, for example, will make some change in the measured density, and may be reflected in the calculated expansion factors. The inclusion of NGL spike into the crude oil stream will also be accounted for in this way.

The compensation for changing process conditions happens automatically, to all intents and purposes 'in real time' (independent of operator or technical action, independent of sampling or analysis error), and is incorporated immediately into the on-line determination of quantities.

Clearly, its efficacy depends upon good density measurement.

FLOW COMPUTER ROUTINES

The earlier generation of flow computers tended to have a straight implementation of IP Paper No 2 built into the software. Models currently being offered may include a variant of the Paper No.2, in that the Downer equation for compressibility has been replaced with the API 11.2.1M equation instead.

RESOLUTION OF CALCULATION

An integral part of the API 2540 calculation implementation is a specific approach to the rounding or truncation of values. These are carried through in Paper No 2, and some new rounding is added. The value of K_0 given in API 2540 for crude oil, for example, is 613.97226 ; Paper No 2 rounds this to 613.9723. This rounding and truncation was specified to ensure that identical results, within the uncertainty of the Standard, would be obtained regardless of the variety of the computer used to perform the calculations: current flow computers tend to use the values at their full resolution.

METER K-FACTOR CALCULATION ANOMALIES

The meter K-Factor calculation is defined in IP Part X, as follows:

$$K = [(n/V_b) \times (C_{tm}/C_{tp}) \times (C_{plm}/C_{plp})]$$

where

K is the meter K-factor, pulses/m³

n is the number of pulses from the turbine meter during the proving run

V_b is the volume of the prover during the proving run, m³

C_{tm} and C_{tp} are corrections for the effect of temperature on the liquid, at meter and prover conditions respectively

C_{plm} and C_{plp} are corrections for the effect of pressure on the liquid, at meter and prover conditions respectively.

Some systems use a variation of this equation

$$K = [(V_b/n) \times (C_{tm}/C_{tp}) \times (C_{plm}/C_{plp})]$$

This has the effect of having the K-factor in units of m³ per pulse, the "one pulse volume".

The implementation of the full equation depends upon the calculation of the liquid expansion factors at the various locations: density transducer to turbine meter in the first case, meter to prover conditions in the second.

The first of these is not shown explicitly in the equation above, but may participate nevertheless in that the value of "density at meter conditions" depends upon the notional expansion of the liquid from density transducer to turbine meter conditions of temperature and pressure.

It follows, therefore, that any error in the calculation of the liquid expansion factors will contribute to an error in the value of any meter K-factor based upon them. The nature of the calculation of, say, C_{pld} will be included also in the calculation of C_{plm} and C_{plp}.

Since the meter K-Factor calculation is central to all the subsequent determination of quantities, it is clearly vital that the expansion calculations be as accurate as possible.

THE EFFECT OF WATER

It is not clear *from the Standards* if the crudes which formed the database studied had any appreciable water content. Water content is not even mentioned, suggesting that it was not a significant consideration in respect of their samples tested. In addition, the only North Sea crudes included in the study are samples from Shell's Auk and BP's Forties fields. Whether these crudes were at all 'wet' at the time of the study (late 1970s) is irrelevant in so far as the Standard is concerned.

In fact, one has to go behind the Standard to the paper published by NBS describing the original research to find that water content was very much a factor in the selection of the crudes investigated.

No sample of crude which contained more than 0.38% of water was investigated, so there is real doubt as to the applicability to (typically wet) North Sea fluids.

In addition, the research samples were of 'stable' crude : the typical North Sea crude contains some proportion of components which are naturally gaseous at Standard Temperature and Pressure. The 'natural drip gasolines' are specifically treated in the Guidelines (see below).

A typical expansion factor for *fresh water* may be calculated from IP Part X Section 3 (which refers to either ISO 3838 or ISO 8222). At 46 °C and 70 bar g, a combined expansion coefficient for fresh water is 0.9937.

At the same temperature and pressure, a typical value for crude oil is 0.9790. This represents a difference of approximately 1.5%.

Even if the values had been similar to those for crude, we would be left with the problem that the values given by the IP are for fresh water.

The water content of our crudes is very different from fresh water, containing as they do a variety of mineral salts, and frequently contain amounts of process chemicals.

This being so, it is pointless to suppose that there could be some way of applying these values for pure water into any calculation involving the water content of the metered liquids.

THE EFFECT OF SPIKED NGL

We know that NGLs behave differently from crude oil in terms of temperature and pressure.

IP Measurement Paper No 2, in its section giving guidance on the use of API 2540, specifically excludes NGLs from the applicability of the Standard, if the NGLs are *pure components*, e.g., pure butane or pure propane. It allows their inclusion if they are "drip gasolines.....the paraffinic condensate from gas well production". The liquids spiked into the crude in the North Sea fall into this latter category, in which case API 2540 states that they should be treated as if they were crude oil.

In addition, Paper No 2 states explicitly that its calculation routine is for crude oil or condensate.

The effect of adding NGLs into the crude stream will be to decrease the value of the measured and the base density. This is the sort of change which is accounted for automatically if one uses the Paper No 2 method, based upon measured density.

A recent revision of the API Manual of Petroleum Measurement Standards Chapter 12.2 suggests the use of the Historical 1952 Edition of API 2540 for condensates. It is interesting to note that while IP Paper No 2 stated explicitly that API 2540 constants should not be applied to pure NGLs, the 1952 Standard was based upon laboratory investigation of the characteristics of pure NGLs. Either way, this is of no help in the treatment of crude / condensate mixes.

CHOICES AVAILABLE

It is clear that the current regime of using the API / IP / ASTM / ISO methods described have several shortcomings when applied to our North Sea crudes. To summarise these:

API 2540 makes no provision for the presence of water
API 2540 is not applicable to lively crudes

There are several methods available to calculate for crude oil expansion. There are three factors to be considered:

The Operator's commercial interest
The Department of Trade and Industry's requirements
Pipeline operating agreements.

The first of these could sometimes be at variance with the other two.

The choices available are:

Ignore β (F)
Use IP Paper No 2
Use a modified version of IP Paper No 2
Use pre-set correction factors
Use a modified version of IP Paper No 2, with custom values for K0 and K1

IGNORE β (F)

The Department of Trade and Industry standards state that they may allow UKCS operators to ignore the effects of pressure of the crude, presumably on the basis that crude itself is not very compressible.

This may be true at fairly low pressures. At higher levels, pressure is likely to have an increasing effect upon the volume of the crude. At higher pressures, and certainly for crude/condensate mixtures, it would not be considered wise to ignore the effects of pressure.

In any event, pipeline agreements frequently require that the compressibility be taken into account.

IP PAPER NO 2

It is a requirement of the Department of Trade and Industry that "good oilfield practise" be followed in one's metering effort. This probably involves some form of implementation of IP Measurement Paper No 2, in the general sense that it may be the most common approach in the industry. In addition, the DTI Standards specifically mention API 2540 and IP Paper No 2.

All the rounding and truncation is designed to achieve results within the uncertainty of the original, which is the best that any user of the API standard can claim for any implementation.

The fact that the original standard was generated to be used with the computers commonly-available in the late 1970s and early 1980s may make the provisions unnecessarily restrictive today : they are being widely ignored.

I P PAPER NO 2 MODIFIED

A major part of the IP Paper No 2 routine, the use of the "Downer" equation for the calculation of the compressibility of the crude oil, has been superseded, however. The equation and constants from API Chapter 11.2.2M are being used instead.

Its use has been sanctioned by the Department of Trade and Industry and by the Institute of Petroleum. (It is, in fact, included in its recently published revisions of parts of the Petroleum Measurement Manual, e.g. Part X. (It is also, I am told, included in a revised version of Part VII Section 2, due to be published 1992!)). Its use has been approved by Mr Lionel Downer himself, and it has been incorporated in BS 7340 / ISO9770.

PRESET α AND β (F)

It is possible have the major inputs to the expansion calculations, α_{15} and β (or F), input into the flow computers as pre-set constants.

In this method, α_{15} , and β (or F), can be established by laboratory analysis on the basis of a periodic flow-proportional sample. The values can be set into the flow computers as soon as possible after the results of the analysis have been obtained and checked, and up-dated as required.

It may be considered that this approach contributes no more uncertainty to the overall determination of quantities than any other method. If conditions vary randomly, within very small limits, this could be the case. However, the uncertainty of the laboratory evaluation of compressibility is estimated as $\pm 5\%$.

In a situation where any single input parameter may vary by an order of magnitude for an appreciable period (e.g. water or NGL content going from 1% to, say, 10% for several hours, or even days) this assumption is not tenable. This would require the pre-set values to be updated to match the new circumstances.

Technicians or operators may be unable, for whatever reason, to input updated values at the prescribed time, or even forget to have the values updated for long periods, regardless of the results of analysis. In these situations, the potential for mis-measurement is greatly increased.

This can give rise to the use of inappropriate meter K-Factors. While the magnitude of the error in meter K-Factor is generally small, it is systematic, and should not be lightly ignored.

METER K-FACTOR CALCULATIONS

A set of calculations has been done to assess the implications of using pre-set expansion constants, as opposed to allowing the (effectively "real time") updated calculation of these using the IP Paper No 2 method.

- a A baseline calculation where the assumption is that the constants are entirely appropriate for the conditions, is done for typical conditions.

Thus for example, with 30000 pulses, a prover certified volume of 1.625m^3 , meter temperature of $44\text{ }^\circ\text{C}$, meter pressure of 70 bar, prover temperature of $44.5\text{ }^\circ\text{C}$, prover pressure of 69.5 bar, base density of 825 kg/m^3 , a likely meter K-Factor is approximately $5.424941\text{E-}5\text{ m}^3$ per turbine meter pulse (the "baseline" K-factor).

- b Calculations are repeated where the base density changes by 1% steps (both above and below the nominal 825 kg/m^3 value). The resulting meter K-Factor is compared with the baseline meter K-Factor in each case.

These changes in base density are an attempt to replicate the situation where, for example, water cut or NGL content changes, a situation in which the expansion constants should be changed in the flow computer system.

- c The % error in meter K-Factor per change % in base density is then assessed.

d. Results are as follows:

% Change in Base Density	Base Density (kg/m³)	K-Factor	% Change in KF
-10	742.50	5.4279575e-5	-0.012
-9	750.75	5.4278845e-5	-0.010
-8	759.00	5.4278140e-5	-0.009
-7	767.25	5.4277459e-5	-0.008
-6	775.50	5.4276802e-5	-0.007
-5	783.75	5.4276166e-5	-0.005
-4	792.00	5.4275551e-1	-0.004
-3	800.25	5.4274956e-5	-0.003
-2	808.25	5.4274379e-5	-0.002
-1	816.75	5.4273822e-5	-9.95e-4
+1	833.25	5.4272758e-5	9.64e-4
+2	841.50	5.4272251e-5	1.89e-3
+3	849.75	5.4271759e-5	0.003
+4	858.00	5.4271282e-5	0.004
+5	866.26	5.4270820e-5	0.005
+6	874.50	5.4270371e-5	0.005
+7	882.75	5.4269935e-5	0.006
+8	891.00	5.4269511e-5	0.007
+9	899.25	5.4269099e-5	0.008
+10	907.50	5.4268700e-5	0.008

It is clear that the greater the 'error' in density, the greater will be the error in the meter K-Factor. (NB : This is only true if temperature and pressure at the turbine meter are different from those at the prover, or if density is measured at a different temperature and pressure from those obtaining at the meter, and density is "referred" from one set of conditions to another).

This error in K-Factor is small, and the direction of the error matches the direction of the departure from the accurate density. Under normal operating conditions, variations would be random and could cancel out. A change in base density due to an increased water cut or to a period of NGL spike is not a randomly varying change. Such a change in operating conditions will, instead, be a significant bias in one direction, and liable to be in place for extended periods.

This bias would have the effect of making the metered volumes appear to be different from what they should be otherwise. Whether indicated volumes appear larger or smaller will depend upon the direction of the shift in the base density. If actual base density is larger than that used (e.g. because of a higher water content), calculated volumes will be smaller than actual volumes. If on the other hand actual base density is smaller than the value in use (say because of NGL spiking), calculated volumes will be larger than actual volumes.

STANDARD VOLUME CALCULATIONS

Different considerations apply when one wants to establish the effect of inaccurate expansion constants on calculated Standard Volumes, on which pipeline tariff payments are frequently based.

A set of test calculations was done to determine the likely effect of inappropriate expansion constants on Standard Volumes. The basis of the calculations was the same as used above, i.e., the input of 1% changes in base density followed by a comparison between the resulting Standard Volume and a "correct" baseline value.

Calculated values are based upon a typical situation with 2 meter streams on line, each flowing 280 m³/h for a period of 365 days, i.e. a notional Gross Observed Volume of

$$2 \times 280 \times 24 \times 365 = 4905600 \text{ m}^3 \text{ per annum}$$

With a temperature of 46 °C, a pressure of 70 bar g, base density of 825 kg/m³, this gives a Gross Standard Volume of 4799397 Sm³ for the year.

% Change in Base Density	Base Density (kg/m ³)	Standard Volume	% Change in Standard Volume
-10	742.50	4780706	0.389
-9	750.75	4782588	0.350
-8	759.00	4784482	0.311
-7	767.25	4786380	0.271
-6	775.50	4788278	0.232
-5	783.75	4790169	0.192
-4	792.00	4792049	0.153
-3	800.25	4793914	0.114
-2	808.25	4795763	0.076
-1	816.75	4797591	0.038
+1	833.25	4801180	-0.037
+2	841.50	4802937	-0.074
+3	849.75	4804668	-0.120
+4	858.00	4806372	-0.145
+5	866.26	4808049	-0.180
+6	874.50	4809697	-0.215
+7	882.75	4811317	-0.248
+8	891.00	4812908	-0.281
+9	899.25	4814470	-0.341
+10	907.50	4816003	-0.346

These values are based upon a nominal total for a whole year's flow at the maximum flow rate for each of two meter streams. A situation where a systematic discrepancy remained in place for such an extended period is clearly not likely.

In addition, the likelihood of this level of flow rate for sustained periods is fairly small.

However, the calculated % change is perfectly applicable for the time for which the discrepancy is in place, and is independent of flow rate.

AN ALTERNATIVE

CUSTOM COEFFICIENTS FOR SPIKED OR WET CRUDE

The approach which would offer the optimum in terms of reflecting real operating conditions is to use

A different set of coefficients for each typical fluid mix

Means of placing the appropriate values in use depending upon the actual flowing conditions.

This is not as straightforward as it might appear.

Apart from the problem of acquiring a truly representative sample of each type of mix, there would be a problem in establishing, and agreeing with interested third parties, the specific coefficients for each mix, whose delimiting characteristics would also have to be agreed. There would be the matter, also, of establishing the means of triggering the use of one set of coefficients or the other in the flow computer. Not least, there would be large expense involved. There would be need for a major and complicated research project, including the cost of designing and building the necessary test equipment.

The author's musing on the nature of the test equipment required for such tests prompted the realisation that most North Sea oil platforms already have installed fairly sophisticated, certainly expensive, skid-mounted equipment for the reliable and accurate measurement of the density, and automatic sampling of the quality, of their exported products. Not only that, but the uncertainty of measurement of such equipment is fairly broadly accepted. The equipment is generally maintained to agreed procedures, with the major items being calibrated annually against traceable standards.

This musing prompted the notion of analysing the output of such equipment to see if useful conclusions could be derived.

To be of use, any conclusion would have to be based upon a very large number of samples; ignoring the fact that API 11.2.2 is based upon only 5 tests on each of 6 samples plus 4 tests on the seventh sample, i.e., 34 data points in all! - API 2540 is based upon approximately six hundred data points, gained from a total of over 100 samples.

To use the outputs from offshore metering equipment would necessitate a major data-gathering effort, which might mean many man-hours of technician time taking periodic sets of readings from flow computers or transposing data from periodic printed reports into, say, spreadsheet form - undoubtedly a time-consuming and expensive exercise.

THE DATABASE

The Amerada Hess Ltd (AHL) AMADAES system provided the easy answer to the task of data-gathering.

Every metering supervisory computer in each of the fields operated by AHL sends a minute-by-minute 'snapshot' of its measurement data into a database computer located in Scott House in Aberdeen. The data comprises raw signal data from field equipment (e.g., density transducer periodic time, flow transmitter milliamps, etc.), temperature, pressure, density, base density, flow rates for each meter stream and for the station, calculation constants held in the flow computers, chromatograph analysis and configuration data, accumulated and periodic flow totals, meter proving reports, etc.

Each minute's data is stored for some 40 days, during which time it is available for monitoring and evaluation on the local PC-based network. Thus it is possible to monitor some 10,000 data points every minute. At the end of this 40 day period, it is archived. Even when the bulk of the data has been placed in the archive, a picture of the data is still available on line for ten-minute intervals.

The system arose from the perceived need to be able to offer onshore support to platform technicians who might not have in-depth measurement experience, on the one hand, and to allow readily-accessible data for the verification of daily allocation totals and calculation of mis-measurements. Since its

inception some three years ago, it has proved an invaluable tool for these purposes. It has proved useful, in addition, for the monitoring of quality data (export gas density versus composition, etc.) and of turbine meter performance (each successful proving event is automatically assimilated into trended data, for example).

Thus it is a fairly easy matter to acquire into a desktop personal computer all the data necessary for the evaluation of custom expansion coefficients.

FIELD MEASUREMENTS OF DENSITY AND WATER CONTENT

The combined density measurement / sampling systems, whose data is used in the calculations below, comprise a flow-proportional sampler and two Solartron 7830 or 7835 density transducers mounted in a pumped fast loop drawing its contents from, and returning them to, the inlet header of the metering system. A manual valve and a flow indicator, which are fitted downstream of the sampler, are used to adjust the flow, the ideal rate being that which is isokinetic with the flow through the inlet header.

In the case of one of the platforms, an Endress and Hauser Aquasyst Water-in-oil monitor, whose output is sent into the platform's metering supervisory computer, is also fitted in the fast loop. This monitor is calibrated daily with reference to the water content of a sample taken manually from the location.

On the other installation, a manual sample is taken every 4 hours, and the water content of the sample determined in the platform laboratory. This water content value is manually entered into the platform's metering supervisory computer.

A 4-wire PRT (to BS 1904 Class A) and a high good-quality pressure transmitter are typically installed at the densitometer location, feeding their signals into the flow computer.

A pitot-style probe is installed in the metering inlet header in such a location as to ensure that a representative sample of the crude being exported is introduced to the fast loop system. The loop is insulated to prevent wax build up inside the pipe work.

Density Transducers

The density transducers are Solartron 7830 or 7835 vibrating-tube units with an operating range of 0 - 3000 kg/m³. Each transducer has a single tube through which the pumped fast loop flow passes.

The tube is driven by a pair of electromagnetic coils to vibrate at its resonant frequency. This vibration is detected by a second set of coils, and converted into a pulse train by the instrument's electronics. These pulses are sent to the flow computers, which measure the periodic time of the pulses.

The periodic time is a function of the mass of the vibrating element, which, in turn, is a function of the mass, and therefore the density, of the fluid with which it is filled. The stream flow computers calculate a density value based upon this periodic time, and correct it for the effects of transducer temperature and pressure.

In the calculation, the flow computers use a set of constants which are unique to the transducer, and which have been established at its latest calibration.

Twin Transducers

One of the transducers is designated 'master' or 'fiscal', as the density value derived from its output is the one used in all the flow computers' subsequent calculations. The other is designated the 'tracking' transducer, and its density value is used to check on the health of the other. The output from the 'tracking' transducer may also be used should the 'master' instrument fail.

The density values produced by both transducers are continuously monitored by the stream flow computers. Should a discrepancy, which is greater than a preset value, arise between the two values, an alarm is raised by the flow computer.

Regular re-calibration

Each month an alternate density transducer is removed and air checked in accordance with maintenance procedures.

A regular replacement programme ensures that the density transducers are routinely calibrated.

Every 6 months one of the density transducers is removed from service and replaced by a unit which has recently been calibrated.

The density transducer that has just been fitted after re-calibration, is designated the fiscal transducer and the unit which has been in service is demoted to tracking duty.

This routine ensures that each transducer is changed out every 6 months. When a unit is changed, the one which has been removed is sent to a laboratory for re-calibration.

The Sampler

The sampler is supplied with product from a pumped fast loop system.

The sampler is a pneumatically-operated positive displacement unit which traps a sample in a cup type chamber from the fast loop flow line without interruption to the flow, and discharges it to the pressurised sample receiver.

7-day sample

The requirement is for one representative sample to be gathered over a seven day period.

The metering supervisory computer provides the sampler with a flow proportional pulse rate, to ensure that the acquired sample in the container is representative of the exported fluids.

The sample receiver is pre-charged with nitrogen or argon, to a pressure higher than that in the fast loop, prior to being fitted. This ensures that any sample acquired will be held well above its vapour pressure.

The sample is assayed at an onshore laboratory, the assay results going into the allocation system. The water content is determined as part of the assay.

NGL / CONDENSATE MASS FLOW

In one of the platforms, NGLs / condensates recovered from the gas processing system are 'spiked' (i.e., injected) into the crude oil stream just upstream of the crude oil export metering system. The term 'NGLs' is used in the following text to describe this fluid stream, as that is the common AHL usage. In other companies' installations the fluids may frequently be referred to as 'condensates'.

Their mass, density and temperature are measured by Rosemount Micro Motion coriolis meter, whose data are sent into the metering supervisory computer, prior to their being mixed with the crude oil.

The flow of combined crude oil / spiked NGLs is measured by the platform's three stream and prover turbine meter system, combined with the density measurement system described above. Thus it is simple to derive the percentage of the combined fluids which is from the NGL spike.

The other platform studied has no NGL spike.

THE EXPERIMENTAL CALCULATIONS

The object was to establish the relationships between crude oil density, temperature, pressure, NGL content and water content for the first platform's exported crude oil, and between crude oil density, temperature, pressure, water content for the second platform's exported crude oil.

Coefficients derived from one exporting period would be used to predict the density of crude oil for each of the platforms for other exporting periods.

The experimental procedure was as follows.

A For Platform 1 (NGL Spike and Water Content)

NB: It has not yet been possible to make a satisfactory evaluation of the effects of water content for this platform, as the water content of its exported crude oil is typically below the uncertainty of the method of its determination and therefore taken as zero. However, there is a data set in hand for a period when water content was measurable. This data set has not yet been evaluated.

A1 Using AMADAES, acquire minute-by-minute values for :

Combined crude oil / NGL mass flow rate
NGL mass flow rate
Measured NGL density
Measured crude oil density
Measured crude oil export temperature
Measured crude oil export pressure.

This data is output by AMADAES as a 'Comma Separated Variable' (CSV) file.

A2 Convert the CSV file into a Microsoft 'EXCEL' file.

A3 Remove all data where the minute's set was incomplete or anomalous, or where there was any sign that fixed values (as opposed to measured ones) were in use at the time, or where there was no flow in the system.

Interruptions to the offshore to onshore communications links mean that there are some gaps in the data. These appear to be infrequent, although no attempt has been made to assess the actual frequency, as the information is not relevant to the present study.

Fixed values may appear in the data for two reasons :

They may be used by technicians as part of their routine checks of the flow computers.
They may be adopted automatically by the flow computers in the event of instrument failures.

A4 Using Microsoft 'EXCEL' derive coefficients relating measured crude oil density to :

NGL % of combined exported fluids
Measured NGL density
Measured crude oil export temperature
Measured crude oil export pressure.

The 'LOGEST' function was used for this. This function generates the coefficients a and b for an equation of the form :

$$d = a \times b^P$$

where

d is the density, kg/m³

a and b are coefficients for the parameter being investigated

P is the magnitude of the parameter being investigated

(bar for pressure, % for NGL content, °C for temperature, kg/m³ for NGL density).

The 'LOGEST' function generates these values to fit the data as closely as possible to a non-linear curve.

- A5 Use the coefficients thus derived for pressure, NGL% and temperature to calculate the density from the equation :

$$d_{\text{calc}} = \text{average}((C_1 \times (a_1 \times b_1^{\text{bar}})), (C_2 \times (a_2 \times b_2^{\text{NGL}\%})), (C_3 \times (a_3 \times b_3^{\text{degC}})))$$

where

d_{calc} is the calculated density for the pressure, NGL%, and temperature combination of a minute's data set, kg/m³

C₁ is a constant reflecting the weighting of the pressure effect in the equation

C₂ is a constant reflecting the weighting of the NGL% effect in the equation

C₃ is a constant reflecting the weighting of the temperature effect in the equation.

(The derivation of C₁, C₂, and C₃ is described below)

a₁ and b₁ are the coefficients for the pressure effect on density

a₂ and b₂ are the coefficients for the NGL% effect on density

a₃ and b₃ are the coefficients for the temperature effect on density

bar is the minute set's pressure, bar

NGL% is the minute set's NGL mass flow rate as a percentage of the total combined NGLs and crude oil mass flow rate, %

degC is the minute set's temperature, °C

- A6 Setting C₁, C₂, C₃, and C₄ each to unity , a d_{calc} value was generated for each minute set's combination of pressure, NGL%, NGL density, and temperature.
- A7 The percentage difference between the measured (d_{meas}) and calculated density values for each minute's data set was calculated as follows :

$$\text{Error}\% = 100 \times \frac{|d_{\text{meas}} - d_{\text{calc}}|}{d_{\text{meas}}}$$

- A8 The average of all the Error% values for all the minute data sets was calculated.
- A9 The Microsoft EXCEL 'Solver' function was used to vary the C₁, C₂, C₃ , and C₄ values to achieve the lowest possible average Error% value. The function automatically re-calculates each of the d_{calc}, Error%, and average Error% values.

A10 Investigations into the combinations giving large Error% values led to the awareness that the density of the NGL was a significant factor. A second equation, of the form

$$d_{\text{calc}} = \text{average}((C_1 \times (a_1 \times b_1^{\text{bar}})), (C_2 \times (a_2 \times b_2^{\text{NGL\%}})), (C_3 \times (a_3 \times b_3^{\text{degC}})), (C_4 \times (a_4 \times b_4^{\text{NGLdens}})))$$

where

C_4 is a constant reflecting the weighting of the NGL density effect in the equation
 a_4 and b_4 are the coefficients for the NGL density effect on crude oil density
 NGLdens is the minute set's NGL density, kg/m^3

is also being investigated. Results from this calculation are not yet complete.

B For Platform 1 (Water)

B1 Using AMADAES, acquire minute-by-minute values for :

Measured crude oil density
 Measured crude oil export temperature
 Measured crude oil export pressure.
 Measured crude oil export water content

B2 Convert the file into an 'EXCEL' file, and remove any sets where data was incomplete, anomalous or appeared fixed, or where there was no flow in the system.

B3 Using the Microsoft 'EXCEL' 'LOGEST' function, derive coefficients relating measured crude oil density to :

Measured crude oil export water content
 Measured crude oil export temperature
 Measured crude oil export pressure.

B4 Use the coefficients thus derived for pressure, $\text{H}_2\text{O}\%$ and temperature to calculate the density from the equation :

$$d_{\text{calc}} = \text{average}((C_1 \times (a_1 \times b_1^{\text{bar}})), (C_2 \times (a_2 \times b_2^{\text{H}_2\text{O}\%})), (C_3 \times (a_3 \times b_3^{\text{degC}})))$$

where

d_{calc} is the calculated density for the pressure, $\text{H}_2\text{O}\%$, and temperature combination of a minute's data set, kg/m^3

C_1 is a constant reflecting the weighting of the pressure effect in the equation

C_2 is a constant reflecting the weighting of the $\text{H}_2\text{O}\%$ effect in the equation

C_3 is a constant reflecting the weighting of the temperature effect in the equation. C_1 , C_2 , and C_3 were derived in the same manner as were those in A above.

a_1 and b_1 are the coefficients for the pressure effect on density

a_2 and b_2 are the coefficients for the $\text{H}_2\text{O}\%$ effect on density

a_3 and b_3 are the coefficients for the temperature effect on density

bar is the minute set's pressure, bar

$\text{H}_2\text{O}\%$ is the minute set's crude oil water content

degC is the minute set's temperature, °C

B5 A d_{calc} value was generated for each minute set's combination of pressure, $\text{H}_2\text{O}\%$, and temperature.

B6 The percentage difference between the measured (d_{meas}) and calculated density values for each minute's data set was calculated as follows :

$$\text{Error}\% = 100 \times \frac{|d_{\text{meas}} - d_{\text{calc}}|}{d_{\text{meas}}}$$

B7 The average of all the Error% values for all the minute data sets was calculated.

PRELIMINARY RESULTS

For Platform A

One day's data acquired from AMADAES yielded 1425 minute sets, where

Minimum NGL% value was	1.68*
Average NGL% value was	2.65
Maximum NGL% value was	4.27

*Zero values were excluded for this preliminary test, but will be incorporated in more refined tests.

Minimum temperature value was	42.94
Average temperature value was	46.07
Maximum temperature value was	47.34

Minimum pressure value was	69.74
Average pressure value was	77.56
Maximum pressure value was	82.14

Minimum crude density value was	795.54
Average crude density value was	806.51
Maximum crude density value was	811.75

This gave the equation

$$d_{\text{calc}} = \text{average}((0.9998437 \times (823.07745 \times 0.9997378^{\text{bar}})), (0.997551 \times (810.02934 \times 0.9993505^{\text{NGL}\%})), (1.0006256 \times (806.16877 \times 1.0000091^{\text{degC}})))$$

Applied to each of the sets of data from which the coefficients had been derived, this gave an average Error% value of 0.216, and a maximum Error% value of 1.3436.

Applied to the next day's data, the equation gave an average Error% value of 0.5585, and a maximum Error% value of 2.63.

Applied to the another day's data, the equation gave an average Error% value of 0.1566, and a maximum Error% value of 0.761.

Applied to the third day's data, the equation gave an average Error% value of 0.2337 and a maximum Error% value of 7.463.

These large variations have not yet been investigated.

For Platform B

A set of 10507 minutes' data was acquired from a period of approximately 7.5 days yielded the following data :

Minimum H ₂ O%	0.30
---------------------------	------

Average H ₂ O%	0.91
Maximum H ₂ O%	15.0
Minimum Pressure	8.10
Average Pressure	14.48
Maximum Pressure	16.90
Minimum Temperature	47.10
Average Temperature	54.92
Maximum Temperature	55.80
Minimum Density	789.50
Average Density	794.50
Maximum Density	823.10

$$d_{\text{calc}} = \text{average}((-0.032 \times (802.8595 \times 0.999274^{\text{bar}})), (0.999274 \times (792.4156 \times 1.002847^{\text{H}_2\text{O}\%})), (0.023154 \times (810.309 \times 0.999274^{\text{bar}})))$$

This equation gave a Maximum Error% of 0.719, and an Average Error% of 0.052 when applied to its own data.

The Maximum Error% of 0.719 was found to be from the minute with the highest water content and highest measured density values. It may be noted that, while the *average* water content value was found to be below 1%, this *highest* water content was 15%.

DISCUSSION OF RESULTS

The results so far indicate that the method is potentially a very useful one.

The data acquired so far for each of the platforms comprises many thousands of minute sets. It has not been possible to process more than a very small part of these, so it is not wise to give firm conclusion at this time. We estimate that another month's work, which would include some test of the results on data from other installations, is required before firm conclusions and recommendations can be made.

We have made no serious attempt so far to quantify the uncertainty of our proposed system of coefficients.

The uncertainty of the measurements on which the equations are based are likely to be dominated by the uncertainty of the water-in-oil determination and of the NGL density for Platform A, and by the uncertainty of the water-in-oil monitor for Platform B. (However, if we remind ourselves that the API coefficients and equations currently in use make no allowance whatever for water or NGLs, we can retain some perspective).

It will be clear also that one of the basic tenets of API 2540, namely that the density at 15 °C is a vital measurement point, may not be achievable using our alternative method. We may retain some useful perspective, again, however, when we remind ourselves that some North Sea crudes are liable to show wax precipitation at this temperature!

There remains the basic philosophical question of the validity of using API 2540 or API 11.2M on crude oil containing substantial admixtures of water or NGLs, when they were derived from experimental work on what was effectively dry, stock tank crude.

ACKNOWLEDGEMENTS

I am grateful for the assistance I have received from management and staffs at Amerada Hess Ltd and Rhomax Engineering . I must mention especially Margaret Low, Librarian at AHL, whose help has been ready and patient.

UNPREDICTED BEHAVIOUR OF VENTURI FLOWMETER IN GAS AT HIGH REYNOLDS NUMBERS

by

A. W. Jamieson (Shell Exploration and Production), P. A. Johnson (NEL),
E. P. Spearman (NEL) and Mrs J. A. Sattary (NEL)

SUMMARY

A Venturi flowmeter is expected to produce a discharge coefficient of less than unity. Laboratory work at NEL, for Shell Expro, on a series of 150 mm (6 inch) diameter Venturi flowmeters, has resulted in discharge coefficients of several percentage points higher than predicted, according to ISO 5167-1; 1991. This work was performed in high pressure air up to 70 bar, Reynolds Numbers up to 8×10^6 and throat velocities up to 125 m/s. Calibration work previously undertaken with the same Venturi flowmeters in water, at lower Reynolds numbers, resulted in behaviour as expected with discharge coefficients near 0.9950.

The paper describes the laboratory investigation that was undertaken to determine the apparent source of error with a view to providing a straightforward solution.

The NEL high pressure recirculating loop facility was utilised, with a reference mass flowrate traceable to the UK Primary Standard Gravimetric facility. Brief details are included on integrity checks performed on the loop and its instrumentation.

Observations during testing are discussed, for example the audible whistle that occurred for certain flow conditions and the significance of throat velocity as a parameter to describe the flowmeter behaviour. The paper explains the justification for the various differential pressure tapping modifications made during the investigation.

This investigation into Venturi flowmeter behaviour has shown some surprising phenomena which, as yet, have not been fully explained. With the increased interest of the oil and gas industry in using Venturi meters in their own right and as part of multiphase flow metering systems, further work is essential to clarify these phenomena.

1 INTRODUCTION

This paper is a follow up to "High accuracy wet gas metering" presented in the 1993 North Sea Flow Metering Workshop¹. A High accuracy metering system for wet gas was described using Venturis as the primary elements and making corrections based on the Murdock equation² for the relatively low quantities of liquid (less than 1 per cent by volume) that would be experienced in the application under consideration. It is worthwhile noting here that for higher liquid contents, Chisholm's equation^{3,4} is better as it can cope with changes in pressure, whereas Murdock's equation is pressure independent.

The installation for which this system was designed is now installed, with start-up scheduled for the fourth quarter of 1996. The aim was to provide a metering system with overall accuracy close to that for gas fiscal metering systems. The Venturi meters will be operating at Reynolds Numbers in the range 10^6 to 10^7 , above the upper range limit of 10^6 stated in ISO 5167-1⁵ for machined Venturi meters. To keep things simple, Shell Expro wanted to modify the standard Venturi design as little as possible. The only modification that was introduced was to use a single tapping at upstream and throat tapping positions instead of the four tapping points, joined by a piezometer ring called for in ISO 5167-1. Shell Expro had accepted that the Venturi meters should be calibrated with liquid and gas to give baseline discharge coefficients. A test separator is installed on the facility, so there was the capability of comparing the flowline meters with the test separator meters to monitor for possible shifts in the discharge coefficients.

For various reasons the Venturi meters (6 flowline + 1 test separator gas meter) were a critical item on the fabrication plan for the facility. Calibration had to be performed quickly, and NEL was best able to carry out both sets of calibrations. The liquid calibrations, on water, went well with all discharge coefficients falling well within a ± 1 per cent range centred on 0.995. However, when calibrations on high pressure air were attempted, things went drastically wrong. The first three meters to be calibrated showed high discharge coefficients between about 1.02 and 1.04, with significant variations depending on flowrate. The magnitude of these shifts came as a complete surprise to both Shell Expro and NEL. From Shell Expro's point of view, the reason for calibrating was to confirm that there would not be significant shifts and to confirm the view of other experts who had been consulted that the discharge coefficients of Venturi meters would be around 0.995 at higher Reynolds Numbers. It was evident that if the effects were indeed real and unpredictable, the whole basis on which the facility had been designed was in jeopardy.

We describe the programme of tests undertaken to quantify the problem and to establish whether a practical solution was possible. We relate this more or less as it happened, and hope to indicate the surprise, mounting concern and finally the relief that an acceptable solution was available. We have not tied up all the loose ends. There are many issues concerning the use of Venturis on high pressure gas that are not yet settled.

2 THE PROBLEM EMERGES

Calibrations of the seven Venturis were carried out in the water calibration facility at NEL. The results of these tests were in accordance with ISO 5167-1. Everything appeared to be going well. The Venturis were then transferred to the high pressure gas rig at NEL. This facility was commissioned in 1993 and uses air as the working medium. Pressure in the loop is supplied via compressors, and a high pressure blower circulates the gas between 10 and 70 bar. The flowrate reference is a gas turbine meter calibrated against the Gravimetric primary standard. The differential pressures on the Venturis were measured initially using Rosemount 1151 DP transmitters. After three Venturis had been calibrated, and all three had shown high discharge coefficients, it was clear that something was wrong. Also with the third Venturi, above a critical flowrate a loud whistle could be heard, and this was associated with a step in the discharge coefficient.

What was wrong? Was it the calibration rig? This particular rig had been troublesome since it had been built, and immediately it became a prime suspect. Was it the Venturis? All participants began asking their contacts if similar behaviour had been observed elsewhere. Where did the whistle come from? The noise pervaded the test hall and its source was not at all obvious. There was intense concern by the Shell Expro project team responsible for the facility, as there was a real possibility that the Venturi based metering system would not be viable and there was no real alternative. The only other meters that could reasonably be considered would be orifice meters, and these had been rejected early on. It was considered that the performance of orifice meters installed close to the wellhead would be poor because sand would degrade the sharp edge. Liquids can build up behind the plate, and it is difficult to guarantee that a drain hole in the orifice would remain clear.

3 TESTS PERFORMED

3.1 Confirmation of Problem

The first thing to be done was to find out whether the apparent problem lay with the Venturis or with the NEL facilities. Before calibrating the meters on water, NEL had inspected the seven Venturis carefully, and had removed burrs from the inner edges of the tappings. NEL also carried out an independent metrology of three of the Venturis. This agreed closely with that of the manufacturer. Visual inspection of the Venturis gave rise to some misgivings. The Venturis were made from three sections of Duplex Stainless steel welded together. One of the welds was at the entrance to the convergent section, the other weld was about half way along the divergent section. The surface finish across these weld areas appeared variable, but not so that the Venturis could be rejected. Apart from the single upstream and downstream tappings, the meters were manufactured in accordance with ISO 5167-1.

The Venturi flowmeters include approximately 7D of upstream straight bore. There was a further 30D upstream of this in the test loop. There was no evidence of flow disturbance, including swirl, upstream of the Venturi or reference turbine meter.

One of the Venturis was taken from the high pressure test rig to the Gravimetric rig. Similar results were obtained to those on the high pressure rig, strengthening the view that the high pressure rig was not the source of the problem.

Although all of the instrumentation used was governed by NAMAS procedures for calibration and storage, all of the other instrumentation on the rig was fully checked out. The calibration of the reference turbine meter in the high pressure rig was also checked against the secondary standard sonic nozzles, themselves calibrated against the Gravimetric rig. Its performance was within the range of its last full calibration. The Rosemount DP cells had shown significant zero drift during the first calibrations and were replaced with Mensor DPGII differential pressure gauges rated at 2 and 10 bar.

NEL looked back in their records and found an example of a Venturi nozzle calibrated on water that had shown a step change in discharge coefficient associated with a whistle. Shell Expro had discussed the matter again with metering specialists, and there were stories of Venturis that had had unexpectedly high discharge coefficients.

Thus there was good reason to believe that the problem lay in the meter and not in the NEL test facility. Shell Expro now commissioned a test programme to determine the origin of the problem and to find a solution that would involve as little modification to the Venturis as possible. The time scale demands of the overall Shell Expro project dictated the investigation objectives, and the frequency of reporting. Essentially this investigation was divided into three phases of about ten days, each culminating in a progress meeting at NEL involving NEL, Shell Expro and the metering contractor for the project.

3.2 First Phase

An important detail to be resolved was the source of the audible whistle, as there was still the possibility that this was coming from the test facility. A piece of straight pipe was installed in the rig instead of the Venturi. No whistle could be heard over the whole flow range. Next, it was important to establish the influence of the impulse lines on the whistle. The Venturi which showed the loud whistle and the highest discharge coefficient was reinstalled in the test rig with blanking flanges on the pressure tappings, i.e. without the impulse lines. The whistle was thought to be related to the total volume of the tapping chamber, and removing the impulse lines should show some effect. On flowing gas, the whistle was very much present and thought to be louder for certain flow conditions. A clear plastic tubing was inserted into both upstream and downstream pressure tapping chambers to change the volume of the chamber. The whistle disappeared. The tests were repeated with the impulse lines attached to allow discharge coefficients to be determined. Although the whistle was suppressed, the discharge coefficients remained high. It was clear that the source of the whistle was the Venturi itself, but that it was not directly related to the high values of discharge coefficient observed.

The next stage of phase 1 was to install a different Venturi flowmeter in the test facility and observe the result. Shell Expro had commissioned other work on Venturi meters at NEL which required three 150 mm nominal bore Venturis manufactured in full accordance with ISO 5167-1 with β 0.4, 0.6 and 0.75. The β 0.4 Venturi (for convenience referred to as the research Venturi) was closely comparable to the seven project Venturis (β 0.41). Three of the upstream and throat tappings of the research Venturi were blanked off and a calibration chart was made. Fig 1 shows a step change of about 1 per cent midway across the Re_D range at 3.5×10^6 , from 1.003 to 1.011. An audible whistle also started at this step. It was believed that the acoustic effects in the tapping chamber could be responsible for the step change and the whistle, so attempts were made to modify the throat tapping chamber to try to eliminate the

step. Inserts were made to block up the three redundant throat tappings and were fitted as accurately as possible in the limited time available. A disc drilled with a 0.5 mm hole was fitted in the fourth tapping chamber to act as a dampener for the pressure signal. The discharge coefficient lay between 0.994 and 1.004 as shown in Fig 2. For the first time, discharge coefficients less than unity had been observed, in line with ISO 5167-1.

Buoyed up by this apparent success, the next step was to try to repeat this in the project Venturi, which had different shapes of tapping chambers to the research Venturis. The obvious way to modify the effect of the tapping chamber was to fill the volume. Accordingly inserts were made that filled both tapping chambers, paying attention that they did not protrude into the flow. Carefully cut channels were made on the inserts to allow the pressure signals through. The discharge coefficients measured with this set up were very high, about 1.09, to the disappointment of all. Completion of the tests with inserts that filled each tapping chamber produced variable results and was clearly leading nowhere. This design idea was dropped.

3.3 Second Phase

The second phase of the work started with further effort aimed at attempting to duplicate the pressure tapping arrangement of the research Venturi on the project Venturi. This entailed installation of a drilled disc within the base of the larger upper pressure tapping chamber to simulate the damping effect that had been successful with the research Venturi. The discs were located in both the upstream and throat tappings with hole diameters ranging from 0.5 - 2 mm for separate tests. Because the lengths of the lower sections of the tapping chambers were different between the project and research Venturis, efforts were made to locate a 0.5 mm diameter hole within the lower section of the tapping of the project Venturi. On testing, the discharge coefficients were essentially unchanged and remained high. However, one odd result occurred with 1 mm diameter hole discs where the discharge coefficient decreased to near unity for a small part of the Reynolds number range. The calibration chart is shown in Fig 3; the pressure tapping modification is shown in Fig 4. The abrupt step between high and low discharge coefficient was uncanny and could not be explained. With insufficient time to explore an idea that was unlikely to provide a solution, the modification design was abandoned. Next, it was thought best to decrease the diameter of the pressure tapping at the Venturi internal surface; the region in contact with the flowing gas.

Whilst new pressure tapping modification parts were fabricated, the time was spent investigating acoustic effects within the tapping chambers and impulse lines. It was thought that the acoustic study might provide an insight into the problem. An industrial silencer was fitted at various locations within the throat pressure tapping impulse line, but without changing the high discharge coefficient. Fluidborne noise was also investigated using two piezo-electric pressure transducers fitted at connections normally used for pressure measurement. One of the connections was located close to the throat of the Venturi and the other at the differential pressure sensor. Fig 5 shows pressure ratio plotted against frequency for a throat tapping test performed at 20 bar with a volume flowrate of 600 m³/hr [pressure ratio defined as throat versus sensor pressure]. Large differences resulted between the noise seen at opposite ends of the impulse line. This was due primarily to standing wave effects in the sensing line but it showed that large variations also existed at frequencies as low as 30 Hz. The conclusion from

this work was that a more thorough investigation of the underlying causes was required, which could not be performed at this time.

3.4 Third Phase

Pressure tapping inserts were installed that essentially decreased the diameter of the pressure tapping at the Venturi internal wall surface from 6 mm diameter to both 3 and 4 mm. This configuration was similar to that of the research Venturi which had a 4 mm diameter. The initial tests produced discharge coefficient values ranging from 0.97 - 0.91. This was less than unity but something was obviously wrong. It was thought that during the fitting of these pressure tapping inserts there was a risk that the ends of the inserts were located beyond the internal Venturi wall surface; sticking into the flowing gas stream. On inspection, it was estimated that the throat insert did extend into the Venturi area by 0.5 mm. This further illustrated the extreme sensitivity of the Venturi pressure tapping.

Further modification was made to the pressure tapping inserts in order to ensure that they did not protrude into the Venturi throat area. These new inserts were assembled and inspected prior to pressurisation. The results of these tests are shown in Fig 6, with the corresponding pressure tapping modification shown in Fig 7. It can clearly be seen that real values of low discharge coefficient, with minimal scatter resulted, similar to that obtained for the research Venturi. It was therefore, sensible to conclude that these pressure tapping inserts did not protrude into the Venturi throat area. This was the target that was set at the beginning of the investigation. The problem remained that the effect caused by the Venturi tapping insert was not fully understood and the investigation had demonstrated extreme sensitivity of Venturi pressure tapping alterations. It was concluded that the use of inserts could provide a solution, but that it was not practical to extend the idea to the full metering system.

It was known from the investigation to date that the performance of the Venturi had been repeatable. Shell instructed NEL to establish the repeatability and reproducibility for the project Venturi and the best way in which the data could be presented. Fig 8, a chart of discharge coefficient against pipe Reynolds number, depicts the data collected. A degree of scatter of the order 1.5 per cent existed when the data was represented by Reynolds number, as shown in Fig 8, with no relationship apparent. When the same data was plotted against volumetric flowrate, as shown in Fig 9, the data aligned to produce a trend proportional to volumetric flowrate (or line or throat gas velocity) and independent of line pressure, with scatter less than 0.5 per cent. This relationship could be described mathematically meaning the Venturi, despite having high values of discharge coefficient, could be used in a repeatable manner.

A large quantity of data had been collected for the project Venturi and this was plotted against volumetric flowrate on one chart and is shown in Fig 10. It can clearly be seen that the trend described above existed for the full data set. The shape of the relationship, with a cusp at a volume flowrate of approximately 400 m³/hr [or throat velocity of 50 m/s], cannot be explained at this time. For completeness, Fig 11 shows the same full data set for the project Venturi plotted against pipe Reynolds number. No apparent relationship exists.

It was decided at this point that the Venturi flowmeter could be reliably calibrated, with a method available for describing performance, for use as intended offshore. Each Venturi was calibrated over the full range and a curve fit produced which would ultimately be used in the

field. Fig 12 shows the data collected for the project Venturi with the curve fit, made up of two parts as explained later in the paper, superimposed.

3.5 CFD work

Shell Expro had commissioned NEL to carry out some computational fluid dynamics (CFD) work on Venturi meters. The main objective of this work was to investigate the sensitivity of the discharge coefficient of a Venturi to variations in its critical dimensions and surface roughness. If this sensitivity was small and predictable, then it should be possible to define the accuracy of a Venturi meter from its manufacturing tolerances, and eliminate the need to calibrate Venturi meters empirically.

Interesting results that were difficult to interpret were being obtained from this project just before the high discharge coefficients were discovered. From the computations of flow through a Venturi, profiles (e.g. velocity, pressure, turbulence etc.) were obtained. Spikes were observed in all the profiles close to the pipe wall along the length of the Venturi. These spikes occurred at the intersections of the Venturi sections; in particular at the intersection of the conical convergent and the throat and at the intersection of the throat and the conical divergent sections. These spiky profiles do not just occur along the pipe wall but persist into the flow and decay with distance from the pipe wall; at the centreline all profiles are smooth and there are no spikes. Even when the radius of curvature at these intersections was increased to 15 mm, the maximum permitted by ISO 5167-1, the spikes were still present. The most interesting of these profiles is the static pressure profile at the wall (Fig 13) where, for a Venturi with diameter ratio 0.4, the static pressure at the intersection of the convergent and the throat sections is 41% lower than that at the throat tapping position (centre of the throat section). At 0.25d upstream of the throat tapping position the static pressure has decreased by only 1.2%; this indicates that the positioning of the throat tapping is not critical.

Fig 14 shows the results of a computation for a Venturi of diameter ratio 0.4. It gives turbulent kinetic energy which relates to the fluctuation velocity in the flow. As the flow enters the throat section the turbulence in the centre of the pipe increases to forty times that which would be expected in fully developed flow; the turbulence at the throat tapping is also at a similar level. It indicates that the throat region is one of intense disturbance; it may not be the best place to try to make sensitive measurements.

Rough pipe computations were performed for Venturi meters with a pipe diameter of 0.154 m, Reynolds number of 2×10^7 and a diameter ratio of 0.75. The surface finish of the Venturi in some cases has a significant influence on the discharge coefficient. Certainly a very rough Venturi (roughness criterion, $R_a = 25 \mu\text{m}$) can cause a negative shift in discharge coefficient of the order of 1% compared to that of a smooth Venturi. For a surface finish close to the maximum permissible in ISO 5167-1 ($R_a = 0.8 \mu\text{m}$ for the entrance, the convergent and the throat sections and $3.2 \mu\text{m}$ elsewhere) the computed change in discharge coefficient from that computed for a smooth Venturi was -0.2%. It is clear from these results that pipe roughness effects cannot account for the high discharge coefficients observed in the experimental tests.

4 THE SOLUTION

From the foregoing, once it was clear that the discharge coefficient was a repeatable function of line or throat velocity, and was independent of line pressure, a solution to Shell Expro's immediate problem was available that would not involve modifying the Venturis. Although it is possible to consider tuning the discharge coefficient by inserting inserts into the tapping chambers, Shell Expro considered that this was not practical, as accurate positioning of such inserts would be critical.

The solution chosen was to calibrate the Venturis on high pressure gas at a number of flowrates and find best fit relations between discharge coefficient and flowrate for each Venturi meter. In practice, this was not simple. For some of the meters it was not possible to find a single equation to fit the data. This is best illustrated by the meter on which most of the test data was gathered, shown in Fig 12. At about the flowrate at which the Venturi began to whistle, there appears to be a cusp in the relation between discharge coefficient and flowrate. We decided to fit two curves, one covering the low flowrates and the other the high flowrates. This was also done for some of the other meters.

To enter the data into the stream flow computers, a selection of points from the fitted curves was made and their co-ordinates entered. The flow computer then made an iterative straight line interpolation between the entered points to determine the discharge coefficient and corresponding flowrate from the measured differential pressure.

Recall that the flowline meters could be checked against the test separator meters. In the original scheme of things, Shell Expro did not want to compare the flowline meters with a meter working on a different principle, so a Venturi meter was also installed on the test separator outlet. When the Venturis were shown to be meters whose performance depended on an empirical calibration, it was considered prudent to install a different type of meter on the test separator. The choice was between a multipath ultrasonic meter and an orifice meter. The ultrasonic meter was chosen. It was only slightly more expensive, as an orifice meter would have meant increasing the line diameter. The ultrasonic meter offered greater tolerance to liquid carry over, better diagnostic capability and expected lower maintenance.

5 DISCUSSION

As can be seen from the foregoing, the image that has been building up of a Venturi meter as a simple, robust and highly accurate device is somewhat tarnished. Venturis have become attractive as metering devices because it is reasonable to install them with minimal straight length requirements close to wellheads where they will encounter multiphase fluids, sand, and debris. They are being used as an essential component of some multiphase flowmeters. We can reasonably expect them not to be damaged by these in the way an orifice plate would be. The availability of high precision DP sensors mean that a turndown in flow of close to 10 to 1 is realistic with good accuracy. We had hoped that over a few years experience would show that we could predict the discharge coefficient of a Venturi quite accurately from its dimensions and the manufacturing tolerances. It is evident that this is no longer possible: out of seven nominally identical Venturis we have had a range of discharge coefficients up to 4 per cent high and with a spread of about 3 per cent.

We also showed that by modifying the tapping chambers we could shift the discharge coefficient by ± 10 per cent. Although the modifications that resulted in these shifts were fairly extreme (i.e. tapping chambers almost completely filled leading to + 10 per cent, and protrusions into the throat leading to -10 per cent) it is not unrealistic to expect build up of deposits in the tapping chamber, or round the tapping point into the throat, leading to shifts of 1 per cent or so.

The whole issue of acoustics in the tapping chamber and impulse lines has not been investigated in any detail. We were thankful enough that for our application we had an empirical solution that allowed us to achieve our accuracy requirements without too much modification of the system.

In practice, Venturis for applications such as ours will be sized with low values of β , essentially to give good metering capability over as long a period as possible without changing out the Venturis. This means that with line velocities of 15 m/s, throat velocity is about 90 m/s or 300 km/hr! We have also shown that the throat is an area of extreme turbulence and not the best conditions in which to try to make sensitive and accurate measurements.

Notwithstanding the above, the Venturi is still a very practical device if its limitations are borne in mind. It is not the highly accurate dream solution we had been looking for, but it does offer reasonable accuracy. Indeed if one simply looks at the spread of our data per Venturi, they fall within a 2 per cent range, which is what ISO 5167-1 permits. However, it cannot be used on high pressure gas without calibration.

As Venturis are of interest to several operators, it is worthwhile investigating Venturi performance further on a Joint Industry basis. However the first steps should be to carry out a thorough literature study to find out what really was known about Venturis before they slipped into obscurity.

6 CONCLUSIONS

Venturi meters designed and manufactured to ISO 5167-1 and calibrated on high pressure gas at high Reynolds Numbers show discharge coefficients several percentage points higher than predicted. The project Venturi, the one on which the majority of tests were performed, was shown to produce repeatable and reproducible results independent of line pressure, which could be described mathematically. The other Venturis followed the same pattern. The discharge coefficient is best represented as a function of throat or line velocity (or volumetric flowrate). The relationship between discharge coefficient and throat velocity resulted in a cusp at about 50 m/s which could not be explained.

Both research and project Venturis were sensitive to modification to the pressure tappings. The discharge coefficient is particularly sensitive to changes in the tapping chamber volume (+ 10 per cent) and on small tapping protrusions into the flowing gas stream (- 10 per cent).

When attempting to duplicate the pressure tapping configuration of the research Venturi on the project Venturi, it was possible to reduce the discharge coefficient to near unity. Although this was the investigation aim, the problem remained that the effects caused by Venturi tapping

inserts were not fully understood. It was concluded that it was not practical to extend the idea to the offshore metering system.

Preliminary investigations demonstrated that there were intense acoustic effects in the pressure tapping chambers. Evidently, further study is required to quantify this effect.

Venturi meters are not simple, predictable devices with inherent high accuracy when used on high pressure gas. Further research will be required to establish clearly their limitations and applicability for the future. It is likely that the optimum way forward is with a Joint Industry programme, as Venturi flowmeters are of interest to several operators.

REFERENCES

- 1 DICKINSON, P.F., and JAMIESON, A.W. High accuracy wet gas metering. North Sea Flow Metering Workshop, Bergen, Norway. Oct 1993.
- 2 MURDOCK, J.W. Two phase flow measurement with orifices. Journal of Basic Engineering. Dec 1962.
- 3 CHISHOLM, D. Flow of incompressible two-phase mixtures through sharp edge orifices. Journal of Mechanical Engineering Science. Vol 9, No 1, 1967.
- 4 CHISHOLM, D. Two phase flow through sharp edge orifices. Research Note for Journal of Mechanical Engineering Science. I. Mech.E, 1977.
- 5 INTERNATIONAL ORGANIZATION FOR STANDARDIZATION. Measurement of fluid flow by means of orifice plates, nozzles and Venturi tubes inserted in circular cross-section conduits running full. ISO 5167-1, Geneva: International Organization for Standardization, 1991.

FIGURES

- 1 Calibration of research Venturi with single pressure tappings
- 2 Calibration of research Venturi with plugs in redundant throat tappings and discs in used tappings
- 3 Calibration of project Venturi with 1mm hole discs and metal tube
- 4 Drilled disc located in major pressure tapping chamber of project Venturi
- 5 Pressure ratio between throat and sensor ($600\text{m}^3/\text{hr}$, 20 bar)
- 6 Calibration of project Venturi with modified 4mm neck inserts
- 7 Plugs reducing the 6mm pressure tapping bore to 4mm

- 8 Calibration of project Venturi to assess repeatability and reproducibility
- 9 Calibration of project Venturi with volumetric flowrate
- 10 Calibration of project Venturi with volumetric flowrate
- 11 Calibration of project Venturi with pipe Reynolds number
- 12 Calibration of project Venturi with curve fits
- 13 Profile of static pressure along the length of the Venturi
- 14 Contours of turbulence in the throat region of the Venturi.

Fig. 1 Calibration of research Venturi with single pressure tapplings

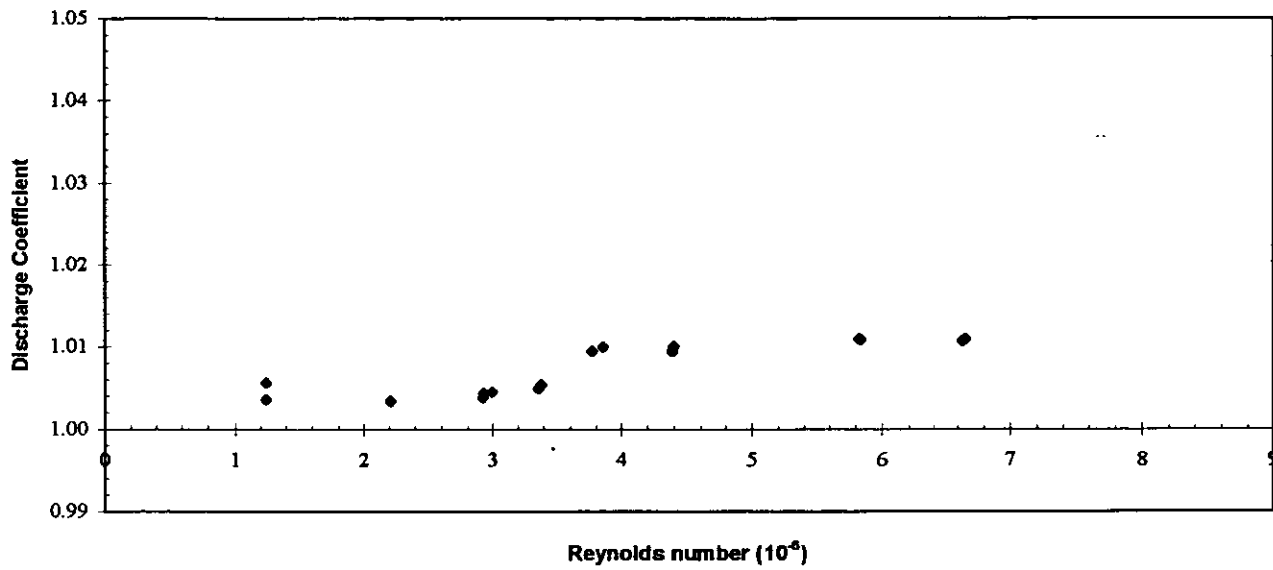


Fig. 2 Calibration of research Venturi with plugs in redundant throat tapplings and discs in used tapplings

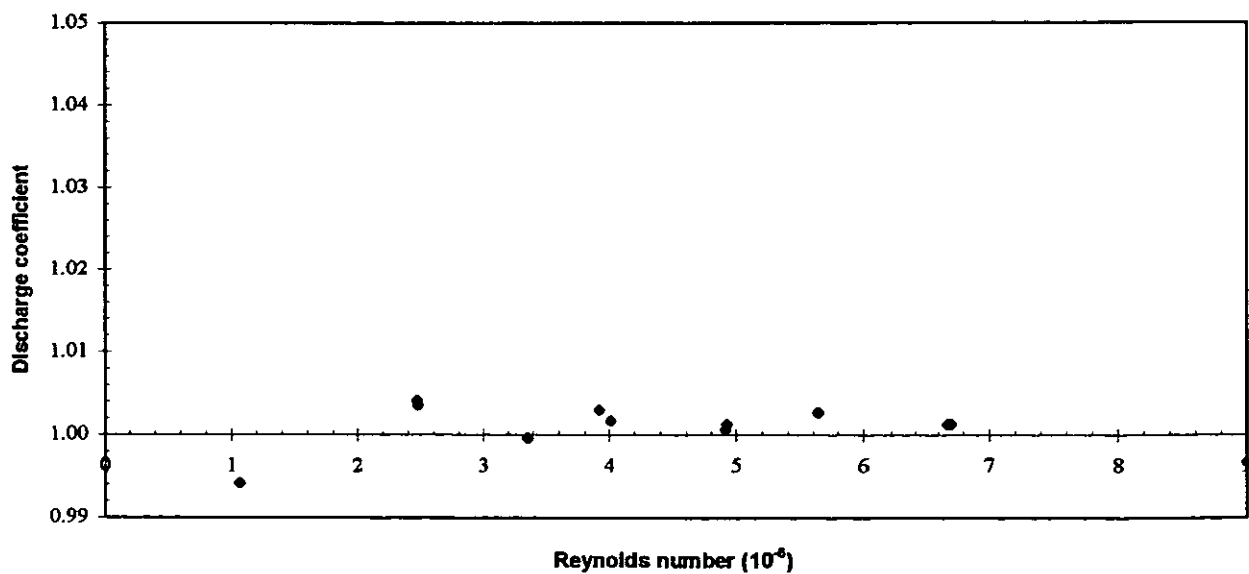


Fig. 3 Calibration of project Venturi with 1mm hole discs and metal tube

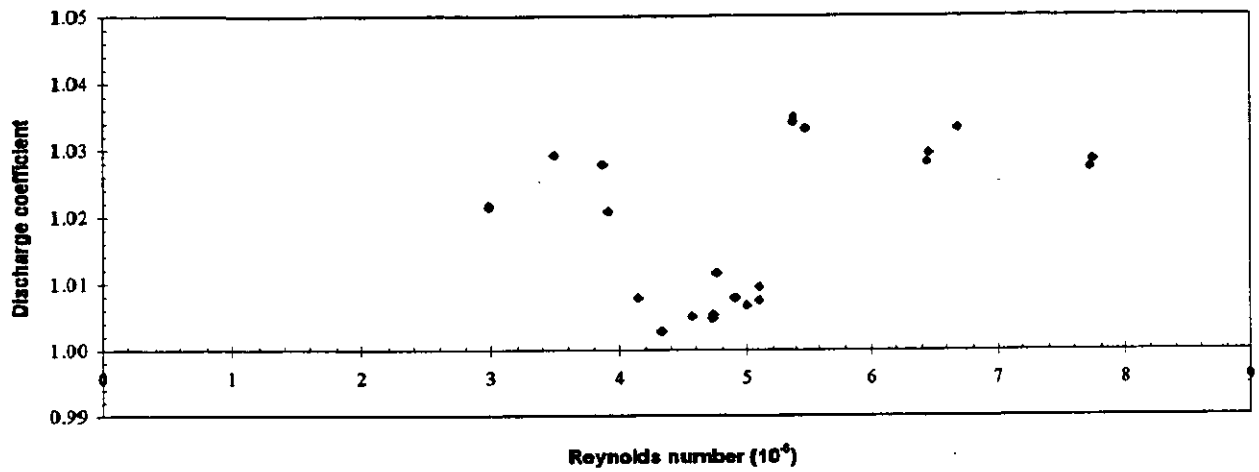
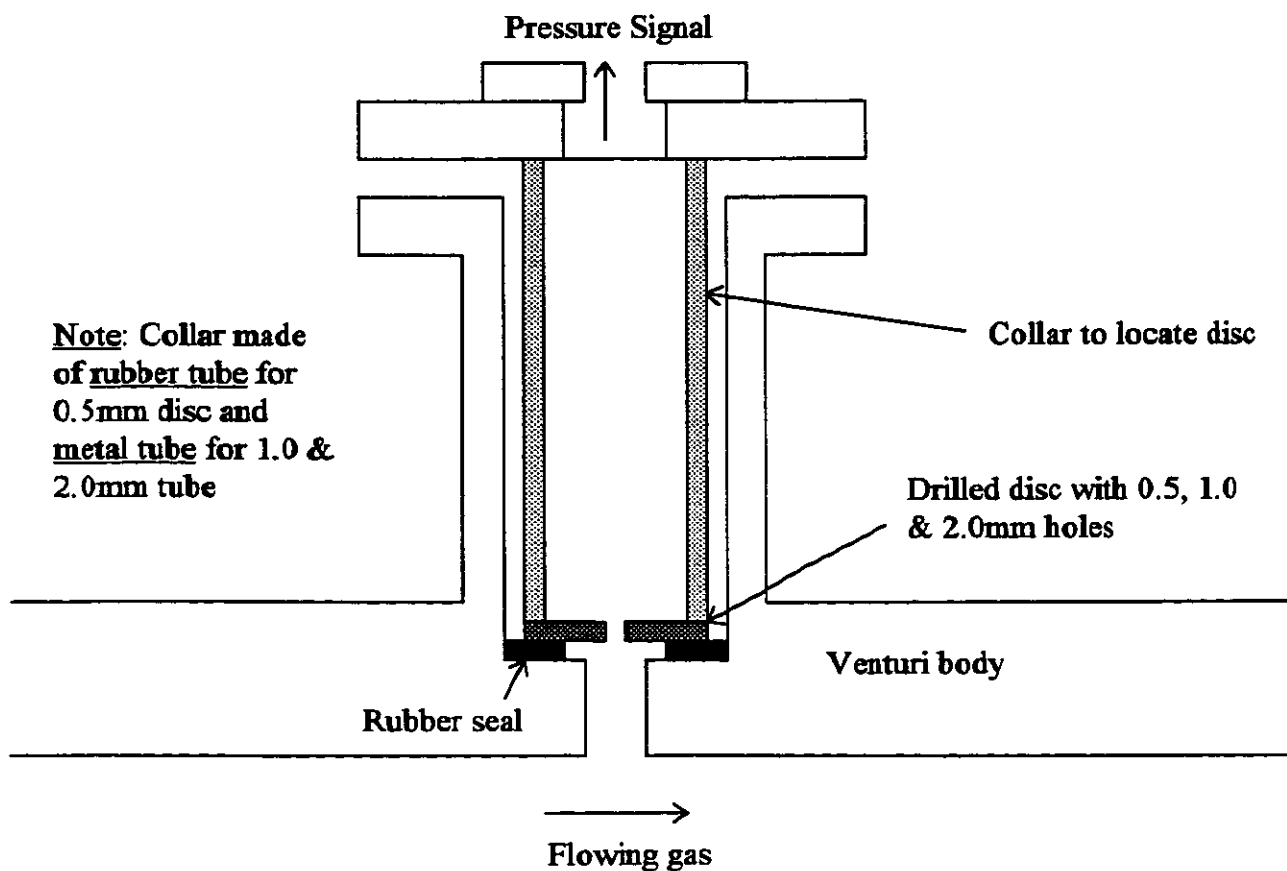
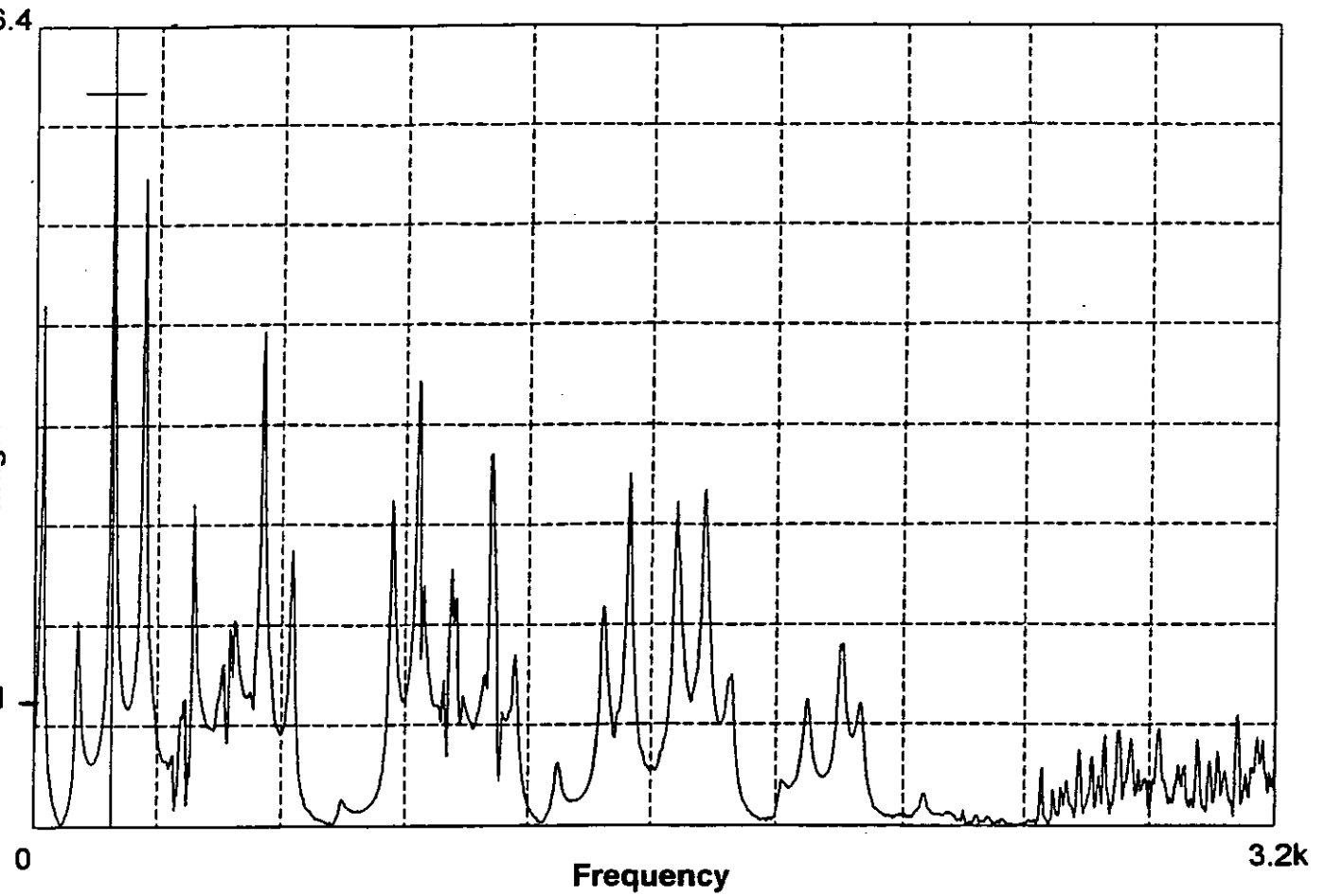


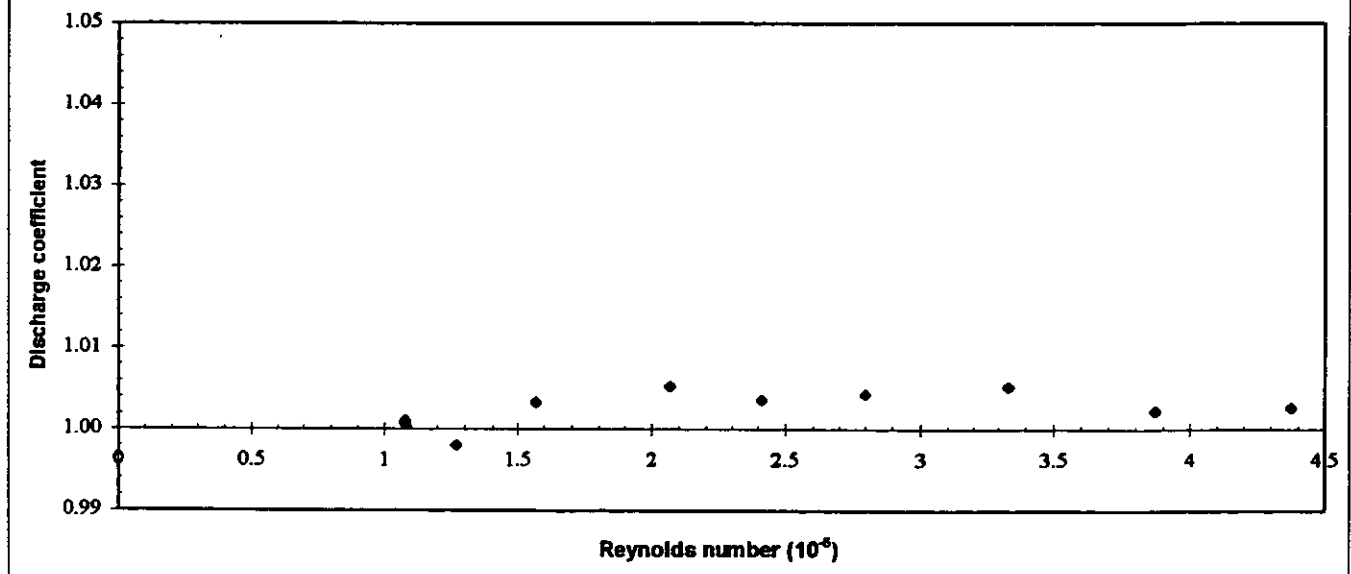
Fig. 4 Drilled disc located in major pressure tapping chamber of project Venturi

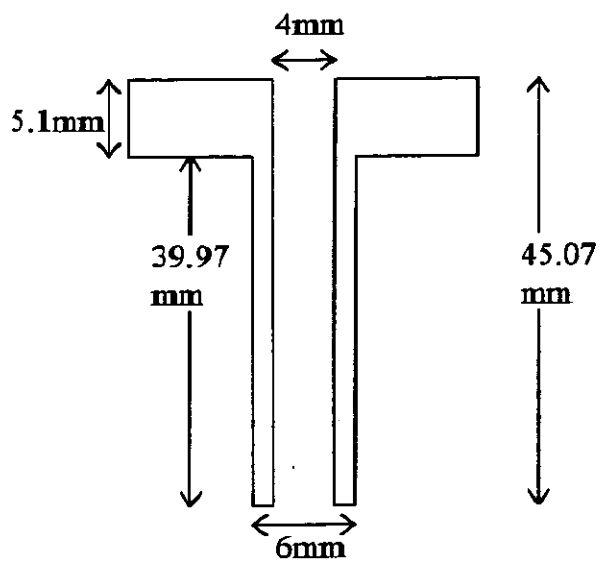


**Fig. 5 Pressure ratio between throat and sensor
(600m³/hr, 20 bar)**

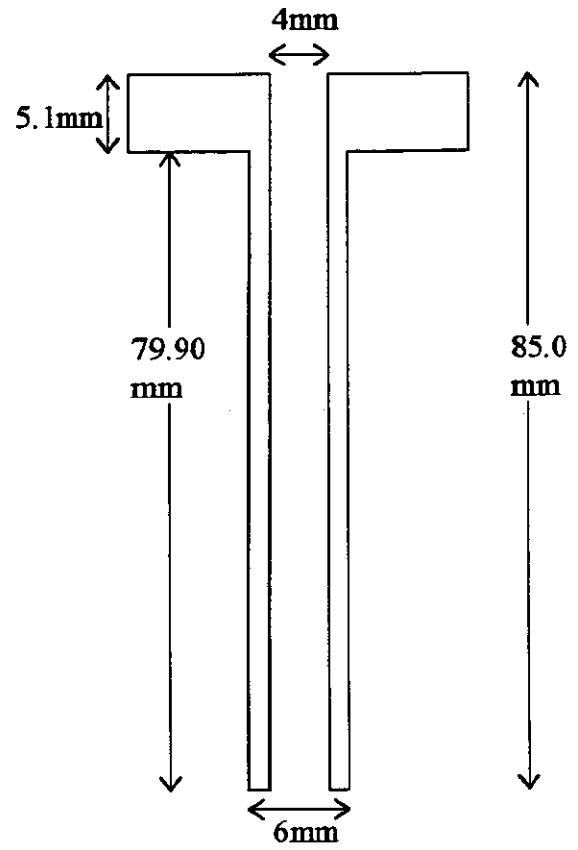


**Fig. 6 Calibration of project Venturi with modified 4mm
neck inserts**





UPSTREAM



DOWNSTREAM

GENERAL INFORMATION

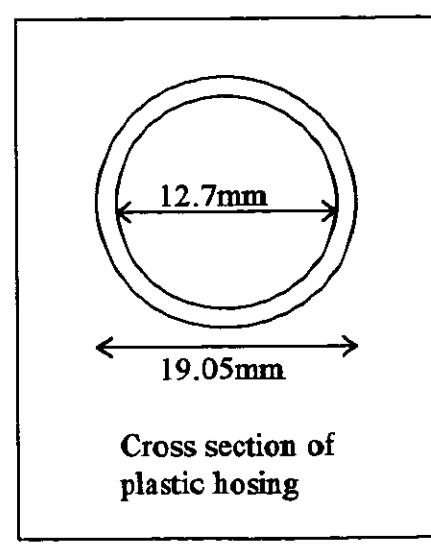
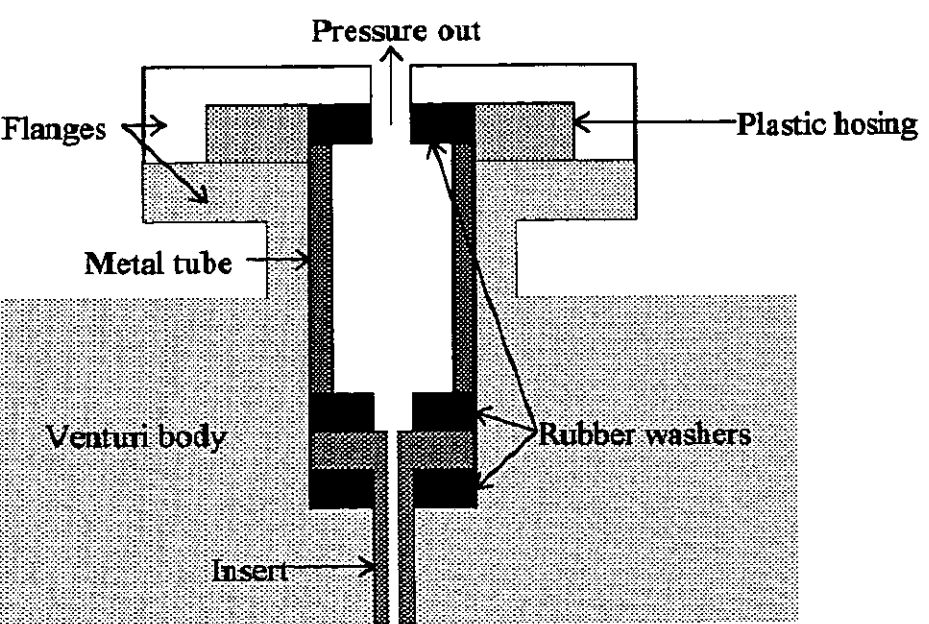


Fig. 7 Inserts reducing the 6mm pressure tapping bore to 4mm

Fig. 8 Calibration of project Venturi to assess repeatability and reproducibility

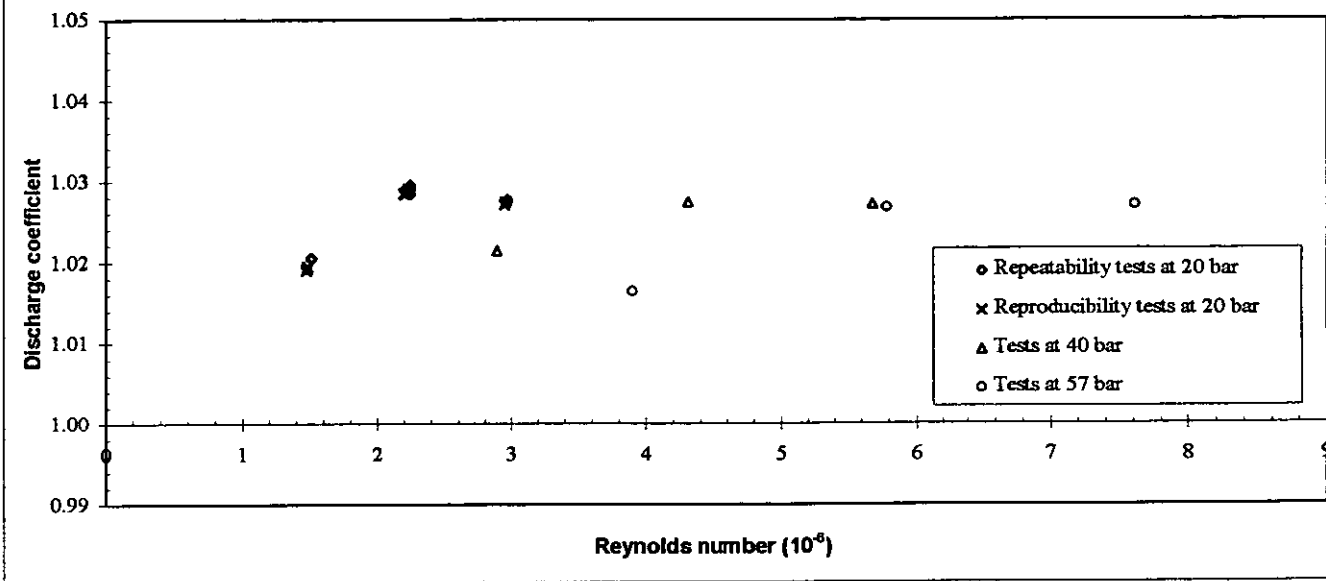


Fig. 9 Calibration of project Venturi with volumetric flowrate

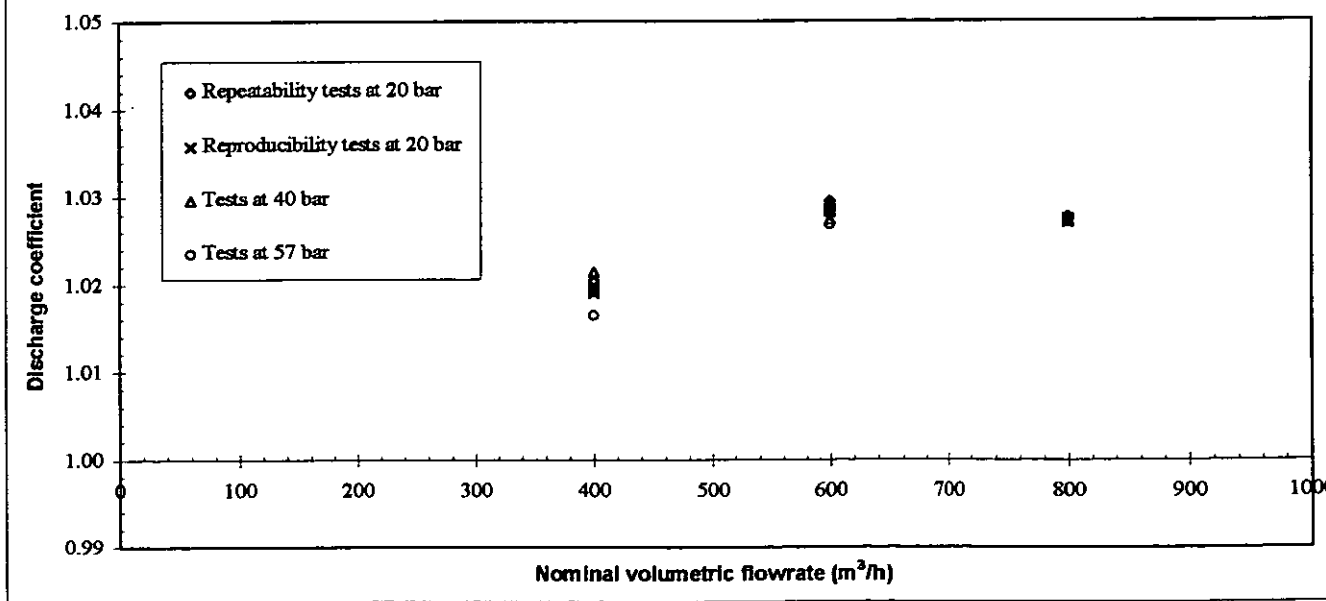


Fig. 10 Calibration of project Venturi with volumetric flowrate

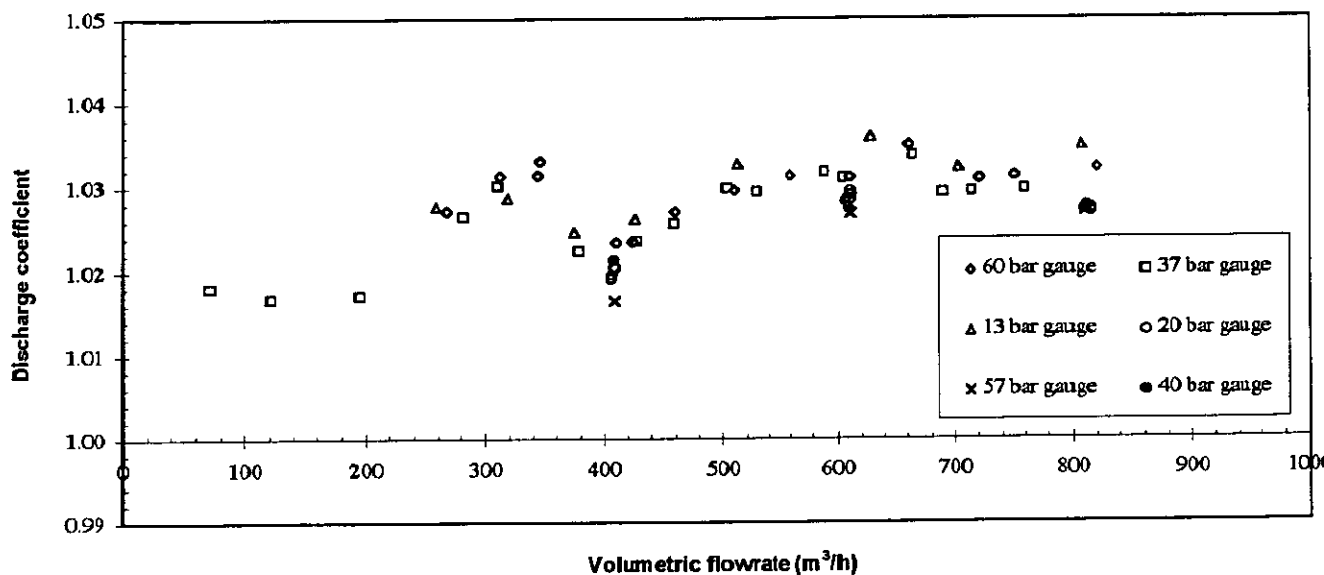


Fig. 11 Calibration of project Venturi with pipe Reynolds number

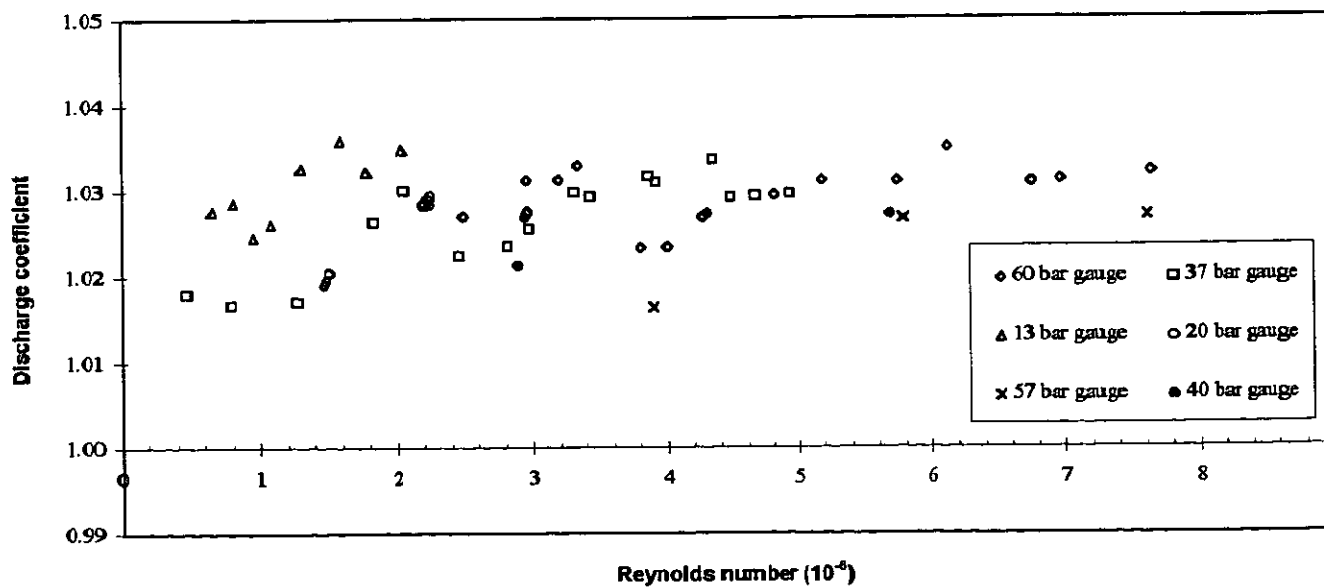


Fig.12 Calibration of project Venturi with curve fits

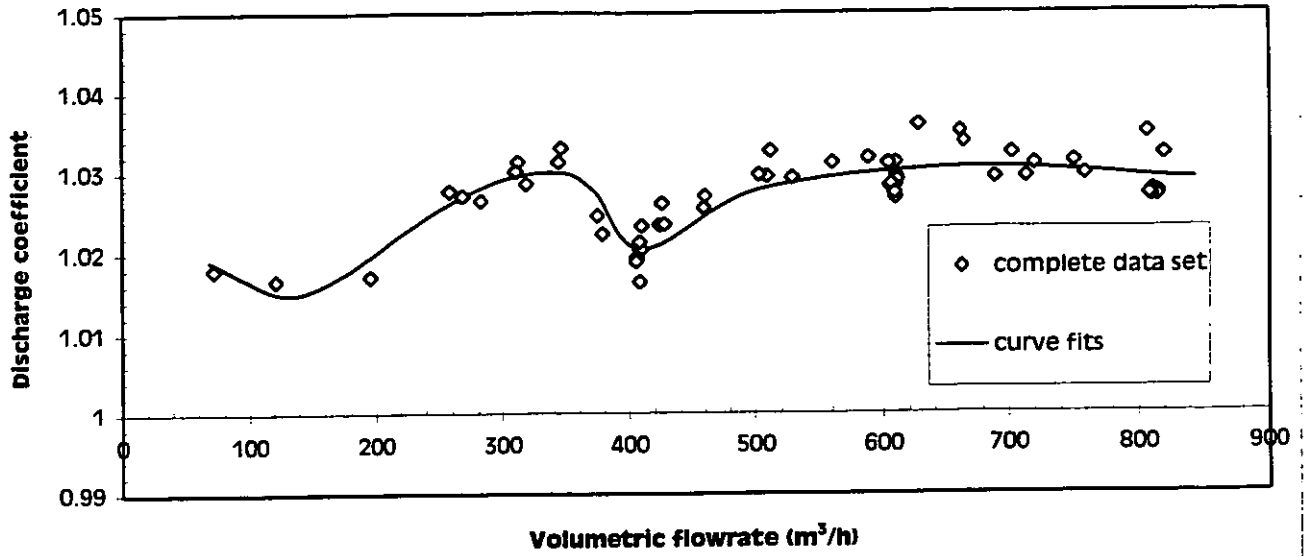
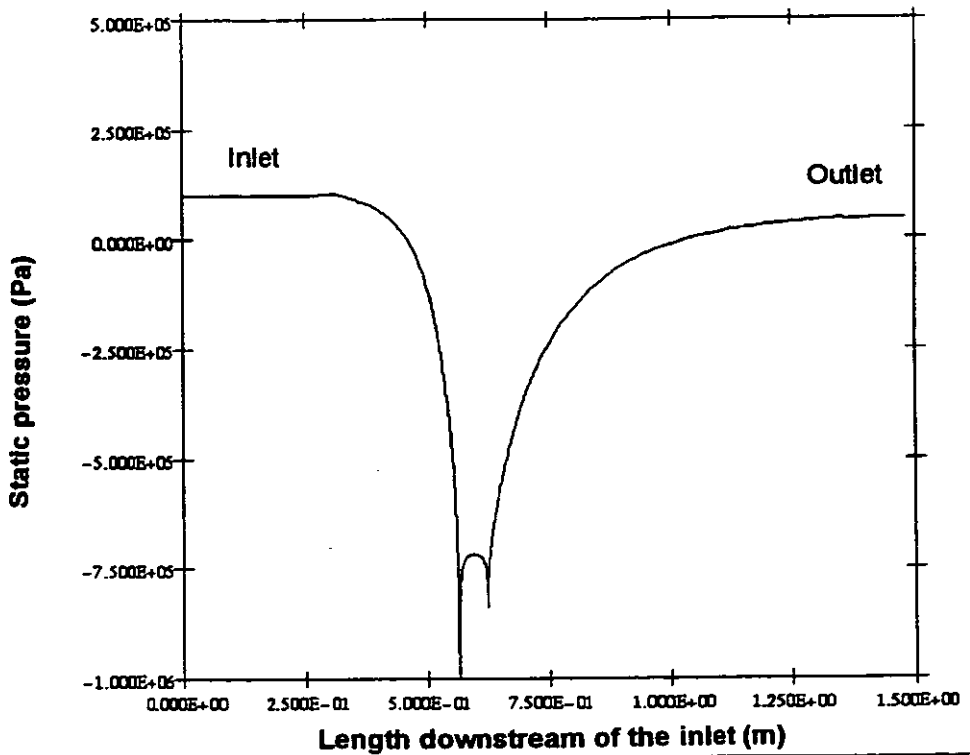


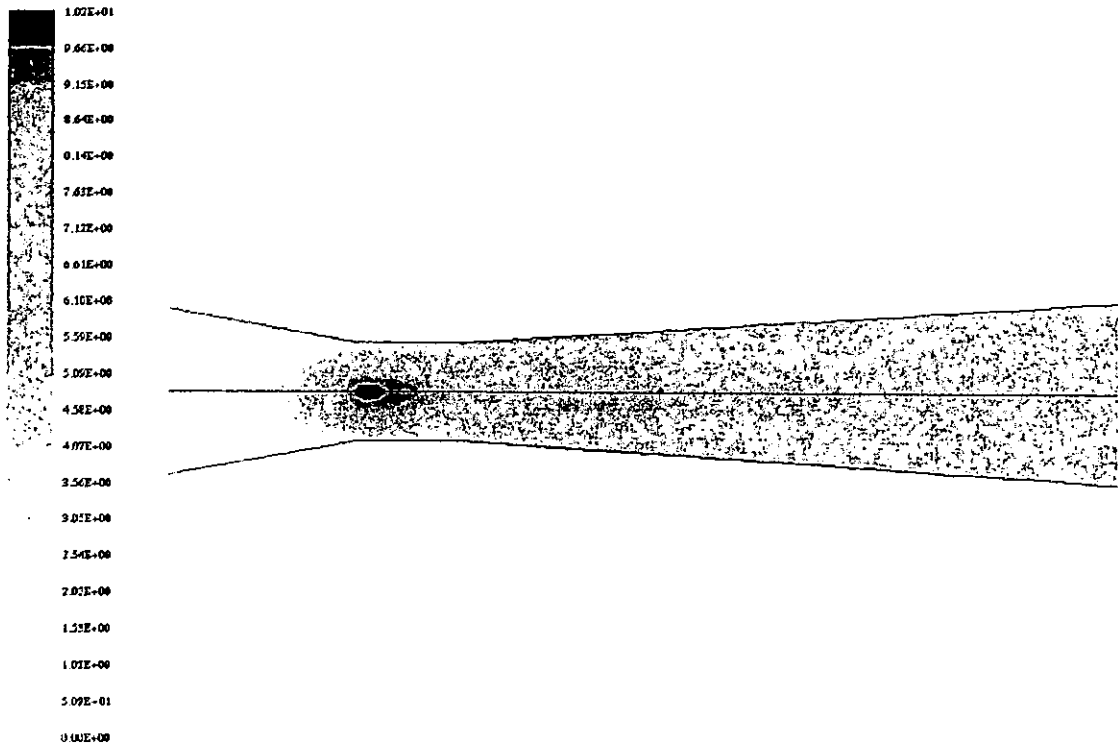
Fig. 13 Profile of static pressure along the length of the Venturi



NEL: Computation of Flow Through a Venturi Meter
 Static Pressure Profile at the Wall
 Beta=0.4, ReD=1E6, D=0.154, U_mean=6.5m/s, Radius=5mm

Sep 12 1996
 Fluent 4.31
 Fluent Inc.

Fig. 14 Contours of turbulence in the throat region of the Venturi



NEL: Computation of Flow Through a Venturi Meter

Key: Kinetic Energy of Turbulence (m^2/s^2)

Beta=0.4, ReD=1E6, D=0.154m, U_mean=6.5m/s, Radius=5mm

Sep 12 1996

Fluent 4.31

Fluent Inc.

SAMPLING 3-PHASE FLUIDS (GAS, HYDROCARBON LIQUID, AND WATER) FOR QUALITY DETERMINATION

Thomas F. Welker
Welker Engineering Company
P. O. Box 138
Sugar Land, Texas 77487

The proper sampling of a 3-phase stream, like measurement, is decidedly more difficult than most engineers and operations people think. In order for this important step in the measurement process to be accomplished properly, the rules of sampling must be followed to the letter.

In order to know what is coming from a produced well, the oil industry is developing the technology to measure 3-phase flow.

To enhance this 3-phase meter, a sampling system has been developed to accurately sample 3-phase flowing streams.

Much study has been involved in the operation of sampling condensate in the Gulf of Mexico, as well as LP and gasoline streams. Both LPG and condensate are streams that have light ends, light liquid hydrocarbons, and water.

The systems that were developed for LPG, gasoline, and condensate years ago were not truly designed to collect a true, representative sample of the total stream. At that time, the systems were looking for hydrocarbons only. Now, however, the importance of the sample being representative of the total stream cannot be overstated.

The total stream includes gas, both hydrocarbon and inert gases, liquid hydrocarbons, and water and particulates. The gas portion of the stream will be gas phase and gas in solution. Considering the ramifications of the sample and its' composition on payment and balance, this mixture of products must be homogeneous at the sample point.

The first consideration is where to take the sample in the line. In order for a sample to be drawn that is representative and repeatable, the line must have enough turbulence to ensure homogeneity of all the products and contaminants. The droplet size should be small enough to allow this uniform mixture to be evenly distributed across the full face of the line.

Since existing facilities are not designed specifically to sample multi-phase streams, the following is an outline of the minimum requirements to perform this task:

1. The system must be equipped with a back pressure control valve that will ensure the multi-phases will be as close to a single phase as possible. This, of course, is as important for measurement as it is for an accurate sample.
2. The line must be conditioned. The proper conditioning of the line may not be done with pumps, strainers, meters, piping, manifolds, or velocity. Velocity alone, or simply changing direction from horizontal to vertical, cannot be expected to cause the proper conditioning of the line at the sample point. As the liquids are moving through a line around an elbow or through a tee, a swirling action or "barber pole" effect might be expected. This centrifugal action will spin the heavier contaminants or components in the line to the outer walls of the lines. The product at the sample point must be a homogeneous mixture. A static mixer specifically designed for your product and flowing conditions is a requirement.

What is proper line conditioning? Proper dispersion and distribution of all the components across the face of the line is the only criteria of adequate mixing in the line. This is small droplets evenly distributed. Small droplets must be described as a droplet that may be captured in a sampling device and pumped from the line to become part of the captured sample (composite). The droplets of the contaminants may not be expected to turn a corner and move out an opening or probe as easily as the general products in the stream.

Laminar or stratified flow: This may be single, double, or even triple layer flow, with the lighter on the top and the heavier on the bottom. This laminar flow is to be expected at flow rates below 4 to 6 feet per second, but may occur even at elevated rates above 6 to 8 feet per second. Velocity, along with elevated Reynolds numbers, will not create adequate dispersion and distribution for sampling.

Dynamic versus Static Mixing:

Dynamic mixing occurs in a line when some type of mechanical device is inserted into the line, or a portion of the stream is drawn out of the line, conditioned, and pumped back into the line through some arrangement of nozzles. There are numerous dynamic styles of mixers available for consideration. Whether or not they are going to create adequate mixing upstream of the sample point is the question the user must ask. Can this stream be proven? Does the streamlining effect of higher velocity have an adverse affect on the dynamic mixing system? This should be properly addressed.

Static mixing is done by building a pressure drop into the pipeline upstream of the sample point (2-4D, no more). A static mixer should be designed to create the dispersion and distribution desired without creating excessive pressure drop. The properly designed static mixer will do this over ranges from 1.5 feet per second and above. If very low flow rates are expected, this information must be passed on to the supplier.

The sampler spool will have the mixer installed with the sample point two pipe diameters downstream of the mixer. The sampler will be installed in a horizontal plane, so the products will flow down and out to the sample container.

3. The sample pump must be designed specifically for the purpose of "grabbing" the sample and pumping that sample from the line regardless of flowing conditions (pressure or temperature) or product properties (viscosity, particulate content, or vapor pressure).

The isokinetic sample probe is designed specifically to trap a sample from the flowing stream and pump that sample into the container.

The sample pump must be designed in a way that will not inhibit the mixed sample from moving freely into the sample head; i.e., inlet check valve. The inlet check valve will cause the mixed sample to separate and the sample pump will vapor lock.

The inlet to the sample collection head should be large enough to inhibit the diversion of sample droplets. The sample head should be self-purging between strokes.

The sampling device must be designed to allow the passage of sand, dirt, pipe debris, or filings that may be in the flowing stream. The sampler must be designed to pump the water and sediment by the check valves, regardless of wax content, viscosity, or pressures.

Since the sample container is normally going to have pressure higher than pipeline pressure on the piston above the product, the sampler must work independently of any associated conditions.

The sampler should be designed to pump all of the trapped sample into the container. Any product retained in the collection head because of clearances from pistons or inlet check valves will most certainly be heavier contaminants, such as water in natural gasoline, debris, or wax.

TIMING OF THE SYSTEM

The multi-phase sampling system, as with all liquid sampling systems, must be actuated proportional to the flowing stream. In order for the components in the sample container to be related to a specific volume of total products moving through the pipeline, the sampling system must be interfaced with the flow.

SAMPLE CONTAINER

There are two types of sample containers in use today.

1. Standard open or atmospheric type container.

This container is equipped with gas pressure or Nitrogen to maintain a pressure head on the product pumped into that container.

The container is equipped with a circulating pump and piping to mix the sample after the composite is collected and ready for conditioning.

It is incorrect to assume that the gas blanket on top of the sample in a sample container will keep the light ends in the liquid phase. Each gas component will seek its own vapor pressure in the head space, allowing the sample to change, which will ultimately change the density and/or API gravity.

2. Constant Pressure Product Container.

The newest method of storing the collected sample is to employ a container that has a sliding piston. The use of the constant pressure sample container allows the sample to be stored and mixed without changing phase.

To retain a collected sample in the same phase as it is in the pipeline, the light ends must be kept as part of the sample. If the light ends are retained, the API gravity and specific gravity will not change.

To use the Constant Pressure Product Container (CPPC) as the sample container, the sampler will be required to capture the sample and pump that collected bite through the tubing and into the cylinder. The cylinder has a precharge gas on the back side of the piston to keep the sample in a single phase. The precharge gas is 50 to 100 psi above the pipeline pressure.

To mix the contents of the CPPC, the valves are opened and the sample is pushed into the mixing piping. The piston will move as the product flows into the mixing piping, keeping the product in a single phase. The mixing manifold includes a circulation pump that is turned on and the sample is circulated through the mixing system.

The sample mixing time is of the utmost importance. The mixing time should be determined for each type of crude or product that is expected, as required by API Chapters 8 and 10.

In order for the sample to be accurately analyzed, it must be kept in the same phase during collection and storage as in the pipeline.

The sample must be collected, stored, and transported in containers specifically designed for this function.

The transportable Constant Pressure (CP) sample container that is used must be capable of the phase control and must have the mixing capability to re-mix the contents of the container to a completely homogeneous mixture, and be D.O.T. Approved.

With gas, water, and hydrocarbon mixtures, the continued mixing of the contents during sample transfer from stationary container to transportation container or container into analytical devices or glassware cannot be stressed enough. These techniques are covered in the latter pages of this paper.

SAMPLE DRAW FROM STATIONARY CONSTANT PRESSURE SAMPLE CONTAINER INTO TRANSPORTABLE CONSTANT PRESSURE CYLINDER FOR RVP & LIGHT END RETENTION

The purpose of the sampling system is to collect a composite sample of a parcel moving through a pipeline or into a truck, tank car, barge, or ship.

Most samples today are taken to ensure product quality. This includes API gravity determination and a chromatographic analysis. The chromatograph will characterize the components from the lights (Butanes) to the heaviest component (1,2,4 - Trimethylbenzene). The only sampling method that can guarantee the accuracy of this analysis is the constant pressure cylinder method.

The sample pump takes the bite of sample and pumps that sample into the constant pressure cylinder for storage. At the end of the parcel or delivery, the composite sample that has been collected in the cylinder must be mixed and transferred to appropriate containers for transportation to a lab for analysis and retention.

The steps for sample transfer are:

If the sample container is equipped with a mixer, attach the mixing handle to the mixing rod and move the mixer through the product 3 to 5 times smartly (not violently). This will ensure the collected sample is homogeneous prior to the transfer. **NOTE:** If water and particulates are contaminants, the mixing is much more important. Mixing must be continued during purge and transferred to a transportation cylinder.

For the API gravity and further analysis on the sample, a transportable constant pressure cylinder should be used.

Proper handling is required for accurate results.

PRODUCTION EVALUATION AND TESTING OF A HIGH VISCOSITY AND HIGH GAS VOLUME FRACTION MULTIPHASE METER.

Bernie Tuss, Conoco, Inc. (Retired)

Abstract

Tests were conducted during November, 1995 on the Agar Corporation Inc. MPFM by Conoco, Inc. and Amoco Corporation at the Conoco Multiphase Test Facility near Lafayette, Louisiana, to determine the performance of this novel high gas volume fraction (GVF) multiphase meter. Tests conducted previously on the this high gas volume fraction meter utilized the standard AGAR MPFM for high viscosity, low gravity multiphase well test measurement. These tests were conducted by Conoco and Maraven (Petrozuata) at the San Diego Norte Pilot Plant near Zuata in the Orinoco Oil Belt of Venezuela and were reported in a paper presented by Intervep, Conoco, and Maraven at "Multiphase 95" in Cannes, France in June of 1995.

Subsequent application and testing was performed by BITOR/JVCO at Camp Morichal, Venezuela during the early part of 1996 on heavy Orinoco Bitumen production. Initial results of that test were presented at the IPC Conference in Calgary, Canada, in July, 1996, Paper No. 629 entitled "Field Tests of a High Viscosity Multiphase Meter".

This paper describes how this multiphase meter works, summarizes the results of the field tests (performance and accuracy), and discusses the application of the meter. The high gas volume fraction meter (MPFM-400 Series) utilizes a patented Fluidic Flow Diverter (FFD™) to divert most of the free gas in a multiphase stream around an MPFM-300 multiphase meter and into an ancillary gas measurement loop. The gas flow rate in the bypass loop is metered accurately and added to the oil, water, and gas volumes measured by the multiphase meter. The result is a high void fraction multiphase meter which can accurately meter flow streams where the gas phase is a dominant component of the flow. This novel concept reduces the size and cost of the multiphase meter while improving its capacity and accuracy. The field tests conducted at the Conoco Multiphase Test Facility determined that the meter can handle flow conditions with the gas-oil ratio (GOR) of 20 to 90,000 SCF/BBL with very good accuracy. The MPFM-400 Series Meter has important applications for metering high GOR wells or wells with moderate GOR that are tested at low pressure.

1. INTRODUCTION

High viscosity fluids measurement necessitates some special consideration for multiphase measurement, primarily in the software and physical attributes. High gas to liquid ratio (GLR) production streams pose a set of special problems to multiphase metering. These problems have been reviewed, and methods for partial separation to deal with high GLR streams have been presented previously (1, 2).

The need for high GLR capabilities of a multiphase meter is illustrated in Figure 1. The graph in Figure 1 shows a sample of well characteristics (gas to liquid ratios) from

different production regions around the world. It should be noted that a significant percentage of the wells have gas fraction above the 90 to 95% gas volume fraction.

The MPFM-400 ("High GVF Meter"), which can measure accurately with a GVF of 99.9%, is an extension of the MPFM-300 Series ("Multiphase Meter"), which is limited to an average GVF of 97.5%. The principles of operation and performance of the Multiphase Meter have been described in detail in References 3, 4 and 5. The Multiphase Meter measures the total volume of the flowing stream utilizing a ruggedized PD (Positive Displacement) meter, a Venturi section to measure gas/liquid flow rates, and a Water Cut Monitor for determination of the water/liquid fraction. The outputs of these devices are fed into a computer which houses the proprietary data management software. The software is designed to provide flow rates of oil, water and gas phases in the multiphase stream.

The High GVF Meter is designed to accurately measure flow streams with very high GLR's. Using the unique FFD™, the meter routes varying amounts of the free gas in the inlet stream into the gas bypass loop as shown in Figure 2. The high viscosity version of the MPFM utilizes only the liquids portion of the meter without provision of any gas diversion. The diverter innovation allows the High GVF Meter to handle a much higher total rate of multiphase fluids. The unique design approach reduces the overall size of the equipment which would otherwise be required, and lowers the overall cost of the system.

Figure 2 is a drawing of the High GVF Meter. The fluid stream enters the meter through the FFD™ which diverts a major portion of the free gas in the inlet stream to the gas bypass loop. The remaining fluids pass into the Multiphase Meter. The FFD™ device is a mechanical device with no moving parts that utilizes the difference in the flow momentum of the gas and liquid to operate as a fluidic diverter. The lower flow momentum of the gas causes the FFD™ to deflect most of the gas in the inlet stream to the gas bypass loop. The higher momentum of the remaining liquid/gas mixture in the stream induces continuation of the flow through the Multiphase Meter.

The diverted gas in the gas bypass loop flows through the gas metering segment where the flow rate is measured. The gas bypass loop stream and the Multiphase Meter stream recombine downstream of the unit and exit the system.

During the above process, the Multiphase Meter has measured the oil, water, and gas phases of the stream running through it. The gas measured by the gas bypass loop is then added to the measurement of the gas phase flowing through the Multiphase Meter to completely account for all fluids in the original stream. The specified accuracy and capacity for a number of common High GVF Meter models are shown in Table 1.

The field tests conducted at the Conoco Multiphase Test Facility used a 2" model of the High GVF Meter. The objective of the field evaluation was to determine that the accuracy specifications shown in Table 1 can be attained under realistic field conditions.

2. THE CONOCO MULTIPHASE TEST FACILITY

The Multiphase Flow Test Facility, which was built for the purpose of evaluating multiphase flow meters, is located within Conoco's North Maurice Field production facility,

approximately 10 miles southwest of downtown Lafayette, Louisiana. In this producing field there are four gas condensate wells that feed into the production facility at a rate of approximately 30 MMSCFPD and 3,000 BFPD. The test facility is capable of handling up to 7,000 barrels per day each of water and oil (combined 14,000 BPD) and 2 MMSCF of gas per day. The facility is unique in that a matrix of tests can be performed for varying flow rates, pressures, volume fractions, GLR, water cuts, and installation effects to simulate various production operations. Table 2 shows the testing capabilities and the fluid properties used in the tests described in this report. Figure 3 shows the schematic of the test facility.

The fluids used in the test facility are produced fluids from the North Maurice Field. A small portion of the gas from the facility process trains is combined with oil and water acquired from volumes accumulated in the field facility tanks and measured by the primary reference meters. The oil and water are drawn from the tanks and surge vessel and mixed with the gas which is injected into the stream. The combined stream is measured by the multiphase meter and then separated. The gas is compressed and routed to the gas sales line. The liquids are separated, with the water being dumped into the facility water disposal system, and the oil accumulated in the surge vessel.

The testing facility is equipped with reference meters so that each single phase is measured before combining into a 3-phase stream. The accuracy of the reference meters is $\pm 0.7\%$. Data readouts are made continuously in the control room.

Provisions are also available to acquire and store heavier crude oils that can be used as an alternative oil phase. In addition, fresh water, from an on-site fresh water tank, can be used as an alternative to produced brine water.

The Conoco facility was used to conduct extensive performance tests on the multiphase meters. These results were published previously (3). The same facility was selected for the High GVF Meter performance tests so that the improvements in the performance of the two meters could be compared under similar testing environments. Figure 4 shows a 2" High GVF Meter (401 Model) similar to the one used in the field tests.

3. PERFORMANCE TESTS AND THE TEST MATRIX

Figure 5 shows the test matrix used in the current performance tests. Each point in the graph represents a test, characterized by the water cut and the GVF of the stream. Since the High GVF Meter is designed to include high GLR conditions, the test matrix was intentionally biased to look at very high gas volume fractions. To illustrate the relationship between the test matrix and typical field conditions, points 1 to 4 in the graph are converted to well flow rates in Table 3. The tests shown in Figure 5 were conducted at an average pressure of 150 psig and temperature of about 120°F. A pressure/temperature correction is therefore used to convert test points 1 to 4 to simulated well conditions in Table 3.

The liquid and gas superficial velocities used in the tests are shown in Figure 6 along with GVF lines. The range of liquid and gas velocities and GVF parameters used in the tests resulted in various flow regimes being tested.

4. TEST RESULTS

The results of the High GVF tests are summarized in Figures 7 through 10. The High GVF Meter readings for oil, water, and gas phases are compared with the single phase data from the loop which is considered as reference. For the purpose of these tests, the loop rates are considered to be 100% accurate. Since the single phase gas rates in the loop are measured under different pressure and temperature conditions than the meter, a PVT and solubility correction was applied to the reference gas measurements to represent the gas rates under actual test conditions.

A total of 157 tests were conducted during the performance evaluation period. Figures 7 through 11 show the High GVF Meter test results plotted against the reference loop rates for oil, water, gas, liquid and total flow rates. In each plot, the upper and lower accuracy specifications (see Table 1) for the High GVF Meter (Model 401-20) are also drawn as the performance boundary lines. As noted by the plots in Figures 7 through 10, the meter can measure oil, water, gas and liquid rates of a multiphase stream within the accuracy specifications stated in Table 1 under the very wide variety of flow conditions represented by the test matrix. Figure 11 shows the total (oil + water + gas) flow rates as determined by the meter to have an accuracy of about $\pm 2\%$ of reading when compared with reference loop tests.

The high viscosity meter has shown exceptional abilities to measure heavy crude (API 10-18 gravity) and viscosities in the 100 to 1200 centistoke range. Tests on Venezuelan Orinoco Belt Bitumen (8, 9) indicate that heavy, high viscosity multiphase fluids can be measured within $\pm 5\%$.

5. CAPACITY OF HIGH GVF METER

The field tests conducted at the Conoco Multiphase Test Facility have shown that the High GVF Meter can handle flow conditions with gas volume fractions up to 99.4% with good accuracy within the vendor's specifications. At the 150 psig pressure used in the Conoco tests, the 99.4% GVF corresponds to the GLR of 9,300 SCF/BBL. Since the meter used in these tests was designed to ANSI 600 pressure rating, the same unit could have handled wells with GLR of up to 90,000 SCF/BBL at the maximum operating pressure of 1,440 (ANSI 600).

The tests conducted at the vendor's test loop, combined with the data from the Conoco tests, have indicated that this technology is applicable to other meter sizes. Utilizing the multiphase flow model of Taitel and Dukler (6) as amended by Xiao (7), the liquid and gas capacities for various size High GVF Meters are calculated as shown in Figure 12. The Flow rates shown in Figure 12 are actual flow rates at 150 psig (10 bars) and 60°F.

6. HIGH GVF AND HIGH VISCOSITY METER APPLICATIONS

The High GVF Meter is intended for applications where gas is the dominant component of the flow stream. This can be in very high GLR wells (gas condensate) or wells with moderate GLR that are tested at low pressure. Figure 13 shows the performance envelope of the 2" High GVF Meter (Model 401-20), with a 4" to 6" gas loop, connected to a 6" flow line operated at 600 psig pressure. The liquid and gas rates are actual rates as seen by the meter. The gas flow rate capacity of the High GVF Meter is a function of the gas bypass loop.

The production rates for 9 wells (Table 4) tested by this meter are also marked in Figure 13 to illustrate the range and turndown capability of the meter. It should be noted that all flow rates shown in Table 4 can be measured with the accuracy stated in Table 1.

As noted by the data in Table 4 and Figure 13, the High GVF Meter can handle total actual fluid flow rates ranging from 100 bbl/d to 29,000 bbl/d. This amounts to a turn down ratio of about 300:1 for the High GVF Meter. Another important improvement in this design is the capability of the High GVF Meter to handle high liquid turndowns at very high gas volume fractions. The importance of these capabilities can be appreciated by the data in Table 4. To handle the 9 wells shown in this table would have required either a very large multiphase meter or multiple small meters at much higher cost than a single 2" High GVF Meter (Model 400-20). The use of the High GVF Meter provides a wide range of capabilities at lower cost.

The gas by-pass loop shown in Figure 2 can be configured as an add-on to the Multiphase Meter to enhance its capacity in production situations where the total flow rates exceed the capacity of the MPFM 300 Series Meter. The addition of the MPFM 400 loop has no effect on the measurement capabilities of the 300 Series Meter. For additional flexibility, the measurement system can be deployed in either the 300 Series or the 400 Series configuration, as the application warrants.

REFERENCES

1. ARPANDI I., JOSHI A.R., SHOHAM, O., and SHIRAZI S., "Hydrodynamics of Two-Phase Flow in Gas- Liquid Cylindrical Cyclone Separators", SPE Paper 30683 presented at the SPE Annual Technical Conference & Exhibition in Dallas, USA , 22-25 October 1995.
2. WEINGARTEN, J.S., KOLPAK, M.M., MATTISON, S.A., and WILLIAMSON M.J.- "New Design for Compact Liquid-Gas Partial Separation: Downhole and Surface Installation for Artificial Lift Applications", SPE Paper 30637 presented at the SPE Annual Technical Conference & Exhibition in Dallas, USA , 22-25 October 1995.
3. MEHDIZADEH, P., and FARCHY, D., "Multiphase Flow Metering Using Dissimilar Flow Sensors - Theory and Field Trials Results", SPE Paper 29847 presented at the SPE Middle East Oil Show, Bahrain, 11-14 March 1995.
4. U.S. Patent 5,099,697 and foreign counter parts, "Two and Three Phase Flow Measurements".
5. U.S. Patent 5,461,930 and foreign counterparts, "Apparatus and Methods for Measuring Two or Three Phase Fluid Flow Utilizing One or More Momentum Flow Meters and a Volumetric Flow Meter".
6. TAITEL, Y. and DUKLER, A.E., "A Model for Predicting Flow Regime Transition in Horizontal and Near Horizontal Gas-Liquid Flow", AIChE. J., 22, No. 1, pp 47-55, 1976.

7. XIAO J.J., SHOHAM, O., and J. P. BRILL, "A Comprehensive Mechanistic Model for Two Phase Flow in Pipelines", SPE Paper 20631 presented at the SPE 65th annual Meeting, New Orleans, September 23-26, (1990).
8. COLMENARES, J., PERRY, D., GUEVARA, E., and PADRON, A. , "Multiphase Flow Metering of Heavy Crude- Oil Field Evaluation", Multiphase 95, Cannes, France, June, 1995.
9. TUSS, B. and MEHDIZADEH, P., "Field Test of a High Viscosity Multiphase Meter", IPC Conference, Calgary Canada, Paper No. 629, July 1996.

**TABLE 1
ACCURACY AND CAPACITY FOR A NUMBER OF
COMMON 400 SERIES METERS**

MPFM-401 Series	Gas Flow Rate Error	Oil Flow Rate Error	Water Flow Rate Error
MPFM-401-20	± 5% of full scale* ± 10% of gas reading	± 90 BBL/D, or ± 10% of oil flow	± 90 BBL/D, or ± 10% of water flow
MPFM-401-30	± 5% of full scale* ± 10% of gas reading	± 180 BBL/D, or ± 10% of oil flow	± 180 BBL/D, or ± 10% of water flow
MPFM-401-40	± 5% of full scale* ± 10% of gas reading	± 480 BBL/D, or ± 10% of oil flow	± 480 BBL/D, or ± 10% of water flow

*Full scale depends on the size of the 400 bypass loop.

**TABLE 2
TESTING CAPABILITIES AND FLUID PROPERTIES**

TEST PARAMETERS		CAPABILITIES	FLUID PROPERTIES	
			Gas Specific Gravity	0.699
Pressure		150 psig	H ₂ S	3 PPM
Temperature		Approx. 80°F - 120°F	CO ₂	2% (mol percent)
Gas Flow		0-2MMSCFPD (2" Flowline) - 0 - 100 ft/sec Superficial Gas Velocity	Condensate	46.5° API 0.7949 sp. gr. 2.1 cSt @ 100° F
Condensate/Crude Produced Water	Oil/	0-7000 BFPD (2" Flowline) - 0-100% Water Cut 0-21 ft/sec Superficial Liquid Velocity	Produced Water	1.0535 sp. gr.

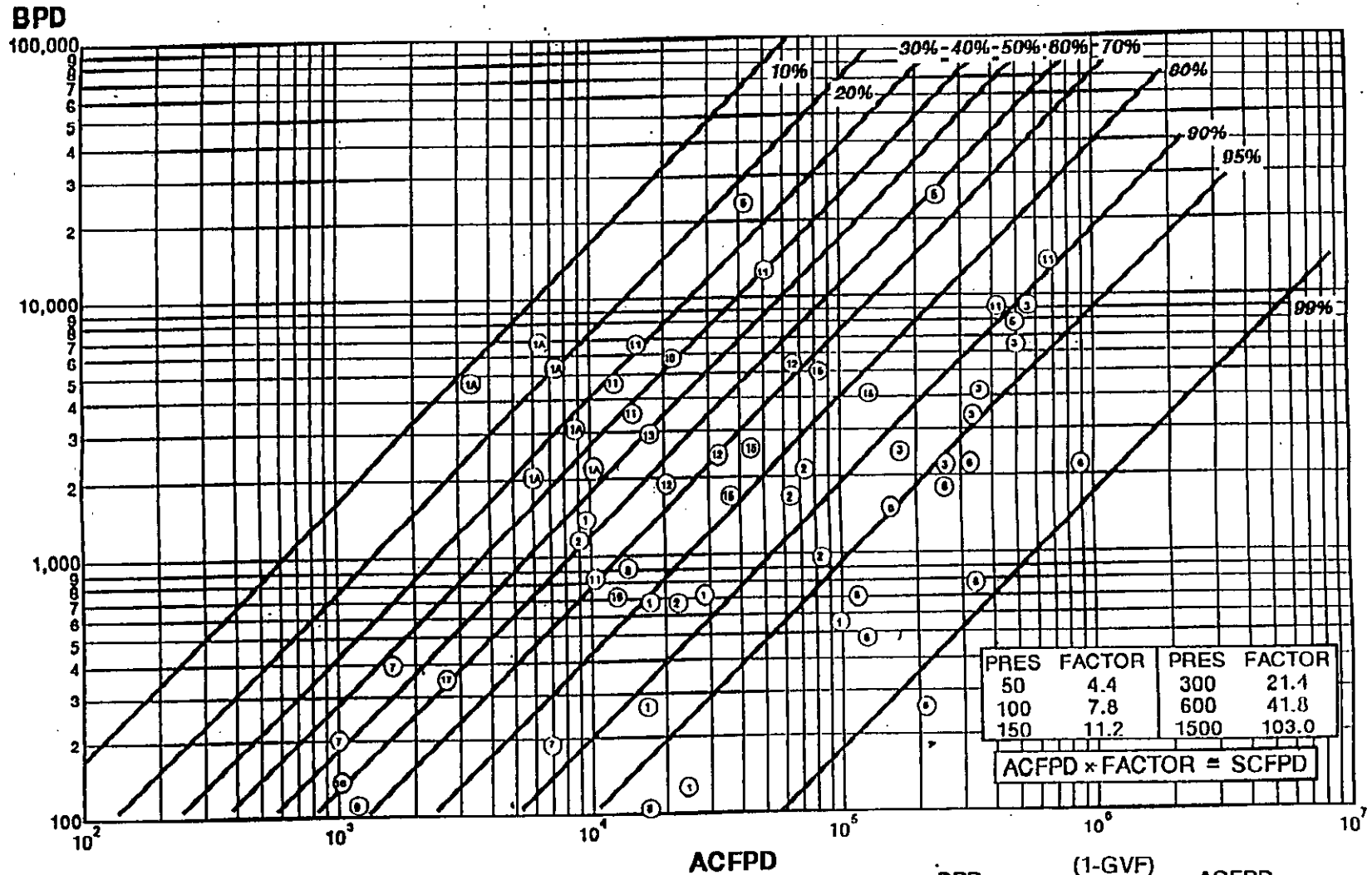
**TABLE 3
WELL FLOW CONDITIONS REPRESENTED BY POINTS 1 TO 4 IN FIGURE 5**

TEST CONDITION POINT IN FIG. 5	WELL FLOW CONDITIONS			
	LIQUID RATE BBL/D	OIL RATE BBL/D	WATER CUT %	GAS RATE MMSCF/D
1	1190	595	50	10
2	396	316	25	20
3	198	50	75	10
4	198	20	90	10

**TABLE 4
WELLS SHOWN IN FIGURE 13
TESTED BY THE MPFM-401-20
WITHIN THE ACCURACIES SHOWN IN TABLE 1**

WELL	PRESSURE	OIL	WATER	GAS	GAS	GOR	GVF	TOTAL FLOW
NAME	PSI	BPD	BPD	MSCF/D	MACF/D	SCF/BO	%	BPD
A1	600	680	350	340	10	500	63	2775
A2	500	680	350	1,360	39	2,000	87	8,010
A3	600	680	350	4,700	137	7,000	96	25,459
A4	600	680	350	8,160	235	12,000	98	42,909
A5	600	680	350	23,800	684	35,000	99	123,177
A6	600	680	350	680	20	1,000	77	4,520
A7	400	680	350	680	29	1,000	84	6,265
A8	200	680	350	680	59	1,000	91	11,500
A9	75	680	350	680	156	1,000	96	28,949

FIGURE 1
WELL CHARACTERISTICS (GAS TO LIQUID RATIOS) FROM
DIFFERENT PRODUCTION REGIONS AROUND THE WORLD



$$BPD_{Lq} = \frac{(1-GVF)}{GVF * 5.614} ACFPD$$

GVF = Actual Gas Volume Fract.

ACFPD = Actual Cubic Feet Per Day

FIGURE 2
SCHEMATIC OF THE MPFM-400 SERIES METER

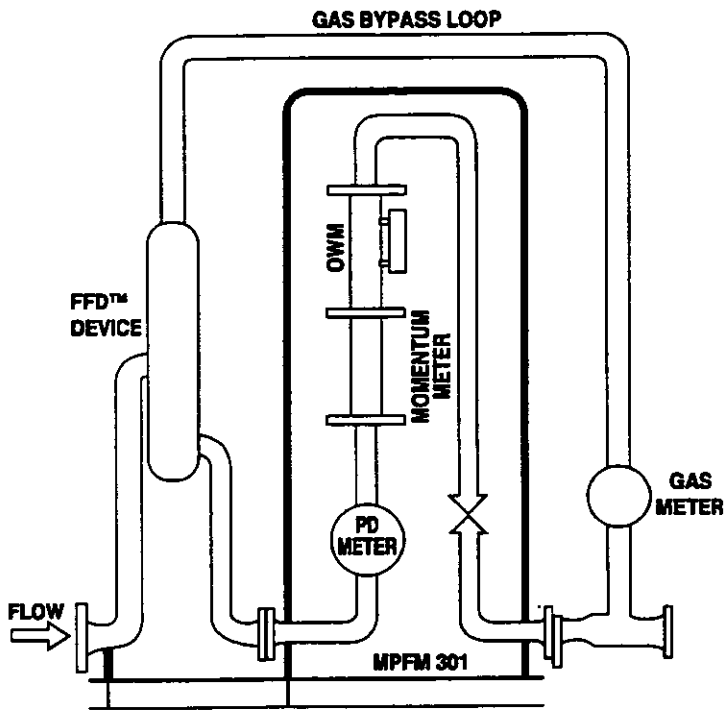
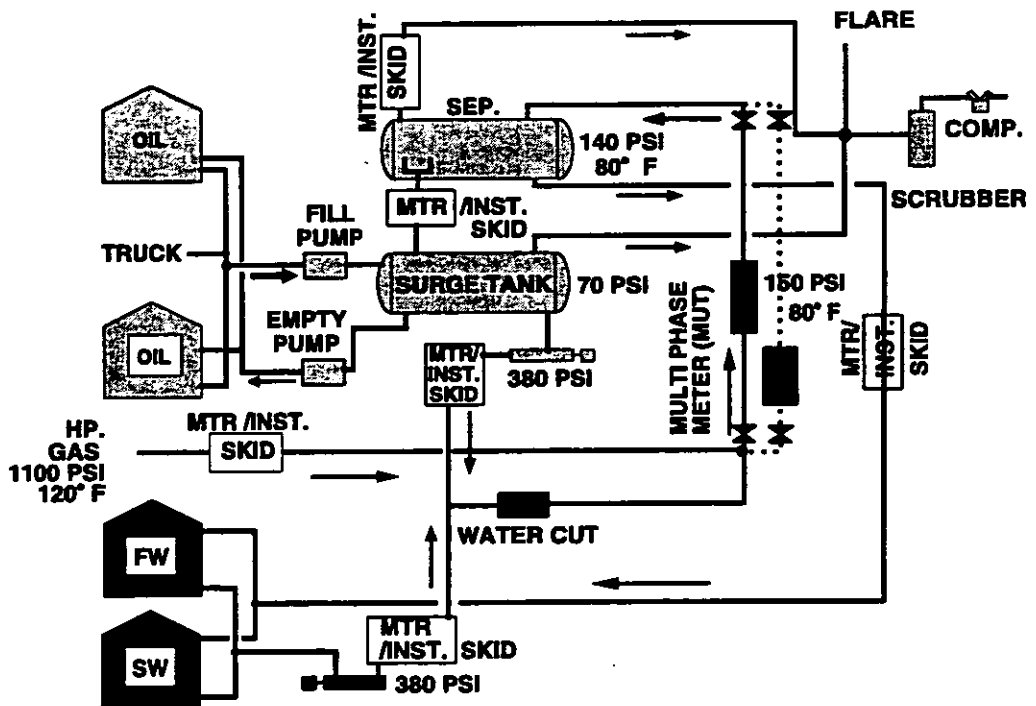


FIGURE 3
MULTIPHASE FLOW TEST FACILITY



MPFD-1 WPG B-7 6896

FIGURE 4
2" MPFM-400 SERIES METER SIMILAR
TO THE ONE USED IN THE FIELD TESTS

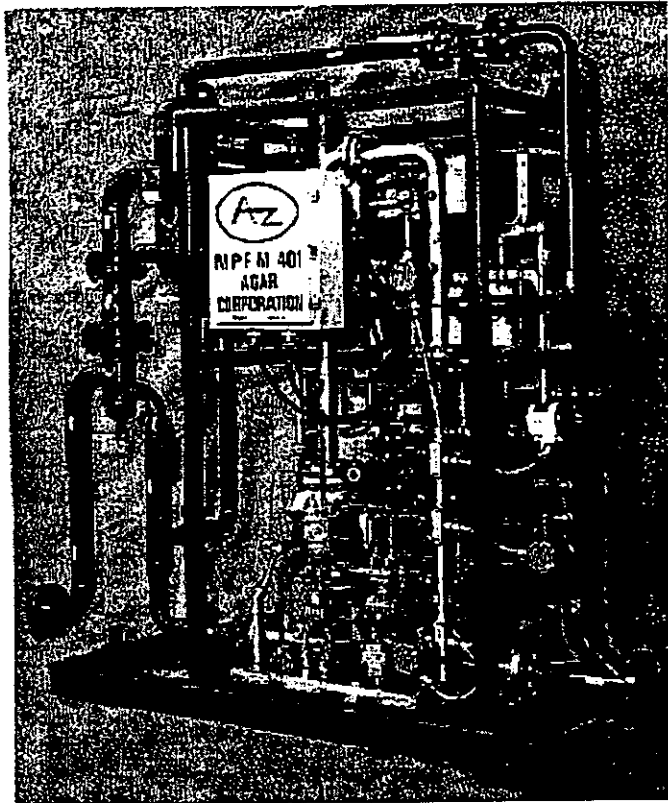


FIGURE 5
TEST MATRIX FOR AGAR MPFM-401 USED AT CONOCO FACILITY

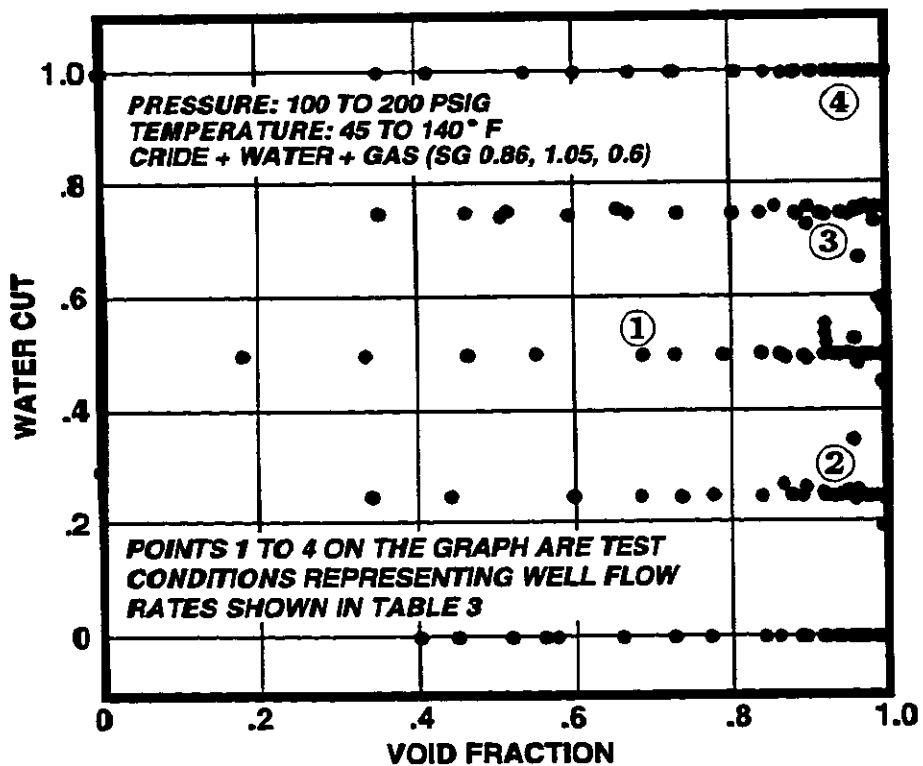


FIGURE 6
LIQUID VERSUS GAS SUPERFICIAL VELOCITY

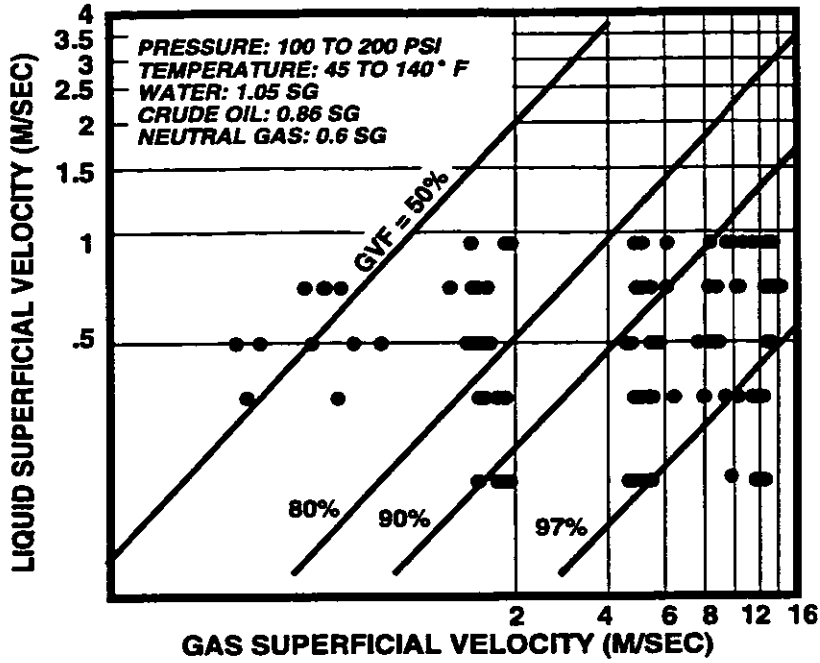


FIGURE 7
AGAR MPFM-401 VERSUS CONOCO LOOP OIL FLOW RATE

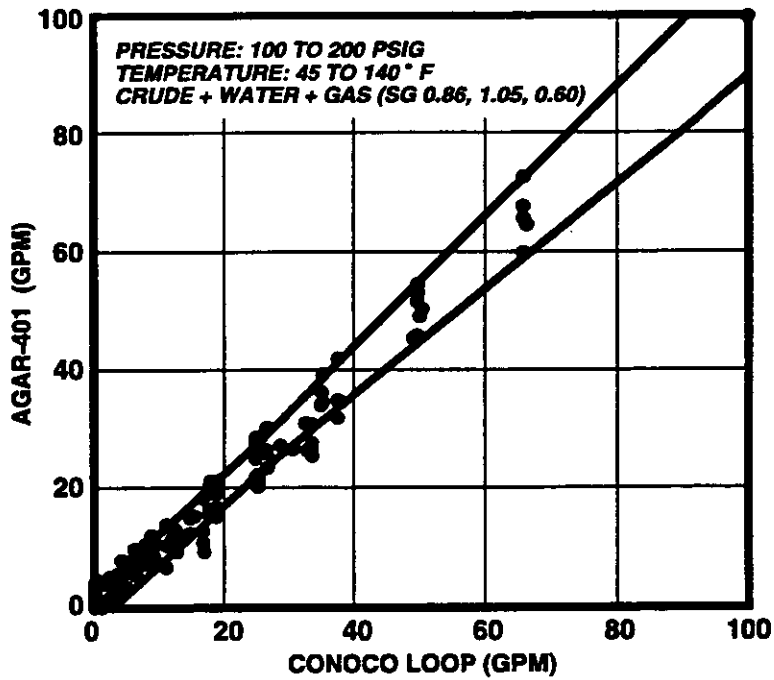


FIGURE 8
AGAR MPFM-401 VERSUS CONOCO LOOP WATER FLOW RATE

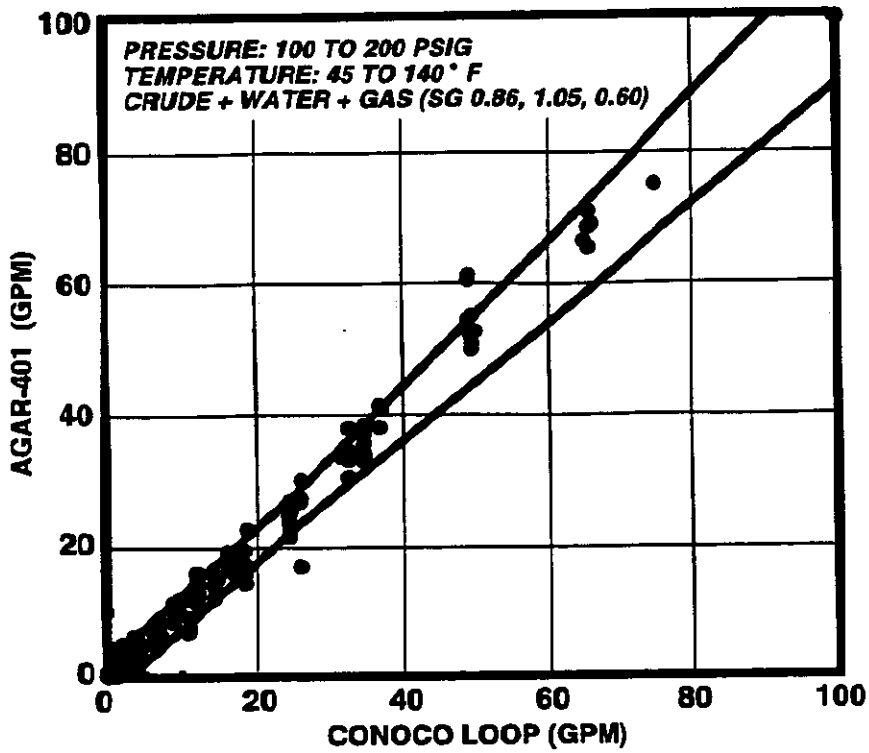


FIGURE 9
AGAR MPFM-401 VERSUS CONOCO LOOP GAS FLOW RATE

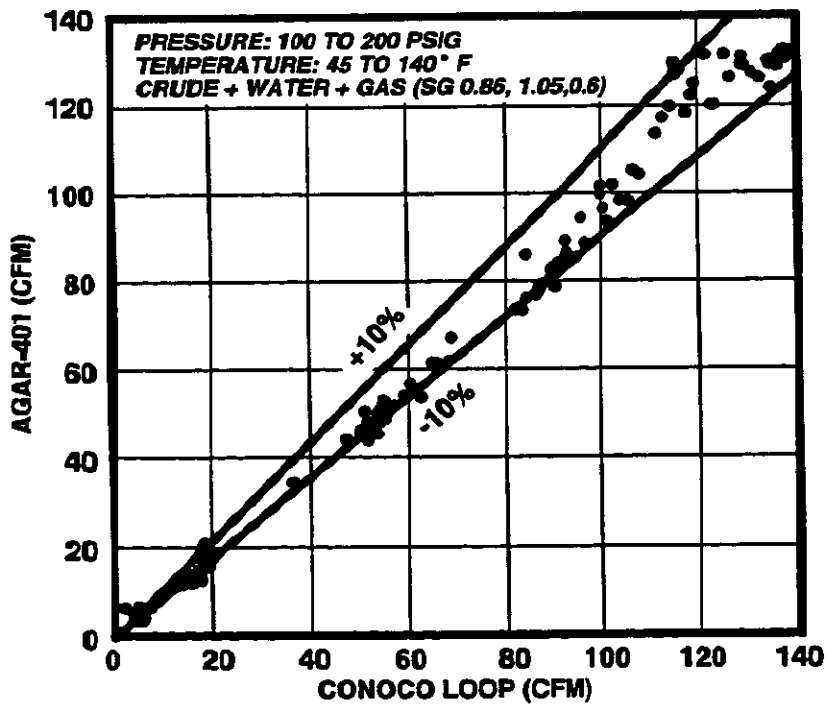


FIGURE 10
AGAR MPFM-401 VERSUS CONOCO LOOP LIQUID FLOW RATE

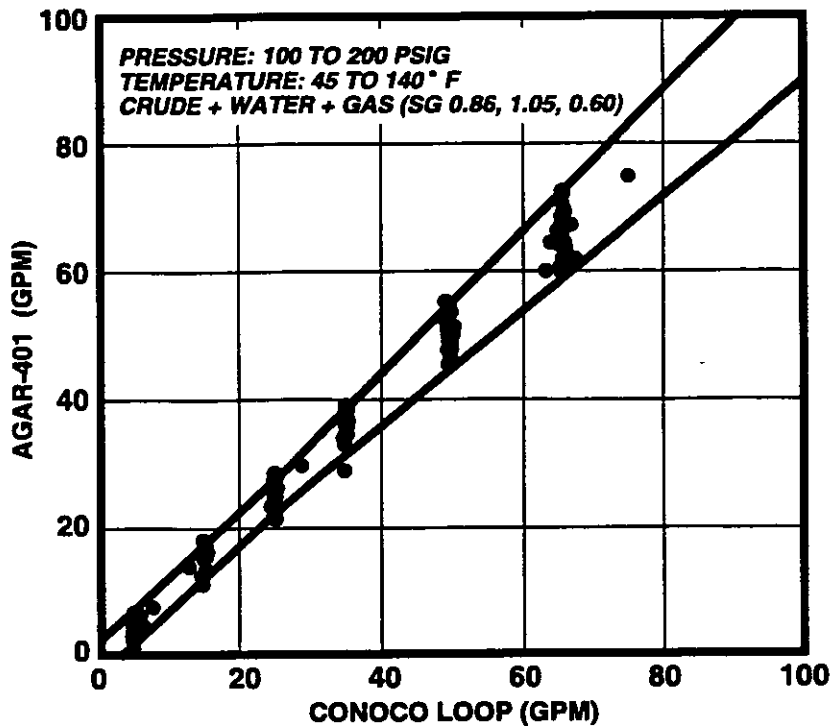


FIGURE 11
AGAR MPFM-401 VERSUS CONOCO LOOP TOTAL FLOW RATE

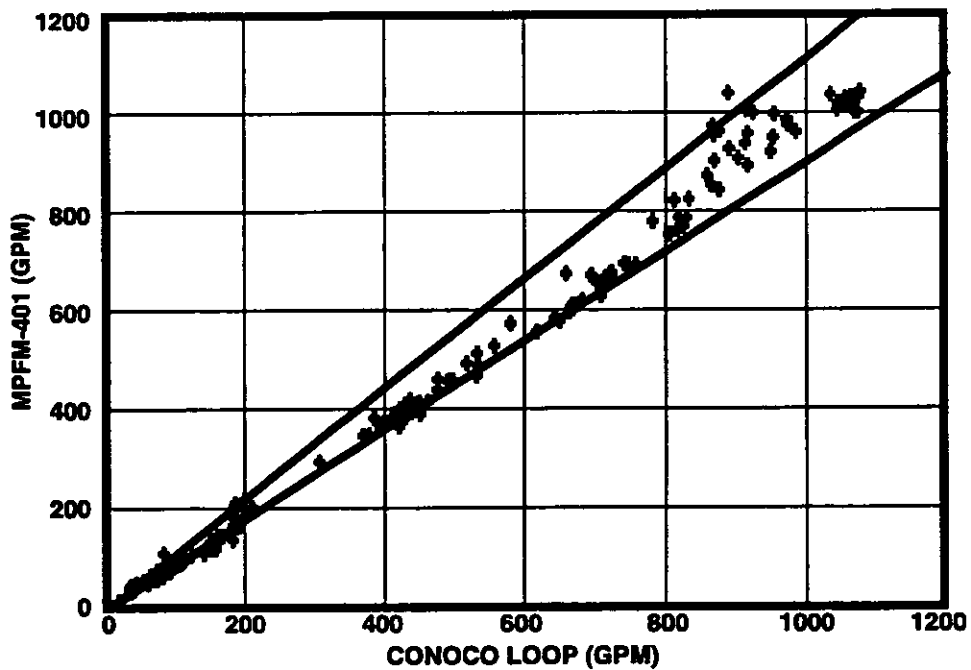


FIGURE 12
GAS AND LIQUID CAPACITIES
MPFM-400 SERIES METER

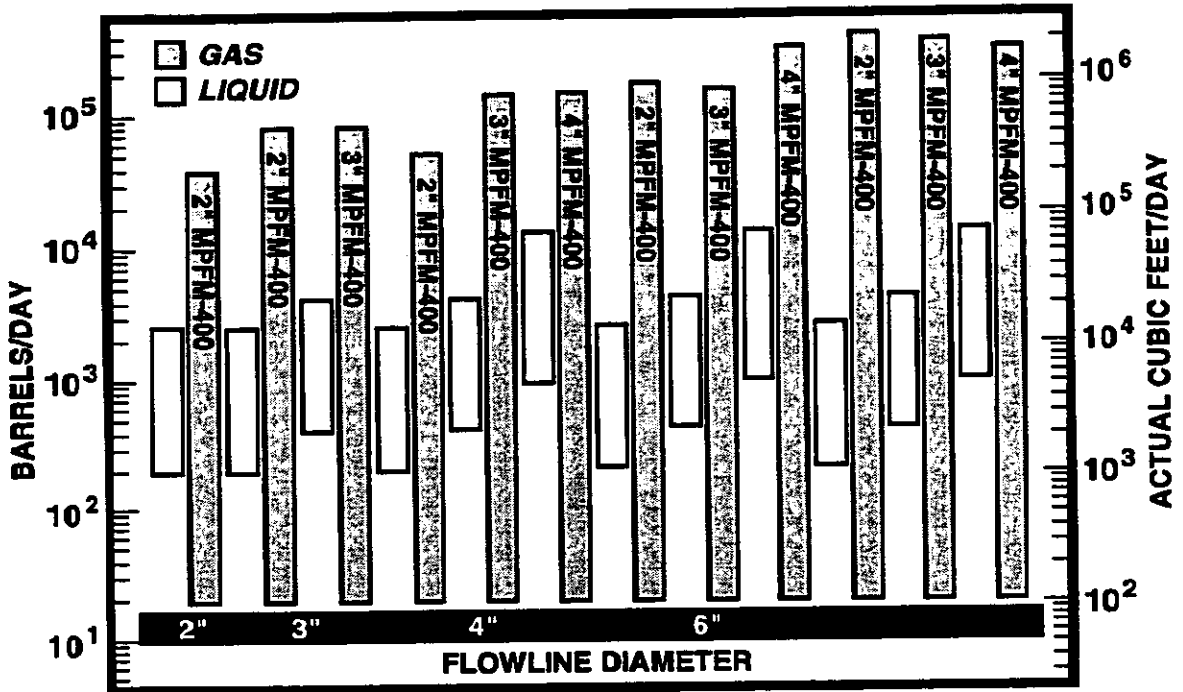
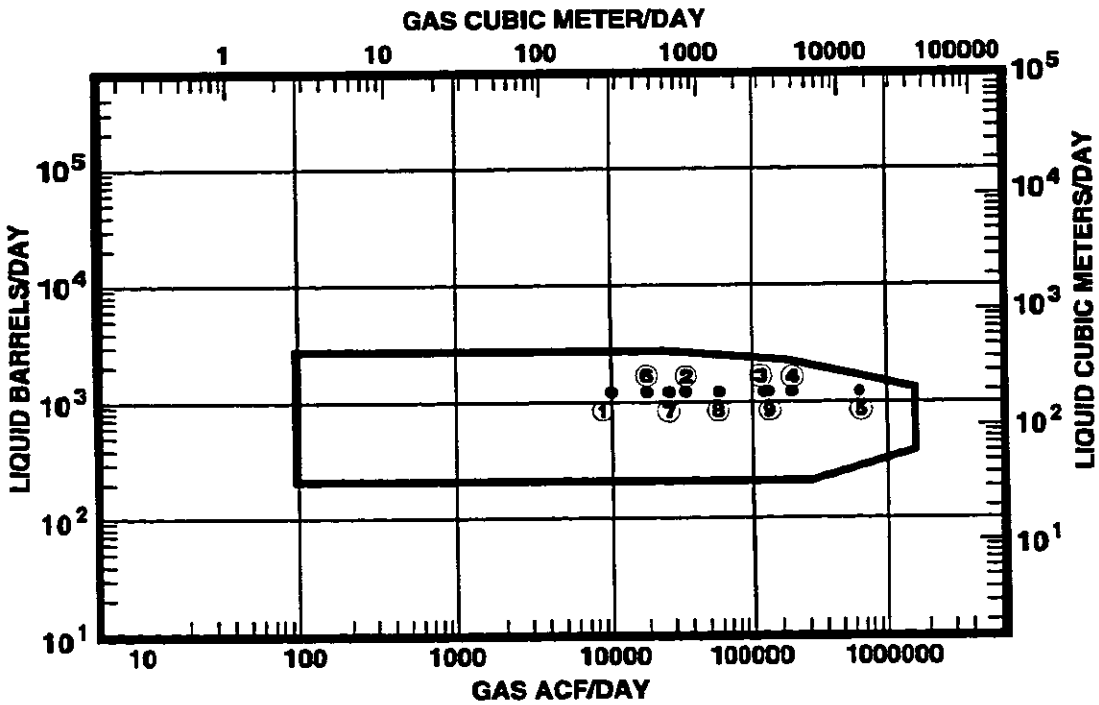


FIGURE 13
PERFORMANCE ENVELOPE FOR MPFM-401-20
4" - 6" LOOP CONNECTED TO 6" FLOWLINE AT 600 PSIG
(Points 1-9 in the Graph refer to the well flow rates in Table 4)



ASSESSMENT OF MULTIPHASE FLOWMETER PERFORMANCE

Dr. Tim Whitaker
Fluids and Process Technologies Division
NEL
East Kilbride G75 0QU

1 INTRODUCTION

The objectives of the Multiflow JIP run by NEL on behalf of Amerada Hess, Brasoil, BP, Exxon, Mobil, Schlumberger and Shell Expro were to characterise the performance of commercially available multiphase flowmeters on a single test bed facility with high quality reference flow rate measurement systems. The results from the project will be used by the sponsoring organisations as benchmark performance data for the selected meters to focus the implementation of multiphase metering strategies in new field developments. Data generated by this project has been utilised by these organisations to assess the likely effectiveness of the meter technology in the field and to assess the performance of the multiphase meter vendors in terms of technical back-up and response to problems with the instrumentation.

The multiphase test facilities at NEL were utilised for the evaluation of the meters, rather than field test data, due to the greater accuracy of the reference flow rate measurements for oil, water and gas. These approach the accuracy attainable with single-phase flow measurements. In addition the use of a laboratory test facility enabled meter performance to be evaluated quickly over a wide range of conditions at a relatively low cost. The evaluation matrix covered 0 to 100% water cut and 0 to 98% gas volume fraction (GVF) over a wide range of flow velocities. An additional benefit was to obtain data for each meter from the same traceable source.

To ensure that the evaluations were as representative as possible of likely field conditions the test fluids used were stabilised Forties blend crude oil, simulated produced water and nitrogen. To establish the effect of changes in water properties on the meter performance, two different concentrations of simulated produced water were used in each case. The concentrations were representative of the mass absorption and density of sea-water and brine, the conductivity of the second solution was approximately twice that of the first. The performance of the multiphase flowmeters was assessed in terms of percentage error relative to the reference oil, water and gas volumetric flow rates and the absolute error relative to the GVF and water cut. In addition to the evaluation of basic accuracy a number of reproducibility tests were run to define the capability of each instrument to return to a previously experienced flow condition and repeat the measurement to within similar levels of accuracy.

The multiphase flowmeters tested at NEL during Multiflow I were the Agar MPFM-301, the Fluenta MPFM 1900VI, the Framo MFM and the MFI LP meters. The bore diameter of the instruments was between 50 mm and 100 mm. These instruments utilised a variety of techniques¹ to measure a number of different parameters associated with oil/water/gas mixtures, such as bulk density, dielectric constant and mixture velocity. These parameters

were then combined to derive the phase flow rates, the water cut and the GVF. All the meters made use of either an intrusive device or some configuration of the pipework upstream of the meter to condition the flow prior to the measurement section. Another feature common to each meter was the use of a differential pressure measurement device at some part of the envelope.

2 MULTIFLOW 2

The second stage of the Multiflow project commenced in September 1996 with completion planned for mid-1998. The main objectives for this project are to complete a further four benchmark multiphase flowmeter evaluations using the same experimental facilities as used in the initial stage of the project and to collate the data from these evaluations and the preceding stage into a single database from which the project sponsors can readily access information to assist in specifying the most suitable meters for particular installations.

The evaluation programme for Multiflow 2 has also been extended to include a second crude oil, in addition to the original Forties blend. These additional tests reflect the concern of the project sponsors that changes in the crude oil properties may influence the ability of multiphase flowmeters to perform accurate measurements. The second oil will be of higher viscosity and density, around API 26. The test matrices from the initial stage will be utilised in the second stage to allow direct comparison of the new data with the benchmark evaluations already collected.

The multiphase flowmeters for evaluation under the Multiflow 2 project will be selected from the Kongsberg MCF351, the MFI Full Range, the CSIRO MFM, the ISA multiphase flowmeter, the Petroleum Software and the Mixmeter projects. The Kongsberg MCF351 utilises intrusive capacitive and resistance sensors to measure water cut and GVF in the multiphase flow, propagation velocity of features is gained by cross-correlation with gas and liquid velocities derived from models. The MFI Full Range meter measures water cut and GVF with microwaves and gamma radiation attenuation, velocity measurement is by cross-correlation. The CSIRO MFM derives phase fractions from dual-energy gamma radiation attenuation, velocity measurement is from cross-correlation of flow features. The ISA meter is essentially a positive displacement meter which can be linked to a phase fraction meter to derive phase flow rates. Petroleum Software have linked a number of instruments which measure pressure drop, capacitance and resistance to a neural network which predicts the individual phase flow rates. The Mixmeter depends on differential absorption of dual-energy gamma radiation and cross-correlation of flow features. The final selection of test meters will be decided by the project sponsors and preference will be given to the most commercially advanced instruments.

3 MULTIFLOW RESULTS

The four multiphase flowmeters were independently evaluated against reference standard single-phase flow measurements, compensated to test section conditions, over a common evaluation matrix. The results from these evaluations indicated the performance of each meter against the accuracy specification claimed by each manufacturer. It is important to consider the results obtained in the light of the complexity of both the multiphase flow structure and number of measurements being made to infer the resultant phase flow rates. Effectively the measurements were tested over a turn-down ratio approaching 100:1 for each of three phases,

and the same degree of absolute accuracy cannot be expected when deriving a small quantity by difference of two much larger quantities as can be achieved by direct measurement. Similarly, the flow rate errors are presented in terms of relative error to the reference phase flow rate, and here the relative error will always increase in significance as the magnitude of the quantity decreases relative to its maxima.

The performance of the meters was assessed in terms of two-phase (gas/liquid) and multiphase (oil/water/gas) flow instruments. In general, the results for total liquid flow rate indicated predictions within $\pm 10\%$ of the reference flow rate over most of the evaluation matrix. For each of the meters there were small localised zones where measurements were found to be less accurate, the location of these zones varied between the meters. The boundaries within which the performance of the meter was within $\pm 10\%$ relative error of the reference are marked on Figure 1.

The gas flow rate predictions were also within $\pm 10\%$ over large regions of the evaluation matrix for each instrument, Figure 2. Local zones of reduced accuracy existed for each meter and covered larger areas of the evaluation matrix than for the liquid flow rates. These zones were, in part, linked to changes in the multiphase flow structure and local gas/liquid distribution. The existence of these zones indicate underlying weaknesses in some of the flow models used in the various instruments, or the inability of flow conditioners to produce consistent downstream conditions as the upstream flow pattern changed.

Each of the multiphase flowmeters evaluated exhibited a performance of better than $\pm 10\%$ relative error for some of the phase flow rates at some of the test matrix conditions. Because of the nature of the measurements the most accurate measure of phase flow rates tended to be at conditions where a relatively high proportion of that phase was present.

For example, the test meters were capable of measuring the oil flow rate to within $\pm 10\%$ relative for most conditions where the water cut was less than 50%, Figure 3. Water flow rate measurements were generally within a similar accuracy once the water cut exceeded 20%, Figure 4.

The data have also been shown on plots of superficial gas and liquid velocity to highlight regions of good and poor performance. The enclosed zones on Figures 5-8 again denote regions within which errors of less than $\pm 10\%$ can generally be expected to occur, this information must also be read in conjunction with the data detailed on the water cut vs. GVF plots to determine the likely performance at a given condition. Flow pattern boundaries for vertical air/water flows² have been overlaid on the plots to illustrate any linkage to flow patterns. Vertical flow pattern boundaries have been used as the majority of the instruments utilise a conditioner prior to vertical up-flow at the measurement section. The differences between Figures 5, and Figures 7 and 8, show that the proximity of the bubble/churn transition boundary may affect the ability of some instruments to distinguish between oil and water, whilst still being capable of more accurate measurement of total liquid flow rate.

In each meter the oil and water flow rates were derived by combining the total liquid flow rate measurement with a measure of the water cut in the liquid phase. It was immediately apparent that, as the total liquid flow measurement was generally within $\pm 10\%$, the increased uncertainty at some conditions for the oil and water flow rate measurement was caused by larger uncertainty in the water cut measurement. On close examination of the data for the individual instruments it was seen that for increasing GVF the magnitude of the error in the water cut

measurement generally increased, Figure 9. For some of the multiphase flowmeters the measurement of the water cut was also affected by the water cut in the flow.

From the data generated during the evaluations it can be seen that multiphase flowmeters are capable of providing the measurement accuracy required for practical applications over some part of the full range of multiphase flows, equally it is apparent that further advances are required before any meter can be claimed to fulfil the complete requirements of the operators. At present the main areas where further improvements are required are at above 85-90% GVF and for flows which are water continuous.

4 CONCLUSIONS

All the multiphase flowmeters tested under the Multiflow JIP were capable of providing phase flow rate measurements to within $\pm 10\%$ relative of the reference measurements for mixtures of crude oil, simulated brine and nitrogen gas over part of the evaluation matrix.

The regions over which the oil, water and gas flow rate measurements provided by the meters were within $\pm 10\%$ relative did not extend over the full matrix of conditions.

All the multiphase meters were capable of measurements within $\pm 10\%$ relative of the reference for gas and liquid flow rates over a wider extent of the evaluation matrix than for individual phase flow rates.

The performance of the multiphase meters was generally strongest in oil continuous flows and for GVF less than 90%. There is scope for improvement in these areas by further development or use of new technologies.

ACKNOWLEDGEMENTS

The author would like to thank the participants in the Multiflow JIP for their kind permission to use data gathered during this project and all the manufacturers who have supported the JIP project by loan of equipment and support staff.

REFERENCES

- 1 Whitaker T.S., Characterisation of the Performance of Multiphase Flowmeters: The Multiflow JIP. North Sea Flow Measurement Workshop 1995.
- 2 McQuillen K.W. and Whalley P.B., Flow Patterns in Vertical Two-Phase Flow. I.J. Multiphase Flow, 1985. Vol. 11, No.2, pp.161-175.

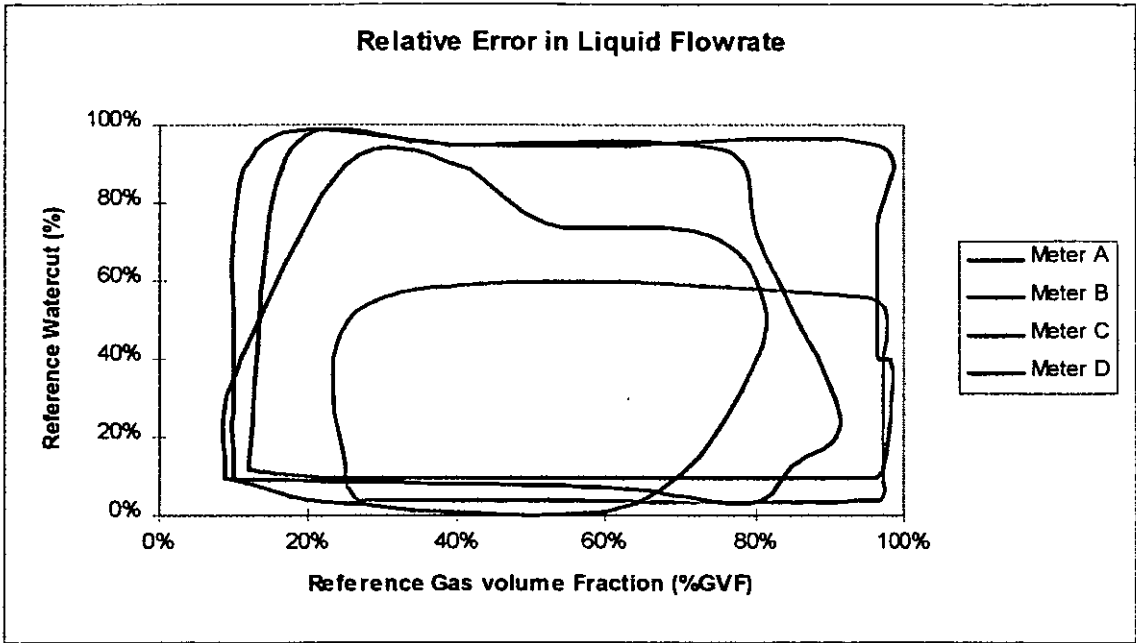


Figure 1: Liquid Flow Rate Prediction

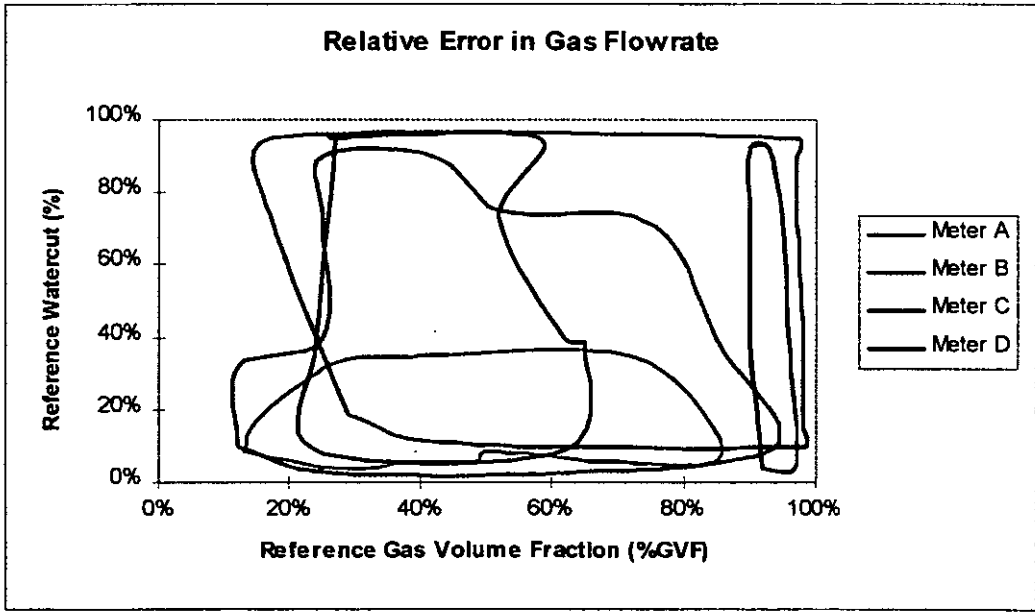


Figure 2: Gas Flow Rate Prediction

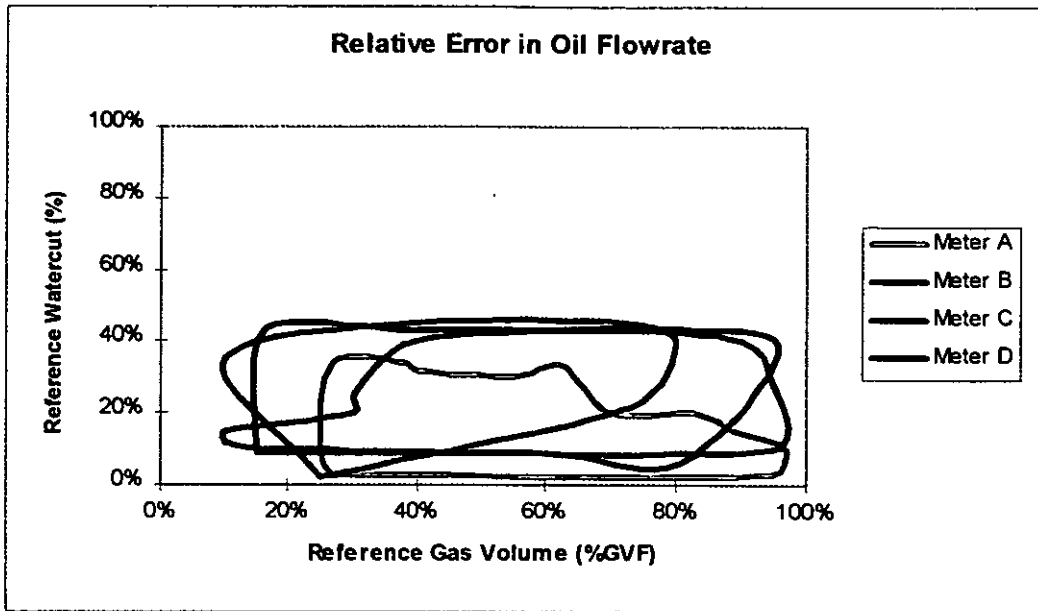


Figure 3: Oil Flow Rate Prediction

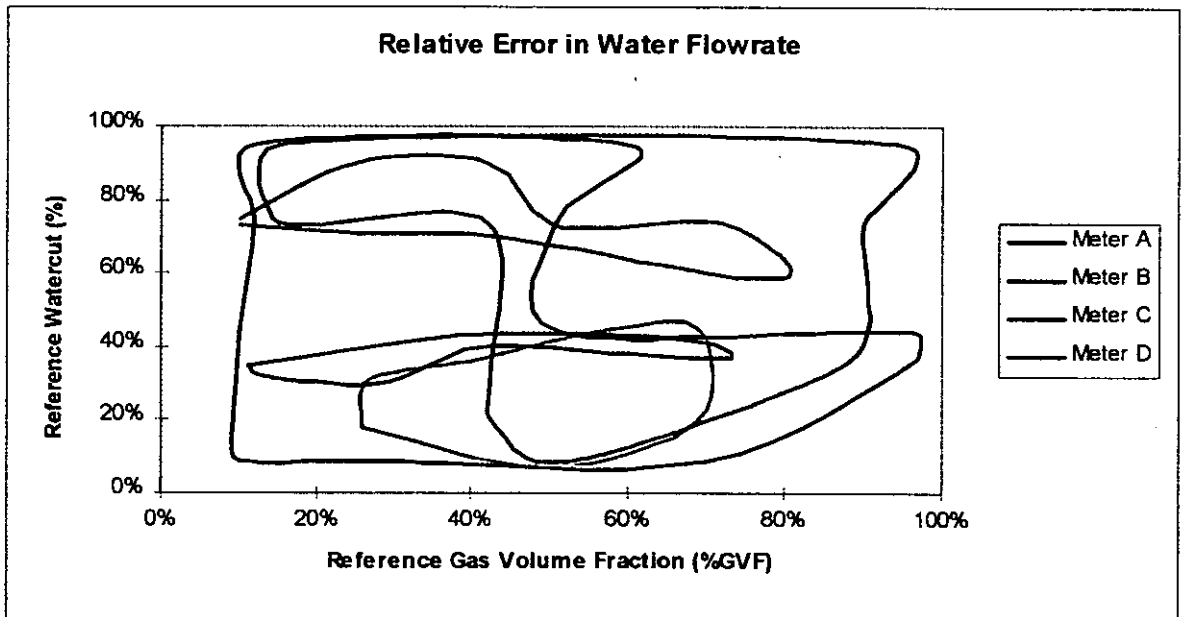


Figure 4: Water Flow Rate Prediction

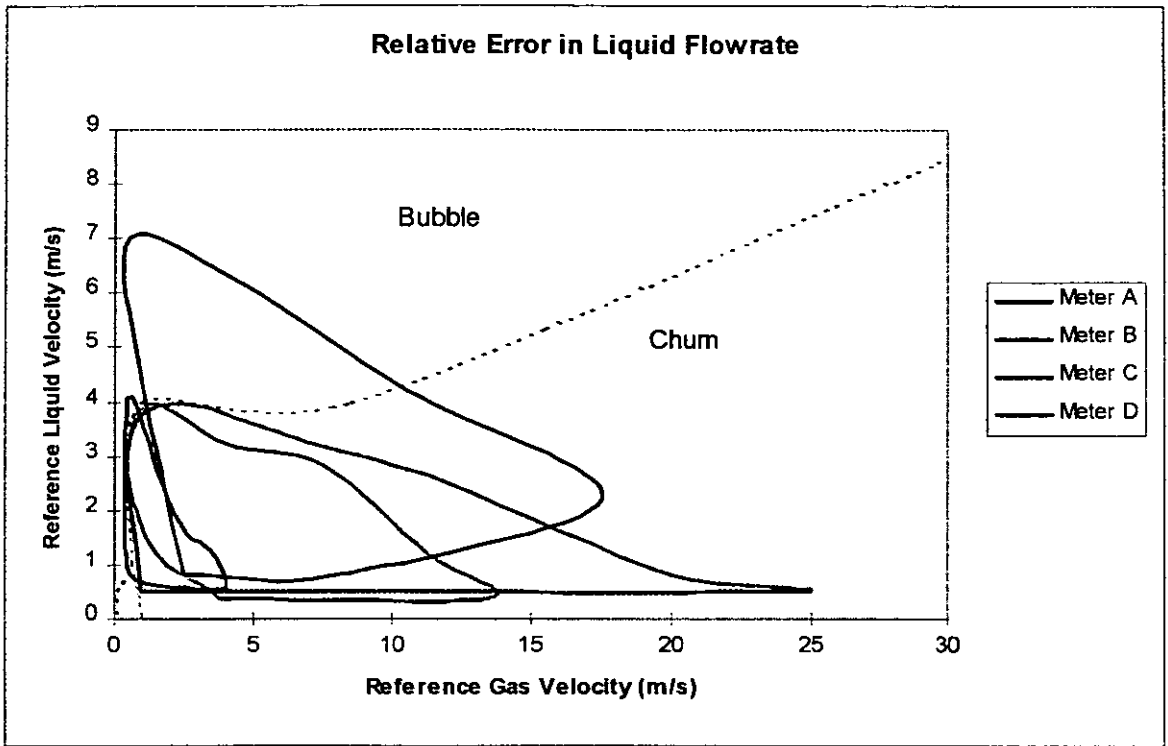


Figure 5: Liquid Flow Rate Error Plots

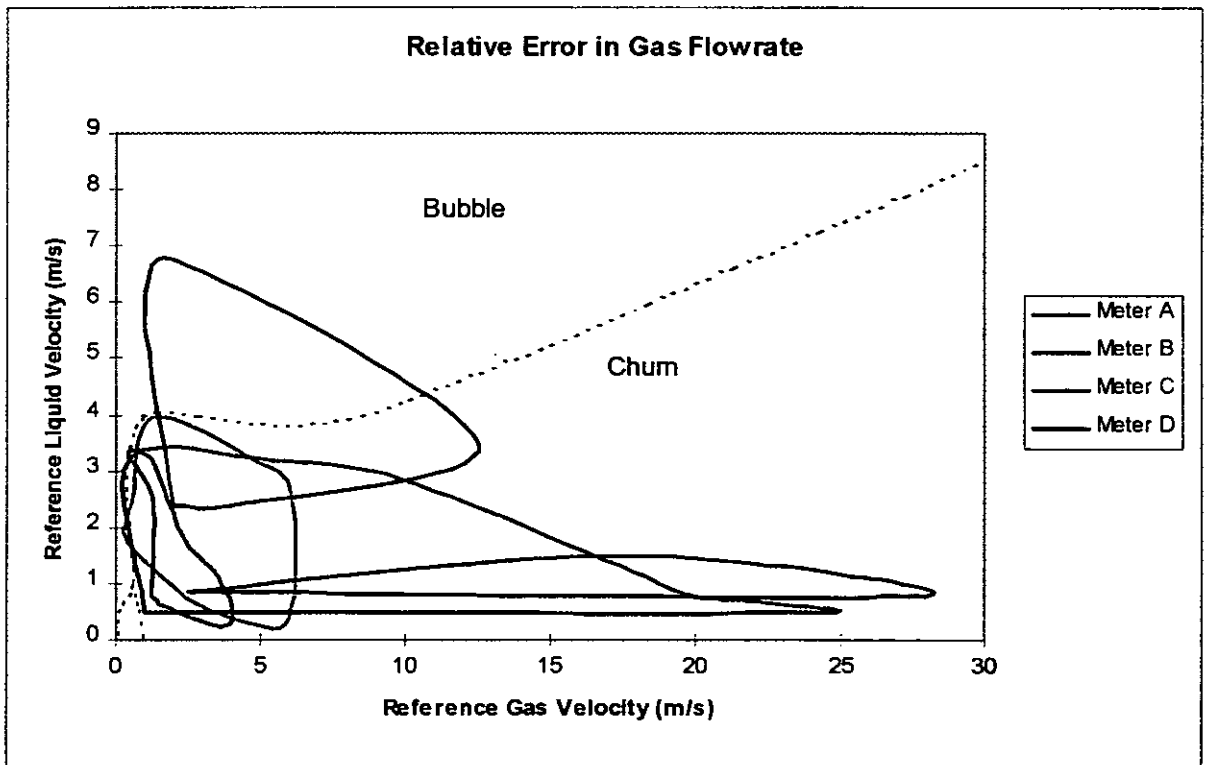


Figure 6: Gas Flow Rate Error Plots

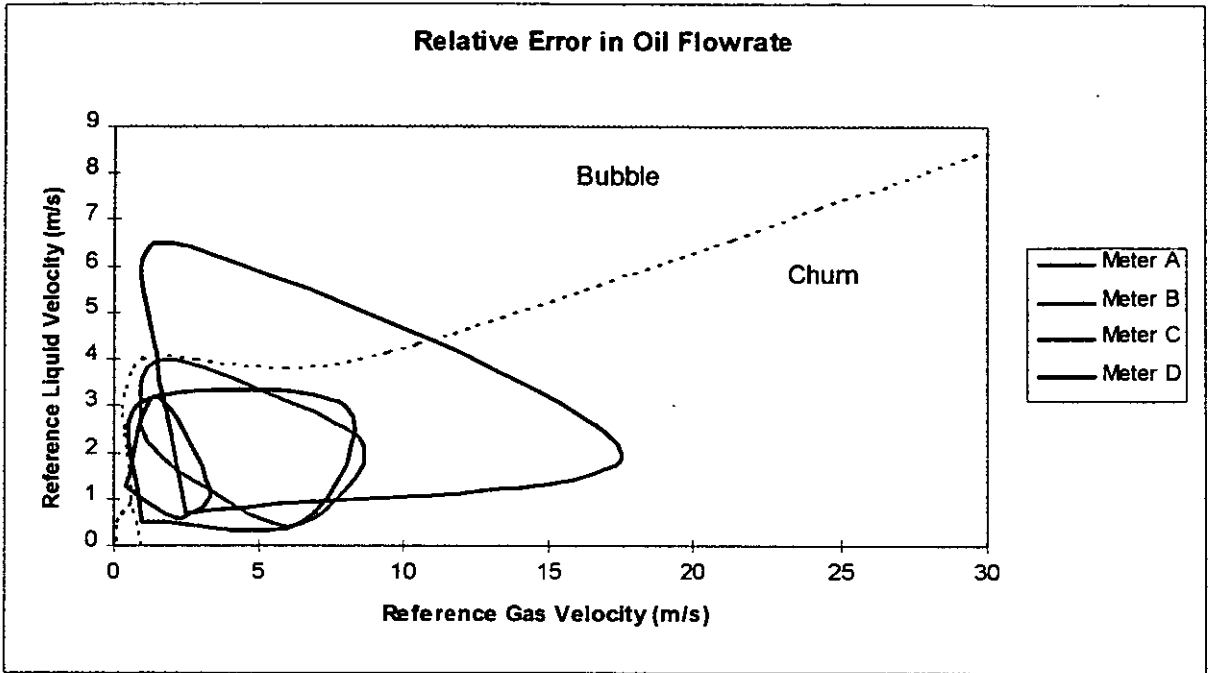


Figure 7: Oil Flow Rate Error Plots

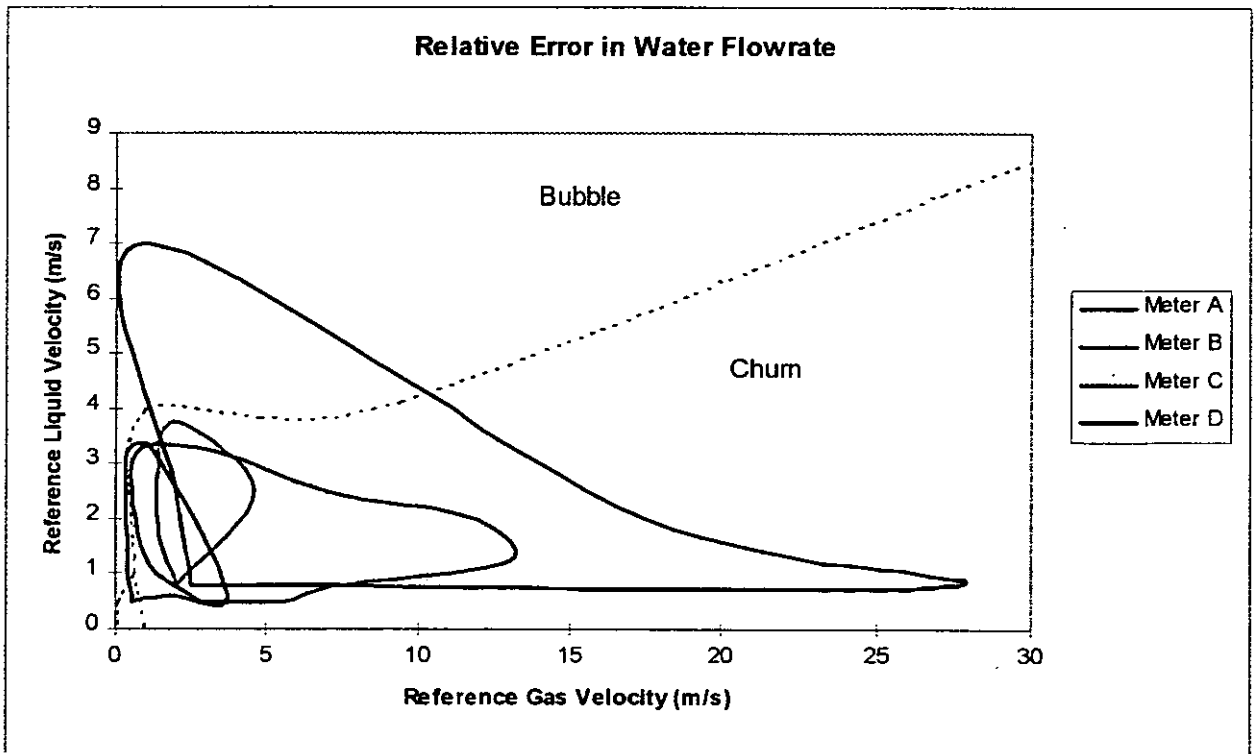


Figure 8: Water Flow Rate Error Plots

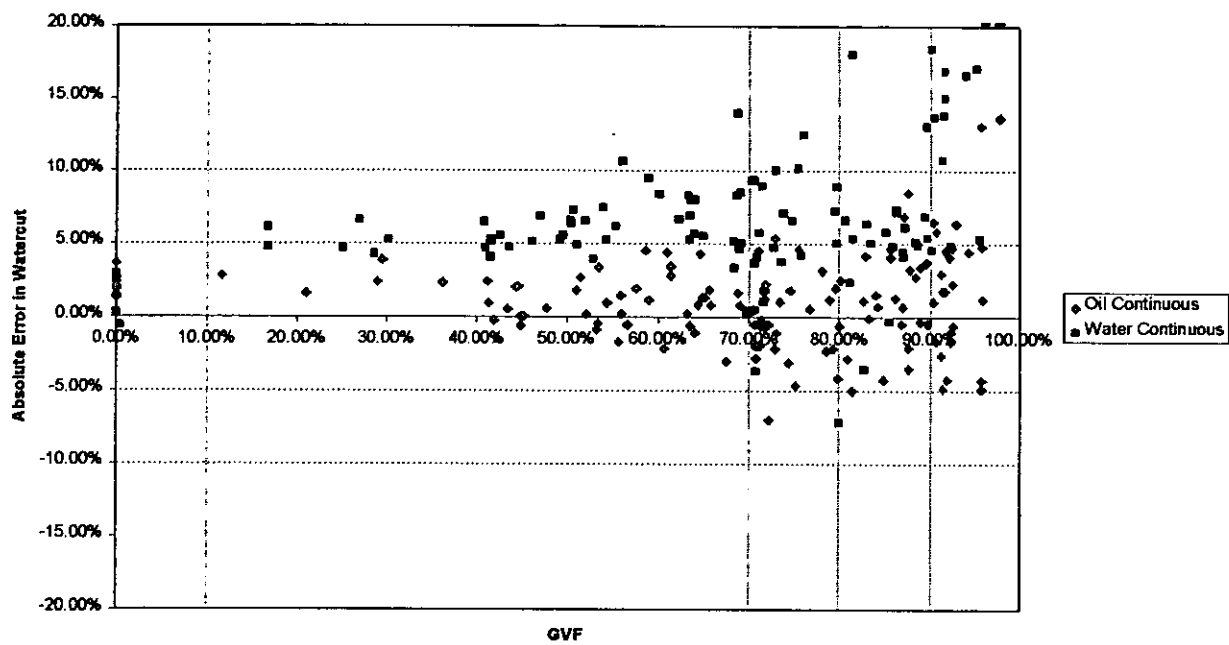


Figure 9: Influence of GVF on Watercut Error

THE IMPORTANCE OF CALCULATING RESULTING PERMITTIVITY AND CONDUCTIVITY IN MIXTURES OF TWO LIQUIDS

Erling A. Hammer, Jarle Tollefsen and Emil Cimpan. University of Bergen, Norway

Summary

Calculation of resulting permittivity and conductivity in mixtures of two liquid components is important for reliable use of capacitance and micro-wave sensors for concentration measurement in mixtures. Especially, in three component flows (e.g. crude/water/gas), a reliable model is necessary for accurate determination of the different component concentrations. There do exist many formulae worked out by i.e. Maxwell (1873), Fricke (1924), Bruggeman (1935), Sillars (1937) and Van Beek (1967), Ramo and Rau (1973) and Hammer (1983) and many other but non of them have shown to be reliable when the continuous component is electrically conducting. A homogeneous mixture of saline water (5 S/m) and crude oil from the Gullfax field has been measured at different frequencies in a homogeneous electric field (Specially designed test cell) with water fractions of 0 - 100% and compared with the results calculated by the different existing formulae. A numerical model has also been developed and data simulations show that the droplet size does not influence on the permittivity of the mixture.

This work shows that Bruggeman's formula for permittivity in two component mixtures agrees best with the eksperimental results on a mixture of crude oil and saline water.

1. INTRODUCTION

Capacitance and microwave transducers are commonly used in multi-component flowmeters to determine the fraction of process water in crude oil/water mixtures. Reliable results are dependent on accurate mathematical models of permittivities in multi-component mixtures. Many models have been developed but they give different results and modification based on empirical data has ben necessary to obtain the demand accuracy.

In this work we have developed a numerical model based on the finite element method and Laplace equation which we have used as the reference in our analyses of the existing formulae together with permittivity measurement on a mixture of Gullfax crude oil and saline water.

A special test cell for measuring the permittivity in mixtures of oil and water has ben developed for obtaining reliable experimental data.

2. SOME EXISTING FORMULAE FOR CALCULATING PERMITTIVITY AND CONDUCTIVITY IN TWO COMPONENT MIXTURES

In 1873 Maxwel [1] published a theory of calculating the permittivity of a mixture of two dielectric materials. He assumed small spheres of one material uniformly distributed in the other. He also assumed a homogeneous electrostatic field, constant diameter of the spheres and that this diameter was small compared with the distance between the spheres. Bruggeman [2] developed, in 1935, a model based on Maxwells theory in which the discontinuous component consisted of spheres of random diameter and distribution.

The Bruggeman's formula is:

$$\frac{\epsilon_2 - \epsilon_m \left(\frac{\epsilon_1}{\epsilon_m} \right)^{\frac{1}{3}}}{\epsilon_2 - \epsilon_1} = 1 - \beta \quad \{1\}$$

Where

ϵ_1 = relative permittivity of the continuous component

ϵ_2 = relative permittivity of the discontinuous component

ϵ_m = relative permittivity of the mixture

β = fraction of component 2

This model has shown to fit very well with experimental results up to 40% water cut and a modified version of this model has therefore been used in most of multi-component meters. This model can be used for mixtures of crude oil and process water. However, since the process water has a conductivity of approximately 5 S/m the water droplet acts as electrical short cuts, equivalent to put the permittivity of the water component (ϵ_2) equal to infinity, if the measurement frequency $f \ll f_d$, where $f_d = 1,3$ GHz is the dispersion frequency of process water.

By introducing $\epsilon_2 = \infty$, the Bruggeman formula then reduces to:

$$\epsilon_m = \frac{\epsilon_{oil}}{(1 - \beta)^3} \quad \{2\}$$

Where ϵ_{oil} is the relative permittivity of the oil.

Many others including Rayleigh [3], Wiener [4], Fricke [5], Sillars [6], van Beek [7] and Hammer [8] have developed formulae for calculating the permittivity and conductivity of mixtures of two different dielectrics.

Ramo and Rao [9] claim, however, that these formulae are inaccurate if one component of the mixture has a high conductivity as i.e. process water in crude oil. Based on a model developed by van Beek, Ramu and Rao have derived formulae which are also valid under such conditions. These formulae have been derived under the assumption that a number of small spheres (material 2) of radius r_2 , permittivity ϵ_2 and conductivity σ_2 are uniformly dispersed in a spherical medium (material 1) of radius r_1 , permittivity ϵ_1 and conductivity σ_1 which in turn is surrounded by continuum of material 1. It is further assumed that $r_1 \gg r_2$. The authors have found that these hold well in the case of low-loss liquid mixtures even if the volume fraction of the dispersed component is as high as 0.4 - 0.45. In the case of high-loss additives, they can only be used with reasonable accuracy when the volume fraction of the dispersed component is less than 0.2 - 0.25. For higher concentrations Ramu and Rao found a considerable difference between the predicted and experimental values. They assumed that this discrepancy was due to higher order interaction between the dispersed particles themselves and between the dispersed particles and the continuum.

These formulae are the only ones developed which can be used for any of the components as the continuous component and can therefore be used for calculation of the permittivity and conductivity of a mixture of oil and water with the water as the continuous component even at saline water with conductivity of 5 S/m (used as substitute for North Sea process water in the laboratory experiment).

For mixtures of oil and process water of $\sigma = 5 \text{ S/m}$, the Ramo and Rao's formulae can be written:

Oil continuous phase:

$$\epsilon_m^o = \epsilon_{oil} \frac{1 + 2\beta}{1 - \beta} \quad (3)$$

Water continuous phase:

$$\epsilon_m^w = \epsilon_w \frac{2\beta}{3 - \beta} \quad (4)$$

where ϵ_w is the relative permittivity of the process water.

3. THE NUMERICAL MODEL FOR CALCULATION OF PERMITTIVITIES AND CONDUCTIVITIES IN TWO COMPONENT MIXTURES

Our numerical model consists of a unit size parallel plate capacitance sensor equipped with sensor screen and guard electrode (Figure 1). The regime between the parallel plate electrodes is a two component mixture where the discontinuous component, i.e., the spheres, is uniformly distributed in the continuous component. The potential, electrical field, and capacitance are calculated by solving the Laplace equation using the Finite Element method (FEM).

Since FEM solves Laplace equation exactly, and thus takes the polarization effect into account, the calculated potential, electrical field distribution, capacitance and thus the permittivity of the homogeneous mixture should be reliable for the droplet distribution simulated. By using guard electrodes in the FEM-model the electrical field in the detector volume will not fringe and, hence, increase the accuracy of the calculations.

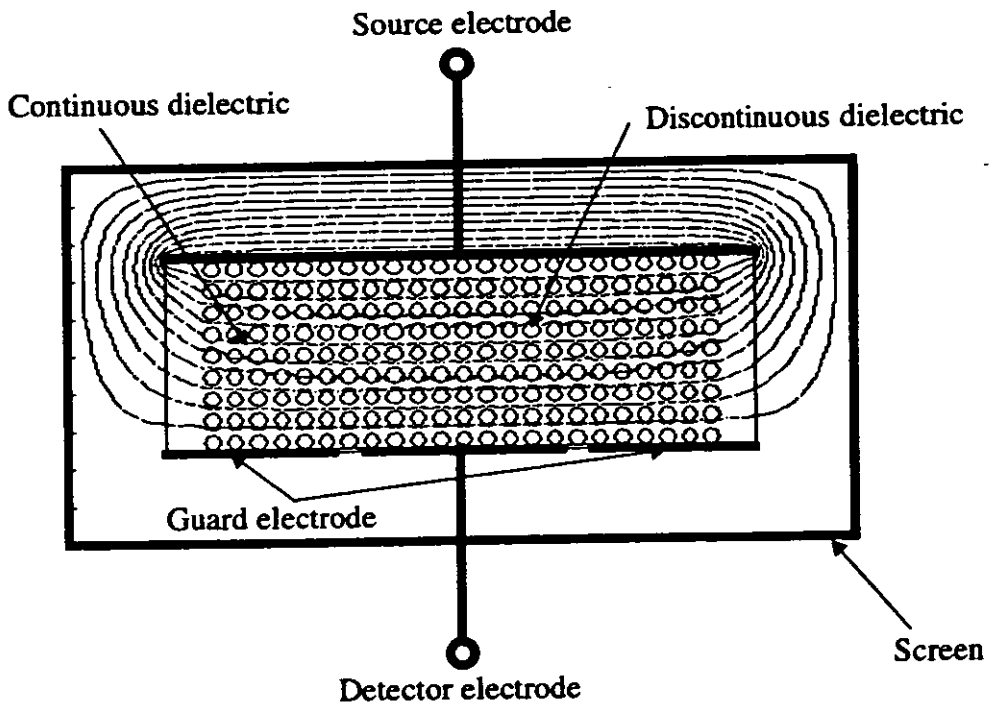


Figure 1. Sketch of the model used for the numerical calculation

4. THE TEST CELL

The test cell arrangement is shown in Figure 2. Two propellers keep the water and oil homogeneously mixed in the test cell.

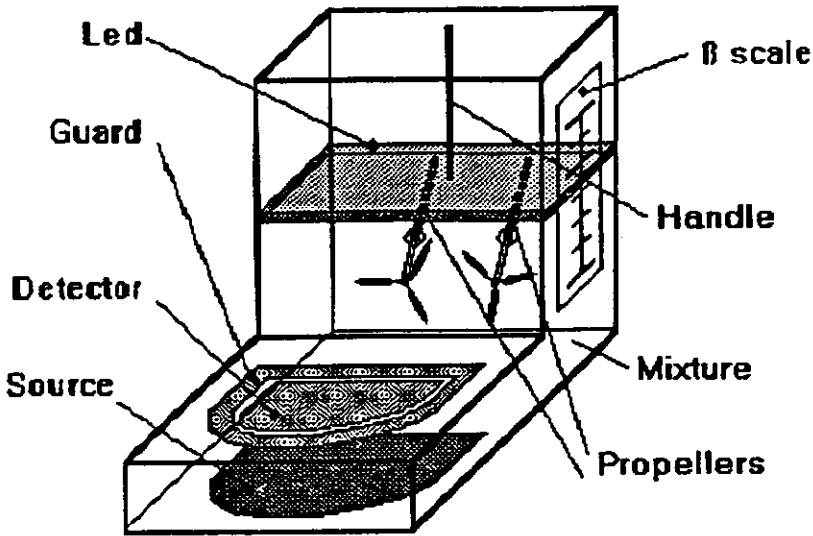


Figure 2. The test cell arrangement

The cell is equipped with a guard electrode surrounding the detector electrode in such a way that the electrostatic field in the measurement volume is kept homogeneous if the mixture is homogeneous. The capacitance and conductance between the electrodes are measured by HP - Impedance Analyzer

The equivalent diagram of this cell is shown in Figure 3.

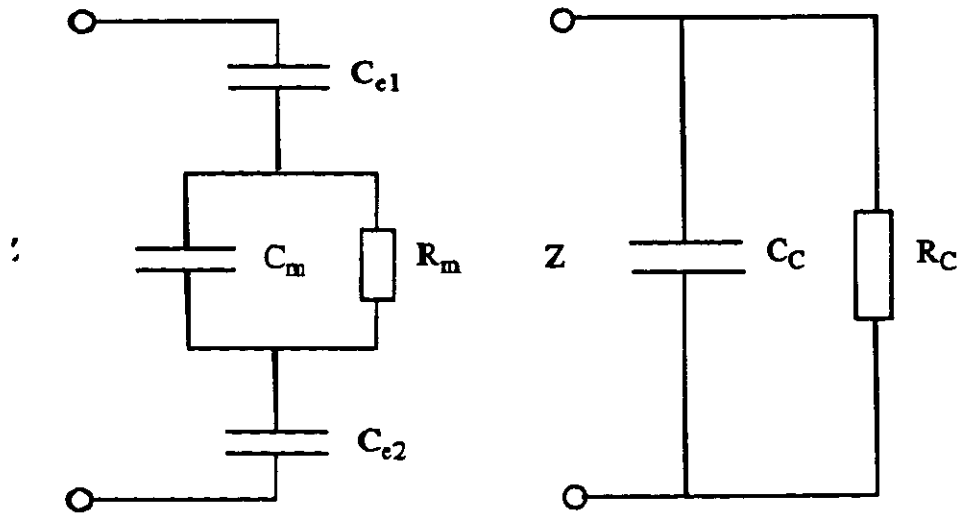


Figure 3. The equivalent diagram of the test cell.

Here C_c and R_c are the measured cell capacitance and resistance, C_{e1} and C_{e2} is the electrode capacitance, e. i. the capacitance between each electrode and the mixture with the electrode

insulation layer as dielectricum. C_m is the capacitance of the mixture and R_m is the resistance of the mixture between the detector electrode and source electrode.

5. CALCULATION OF THE MIXTURE PERMITTIVITY AND CONDUCTIVITY

To calculate the permittivity and conductivity of the mixture, C_m and R_m must be determined from the measurement of C_c and R_c according to the following formulae:

$$C_c = \frac{C_e \{1 + \omega^2 R_m^2 C_m (C_e + C_m)\}}{1 + \omega^2 R_m^2 (C_e + C_m)^2} \quad \{5\}$$

$$R_c = \frac{1 + \omega^2 R_m^2 (C_e + C_m)^2}{\omega^2 R_m C_e^2} \quad \{6\}$$

Where $\omega = 2\pi f$ is the angular frequency of the impedance analyzer and $C_e = 1/2C_{e1} = 1/2C_{e2}$

It is important to be aware of that at oil-continuous phase, R_m is high due to low conductivity in crude oils and if the detector frequency is low the polarization loss in the mixture is negligible. Thus $\omega^2 R_m^2 C_m^2 \gg 1$ and equations {5} and {6} will be reduced to:

$$C_c = \frac{C_e C_m}{C_e + C_m} \quad \{7\}$$

$$R_c = \frac{R_m (C_e + C_m)^2}{C_e^2} \quad \{8\}$$

This means that if the measurement frequency is low so the dielectric loss is low, the permittivity in the mixture will be frequency independent and also independent of the conductivity of the process water when the oil is the continuous phase in the mixture.

The permittivity and conductivity can then be found according to:

$$\epsilon_m = \frac{C_m d}{\epsilon_0 A} \quad \{9\}$$

$$\sigma_m = \frac{d}{R_m A} \quad \{10\}$$

Where d is the distance between the sell electrodes and A is the area of the detector electrode.

When water is the continuous phase the given inequality ($\omega^2 R_m^2 C_m^2 \gg 1$) is not valid and it can be seen that the measurement results will be dependent both on the frequency and the water conductivity.

6. THE CALCULATED AND EXPERIMENTAL RESULTS

6.1 The experimental results

The experimental results are given in Figure 4.

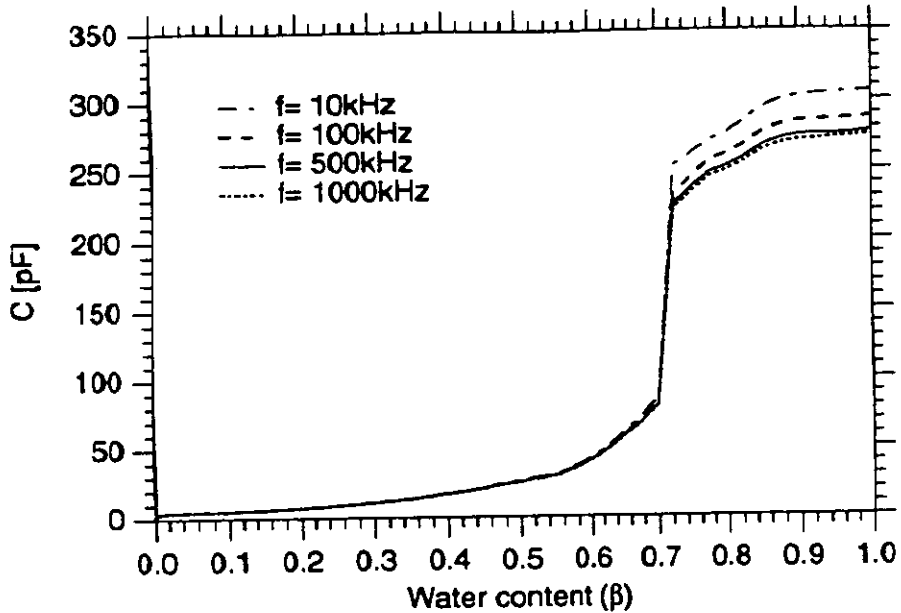


Figure 4. The capacitance of the test cell - homogeneous mixture of Gullfax crude oil and saline water (5 S/m)

The simulation results are shown in Figure 5. together with the result from Bruggeman's, Ramo & Raos', and Hammer's model. The permittivity ϵ_{oil} is 2.2 and ϵ_w is 71. The conductivity of the water σ_w is 5 S/m.

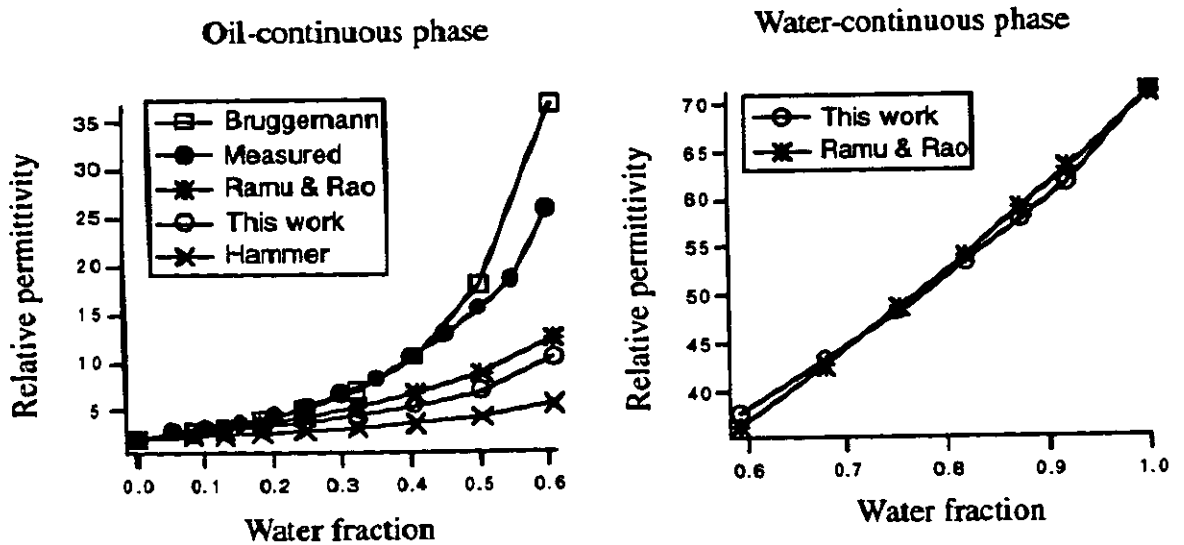


Figure 5. Permittivity of a homogenous mixture of crude oil and water (5 S/m) versus water concentration according to Bruggeman, Ramo & Rao, Hammer, measured capacitance of gull-fax crude and simulation results derived in this work.

Our numerical model also shows that the mixture capacitance is independent of the droplet diameter if the diameter is less than 1/5 of the width of the detector electrode.

7. CONCLUSIONS

From Figure 5 we can see that Bruggeman's formula gives the best result compared with the test cell measurements but even this formula must be modified for water fractions greater than 40%. All the other formulae under-estimate the mixture permittivity and so does our numerical model. The explanation of this is probably that both Ramo and Rao, Hammer and our numerical model are calculating the permittivity in mixtures where the discontinuous phase is arranged in columns between the sensor plates as shown in Figure 1. In a crude oil/process water mixtures the droplets will be randomly distributed resulting in an higher measured capacitance. Bruggeman's formula is based on random distributed diameters and position of the droplets in the mixture and gives therefore the most accurate result among all the existing formulae. Our numerical model must therefore be altered to generate random distributed droplets in the measurement volume.

Figure 4. shows that the capacitance of a mixture of crude oil and saline water is independent of the detector frequency when the mixture is oil continuous. It is also independent of the conductivity of the water component if the frequency is low ($f \ll f_d$) so that polarisation losses are negligible. Above the transition point we can see the frequency dependency and the result will also be dependent on the water salinity.

Figure 4. also shows that the measured capacitance is dependent on the water fraction β even at water-continuous phase. This dependency might be utilized to measure the water content in the mixture even at water-continuous phase but more experiments and analysis have to be done before anything can be said about the reliability.

REFERENCES

- [1] Maxwell, J.C. A Treatise on Electricity & Magnetism. The Clarendon Press, Oxford, Vol. 1, 1st edition, 1973
- [2] Bruggeman, D.A.G. Berechnung verschiedener physikalischer Konstanten von heterogenen Substanzen. Annalen der Physik. 5. Folge, Band 24, 1935.
- [3] Rayleigh, J.W.S.B. On the Influence of Obstacles in Rectangular Order Upon the Properties of a Medium. Phil. mag. 34, 481, 1982.
- [4] Wiener, O. Die Theorie des Mischkörpers für die Feld der Stationären Strömung. Abh. d. Sachs. Ges. d. Wiss., Math.-Phys. K1.32, p. 509, 1912.
- [5] Fricke, H. A Mathematical Treatment of electric Conductivity and Capacity of Disperse Systems. Phy. Rev. 24, p. 575, 1924.
- [6] Sillars, R.W. The Properties of a Dielectric containing semiconducting particles of various shapes. J. Inst.Elec. (Tokyo), Vol. 80, p. 378. 1937.
- [7] Van Beek, L. Dielectric Behaviour of Heterogeneous systems. Progress in Dielectrics, Vol. 7 (1967).
- [8] Hammer, E.A. Three-Component Flow Measurement in Oil/Gas/Water Mixtures using Capacitance Transducers. CMI-Report No. 831251-2, 1983.

- [9] Ramu, T.S., and Narayana Rao, Y. On the Evaluation of Conductivity of Mixtures of Liquid Dielectrics. IEEE Transactions on Electrical Insulation, Vol. EI-8, No. 2, June 1973.
- [10] Dykesteen, E.: "Permittivitet i væskeblandinger". CMI-Report No. 821251-2 1982.

REVIEW OF OPERATION OF ULTRASONIC TIME OF FLIGHT METERS

T. Cousins

Consultant SGS Redwood Technical Services

SUMMARY

The main objectives of this paper are to review Ultrasonic Time of Flight meter design concepts from a theoretical and practical view point. Reviewed are the basic equations used, a discussion of the signal detection problems, path formations and clamp-on meters and their limitations. The author also discusses some of his experiences with the practical operation of Ultrasonic meters, which while not necessarily directly in the oil and gas industry do highlight the practical difficulties of this type of metering.

1.0 INTRODUCTION

There are a number of very pertinent reasons for the current popularity of Ultrasonic Time of Flight techniques.

The technique in various forms can be used on both gases and liquids, and in some cases mixtures, dependant on their format and the transducer and signal processing design.

In general they present little or no obstruction to the flow

They can be insertion or under some circumstances clamp-on, non invasive meters.

They can be designed to a variety of specifications and costs, ie the small domestic gas meter costs around \$60 with a 2% of range performance, whereas a 12" multi-path Fiscal meter would cost approximately \$60000 with a 0.5% of actual flow performance.

Finally the meter physics is such that many improvements in Electronics, particularly speed and processing power impact the performance and cost.

The basic principle for all of the meters described are basically the same, the modification of the time of flight of Ultrasound by the fluid velocity, along the line of the flight path.

2.0 BASIC PRINCIPLES

The ultrasound is usually generated by piezoelectric transducers. The crystals change size when an alternating voltage is applied to the terminal of the piezo material causing it to vibrate at the same frequency as the applied voltage. This produces longitudinal pressure waves in the adjoining fluid. A similar device when subjected to pressure waves has the reverse effect, in that it produces a voltage at the terminals of the piezo material.

The transducers are placed opposite each other, usually but not always, at an angle to the flow, Fig 1.

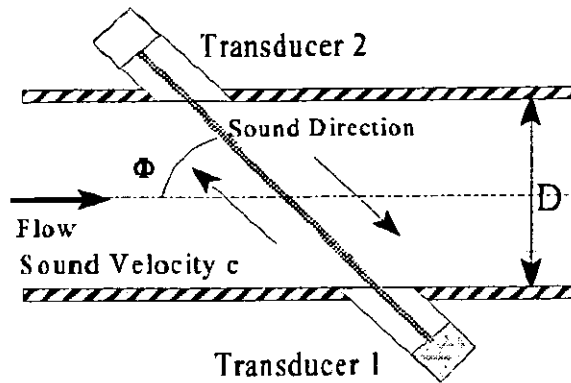


Fig.1 Time of Flight Set-up

The propagation velocity is the sum of the sound velocity, c , and the fluid velocity component in the direction of the transmission path, $v\cos\phi = c \pm v\cos\phi$

The time taken for the sound to travel from one transducer to the other depends therefore on the direction of transmission and fluid velocity and is given by :-

$$T_{12} = \frac{D}{\sin\phi(c - v\cos\phi)}$$

$$T_{21} = \frac{D}{\sin\phi(c + v\cos\phi)}$$

These two basic equations are used in a number of ways to obtain a fluid velocity that is independent of sound velocity.

2.1 SING AROUND (PULSE REPETITION)

This method was used for many years as a way of getting around the problem of the need for high resolution, nanosecond, timing. The basic equations when inverted, form a frequency, that is practically obtained by firing sound from one transducer to the other. When received another pulse is fired, and eventually a repetition frequency is obtained. This is repeated in the opposite direction and in theory the difference in frequency is directly proportional to the fluid velocity. This method is generally not used as the equation should also include the time delay for non-wetted parts and the associated electronics which becomes more significant as the flowrate decreases, causing a large zero offset. For direct timing methods this can be effectively removed.

2.2 DIRECT TIMING

The most common method now is to use direct timing. There are several variations of the above equation that can give flow velocity.

The two most usual forms are :-

$$\frac{1}{T_{12}} - \frac{1}{T_{21}} = \frac{2v \sin \phi \cos \phi}{D}$$

and

$$\frac{\Delta T}{T_{12} T_{21}} = \frac{2v \sin \phi \cos \phi}{D}$$

There are a number of other versions, but these generally contain the velocity of sound, which has to then be removed by some other measurement. **The above equations are essentially independent of velocity of sound, providing that the sound does not change during the flight in both directions.** This usually leads to designs in which the sound is transmitted in both directions at the same time. In both of the above equations the transit time has to be measured, and in the second equation the time difference also has to be calculated.

2.3 PHASE DIFFERENCE METHODS

Phase difference methods are less common than transit time, however there are a number of meters using this method of timing, particularly for "clamp-on" meter design. Instead of direct measurement of the transit time the phase angle of two continuous wave signals is determined. Usually to reduce the power consumption, rather than a continuous wave, packets of continuous wave signals are transmitted and the phase shift measured. In general with this method, the distortion of the signal during transmission is not as important as for the flight time methods, this can be an advantage for clamp-on meters. The measurement method is however fundamentally analogue and is dependant on the velocity of sound, which must be compensated for in the final calculation.

A variant of this type involves keeping the phase constant and vary the frequency, making measurement easier, however, again the velocity of sound of the fluid at rest is required to ensure that the output is directly proportional to fluid velocity.

3.0 SIGNAL DETECTION

The major error in timing derives from detecting the received signal. The transmitted pulse changes its form from the time the electronic pulse is converted into a mechanical pulse in the piezo-crystal. By the time it has reached the receiver it has become a series of pulses, ringing at the resonant frequency of the mechanical system comprising the transducer, its housing and the surrounding fluid, Fig. 2. The envelope of the signal is dependent on the properties and

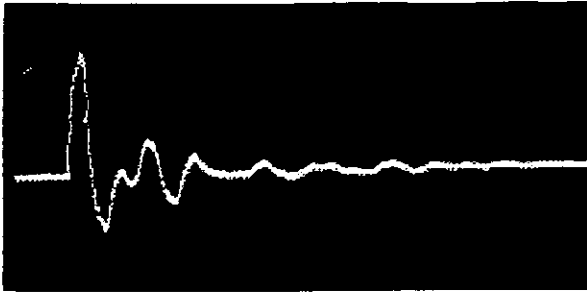


Fig.2a Transmitter Signal

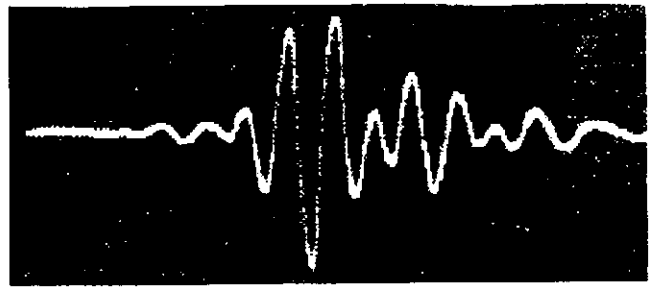


Fig.2b Receiver Signal

acoustic coupling of the various interfaces the signal passes through, as well as the design of the transducers. Generally to retain the shape of the signal the transducer design should have a wide band flat frequency response, as opposed to a high Q, resonant structure. The downside of this design criterion is the loss mechanical signal gain, requiring higher power electronics.

The signal can be regarded as a gating mechanism to start and stop a timer. Obviously, therefore the rise time and consistency of the transmit and received pulses is essential to the accuracy of the meter. The essential point of the received signal is the very start of the envelope. If the resonant frequency is, for example, 1MHz and if the measurement was out by half a cycle then the measurement error would be 500ns before any other errors are taken into account. It is, therefore, in the detection and correct identification of the received signal that much of the design work has progressed.

The design and connection of the transducers is critical to the signal quality, and hence the timing. As a rule, transducers for liquid measurement are operated at a higher frequency than for gases. Around 1MHz for liquid and 100KHz for gases, due largely to the impedance matching problems between gas and the transducers. An advantage of lower frequency operation is that the sound will go through most mediums, whereas the higher frequency signal is severely attenuated by gases. To protect the transducers they are normally potted, and often have a protective stainless steel or titanium cover over the face. Often mechanical amplification is used, such as quarter wavelength resonators, to enhance the signal.

The materials and design used are critical in a number of ways :-

They have to be compatible with the process fluid if wetted. There have been many instances where potted transducers have "dissolved" due to the chemical content of the process fluid. Thus much effort is being put into the development of inert potting materials with the appropriate acoustic properties

An obvious solution is to protect the potting with a material such as stainless steel, this presents two problems, the signal is additionally attenuated and there is always the possibility of the metal diaphragm separating from the potting under the action of temperature changes and the movement of transducers.

The identity and quality of the received signal is very dependant on the stability of the materials used in the transducers. In most cases the action of temperature changes is to change the acoustic properties of the material and the boundaries. To a degree the problem is temperature range, rather than absolute temperature.

One immediate source of error that can be removed is sound either travelling around the pipe,

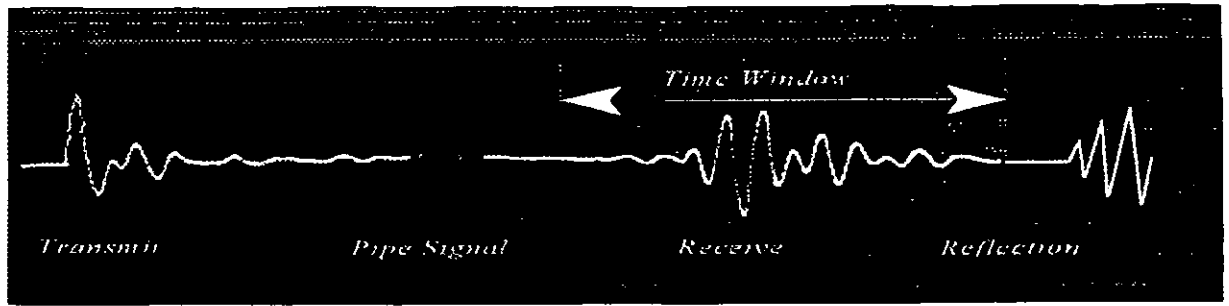


Fig.3 Signal Window

or being reflected in the pipe. This is carried out by ensuring that the receiver only scans the data within an expected time window, Fig. 3.

Correct matching of cable impedances and lengths also contributes toward improved performance.

The received signal is very low amplitude and in many cases buried in surrounding noise. Picking out the signal has produced a number of solutions. Essentially the requirement is to be able to ensure that the signal has as little distortion as possible, so that a position, cross-over point or relative amplitude can be chosen that has a fixed relation to the initial received signal point. The methods are either to set an acceptable trigger level and time from the first zero crossing point, or more successfully to choose a series of zero-crossing points on the most stable part of the signal, determine the period and work back to the first crossing. The alternative is to autocorrelate a burst of transmitted signal with it's received signal, and determine the time delay corresponding to the peak of the correlation function. Another method is to ensure that the shape of the received pulse is as stable and identifiable as possible. By careful design and using digital processing techniques this a very successful and reliable method, particularly using digital fingerprinting.

3.1 CLAMP -ON METERS

Obviously from the forgoing it would be expected that the problems of signal detection are made more difficult when transmitting and receiving the signal through a pipe wall. As one of the main features of a clamp-on system is that there is no requirement to cut the pipe to install the meter, the signal is bound by the vagaries of the pipe wall, its material, composition and any material forming on the inside. As the sound is transmitted it undergoes a series of reflections and refractions, shown at its simplest in Fig.4.

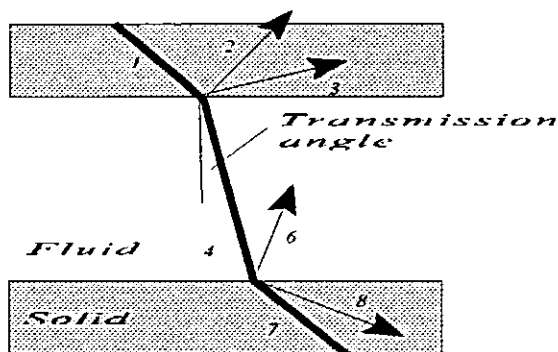


Fig.4 Sound Transmission Through Walls

The diagram describes the path of the signal for a single phase thick walled pipe material. Thin materials for pipe walls may cause waves to form in the pipe walls in plate mode, and longitudinal waves are produced in the fluid. The walls appear transparent to the sound. In the majority of cases the pipe wall is thick walled, and using Snell's law the maximum angle of transmission for different combinations of pipe and fluid materials can be obtained. Typically for stainless steel and water this will be 14.5° for longitudinal waves and 27° for transverse waves. These angles clearly limit the sensitivity of the transit time of flight meter, as the flight time equations show that the difference increases with increased angle. There is therefore often a higher minimum velocity than for wetted transducer meters.

A further problem results from the nature of the pipe material. Many materials attenuate the ultrasonic signal. Further, often there are layers of material that ensure that the signal is either heavily attenuated or is totally reflected.

4.0 VELOCITY MEASUREMENT

Much has been written about the way in which time of flight meters interpret the velocity along the path of transmission, and how this can be developed to produce a volume flow measuring device. In this paper the concepts will only be touched on as a guide to what is possible for practical measurement.

Essentially the final velocity determined along the path of the sound is a line integral of the varying velocities along that path. The beam width will obviously have some influence on the value of the velocities that go towards this final velocity Fig.5.

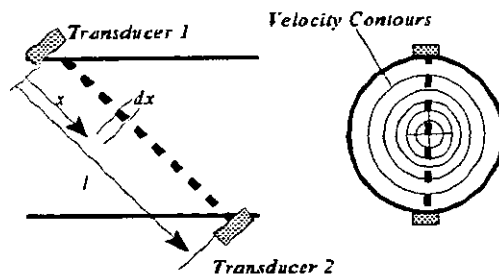


Fig.5 Velocity Averaging

The total transit time is given by :-

$$T_{12} = \int_0^l \frac{dx}{c+v(x)} = \frac{l}{c} \left(1 - \frac{v_{mean}}{c}\right)$$

Where v_{mean} is the average velocity in the direction of the beam along its length. This is not the same as the mean velocity over the complete volume. If as is common place the beam is fired across the centreline then the resultant velocity is weighted towards the centreline, and so reads high, relative to the volume weighted mean velocity. It can be shown theoretically that for a laminar flow the ratio of the ultrasonic mean velocity to the volume weighted mean is 1.33, that is it reads 33% high. For turbulent profiles it is approximately 1.05, that is 5% high dependant

on the profile. It can be shown that is of the order of 1% change per decade in the Reynolds number range of 10^3 to 10^6 .

The implications of this are that the single path meter is not only installation dependant but has to be corrected for profile under ideal conditions if a reasonable level of uncertainty is to be maintained. The possible effect of installation is admirably demonstrated by the use of an eccentric orifice as the flow disturber, Fig .6. The effect on the calibration depends on the plane of the beam relative to the profile.

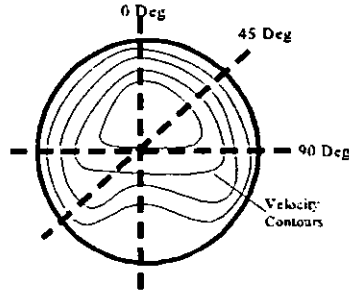


Fig.6 Path Positions

The changes in reading from the calibration under fully developed flow conditions are:-

0°	-----	16.3%
45°	-----	10.3%
90°	-----	5.2%

Detailed data is available for different combinations of installations in the list of references. The point at issue is that for single path meters, care must be taken with installation in relation to the fittings, further for gas measurement where the pipe is large it is common practice to fire the sound across an offset chord. There is data for the effect of installation on this method, but it is not as well documented as the centreline chord.

One method available to alleviate the effect of swirl flow is to reflect the signal from the opposite wall, the effect of rotational flow on the initial path is largely cancelled out on the reflected path. **The effect of distorted flow profile is not however removed.**

4.1 MULTI-PATH METERS

As with single path meters there are now a very detailed papers describing the basic concepts of the various multi-path meters. It is interesting that much of the basic data has been available for many years, the Westinghouse multi-path meter was successfully tested in 1970, and shown to have considerable benefits with regard to installation. Only in the last 10 years has technology caught up enough to make such meters a viable proposition.

There are currently two methods employed which take a fundamentally different approach to the problem of multi-path metering, both are shown in Fig.7. The more conventional approach is to use chordal paths, the positions of which are either obtained by experiment or by giving weighting factors to the various paths using a numerical quadrature method to obtain the least variation of calibration for a number of theoretical profiles. The other method is to use a series of paths, which by a combination of reflections can determine individual features of the flow.

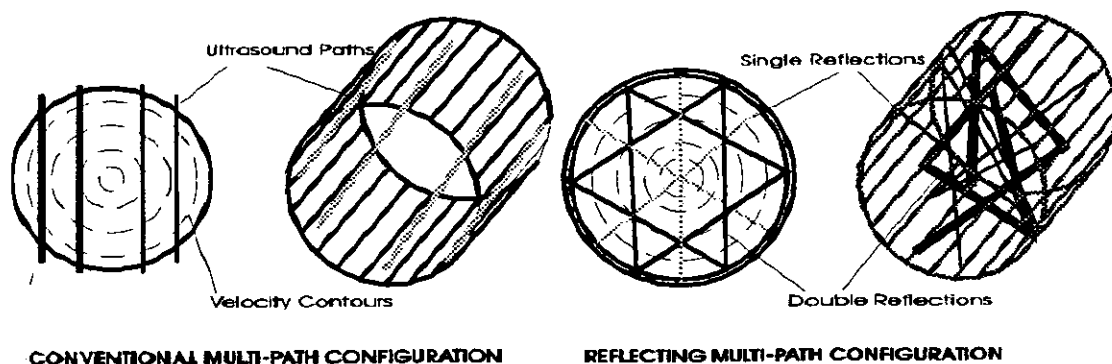


Fig. 7 Different Types of Multi-Path Configurations

For example the degree of swirl and the asymmetry can be estimated as a contribution towards the final answer.

Both methods have currently have their advantages and disadvantages:-

Method	Advantages	Disadvantages
Chordal	<p>The information Required about the flow profile is fixed</p> <p>The weighting factors are fixed, reducing the computational requirements</p> <p>A loss of a path is easier to compensate for</p>	<p>The flow velocity is assumed as axisymmetric</p> <p>Additional information with regard to the flow is lost</p> <p>As the profile deviates from the theoretical errors occur</p>
Reflecting	<p>The close spacing of the paths gives high cross sectional coverage</p> <p>Measurement is insensitive to orientation for single phase fluids</p> <p>Paths are generally longer making timing resolution better</p> <p>More detailed data available for assessing the meter uncertainty</p>	<p>Much harder to manufacture</p> <p>Needs continuous update of algorithms for flow computation</p> <p>At present loss of certain paths causes larger uncertainties</p> <p>Concern over the reflection remaining stable in operation</p>

In the following papers there will be a large amount of data provided on both meters for gas measurement. It is not clear whether it is possible to use reflecting methods for liquids successfully, as the acoustic mis-match between the liquid and the wall is generally low, thus reducing the reflectivity of the signal. Data shows that for small liquid meters there is an optimum design of two path-chordal meter, that significantly reduces the effect of installation, although such a meter would struggle to meet fiscal levels of metering.

It worth making the point that the multi-path meters do have the possibility, particularly the reflecting path meters, of being true "smart" meters. It is feasible that in combination with such technology as neural networks that the meters can start to learn about the flow and improve with time. Further it very feasible to produce a meter that can give a good running estimate of its own uncertainty.

5.0 SOME PRACTICAL OPERATIONAL ASPECTS

The comments in this section are divided into application areas, with some notes from the authors experience on possible problems.

5.1 CLAMP-ON METERS

As previously described, clamp-on meters are generally used for liquid measurement either as a permanent installation or as a check meter.

Recently the author performed a series of eight meter checks of magnetic flow meter installations using a commercial clamp-on meter. It is probably one of the best designs, but of the eight installations only three worked fully and one intermittently. Two that worked well were with single phase plastic and the other a new steel pipe. An old cast iron pipe gave some results after thorough cleaning of the outer surfaces. The other pipes, multi-phase pipes with a liner and possibly internal build-up gave no results at all. The software was designed to cope with multi-phase materials, but no signal was ever found. Where results were obtained the best correlation obtained was of the order of 5%, with the magnetic flow meters. The errors in measurement of this type are very clear, the major uncertainty is usually the pipe diameter, which doubles when applied to volume. Practically, particularly within the confined spaces often available installation of the clamp-on meter is difficult to achieve with any degree of accuracy, in fact it was almost impossible to install single handed, with the problems of putting on the acoustic couplant, lining up the transducers and tightening them up.

With permanent installations life is marginally easier, as you can generally get someone else to install it. There are still a number of points of which to be aware :-

Always check the sound will go through the pipe walls and fluid before purchasing.

Do not assume that two nominally similar installations will work

Check that during operation the acoustic couplant does not deteriorate with time

For an uncalibrated installation the diameter of the calibration section can represent a large error

All of the above the author has encountered in recent audits of clamp-on installations. There is also a temptation, because of the theoretical ease of installation to mount the meters without regard to flow profile.

The uncertainty of clamp-on meters can be improved by on-site calibration, although for single path meters the calibration should be over the operational range. Under such circumstances the good repeatability of the meters will give favourable results.

5.2 FLARE/ FLUE GAS METERS

The ultrasonic time of flight meter is almost the only meter capable of reliably metering Flare gas, there are however several problems encountered by the author for which potential users should be aware. Generally the gas for Flares is operating at a relatively low pressure. It becomes more difficult to send sound into the gas as the pressure reduces. This can be made worse if there is a large quantity of Carbon Dioxide present which attenuates signal. In several cases investigated by the author the presence of CO₂, has effectively killed the application. Sometimes it is possible to reduce the distance between the transducers by inserting them into

the flow. This is done, however, at the cost of uncertainty, as the knowledge of the relationship between the path velocity and the fluid velocity is often unknown. A further problem encountered is the presence of noise. This is a problem throughout Ultrasonic metering, particularly noise produced by fittings, such as pressure reducer valves that is in the frequency range of the transmitted ultrasound. This can effectively "kill" the received signal.

5.3 LIQUID METERS

In general high performance liquid meters have taken longer to achieve their full potential than Gas meters. This is due probably to the operational problems encountered when moving away from water measurement. Water is a relatively continuous medium, and does not in general carry gas, air, mixed in the fluid for very great distances. Oil on the other hand does form easily into emulsions of gas and liquid, which are almost impenetrable to sound. It has been the authors experience that the most destructive mixture of gas and liquid is the presence of continuous small particles of gas, causing "Rayleigh" scattering.

5.4 REFERENCES

a Paper

- 1 Cousins. T and Huisman F. The Effect of Different Path Configurations on Ultrasonic Flow Measurement. North Sea Workshop 1994
- 2 Lynnworth L.C. Ultrasonic Flowmeters Physical Acoustics Vol. 14.
- 3 Sanderson M.L & Hemp J. Ultrasonic Flowmeters a Review of the State of the Art. Advances in Flow Measurement Techniques Warwick University 1981.
- 4 Cranfield University Flow Measurement Lectures

ULTRASONIC METERING ON AN OFFSHORE GAS PLATFORM

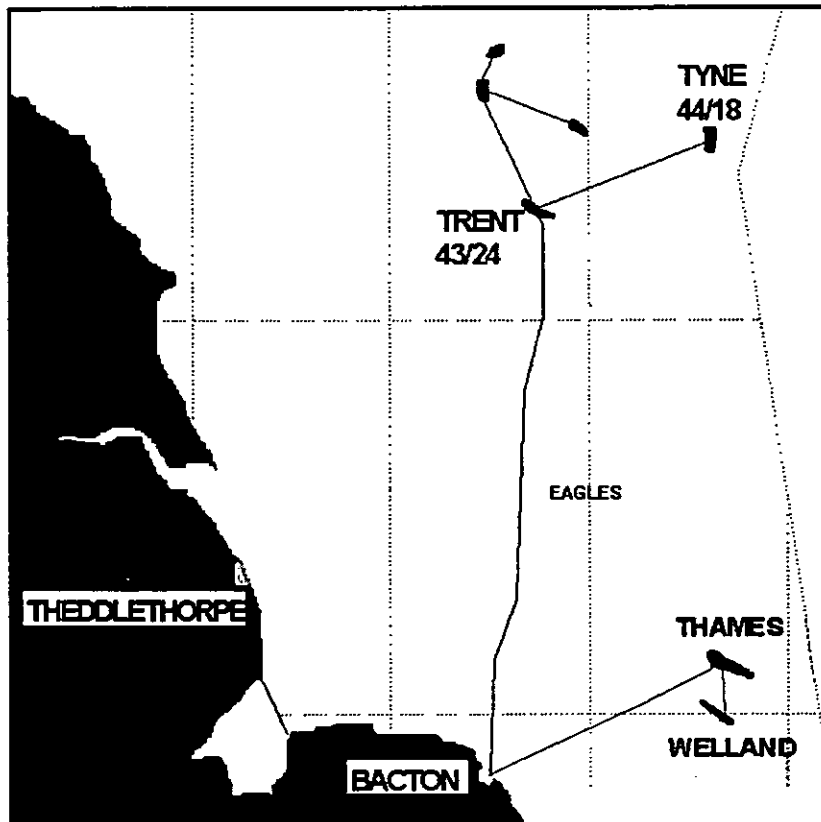
Phil Robbins

Metering & Allocation Supervisor
ARCO British Limited

1.0 Summary

A trial was conducted on the ARCO British Limited (ABL) operated Thames Alpha gas gathering platform to evaluate the accuracy and performance of a multi-path USM (UltraSonic Meter) downstream of a production separator and in series with a orifice plate metering station. Throughout the trial the test meter performed without failures of any kind and demonstrated a very high degree of accuracy and repeatability.

The success of this trial has permitted the use of USM's on two new ABL operated platforms, Trent & Tyne, that are due on stream during September 1996.



Glossary of Terms

USM	Ultrasonic Meter - In this case the multipath ultrasonic meter manufactured by Instromet Ultrasonics bv.
ABL	ARCO British Limited
MAG	ABL Metering and Allocation Group based at Gt Yarmouth.
AGA-8	American Gas Association Transmission Measurement Committee Report Number 8, for the determination of Compressibility and Supercompressibility for Natural Gas and other Hydrocarbon Gases.
S500	Spectra-Tek Limited flow computer for USM's
S1000	Spectra-Tek Limited metering database.
SCI	Rosemount Supervisory Computer Interface
PCS	Rosemount Production Control System - Series 3
EAGLES	East Anglian Gas & Liquid Evacuation System
Swirl Path	Double bounce ultrasonic path unique to the Instromet Q-Sonic USM
Single Path	Single bounce ultrasonic path unique to the Instromet Q-Sonic USM
Msm3	One Million Standard Cubic Meters
mmscf	One Million Standard Cubic Feet

2.0 Introduction

This report details the USM trial conducted on the Thames platform. *(Please note that at the beginning of the trial the meter manufacturer was Stork Servex b.v. however during the course of the trial the company has changed names and is now known as Instromet Ultrasonic Technologies)*

During the design phase of the Trent and Tyne platforms it became apparent that technology had progressed enough to enable ultrasonic metering (USM) to bid alongside more traditional orifice plate metering systems and that USM met fully the high accuracy needs of allocation metering.

Indeed, the benefits of USM soon became so obvious that, unless contractually instructed to use orifice plate metering, ARCO would not have been acting as a reasonable and prudent operator if it had not have chosen USM. The cost savings to ARCO and its partners in providing a far more compact metering station that would require far less maintenance over its orifice plate counterpart fully justified the decision to choose USM. Coupled with the superior diagnostics of the

USM, that allows for remote (from the beach) interrogation of the meters to monitor performance and reliability, and the option of being able to have the whole meter sent away and check calibrated by an internationally traceable test centre all adds to the "feel-good" comfort factor that USM provides over orifice plate metering.

As part of the Trent & Tyne DTI design approval process, the ARCO Metering & Allocation Group (MAG) have purchase a 12" Instromet Q-Sonic 5-path ultrasonic meter in advance of Trent & Tyne coming on line and placed it in series with an existing orifice plate metering station on the ARCO Thames Alpha platform (downstream of the production separator and upstream of the orifice plate metering station). This meter has provided MAG with valuable information as to how USM's perform in an offshore environment and, perhaps more importantly, how USM's compare with a traditional orifice plate metering system.

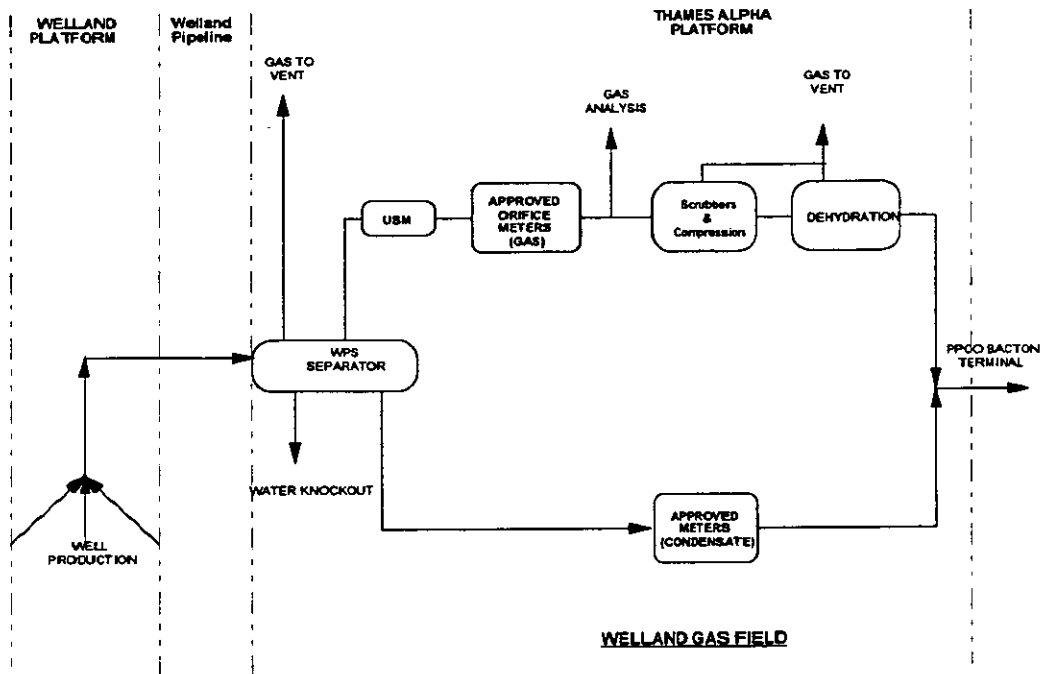
3.0 Trial Programme on Thames.

(Comparison of USM's against orifice plate meters.)

The measurement philosophy for the Trent and Tyne Fields Development specifies the use of multi-path ultrasonic flow meters for the gas allocation measurement. As yet this technology is relatively untried to the standard required for fiscal or allocation gas measurement, particularly in the UK sector of the offshore oil & gas industry. *(However, NMI and PTB approval for the meter has been received for custody transfer metering).* A 12" multi-path ultrasonic meter was installed on the Thames Alpha Platform on the Welland Pipeline System reception metering station to carry out accuracy tests in comparison with an existing fiscal standard, gas orifice measurement station which was designed and is operated in accordance with Dept. Trade & Industry guidelines and ISO 5167. The only departure from ISO 5167 being that for the use of orifice plates with drain holes.

The Thames Alpha platform is located in block 49/28 of the North Sea and the Welland platform in block 53/4a. The not-normally-manned Welland platform exports it's gas and liquids via the Welland Pipeline System (16" diameter, 17.5 km) to the Thames Alpha platform for minimal processing, metering, compression & dehydration before entering the Thames Pipeline System for transportation to the Phillips Petroleum Company (PPCO) operated terminal at Bacton in Norfolk.

(Fig 1) A process schematic of the Welland gas from well extraction to import at the PPCo terminal.



The process conditions experienced throughout the trial were as follows:

Typical Gas Composition

N ₂	4.49 %	Max pressure	90 barG
CO ₂	0.48 %	Min pressure	22 barG
C1	90.21 %	Max temperature	20 degC
C2	3.34 %	Min temperature	8 degC
C3	0.83 %		
C4	0.35 %		
C5	0.12 %		
C6	0.18 %		

Typical water to gas (WGR) and condensate to gas (CGR) ratios pre-separation are as follows:-

WGR	7092 kg/Msm ³	1.24 BBLs/mmscf
CGR	7489 Litres/Msm ³	1.31 BBLs/mmscf

Furthermore, an analysis was carried out of the gas at the conditions prevailing at the gas chromatograph 1st stage let down to determine the amount of water vapour present in the flowing gas. The quantity of water in flowing gas was then calculated. The results were 2150 kg/Msm³ or 0.38 BBLs/mmscf.

The tests carried out have allowed comparison of the different measurement techniques under a wide range of flow conditions. Additional tests provided information on the meter's operation in the event of process problems and instrument failures, specific to the operation of ultrasonic meters.

The tests can be broken down to four distinct parts; onshore calibration, offshore accuracy monitoring, offshore operational checks and an additional post test program.

The meter under test was a 12" Instromet Ultrasonic Technologies Q.Sonic 5-path ultrasonic flow meter. This has been installed in series with the Welland Pipeline System (WPS) metering station located on the Thames Alpha platform. The meter was installed on the 18th September 1995 after onshore calibration of the meter took place at Ruhrgas's test centre in Dorsten - Germany on the 11th September 1995.

Due to initial commissioning problems encountered with the flow computer and coupled with an extended period of zero nominations from the buyer of the gas, the trial did not formally commence until the 5th November 1995.

Because this technology is relatively untried in high accuracy gas measurement applications, there are no recognised standards or guide-lines to assist in the installation and operation of meters of this type. Arco British Ltd have prepared a guide-line to the installation and operation of multi-path ultrasonic flow meters. The tests have been set up in accordance with the methods detailed in this document.

3.1 Onshore Tests

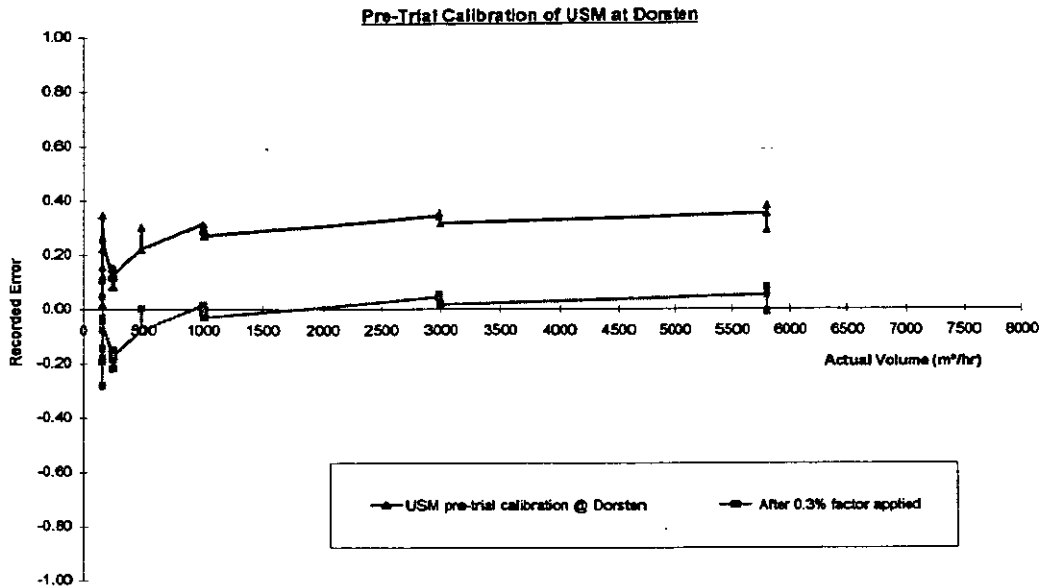
Prior to the meter being installed on Thames platform, it was calibrated and tested at an approved onshore test facility. The calibration was carried out at six flow rates with process conditions of 50.6 barA and 14.8 degC. At the two lowest flowrates (160 & 250m³/hr) six repeat runs were performed and for all other flowrates only three repeat runs were performed.

The results of the pre-trial calibration can be viewed in Figure 2. As can be seen the repeatability and accuracy of the meter was well within the manufacturer's stated limits.

After the meter had been calibrated across its flow range, one of the transducers located in a single path and one located in a swirl path

were swapped around. The calibration run was then repeated at two of the flowrates, 160 & 1000m³/hr. Three repeat runs were carried out at these two flowrates and no shift in accuracy could be detected.

(Fig 2) Pre trial calibration at Dorsten

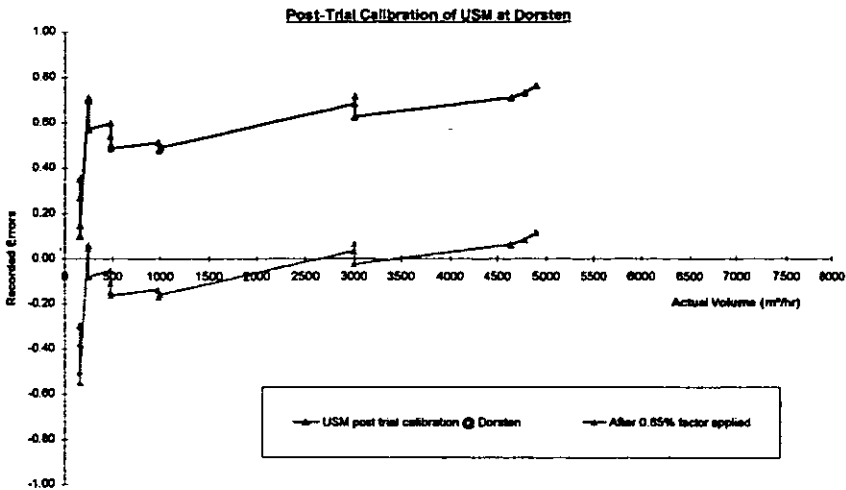


The post trial calibration at Dorsten in Germany was intended to evaluate whether there was any potential long term drift in the accuracy of the meter. The meter was removed from the platform during our annual shutdown. Strict instructions were issued to ensure that, under no circumstance were the transducers to be removed or touched in any way.

To my surprise, when I arrived in Germany with Instromet to witness the re-calibration, we found that every transducer cable had been cut. To make matters worse, the cables had been cut at the point of entry to the transducer housing.

To try to rescue this part of the trial, the transducers were carefully labelled to ensure that a record of which slot and what orientation each were in. Instromet then manufactured some special new glands and repaired the transducers. The transducers were then refitted to the spool piece and the re-calibration was conducted on the 23rd July 1996. (Instromet confirmed that as a result of the repairs no effect on the accuracy would be detected.) The subsequent calibration results were obtained. - see figure 3.

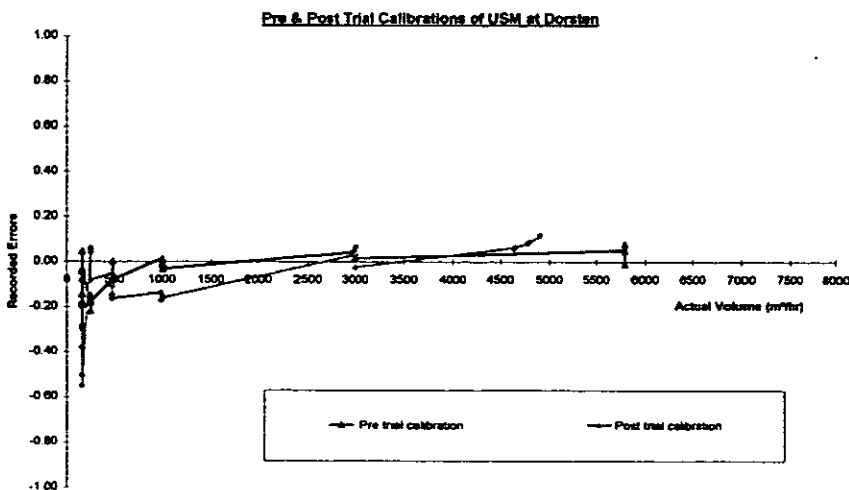
(Fig 3) Post trial calibration at Dorsten.



As can be seen, there is an approximated shift of + 0.35% from the original calibration carried out during September 1995. Whilst this size of shift is still within the design accuracy of the meter, it remains to be seen whether the shift is systematic or random. After discussions with the manufacturer, it would appear that this size of shift is not uncommon, however, in their experience, the shift can be positive or negative.

Obviously, with the data available to date, I cannot justify not sending the meters away for re-calibration on an annual basis. Only by monitoring the result of repeat calibration over the next year or two can we confirm the need or otherwise of annual calibrations.

(Fig 4) Pre & Post trial calibrations at Dorsten combined.



3.2 Offshore Installation of Trial Meter

The meter was installed on Thames platform, upstream of the WPS fiscal metering station. The installation was carried out in accordance with the ARCO British Ltd "Code of Practice for Multi-Path Ultrasonic Flow Meters", Revision 1 May 1995. A copy of which has been submitted to the BSI panel on Ultrasonic Flowmeters [CPL'30'S'1].

The meter run consists of a straight pipe length for 10 diameters upstream and 5 diameters downstream of the meter spool the pressure measurement instrument installed and a further 1 diameter downstream the temperature element was installed. The pipework was not lagged. See Appendix A3 for detailed pipework configuration.

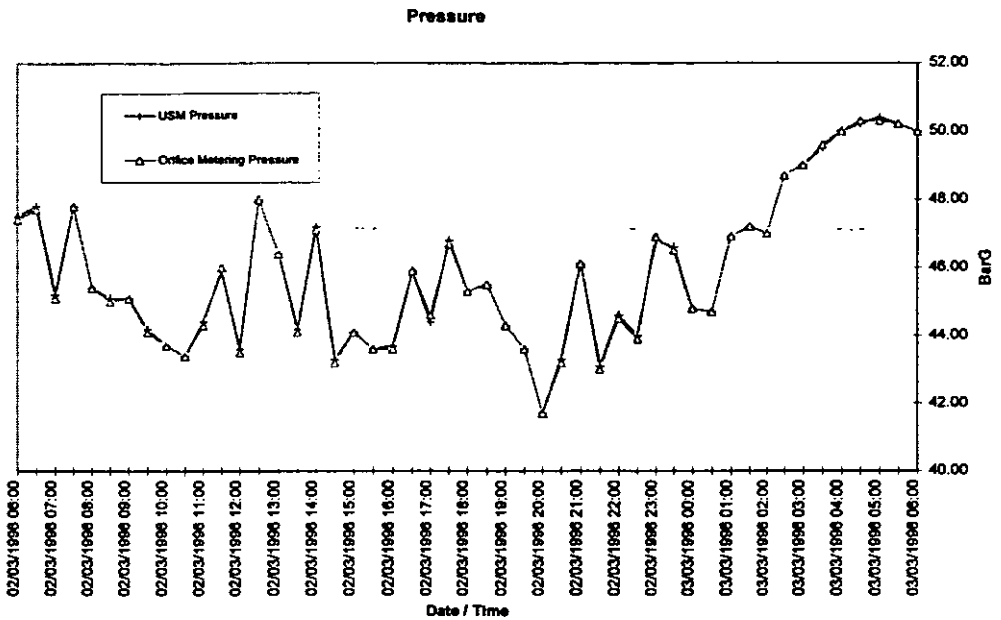
The control electronics for the ultrasonic meter are field mounted at the meter with cabling for power, frequency flow signal, data valid signal and serial diagnostics link run to the control room. Cabling from the temperature and pressure instruments have also been run to the control room.

A Spectra-Tek S500, ultrasonic meter flow computer takes the frequency input from the USM, together with temperature, pressure from field mounted transmitters and density from WPS Stream 1 flow computer to calculate and totalise actual volume flow and mass flow. Please refer to Figure 6 for full details of the instrumentation set up.

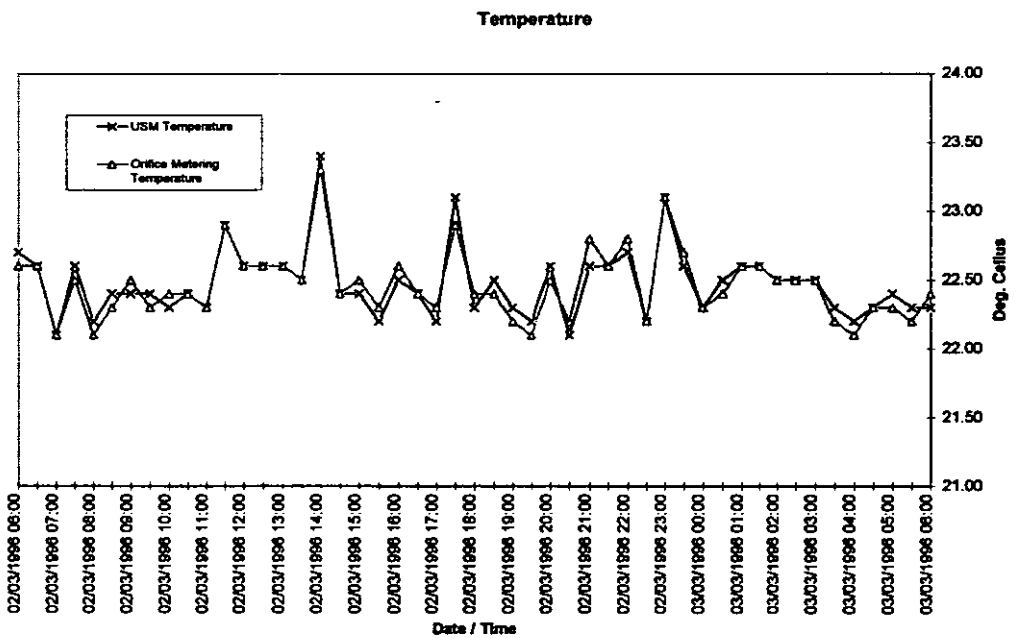
WPS gas orifice stream 1 flow computer has had its configuration modified to give a 4-20 mA output for gas calculated density. (The density being determined from on-line gas chromatograph and using AGA8 - 1985 equation of state). This has been input to the ultrasonic flow computer via a Protech input isolator to enable the calculation of mass flow. The sensitivity of WPS gas density to differences in temperature and pressure between the ultrasonic meter run and WPS gas stream 1 has been closely monitored and it has been felt that no off-line correction of the density is necessary.

Figure 5 (A&B) below shows a typical daily profile of the two metering stations pressures and temperatures.

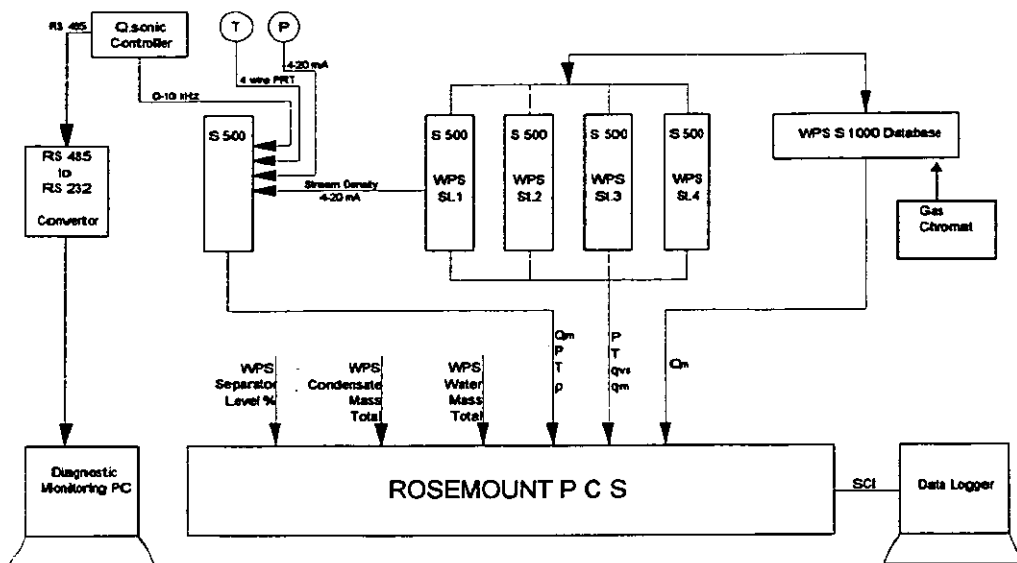
(Fig 5a)



(Fig 5b)



(Fig 6) Instrumentation and data logging schematic.



Secondary instrumentation and the flow computer fitted to the ultrasonic flow meter run have been calibrated monthly as part of the normal maintenance routines. The procedures implemented have been as for the fiscal metering station calibration routines. An additional procedure was developed to enable the calibration of the flow computer frequency input and calculations of flowrates.

3.3 Performance Tests

Offshore performance testing of the meter has been carried out in two parts. For the initial period of three months, testing has been restricted to monitoring the accuracy of flow measurement by the meter. This then continued for the second period but during this time additional tests specific to the operation of ultrasonic meters were carried out.

3.3.1 Accuracy Comparison

The metered throughput of the ultrasonic flow meter has been compared at half hourly and daily intervals with the total metered throughput of the WPS gas orifice metering system. Comparisons have been made on a total mass and actual volume basis.

Separator Levels and Condensate process data have been recorded to enable any correlation between variance in system performance with changes in process conditions to be investigated.

A typical example of the daily data recorded is provided in Appendix A1.

3.3.2 Meter Recovery from Liquid Contamination

Although not deliberately planned, this test has been carried out successfully on at least three occasions:-

- 1) During one week of the test the chromatograph used on the WPS metering station was out of action due to liquid contamination. In fact the chromat was completely flooded following a large increase in nomination for the Welland field. For the previous 4 months the gas flow rate through the system had been very low and excessive liquid build up had occurred in the inter field pipeline.

With the increase in nomination and subsequent increase in gas velocity a lot of the excess liquid was carried into the WPS separator. The separator was unable to cope with the large intake of liquids and liquid carry over occurred into the meter tubes.

As the gas chromatograph is the highest point within the whole of the orifice and USM metering systems it is safe to assume that very large quantities of liquid were present for a short time in the USM.

- 2) On a separate occasion, whilst observing the USM diagnostics in the office, it was noticed the average performance value of the transducers had fallen from 100% down to 85%. This loss in performance (but apparently not accuracy) was directly attributed to a high high water level in the WPS separator and subsequent liquid carry over.

Once the level was lowered the performance of the transducers immediately returned to 100%.

(Note: Performance value in this instance is an indication of the number of pulses of ultrasound received compared to those transmitted by a pair of transducers.)

- 3) On the 5th January 1996, again whilst observing the USM diagnostics in the office, it was noticed that the average performance value of the transducers had fallen from 100% to around 85%.

Initial enquiries with the Control Room Operators revealed that the separator levels were healthy. However, after inspection of the sight glasses on the side of the separator, a condensate level of 100% was found, as can be seen in Figure 7 below.

(Fig 7) Trend showing separator levels on Contract day 5th Jan 1996.

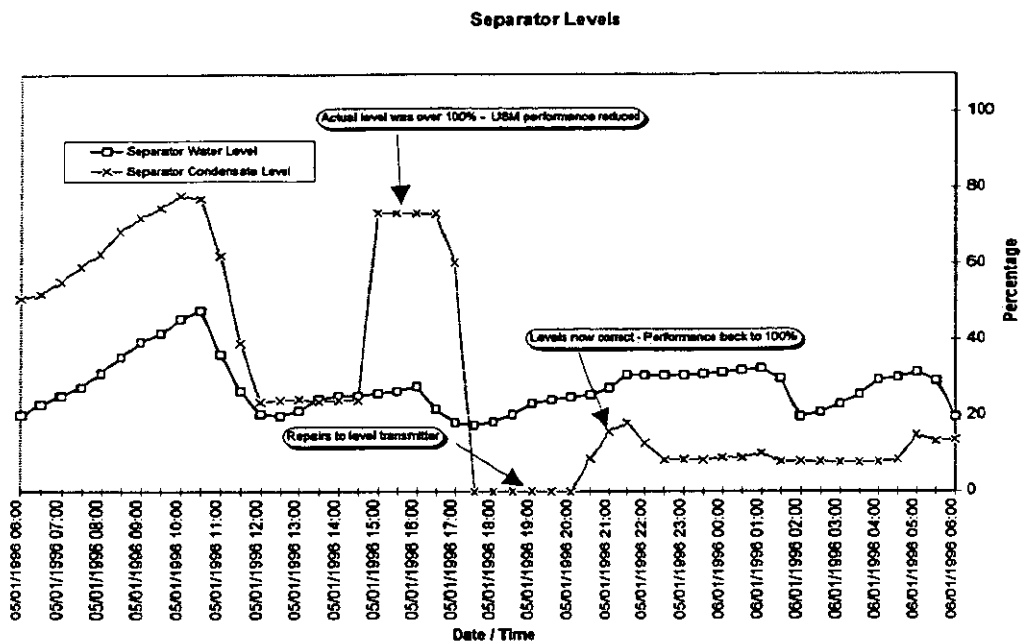
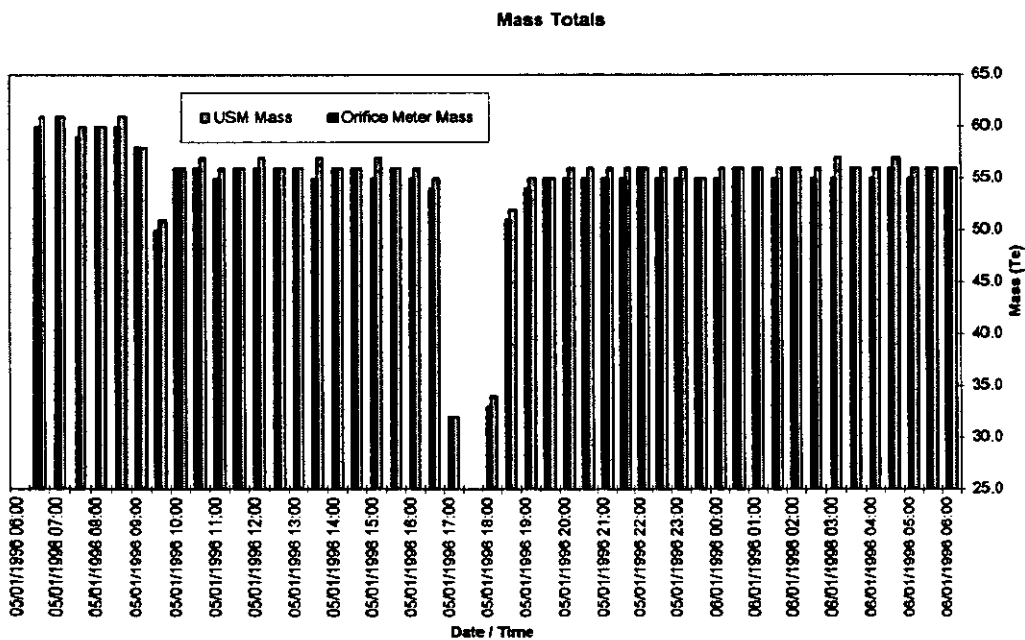


(Fig 8) Mass totals of USM versus orifice plate system every half hour for Contract day 5th Jan 1996.



Whilst the performance was reduced, interrogation of the individual transducer performance levels was carried out. It was

found that transducer pairs 1, 3, 4 & 5 were all at 100% but pair number 2 was around 35%. Pair number 2 is a swirl path pair that out of all the transducers bounces nearest the bottom of the spool.

The performance of transducer pair number 2 was monitored as the separator level was brought down and the effect was noticed immediately.

Some conclusions to be drawn from this is that the USM is capable of detecting liquid content travelling along the pipe without apparent loss in accuracy. (See Figure 8). It has also been useful in monitoring the effectiveness of our production separators.

An orifice plate system (particularly without drain holes) would be building up this liquid content and manual intervention would be required to drain the orifice fittings upstream of the plate, thereby increasing the measurement error.

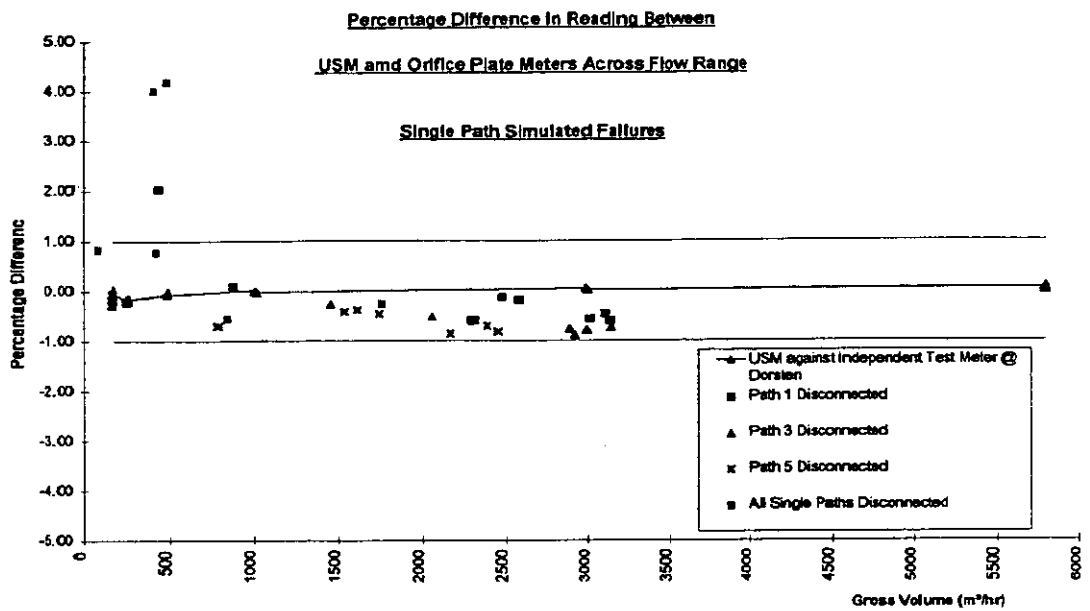
3.3.3 Additional Testing

During the second period, a number of tests specific to the operation of ultrasonic meters were carried out as follows:

Effect of Path Failure on Measurement Accuracy

This test verified the effect that the failure of an individual pair of transducers would have on measurement accuracy. Each pair of transducers were isolated (to simulate transducer failure) individually for a period of at least one week. The change in system difference was monitored to identify the effect on measurement accuracy of a path failure and show any differences between the effect of failure by the single and double (swirl) reflection chords.

(Fig 9) Effects of single path simulated failures



The effects of individual single path pair failures demonstrated that the meter continued to perform to within +/- 1% of the orifice plate system. Unfortunately by the time we got round to deliberately failing all single path transducers the flowrates had dropped significantly and the errors appeared to increase. However, as can be seen from Figure 11, these sort of errors are not untypical for the very small flowrates encountered. Remember, the differences are of percentage reading. My overall conclusions about failures of single paths are that no significant measurement errors are likely to be encountered and therefore change-out of faulty transducers can be arranged to coincide with planned visits to the platform. Given the fact that the Trent & Tyne platforms will be not-normally-manned, this has proved to be a very valuable evaluation.

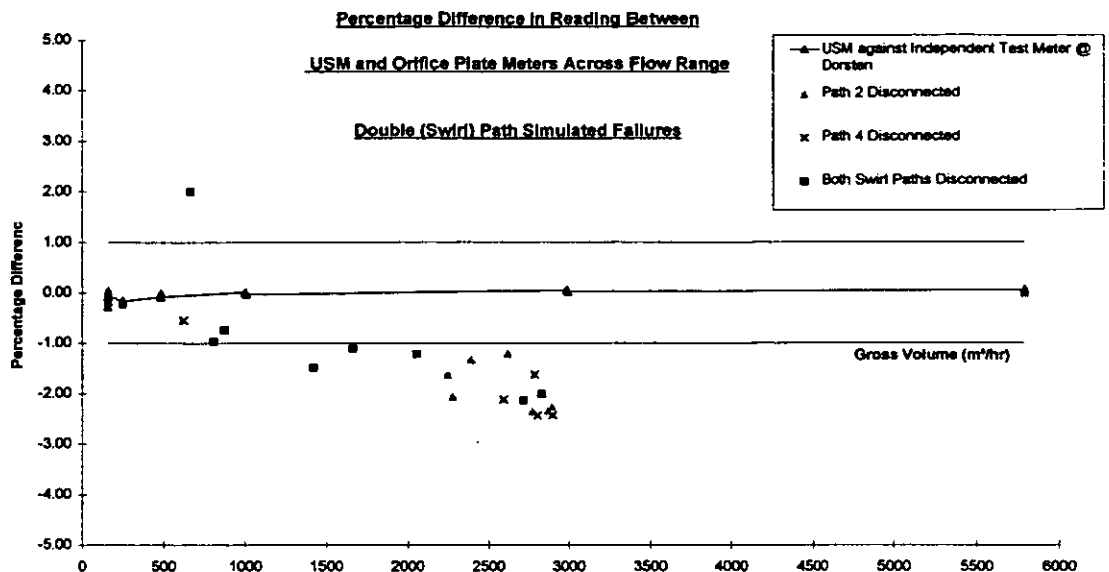
The effects of simulated failure of swirl paths produced a different set of results. (See figure 10). Generally, whether one or both paths were switched off the results showed an under measurement of approximately 1 - 1.5 %.

After consultation with Instronet Ultrasonic BV. , they confirmed that the electronics would automatically switch off a "good" pair of swirl paths if it detected the other pair had failed.

Obviously, should we encounter a swirl path failure with either of the Trent & Tyne meters we need to consider carefully how quickly we need to get out and make repairs.

Should we be in a position that no spare transducers are available, it should be possible to use a single path pair for a swirl path as all the transducers are identical and interchangeable.

(Fig 10) Effects of double (swirl) path simulated failures



Effect of On-Site Transducer Replacement

Unfortunately it is was operationally impractical with the test meter to change out or swap around one of the transducers.

3.4 Data Logging and Analysis

All the data for the above tests (with the exception of some high level diagnostics) were logged onshore via the Rosemount PCS system. This data has been logged on an half hourly basis on a personal computer via an SCI link from the PCS. (See figure 5). The data was then transferred daily via a floppy disk to an "Microsoft Excel" spreadsheet to enable the data to be trended and analysed.

The analysis of data was carried out daily by onshore metering personnel. This has enabled any adjustment to the test procedures to be carried out quickly.

The data logged and analysed via the PCS is as follows:

<u>Data Source</u>	<u>Description</u>	<u>Units</u>
--------------------	--------------------	--------------

USM Flow Computer	Mass Total	tonnes
	Pressure	bar g
	Temperature	°C
	Density	kg/m ³
Stream Flow Computers (data for each stream)	Pressure	bar g
	Temperature	°C
	Mass Flow Rate	t/hr
	Std Volume Flow Rate	ksm ³ /hr
WPS Database	Station Mass Total	tonnes
WPS Prod. Condensate	Mass Total	tonnes
WPS Separator	Water & Cond. Level	%

Additional high level diagnostic data has been available onshore and offshore from the ultrasonic meter controller via an RS485 serial link. This has provided invaluable information on the operation of individual transducers as well as specific process data such as flow velocity and fluid speed of sound.

The primary comparison made using the data supplied is of total measured mass throughput by each method.

3.5 Q.Sonic Diagnostics Link

This link can provide measurement and process data as well as additional diagnostic data.

It was intended that the following parameters would be logged, as a minimum, on a daily basis by interrogation of the Q.sonic diagnostics:

- Automatic Gain Control (AGC) Level for each transducer pair.
- AGC Limit for each transducer pair.
- Measured flow velocity
- Measured fluid speed of sound.

and that during the additional meter operational checks, these readings would be logged at a greater frequency.

However, it was found that this was not serving any real purpose. Taking daily spot readings of VOS and transducer performance was not truly representative and it is felt that a more automated system of logging was required such as continuous logging of individual transducer performance and calculated VOS together with averaged transducer performance and averaged calculated VOS.

During the development of the metering database for Trent & Tyne automatic monitoring will be built into the database functionality with alarms to warn the operator in the event that a transducer is potentially failing.

4.0 Analysis of Results Obtained from Trial.

Refer back to Section 2.4 for details of the data that was logged every half an hour:

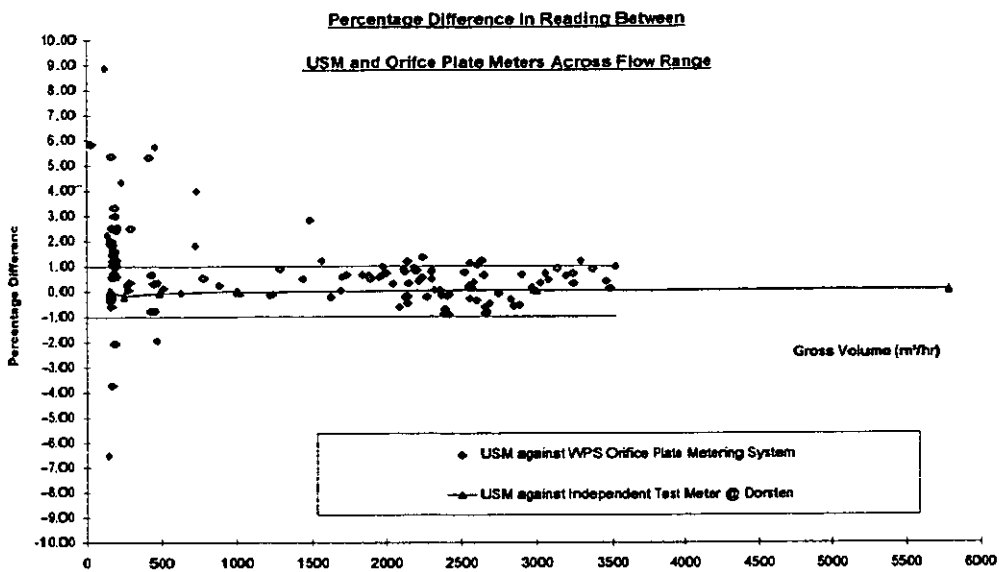
At the end of each day all the data has been transferred to disk for importing into an Microsoft Excel spreadsheet. Once this spreadsheet has been generated, the various data sets are trended and charts produced daily. The daily mass total of the USM and the orifice plate system together with the days average line density are then input into a separate spreadsheet (USM_MASS.xls) for day by day monitoring of percentage errors between the two systems. For the purposes of this trial the errors stated refer to the difference between the gross volume total of the USM against that of the orifice plate system and have been calculated using the following formula:

$$\frac{(\text{USM Actual vol. (m3/hr)} - \text{Orifice Actual vol. (m3/hr)})}{\text{Orifice Actual vol. (m3/hr)}} \times 100 \% \quad (\text{Eq 1})$$

The results have been monitored using a number a trends. Firstly, using the results of equation (1) above and plotting these results using a scatter diagram as illustrated in Figure 11 below:

(Note: Data from the trial obtained during some of the additional testing such as deliberate failure of transducer has been excluded from these results.)

(Fig 11) Daily percentage differences.



From Figure 11 above it can be seen that the results obtained generally fall between +/- 1% once away from the lower volumes. It was felt to be a useful exercise to trend these differences on the same chart as that of the flowrates.

The following two figures (Figures 12 & 13) show the difference between the two metering system against flowrate:

(Fig. 12) Difference in terms of actual volume flows.

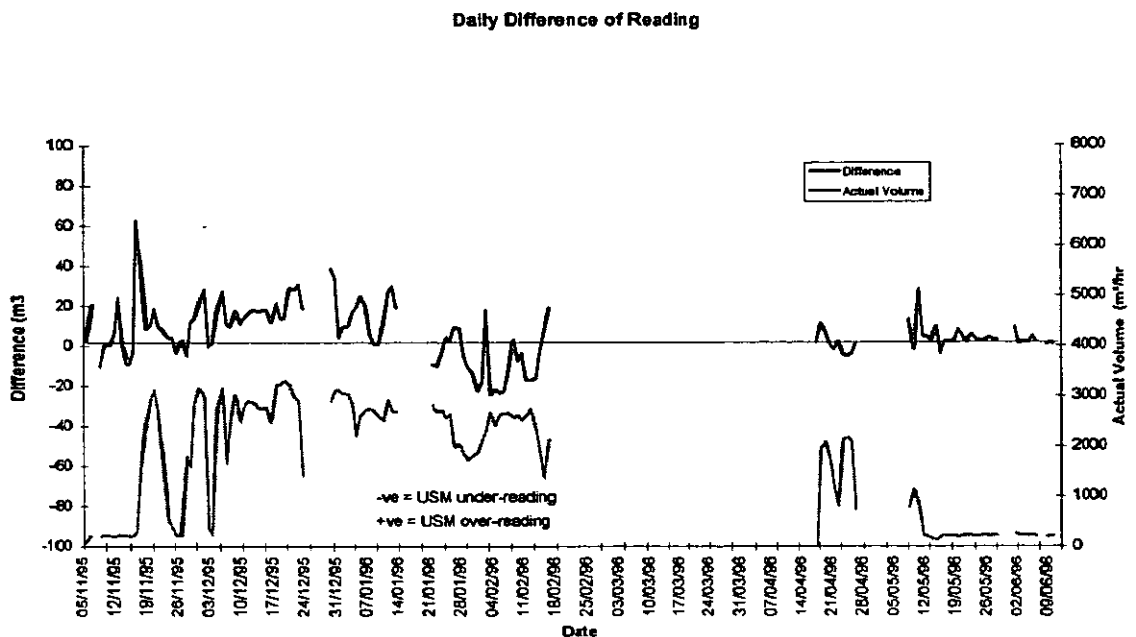
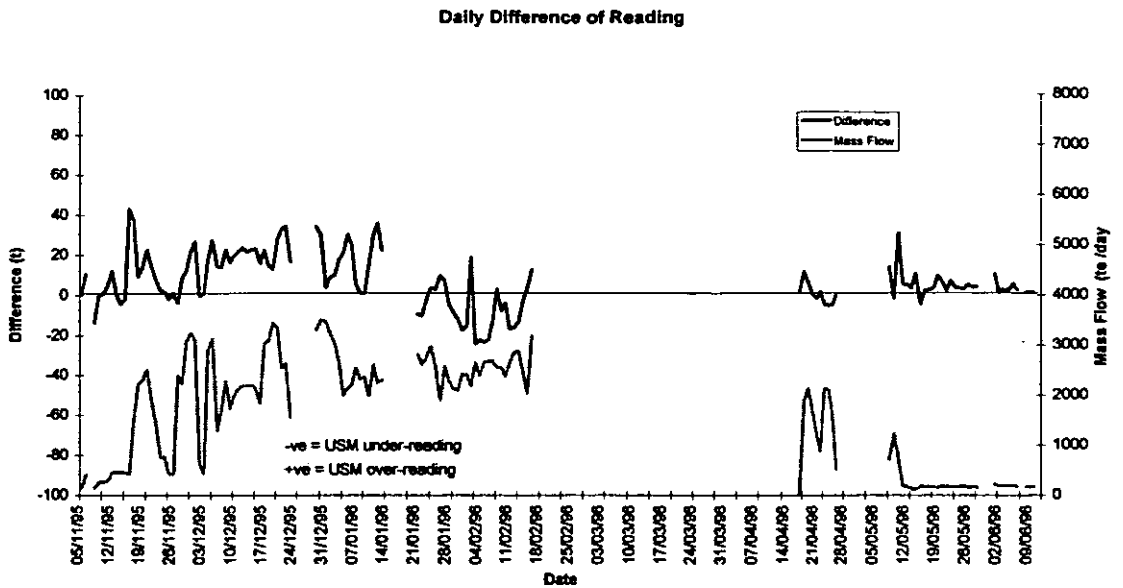
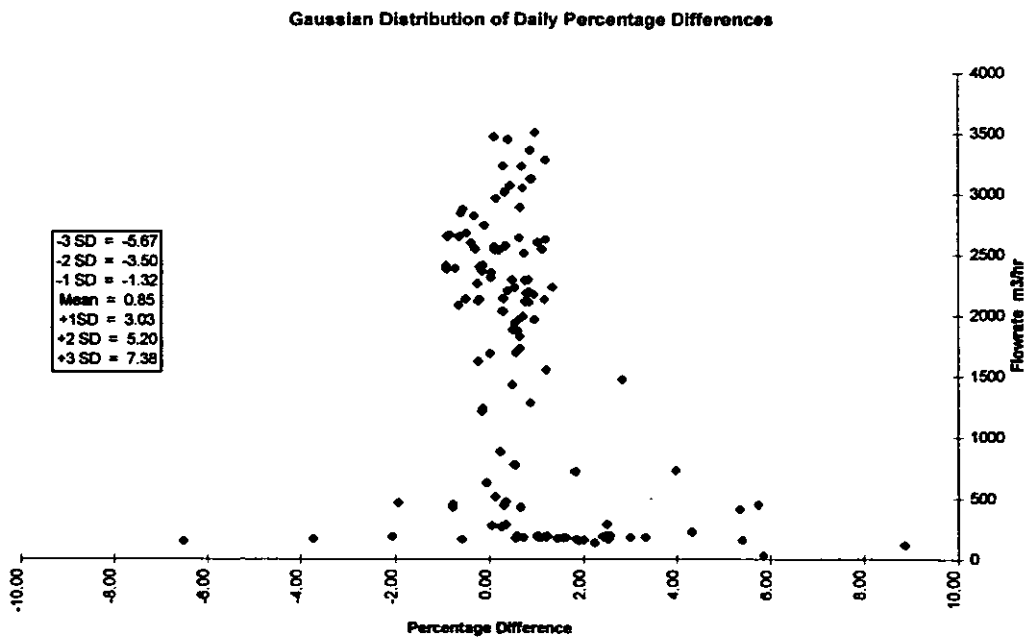


(Fig 13) Difference in terms of mass flows.



The following chart (Figure 14) is a Gaussian normal distribution of the results obtained. For reference, the mean value obtained was +0.8519, one standard deviation was 2.1751 and a 95% confidence level of 0.373 was also calculated.

(Fig 14) Gaussian distribution of results.



The following eight bar charts (Figure 15.1 - 15.8) show the day-by-day differences between the two metering systems. :

Figure 15.1 November 1995

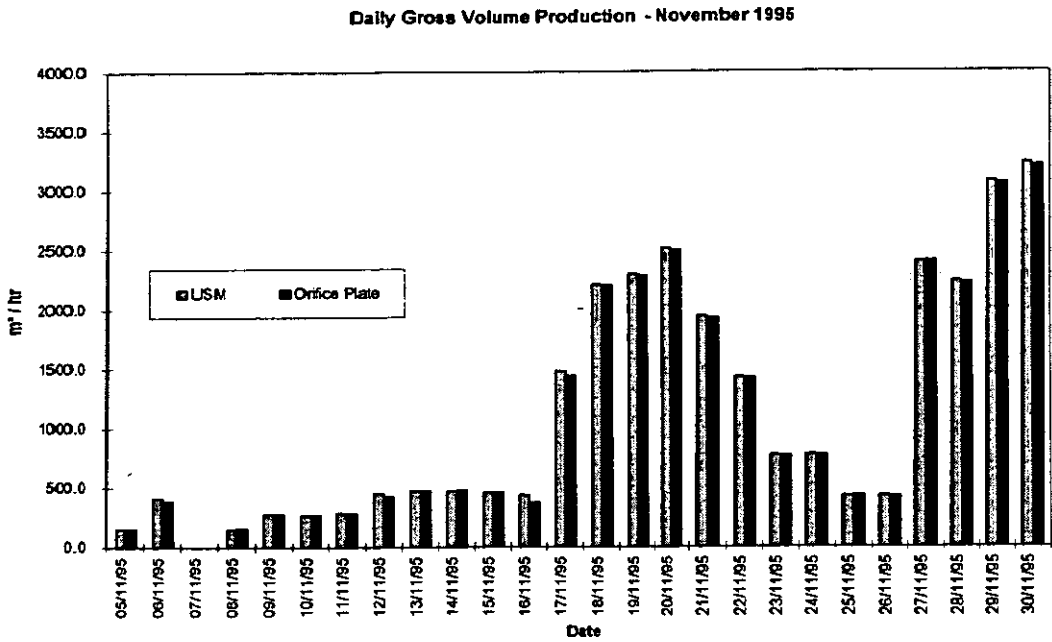


Figure 15.2 December 1995

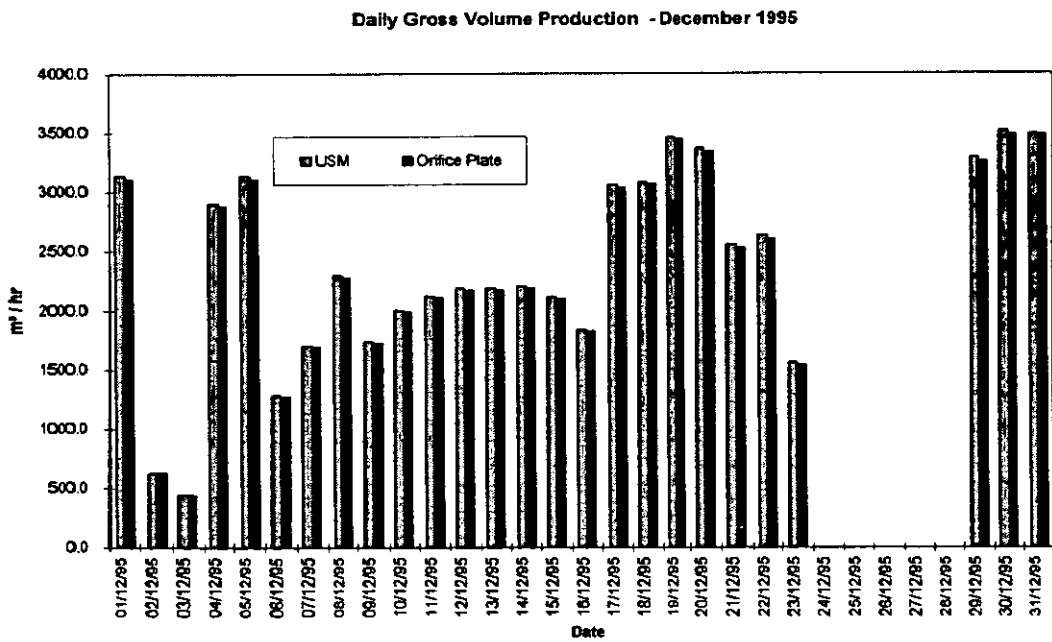


Figure 15.3 January 1996

Daily Gross Volume Production - January 1996

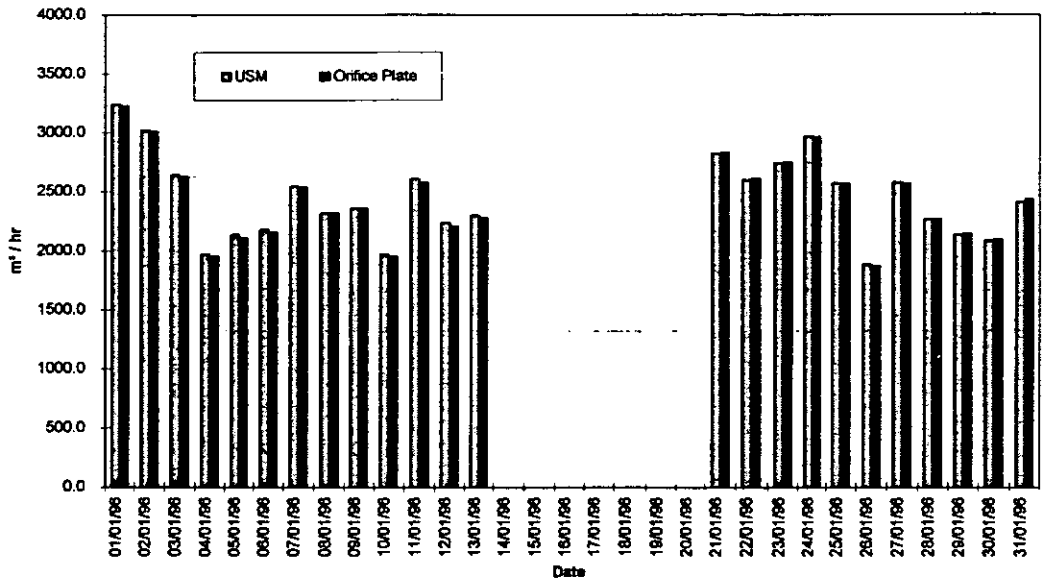


Figure 15.4 February 1996

Daily Gross Volume Production - February 1996

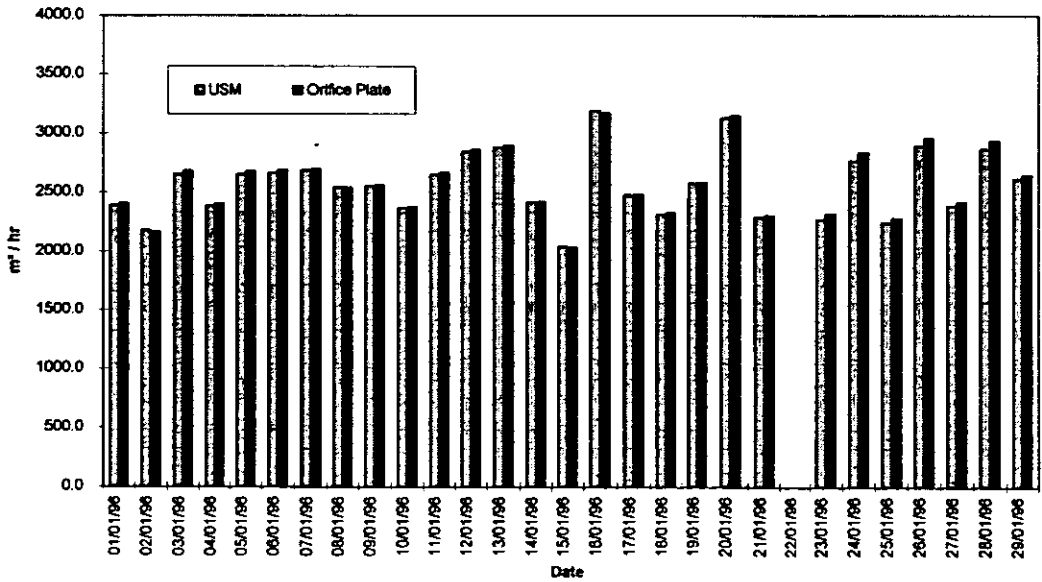


Figure 15.5 March 1996

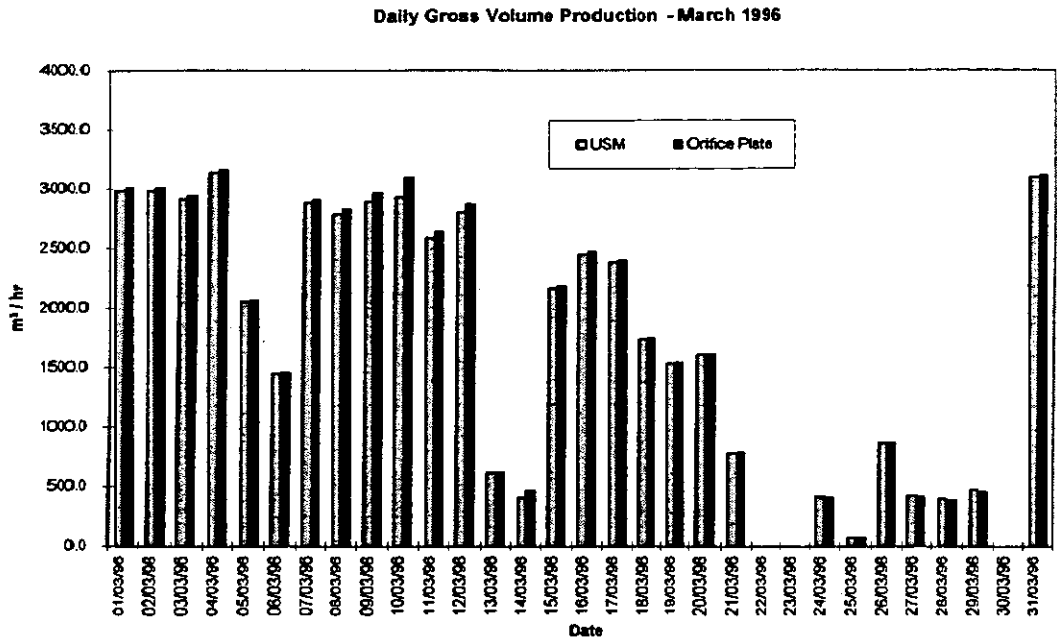


Figure 15.6 April 1996

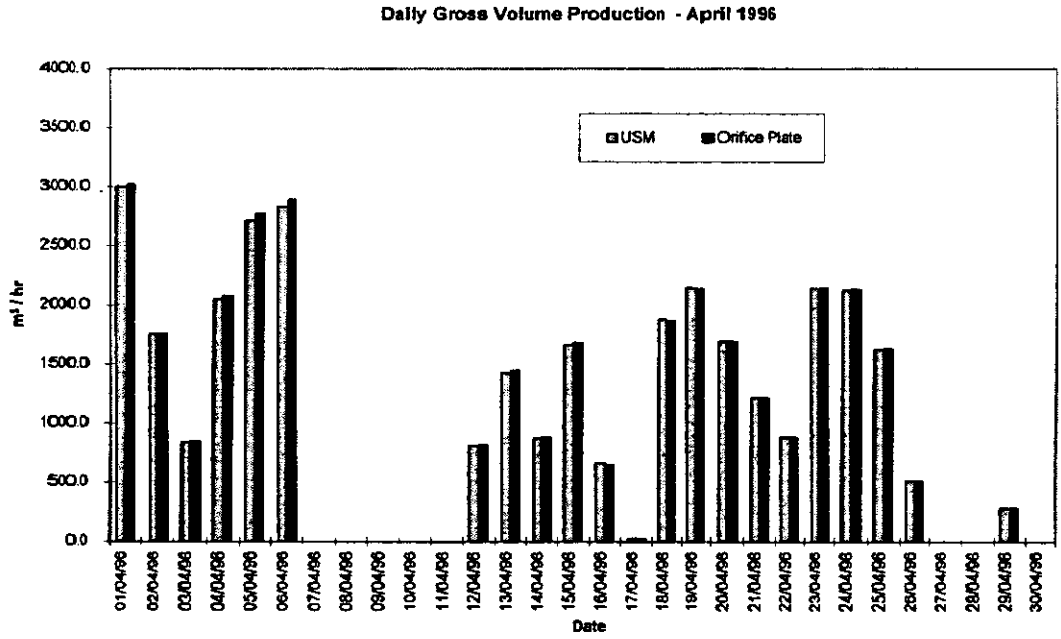


Figure 15.7 May 1996

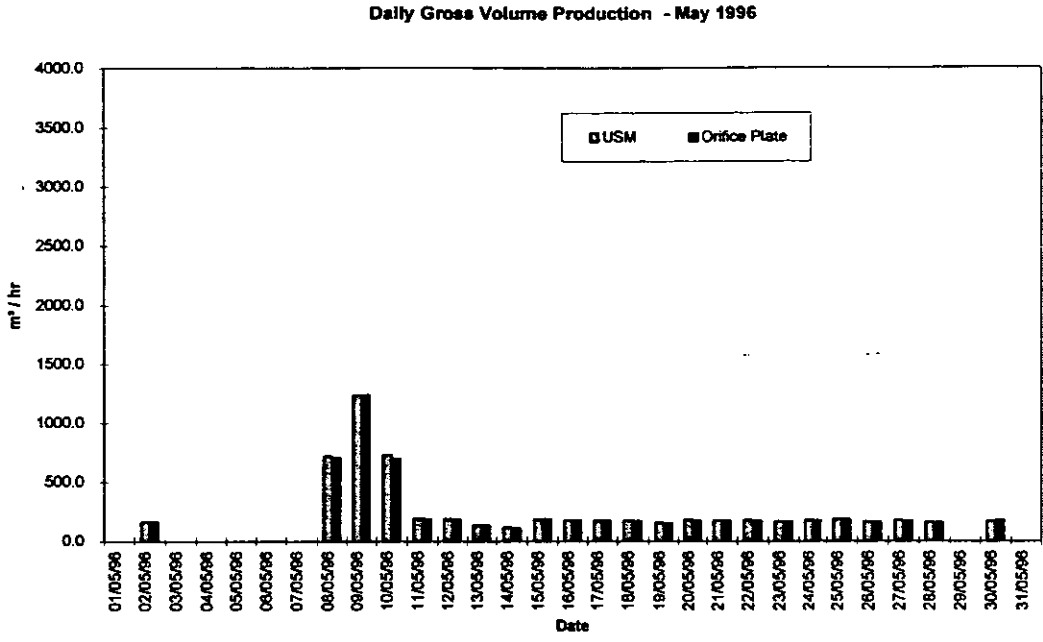
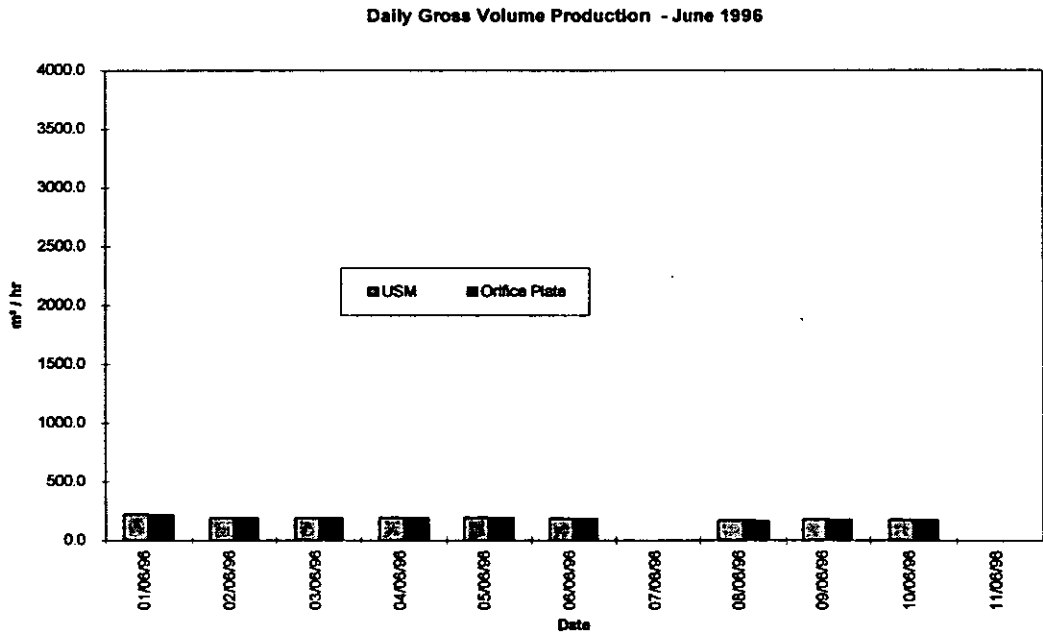


Figure 15.8 June 1996



Data for the following days has not been included :

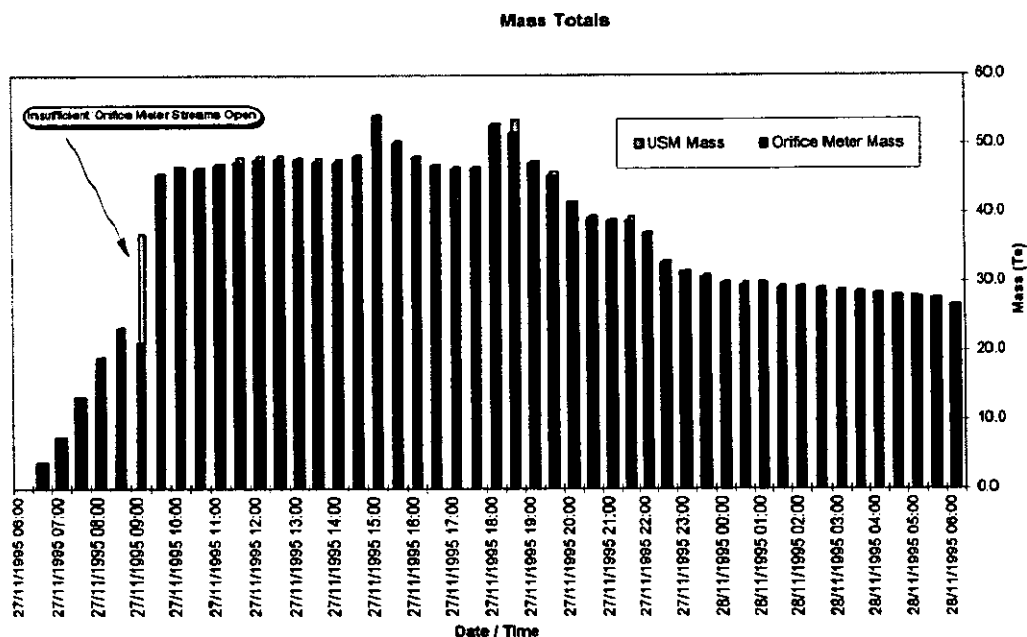
7th November 1995 - No production.

24th - 28th December 1995 inclusive - Stream 1 mistakenly taken off-line. (The USM flow computer uses the density supplied by the flow computer.)

14th - 20th January 1996 - S500 flow computer failure due to circuit board component failure.

On some occasions minor alterations to the WPS orifice readings have been implemented as a result of plant operators not opening or closing orifice plate streams quick enough after changes in production rates. (See figure 16). As the USM is a single stream it never misses any flow, however the orifice plate systems utilises four streams and relies on operator intervention to select the appropriate number of streams. An example of this is given in Figure 16 below:

(Fig 16) Example of effects of not opening orifice streams in time.



During the trial numerous problems were encountered with the S1000 database. One of the most common faults was that the outputs driven by the database to the PCS would on some occasions be very erratic. On these days only the end of day totals have been used and the data logged by the PCS has been ignored.

After the new flow computer was installed on the 20th January a full set of calibrations were carried out. During this time it was noticed that the

density displayed on Stream 1 flow computer did not match exactly that of the USM flow computer. The Protech input isolator was found to be in need of adjusting. After adjustment the density input to the USM matched exactly that of Stream 1 through the range.

For all remaining days the errors are as recorded with no adjustments.

5.0 Conclusions.

As can be seen quite clearly from the Scattergram (Fig 9) and the trend of errors reported each day, the USM has demonstrated repeatable and accurate results. From the initial start date through to the 13th January (pre density input calibration) the average error, or rather difference of reading between the two types of meters, was +0.9264 %. The average difference of reading after the density input calibration was +0.7802 %. The overall average of the results obtained (excluding periods of deliberate simulated transducer failures) was +0.8506 %.

The overall average percentage difference of reading of all the results obtained was +0.3538 %.

(It is comforting to know that our orifice plate metering systems are so accurate !)

Apart from the accuracy of the results, some of the other benefits / conclusions to be drawn so far are as follows:-

The USM has proved to be more reliable and versatile than its orifice plate counterpart. Its ability to detect liquids travelling along the spool pipe with apparently no loss in accuracy is an excellent feature that orifice plate systems cannot compete with as illustrated in BSI 1042 Part 1 Section 1.5 Guide To The Effects of Departure From Conditions Specified in Section 1.1

The comprehensive remote diagnostic tools enables the user to carry out detailed examination of the performance of individual transducer pairs from remote (onshore) locations.

The reduced maintenance / calibrations associated with an USM system (no need for DP cell or orifice calibrations/ inspections of multiple streams) contributes to reducing the number of personnel exposed to working offshore.

The amazing 100:1 turn down ratio and built in redundancy enables metering stations to consist of little more than a single USM and a short upstream and downstream spool piece.

The ability of the meters to be upgraded with minimal costs in years to come by having revised software uploaded or new transducers or new circuit boards fitted contributes to a far more flexible metering system .

The long term evaluation into the issue of whether the meters need to be re-calibrated each year has yet to be concluded. More data and results are needed, however, initial results look positive.

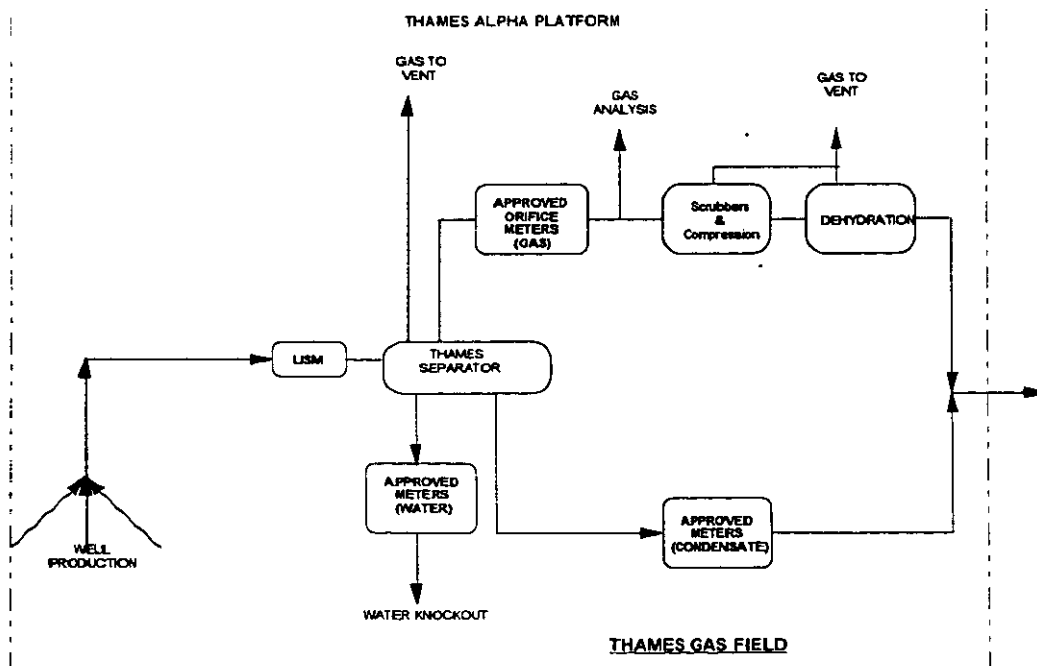
6.0 Future Trials

The trial involving the comparison of the USM against the orifice plate system downstream of separation has now finished. The meter purchased to carry out the trial has been retained and re-located upstream of separation. A new trial is now underway to evaluate the performance and accuracy of the meter on three phase wet gas. The meter has been placed upstream of the Thames field Production Separator, again on the Thames Alpha platform.

We know from the previous trial that the meter is capable of detecting free liquids within the pipe spool, we should be able to use this information and use the various paths as level detectors within the spool and try to compensate the gas flow rate accordingly.

A process schematic of the three phase trial is provided below.

(Fig 16) Three Phase Ultrasonic Trial



A further trial will be commencing with the two Trent & Tyne meters to evaluate the calculated line density from velocity of sound from the USM and comparing this density with that of the gas chromat / AGA8 route. The metering database developed for the Trent & Tyne metering has the ability to continuously monitor and log both calculated densities.

I look forward to sharing the results of these new trials in the near future. Watch this space !!!!!!!

7.0 Acknowledgements:

Kevin J Robinson: Who, during his time as Metering Supervisor within ABL recognised the potential opportunity to make use of USM's and then had the commitment to ensure that the Trent & Tyne project team made use of this (at the time) untried technology on an offshore gas platform.

Instromet Ultrasonics BV: for their efforts in repairing the transducers damaged by the platform staff and in rescuing the evaluation into the long term accuracy of the meter.

The DTi - GOMB : for their encouragement and support of the proposal to use USM's for Trent & Tyne platforms.

Gwilym Foulkes
(SGS Redwood Ltd) for his technical support throughout the trial and in particular in preparing the draft Code of Practice for the Installation of USM's

ARCO British Ltd for funding the trial meter used on Thames.

And finally, to all those who provided very constructive feedback to my Preliminary Report (date 6th February 1996), in particular Jacques Agricola (NAM)

Today's E.O.D Mass
 Yesterday's E.O.D. Mass
 01/02/1996

USM
 173883.0
 171762.0
 2121.0

WPS
 186752.0
 184605.0
 2142.0

te
 te
 te

Ultrasonic Flow Computer			
Density kg/m3	Temper. degC	Press. barG	Mass Te
36.97	11.87708	44.0938	2121.0
02/02/1996 06:00	43.84	10.30	173883.00
02/02/1996 05:30	43.84	10.30	173828.00
02/02/1996 05:00	43.51	10.30	173773.00
02/02/1996 04:30	42.79	10.30	173718.00
02/02/1996 04:00	42.39	10.20	173665.00
02/02/1996 03:30	42.75	10.20	173611.00
02/02/1996 03:00	42.85	10.20	173557.00
02/02/1996 02:30	42.92	10.20	173503.00
02/02/1996 02:00	42.90	10.30	173450.00
02/02/1996 01:30	42.95	10.20	173396.00
02/02/1996 01:00	42.84	10.20	173342.00
02/02/1996 00:30	42.68	10.20	173289.00
02/02/1996 00:00	42.35	10.20	173235.00
01/02/1996 23:30	42.33	10.20	173181.00
01/02/1996 23:00	42.32	10.20	173127.00
01/02/1996 22:30	42.14	10.20	173073.00
01/02/1996 22:00	42.07	10.30	173020.00
01/02/1996 21:30	41.71	10.40	172966.00
01/02/1996 21:00	40.77	10.40	172914.00
01/02/1996 20:30	37.61	9.70	172864.00
01/02/1996 20:00	37.45	9.70	172809.00
01/02/1996 19:30	37.84	9.70	172752.00
01/02/1996 19:00	38.31	9.60	172696.00
01/02/1996 18:30	38.63	9.80	172639.00
01/02/1996 18:00	39.41	9.80	172581.00
01/02/1996 17:30	40.18	10.30	172523.00
01/02/1996 17:00	39.94	10.60	172463.00
01/02/1996 16:30	36.77	12.40	172410.00
01/02/1996 16:00	31.07	11.50	172367.00
01/02/1996 15:30	23.79	15.50	172336.00
01/02/1996 15:00	20.84	23.60	172318.00
01/02/1996 14:30	21.12	23.40	172308.00
01/02/1996 14:00	26.46	8.80	172294.00
01/02/1996 13:30	34.25	7.40	172270.00
01/02/1996 13:00	30.70	5.70	172248.00
01/02/1996 12:30	43.07	11.00	172212.00
01/02/1996 12:00	40.09	12.10	172173.00
01/02/1996 11:30	23.11	11.70	172152.00
01/02/1996 11:00	24.62	14.80	172152.00
01/02/1996 10:30	32.28	16.60	172143.00
01/02/1996 10:00	31.87	15.80	172115.00
01/02/1996 09:30	33.42	15.60	172077.00
01/02/1996 09:00	33.45	15.50	172032.00
01/02/1996 08:30	33.44	15.50	171987.00
01/02/1996 08:00	33.51	15.40	171943.00
01/02/1996 07:30	33.57	15.50	171898.00
01/02/1996 07:00	33.75	15.70	171852.00
01/02/1996 06:30	34.06	15.70	171807.00
01/02/1996 06:00	34.24	15.70	171762.00

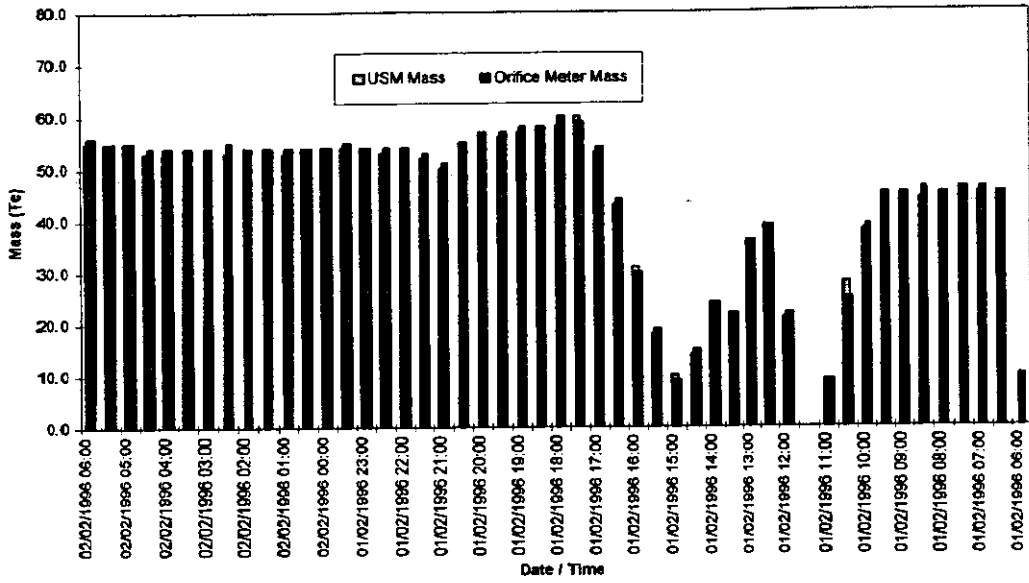
WPS Separator		
Sep. Water Level %	Sep. Condy Level %	Condy Mass kg
		0.00
20.59	17.50	0.00
19.53	17.10	47393.20
18.77	17.20	45845.10
17.74	17.60	44005.60
7.97	23.10	42100.90
7.82	21.20	41953.40
7.73	17.00	41486.00
7.64	17.00	40800.80
7.66	17.50	39344.70
7.59	16.90	37920.20
7.56	17.10	37274.40
7.53	16.70	36051.60
0.00	16.60	35389.30
0.00	16.70	34663.80
0.00	16.60	33893.30
0.00	16.40	33067.30
0.00	16.40	32422.10
0.00	16.40	31229.30
0.00	16.40	30499.90
0.00	16.60	29933.90
0.00	16.50	28884.00
38.67	36.60	26420.50
38.70	39.30	23419.30
38.66	42.70	20686.10
38.73	43.80	18903.80
38.66	2.40	17970.00
38.41	25.10	17400.30
37.23	58.30	16867.00
36.74	0.00	15796.70
36.38	0.00	15272.00
36.33	0.00	14761.50
36.29	6.30	14228.50
36.19	0.00	13737.70
35.97	0.00	13737.70
35.82	7.20	13225.90
35.71	7.00	12662.30
35.61	69.60	11094.30
35.77	98.30	8376.72
36.08	38.10	6956.98
35.10	37.50	5615.21
34.26	35.80	4947.78
32.95	33.70	3082.10
30.84	31.00	1654.81
29.97	24.10	1369.59
29.26	12.30	1369.59
28.22	7.20	949.62
25.57	7.20	498.17
22.39	7.10	498.17
19.59	7.10	0.00

WPS Stream One	
Press. barG	Temper. degC
44.66208	11.91678
52.1	10.3
52.0	10.4
51.7	10.4
51.0	10.4
50.5	10.2
50.8	10.2
51.0	10.3
51.0	10.3
51.0	10.3
51.1	10.3
51.0	10.3
50.8	10.3
50.4	10.3
50.5	10.2
50.4	10.3
50.2	10.3
50.2	10.3
49.8	10.4
48.7	10.4
45.1	9.8
44.9	9.7
45.4	9.7
45.9	9.7
46.4	9.8
47.1	9.9
48.1	10.3
47.9	10.7
44.5	11.2
38.1	11.7
30.2	16.4
27.1	22.3
27.0	18.4
31.9	7.0
40.8	7.5
36.7	6.7
51.4	11.1
48.5	12.3
29.1	15.3
31.1	16.6
40.4	16.7
39.6	15.4
41.5	15.5
41.5	15.5
41.5	15.4
41.5	15.3
41.7	15.4
41.9	15.3
42.3	15.6
42.5	15.7

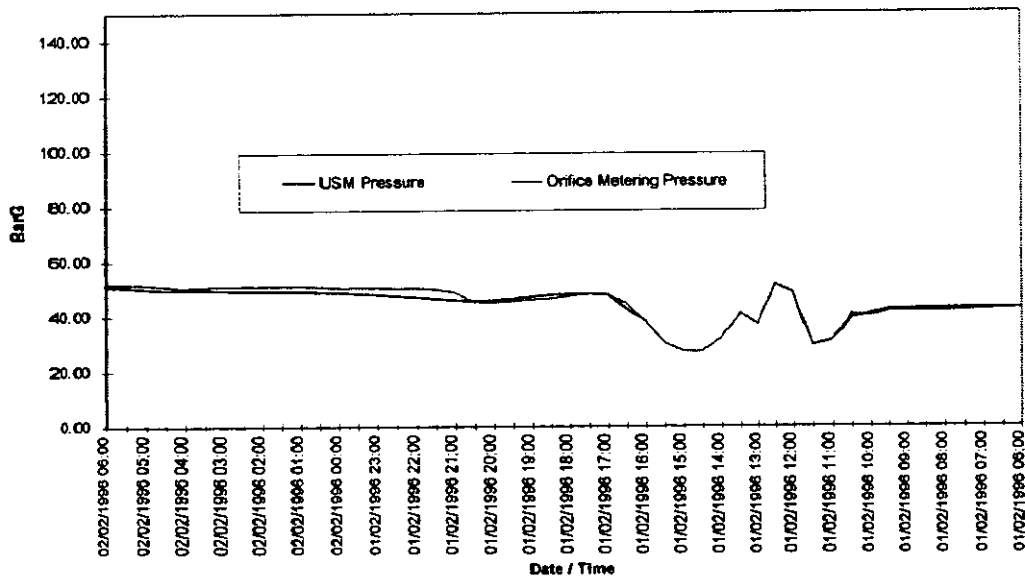
WPS D/b
Mass Te
2137.0
186752.0
186696.0
186641.0
186586.0
186532.0
186478.0
186424.0
186370.0
186315.0
186281.0
186207.0
186153.0
186099.0
186045.0
185990.0
185936.0
185882.0
185828.0
185775.0
185724.0
185669.0
185612.0
185555.0
185497.0
185439.0
185379.0
185320.0
185266.0
185222.0
185192.0
185173.0
185164.0
185149.0
185125.0
185103.0
185067.0
185028.0
185006.0
185006.0
184997.0
184972.0
184933.0
184888.0
184843.0
184797.0
184752.0
184706.0
184660.0
184615.0

USM	WPS	Condy
Mass Te	Mass Te	Mass kg
		0.00
55.0	56.0	0.00
55.0	55.0	1548.10
55.0	55.0	1839.50
53.0	54.0	1904.70
54.0	54.0	147.50
54.0	54.0	487.40
54.0	54.0	685.20
53.0	55.0	1456.10
54.0	54.0	1424.50
54.0	54.0	645.80
53.0	54.0	1222.80
54.0	54.0	662.30
54.0	54.0	725.50
54.0	55.0	970.50
54.0	54.0	626.00
53.0	54.0	645.20
54.0	54.0	1192.80
52.0	53.0	729.40
50.0	51.0	566.00
55.0	55.0	1049.90
57.0	57.0	2463.50
56.0	57.0	3001.20
57.0	58.0	2733.20
58.0	58.0	1782.30
58.0	60.0	933.80
60.0	59.0	569.70
53.0	54.0	533.30
43.0	44.0	1070.30
31.0	30.0	524.70
18.0	19.0	510.50
10.0	9.0	533.00
14.0	15.0	490.80
24.0	24.0	0.00
22.0	22.0	511.80
36.0	36.0	563.60
39.0	39.0	1568.00
21.0	22.0	2717.58
0.0	0.0	1419.74
9.0	9.0	1341.77
28.0	25.0	667.43
38.0	39.0	1865.68
45.0	45.0	1427.29
45.0	45.0	285.22
44.0	46.0	0.00
45.0	45.0	419.97
46.0	46.0	451.45
45.0	46.0	0.00
45.0	45.0	488.17
0.0	10.0	0.00

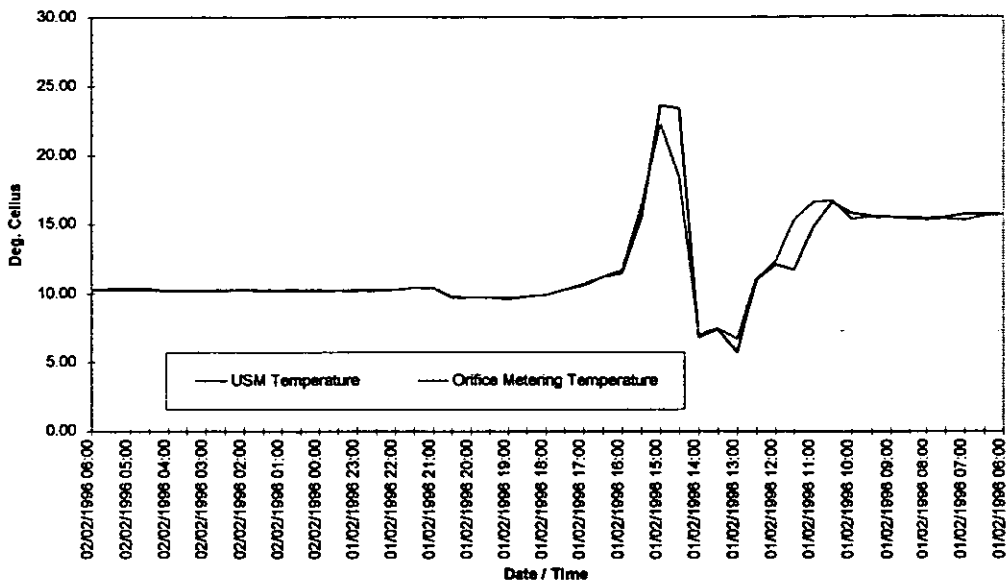
Mass Totals



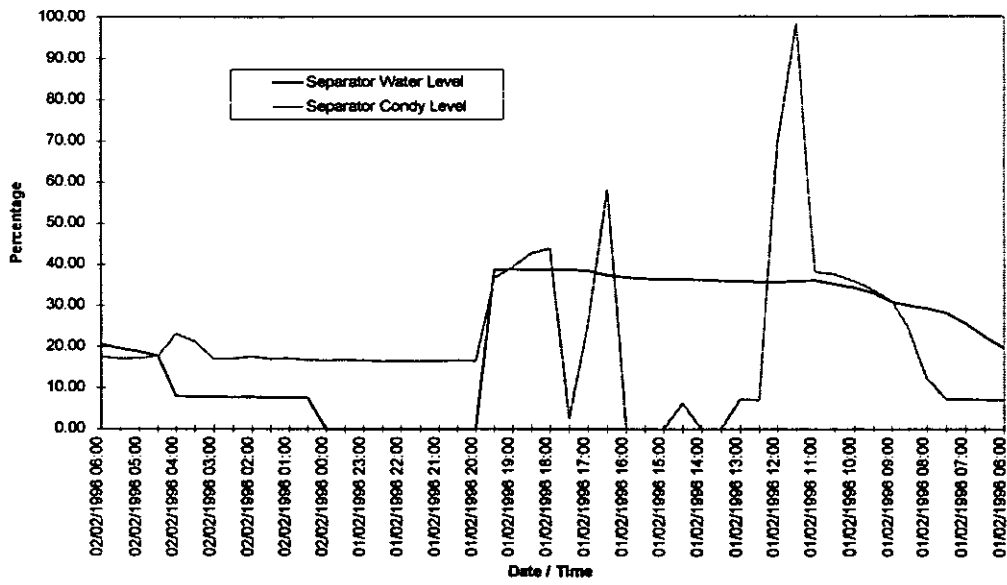
Pressure



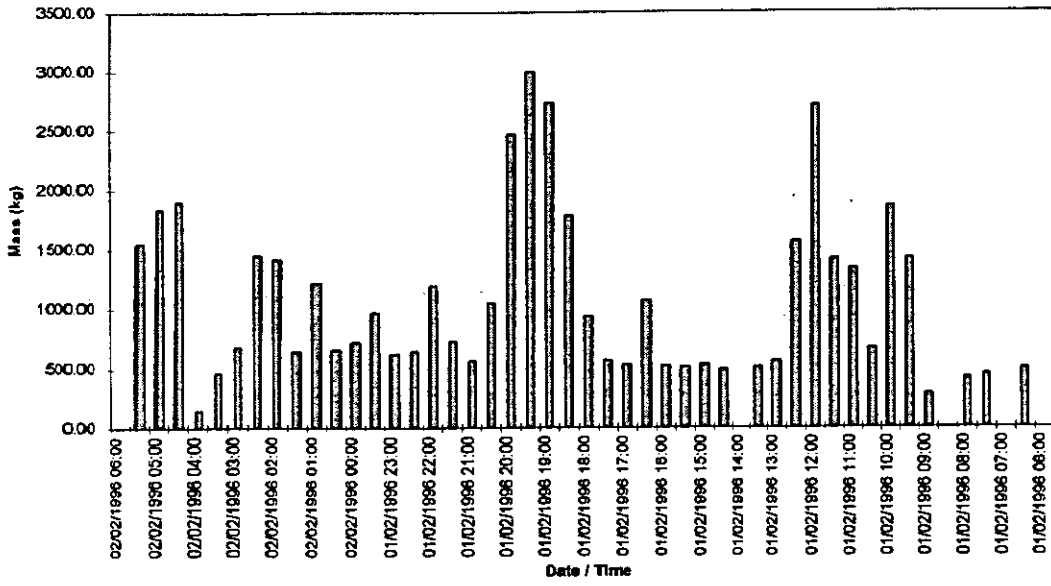
Temperature



Separator Levels



Condensate Mass



Appendix A1

Example of Daily Data Logged During Trial

Appendix A2
Full List of Results

Contract Day	Measured Density (kg/m ³)	USM Mass (t)	Orifice Plate Mass (t)	USM GYOL (m ³ /hr)	Orifice Plate Gvol (m ³ /hr)	% Difference of Reading (Volume) **	% Difference of Reading (Volume) ***	Physical Difference (Volume) (m ³)	Physical Difference Mass (t)	Comments
										** = Results obtained during normal operation *** = Results obtained during deliberate failure of transducers
05/11/95	17.5	64.7	63.5	154.0	151.2	1.8984		2.8696	1.2053	Very low velocities encountered ... below Qmin at times
06/11/95	21.4	211.7	201.0	411.5	390.8	5.3050		20.7308	10.6631	Very low velocities encountered ... below Qmin at times
07/11/95										No data available
08/11/95	55.6	199.6	213.5	149.7	160.1	-6.5108		-10.4254	-13.9006	Very low velocities encountered ... below Qmin at times
09/11/95	33.5	223.6	223.5	277.8	277.6	0.0569		0.1579	0.1271	Very low velocities encountered ... below Qmin at times
10/11/95	33.6	216.7	216.2	268.9	268.2	0.2534		0.6797	0.5478	Very low velocities encountered ... below Qmin at times
11/11/95	29.0	200.9	196.0	289.1	282.1	2.4977		7.0454	4.8955	Very low velocities encountered ... below Qmin at times
12/11/95	21.1	227.5	215.2	448.9	424.6	5.7228		24.2980	12.3154	Very low velocities encountered ... below Qmin at times
13/11/95	19.2	217.6	216.9	471.3	469.7	0.3435		1.6136	0.7451	Very low velocities encountered ... below Qmin at times
14/11/95	19.7	220.8	225.2	466.1	475.3	-1.9381		-9.2122	-4.3645	Very low velocities encountered ... below Qmin at times
15/11/95	19.4	211.8	213.4	453.9	457.4	-0.7672		-3.5091	-1.6372	Very low velocities encountered ... below Qmin at times
16/11/95	28.6	299.2	256.0	435.3	372.5	16.8749		62.8518	43.1997	Very low velocities encountered ... below Qmin at times
17/11/95	38.6	1370.9	1333.3	1479.7	1439.1	2.8182		40.5578	37.5750	
18/11/95	45.9	2433.3	2423.9	2210.3	2201.8	0.3869		8.5189	9.3782	
19/11/95	53.6	2956.8	2942.7	2298.0	2287.1	0.4793		10.9607	14.1029	
20/11/95	51.8	3129.4	3106.4	2519.6	2501.0	0.7399		18.5047	22.9836	Low frequency cut off set
21/11/95	58.2	2714.7	2699.9	1944.3	1933.7	0.5493		10.6221	14.8313	
22/11/95	48.9	1682.9	1674.8	1433.0	1426.0	0.4858		6.9275	8.1360	Adjusted Orifice plate reading - 3 streams online with very little flow
23/11/95	27.9	517.8	515.0	773.9	769.6	0.5518		4.2469	2.8418	Stream selection problems (WPS original mass = 505.0te)
24/11/95	19.4	362.1	360.2	779.5	775.4	0.5304		4.1125	1.9104	Stream selection problems (WPS original mass = 352.6te)
25/11/95	22.3	228.9	230.7	428.3	431.7	-0.7754		-3.3473	-1.7888	Stream selection problems (WPS original mass = 217.7te)
26/11/95	21.2	217.8	216.4	428.8	426.0	0.6675		2.8434	1.4445	
27/11/95	30.9	1783.9	1787.6	2404.8	2409.8	-0.2052		-4.9445	-3.6679	Orifice readings for 09:00 26/11 adjusted
28/11/95	29.9	1602.1	1593.5	2236.0	2224.1	0.5384		11.9742	8.5793	
29/11/95	38.3	2833.9	2821.4	3079.3	3065.8	0.4421		13.5531	12.4728	
30/11/95	40.6	3157.1	3135.6	3236.6	3214.6	0.6857		22.0417	21.5002	Factor of 0.997 set in USM as per calibration results
01/12/95	39.8	2991.2	2964.3	3134.7	3105.5	0.9075		28.1901	26.9000	
02/12/95	23.5	354.2	354.4	628.9	629.2	-0.0564		-0.3551	-0.2000	
03/12/95	21.5	228.5	227.8	442.7	441.4	0.3073		1.3563	0.7000	Welland Database changed - pulses missed & incorrect stream selection

04/12/95	39.3	2733.3	2715.7	2897.3	2878.7	0.6481	18.6583	17.6000	Stream selection problems (WPS original mass = 2704.2te)
05/12/95	42.0	3159.0	3131.5	3132.7	3105.4	0.8782	27.2707	27.5000	
06/12/95	54.0	1661.6	1647.1	1283.3	1272.1	0.8803	11.1984	14.5000	
07/12/95	60.3	2461.8	2447.9	1699.8	1690.2	0.5678	9.5976	13.9000	Stream selection problems (WPS original mass = 2437.6te)
08/12/95	55.0	3030.7	3007.7	2295.3	2277.9	0.7647	17.4188	23.0000	
09/12/95	59.8	2492.6	2476.3	1735.8	1724.4	0.6582	11.3508	16.3000	
10/12/95	58.2	2792.0	2772.2	1999.1	1984.9	0.7142	14.1767	19.8000	
11/12/95	56.9	2899.7	2877.7	2121.9	2105.8	0.7645	16.0992	22.0000	
12/12/95	54.6	2888.5	2844.8	2188.4	2170.3	0.8331	18.0806	23.7000	
13/12/95	52.6	2760.9	2739.2	2188.2	2171.0	0.7922	17.1984	21.7000	
14/12/95	52.0	2751.0	2728.3	2205.0	2186.8	0.8320	18.1948	22.7000	
15/12/95	54.3	2759.3	2736.0	2116.0	2098.1	0.8516	17.8677	23.3000	
16/12/95	56.2	2472.5	2456.6	1834.6	1822.8	0.6472	11.7980	15.9000	Stream selection problems (WPS original mass = 2357.9te)
17/12/95	43.8	3217.0	3194.4	3057.0	3035.6	0.7075	21.4763	22.6000	Stream selection problems (WPS original mass = 3161.1te)
18/12/95	43.6	3224.1	3209.7	3079.3	3065.6	0.4486	13.7534	14.4000	Database problems - WPS original mass = 2825.9te)
19/12/95	39.7	3293.4	3280.5	3458.0	3444.5	0.3932	13.5447	12.9000	
20/12/95	40.1	3242.0	3214.1	3368.0	3339.0	0.8681	28.9842	27.9000	
21/12/95	48.4	2965.5	2932.5	2551.9	2523.5	1.1253	28.3976	33.0000	
22/12/95	45.8	2894.3	2860.1	2631.0	2599.9	1.1958	31.0889	34.2000	
23/12/95	37.3	1394.7	1378.0	1558.6	1539.9	1.2119	18.6627	16.7000	
24/12/95									Stream 1 off-line therefore incorrect density used
25/12/95									Stream 1 off-line therefore incorrect density used
26/12/95									Stream 1 off-line therefore incorrect density used
27/12/95									Stream 1 off-line therefore incorrect density used
28/12/95									Stream 1 off-line therefore incorrect density used
29/12/95	36.7	2897.5	2863.3	3289.4	3250.6	1.1944	38.8261	34.2000	Stream selection problems (WPS original mass = 2792.8te)
30/12/95	36.9	3110.2	3080.2	3515.6	3481.7	0.9740	33.9108	30.0000	
31/12/95	37.3	3121.7	3118.3	3483.0	3479.2	0.1090	3.7935	3.4000	
01/01/96	39.3	3054.8	3045.9	3241.3	3231.9	0.2922	9.4434	8.9000	
02/01/96	41.9	3043.0	3033.1	3022.6	3012.8	0.3264	9.8337	9.9000	15 - 17:00 hrs Stream 1 plate changed and wrong density used by USM
03/01/96	44.9	2851.7	2833.8	2644.7	2628.1	0.6317	16.6005	17.9000	
04/01/96	46.4	2198.5	2177.5	1973.4	1954.5	0.9644	18.8498	21.0000	
05/01/96	50.7	2604.4	2574.1	2139.3	2114.4	1.1771	24.8893	30.3000	Liquids present in meter tubes - Separator levels not working correctly

06/01/96	52.0	2720.3	2694.9	2179.0	2158.6	0.9425	20.3457	25.4000	Liquids present in meter tubes - Separator levels not working correctly
07/01/96	45.0	2748.9	2743.3	2544.8	2539.6	0.2041	5.1843	5.6000	
08/01/96	48.6	2703.7	2702.7	2318.7	2317.8	0.0370	0.8576	1.0000	
09/01/96	45.7	2586.5	2585.5	2358.8	2357.9	0.0387	0.9120	1.0000	
10/01/96	53.2	2513.3	2498.0	1968.0	1956.1	0.6125	11.9806	15.3000	WPS Database fault for half of day - see printouts
11/01/96	46.7	2922.9	2893.0	2606.6	2580.0	1.0335	26.6646	29.9000	WPS database problems and liquids detected
12/01/96	50.2	2694.2	2658.4	2238.4	2208.7	1.3467	29.7434	35.8000	Liquids detected again
13/01/96	48.6	2683.0	2660.8	2300.1	2281.1	0.8343	19.0316	22.2000	
14/01/96						0.9264			Flow computer u/s
15/01/96									Flow computer u/s
16/01/96									Flow computer u/s
17/01/96									Flow computer u/s
18/01/96									Flow computer u/s
19/01/96									Flow computer u/s
20/01/96									New computer fitted & density input calibrated
21/01/96	41.4	2810.8	2820.0	2826.4	2835.6	-0.3262	-9.2510	-9.2000	WPS mass from ETC / Database problems
22/01/96	43.1	2688.9	2699.3	2601.7	2611.8	-0.3853	-10.0627	-10.4000	
23/01/96	41.3	2726.2	2729.0	2747.4	2750.2	-0.1026	-2.8217	-2.8000	
24/01/96	35.8	2549.6	2545.9	2969.5	2965.1	0.1453	4.3093	3.7000	
25/01/96	42.8	2641.0	2638.3	2573.5	2570.9	0.1023	2.6310	2.7000	
26/01/96	43.7	1980.7	1971.0	1887.9	1878.6	0.4921	9.2453	9.7000	
27/01/96	33.1	2049.8	2042.8	2581.1	2572.3	0.3427	8.8145	7.0000	
28/01/96	34.0	1851.2	1855.8	2267.8	2273.5	-0.2479	-5.6353	-4.6000	
29/01/96	33.4	1714.8	1723.4	2140.4	2151.1	-0.4990	-10.7345	-8.6000	
30/01/96	35.8	1793.5	1805.2	2087.9	2101.6	-0.6481	-13.6207	-11.7000	
31/01/96	32.4	1876.7	1894.2	2416.5	2439.0	-0.9239	-22.5337	-17.5000	
01/02/96	37.0	2121.3	2136.9	2390.8	2408.4	-0.7300	-17.5818	-15.6000	
02/02/96	44.0	2303.6	2285.0	2181.7	2164.1	0.8140	17.6156	18.6000	Database error during stream flow computer change-out
03/02/96	41.7	2663.4	2687.8	2660.3	2684.6	-0.9078	-24.3714	-24.4000	
04/02/96	42.3	2424.6	2446.9	2386.1	2408.0	-0.9114	-21.9457	-22.3000	
05/02/96	41.5	2647.9	2671.3	2656.5	2680.0	-0.8760	-23.4759	-23.4000	
06/02/96	41.2	2642.4	2664.8	2670.3	2693.0	-0.8406	-22.6369	-22.4000	
07/02/96	41.3	2660.0	2673.1	2686.6	2699.8	-0.4901	-13.2310	-13.1000	
08/02/96	42.2	2574.4	2571.4	2544.9	2541.9	0.1167	2.9656	3.0000	

09/02/96	42.7	2618.0	2625.8	2553.6	2561.2	-0.2971	-7.6081	-7.8000	USM adjusted slightly (original 2670.9 te)
10/02/96	43.9	2498.0	2501.9	2370.0	2373.7	-0.1559	-3.7002	-3.9000	
11/02/96	40.7	2593.4	2610.2	2653.8	2671.0	-0.6436	-17.1910	-16.8000	
12/02/96	40.0	2733.7	2750.2	2847.5	2864.7	-0.6000	-17.1871	-16.5000	
13/02/96	33.9	2342.4	2355.6	2882.3	2898.5	-0.5604	-16.2424	-13.2000	Database error warm start for Spectra-tek 16t lost
14/02/96	32.8	1901.8	1904.4	2418.7	2422.0	-0.1365	-3.3066	-2.6000	
15/02/96	27.9	1365.1	1361.2	2042.0	2036.2	0.2865	5.8339	3.9000	
16/02/96	27.9	2135.3	2122.8	3194.1	3175.1	0.5983	18.9975	12.7000	Path 1a Disconnected
17/02/96	36.5	2169.3	2172.3	2478.4	2481.8	-0.1381			
18/02/96	38.6	2143.4	2156.2	2313.6	2327.4	-0.5936			
19/02/96	32.1	1987.2	1991.0	2579.9	2584.8	-0.1909			
20/02/96	26.8	2016.5	2028.7	3131.3	3150.3	-0.6014			
21/02/96	27.4	1504.3	1513.4	2290.6	2304.4	-0.6013			
22/02/96									No data available
23/02/96	34.4	1875.1	1914.5	2273.6	2321.4	-2.0580			No1 connected - No2 Disconnected
24/02/96	38.7	2574.0	2636.1	2772.5	2839.4	-2.3558			
25/02/96	34.2	1842.4	1872.8	2243.5	2280.6	-1.6232			
26/02/96	37.8	2626.0	2687.0	2895.3	2962.5	-2.2702			
27/02/96	37.1	2127.0	2155.7	2388.0	2420.3	-1.3314			
28/02/96	37.7	2597.9	2660.2	2871.6	2940.4	-2.3419			
29/02/96	36.4	2287.2	2315.2	2616.9	2648.9	-1.2094			
01/03/96	36.1	2588.1	2608.6	2990.9	3014.6	-0.7859			No 2 connected - No3 Disconnected
02/03/96	36.1	2588.1	2608.6	2990.9	3014.6	-0.7859			
03/03/96	38.2	2670.8	2694.8	2916.9	2943.1	-0.8906			
04/03/96	30.0	2259.9	2276.6	3137.3	3160.5	-0.7336			
05/03/96	24.0	1184.7	1190.9	2052.6	2063.3	-0.5206			
06/03/96	32.6	1137.9	1141.0	1452.6	1456.6	-0.2717			
07/03/96	34.1	2363.8	2381.9	2888.0	2910.1	-0.7599			
08/03/96	40.0	2676.2	2720.4	2787.7	2833.8	-1.6248			No3 connected - No 4 Disconnected
09/03/96	38.5	2678.5	2745.2	2897.9	2970.0	-2.4297			
10/03/96	35.3	2487.7	2625.0	2933.2	3095.1	-5.2305			Suspect finger trouble on platform
11/03/96	39.5	2457.5	2510.6	2591.5	2647.5	-2.1150			
12/03/96	38.3	2581.6	2646.1	2805.5	2875.6	-2.4375			
13/03/96	30.7	458.1	460.6	622.0	625.4	-0.5428			

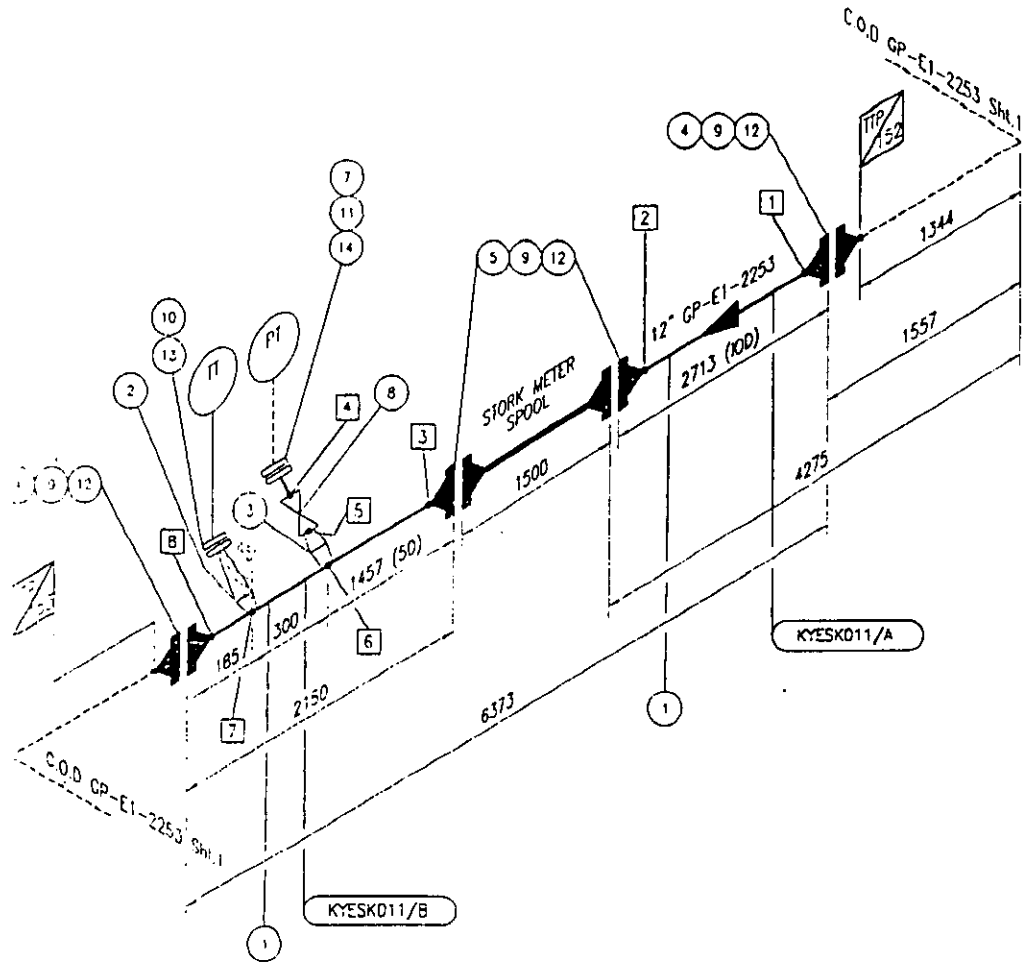
14/03/96	38.9	382.2	437.5	409.5	468.8	-12.6400	Suspect finger trouble on platform
15/03/96	41.0	2133.4	2152.0	2166.7	2185.5	-0.8643	No 4 Connected - No 5 Disconnected
16/03/96	43.1	2533.9	2554.8	2451.3	2471.5	-0.8181	
17/03/96	43.6	2494.2	2512.0	2384.7	2401.8	-0.7086	
18/03/96	42.6	1777.5	1785.9	1740.5	1748.7	-0.4704	
19/03/96	44.3	1633.7	1640.6	1535.3	1541.8	-0.4206	
20/03/96	41.2	1592.9	1599.1	1610.3	1616.6	-0.3877	
21/03/96	42.8	805.6	811.3	785.1	790.6	-0.7026	
22/03/96							No 1, 3 & 5 disconnected - No production
23/03/96							No production
24/03/96	44.1	443.0	439.6	418.6	415.4	0.7734	
25/03/96	47.2	85.0	84.3	75.1	74.5	0.8304	
26/03/96	45.9	963.0	962.0	873.8	872.9	0.1040	
27/03/96	43.5	451.0	442.0	431.5	422.9	2.0362	
28/03/96	42.8	416.0	400.0	404.9	389.3	4.0000	
29/03/96	36.2	416.6	399.9	479.3	460.1	4.1760	
30/03/96							No production
31/03/96	28.9	2151.0	2161.0	3100.9	3115.3	-0.4627	
01/04/96	24.7	1784.9	1795.0	3005.2	3022.3	-0.5627	
02/04/96	26.9	1131.0	1134.0	1754.3	1759.0	-0.2646	
03/04/96	39.0	786.0	790.4	840.0	844.7	-0.5567	No 2 & 4 Disconnected - No 1, 2 & 3 Connected
04/04/96	23.1	1140.4	1154.4	2053.6	2078.8	-1.2128	
05/04/96	22.7	1479.7	1511.9	2717.4	2776.5	-2.1298	
06/04/96	22.5	1532.0	1563.4	2833.6	2891.7	-2.0084	
07/04/96							No production
08/04/96							No production
09/04/96							No production
10/04/96							No production
11/04/96							No production
12/04/96	17.4	338.8	342.1	811.0	818.9	-0.9646	
13/04/96	14.5	497.5	505.0	1425.0	1446.5	-1.4851	
14/04/96	47.0	985.0	992.3	673.6	680.1	-0.7357	
15/04/96	44.8	1786.0	1806.0	1662.2	1680.8	-1.1074	
16/04/96	43.7	698.7	685.0	665.7	652.7	2.0000	All paths reconnected

17/04/96	44.2	30.8	29.1	29.0	27.4	5.8419	1.6015	1.7000	
18/04/96	43.3	1951.7	1939.9	1879.8	1868.5	0.6083	11.3654	11.8000	
19/04/96	40.5	2084.6	2078.4	2144.7	2138.3	0.2983	6.3786	6.2000	
20/04/96	41.8	1698.4	1698.0	1691.8	1691.4	0.0236	0.3984	0.4000	
21/04/96	38.9	1133.9	1135.6	1214.9	1216.7	-0.1497	-1.8214	-1.7000	
22/04/96	38.1	808.0	806.1	883.2	881.1	0.2357	2.0768	1.9000	
23/04/96	41.5	2131.8	2136.3	2139.3	2143.8	-0.2106	-4.5159	-4.5000	
24/04/96	42.6	2172.9	2178.2	2125.8	2131.0	-0.2433	-5.1851	-5.3000	
25/04/96	53.2	2076.8	2081.7	1626.6	1630.4	-0.2354	-3.8377	-4.9000	
26/04/96	59.1	729.0	728.1	514.0	513.4	0.1236	0.6346	0.9000	
27/04/96									No production
28/04/96									No production
29/04/96	42.2	289.0	288.0	285.1	284.2	0.3472	0.9867	1.0000	
30/04/96									No production
01/05/96									No production
02/05/96	43.2	171.0	172.0	165.0	166.0	-0.5814	-0.9650	-1.0000	
03/05/96									No Production
04/05/96									No Production
05/05/96									No Production
06/05/96									No Production
07/05/96									No Production
08/05/96	45.0	780.0	766.0	723.0	710.0	1.8277	12.9774	14.0000	Scaling factor changed (0-4ksm3/hr = 0-4kHz) was (0-8ksm3hr = 0 - 8kHz)
09/05/96	38.5	1144.3	1145.8	1238.7	1240.4	-0.1309	-1.6238	-1.5000	
10/05/96	46.1	809.4	778.4	731.6	703.6	3.9825	28.0200	31.0000	
11/05/96	46.5	219.2	213.9	196.4	191.6	2.4778	4.7477	5.3000	
12/05/96	48.8	221.0	215.8	188.8	184.4	2.4096	4.4424	5.2000	
13/05/96	48.7	160.1	156.6	136.9	133.9	2.2350	2.9933	3.5000	
14/05/96	47.7	135.0	124.0	118.0	108.4	8.8710	9.6187	11.0000	
15/05/96	49.6	223.3	228.0	187.4	191.3	-2.0614	-3.9443	-4.7000	
16/05/96	51.9	222.3	219.9	178.3	176.4	1.0914	1.9251	2.4000	
17/05/96	52.8	225.2	222.5	177.6	175.5	1.2135	2.1293	2.7000	
18/05/96	53.5	223.1	219.9	173.9	171.4	1.4552	2.4943	3.2000	
19/05/96	51.5	196.5	186.5	159.1	151.0	5.3619	8.0971	10.0000	
20/05/96	51.8	227.2	220.6	182.7	177.3	2.9918	5.3060	6.6000	

21/05/96	52.4	224.0	221.7	178.0	176.2	1.0374	1.8281	2.3000	
22/05/96	52.3	226.7	219.4	180.7	174.9	3.3273	5.8199	7.3000	
23/05/96	52.1	209.8	206.0	167.8	164.0	1.8447	3.0395	3.8000	
24/05/96	52.4	225.3	221.8	179.1	176.3	1.5760	2.7822	3.5000	
25/05/96	52.7	238.9	236.0	188.9	186.6	1.2288	2.2932	2.9000	
26/05/96	56.2	223.5	218.0	165.8	161.8	2.5229	4.0810	5.5000	
27/05/96	55.4	236.2	232.4	177.6	174.8	1.6351	2.8579	3.8000	
28/05/96	55.5	213.9	209.7	160.6	157.5	2.0029	3.1542	4.2000	
29/05/96									No production
30/05/96	54.4	225.0	233.7	172.3	178.9	-3.7227	-6.6616	-8.7000	
31/05/96									No production
01/06/96	47.5	258.4	247.7	226.5	217.1	4.3197	9.3796	10.7000	
02/06/96	48.3	225.6	224.3	194.5	193.4	0.5796	1.1206	1.3000	
03/06/96	49.7	227.9	225.1	191.2	188.9	1.2439	2.3493	2.8000	
04/06/96	48.4	226.8	224.5	195.3	193.3	1.0245	1.9802	2.3000	
05/06/96	49.2	233.2	227.4	197.6	192.6	2.5506	4.9134	5.8000	
06/06/96	47.4	213.1	210.6	187.3	185.1	1.1871	2.1970	2.5000	
07/06/96									No production
08/06/96	48.2	197.4	196.3	170.6	169.6	0.5604	0.9506	1.1000	
09/06/96	48.8	209.8	208.3	179.0	177.7	0.7201	1.2798	1.5000	
10/06/96	49.7	209.7	208.5	175.9	174.9	0.5755	1.0066	1.2000	
11/06/96									S500 failed - end of trial

Appendix A2
Test Meter Spool Sketch

UP
DOWN



ITEM No.	QUANTITY		SIZE	RATING SCH	DESCRIPTION	CAST No.	CERT. No.
	SHOP	FIELD					
1	6M		12"NB	120	PIPE ASTM A333 GR.5		
2	1		12"x1 1/2"	XXS	"PROMAT" WELDOFLANGE 1500# RTJ LTFCS A350 LF2 - SCH 120		
3	1		12"x1"	XXS	"PROMAT" NIPOLET 6000# BW LTFCS A350 LF2 - SCH 160		
4	2		12"NB	120	FLANGE 900# RTJ WN BW LTFCS A350 LF2		
5	2		12"NB	140	FLANGE 900# RTJ WN BW LTFCS A350 LF2		
6	1		1"NB	XXS	FLANGE 1500# RTJ BW WN LTFCS A350 LF2		
7	1		1"NB	XXS	FLANGE 1500# RTJ BLIND LTFCS A350 LF2 (DRILL & TAP 1/2" NPT CENTRALLY)		
8	1		1"NB	XXS	GATE VALVE 1500# BW LTFCS GA.13		
9	4		12"NB	R57	OCT. RING GASKET SS TYPE 316 ABOVE TO SUIT 900# RTJ FLANGES		
10	1		1 1/2"NB	R20	OCT. RING GASKET SS TYPE 316		
11	1		1"NB	R16	OCT. RING GASKET SS TYPE 316 ABOVE TO SUIT 1500# RTJ FLANGES		
12	80		1/2"	-	STUDBOLTS X 290 LONG C/W 3 NUTS		
13	4		1"	-	STUDBOLTS X 140 LONG C/W 2 NUTS		
14	4		2 1/2"	-	STUDBOLTS X 125 LONG C/W 2 NUTS STUDBOLTS - A320 GR.L7 NUTS-A194 GR.7 SF HVY HEX FCC		

LAST WELD No. THIS DRG.		8	RADIOGRAPHY	
REINFORCEMENT	STRESS RELIEVING	STRESS SKETCH No.		
NO	YES	FULL PART		
INSULATION	TRACING	PRESSURE TEST	PAINT COLOUR	
TYPE	THICKNESS	MEDIUM	PRESSURE	
-	30	WATER	222	BARG

REFERENCE DRAWINGS		REV. No.	REVISION	BY	DATE	CHKD	APPVD	CHECKED	PROJECT
NUMBER	TITLE					AV	PL		
E1-2253-SHT 1	8090 ISO 12" E1-2253-SHT 1	1	ISSUED FOR CONSTRUCTION						DESIGN ENGINEERING SERVICES FOR KYE LTD
									TITLE
									TEST METER SPOOL SKETCH
DRAWING		CHECKED	APPROVED	CLIENT APPVD.	SCALE	DRAWING NUMBER		REV.	
A FINCH		A. WPOHO	P. LAFFERTY		NTS	9095-G06		1	
2.08.95		2.08.95	2.08.95						

0 drawing - no modified by hand

Frøysa, Lunde, Sakariassen, Grendstad & Norheim, "Operation of multipath ultrasonic gas flowmeters in noisy environments".
North Sea Flow Measurement Workshop, Peebles, Scotland, October 28-31, 1996.

OPERATION OF MULTIPATH ULTRASONIC GAS FLOW METERS IN NOISY ENVIRONMENTS

Kjell-Eivind Frøysa,
Per Lunde¹,
Reidar Sakariassen,
Jens Grendstad,
Rune Norheim,

Christian Michelsen Research AS (CMR), Bergen, Norway.
Christian Michelsen Research AS (CMR), Bergen, Norway.
Statoil K-Lab, Kårstø, Norway.
Kongsberg Offshore AS (KOS), Kongsberg, Norway.
Fluenta AS, Bergen, Norway.

SUMMARY

A 12" KOS FMU 700 multipath ultrasonic transit time gas flow meter (USM) has been used in testing at Statoil's K-Lab, in order to investigate the ultrasonic noise radiated by a 6" control valve with silencer trim in the operational frequency band of USMs, and the characteristic influence of the valve noise on the performance of USMs, when installed in the vicinity of such valves. The paper discusses the frequency contents of the valve noise, the signal-to-noise ratio (SNR), and the dependence of these parameters to gas/flow/valve parameters such as the gas pressure, the pressure drop of the valve, the flow rate, upstream/downstream operation of the USM relative to the valve, the distance from the valve, the lateral position of the acoustic paths in the USM, and the piezoelectric transducer orientation and directivity. Possible methods for noise suppression in USMs are discussed.

ABBREVIATION AND SYMBOL LIST

USM:	Multipath ultrasonic transit time gas flow meter.
SNR:	Signal-to-noise ratio (Eq. (6)).
P:	Hydrostatic pressure upstream of the control valve [bar].
ΔP :	Hydrostatic differential pressure (pressure drop) over the valve [bar].
v:	Average axial gas flow velocity, at line conditions [m/s].
v_{\min} , v_{\max} :	Minimum and maximum average axial gas flow velocity specified for the meter, respectively [m/s].
v_i :	Average axial gas flow velocity along path no. i, at line conditions, $i = 1, \dots, N$ [m/s].
D:	Pipe diameter (here, D refers to a 12" pipe) [m].

1. INTRODUCTION

The use of multipath ultrasonic transit time gas flow meters (USM) is by the gas industry today seen as a realistic, competitive and cost-saving alternative to the use of more conventional technologies for fiscal metering of natural gas [1], [2], [3], [4], [5], [6]. The USM technology offers significant advantages such as high accuracy, compactness, bi-directionality, short upstream

¹ Presenting author

and downstream requirements with respect to bends, no pressure loss, short response time, and large turn-down ratio (1:50).

Through testing and operation of first generation USMs it has been demonstrated that ultrasonic noise generated by flow control valves deteriorates the performance of such meters [7]. For certain applications, valves may be installed close to the USM, and ultrasonic noise radiated by the valve may interfere with the flow meter signals. In testing with high pressure drops over the control valves, it has been experienced that USMs may fail to operate. Current industrial requirements as specified by European gas companies (i.e., GERG, the European Group for Gas Research) [1] state that USMs installed upstream of a control valve should tolerate relative pressure drops of $\Delta P/P \approx 25\%$ and 15% , at v_{\min} and v_{\max} , respectively.

In a commercial USM, problems with valve noise are being reduced by implementing a noise suppression algorithm, based on a signal averaging method ("stacking"). Significant improvements have been reported using this technique [7]. However, current noise suppression methods have potentials for further improved with respect to robustness and response time, to enable the following of rapid changes in the gas flow rate to the same high extent as has been demonstrated for USMs in test lines without valve noise present [8], [9]. Development work within this field is ongoing, by several manufacturers.

In order to further improve the robustness and response time of USMs operating in valve noise, the knowledge about such noise and its influence on USM should be improved, in the range of ultrasonic signal frequencies where such meters are operated [1]. That means, typically, in the 100 - 200 kHz range. A number of parameters or conditions may be expected to influence on the sensitivity of USMs to control valves, such as

- (a) The frequency content of the valve generated noise (i.e., the type of valve) in the operational frequency band of the USM.
- (b) The frequency filtering used in the USM.
- (c) The relative differential pressure of the valve, $\Delta P/P$.
- (d) The hydrostatic pressure in the pipeline, P .
- (e) The average axial gas flow velocity, v .
- (f) USM installed upstream / downstream relative to the valve.
- (g) The distance of the USM from the valve.
- (h) Receiving transducer facing the valve / facing away from the valve.
- (i) The lateral position in the pipe of path no. i .
- (j) The inclination angles of the acoustic paths, relative to the pipe axis.
- (k) The directivity of the piezoelectric transducers (beam width and side lobe level), at the dominating noise frequencies, in gas at operational pressure and temperature conditions.
- (l) The conversion efficiency and signal level of the piezoelectric transducers.
- (m) The transit time detection method implemented in the actual meter, including possible noise suppression methods.
- (n) The degree of flow profile disturbance caused by the valve (primarily for USMs installed downstream of the valve).
- (o) Whether the noise is primarily gas borne or pipe borne, or both. For significant pipe borne noise, the degree of acoustic isolation between the piezoelectric transducers and the spoolpiece (i.e., the transducer mounting) is an essential factor.

From practical operation and testing of USMs close to valves, some qualitative information on the influence of such parameters has been gained. It has been observed that [7]

- Valves equipped with silencer moves the noise towards ultrasonic frequencies,
- The more efficient the silencer is, the more energy is radiated at higher frequencies,
- The noise level at a given frequency increases with differential pressure and flow rate,
- More noise is radiated in the downstream direction than in the upstream direction,
- High frequency ultrasonic noise from the valves can interfere with the acoustic signals in the flow meter, resulting in degraded or even ruined measurement signals.

In general, the high-frequency distribution of the radiated acoustic noise from valves, and the characteristic influence of valve noise on the performance and accuracy of USMs installed close to a valve, is currently not well known. As part of a work to improve the robustness and accuracy of USMs installed close to valves, better information about the noise and its influences on USM signals is of interest.

In the present paper, the influence of some of the above mentioned factors are investigated experimentally. Noise characteristics of a 6" control valve with silencer trim are investigated in a frequency band of relevance for USMs, and its influence on a commercial 6-path USM (the KOS FMU 700 meter) is examined, in the case where noise suppression algorithms are not activated. The recorded information serves as a base to improve noise suppression methods. The paper discusses the frequency contents of the valve noise, the signal-to-noise ratio (SNR), and the dependence of these parameters to gas/flow/valve/installation parameters such as (c)-(i) listed above. Possible methods for noise suppression in USMs are discussed.

2. FLOW TESTING AT K-LAB

The 12" KOS FMU 700 six path USM [9] was installed in a gas test loop at Statoil's K-Lab, in series with a 6" control valve with silencer trim. In the tests, the USM was installed 10D and 5D upstream of the valve² (2.6 m and 1.3 m, respectively), and 10D downstream of the valve, cf. Fig. 1. (Here D here refers to the USM diameter, 12".) No flow conditioner was used. Sonic nozzles were used as the reference flow meter, with a 8" Instromet turbine meter as a backup reference (installed downstream of the valve and the USM). The gas temperature and pressure were measured upstream of the valve and downstream of the valve. For the USM installed upstream of the valve, the gas temperature at the USM was in the range 37-39 °C. For the USM installed downstream of the valve, the temperature at the USM varied more, in the range 29-37 °C.

Table 1 shows the run matrix, i.e. the combinations of parameter settings (USM position / pressure / differential pressure / velocity) used in the test. In the table, "nominal" refers to the approximate, desired parameter setting, and "actual" refers to the actual (measured) parameter setting achieved in the test.

For each parameter setting (run) of Table 1, the analog output voltage signal delivered by each of the 12 piezoelectric transducers in the USM was sampled (digitized, at 10 MHz sampling rate and 8 bits resolution) and stored for later signal processing. The transducers were mounted in their transducer ports, as for ordinary flow metering operation of the USM. For each piezoelectric transducer, up to 32 succeeding signal traces were logged per run, for the purpose of SNR estimation, and the study of noise suppression techniques. Each recorded signal trace contains the received ultrasonic signal transmitted from the corresponding (opposite) transducer in the path, and the ultrasonic noise signals received by the transducer (cf. Figs. 2 and 3). It should be noted that the signal traces are of course influenced (filtered) by the frequency response of the piezoelectric transducers, and the frequency filter settings used in the meter electronics.

² More precisely: upstream of the 12"-to-6" conical diffuser installed at the valve spool, cf. Fig. 2.

Consequently, from a viewpoint of characterizing the valve noise only, an alternative measurement setup would be preferred, using a broadband high-pressure microphone (with a preferably flat and calibrated response to at least 200 kHz). However, the present setup, with recordings of signal and noise using the FMU 700 piezoelectric transducers, enables a more flexible and extended application of the recorded data. In addition to be used for "characterizing" the valve noise (at least to some extent), information about the SNR ratio in the meter is obtained, as a function of several flow parameters listed in the Introduction, cf. Section 3. In addition, the recordings are used directly in the study of noise suppression methods in the meter, cf. Section 4. Microphone recordings would not be so useful for the two latter purposes. The present setup is therefore used as a reasonable compromise.

The recorded signal traces are used to estimate the signal and noise levels, $V_{\text{signal}}^{\text{rms}}$ and $V_{\text{noise}}^{\text{rms}}$, respectively (both expressed as root-mean-square (rms) voltages), and the signal-to-noise ratio, SNR. Each recorded voltage trace, $V_m(t)$, $m = 1, 2, \dots, M$, consists of a time window containing essentially noise ("noise window"), and a time window containing the ultrasonic signal superposed with noise ("signal window"), cf. Fig. 3. To estimate the rms noise level, $V_{\text{noise}}^{\text{rms}}$, the rms noise level of trace no. m is first calculated over a time window of $T_1 = 350 \mu\text{s}$ within the noise window of the trace, i.e. as

$$V_{\text{noise},m}^{\text{rms}} = \sqrt{\frac{1}{T_1} \int_{t_1}^{t_1+T_1} V_m^2(t) dt}, \quad (1)$$

where t is the time, and t_1 is a time in the beginning of the noise window. The rms noise level is then found by averaging over a number of N traces, i.e. as

$$V_{\text{noise}}^{\text{rms}} = \frac{1}{N} \sum_{m=1}^N V_{\text{noise},m}^{\text{rms}}. \quad (2)$$

To estimate the signal level, $V_{\text{signal}}^{\text{rms}}$, up to $M = 32$ signal traces are first averaged ("stacked") in order to suppress the superposed noise, giving an averaged voltage trace,

$$V_{\text{average}}(t) = \frac{1}{M} \sum_{m=1}^M V_m(t). \quad (3)$$

The rms signal level is then calculated over a time window of $T_2 = 100 \mu\text{s}$ within the signal window, on the resulting averaged signal trace, i.e. as

$$V_{\text{signal}}^{\text{rms}} = \sqrt{\frac{1}{T_2} \int_{t_2}^{t_2+T_2} V_{\text{average}}^2(t) dt} \quad (4)$$

where t_2 is a time in the stationary part of the signal. The signal-to-noise ratio is then calculated as

$$\text{SNR} = \frac{V_{\text{signal}}^{\text{rms}}}{V_{\text{noise}}^{\text{rms}}} \quad (5)$$

This is done for most of the parameter settings (runs) shown in Table 1, for several selected piezoelectric transducers of each run.

3. RESULTS

Selected results from the flow tests of the USM in valve noise at K-Lab are presented in the following. The results should be considered as preliminary, since data are presented for selected transducers only, in the two paths marked A and B shown in Fig. 2a.³

Fig. 2b show an example of a voltage signal trace for a low noise metering situation (recorded with the USM 10D upstream of the valve, $P = 23$ bar, $v = 0.5$ m/s, and $\Delta P/P = 1$ %). Traces of this type form the basis for measurement of transit times in USMs. The trace shown here, with a high signal-to-noise ratio, SNR, may be representative for the combination of low flow velocity and low pressure drop of the valve (as shown here), or for USM flow metering without valves installed in the line. For the latter case, a measurement accuracy of 0.5 % or better has been reported using the present meter [9].

With valves installed in the line, the signal is more influenced by valve noise as the flow velocity or the pressure drop increases, as discussed in the following.

3.1 Frequency content of valve noise

Fig. 3 shows single voltage signal traces recorded at one of the piezoelectric transducers, for the USM mounted 10D upstream of the valve, $P \approx 100$ bar and $\Delta P/P \approx 19$ %. Traces are shown for three different gas flow velocities: $v \approx 0.24$, 2.26 and 6.76 m/s. The transducer is facing towards the valve, at an oblique angle relative to the pipe. The same time and amplitude scales are used for all three traces. The noise window extends to about 1.05 ms, at which time the ultrasonic signal arrives. The figure clearly demonstrates that the noise level increases with increasing flow velocity, v , while the signal level is kept essentially constant. For the three velocities shown in Fig. 3, the SNR is calculated to about 22, 9 and 2 dB, respectively (cf. Fig. 5a). Additional results (not shown here) reveal that the noise level increases also with $\Delta P/P$, with a corresponding reduction in SNR (cf. also Fig. 5).

Fig. 4 shows the magnitude FFT (Fast Fourier Transform) spectrum of the noise signals given in Fig. 3, taken within the noise window of the respective traces, in the frequency band 100-200 kHz. The average of 10 magnitude FFT spectra are shown here. When using these results for noise characterization, one should be aware that the noise spectrum is influenced both by the filter setting used in the USM, and the frequency response of the receiving transducer (cf. the discussion of Section 2), so that the present results do not give the correct frequency spectrum of the noise. In spite of that, the results reveal important noise components in the frequency band 110-150 kHz, for the present valve. The results also show that the frequency contents of the noise is essentially the same at the three flow velocities.

Other results of the study (not shown here) indicate that the frequency contents of the noise is essentially invariant to the parameter $\Delta P/P$ as well; that it is essentially the same at 10D upstream and 10D downstream of the valve; and that it is independent of the transducer facing the valve or facing away from the valve.

3.2 Pressure, differential pressure and flow velocity effects

Fig. 5a shows the SNR (plotted on a dB scale, i.e., $20\log_{10}(\text{SNR})$) as a function of the flow velocity, v , at different values of $\Delta P/P$, for the transducer facing towards the valve. (Note that the

³ Note that the two paths A and B shown in Fig. 2a are located at different lateral positions in the pipe. This is shown in the left part of the figure, but not in the right part, which has been simplified in this respect.

curve for $\Delta P/P = 19\%$ corresponds to time traces as shown in Fig. 3.) The SNR is observed to decrease systematically with increasing v , and with increasing $\Delta P/P$, due to an increasing level of the valve noise. The corresponding results at 23 bar (not shown here) are to a large extent equal, within less than 3 dB for most of the runs. This result (which has been observed for transducers facing towards and away from the valve, and for different paths) indicate that the pressure dependence of the SNR appears essentially through the parameter $\Delta P/P$.

The observed increase of the valve noise level by increasing ΔP and v (and the corresponding decrease of the SNR) is probably explained by the increase of the gas flow velocity in the narrow opening slit of the control valve which follows from increasing the pressure drop, ΔP ; increasing gas the flow velocity in the pipe, v ; or both.

3.3 Transducer orientation effects

Fig. 5a and 5b show SNR results for path A, for the two transducers which are facing towards the valve and facing away from the valve (nos. 4 and 7), respectively. A systematically higher SNR is observed for the transducer facing away from the valve. For the present path example, the difference is approximately in the range 9-13 dB.

This result may probably be explained by the directivity properties of the transducer, cf. Fig. 6. Assumed that the noise propagates essentially in the direction of the pipe, the noise will probably be received primarily through the 1st side lobe for the transducer facing towards the valve, since the main lobe will not be very sensitive to the direction of the noise, and since the level of the higher-order side lobes is expected to be lower than for the 1st side lobe.

On the other hand; for the transducer facing away from the valve, the noise will probably be received primarily through the higher-order side lobes, since both the main lobe and the 1st side lobe will not be sensitive to the direction of the noise (unless a considerable amount of the noise is reflected at the pipe wall or the opposite transducer).

Thus, since the level of the higher-order side lobes is expected to be significantly lower than the level of the 1st side lobe, the noise level will be higher for the transducer facing towards the valve.

One should be aware that there are factors which complicate the above qualitative analysis, and which are not controlled at present. These are the directivity properties of the transducers at the gas/pressure/temperature conditions used, and the influence on the directivity of the geometry of the transducer mounting ports. The effective directivity of the transducers in the pipe, under the actual test conditions, is thus not sufficiently known. In spite of that, the above analysis is expected to hold, qualitatively.

It follows from such an analysis that the noise level will also vary with the inclination angle of the path, ϕ . The variation will depend on the actual transducer directivity under the operational gas/pressure/temperature/mounting conditions.

3.4 Influence of lateral position of path

Figs. 7a and 7b show SNR results for transducers facing towards the valve, for the acoustic paths A and B, respectively. A higher SNR is observed for path B, by about 6-7 dB. About half of this increase is probably explained by the shorter propagation length of path B, giving a higher signal level. It is also expected that for the outer path (path B), the effective transducer directivity will be more influenced by the transducer mounting port than for path A, giving a larger "shadowing effect" of the noise for path B than for A, due to the geometry of the port. This may contribute to

the observed higher SNR ratio for path B. A third factor is of course the possibility of lateral variation of the noise level in the pipe. This factor is not known at present, however.

3.5 Installation effects

In Fig. 8, SNR results are compared for the USM installed 10D and 5D upstream of the valve (i.e. 1.3 m and 2.6 m upstream, respectively). For the lower velocities, an increase of the SNR of up to about 4-5 dB has been observed for the path shown here, by moving the USM from 1.3 m to 2.6 m from the valve. No significant increase of the SNR has been found for the upper part of the velocity range ($v = 6-8$ m/s), however. This observed difference in the increase of SNR over the flow velocity range has not been explained so far, and is to be investigated also for the other paths of the meter.

Fig. 9 illustrates the influence of installing the USM 10D (2.6 m) upstream or 10D downstream of the valve. Signal traces are shown for each of the two cases, for the case of $P \approx 100$ bar, $v \approx 2.5$ m/s, and a relatively large pressure drop, $\Delta P/P \approx 19$ %. A significant reduction of the SNR is observed for the USM installed downstream of the valve, relative to the upstream installation, due to a higher noise level downstream. Similar results have been observed also for other transducers and paths, and are qualitatively in agreement with results reported in ref. [7]. The results may indicate that the present valve type radiates more strongly downstream than upstream. The results also suggest that if possible, USMs should be installed upstream of the valve, in order to reduce the noise level and increase the SNR.

4. DISCUSSION

Various strategies for improving the SNR of USMs operating in valve noise may be considered, as discussed in the following. Combined techniques for raising the received signal amplitude, and for noise suppression, are of interest.

4.1 Received signal amplitude

For piezoelectric transducers working in the linear range, the SNR can of course be increased by *increasing the input voltage signal amplitude*. The maximum input voltage that can be used is, however, limited by at least three factors: safety requirements, nonlinearity in the piezoelectric transducers, and nonlinearity in the gas under the operating pressure and temperature conditions.

With respect to possible nonlinearity in the transducers and the gas, both increase by increasing input voltage. In high-precision applications of USM, such as fiscal gas metering, the transducers are recommended not to be driven in the nonlinear range, which might introduce problems with reciprocity and signal distortion. It appears that the input voltage limit will in general depend on the design and properties of the transducer, and is thus meter dependent. It will also depend on the gas properties (pressure, temperature, gas composition). For a given transducer design, the limiting input voltage (with respect to nonlinearity) should be determined experimentally. For the FMU 700 transducers, such measurements have been made in air at 1 atm. conditions. At present, documentation with respect to possible nonlinearity effects in the operational pressure, temperature and gas compositional ranges of the commercial USMs does not seem to be available.

For certification in the safety class EEx ia IIB T4, the maximum allowed electrical power delivered to the zone 0 area is about 4.8 W. This maximum power puts restrictions on the input

voltage which can be delivered to the piezoelectric transducer. The allowed voltage depends on the electrical input impedance of the transducer, and will depend on the specific transducer design used in the meter. However, for a given maximum power delivered to the transducer, the SNR can be increased by *improving the conversion efficiency of the transducer*, assumed that nonlinearities in the transducer and the gas do not occur (as discussed above).

The signal level (and thus the SNR) can also be increased by *increasing the transducer directivity*, i.e., by narrowing the main lobe. This will give a higher signal level for the same input voltage to the transducer, i.e., for the same power consumption.

4.2 Noise suppression

With respect to noise suppression, the use of *more optimal frequency filtering* of the time signals may be advantageous. That means, to remove as much as possible of the valve noise by filtering, without severely influencing the amplitude and time delay of the ultrasonic signal. Even for USMs using signal frequencies in the vicinity of a dominant frequency band of the valve noise (such as 110-150 kHz, for the present valve, cf. section 3), the SNR may possibly be somewhat improved by such filtering.

For directive transducers, as used here, the results indicate that a significant part of the noise may be received through the transducer's side lobes (the first side lobe and the higher side lobes, for transducers facing towards and away from the valve, respectively). Since the signal is received through the main lobe, the SNR ratio may thus probably be increased by *lowering the side lobe level of the transducers* (at the dominating noise frequencies) relative to the main lobe (at the signal frequency), especially for the first side lobe. To evaluate the degree of noise suppression which can be obtained by such *spatial filtering*, information is necessary about the transducer directivity (beam width and side lobe level), at the signal frequency and the dominating noise frequencies, and at the operational pressure, temperature and gas compositional conditions. This directivity may be significantly different from the directivity in air at 1 atm. and room temperature conditions. For the FMU 700 meter, the transducer properties have been measured for the most part in air at 1 atm. conditions, supplied with measurements at various pressure and temperature conditions. At present, documentation of the transducer directivity of commercial USMs, in the operational pressure, temperature and gas compositional ranges of these meters, and over the relevant frequency band, does not seem to be available.

A complicating factor here is of course the *influence of the transducer mounting port on the transducer directivity*. Due to such influence, the "effective directivity" (beamwidth and side lobe level) of the transducer mounted in the spoolpiece is not the same as the transducer's directivity in freefield (measured without mounting in the port), and this influences on the meter's sensitivity to valve noise. Since the geometry of the various ports are different, the "effective directivity" of the various transducers mounted in a USM may also be different. However, transducers with a low side lobe level will be less influenced by the port than transducers with a higher side lobe level. To evaluate possibilities for noise suppression by lowering the side lobe level, the influence of the transducer ports on the transducer directivity should be investigated experimentally.

Significant noise suppression can also be obtained using *digital signal processing* methods. *Signal averaging ("stacking")* methods have been used successfully in a commercial USM. The tolerated differential pressure, ΔP , may be increased by a factor 2-5 using such methods [7]. Fig. 10 shows an example of how a signal largely influenced by valve noise (SNR \approx 9 dB; cf. Figs. 3 and 5a) can be recovered to a large extent using a signal averaging technique. The averagings shown in Fig. 10 are made according to Eq. (3), with averaging number $M = 1, 5$ and 27 ,

respectively. In the present example, the SNR is increased by about 16 dB by averaging 27 signals. Using such averaging, the robustness of the time detection may be improved considerably, and the meter operated in more noisy environment.

However, sampling and averaging of signal traces is very time consuming, and with up to about 30 traces averaged, as considered in the present study, the response time of the meter may be significant (several tens of seconds). That means, the meter may not be able to follow rapid changes in the flow rate, or may even fail to operate over a certain time period, after which the meter is again operating [7].

Consequently, there is today an interest in developing a signal processing method for noise suppression which is at least as powerful as the signal averaging method with respect to the suppression of noise, but which has considerably shorter response time. Work in this direction is ongoing, in a cooperation between KOS and CMR. Fig. 11 shows a comparison of (1) a time detection method based on averaged ("stacked") signals (as illustrated in Fig. 10), and (2) an *alternative signal processing method* for time detection which is under development and testing. The figure shows the relative difference in the transit time difference, Δt_i , for the two methods (1) and (2), for a single path (no. i) in the meter (here chosen as approximately a "worst case" path with respect to the SNR, cf. Fig. 5a)⁴. The figure indicates that with respect to the measurement of Δt_i for path no. i , the alternative method (2) has an accuracy similar to the "stacking" method (1). For the present example, the difference is less than 0.08 %. Due to the relation between Δt_i and v_i (cf. Fig. 11) it follows that the alternative method (2) may have an accuracy similar to the "stacking" method (1) also for measurement of v_i , the average axial flow velocity along path no. i . The main advantage of the alternative method (2) is the significantly reduced processing time relative to method (1). The promising potentials of the present method with respect to retaining similar measurement accuracy in valve noise as the "stacking" method, while significantly improving the response time of the meter relative to the "stacking" method, are being further explored.

5. CONCLUSIONS

In testing over several years, USMs have demonstrated to be accurate instruments for measurement of gas flow, with a number of advantages for the gas industry. However, when installed close to control valves, the ultrasonic noise radiated by the valve represents a problem for the first generation of USMs, and work is ongoing to overcome such problems.

In the present work, a 12" USM (the KOS FMU 700) is used for measurement of valve noise, and to study characteristic performances of USMs in valve noise, over the parameter range $P \approx 23$ and 100 bar, $v \approx 0.5$ -8 m/s, and $\Delta P/P \approx 1$ -19 %. Some conclusions of the work are:

- Important noise components are found in the frequency band 110-150 kHz, for the present 6" control valve with silencer trim.
- In the frequency range of the meter, the frequency content of the valve noise is found to be independent of P , $\Delta P/P$, v , transducer orientation, distance from the valve, and upstream/downstream installation of the USM.

⁴ The transit time difference of path no. i , Δt_i , is defined in the figure as the difference between the upstream and downstream transit times of the path, $t_{up,i}$ and $t_{down,i}$, respectively. Note that in the axis text of Fig. 11, $(\Delta t)_1$ and $(\Delta t)_2$ are replaced by $(\Delta t)_1$ and $(\Delta t)_2$, for simplicity in notation.

- The pressure dependence of SNR appears essentially through the parameter $\Delta P/P$.
- The SNR is significantly reduced by increasing v , and by and increasing $\Delta P/P$.
- The SNR is significantly lower upstream of the valve than downstream, which suggests that USM should preferably be installed upstream of a valve, if possible. However, with improved noise suppression methods, installation downstream of the valve may be feasible, possibly at a reduced accuracy.
- The SNR varies with distance from the valve, but more work is needed to clarify the effects.
- The SNR is higher for a receiving transducer facing away from the valve than for the corresponding receiver facing towards the valve. The result may be explained by the transducer directivity. The noise is probably received primarily through the side lobes of the transducer.
- The SNR depends on lateral position of the path. Parts of this effect may be explained by the difference in path length, and possibly by the geometry of the transducer mounting port.
- Results from the study (not shown here) show that the SNR depends on the inclination angle of the path.

These results are based on the use of a commercial USM, but are expected to be reasonably representative for other USM as well, at least qualitatively, in the range of ultrasonic signal frequencies where such meters are operated (typically in the 100-200 kHz range), and for the present valve type. Similar investigations should be carried out also for other valve types.

For robust metering in strong valve noise, a combination of several of the possible remedial actions discussed in Section 4 may be advantageous, for sufficient improvement of the SNR. For certain of these actions, the SNR may possibly be raised by several dB, while others might give only a few dB increase of the SNR. In sum, the total increase of the SNR may be significant by combining several remedial actions. In case of marginal operating conditions, a SNR increase of the SNR by even 10 dB (say), may be a significant improvement, which can extend the range of applications for the USM.

Results of the work indicate that robustness against valve noise can be significantly improved by a noise suppression algorithm, so that the USM can operate with an accuracy similar to a signal averaging ("stacking") method, but with a significantly reduced response time relative to a conventional "stacking" method. The noise suppression algorithm is currently being refined and tested, in order to be implemented in the KOS FMU 700 multipath gas flow meter. The accuracy of improved USMs installed near valves will be continuously addressed as the methods for noise suppression improves.

6. ACKNOWLEDGMENTS

In addition to the authors, Atle A. Johannessen, Reidar Bø, Gunnar Wedvich, Morten I. Andersen, Ørjan Villanger, Hans Ingebrigtsen and Svein Værholm at CMR; Asle Lygre at Aanderaa Instruments, Bergen; and Magne Vestrheim at the University of Bergen, Dept. of Physics, have given contributions to the development of FMU 700. Tore Tjomsland, CMR, has contributed to the project by aquisition and processing of the data. The present work has been

carried out in a cooperation between CMR, KOS, Statoil, The Research Council of Norway (NFR) and Fluenta AS. From May 1996, the FMU 700 meter is developed, produced, delivered and marketed by KOS a.s.

7. REFERENCES

- [1] LYGRE, A., LUNDE, P. and FRØYSA, K.-E. "Present status and future research on multi-path ultrasonic gas flow meters". GERG Technical Monograph TM8, Groupe Européen de Recherches Gazières, Groningen, The Netherlands, 1995. Also issued as: CMR Report no. CMR-95-A10037, Christian Michelsen Research AS, Bergen, December 1995.
- [2] ISO/CD-TR 12765. "Measurement of fluid flow in closed circuits - Methods using transit time ultrasonic flowmeters". ISO Technical Report, Berlin, May 1996.
- [3] "Measurement of gas by ultrasonic meters". Transmission Measurement Committee, Report no. 9, American Gas Association (A.G.A.), February 9, 1996 (Draft no. 2).
- [4] SAKARIASSEN, R. "Gas measurement by use of ultrasonic flowmeters". 19th World Gas Conference, Milan, 20-23 June 1994. International Gas Union, Round Table Committee C, Measurement Accuracy (IGU/RC7-94), 1994.
- [5] SAKARIASSEN, R. "Why we use ultrasonic gas flow meters". *Proc. of The North Sea Flow Measurement Workshop, Lillehammer, Norway, October 23-26, 1995.*
- [6] BOSIO, J. "Opening address", *Proc. of The North Sea Flow Measurement Workshop, Lillehammer, Norway, October 23-26, 1995.*
- [7] SAKARIASSEN, R. "Real life experience with multipath ultrasonic gas flow meters". In: *Proc. of International Pipeline Conference, Calgary, Canada, June 9-14, 1996.*
- [8] LYGRE, A., FOLKESTAD, T., SAKARIASSEN, R. and ALDAL, D. "A new multi-path ultrasonic gas flow meter", *Proc. of The North Sea Flow Measurement Workshop, NEL, Glasgow, October 27-29, 1992.*
- [9] LYGRE, A., JOHANNESSEN, A.A., DYKESTEEN, E. and NORHEIM, R. "Performance test of a 6 path USM". *Proc. of The North Sea Flow Measurement Workshop, Lillehammer, Norway, October 23-26, 1995.*

Table 1. Parameters settings for the USM valve noise testing at K-Lab using FMU 700.

Nominal				Actual			
Meter position rel. valve	P [bar] (upstrm)	v [m/s]	ΔP [bar]	$\Delta P/P$ [%]	v [m/s] ⁵		
10D up	100 bar	0.5 m/s	≈ 0 bar	0.12 %	0.47 m/s		
			5 bar	5.5 %	0.44 m/s		
			10 bar	10.1 %	0.42 m/s		
			20 bar	19.6 %	0.24 m/s		
		3 m/s	1 bar	0.9 %	2.92 m/s		
			5 bar	4.9 %	2.80 m/s		
			10 bar	9.9 %	2.65 m/s		
			20 bar	19.2 %	2.26 m/s		
		6-8 m/s	6 bar	5.9 %	8.21 m/s		
			10 bar	10.3 %	7.82 m/s		
			20 bar	19.4 %	6.76 m/s		
			23 bar	0.5 m/s	≈ 0 bar	0.74 %	0.49 m/s
	1 bar	4.5 %			0.47 m/s		
	2 bar	8.6 %			0.45 m/s		
	4 bar	16.8 %			0.32 m/s		
	3 m/s	≈ 0 bar		1.6 %	3.09 m/s		
		1 bar		4.0 %	3.01 m/s		
		2 bar		8.9 %	2.85 m/s		
		4 bar		17.1 %	2.60 m/s		
	6-8 m/s	1 bar	6.5 %	8.57 m/s			
2 bar		9.1 %	8.34 m/s				
4 bar		16.7 %	7.05 m/s				
5D up		100 bar	0.5 m/s	10 bar	8.6 %	0.84 m/s	
	20 bar			19.6 %	0.74 m/s		
	3 m/s			1 bar	0.88 %	2.94 m/s	
				5 bar	5.2 %	2.81 m/s	
			10 bar	10.2 %	2.66 m/s		
			20 bar	19.9 %	2.37 m/s		
	6-8 m/s		6 bar	5.9 %	8.27 m/s		
			10 bar	9.6 %	7.94 m/s		
			20 bar	19.2 %	5.20 m/s		
			10D dwn	100 bar	0.5 m/s	≈ 0 bar	0.20 %
	5 bar					4.9 %	0.47 m/s
	10 bar					9.7 %	0.46 m/s
20 bar	19.2 %	0.27 m/s					
3 m/s	1 bar	0.38 %			2.96 m/s		
	5 bar	4.8 %			2.95 m/s		
	10 bar	9.7 %			2.93 m/s		
	20 bar	19.0 %			2.59 m/s		
6-8 m/s	6 bar	5.5 %			8.73 m/s		
	10 bar	9.6 %			8.70 m/s		
	20 bar	18.7 %			6.34 m/s		

⁵ For the large majority of runs given in Table 1, the average axial gas flow velocity given in the table, v, was measured using the sonic nozzle bank. In some runs, however, the nozzles were operated subsonic, in which case the turbine meter reading for v is given.

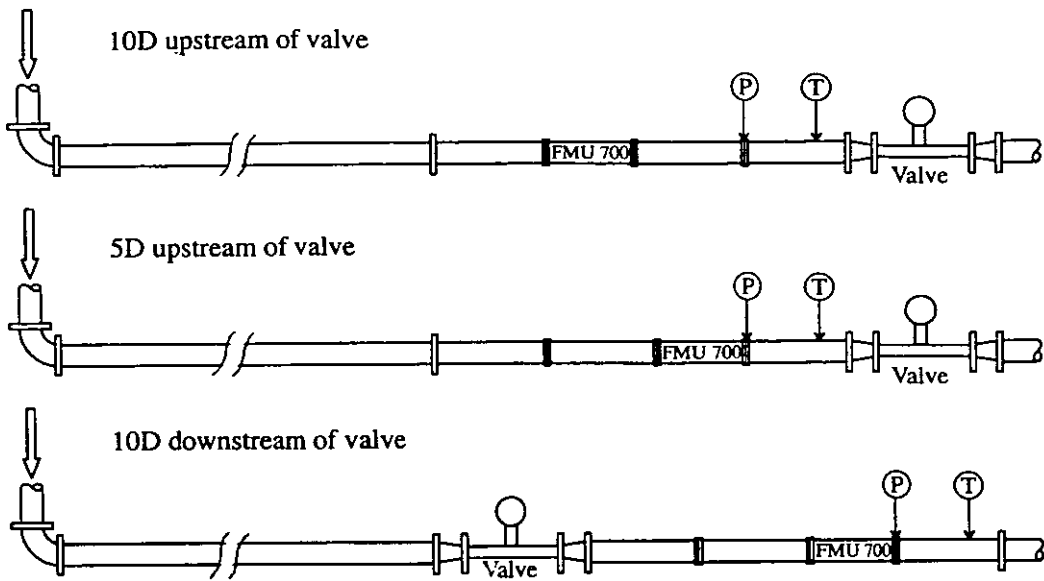


Fig. 1. Sketch of test section used at K-Lab, with the three different installation conditions.

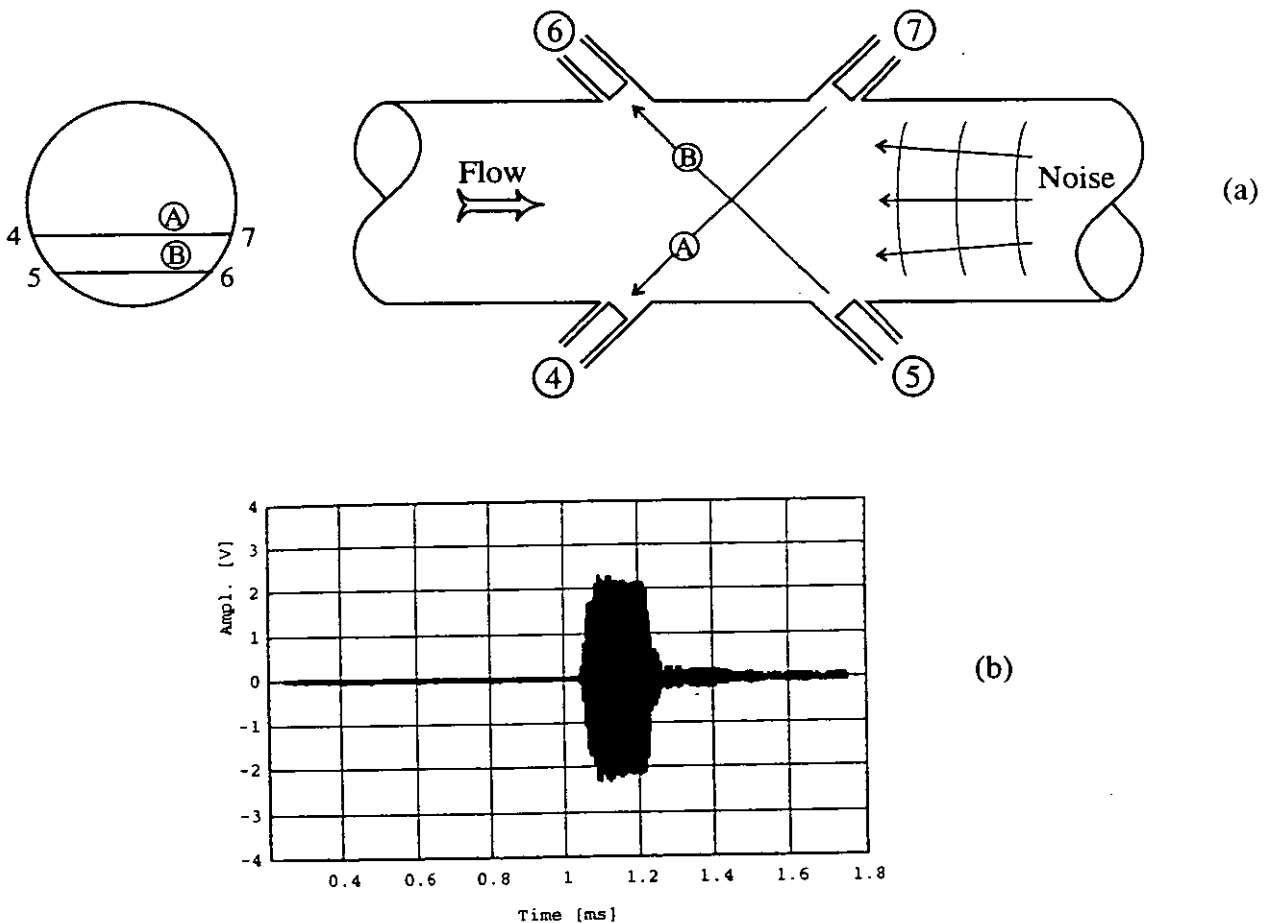
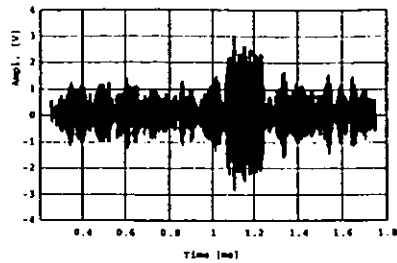
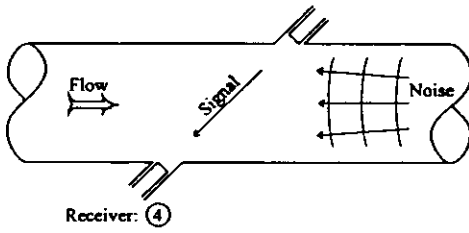


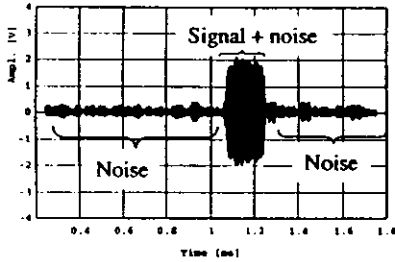
Fig. 2. (a) Sketch of the two acoustic paths A and B of the USM which are used in the results presented here, with the transducer numbering used here (for the case of the USM installed upstream of the valve).
 (b) Example of a recorded voltage-vs-time signal trace, for a low-noise metering situation (USM installed 10D upstream of the valve, $P \approx 23$ bar, $v \approx 0.5$ m/s, and a low pressure drop, $\Delta P/P \approx 1\%$).

SIGNAL TRACES

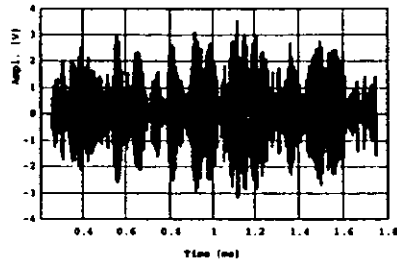
10D upstream, 100 bar, $\frac{\Delta P}{P} \approx 19\%$



$v \approx 2.3$ m/s



$v \approx 0.2$ m/s



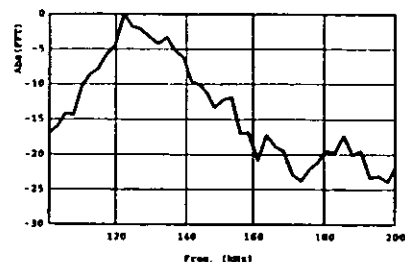
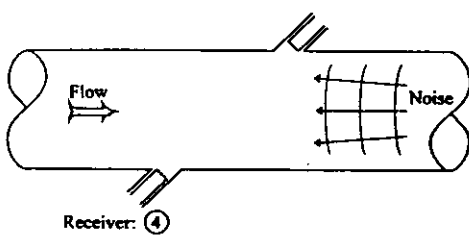
$v \approx 6.8$ m/s

Per Lundt-p3 pp-pp-23 10 96

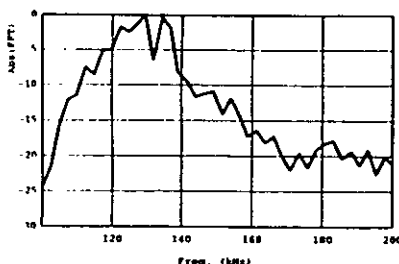
Fig. 3. Voltage signal traces, recorded at one of the piezoelectric transducers of the USM (no. 4), for different flow velocities; $v = 0.2, 2.3$ and 6.8 m/s. Installation conditions: USM 10D upstream of the valve, $P = 100$ bar, $\Delta P/P \approx 19\%$, transducer facing the valve, acoustic path A.

"NOISE FREQUENCY SPECTRUM"

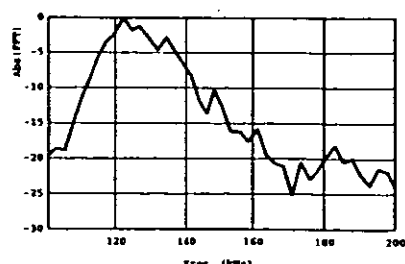
10D upstream, 100 bar, $\frac{\Delta P}{P} \approx 19\%$



$v \approx 2.3$ m/s



$v \approx 0.2$ m/s



$v \approx 6.8$ m/s

Per Lundt-p3 pp-pp-23 10 96

Fig. 4. Magnitude FFT spectrum of the voltage signal traces shown in Fig. 3, taken within the noise window of the traces.

Influence of transducer side lobes (spatial filter)

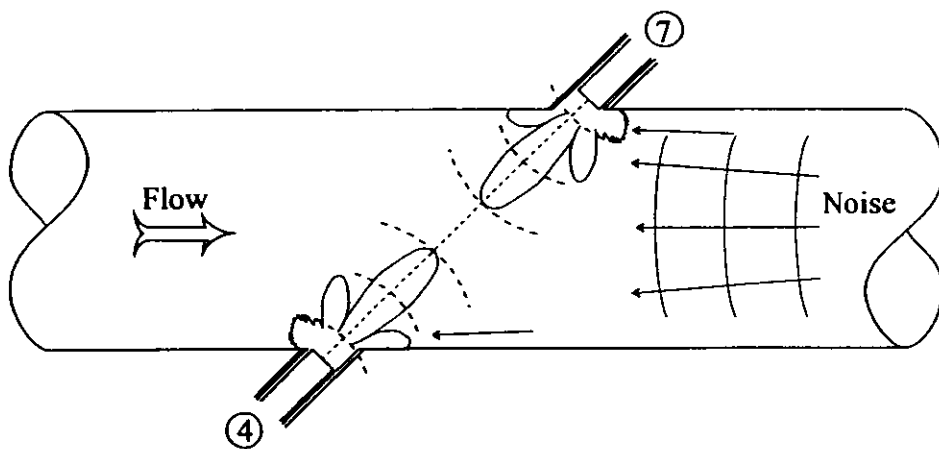


Fig. 6. Qualitative sketch of the transducer directivity (tentative direction and relative levels of main lobe, first side lobe, and higher-order side lobes), for two transducer mounted in the pipe (facing towards and away from the valve, respectively); relative to the expected noise propagation direction.

SNR Influence of ΔP , P , v and transducer orientation

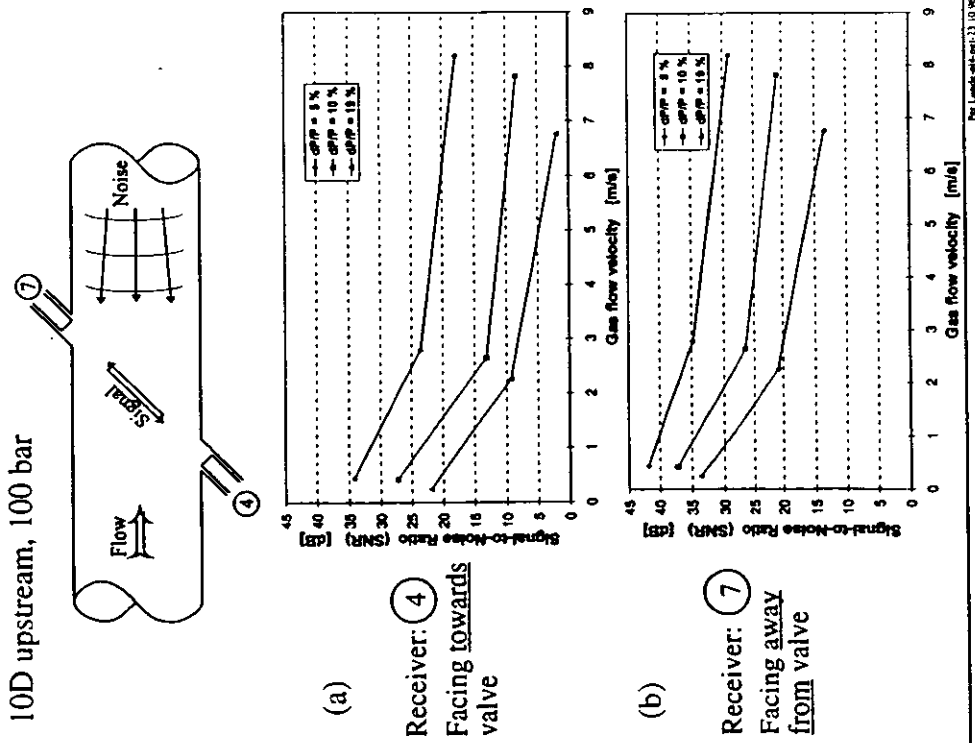


Fig. 5. SNR plotted vs. flow velocity, v , for different $\Delta P/P$.
 Conditions: USM installed 10D upstream of valve, $P \approx 100$ bar.
 (a) Path A, transducer facing towards the valve (no. 4).
 (b) Path A, transducer facing away from the valve (no. 7).

SNR

Influence of lateral position of path

10D upstream, 100 bar

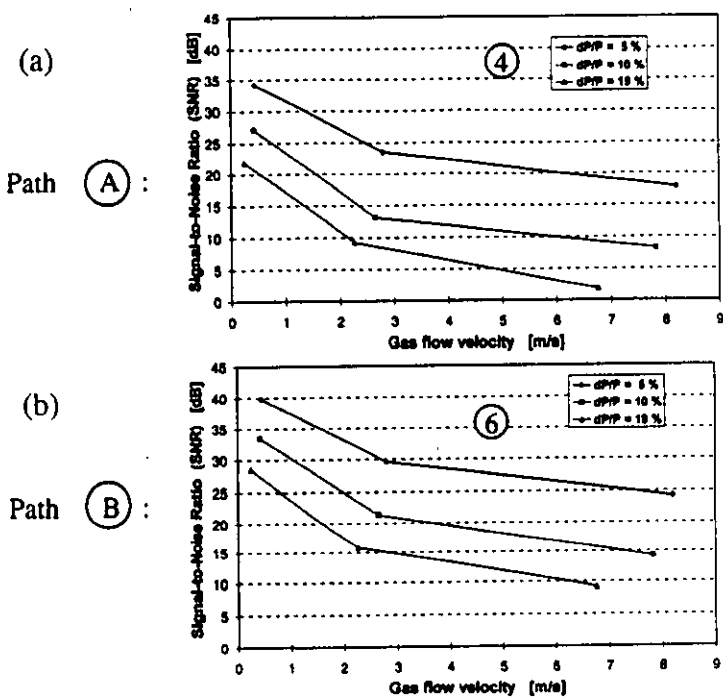
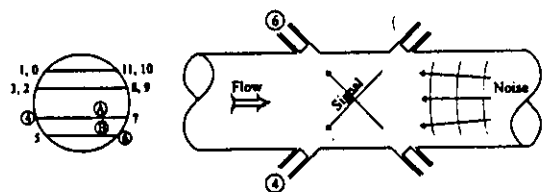


Fig. 7. SNR plotted vs. flow velocity, v , for different $\Delta P/P$.
 Conditions: USM installed 10D upstream of valve, $P \approx 100$ bar.
 (a) Path A, transducer facing towards the valve (no. 4).
 (b) Path B, transducer facing towards the valve (no. 6).

SNR

Influence of distance from valve

100 bar, transducer (4) (facing towards valve)

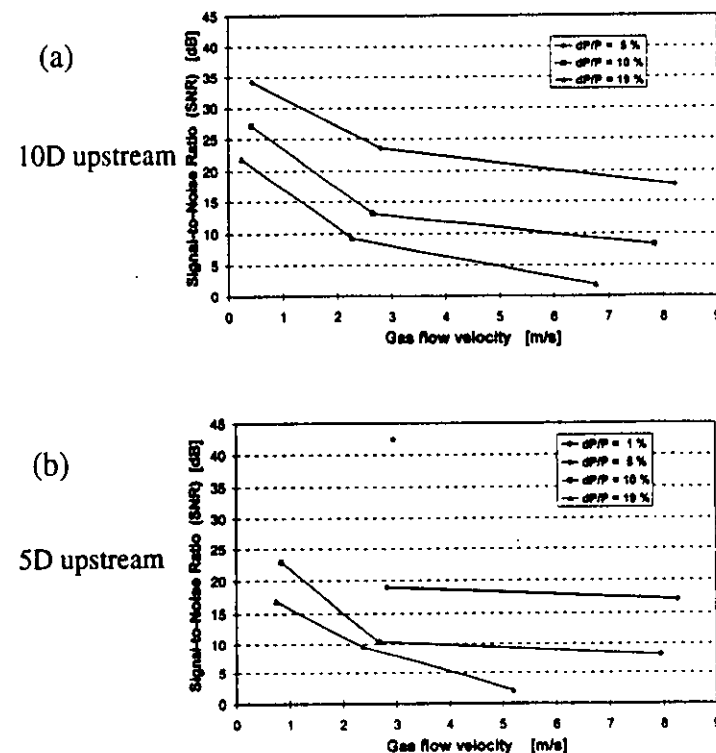
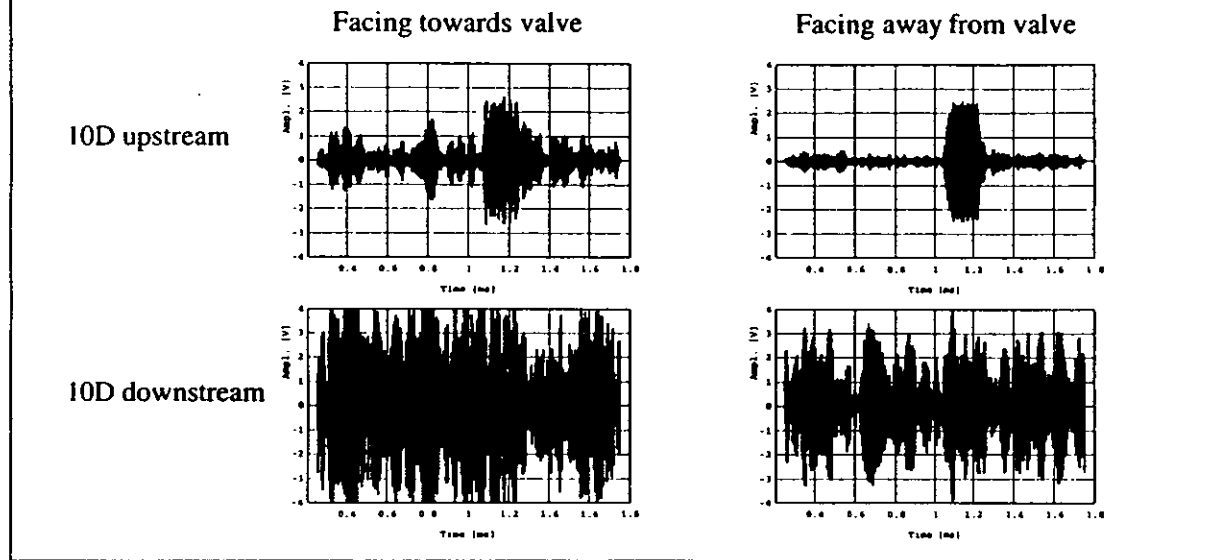


Fig. 8. SNR plotted vs. flow velocity, v , for different $\Delta P/P$.
 Conditions: $P \approx 100$ bar, path A, transducer facing towards the valve (no. 4).
 (a) USM installed 10D upstream of valve.
 (b) USM installed 5D upstream of valve.

USM upstream / downstream of valve

100 bar, $v \approx 2.5$ m/s, $\frac{\Delta P}{P} \approx 19\%$



Per Landa-p13 ppt-pg1-23 10 96

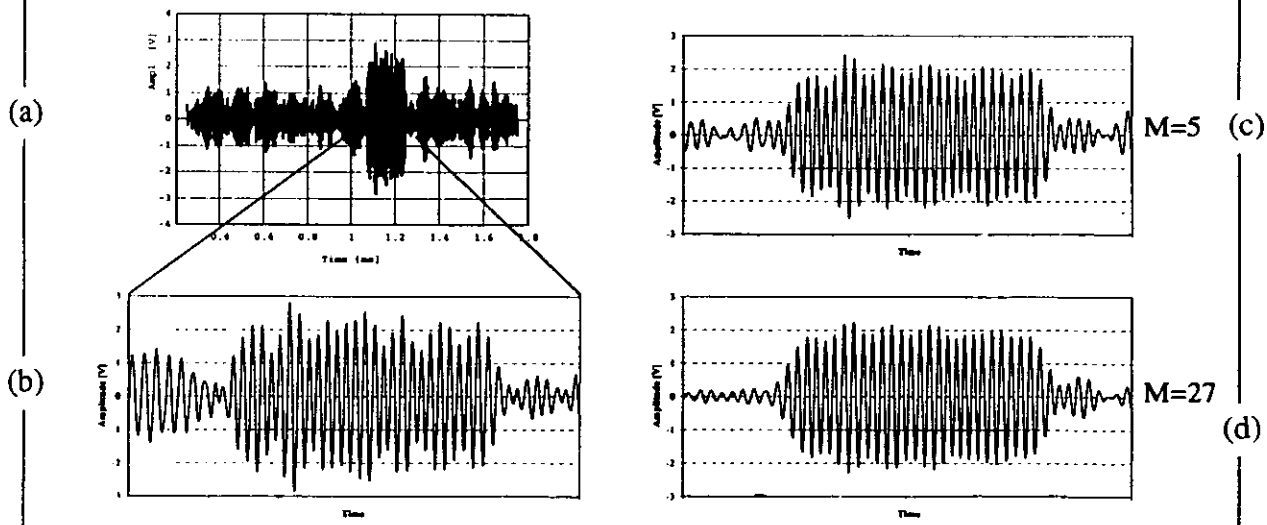
Fig. 9. Voltage signal traces, recorded for different installation conditions, as explained in the figure. For all traces: $P \approx 100$ bar, $v \approx 2.5$ m/s, $\Delta P/P \approx 19\%$.

Signal averaging ("stacking")

10D upstream, 100 bar, $\frac{\Delta P}{P} \approx 19\%$, $v \approx 2.3$ m/s, Receiver ④

No averaging: (SNR ≈ 9 dB):

With averaging:



Per Landa-p13 ppt-pg1-23 10 96

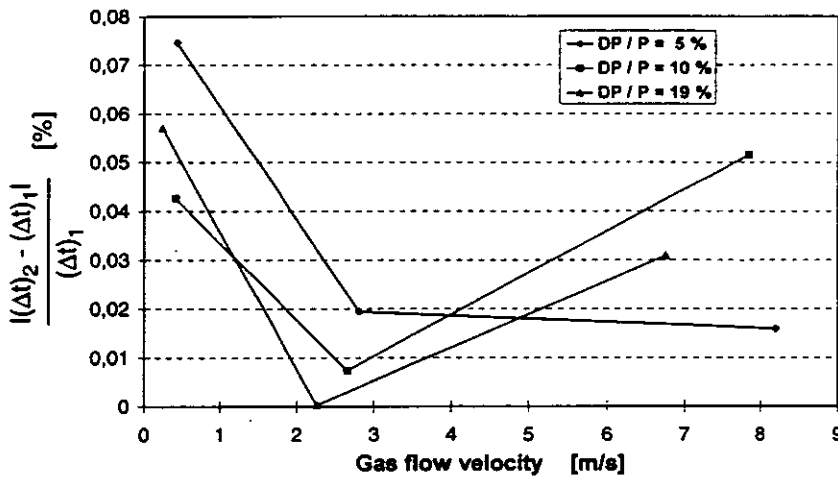
Fig. 10. Effect of averaging signal traces, recorded at one of the piezoelectric transducers of the USM (no. 4), for the following installation conditions: 10D upstream of the valve, $P \approx 100$ bar, $\Delta P/P \approx 19\%$, $v \approx 2.3$ m/s, transducer facing the valve. (a) No averaging; (b) blow-up of the signal part of the trace shown in (a); (c) average of 5 traces; (d) average of 27 traces.



COMPARISON OF TIME DETECTION METHODS IN VALVE NOISE

- (1) Signal averaging ("stacking")
- (2) Alternative signal processing method

≈ "Worst case" path:



$$v_i = \frac{L_i \Delta t_i}{2 t_{1i} t_{2i} \cos \phi_i}, \quad \Delta t_i \equiv t_{up,i} - t_{down,i}$$

$$v = \sum_{i=1}^N w_i v_i$$

For Lunde-p44-pg1-23.10.96

Fig. 11. Comparison of (1) signal averaging method ("stacking") and (2) "alternative signal processing method" for transit time detection, for USM installed 10D upstream of the valve, $P = 100$ bar, and for path A (cf. Fig. 5a). The figure shows the relative difference in Δt_i between the two methods, for a single path. Expressions for the average axial flow velocity along path no. i , v_i ($i = 1, \dots, N$), and the average axial (integrated) flow velocity in the pipe, v , are also given.

PRACTICAL EXPERIENCE WITH GAS ULTRASONIC FLOW METERS

K. J. Zanker Daniel Industries UK
W. R. Freund Jr. Daniel Instruments USA

1. SUMMARY

Two very different situations are reported: type approval testing of a small 6" meter; and calibration of a large 30" meter. The small meter was chosen for its sensitivity to dimensional and timing errors, whereas the large meter (5 times larger) should be immune to such influences. However when calibrating the 30" meter some unexpected effects were experienced: at one extreme, due to the difficulty in obtaining large flows in the calibration facility and maintaining them long enough to reach thermal equilibrium; and at the other, due to solar radiation, stratification and convection currents distorting the low flows.

Type testing showed that: the meter functioned equally well in both the forward and reverse flow direction; and that it is possible to exchange transducers with little loss in accuracy.

The 30" meter calibration showed that: the diagnostic ability of the ultrasonic meter can recognise unusual conditions; that more care must be taken to reach thermal equilibrium during calibration; and that the meter design could be refined.

2. NOTATION

NMI	Netherlands Measurement Institute
VOS	Velocity of sound in the gas
D	Pipe internal diameter
t_1	Transit time against flow component
t_2	Transit time with flow component
$\Delta\tau$	Transit time difference ($t_1 - t_2$)
Tamb	Ambient temperature
Tult	Temperature in the ultrasonic meter
ChdVel	Chord velocity
AveVel	Average velocity

3. INTRODUCTION

The multipath meter was developed by British Gas in the early 1980's and licensed to Daniel Industries in 1986. The first commercial production meters were sold in 1989, thus there is 7 years of field experience and many publications (Ref. 1,2,3,4,5) describing meter theory, performance, application and special features. Despite this, ultrasonic technology for gas flow measurement is relatively new, especially compared with the orifice plate, and not yet well established. There is no recognised standard at present although there is a draft ISO technical report (Ref. 2). The information given here is presented with the intention of advancing the acceptance and standardisation of Ultrasonic gas flow measurement.

4. TYPE APPROVAL TESTING OF A 6" METER

As part of the NMI type approval process for the ultrasonic meter the following tests were performed:

- Calibration of the meter with flow in the normal forward direction
- Calibration with the flow in the reverse direction (meter rotated 180 degrees)
- Re-calibration after exchanging one pair of transducers (one chord)
- Re-calibration after exchanging two pair of transducers (two chords)

A 6" meter was chosen for these tests because it is the smallest in the range and hence the most sensitive to dimensional ($D = 150 \text{ mm}$) and timing ($t = 600 \mu\text{s}$) errors.

The results are shown in Figs 1, 2, 3 & 4, as % Error from the reference meter against Velocity, with the open points showing all the repeated tests and the closed points showing the average error. To help comparison of these results, all four average errors are plotted on the same graph in Fig 5.

The scattering of the results increases at the lower velocity flows, which is to be expected as the transit time difference $\Delta\tau$ decreases. In fact at 1 m/s velocity in the 6" meter, $\Delta\tau = 1 \mu\text{s}$ for chords A & D (outside) and $\Delta\tau = 2 \mu\text{s}$ for chords B & C (inside), giving a weighted average of $\Delta\tau = 1.7 \mu\text{s}$. Thus a timing error of just 17 ns is sufficient to give a 1% error in velocity and is in line with the Daniel claimed timing accuracy of 20 ns. At higher flows the typical scatter, or repeatability, is 0.2%, coming from both the meter and test facility.

The results from Fig 1 & 2 show that the meter is reversible without the need to change any meter factor for the different flow directions. The results from Fig 3 & 4 show that transducers can be exchanged using the factory "dry" calibration procedure, with negligible deterioration in performance. Fig 5 shows that all four tests give basically the same result within the scatter and repeatability of any individual test.

4.1 Comments

The dry calibration determines the physical size of the transducer and the delay times associated with the transducers and electronics. The average delay time for a pair of transducers ($AveDly = [t_1 + t_2]/2$) is typically $24 \mu\text{s}$, is known to about 1% or $0.24 \mu\text{s}$, and thus should contribute $0.48/600 = 0.08\%$ to the velocity measurement error (VOS**2). The delta delay ($DltDly = t_1 - t_2$ at zero flow) can only be determined to $0.02 \mu\text{s}$ and is the cause of any zero offset error and the scatter at low flows.

The exchangeability of the transducers suggests that the AveDly and DltDly are basically associated with the transducers and not the electronics. This is in line with the design of the new and improved MK II electronics.

With these transducer exchange tests only the factory dimensions and delays were entered into the software. In practice these can be further verified in the field by checking the VOS and

velocity profile before and after the exchange.

5. CALIBRATION OF A 30" ULTRASONIC METER

The 30" meter with $D = 670$ mm, $t = 4000$ μ s and $\Delta\tau = 10$ μ s at 1 m/s was expected to give a good calibration, but that was not found to be the case, as shown in Fig 6. One immediate pointer to a possible reason was the temperature difference between ambient and the gas ($T_{amb} - T_{ult}$), also shown in Fig 6. When the temperatures are not the same it gives rise to two potential problems:

- what temperature should be used to correct the reference meter flow to the actual flow through the ultrasonic meter ?
- what effect does the temperature gradient over the acoustic path have on the operation of the ultrasonic meter ?

The calibration was performed on a relatively rare warm and sunny day ($T_{amb} = 16$ C) and at high flow the gas temperature dropped to $T_{ult} = 4$ C, as a result of expansion due to the pressure drop required to achieve the large flow. The maximum flow of 11 m/s (not 15 m/s velocity) could only be held for 15 min, both limited by the test facility, and hence thermal equilibrium was never reached. Furthermore the max flow was the first flow of the day, due to the test facility being part of the national grid, it would have been better to increase the flow slowly up to the max, to try to cool down all the pipework and meter body to the gas temperature, but then there would be no guarantee of still being able to reach the max flow.

At low flows temperature effect become very pronounced, both on the velocity profile and the VOS profile across the chords.

Figs 7 & 8 show the same non-dimensional chord velocity ratio data in two different ways:

- Fig 7 plots the individual chord velocity ratio against the flow velocity
- Fig 8 plots the velocity profile across the pipe diameter for different flow velocities

At high flows the profile is normal, but at low flows the velocity at the top of the pipe (Chord-A) decreases while the velocity at the bottom of the pipe (Chord-D) increases.

Figs 9 & 10 show the same velocity of sound (VOS) data in two different ways:

- Fig 9 plots the individual chord VOS against the flow velocity
- Fig 10 plots the VOS profile across the pipe diameter for different flow velocities

At high flows the VOS becomes uniform across the pipe, but at low flows the VOS increases, with the greatest effect noticeable at the top of the pipe (Chord-A), next on Chord-B and so on.

It was observed that at flows below 1 m/s the temperature in the pipe rose to 22 C (measured near the top) as a result of solar radiation on the un-insulated steel pipes. VOS is a measure of temperature for constant gas composition, a 1% change in VOS (4/400) corresponds to a 2% change in temperature (6/300) as $VOS = T^{*0.5}$. Thus the 10 m/s VOS gradient corresponds to a 15 Deg C temperature gradient from 7 to 22 Deg C and seems reasonable.

The max VOS (and temperature) occurs at 1 m/s and not at Zero flow, presumably this is because the heat transfer with the pipe wall is better.

It is most likely that the VOS and velocity profiles are related via convection effects. One can postulate that cold gas (from the mains) enters a hot meter (from solar radiation) and tends to fall towards the bottom of the meter giving the observed higher velocity on the D-Chord.

A crude estimate of the convection current magnitude, based on a density difference of 3% and a 600 mm fall, gives a velocity of $(20 \times 3\% \times 0.6)^{0.5} = 0.6$ m/s (where 20 = 2g m/s/s). The calculation shows that the large size (30") contributes as much as the temperature difference (density difference) to the problem of convection. Thus the large meter size magnifies any problems due to a lack of thermal equilibrium.

Apart from this vertical VOS and temperature gradient, there is a horizontal VOS gradient because the gas in the transducer ports and isolating valves will be closer to T_{amb} than to T_{ult} . The effects of these gradients on the meter performance are difficult to estimate. Simple theory assumes that the VOS is the same throughout the meter, not only does the gradient upset this, but it also produces other effects due to refraction and distortion of the ultrasonic signal.

5.1 Comments

The problems described above are associated with calibration and will not occur in the actual 30" meter application. In use the meter and pipework will be insulated and the flow will be continuous such that thermal equilibrium will be achieved and maintained. The diagnostic ability of the meter will recognise any peculiarities in velocity profile or VOS distribution and confirm that the meter is functioning correctly

There is a need to improve the calibration facility for these large meters, but this is not straightforward. The 30" meter can easily handle the total national grid flow at the British Gas, Bishop Auckland facility. Insulating all the pipework would considerably reduce the flexibility of the test site. Covering the pipework, to shield it from direct sunlight, would reduce access with cranes and equipment. Increasing the flow rate and holding it for a longer time would require another mode of operation, with the cooperation of Transco and require three reference 12" turbine flow meters, instead of the two used at present.

Alternatively it can be argued that there is no need to calibrate large meters, as their performance could be predicted, with sufficient accuracy, based on theory and model testing of smaller meters. It is the ultimate goal to produce an ultrasonic meter that does not require flow calibration.

Another approach is to modify the ultrasonic meter design. The 6" meter is too small to fit transducer isolation valves, but the 30" meter has 1500# double block & bleed isolation valves fitted to all eight transducer ports, making a very much longer acoustic path, 4000 μ s compared with 2680 μ s (= $600 \times 670 / 150$) for a scaled up 6" meter, with much of the path outside of the flow and hence influenced more by the ambient temperature.

The idea of isolating valves is attractive, to be able to change transducers without shutting down the flow, but can increase potential temperature gradient effects and act as a moisture trap. The present tendency is to place the transducer close to the pipe bore (not in a cavity) to eliminate temperature gradients in the ultrasonic path and avoid liquid traps thus making wet gas

measurement possible. An extractor mechanism is being designed to remove transducers from the meter under pressure one at a time, with the added advantage that only one extractor is necessary, not eight isolation valves.

6. CONCLUSIONS

It has been demonstrated that the ultrasonic meter is reversible, with the same performance in both directions.

It is possible to change transducers, without the need for re-calibration, with negligible (0.1%) loss of accuracy.

It proved to be quite difficult to calibrate the large 30" meter, mainly because it was impossible to reach thermal equilibrium in the flow facility

The calibration did reveal that the diagnostic ability of the meter was able to recognise this unusual situation and would be able to confirm correct operation in actual practice.

The calibration did suggest that some modifications to meter design could partly alleviate these difficulties.

The strange effects are a result of the calibration process and would not occur in actual use.

It might be both more expedient and more accurate to accept "dry" calibration of large meters.

The small meter magnifies the effects of dimensional and timing errors, where as the large meter magnifies any effects due to temperature differences.

7. REFERENCES

1. BLOEMENDAAL K. van and KAM P.M.A. van der " Installation Effects on Multi-Path Ultrasonic Flowmeters: The Ultraflow Project" North Sea Flow Metering Workshop 1994
2. ISO/TR 12765, Draft Standard, " Measurement of Fluid Flow in Closed Conduits - Methods using Transit Time Ultrasonic Flowmeters" May 1996
3. ZANKER K.J. and FREUND W. R. "Developments of Multipath Transit Time Ultrasonic Gas Flow Meters" North Sea Flow Metering Workshop 1994
4. FREUND W.R. and WARNER K.L. "Performance Characteristics of Transit Time Ultrasonic Flow Meters" 3RD Int. Symp. on Fluid Flow Measurement, San Antonio, 19-22 Mar 1995
5. ZANKER K.J. "Ultrasonic Transit Time Gas Flow Meters" I M & C, May 1995

Fig 1. Calibration of 6" USM

Normal Flow

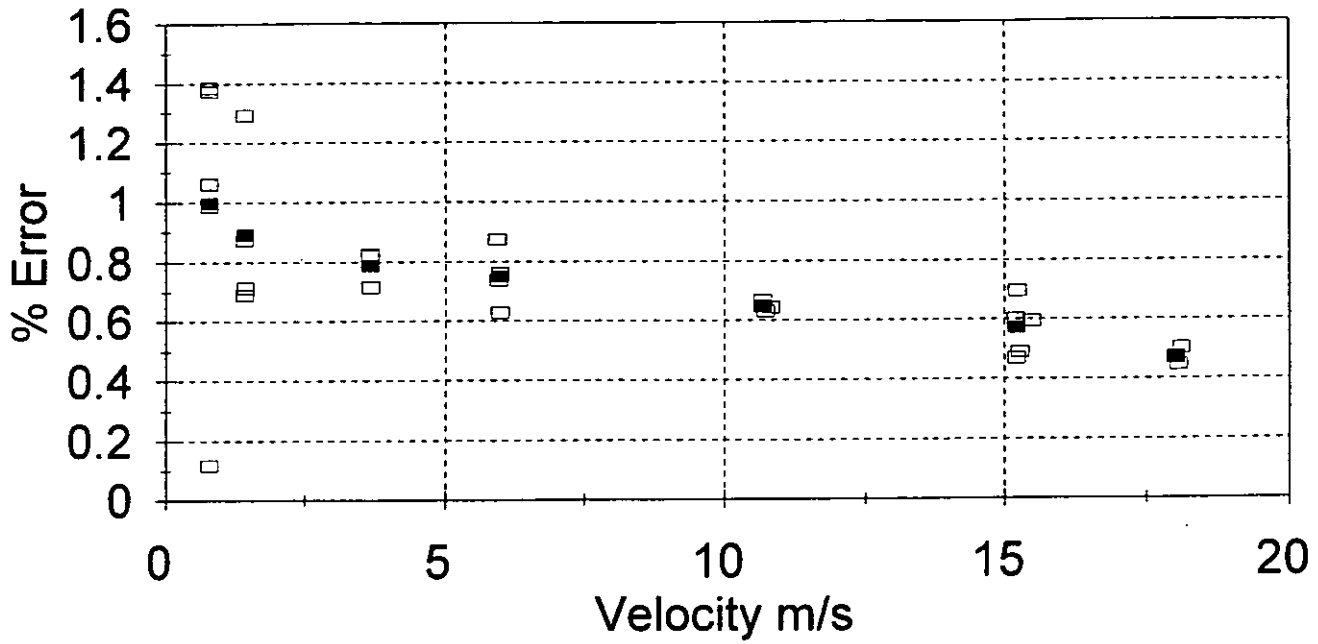


Fig 2. Calibration of 6" USM

Reverse Flow

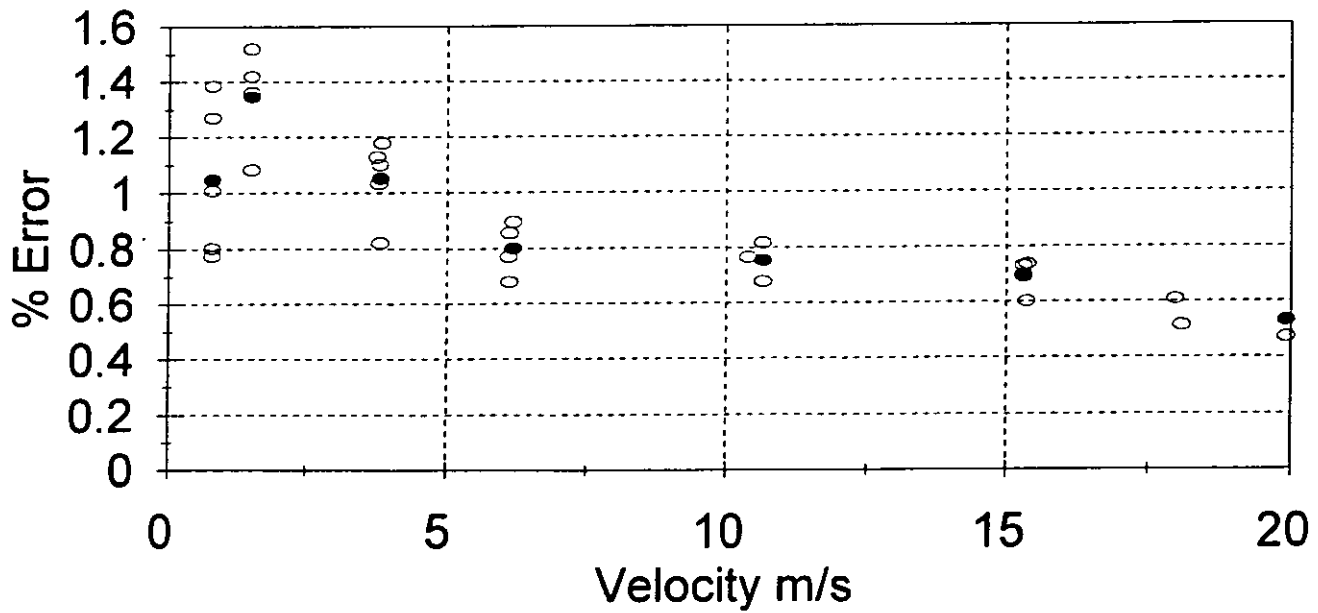


Fig 3. Calibration of 6" USM

Exchange Chord A Transducers

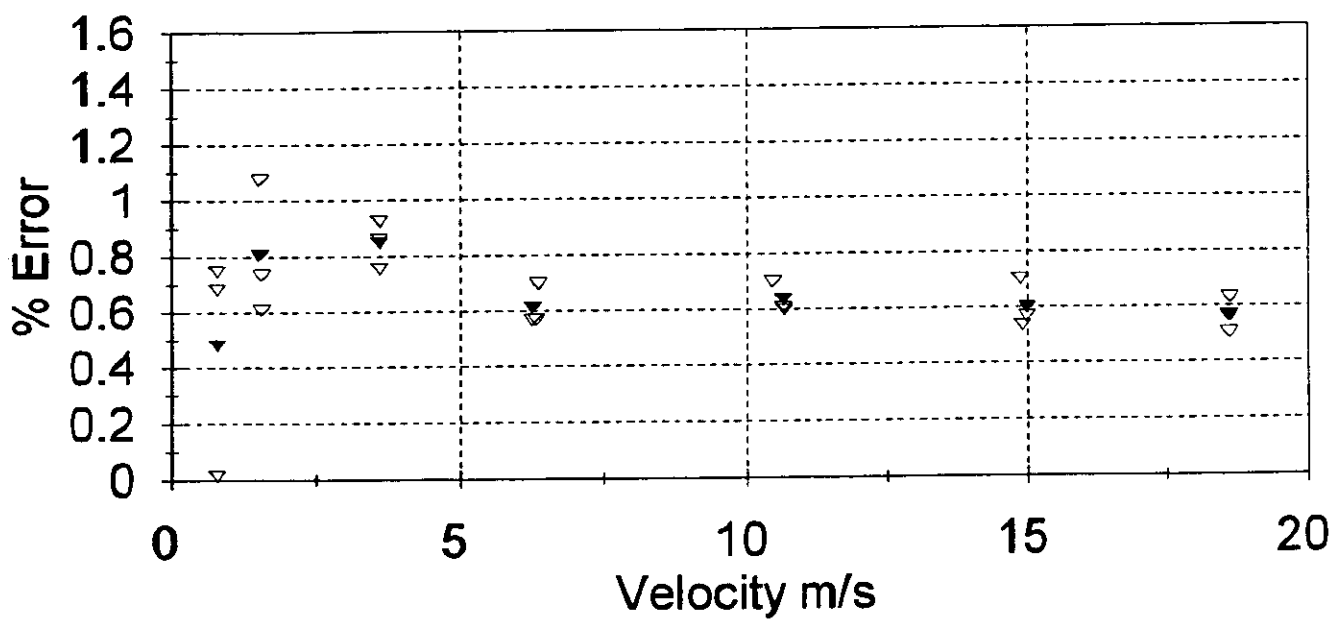


Fig 4. Calibration of 6" USM

Exchange Chord A & D Transducers

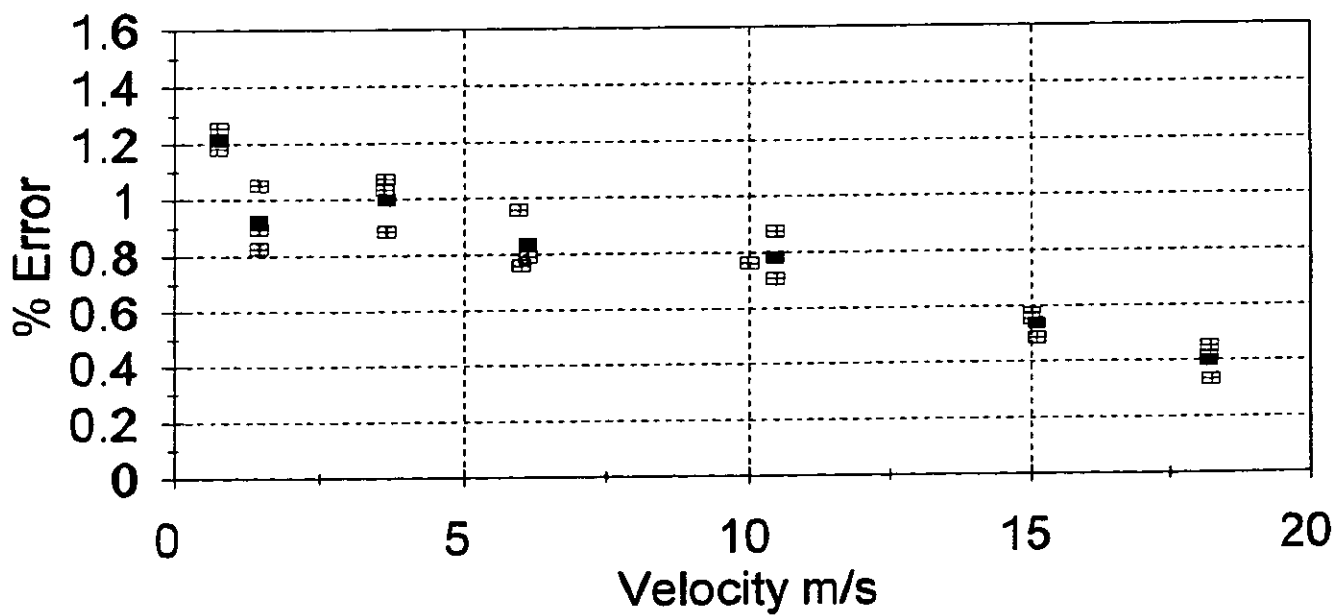


Fig 5. Calibration of 6" USM

Average Error

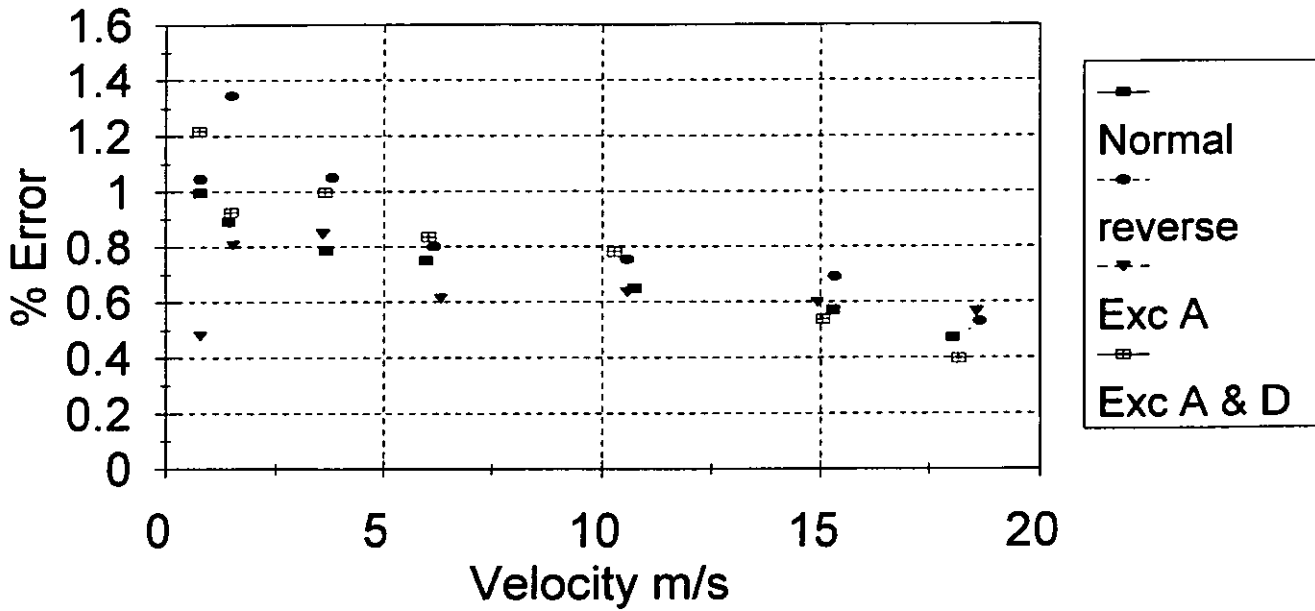


Fig 6. Calibration of 30" USM

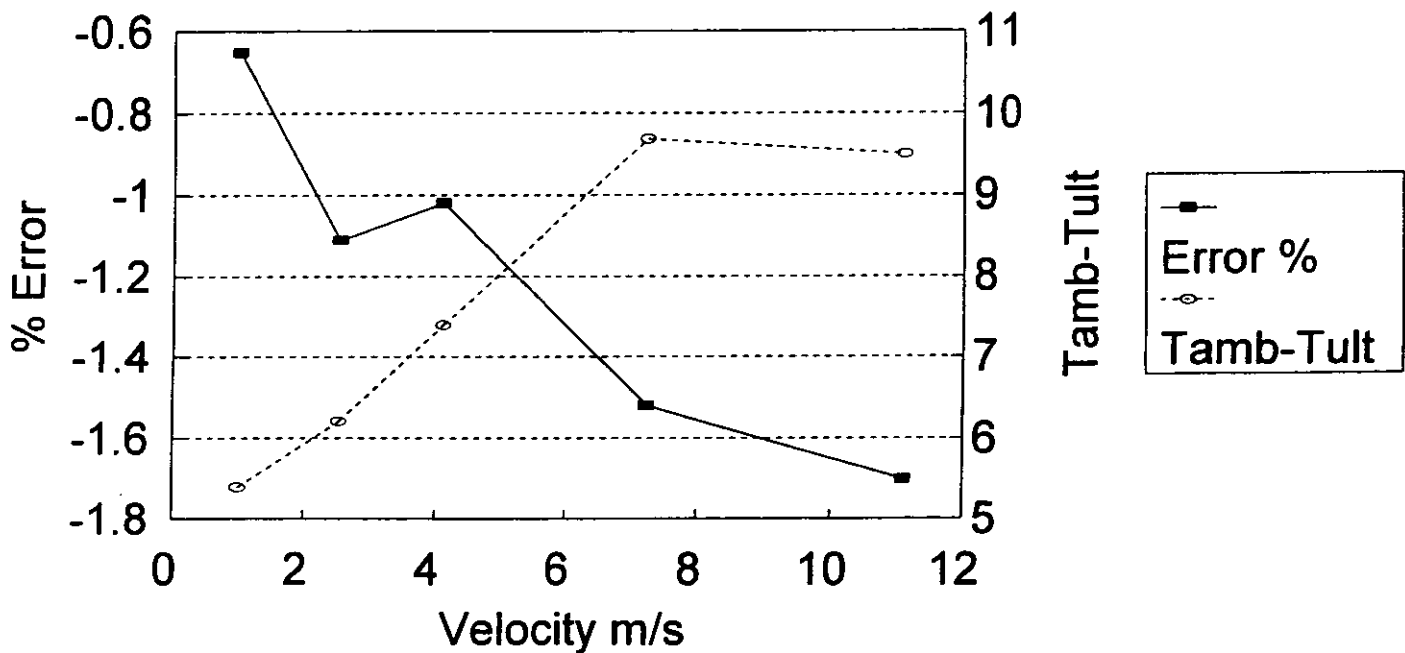


Fig 7. 30" USM Chord Velocities

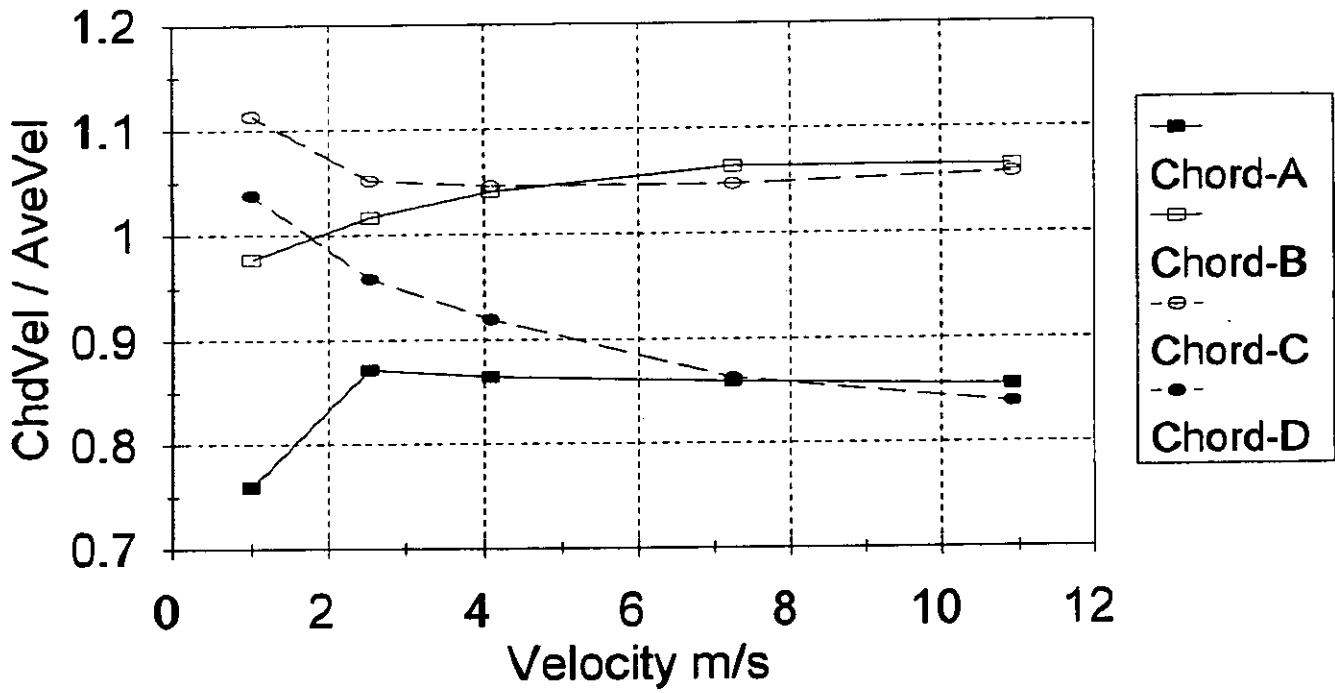


Fig 8. 30" USM Velocity Profile

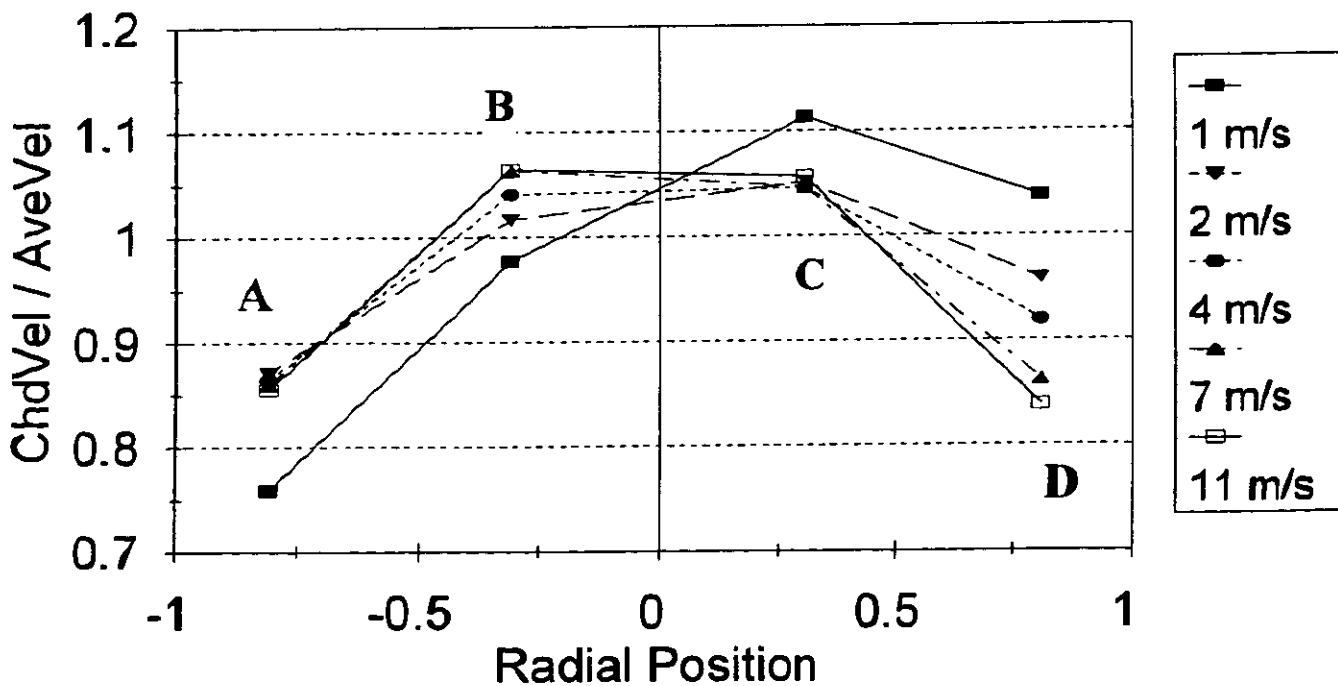


Fig 9. 30" USM Chord VOS

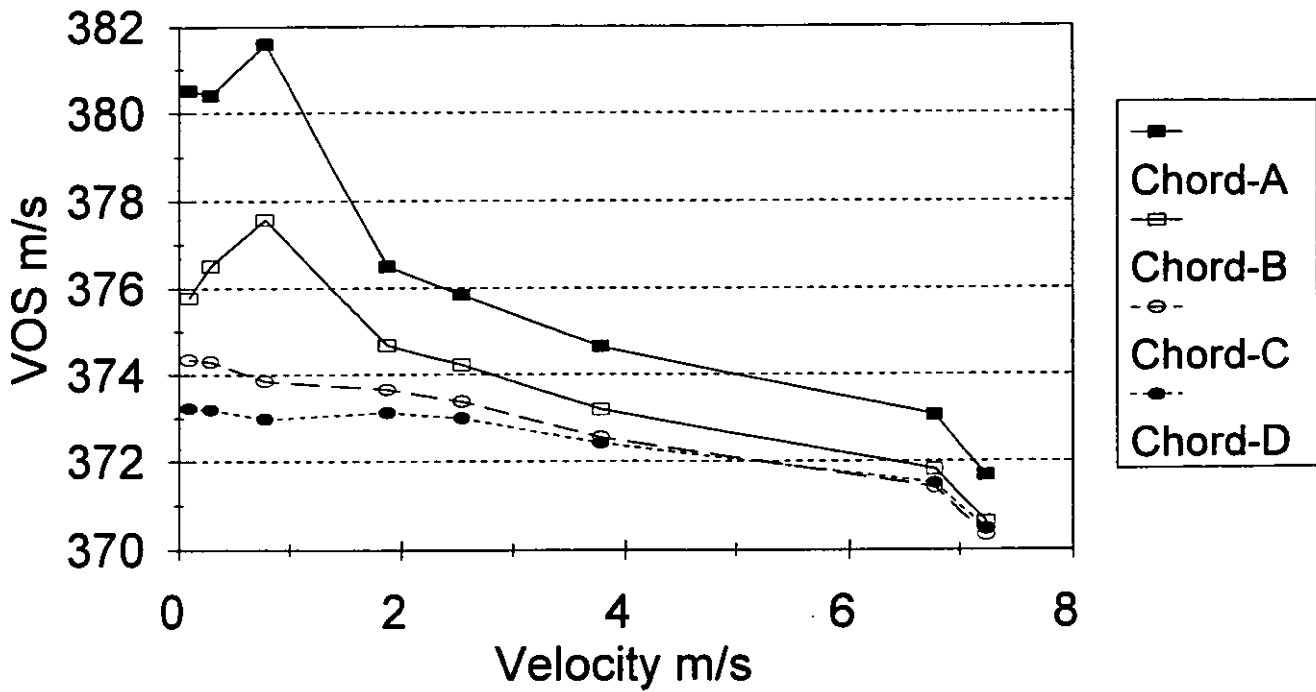
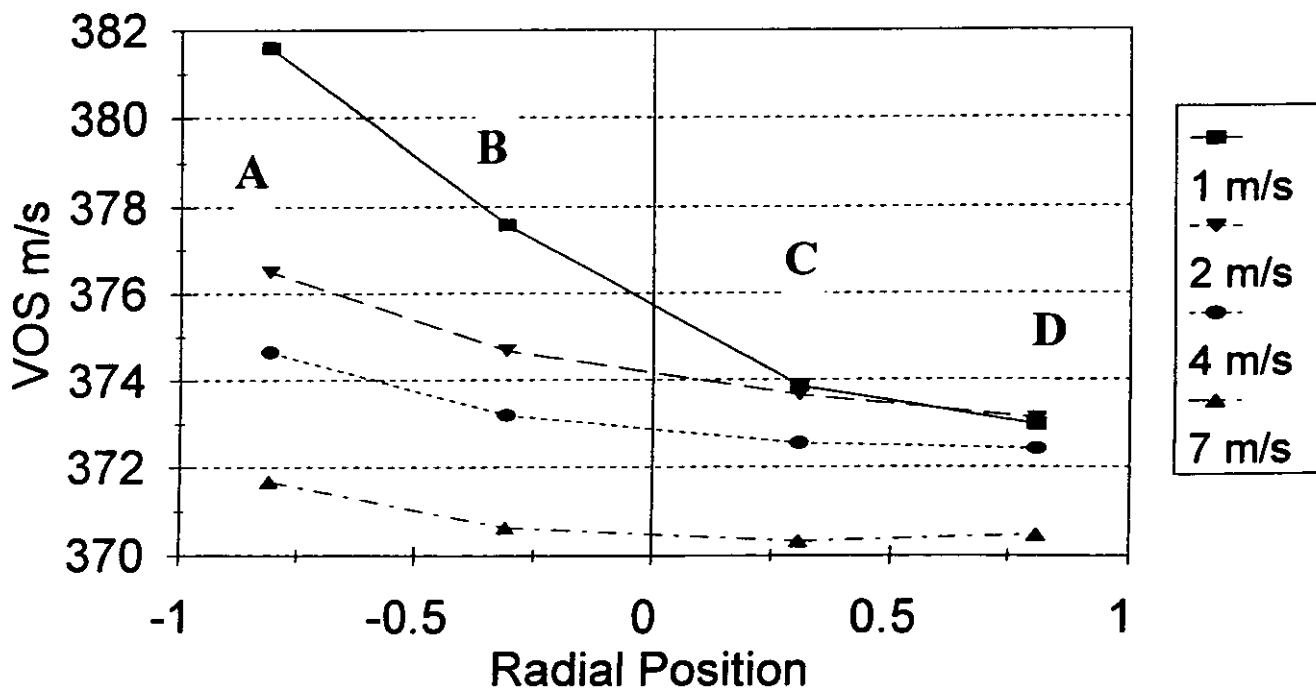


Fig 10. 30" USM VOS Profile



MULTIPATH ULTRASONIC FLOW METER PERFORMANCE

Terrence A. Grimley, Southwest Research Institute
Southwest Research Institute, San Antonio, Texas, USA

SUMMARY

Commercially available Daniel and Instromet 12-inch multipath ultrasonic flow meters have been tested at the Gas Research Institute (GRI) Metering Research Facility (MRF) in baseline and disturbed flow installations. This paper presents test results to assess baseline accuracy and repeatability over a range of flowrates and pressures, and the influence of one piping configuration on meter performance. Comparisons are also made between the speed of sound as measured by the test meters and values calculated based on gas composition.

1. BACKGROUND

Ultrasonic flow meters (USM) are of interest because they offer the potential to significantly reduce installation and operating costs of meter stations while providing accuracy levels consistent with, or better than, other traditional metering methods (Beeson,⁽¹⁾ Sakariassen⁽²⁾). A significant barrier to wide-spread use of ultrasonic meters in the natural gas industry is the lack of a standard covering their use for custody transfer applications. There is work in progress at both the American Gas Association (A.G.A.) (Ultrasonic Meter Task Group of the Transmission Measurement Committee) and the American Petroleum Institute (API) (Alternate Meters Working Group) to assess USM technology and establish a direction for the potential development of a standard. The A.G.A. recently published an Engineering Technical Note⁽³⁾ covering a range of topics related to the use of ultrasonic meters for natural gas applications. A significant contribution to the development of an ISO standard is the Groupe Européen de Recherches Gazières (GERG) Technical Monograph 8,⁽⁴⁾ "Present Status and Future Research on Multi-path Ultrasonic Gas Flow Meters," which suggests functional requirements for manufacturers to target and identifies "gaps" in the available information.

Of the 193 publications listed in the GERG monograph, only 21 concern testing, calibration,

installation effects, and long term performance. This suggests that, as compared to other commonly used natural gas meter types (orifice, turbine), there is not a large published information base on the performance of ultrasonic flow meters. The tests published to date (including those by van Bloemendaal and van der Kam,⁽⁵⁾ van der Kam et al.,⁽⁶⁾ Vulovic et al.⁽⁷⁾) have been conducted on a variety of upstream disturbances and on different meter types and sizes.

Overall, the published results indicate that under good flow conditions the meters provide measurements well within $\pm 1\%$, and in typical disturbed flow configurations (without pressure reducing flow control valves) the deviation of the meter from the good flow results is on the order of 0.5%. Performance test results show that the meter type, particular installation configuration, and meter size can all influence the amount of meter deviation from baseline or reference conditions. Therefore, the need remains for more information on ultrasonic flow meter performance over a wide range of operating and installation conditions.

The purpose of the tests reported here was to expand the information available on the performance of ultrasonic flow meters over a range of operating conditions and configurations. These test data are intended to contribute to standards development efforts.

2. INTRODUCTION

Ultrasonic flow meters use measurements of the transit time of high frequency pulses between one or more pairs of transducers to determine the volumetric flowrate in the meter. The relationship between the measured transit time of an ultrasonic pulse and the average velocity along the pulse path has been well described by others (including Freund and Warner,⁽⁸⁾ Drenthen,⁽⁹⁾ van Dellen,⁽¹⁰⁾ and A.G.A.⁽³⁾). A weighting function is typically used to combine the individual path velocities to form the meter average axial velocity, which is used to calculate the volumetric flowrate.

Although the basic relationships are common to all transit time ultrasonic flow meters, there is considerable variation in path configuration, transducer type and placement, transit time measurement algorithm, and flow calculation method used by the different commercially available meters. These differences are the result of the use of different strategies to achieve the meter's target accuracy, which is typically stated as 0.5 to 1.0%. Differences in meter configuration and data processing methods can affect meter accuracy, rangeability, repeatability, and susceptibility to error due to less-than-ideal installation configurations.

The Daniel multipath ultrasonic meter, which is designed around the use of four-parallel chordal paths, exploits a numerical integration technique to form a weighted average of the path measurements without an assumption of the velocity profile. The method, described by several references including the GERG Technical Monograph 8⁽⁴⁾, specifies the transducer locations and results in a fixed set of weighting coefficients. The Instromet five-path ultrasonic meter utilizes the measurements from three single-reflection diametral paths and two double-reflection chordal (mid-radius) paths to form an average velocity based on a combination of theoretically and experimentally determined weighting factors (Drenthen⁽⁹⁾).

3. TEST METHODS

Tests for this program were conducted in the GRI MRF High Pressure Loop (HPL) located at Southwest Research Institute. Test meters were installed in the 12-inch reference flow leg of the MRF HPL and tested with pipeline quality natural gas. Data were collected simultaneously on the ultrasonic meters and on the HPL critical flow nozzle bank, which served as the flow reference. The five binary weighted sonic nozzles were calibrated in situ at different pressures against the HPL weigh tank system (described by Park et al.⁽¹¹⁾). The total uncertainty for the nozzles is estimated to be approximately 0.2%. An on-line gas chromatograph and equations of state from A.G.A. Report 8⁽¹²⁾ were used to determine gas properties for all calculations. Static pressure and temperature were measured at the meters. The volumetric flowrate reported by the ultrasonic meter was acquired using different methods, depending on the meter options available from the manufacturer. For the Daniel USM, a "calibration mode" was used, whereby the meter internally totaled the gas volume and the time during which a specific register was toggled. The average flowrate was then calculated from the totaled

numbers. For the Instromet USM, reported values of actual flowrate (which were provided at a rate of one per second) were averaged to determine the average volumetric flowrate. Speed of sound measurements taken by both meters were also recorded.

A typical test sequence consisted of recirculating gas through the flow loop for a period of time to allow the gas temperature to stabilize. Steady flow was established by selecting and choking different nozzle combinations. A test point consisted of the average values of flowrate and other variables, computed over a period of 90 to 120 seconds. Test points were repeated a minimum of five to ten times to calculate an average value and standard deviation. Data were collected simultaneously from other flow measurement devices in the flow loop (typically one 10-inch orifice meter and two 12-inch turbine meters), which aided in establishing the validity and consistency of the data.

The ultrasonic meters were tested as received from the manufacturers, and all tests were conducted without the use of flow conditioners. The Daniel four-chordal path USMs were "dry calibrated" by the manufacturer. The dry calibration included measuring the various lengths required for the calculations and characterizing the timing delays for the ultrasonic transducer pairs. These meters had not been exposed to flowing gas prior to installation at the MRF. The Instromet five-path USM (two double-reflecting chordal paths and three single-reflecting diametral paths) had previously been flow calibrated and tested at several European laboratories. As received, the meter was set up for approximately 2.8 MPa operating conditions by the specification of density and viscosity values that are used for a Reynolds number calculation, which is part of the algorithm for calculation of the flowrate.

4. TEST RESULTS

4.1 Baseline Tests

The baseline tests were conducted with the meters installed approximately 68 diameters downstream of an in-plane tee. This corresponds to meter location 3, as shown in plan-view in Figure 1. The pipe 17 diameters upstream of the meter had a surface roughness of approximately 3.8 μm and an inside diameter of 304.8 mm, which matched the diameters for Daniel meters A1 and A2 and was slightly smaller than the 306.3 mm inside diameter of Instromet meter B. The baseline testing for meters A1 and A2 was conducted with the two meters in series. The first meter was located at location 3 (Figure 1),

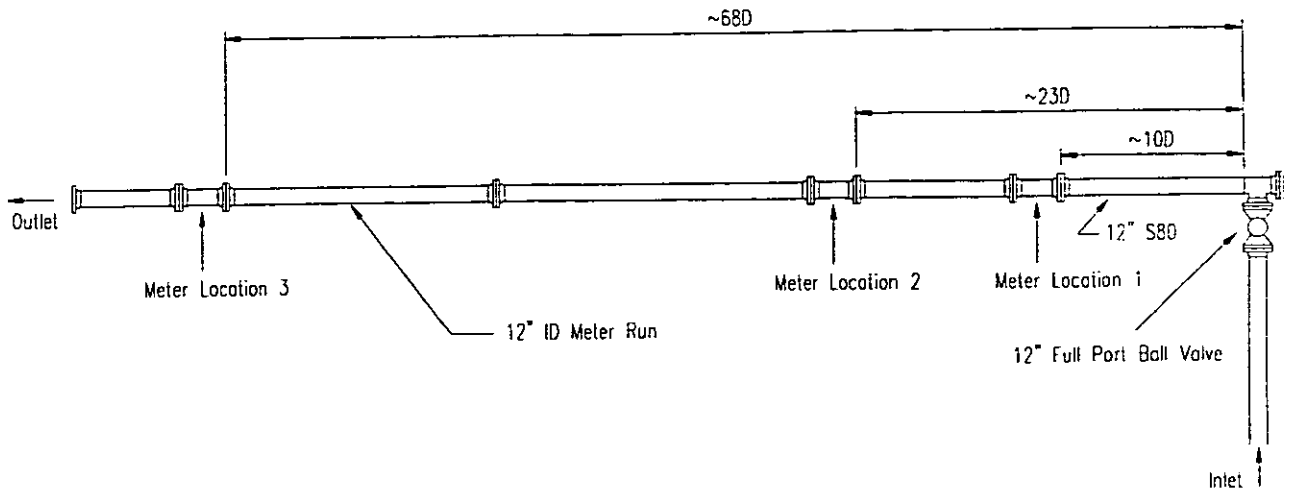


Figure 1. Meter installation for baseline and disturbed flow conditions.

and the second meter was located 10 diameters downstream from the first. The meters were oriented such that the chords were aligned in a horizontal plane. Baseline testing on meter B was conducted while meters A1 and A2 were installed at locations 1 and 2 (Figure 1).

Figure 2 shows the baseline performance of meters A1, A2, and B over the range of flowrates achievable in the MRF (which is 30 to 40% of full scale for a 12-inch meter). The error percentages shown are calculated relative to the nozzle bank reference flowrate.

It is apparent from the curves that all the meters are well within a 1% error tolerance, and for all but the lowest velocity, the points fall within a 0.5% band. The error bars shown on the data represent two standard deviations calculated from the data scatter at each velocity. The repeatability is similar for all the meters, having a value of less than 0.25% above approximately 1.5 m/sec. At low velocities there tends to be more scatter in the data, which is likely an effect of the resolution of the transit time measurements.

Figure 2 also shows that for meter A1, there is a small zero offset present in the meter. The offset is indicated by curvature in the meter error curve. The error changes steadily, from 0.3% when the velocity is above 1.5 to 3 m/sec, to -0.5% as the velocity approaches 0.5 m/sec. It is important to note that the zero offset present in this meter, which would normally be eliminated during the dry calibration at

the factory, was knowingly left in this meter to verify its effect on the meter calibration curve. At 6.2 MPa, the estimated offset for meter A1 is 0.003 m/s.

Baseline testing was conducted at line pressures of 1.7, 2.8, and 6.2 MPa to assess any effect of pressure on the meter calibration. Figure 3 indicates the average meter error, for velocities above 2.7 m/s as a function of pressure. The data reflect a shift in the average error of about 0.4% over the 4.5 MPa range of pressures tested.

As the pressure is increased, the gas density, and therefore the Reynolds number, will also increase. Since the velocity profile will change as a function of the Reynolds number, profile dependent errors should collapse when the error data are plotted against the Reynolds number. Figures 4, 5, and 6 present the same data with the percent error plotted as a function of Reynolds number. Since the zero offset in meter A1 would somewhat obscure the Reynolds number dependence, the data in Figure 4 has been corrected for a 0.003 m/s offset (assumed to be independent of pressure.) The figures show some Reynolds number dependence and tend to collapse slightly as the Reynolds number increases; however, the curves for individual pressures remain separate.

The calculation method employed by meter B uses corrections that are dependent on the velocity profile and therefore dependent on the Reynolds number. Because the density and viscosity values used by the meter were set to values appropriate for

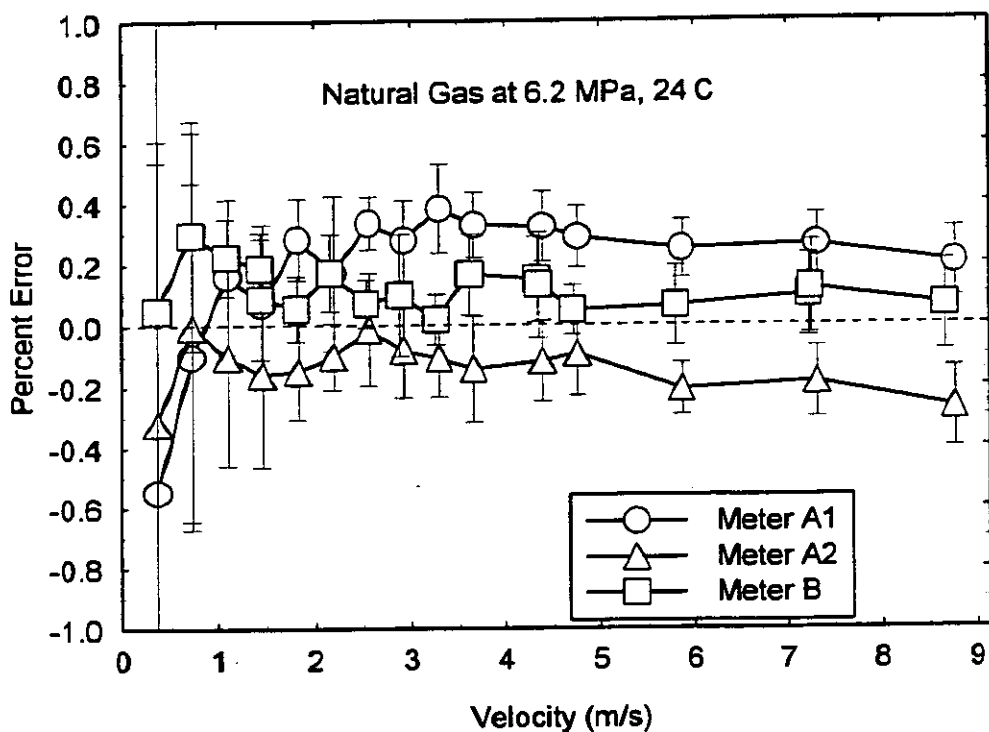


Figure 2. Baseline results at 6.2 MPa for meters A1, A2, and B.

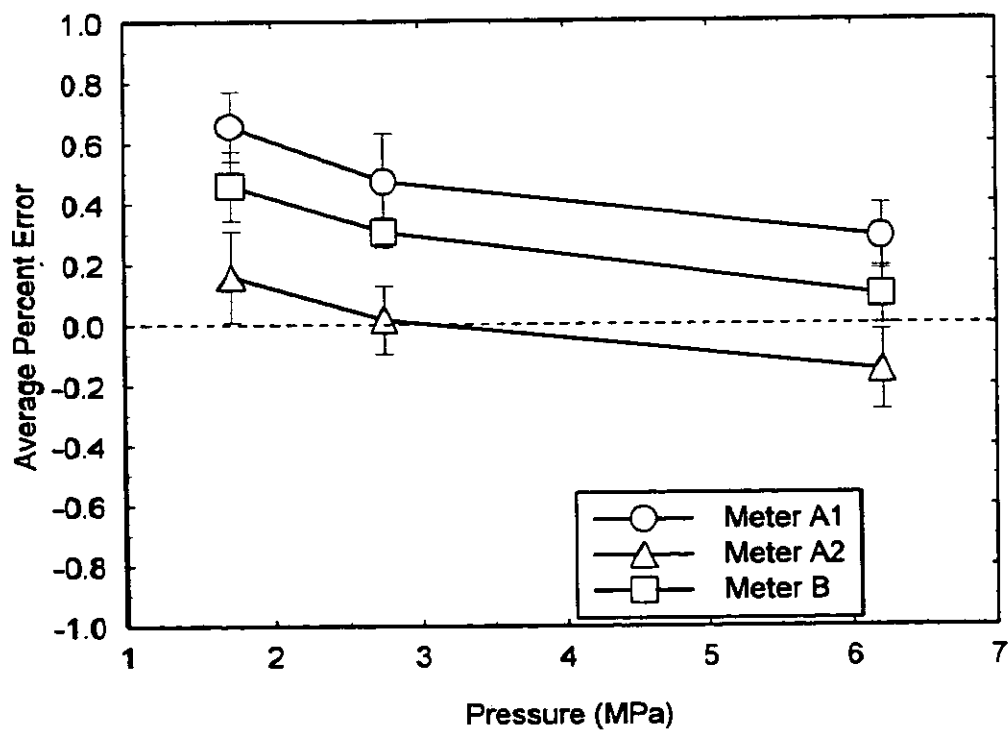


Figure 3. Average meter error as a function of pressure.

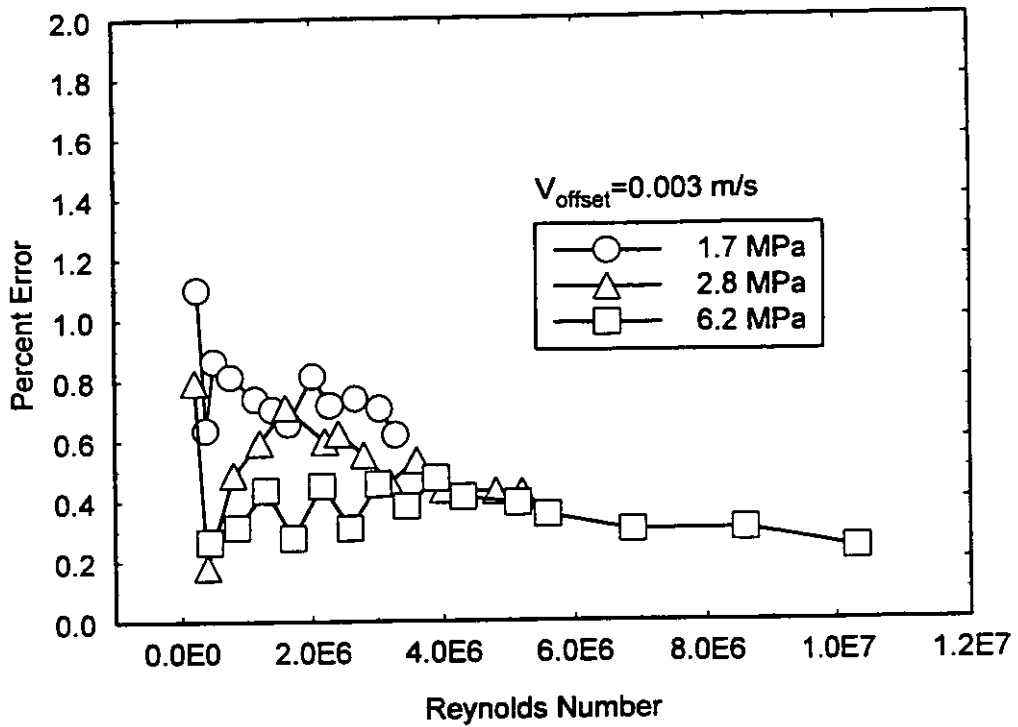


Figure 4. Effect of pressure on meter A1 after correcting for velocity offset.

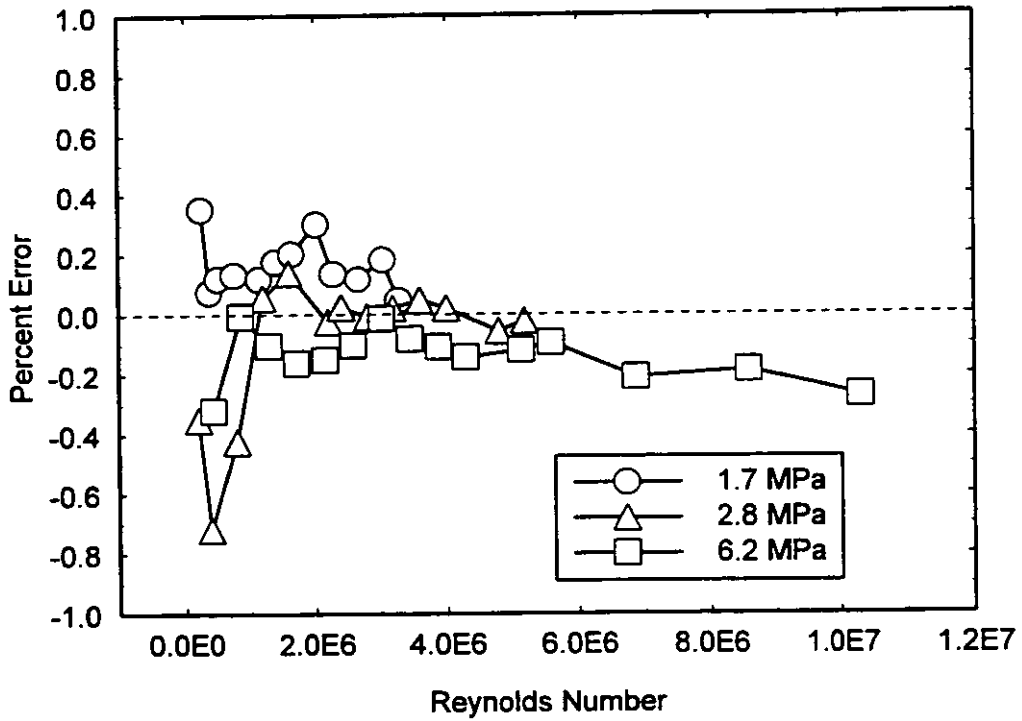


Figure 5. Effect of pressure on meter A2 plotted as a function of pipe Reynolds number.

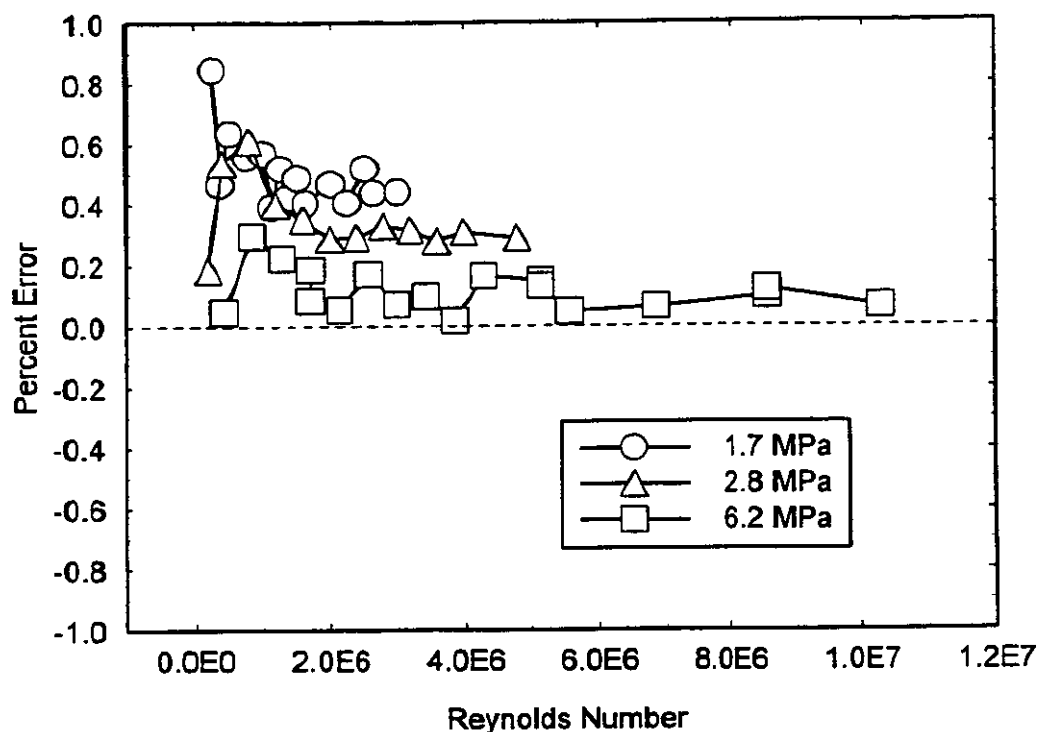


Figure 6. Effect of pressure on meter B plotted as a function of pipe Reynolds number.

2.8 MPa operation, a portion of the pressure shift for meter B can be attributed to the fixed values, preventing the meter from making proper corrections. A limited set of additional tests were conducted with meter B at 1.7 and 6.2 MPa, with the baseline values for the density and viscosity and then with property values, consistent with the pressure. The data indicate shifts of roughly 0.1 percent towards the 2.8 MPa line for the 1.7 MPa case and essentially no change for the 6.2 MPa case. These results, and Figure 6, suggest that the Reynolds number based profile correction does not completely account for the effect of pressure on the meter error. Calculations, similar to those done by van Dellen,⁽¹⁰⁾ demonstrate that the theoretical performance of the integration method used by meters A1 and A2 is largely independent of velocity profile over the Reynolds number range (and therefore the pressure range) involved in these tests. Calculations to assess the profile dependence were made by integrating an assumed profile (Bogue and Metzner⁽¹³⁾) for different Reynolds numbers and different path locations. Figure 7 shows the "path factor" for several different locations as a function of Reynolds number for the locations used by the Daniel and Instromet meter designs. The path factor is

calculated from the ratio of the average velocity to the calculated velocity along a path. Figure 8 shows the overall calculated meter factor using the method of meters A1 and A2 and the path factor for the mid-radius path (believed to have the most importance in the calculation method for meter B.) Since the method used by meter B to calculate the average velocity is proprietary, the curve in Figure 8 is a path factor and not an overall meter factor. The curves indicate the four-path weighted method should have very little pressure shift over the 4.5 MPa range of pressures. The mid-radius path has a shift in the path factor of about 0.05% over the 4.5 MPa range. These calculations indicate that the meter variation with pressure observed in the test data is not explained by changes in velocity profile shape.

The path calculations are based on the assumption that the transducers are located at the exact design location and that the transit times are measured from a point at the center of the transducer. A further assumption is that the ultrasonic beam has no thickness (volume.) These assumptions should be investigated further to assess their validity and their effect on the calculations.

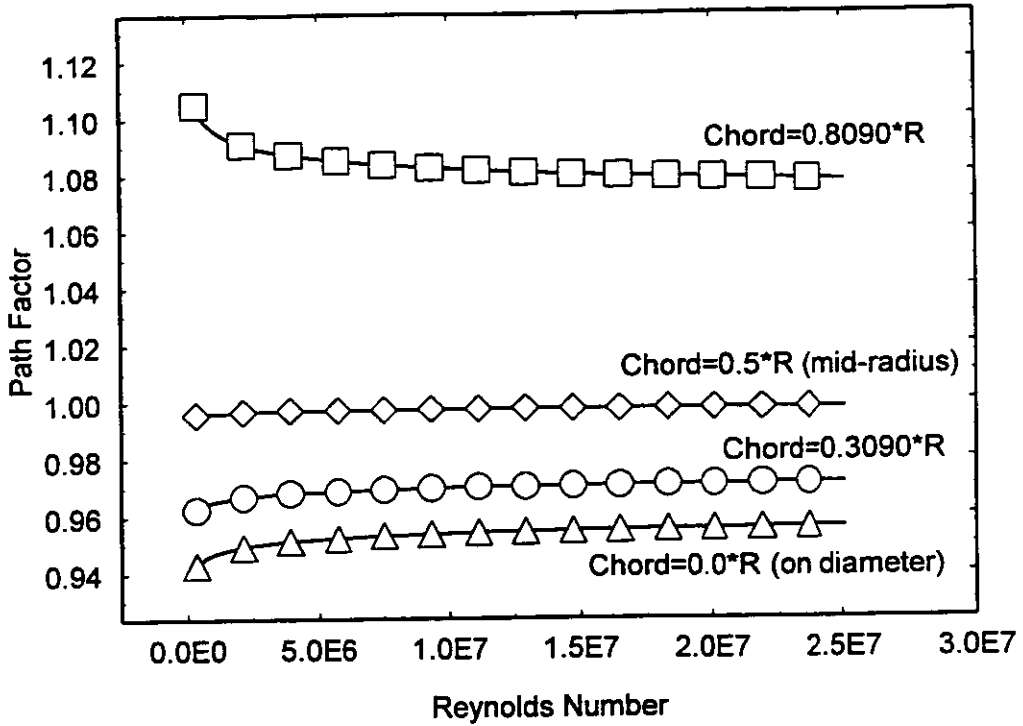


Figure 7. Calculated path factors as a function of Reynolds number for different path locations.

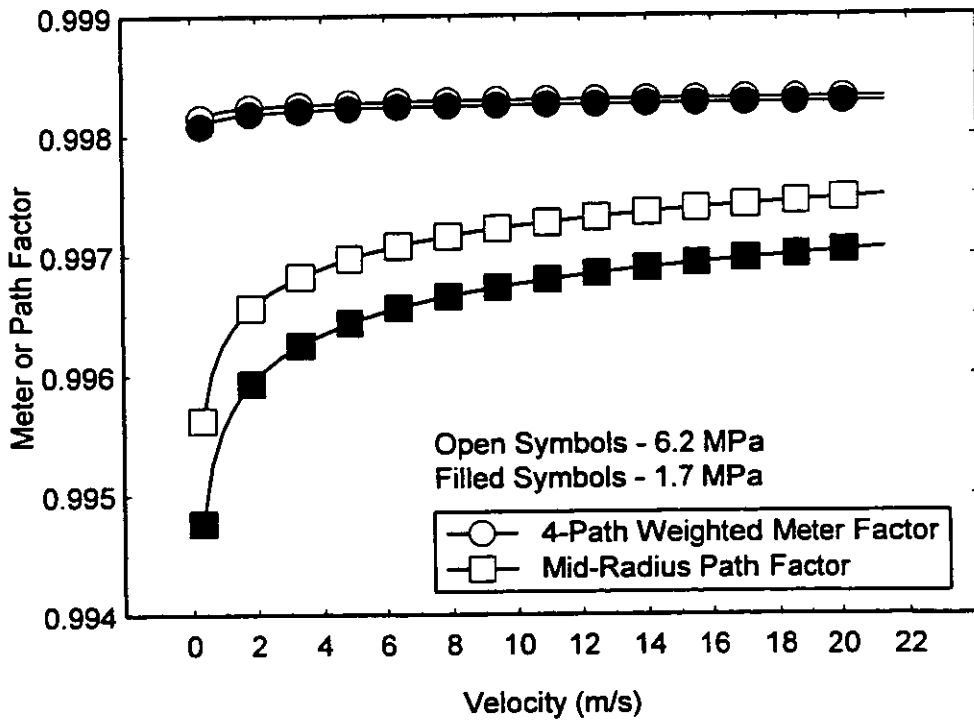


Figure 8. Calculated effect of pressure on meter or path factor.

The change in the path length and meter body diameter as the pressure is increased also introduces an error into the measurement. However, the estimated change in calibration, due to mechanical deformation, is less than 0.05% for the 4.5 MPa change in pressure. These results are contrary to the findings of other testing (van Bloemendaal and van der Kam,⁽⁵⁾ Vulovic et al.⁽⁷⁾) where no consistent dependence on pressure was identified (although there were variations in the mean error at different pressure levels.) Because the data available in the aforementioned studies came from multiple laboratories and were presented in summary fashion, it is difficult to distinguish differences that are related only to pressure versus differences that are a result of small biases between laboratories. The results from the five test facilities show variations of about $\pm 0.6\%$ over a 10:1 turndown in the meter operating range for pressures between 1 and 6 MPa. The effect of pressure needs to be investigated further to fully explain the data. Additional work to accurately model the measurement process used by ultrasonic meters may offer possible explanations.

4.2 Speed of Sound

Figure 9 shows the percent error between the speed of sound reported by the meters and that derived from A.G.A. Report 8⁽¹²⁾ density calculations based on the measured pressure, temperature, and gas composition. The figure shows that the error is typically less than 0.2% for both test meter types, with each meter type having its own bias relative to the calculated value. The figure confirms that the reported speed of sound is not dependent on the gas velocity. The meter velocity was used as the independent axis in the figure because of the limited range of speed of sound information available from the data shown in Figure 9 (sound velocities ranged from 414 to 430 m/sec). The data for meter A1 show more scatter than the meter B data. Although not presented, the data for meter A2 were similar to those for meter A1. There does not appear to be a large dependence on pressure, with about 0.1% shift between the 6.2 MPa data and the results for the other pressures.

These results indicate the level of agreement that can be expected under controlled conditions is on the order of the uncertainty in the speed of sound calculated from the gas composition. It should be recognized, however, that because of the relationship between the path velocity and path speed of sound measured by the meter, good agreement between the calculated speed of sound and that reported by the

meter is not a sufficient condition for accurate flow measurement.

4.3 Disturbance Tests

Figure 1 showed that the location of the meters for the disturbance tests was 10 diameters downstream of a tee (i.e., meter location 1 on Figure 1) that was located just downstream from a 12-inch diameter full-port ball valve. Tests were conducted with the ball valve open, and at two partially closed positions (to increase the level of flow disturbance entering the test meter). No flow conditioner was installed upstream of the meter. The piping between the tee and the meter was 12-inch schedule 80 pipe having a nominal inside diameter of 288.9 mm (and surface roughness of approximately 8.9 μm). Therefore, when located at the position 10 diameters down from the tee, the meter was subjected to a combination of the effects of the 15.9 mm concentric step in diameter (an 11% increase in area), the tee, and for some tests, a partially closed valve. Tests were conducted at the same three pressures used for the baseline calibrations. A set of scoping tests were also performed with the meter located 23 diameters downstream from the tee (meter location 2 on Figure 1.)

Meter A1 was tested in two different orientations relative to the tee. The 0 degree position had the chords aligned in a horizontal plane along with the tee. The meter was also rotated 90 degrees, so that the chords were aligned in a vertical plane. Meter B was tested in only one orientation.

Figure 10 displays the results for the upstream disturbance testing at 2.8 MPa. Although the data appear to differ from the initial baseline, additional baseline data collected just prior to the initiation of the disturbance tests revealed a shift. (It was later discovered that this shift may have been due to a failing chord.) The data at 23D can be considered as the revised baseline. Relative to the 23D (revised baseline) results, the data for 10D with the chords horizontal (0°) are shifted by about 0.1% to 0.2%. The results for the dependence on the meter orientation indicated a shift of about -0.4% when the chords are vertical (90°). The fact that there are differences dependent on the chord orientation relative to the disturbance is not surprising, and these differences have been measured by others (van Bloemendaal and van der Kam⁽⁵⁾). Since the transit time measured by the meter for a particular path is dependent on the average velocity along the path, the paths cutting across the disturbance tend to average out the effect of

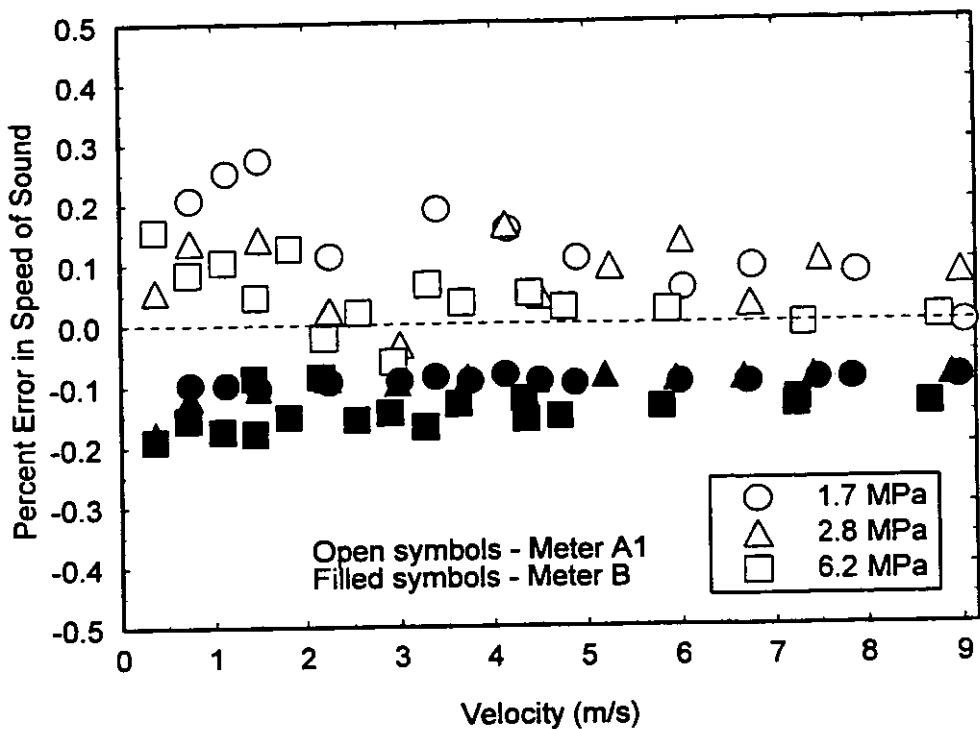


Figure 9. Comparison of speed of sound for meters A1 and B.

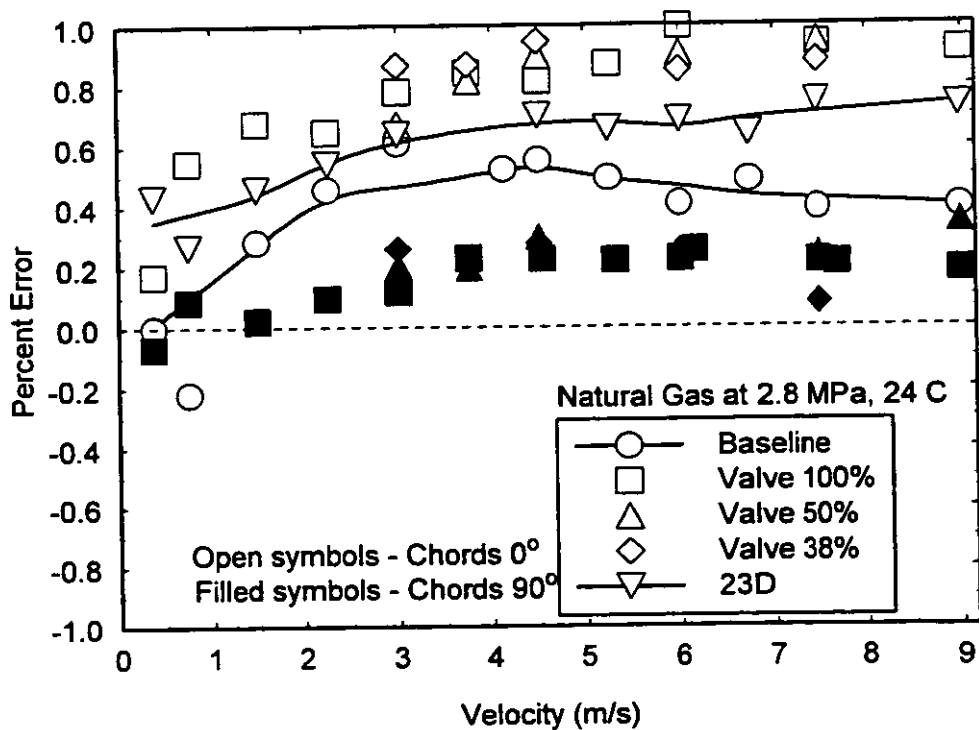


Figure 10. Performance of meter A1 10D downstream of a tee at 2.8 MPa.

the disturbance. When the paths are vertical and the primary direction of velocity disturbance is horizontal, the ability of the integration method to accurately resolve the average velocity has more of an effect on the results.

Also shown in Figure 10 is the effect of the partially closed valve on the meter performance. The results indicate that the valve position had little effect on the average error of the repeated runs, but there was a small increase in the data scatter, suggesting that turbulence levels were increased as a result of closing the valve. Table 1 lists, for velocities above 2.7 m/sec, the average percent error and twice the average standard deviation (2σ) of the data for the different axial installation locations, meter orientations, and valve positions.

Figure 11 gives the results for meter B installed 10D down from the tee. The results show a shift of about 0.6% from the baseline with the valve fully open and a shift of about 0.4% from the baseline when the valve is partially closed (50% and 38% open). The result was unanticipated, since the partial blockage by the valve was expected to increase the flow distortion. Table 2 shows that although the valve position did influence the absolute value of the error, it did not have a significant effect on the data scatter of the

repeated runs. Data reported by Vulovic, Harbrink, and van Bloemendaal⁽⁷⁾ showed a deviation of 0.3% relative to the baseline when the meter was installed 10D down from an elbow. The effect of the 15.9 mm step change in pipe diameter in the MRF installation may account for the difference in results as compared to those of Vulovic et al., where no step was indicated in the description of the test.

Table 1. 2.8 MPa data for meter A1.

Dist D	Valve %	Orient °	Error %	Error 2σ
10	100	0	0.880	0.205
10	50	0	0.875	0.286
10	38	0	0.883	0.329
10	100	90	0.208	0.222
10	50	90	0.253	0.250
10	38	90	0.217	0.332
23	100	0	0.684	0.167
68	100	0	0.288	0.114

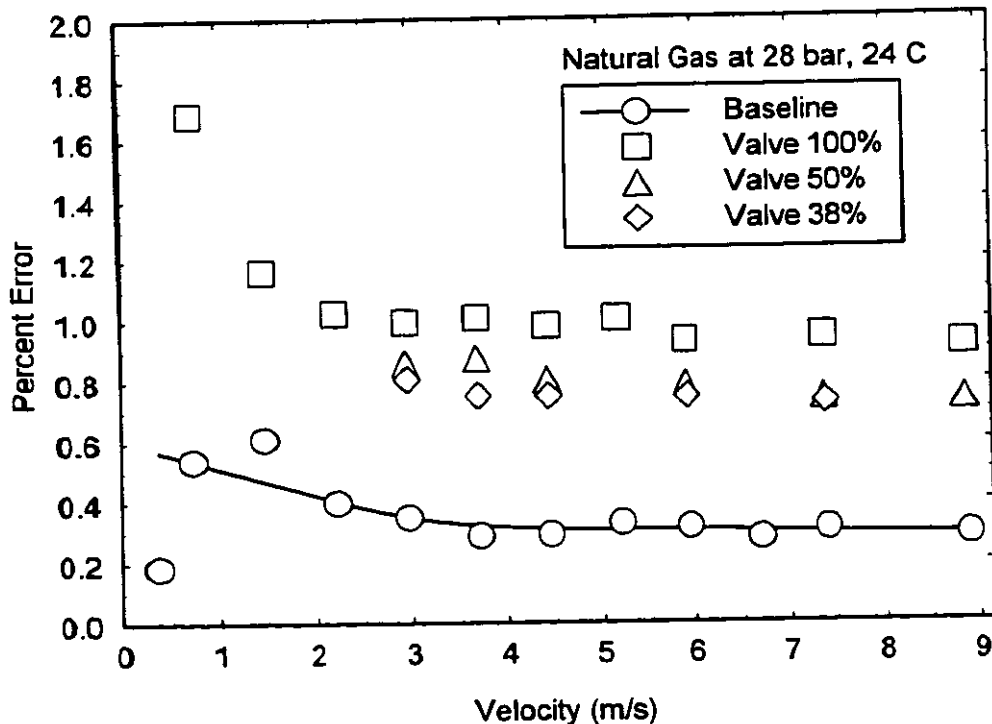


Figure 11. Performance of meter B 10D downstream of a tee at 2.8 MPa.

Table 2. 2.8 MPa data for meter B.

Dist D	Valve %	Orient °	Error %	Error 2σ
10	100	0	0.969	0.097
10	50	0	0.800	0.106
10	38	0	0.755	0.126
68	100	0	0.306	0.134

The results of the disturbance testing conducted at 1.7 and 6.2 MPa indicate results similar to those shown here for 2.8 MPa for both meter types.

5. CONCLUSIONS AND RECOMMENDATIONS

These data demonstrate that the test meters are capable of accuracies well within a 1% tolerance and have repeatability of better than 0.25% when the flowrate is above about 5% of the meter capacity. The data indicate that pressure may have an effect on meter error. Both meter types showed shifts of 0.4% over a 4.5 MPa static pressure variation, but remained within a 1% tolerance. These results suggest that flow calibration of each meter at or near the field operating conditions may be necessary for reducing any unacceptable measurement bias. If the target is to produce a dry calibrated meter with a bias error on the order of a few tenths of a percent, then a more complete understanding of the relationships between various operating parameters and the meter design may be required.

The data suggest that both the magnitude and character of errors introduced by flow disturbances are a function of meter design. Shifts of up to 0.6% were measured for meters installed 10 diameters from a tee without a flow conditioner. Better characterization of the effects of flow disturbances on the measurement accuracy is needed to more accurately define the installation requirements necessary to achieve meter performance within a specified tolerance. This should involve additional tests of different installations with and without flow conditioners.

Additional details on these results can be found in GRI Topical Report GRI-96/0291⁽¹⁴⁾. Plans to extend this work include addressing the effects of flow disturbances on meter performance with and without flow conditioners. This work will utilize smaller meters, which can be tested over more of their velocity range. This work may also be extended to include testing specific to the application of ultrasonic meters

to gas storage reservoirs, with funding provided by the U.S. Department of Energy.

6. REFERENCES

1. BEESON, J. Ultrasonic Metering – A Field Perspective. A.G.A. Operations Conference, 1995.
2. SAKARIASSEN, R. Why We Use Ultrasonic Gas Flow Meters. North Sea Flow Measurement Workshop, 1995.
3. AMERICAN GAS ASSOCIATION. Ultrasonic Flow Measurement for Natural Gas Applications. A.G.A. Transmission Measurement Committee Engineering Technical Note, Arlington, Virginia, USA, May 1996.
4. GROUPE EUROPÉEN DE RECHERCHES GAZIÈRES. Present Status and Future Research on Multi-path Ultrasonic Gas Flow Meters, GERG Technical Monograph 8. 1995.
5. VAN BLOEMENDAAL, K. and VAN DER KAM, P. M. A. Installation Effects on Multi-Path Ultrasonic Flow Meters: The "ULTRA-FLOW" Project. Third International Symposium on Fluid Flow Measurement, San Antonio, Texas, USA, March 19-22, 1995.
6. VAN DER KAM, P. M. A., DE JONG, S. and DAM, A. M. The Effects of Dirt and Swirling Flow on Multipath Ultrasonic Gas Flow Meters. Third International Symposium on Fluid Flow Measurement, San Antonio, Texas, USA, March 19-22, 1995.
7. VULOVIC, F., HARBRINK, B. and VAN BLOEMENDAAL, K. Installation Effects on a Multipath Ultrasonic Flow Meter Designed for Profile Disturbances. North Sea Flow Measurement Workshop, 1995.
8. FREUND, W. R., JR., and WARNER, K. L. Performance Characteristics of Transit Time Ultrasonic Flow Meters. Third International Symposium on Fluid Flow Measurement, San Antonio, Texas, USA, March 19-22, 1995.
9. DRENTHE, J. G. The Q.Sonic Ultrasonic Gas Flowmeter for Custody Transfer. Third International Symposium on Fluid Flow Measurement, San Antonio, Texas, USA, March 19-22, 1995.
10. VAN DELLEN, K. Multipath Ultrasonic Gas Flow Meters. Daniel Industries (undated private communication).

11. PARK, J. T., BEHRING, K. A. II and GRIMLEY, T. A. Uncertainty Estimates for the Gravimetric Primary Flow Standards of the MRF. Third International Symposium on Fluid Flow Measurement, San Antonio, Texas, USA, March 19-22, 1995.
12. AMERICAN GAS ASSOCIATION. Compressibility of Natural Gas and Other Related Hydrocarbon Gases. A.G.A. Transmission Measurement Committee Report No. 8, Arlington, Virginia, USA, 1985.
13. BOGUE, D. C. and METZNER, A. B. Velocity Profiles in Turbulent Pipe Flow. I. and E.C. Fundamentals, Vol. 2, No. 2, 1963.
14. GRIMLEY, T. A. Metering Research Facility Program: Performance Tests of 12-Inch Multipath Ultrasonic Flow Meters. Topical report to Gas Research Institute, Report No. GRI-96/0291, Chicago, Illinois, USA, August 1996.

OIL FLOW PERFORMANCE OF ULTRASONIC METERS

Gregor J Brown
Oil Flow Measurement Section
Fluids & Process Technologies Division
NEL, East Kilbride, Glasgow.

SUMMARY

Ultrasonic meters have significant potential for application in the oil industry due to their non-intrusive design, low maintenance requirements and diagnostic capabilities. For a number of reasons the industry's use of this technology for oil flow measurement is limited at present. Over the past year NEL have completed a DTI funded project to investigate the capabilities and limitations of current ultrasonic techniques for oil flow measurement. A series of tests were carried out in order to evaluate the performance of a selection of modern transit-time ultrasonic flowmeters. These meters included both wetted and clamp-on designs. Basic calibrations were performed using the NEL oil flow primary standard with kerosene, gas oil and 30 cSt oil. As offshore applications may not always be single-phase oil, the test programme was also designed to establish limitations with respect to the presence of gas and water components. The performance of the meters under evaluation is described in terms of repeatability and deviation from the reference flow rate.

1 INTRODUCTION

Ultrasonic flow measurement technology based on the transit-time principle offers a compact non-intrusive alternative for oil flow measurement. Combined with low maintenance requirements and stable long term operation, considerable cost savings may be achieved over turbine and prover loop systems. Potential uncertainties of ± 0.5 to 1 % of rate for calibrated systems and independence of changing fluid properties are generally claimed, indicating suitability for allocation metering duties. Such claims however are not well supported by independent evaluation data. Where such evaluation data exists it tends to be limited either in terms of the range of conditions to which the meters are subjected or in the number of meters which are evaluated under common conditions.

The report of a project co-ordinated by NEL and published in 1989 by Heritage [1] describes one of the most comprehensive ultrasonic flowmeter evaluations to date. Meters of nominal internal diameter of 100 mm from seven sources were calibrated in water over a flowrate range of approximately 8 - 80 l/s. Of eleven meters, three failed to complete the test programme, two performed within the manufacturers specification, five performed within specification only over part of the range, and one performed outside of the specification over the entire range. A summary of performance of nine meters which completed all or part of the first phase, 'ideal installation' tests, is given in Table 1 below. The conclusion drawn from these results was that the majority of 100 mm ultrasonic flowmeters were likely to be out of specification.

Maximum error (% rate)	Number of meters
error \leq 2 %	2
2 % < error \leq 5 %	3
5 % < error \leq 10 %	2
error > 10 %	2

Table 1 A summary of past ultrasonic meter performance

The second phase of the project addressed the important issue of installation effects. However, as the 'ideal installation' tests were conducted only with water as the test fluid and no investigation into the effect of changes in fluid and temperature related properties was carried out, the results can not be considered exhaustive.

With the advent of new developments in design and a number of economic advantages to the oil industry, in 1995 NEL, under the DTI NMSPU Flow Programme, initiated a project to investigate the capabilities and limitations of ultrasonic meters for oil flow measurement. The remit of the project was to evaluate the oil flow performance of a range of ultrasonic meters in 'ideal' flow conditions and to determine limitations in terms of secondary flow components. Meters of 100 mm nominal diameter were specified in order that a velocity range of approximately 0.5 to 10 m/s could be covered using the primary flow loops of the oil flow National Standard and to give good comparison with the results of Heritage. Meters of clamp-on and wetted types were to be included due to oil industry interest in both types. In conjunction with this project, Amerada Hess Ltd commissioned some specific tests which have been included with the main project results.

At the time of writing this paper, basic oil calibrations and oil/gas tests have been concluded. The water-in-oil evaluations are underway and will be reported at a later date.

2 TEST FACILITIES AND METHOD

The tests reported in this paper were conducted in the main oil flow measurement standard facility of the NEL Oil and Multiphase Flow Laboratory. The facility comprises three separate flow circuits each with a 100 l/s flow rate capability using kerosene, gas oil and 30 cSt (velocite) oils respectively. Figure 1 shows a schematic diagram of one of these circuits. The oil for each circuit is stored in 30 m³ tanks and is maintained to within $\pm 1^\circ\text{C}$ of a pre-determined temperature within the range of 5 to 50 $^\circ\text{C}$ by a conditioning circuit linked to each tank. The test lines themselves can each accommodate 30m of horizontal straight lengths or other configurations as required. At the outlet of each test section a manifold directs the fluid either back to the storage tank or to one of the weigh tanks. Line temperature and pressure are monitored both upstream and downstream of the test section.

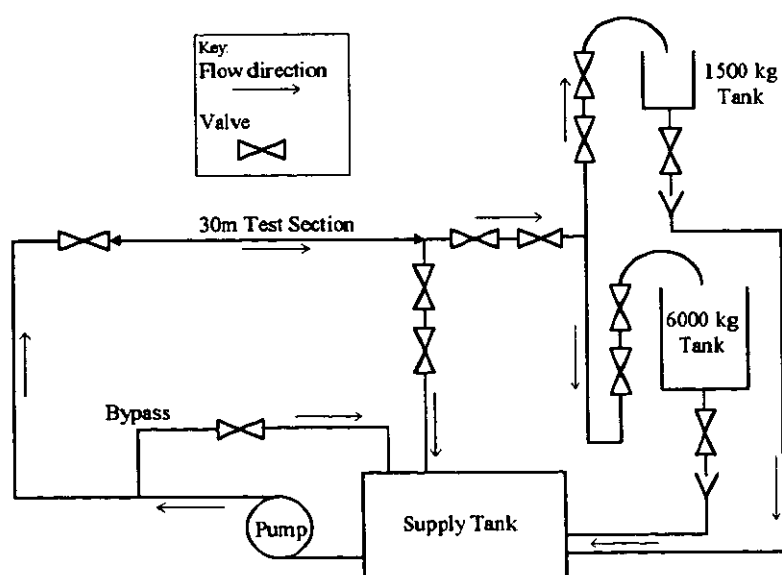


Figure 1 A Schematic Diagram of the Test Facility

The standard calibration method is a gravimetric standing-start-and-finish method by which the flow through the test section starts from zero at the opening of the inlet valve to the tank and returns to zero when the inlet is closed, during which time a quantity of fluid is collected in the weigh tank. For volumetric meters the calculated volume of liquid is then compared with the indicated volume passed through the meter, either in the form of a totalised pulse/frequency output or internal totaliser result. Alternatively calibration can be performed by a master-meter method using a sliding-vane positive displacement (PD) meter.

The facility is fully traceable to Primary National Standards and is accredited by the National Accreditation of Measurement and Sampling (NAMAS). The uncertainty in the measurement of the quantity of fluid passed through the meter is $\pm 0.03\%$ for the gravimetric method and $\pm 0.08\%$ for the master meter method, these uncertainties being estimated at a confidence level of not less than 95%.

For the two-phase oil/gas tests a skid comprising a manifold and $\frac{1}{2}$, $\frac{3}{4}$ and 1 inch gas turbines was used to inject nitrogen from a pressurised supply into the test line on the downstream side of the reference PD meter prior to the meters under test. Measurement of line temperature and pressure were made at the gas meter skid and in the main test line to determine the volumetric gas fraction at the start of the 4-inch section and perspex sections were installed to enable viewing of the flow.

3 TEST CONDITIONS

The test programme was designed to determine meter performance in 'ideal' conditions and to quantify effects due to changes of temperature and fluid related parameters and the presence of second flow components. The key tests to which meters were subjected were calibrations in kerosene and velocite oil at a nominal temperatures of 16 and 20 °C and the second-phase tests. Where time has allowed, due to the prompt delivery of a meter, further tests have been conducted in gas oil and at additional temperatures.

An approximate specification for each of the oil calibrations reported is given in Table 2 below. A nominal pressure of 1.5 Bar gauge was maintained downstream of the test section throughout the tests.

Test identifier	ID1	ID2	ID3	ID4	ID5	ID6
Fluid name	Kerosene	Kerosene	Velocite	Velocite	Gas oil	Velocite
Calibration method	Gravimetric	Master meter	Gravimetric	Master meter	Gravimetric	Master meter
Test temperature (nominal)	16 °C	20 °C	20 °C	20 °C	47 °C	45 °C
Density @ test temperature	803 kg/m ³	800 kg/m ³	852 kg/m ³	852 kg/m ³	798 kg/m ³	836 kg/m ³
Viscosity @ test temperature	2.75 cSt	2.56 cSt	31.2 cSt	31.2 cSt	2.75 cSt	12.0 cSt
Velocity of sound @ test temp.	1340 m/s	1330 m/s	1420 m/s	1420 m/s	1250 m/s	1340 m/s
Reynolds number range	46,000 - 440,000	25,000 - 350,000	6,000 - 27,000	2,000 - 37,000	70,000 - 320,000	10,000 - 95,000

Table 2 An approximate specification of test conditions

The oil/gas tests were conducted in the velocite line of the oil flow primary standard at a nominal temperature of 20 °C. Preliminary trials were carried out prior to the specification of the tests. The following test matrix was constructed in light of the trial results.

Nominal flowrate	Nominal gas fractions by volume (GVF)		
	5 %	10 %	20 %
10 l/s	5 %	10 %	20 %
30 l/s	1 %	2 %	5 %
50 l/s	0.5 %	1 %	2 %
70 l/s	-	0.5 %	1 %

Table 3 Nominal conditions for the oil/gas tests

4 DESCRIPTION OF TEST METERS

A number of companies were invited to provide meters for the duration of the project. These companies products were chosen to represent the state-of-the-art in ultrasonic flow measurement. Meters were supplied from five sources covering a range of technological aspects. In each case the meter supplied represented the manufacturers most recent product generation. The following sections are intended to provide a brief description of features relevant to the discussion of test results.

4.1 DANFOSS Sonoflow

The SONO3300 is a sensor tube with four wetted transducers forming two parallel tilted chordal sound paths. Each path is formed at a mid-radius position in the cross-section and is inclined at an angle of 39° to the tube axis. This configuration is represented schematically in Figure 2(a). The transducers are metal encapsulated piezoelectric crystals which are mounted in the cast body by means of a screw fitting. A memory chip which is pre-programmed with the primary physical parameters and factory calibration factor is provided with the meter tube. The meter provided by Danfoss for the project was taken from their normal production stream.

The excitation and detection of ultrasonic signals and subsequent processing and flow computation are performed by the SONO3000 signal converter. The transducers are excited by a sine wave of 8 cycles duration and a frequency of around 1 MHz. The received upstream and downstream signals are digitised and stored for processing. Automatic gain control (AGC) is utilised to optimise the analogue to digital conversion. The flow computation is based on measurement of the overall transit-time and the upstream-downstream transit-time difference, which are both treated separately by a correlation technique. The transit-time difference is determined by cross-correlating the upstream and downstream signals whereas the overall transit-time is determined by cross-correlating one of the received signals with a stored reference signal. This stored reference signal is dynamically adapted to the operation conditions.

The mid-radius position of the measurement paths is chosen to minimise sensitivity due to Reynolds number dependent changes in flow profile [2]. The SONO3300/3000 therefore does not require user-input viscosity data.

4.2 ULTRAFLUX UF322-2

The Ultraflux UF322-2 is a dual path signal converter for use with clamp-on or wetted transducers. The meter was supplied with 1 MHz clamp-on transducers which were installed by a representative of Ultraflux on a 4-inch nominal bore stainless steel spoolpiece provided by NEL. The transducers were coupled to the outside of the spoolpiece using Polyken elastomer and secured in position with jubilee clips to form two tilted-diameter single-reflection sound paths in perpendicular planes, as illustrated schematically in Figure 2(b). The axial distance at which the transducers should be set apart is displayed by the converter following entry of transducer configuration, pipe dimensions and fluid velocity of sound parameters. Prior to the transducer installation, an approximately mid-range value for fluid sonic velocity and the tabulated dimensions for the Schedule 40 pipe had been entered into the converter.

The upstream and downstream transit time measurements are performed by detecting the first zero crossing in the received digitised pulse signals. The UF322-2 has an automatic flow profile compensation feature which was utilised to compensate for the difference between the measured diametrical velocity and the mean velocity in the cross-section. This feature requires fully developed symmetrical flow at the meter and that values for viscosity and for roughness of the pipe interior be input during set-up. For tests ID1, ID3 and ID5, performed by the standing-start and finish method, a constant value of 20 cSt was entered for the dynamic profile compensation. For tests ID4 and ID6, performed by the master meter method, viscosity values of 31.2 and 12.0 cSt respectively were entered. The roughness was entered as 0.1 mm.

4.3 PANAMETRICS XMT868

The Panametrics XMT868 is a dual channel flow transmitter for use with clamp-on or wetted transducers. Two XMT's were provided by Panametrics with a carbon steel spoolpiece comprising both wetted and clamp-on transducer configurations. The wetted transducers were 1 MHz 1 inch NPT 'extended-well' type transducers which are threaded into a welded boss such that the centre of the transducer face is aligned with the interior of the spoolpiece. The clamp-on transducers were 1 MHz shear wave transducers which were each mounted on the exterior of the spoolpiece by means of a welded yoke and coupled to the pipe wall using a silicon vacuum grease. Both wetted and clamp-on path configurations were dual tilted-diameter single-reflection sound paths in perpendicular planes as illustrated schematically in Figure 2(b). Each meter was flow calibrated prior to arrival at NEL.

The Panametrics XMT868 uses a coded excitation and correlation detection scheme to determine the transit time of the ultrasonic signals [3]. The excitation signal, rather than an impulse or sinusoid, is a phase-coded square-wave burst. AGC is utilised to optimise the signal level before digitisation and averaging of several successive signals. The digitised receive signals are then cross correlated with a stored version of the excitation signal to determine the upstream and downstream transit times.

As both clamp-on and wetted configurations employed diametrical paths, the flow profile compensation feature of the XMT868 was utilised in each case. This feature requires fully developed symmetrical flow at the meter and that a value of viscosity be entered in the meter during set-up. A value of 20 cSt was entered for both meters throughout the tests.

4.4 PEEK MEASUREMENT Polysonics DCT-6088

The Polysonics DCT-6088 is Peek's latest generation of transit-time ultrasonic flowmeter. It is a single-beam meter with 1 MHz clamp-on transducers which for the project were mounted on a 4 inch nominal bore carbon steel spoolpiece provided by NEL. The transducers were coupled to the outside of the spoolpiece using a mineral oil based couplant and secured in position with jubilee clips to form a tilted-diameter double-reflection sound path, as illustrated schematically in Figure 2(c). The axial distance at which the transducers should be set apart is displayed by the converter following entry of transducer configuration, pipe dimensions and fluid velocity of sound parameters. Prior to the transducer installation, an approximately mid-range value for fluid sonic velocity and the tabulated dimensions for the Schedule 40 pipe had been entered into the converter.

The DCT-6088 uses digital correlation to determine the transit-time of the ultrasonic signals. Several different signal types are used for excitation of the transducers including coded and modulated waveforms. Specific detail regarding the methods used was not available at the time of writing this paper.

The Polysonics meter has an automatic flow profile compensation feature which is utilised to compensate for the difference between the measured diametrical velocity and the mean velocity in the cross-section. A viscosity value of 20 cSt and bore roughness of 0.21 mm were utilised for this feature throughout the tests.

4.5 KROHNE ALTOMETER UFM Multi-channel

Krohne Altometer provided a 5-beam version development prototype of their UFM Multi-channel flowmeter. The sensor head of the 5-beam meter is constructed such that ten wetted transducers are paired to form measurement paths in two planes as illustrated schematically in Figure 2(d). Excitation and signal detection for each transducer pair is at present achieved by use of one of five UFC 500 signal converters, these being standard signal converters as employed in the single and dual beam ultrasonic flowmeter designs available from Krohne Altometer. Upstream and downstream transit-time measurements are performed by a threshold-armed zero-crossing detection technique. The five signal converters each produce a frequency output proportional to flow velocity which are input to a PC controlled data acquisition and transmission board. Computation of the volumetric flowrate from the five frequency inputs is performed in the software and the result output as a frequency at the PC controlled board.

The computation of volumetric flowrate is similar to multi-path meters based on Gaussian or Chebychev integration techniques [4] in that the individual path measurements are individually weighted and then summed. The meter also has the facility to reduce the non-linearity inherent in such techniques by identifying Reynolds number and applying a corresponding profile correction factor for fully developed flow. The Reynolds number/profile identification is performed by computing the difference in fluid velocity at two distinct radial positions in a manner similar to that described by Jackson et al [5]. It is also claimed that the meter should be able to compensate for asymmetric profiles and non-axial velocity components. However, such claims have not yet been tested by NEL.

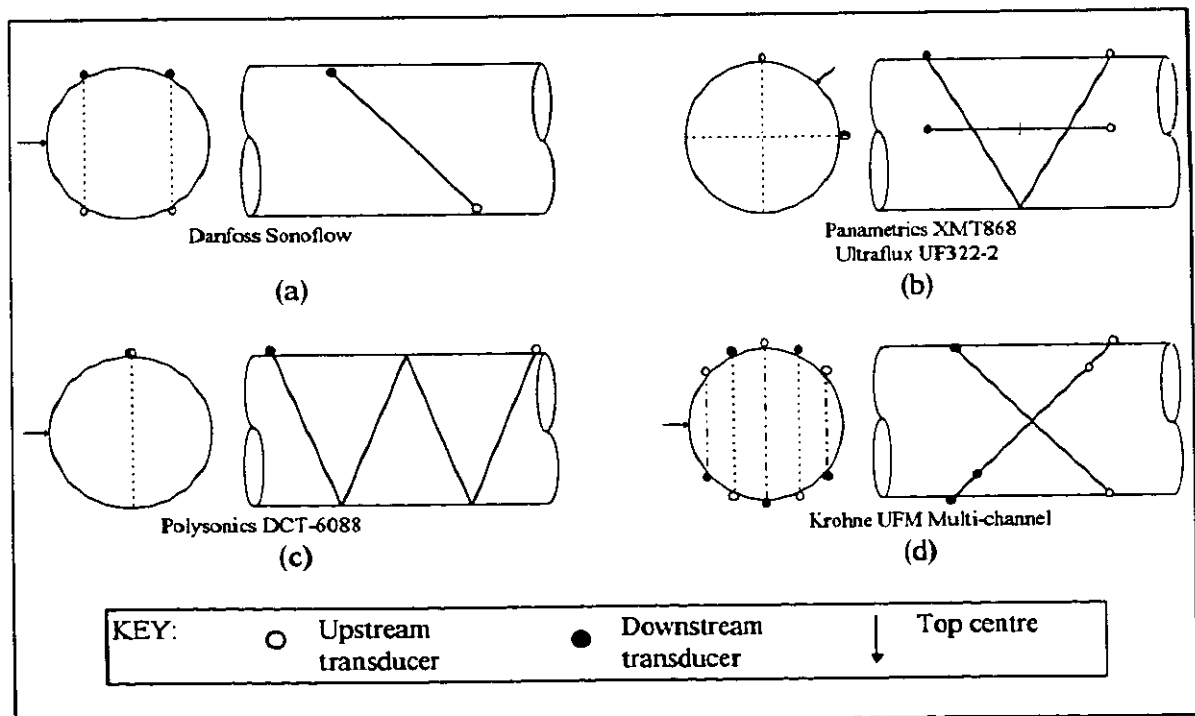


Figure 2 The schematic diagrams of meter path configurations

5 PRECURSIVE DISCUSSION

The following general points should be considered in relation to the results which follow.

5.1 The effect of meter size

Ultrasonic transit-time flowmeters generally utilise nominally identical primary elements (i.e. transducers and electronics) for all sizes of meter. However, a change in meter diameter can affect the performance in a number of ways. Such effects are not discussed in detail here but should be considered carefully when selecting an ultrasonic meter for a specific application. If similar velocities are maintained it is generally true to say that meter performance improves with increasing size.

5.2 The use of dynamic profile correction

Dynamic profile correction utilises an iterative process to compensate for difference between the measured diametrical velocity and the mean velocity in the cross-section.

$$\bar{v} = k_h v_{meas}. \quad (1)$$

where k_h is the profile correction factor. For the majority of results from meters employing only diametrical beams and dynamic profile correction, a nominal viscosity value of 20 cSt was entered into the meter software though out the tests. Therefore the results are in some cases artificially worse than they would have been had an appropriate viscosity value been entered for each test. To illustrate this two graphs have been constructed, Figure 3 showing theoretical curves of profile correction factor versus flowrate for viscosity values of 2.65, 20 and 31.2 cSt, and Figure 4 showing the approximate error introduced into kerosene and velocite calibrations for the diametrical meters. The analytical expression for the turbulent profile factor k_{turb} used here is derived from the power law for velocity distribution in a smooth pipe [6].

$$k_{turb}(R_{eD}) = \frac{1}{1.119 - 0.001 \times \log R_{eD}} \quad (2)$$

Where R_{eD} is the diametrical Reynolds number. In laminar flow conditions assuming a parabolic profile the factor is constant at $k_{lam} = 0.75$ [6]. In the transition between laminar and turbulent flow, the profile correction factor can not be defined without ambiguity. For illustrative purposes the switching function S of Pannell *et al* [4] has been adopted.

$$S(n, R_{eD}, R_c) = \frac{1}{1 + (R_{eD}/R_c)^n} \quad (3)$$

The function for the profile correction factor across all regimes can now be given as

$$k_h(R_{eD}) = [1 - S(n, R_{eD}, R_c)]k_{turb}(R_{eD}) + S(n, R_{eD}, R_c)k_{lam} \quad (4)$$

Here R_c , the critical Reynolds number at which transition occurs, was taken as 3200 and n which defines the width of the transition region was taken as 5 such that k_h is approximately 10 % k_{turb} at $R_{eD} = 2000$ and 10 % k_{lam} at $R_{eD} = 5000$.

It must be stressed that this k_h function is not strictly correct but is used only to illustrate the nature of error that can be incurred by inaccurate entry of the viscosity value for dynamic profile correction. Equally important is the fact that not only viscosity but other factors such as vibration, bore roughness and diameter will affect the flow profile and the point at which the flow regime transition occurs.

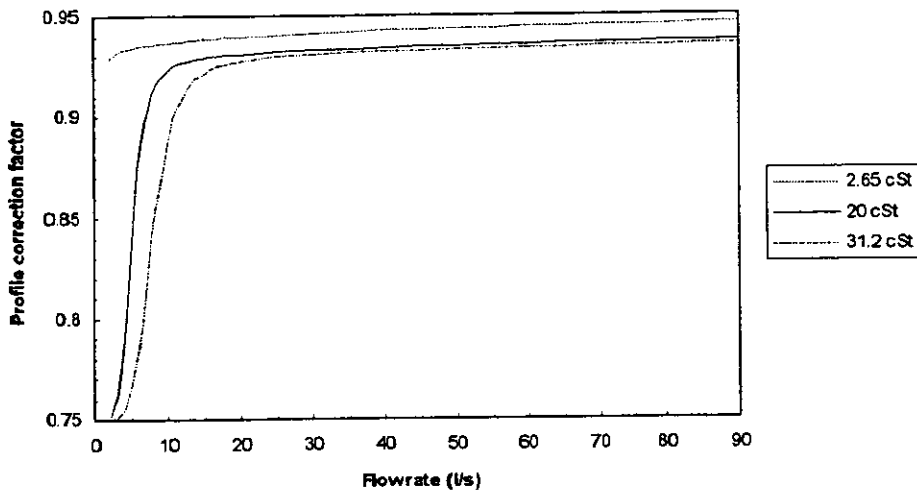


Figure 3 Viscosity dependence of profile correction for 100 mm bore diametrical meters

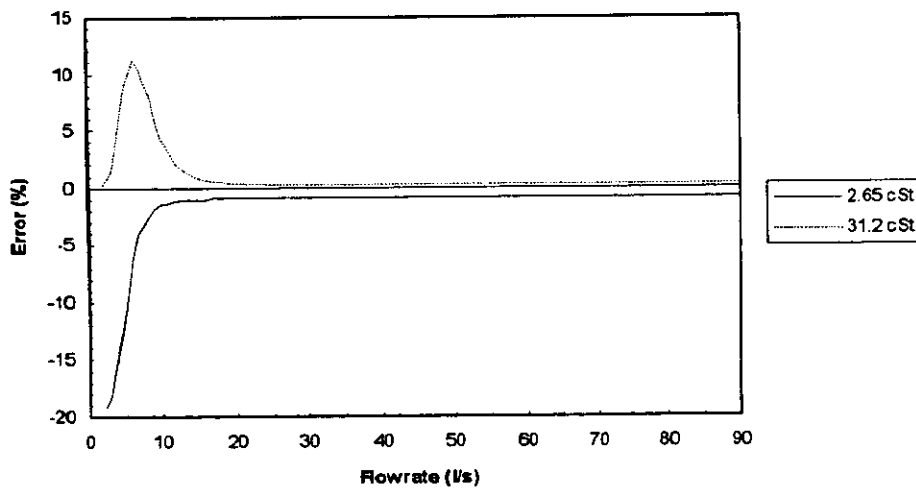


Figure 4 Error introduced by entry of the viscosity as 20 cSt

5.3 The effect of gas in liquid

The oil/gas testing was carried out to examine the potential of the meters to cope with gas content in an oil stream. The meters were not modified in any way between single-phase and two-phase tests and as such the results reflect indicative behaviour rather than the limitation of the technology if 'tuned' to specific application conditions.

The acoustic impedance (product of density and velocity of sound) of gases is significantly less than that of liquids (~ 3000:1). The consequence of this *acoustic impedance mismatch* is that extreme reflection/scattering occurs when ultrasound encounters gas in a liquid, this being the main mechanism of attenuating the received signals. Another point to note is that the low acoustic impedance of gases means that transducers designed for liquid use are not suitable for gas measurements. Therefore a transmitter-receiver pair will register signal loss when the fluid path between them is gaseous.

Johannessen [7] presented results which showed meter failure with as little as 0.4 % gas by volume at a flowrate of approximately 11 l/s. It was stated that the gas fraction could even have been less due to entrapment of gas in cavities in the closed-loop system. The meters tested were a Panametrics model 6468 and a Danfoss SONO 2000. Transit-time measurement in the wetted SONO 2000 was performed by threshold-armed zero-crossing detection. The Panametrics 6468 utilised digital correlation processing. It was not stated whether the 6468 was used with wetted or clamp-on transducers.

Different gas fractions were specified for each nominal flowrate during the oil/gas tests due to the effect of the flow velocity on the gas distribution and resultant behaviour of the meters. At the highest velocities the gas appeared to be fairly evenly distributed in the cross-section in the form of many sub-millimetre bubbles. As the velocity was decreased, the bubbles increased in size, decreased in number and were less evenly distributed with greatest concentrations in the upper area of the cross-section. At the lowest velocity the gas and liquid were clearly stratified with only a few bubbles present in the lower areas of the pipe. Throughout the tests no recirculation of gas was observed at a perspex viewing section upstream of the gas injection point.

6 PRESENTATION

Results are presented in graphical and tabular form and described in the following terms:

- *Error*: The difference between the total volume indicated by the meter under test and the recorded reference volume, expressed as a percentage and plotted against flowrate. In the oil/gas tests the reference volume is considered to include both liquid and gas components.

$$E = \left(\frac{V_{ind} - V_{std}}{V_{std}} \right) \times 100\% \quad (5)$$

- *Deviation*: The difference between the error at test and reference conditions.

$$D = (E_{test} - E_{ref}) \quad (6)$$

- *Repeatability*: A measure of the random uncertainty in measurement defined [8] as:

$$R = 2.83s_E, \text{ where } s_E = \sqrt{\frac{\sum (E - \bar{E})^2}{n - 1}} \quad (7)$$

and n , the number of repeat measurements at a single test condition, is five.

7 RESULTS

7.1 DANFOSS Sonoflow

The Danfoss Sonoflow exhibited a well defined and repeatable dynamic response to the transient changes in flowrate inherent in the standing-start and finish method.

7.1.1 Baseline calibration

The results of calibration in kerosene at 20 °C are presented in Figure 4 which also shows by a dashed line the bounds of the manufacturers accuracy statement; *Accuracy better than $\pm 0.5\%$ of reading over a dynamic range with a turndown of 20:1*. The figure shows maximum and minimum errors of 1.2 and -0.5% at flowrates of 14 and 51 l/s respectively. The results are within the bounds of the manufacturers accuracy statement for flowrates of 24 l/s and above.

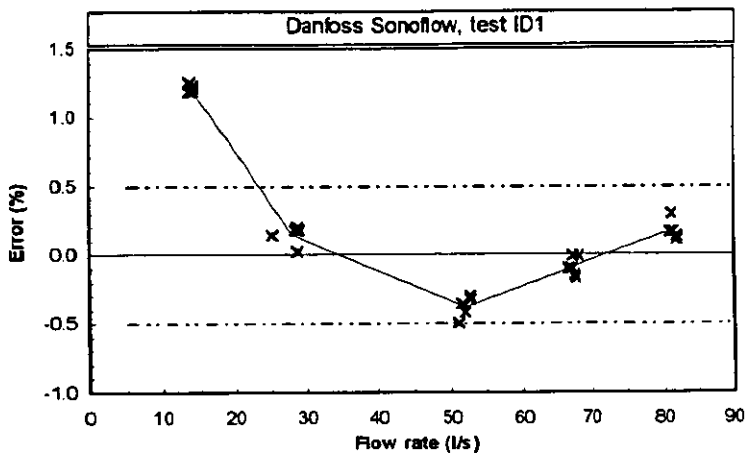


Figure 4 Kerosene calibration at 16 °C

7.1.2 Viscosity tests

The results of calibration in velocite oil at 20 °C are presented in Figure 5 which also shows by dashed lines the baseline calibration and manufacturers accuracy limits. The figure shows maximum and minimum errors of 4.8 and -0.68% at flowrates of 9 and 51 l/s respectively. The results are within specification at flowrates of 70 l/s and above. The deviation from the baseline calibration is a maximum of approximately 1.5 % at 14 l/s and within $\pm 0.7\%$ at flowrates of 30 l/s and above.

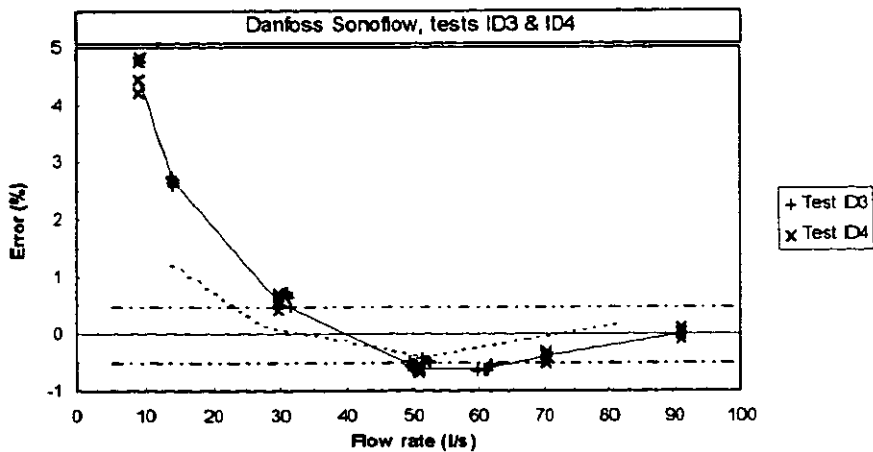


Figure 5 Velocite calibration at 20 °C

The results of calibration in velocite oil at 45 °C with are presented in Figure 6. The figure shows maximum and minimum errors of 2 and -0.65 % at flowrates of 10 and 50 l/s respectively. The results are within specification at 30 l/s and at 70 l/s and above. The deviation from the baseline calibration is within approximately ± 0.4 % across the range.

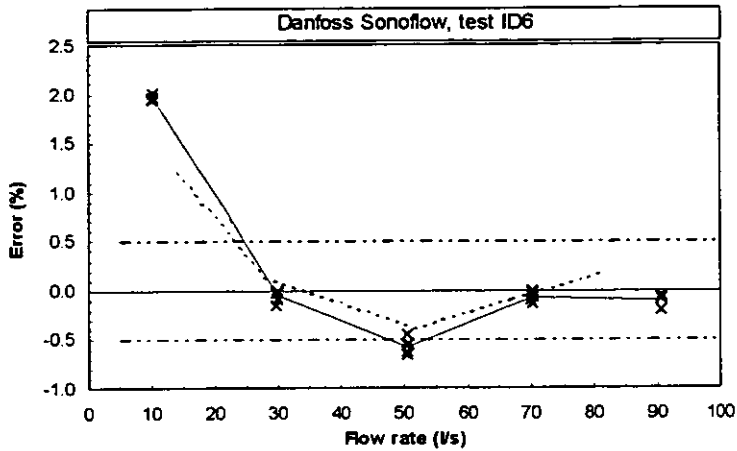


Figure 6 Velocite calibration at 45 °C

7.1.3 Temperature test

The gas oil test at 47 °C subjected the meter to a temperature change of 31 °C and a change in fluid sonic velocity of approximately 7 % whilst nominally maintaining viscosity with reference to the baseline calibration. The results of this test are presented in Figure 7 which also shows by a dashed line the baseline calibration. The figure shows maximum and minimum errors of 1.2 and -0.36 % at flowrates of 15 and 50 l/s respectively. The deviation from the baseline calibration is within ± 0.25 % across the majority of the range.

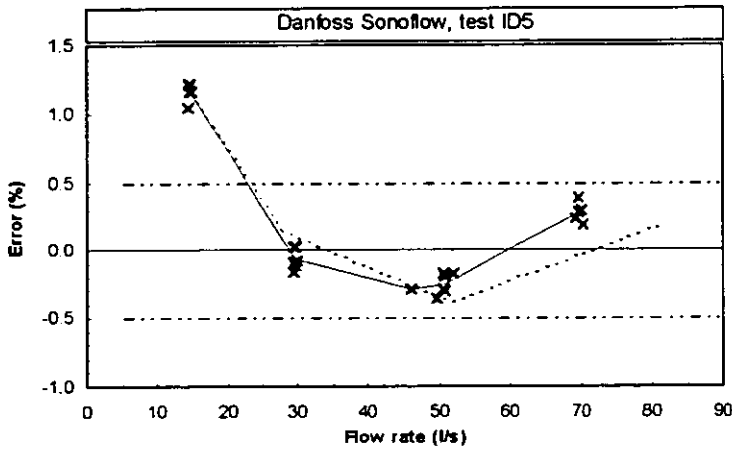


Figure 7 Gas oil calibration at 47 °C

7.1.4 Repeatability

Figure 8 shows the repeatability of the meter as determined during each of the oil calibrations. There is no clear relationship between flowrate and repeatability. The repeatability is better than 0.3 % for all but one point, which was calculated from results in the transition region of test ID4.

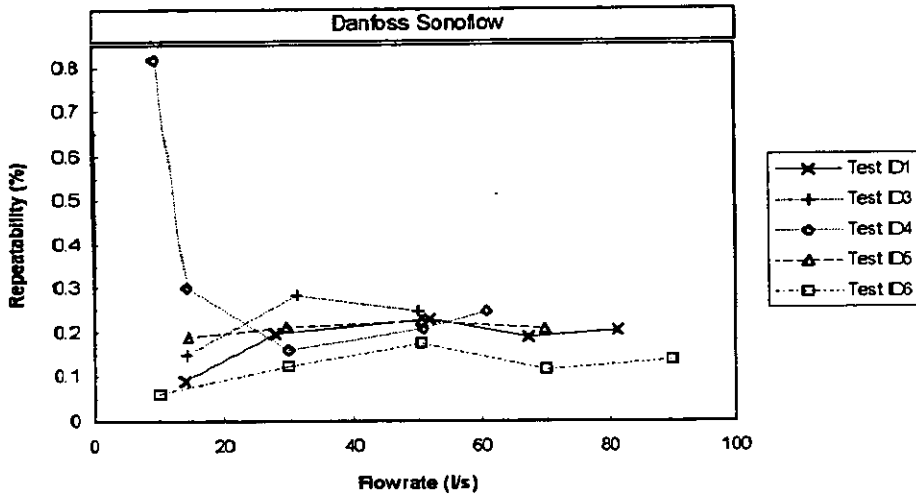


Figure 8 Repeatability versus flowrate

7.1.5 Oil/gas tests

During the oil/gas tests, the SONO3000 converter was observed at each test condition. The occurrence of fault conditions are recorded in Table 4 along with the range within which the maximum deviation from the 0 % GVF results occurred. The fault conditions observed corresponded to a *weak received signal* or an *unstable signal due to the presence of gas bubbles*.

Nominal flowrate	GVF	Converter fault indication	Max. deviation
10 l/s	2.5 %	no	$\pm 1 \% < d \leq \pm 5 \%$
	7.5 %	no	$\pm 1 \% < d \leq \pm 5 \%$
	22.5 %	yes	$d > \pm 10 \%$
30 l/s	0.75 %	no	$\pm 5 \% < d \leq \pm 10 \%$
	1.5 %	intermittent	$d > \pm 10 \%$
	4 %	yes	$\pm 5 \% < d \leq \pm 10 \%$
50 l/s	0.35 %	no	$d \leq \pm 1 \%$
	0.7 %	no	$\pm 1 \% < d \leq \pm 5 \%$
	1.5 %	yes	$d > \pm 10 \%$
70 l/s	0.4 %	no	$\pm 1 \% < d \leq \pm 5 \%$
	0.8 %	intermittent	$d > \pm 10 \%$

Table 4 Summary of oil/gas performance

From the table it can be seen that fault free operation with deviation within $\pm 10 \%$ is achieved at 10 l/s up to 7.5 % GVF, 30 l/s at 0.75 % GVF, 50 l/s up to 0.7 % GVF and 70 l/s at 0.4 % GVF.

7.2 ULTRAFLUX UF322-2

The Ultraflux UF322-2 exhibited a reasonably prompt and repeatable response to the transient changes in flowrate inherent in the standing-start and finish method.

7.2.1 Baseline calibration

The results of calibration in kerosene at 20 °C are presented in Figure 9 which also shows by a dashed line manufacturers accuracy limits. The figure shows maximum and minimum errors of -5.3 and -3.4 % at flowrates of 14 and 52 l/s respectively. The error is clearly greater than the manufacturers stated *Typical accuracy: 0.5 % at 10 to 100 % of the scale*. Also the magnitude of the error greater than the predicted deviation due to the entry of the viscosity as 20 cSt implying an error due to the uncertainties in pipe dimensions.

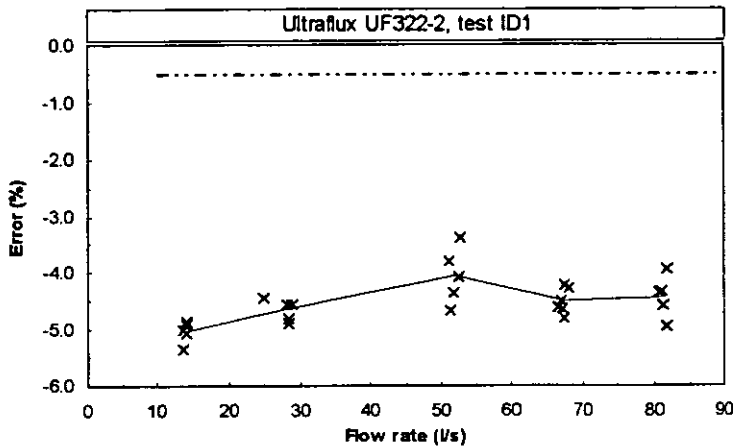


Figure 9 Kerosene calibration at 16 °C

7.2.2 Viscosity tests

The results of calibration in velocite oil at 20 °C are presented in Figure 10 which also shows by a dashed line the baseline calibration and manufacturers accuracy limits. The figure shows maximum and minimum errors of 1.5 and -1.8 % at flowrates of 14 and 60 l/s respectively. The deviation from the baseline calibration is reasonably constant at approximately 3.5 % for flowrates greater than 30 l/s. At 14 l/s the deviation has increased to approximately 6%.

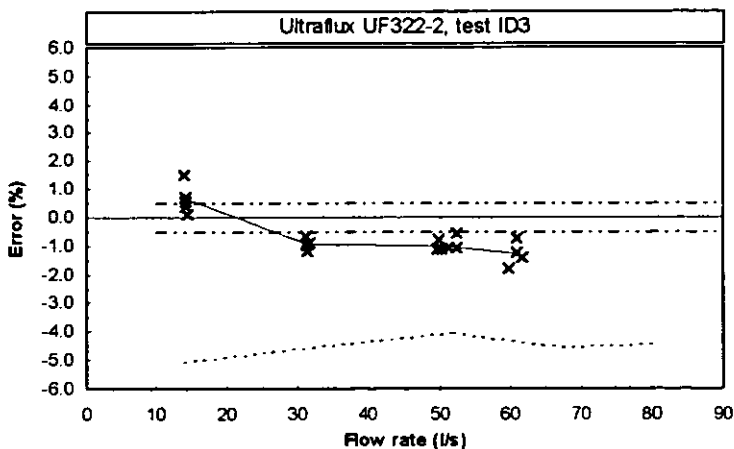


Figure 10 Velocite calibration at 20 °C

Two further tests were conducted by the master meter method in velocite at temperatures of 20 and 45 °C. For both of these tests the appropriate viscosity was entered so as to remove any 'artificial' error source. The results of these tests are presented in Figure 11. The figure shows average errors of -1.2 and -1.7 % at flowrates greater than 30 l/s for the 31.2 and 12 cSt calibrations respectively, supporting the hypothesis that a component of the error is due to dimensional uncertainties. The deviation between calibrations reaches a maximum of approximately 11 % at 10 l/s.

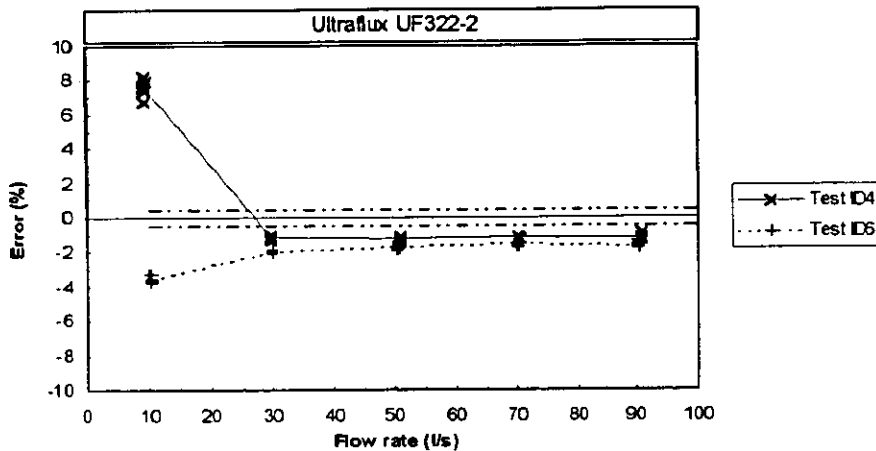


Figure 11 Velocite calibrations at 20 and 45 °C

7.2.3 Temperature test

The gas oil test at 47 °C subjected the meter to a temperature change of 31 °C and a change in fluid sonic velocity of approximately 7% whilst maintaining viscosity with reference to the baseline calibration. The results of this test are presented in Figure 12 which also shows by a dashed line the baseline calibration. The figure shows maximum and minimum errors of -2.2 and -4.0 % at flowrates of 51 and 30 l/s respectively. The deviation from the baseline calibration is reasonably constant at approximately 1 % for flowrates greater than 30 l/s. At 14 l/s the deviation has increased to approximately 2 %.

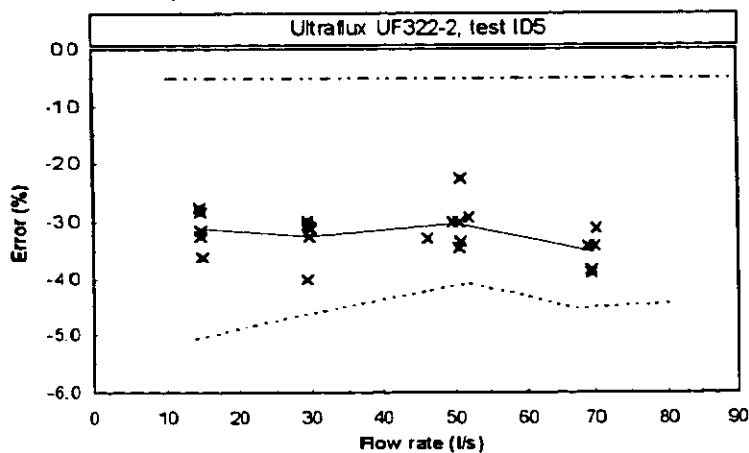


Figure 12 Gas oil calibration at 16 °C

7.2.4 Repeatability

Figure 13 shows the repeatability of the meter as determined during each of the oil calibrations. The expected trend of an improvement in repeatability with increased flowrate is seen for the master-meter tests, but is not apparent in the standing-start and finish tests. The significant difference in results between methods is due to the variation in test times in addition to the effects of the transients.

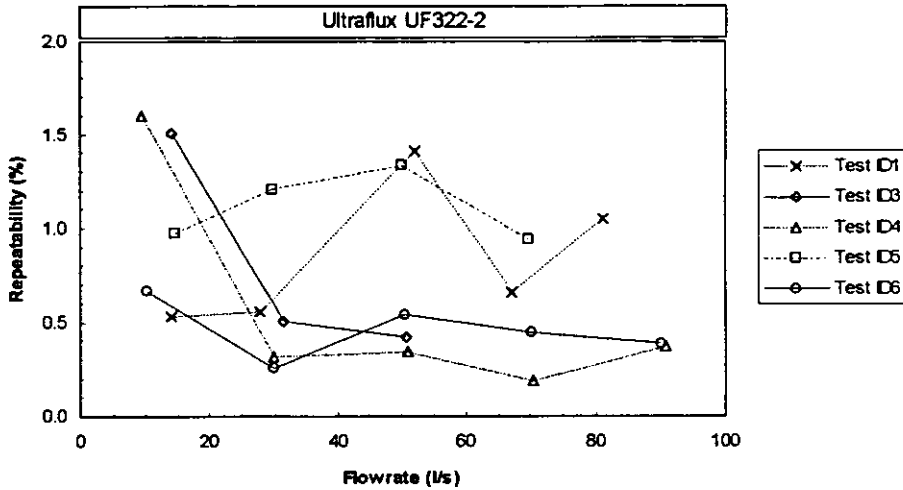


Figure 13 Repeatability versus flowrate

7.2.5 Oil/gas tests

During the oil/gas tests, the UF322-2 converter was observed at each test condition. The occurrence of 'echo loss' fault conditions are recorded in Table 5 along with the range within which the maximum deviation from the 0 % GVF results occurred. When echo loss faults occurred on both paths the flowrate indication was forced to zero.

Nominal flowrate	GVF	Converter fault indication	Max. deviation
10 l/s	2.5 %	none	$\pm 5 \% < d \leq \pm 10 \%$
	7.5 %	frequent	$d > \pm 10 \%$
	22.5 %	frequent	$d > \pm 10 \%$
30 l/s	0.75 %	intermittent	$\pm 1 \% < d \leq \pm 5 \%$
	1.5 %	frequent	$d > \pm 10 \%$
	4 %	continuous	$d > \pm 10 \%$
50 l/s	0.35 %	intermittent	$\pm 1 \% < d \leq \pm 5 \%$
	0.7 %	continuous	$d > \pm 10 \%$
	1.5 %	continuous	$d > \pm 10 \%$
70 l/s	0.4 %	continuous	$d > \pm 10 \%$
	0.8 %	continuous	$d > \pm 10 \%$

Table 5 Summary of oil/gas performance

From the table it can be seen that operation with deviation less than $\pm 10 \%$ is achieved at 10 l/s with 2.5 % GVF, 30 l/s with 0.75 % GVF and 50 l/s with 0.35 % GVF.

7.3 PANAMETRICS XMT868

During initial standing-start and finish tests on the XMT868, it was noted that the repeatability of the meter was poorer than expected due to the transient changes in flowrate inherent in the method. In order that the meter was not subjected to these transients the calibrations were performed by the master-meter method.

7.3.1 Baseline calibration

7.3.1.1 Wetted transducers

The results of calibration in kerosene at 20 °C are presented in Figure 14 which also shows by a dashed line the lower bounds of the manufacturers accuracy statement; *pipe diameter ≤ 150 mm, velocity > 0.3 m/s, $\pm 2\%$ to 5% of reading typical*. The figure shows maximum and minimum errors of -1 and -8.8 % at flowrates of 10 and 5 l/s respectively. At flowrates of 10 l/s and above, the calibration meets the manufacturers specification, even with the additional error predicted by entry of the viscosity as 20 cSt.

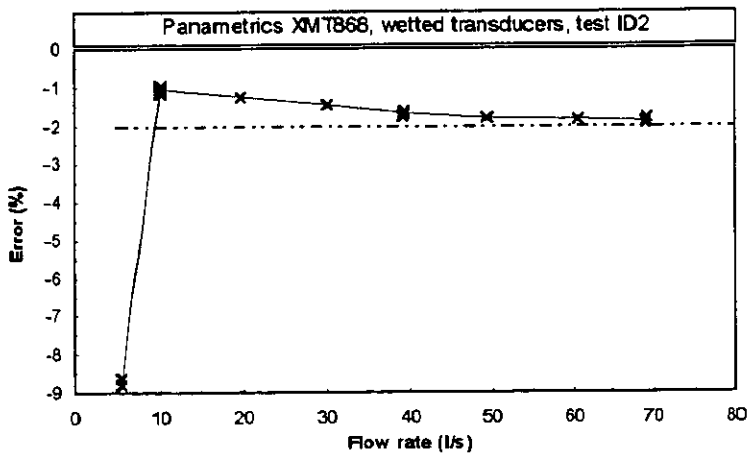


Figure 14 Kerosene calibration at 20 °C

7.3.1.2 Clamp-on transducers

The results of calibration in kerosene at 20 °C are presented in Figure 15 which also shows by a dashed line the lower bounds of the manufacturers accuracy statement. The figure shows maximum and minimum errors of -0.5 and -9.1 % at flowrates of 10 and 5 l/s respectively. Again the manufacturers specification is satisfied at flowrates of 10 l/s and above.

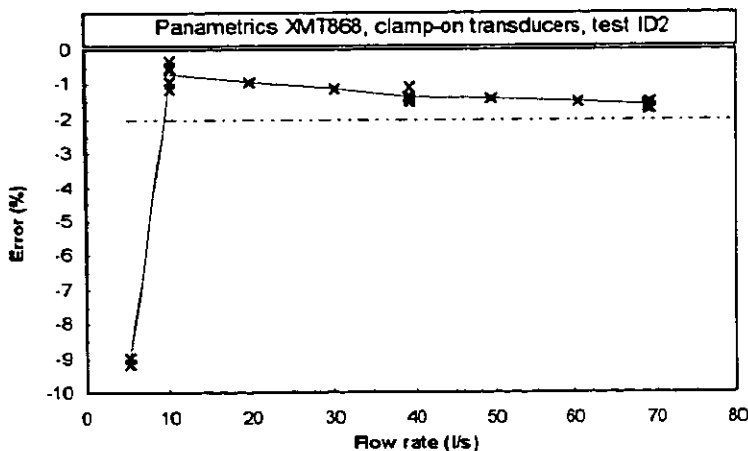


Figure 15 Kerosene calibration at 20 °C

The under-estimation at 5 l/s in both clamp-on and wetted meters is most probably due to the meters predicting the flow to be in transition between turbulent and laminar conditions, as a result of the entry of viscosity as 20 cSt, when indeed the flow was fully turbulent.

7.3.2 Viscosity test

7.3.2.1 Wetted transducers

The results of calibration in velocite oil at 20 °C are presented in Figure 16 which also shows by dashed lines the baseline calibration and the lower bounds of the manufacturers accuracy statement. The figure shows maximum and minimum errors of 10.1 and 0.7 % at flowrates of 5 and 69 l/s respectively. For flowrates of 20 l/s and above, the manufacturer's specification is satisfied and the deviation from the baseline calibration is reasonably constant at approximately 2.5 %.

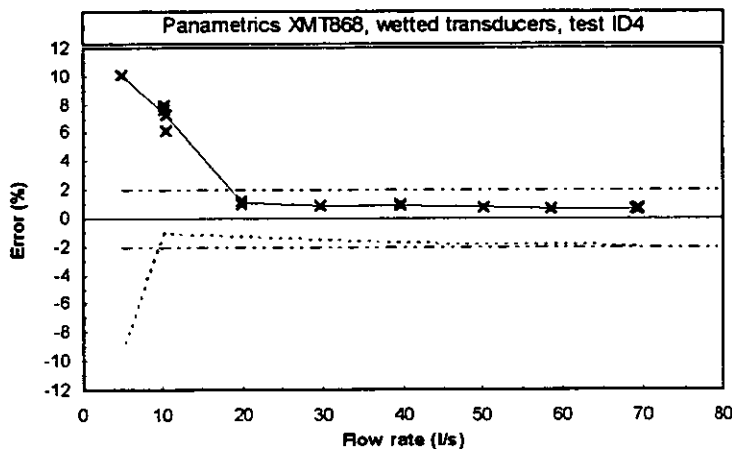


Figure 16 Velocite calibration at 20 °C

7.3.2.2 Clamp-on transducers

The results of calibration in velocite oil at 20 °C are presented in Figure 17 which also shows by dashed lines the baseline calibration and the lower bounds of the manufacturers accuracy statement. The figure shows maximum and minimum errors of 11 and 0.2 % at flowrates of 5 and 40 l/s respectively. The deviation from the baseline calibration is reasonably constant at approximately 1.8 % for flowrates of 20 l/s and above. Again, the manufacturers specification is also satisfied at these flowrates.

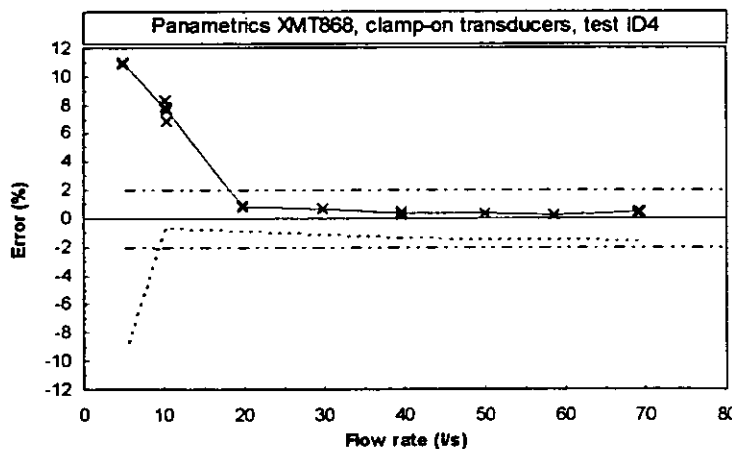


Figure 17 Velocite calibration at 20 °C

The over-estimation at 5 and 10 l/s in both clamp-on and wetted meters is most probably due to the meters predicting the flow to be nearer fully turbulent than laminar conditions, as a result of the entry of viscosity as 20 cSt.

7.3.3 Repeatability

7.3.3.1 Wetted transducers

Figure 18 shows the repeatability of the meter as determined at three flowrates across the range during both the kerosene and velocite calibrations and the bounds of the manufacturers repeatability statement; *Wetted transducers: $\pm 0.2\%$ of full scale (12.2 m/s)*. The results are within the manufacturer's specification with the exception of the point from the velocite calibration at 10 l/s. This point lies practically on the boundary of the manufacturers limits and was determined when the flow was probably in laminar/turbulent transition.

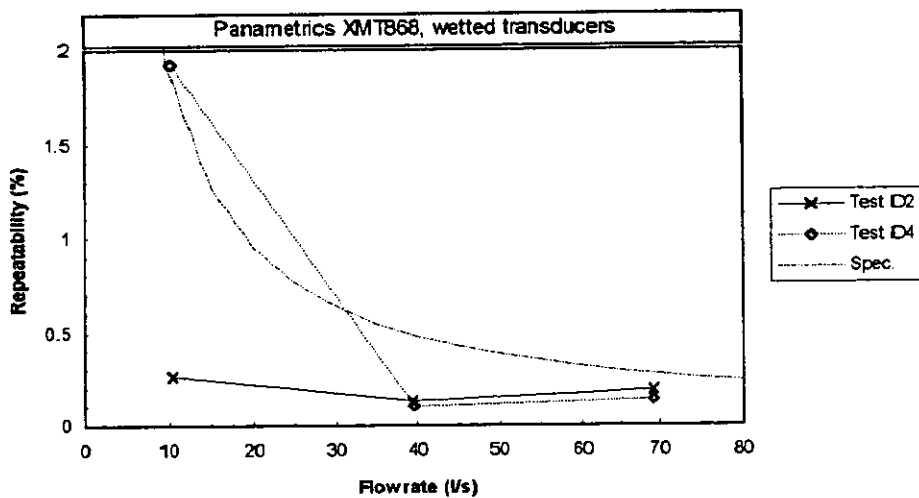


Figure 18 Repeatability versus flowrate

6.3.3.1 Clamp-on transducers

Figure 19 shows the repeatability of the meter as determined at three flowrates across the range during both the kerosene and velocite calibrations and the lower bounds of the manufacturers repeatability statement; *Clamp-on transducers: $\pm 0.2\%$ to 0.5% of full scale (12.2 m/s)*. The results are all within the manufacturer's specification and the display the expected trend of an improvement in repeatability with increasing flow velocity.

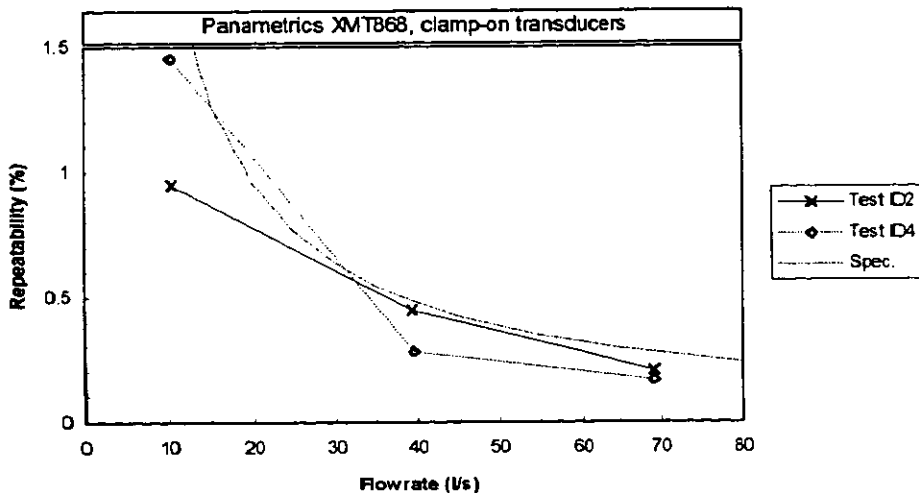


Figure 19 Repeatability versus flowrate

7.3.4 Oil/gas tests

During the oil/gas tests, the XMT868 converters were observed at each test condition. The occurrence of low signal fault conditions are recorded in Table 6 along with the range within which the maximum deviation from the 0 % GVF results occurred. During fault occurrence the flowrate indication of the XMT's were forced to zero.

Nominal flowrate	GVF	Wetted fault	Wetted max. deviation	Clamp-on fault	Clamp-on max. deviation
10 l/s	2.5 %	none	$\pm 1 \% < d \leq \pm 5 \%$	none	$\pm 1 \% < d \leq \pm 5 \%$
	7.5 %	intermittent	$d > \pm 10 \%$	none	$\pm 5 \% < d \leq \pm 10 \%$
	22.5 %	frequent	$d > \pm 10 \%$	frequent	$d > \pm 10 \%$
30 l/s	0.75 %	intermittent	$d > \pm 10 \%$	none	$d \leq \pm 1 \%$
	1.5 %	continuous	$d > \pm 10 \%$	none	$\pm 1 \% < d \leq \pm 5 \%$
	4 %	continuous	$d > \pm 10 \%$	continuous	$d > \pm 10 \%$
50 l/s	0.35 %	none	$d \leq \pm 1 \%$	none	$d \leq \pm 1 \%$
	0.7 %	continuous	$d > \pm 10 \%$	none	$\pm 1 \% < d \leq \pm 5 \%$
	1.5 %	continuous	$d > \pm 10 \%$	continuous	$d > \pm 10 \%$
70 l/s	0.4 %	continuous	$d > \pm 10 \%$	none	$d \leq \pm 1 \%$
	0.8 %	continuous	$d > \pm 10 \%$	continuous	$d > \pm 10 \%$

Table 6 Summary of oil/gas performance

From Table 6 it can be seen that fault free operation of the wetted meter with deviation less than $\pm 5 \%$ is achieved only at 10 l/s with 2.5 % GVF and 50 l/s with 0.35 % GVF. The performance of the clamp-on meter is considerably better with fault free operation with deviation less than $\pm 5 \%$ being achieved only at 10 l/s with 2.5 % GVF, 30 l/s at up to 1.5 % GVF, 50 l/s at up to 0.7 % GVF and 70 l/s at 0.4 % GVF. The difference in performance between the clamp-on and wetted meters is most probably due to gas collecting in the small cavities at the faces of the wetted transducers.

7.4 PEEK MEASUREMENT Polysonics DCT-6088

The Polysonics DCT-6088 was included in the series of basic oil calibrations and oil/gas tests. These results have been withheld at the request of Peek Measurement Ltd until further consideration can be given to the findings. The results should be available for future publication.

7.5 KROHNE ALTOMETER UFM Multi-channel

The Krohne Altometer UFM Multi-channel was improperly set up during initial oil calibrations at NEL, and it has been agreed between Krohne Altometer and NEL to withhold these results as they are not truly representative of the meter's performance.

7.5.1 Baseline calibration

Subsequent to ensuring proper grounding and electronic set-up of the meter, a test was performed in velocite oil at 20 °C to determine accurate values for Reynolds number compensation. Parameters of the Reynolds number compensation curve were then entered into the meter software and a calibration in velocite oil at 20 °C performed. The results of the calibration are presented in Figure 23 which also shows the manufacturers uncertainty specification of $\pm 0.15\%$ of rate. The figure shows maximum and minimum errors of 0.11 and -0.04% at flowrates of 5 and 31 l/s respectively. The meter showed good dynamic response to the transient changes in flowrate inherent in the standing-start and finish method and the repeatability was determined as 0.033 % at 58 l/s.

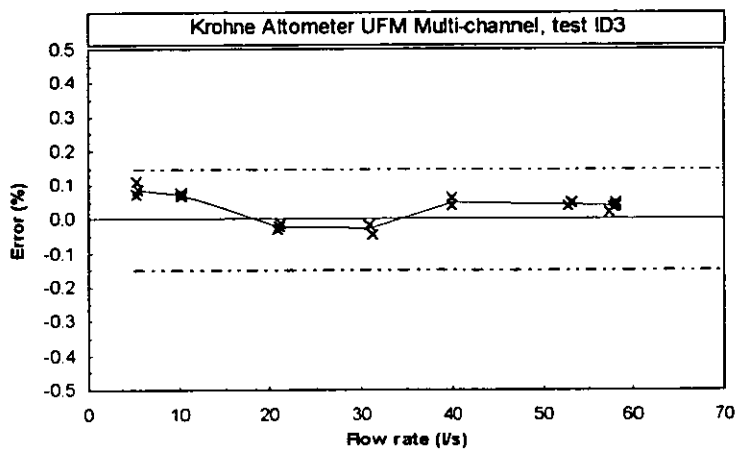


Figure 23 Velocite calibration at 20 °C

7.5.2 Viscosity

This meter determines Reynolds number and the corresponding profile correction without the necessity of user-input values of viscosity and bore roughness, and in principle deviations due to changes in fluid viscosity should be minimal. However, further laboratory evaluation is required and therefore results presented here should be considered only as an indication of the performance that may be achieved.

7.5.3 Oil/gas tests

The UFM Multi-channel ultrasonic flowmeter was included in the series of oil/gas tests. The results from these tests have been withheld at the request of Krohne Altometer until further evaluation can be carried out.

8 DISCUSSION & CONCLUSIONS

8.1 Baseline calibration

From the results reported, one meter performed within specification across the range, three performed within specification across the majority of the range and one performed outside its specification across almost the entire range.

8.2 Viscosity

The viscosity of the fluid influences the velocity profile. Meters employing only diameter paths are most sensitive to these profile changes. Modern meters employ dynamic profile compensation and utilise user-input values of diameter, viscosity and roughness and measured velocity to determine a profile correction factor. Results in the turbulent regime show deviations of the order of a few percent when the viscosity was varied from approximately 2.65 cSt to 31.2 cSt and the input viscosity was constant. Both clamp-on and wetted meters performed very similarly in this respect. If the viscosity input is adapted to application conditions the influence in the turbulent regime should be minimal. From equation 3 it can be shown that a $\pm 10\%$ uncertainty in viscosity will give rise to an uncertainty of less than $\pm 0.05\%$ in the correction factor.

It has been illustrated that inaccuracy of the profile compensation in transition from turbulent to laminar flow can result in uncertainties of up to approximately $\pm 20\%$. It is important to stress that the velocity profile, particularly in transition, is dependent not only on Reynolds number but on bore roughness and vibration [6].

Mid-radius positioning of the measurement paths is chosen to minimise the effect of viscosity dependent changes in velocity profile. The results from the mid-radius pathed meter show that in the turbulent regime the deviation was within $\pm 0.7\%$ when the viscosity was varied from 2.75 cSt to 31.2 cSt and within $\pm 0.4\%$ when the viscosity was varied from 2.75 cSt to 12.0 cSt. At Reynolds numbers close to accepted values for the transition region, the deviation was increased to approximately 1.5%.

The five-beam meter exhibited excellent linearity when calibrated with velocite oil. As the methodology applied is to identify the profile and compensate on the basis of measured variables, viscosity effects should be minimal. However, until this has been thoroughly evaluated, the magnitude of possible effect cannot be quantified.

8.3 Temperature

Two of the meters, one clamp-on, one wetted, were subjected to a calibration in gas oil at 47 °C in an attempt to quantify temperature effects independent of viscosity. The deviation of the clamp-on meter was between 1 and 2%. The deviation of the wetted meter was within approximately $\pm 0.25\%$. The major difference in design, aside from the path configuration, is that the ultrasonic beam in the clamp-on design undergoes refraction at each interface between the transducer crystals and flowing fluid. As a result, the angle of the beam in the flow changes and must be dynamically calculated, and this introduces a further source of uncertainty into the measurement.

8.4 Repeatability

The repeatability of the meters varied from design to design. Best performance was achieved by the 5-beam meter although this was assessed only at one high flowrate. The repeatability of the mid-radius pathed meter was better than the diametrical meters. Among the diametrical meters, the repeatability of the wetted meter showed slight improvement over the clamp-on designs. Repeatability points calculated in the transition region were significantly poorer.

Repeatability is dependent on environmental factors, and temperature affects the flow profile, thus linking repeatability and path configuration. Also, as the 5-beam meter employs a converter for each path, rather than multiplexing, the number of transit-time measurements in a given period is increased, thus improving repeatability.

8.5 Oil/gas Performance

The performance in the presence of free gas is varied but generally poor and is critically dependent on the distribution of the gas in addition to the volume fraction. The reason for this is twofold, firstly, the gas has to actually be in the path between transducers to affect measurement of the transit time, and secondly, how the fluid velocity profile departs from gas-free conditions is dependent on the gas distribution. However, erroneous readings can be identified by fault indications. The signal limits for fault indication can generally be adjusted to tailor the uncertainty limits to specific applications. The performance, although poor, appears to have improved in some cases since the work of Johannessen [7] was carried out. This is almost undoubtedly due to the adoption of techniques based on digital correlation. This is supported by comparison of the results of the two clamp-on meters as one employs correlation detection and the other utilises zero-crossing detection.

Also of interest is to compare the results of the otherwise nominally identical wetted and clamp-on meters. The wetted meter, contrary to the expectation of maintaining a greater signal-to-noise ratio and hence performing better, actually performs worse. This is most likely due to inexpedient positioning of the transducer wells in the upper quadrant of the pipe, and may have been prevented simply by rotating the spoolpiece through 180°.

8.6 Clamp-on versus Wetted Transducers

The discussion of clamp-on versus wetted transducers covers many aspects of performance as well as ease of installation and maintenance. In considering high accuracy applications the following points are probably the most important of those which should be considered.

By comparison of results from the XMT868 with wetted and with clamp-on transducers it is clear that if care is taken in setting up the clamp-on meter similar performance can be achieved. However, what is not obvious is that the limitations of current ultrasonic technology constrains the use of clamp-on transducers to diametrical paths. This means that for the foreseeable future, the problems of dynamic profile compensation must be tolerated. On-line determination of viscosity, either by a viscometer or inferentially by measurement of temperature and/or velocity of sound in the fluid, is one way of improving the situation. However, the effectiveness of either of these solutions must be evaluated.

Perhaps more important is the issue of dimensional uncertainties. Considering that a 1 % uncertainty in the determination of the inner diameter gives rise to a 2 % uncertainty in the cross-sectional area, it is easy to see the importance of the dimensional uncertainties. This is supported by the results shown in Figure 11. Obviously the electronics and spoolpiece with transducers in place can be calibrated in a laboratory, however, when the meter is installed in the field the validity of the calibration must be called into question, especially if the transducers have been removed from the calibrated spoolpiece.

The following conclusions can be drawn from this work:

- Manufacturers specifications in many cases should be more detailed, specifically in relation to pipe dimensions, transducer configurations, calibrated and uncalibrated uncertainties.
- The number and positioning of paths in addition to the manner of processing the individual velocities considerably effects the performance of ultrasonic meters.

- Mid-radius paths are less sensitive than diametrical paths to viscosity dependent changes in velocity profile.
- When specifying either a mid-radius or diametrical beam ultrasonic meter the diameter should be chosen so as to avoid the transition region.
- Clamp-on meters are susceptible to additional sources of uncertainty over wetted meters.
- Transit-time meters should not be utilised if it is expected that free gas could be entrained in the liquid. The velocity as well as the volume fraction should be considered. A useful rule of thumb is that the gas component should be less than 0.5 % by volume.

Ultrasonic flowmeters have been subject to progressive development. Advances in transducer technology, signal processing and high speed electronics have all assisted in the process. It is important that progress continues and this will require a structured programme of development and evaluation both by the manufacturers and on behalf of the end-users. Equally important is that the standards organisations and independent bodies are apprised of developments. Issues such as reliability and installation effects must be addressed and new developments tested. The performance of currently available meters is sufficiently encouraging to suggest that ultrasonic technology will be widely adopted for allocation and eventually fiscal metering duties.

ACKNOWLEDGEMENTS

The work described in this paper was carried out as part of the Flow Programme, under the sponsorship of the DTI's National Measurement System Policy Unit. The author would also like to thank Amerada Hess Ltd, Danfoss Ltd., Krohne Altometer, Krohne Measurement & Control Ltd, Flowline Manufacturing Ltd., Panametrics Ltd., Peek Measurement Ltd., and Ultraflux for their co-operation.

REFERENCES

- [1] HERITAGE, J. E. *The performance of transit time ultrasonic flowmeters under good and disturbed flow conditions* Flow Meas. Instrum., 1(1), pp. 24-30, 1989.
- [2] THOMPSON, E. J. *Mid-radius ultrasonic flow measurement* Flow Measurement of Fluids, Ed. Dijstelbergen, H. H., and Spencer, E.A., North-Holland Publ. Co., pp. 153-161, 1978
- [3] SCELZO, M. and JACOBSON, S. *Transit-time ultrasonic flowmeter with patented signal-coding* Measurements & Control, 28(2), pp. 84-87, 1994
- [4] PANNELL, C. N., EVANS, W. A. B., and JACKSON, D. A. *A new integration technique for flowmeters with chordal paths* Flow Meas. Instrum., 1(4), pp. 216-224, 1990.
- [5] JACKSON, G. A., GIBSON, J. R. and HOLMES, R. *A three path ultrasonic flow meter with fluid velocity profile identification* Meas. Sci. Technol., 2, pp. 635-642, 1991.
- [6] LYNNWORTH, L. C. *Ultrasonic Flowmeters* Physical Acoustics Volume 14, Ed. Mason, W. P., and Thurston, R. N., Academic Press, pp. 488-492, 1979.
- [7] JOHANNESSEN, A. A., *Evaluation of ultrasonic liquid flowmeters* Proc. North Sea Flow Measurement Workshop, 26 -28 October, Bergen, Norway, 1993.
- [8] BRITISH STANDARDS INSTITUTION *Precision of test methods. Part 1: Guide for the determination of repeatability and reproducibility for a standard test method* BS 5497 : Part 1 : 1987.

North Sea Flow Measurement Workshop 1995**DEVELOPMENT OF AN IN-SITU CALIBRATION METHOD FOR MULTIPHASE FLOW METERS USING A RADIOACTIVE TRACER TECHNIQUE**

Torben Sevel, Niels Hald Pedersen, Claus Erik Weinell and Birger Lind-Nielsen
FORCE Institute, Brøndby, Denmark

SUMMARY

A novel technique for in situ calibration of multiphase flow meters is currently being developed at the FORCE Institute.

The method implies injection of a mixture of 3 radioactive tracers each being distributed into one of the 3 phases. From measurements of tracer concentrations by spectral detectors outside the pipe at a downstream position the flows are calculated from the dilution of the injected tracers.

Experiments have been made with tracers in gas, oil and water being present in a static laboratory set-up in various amounts and concentrations. A simulation model for generating supplementary data has been developed and verified. A statistical data treatment method has been applied to estimate tracer concentration from detector measurements with promising results.

The design of a dynamic flow test facility for tracer measurements is presented together with considerations regarding future offshore operation of the calibration method.

1 INTRODUCTION

Multiphase flow meters for measuring mixtures of gas, oil, and water in pipe-lines are rapidly developing and their use in offshore installations increases accordingly. No method has so far been operated for in situ control and calibration of such meters. A development project has been initiated with the aim of providing a method that ultimately can be implemented as a routine calibration method for permanently installed multiphase flowmeters. The method is based on application of radioactive tracers and requires that the phases are separated and arranged according to density difference over the measurement cross section in a horizontal pipe at the measuring point. The method has no inherent limitation of accuracy obtainable, however the target set for initial operations is an uncertainty of $\pm 10\%$ for each phase. The method is intended to be able to control and calibrate both platform and sub sea installed flowmeters.

The development project is supported by a research grant from the Danish Ministry of Energy.

2 FLOW MEASUREMENT BY THE USE OF RADIOACTIVE TRACERS

2.1 The concept of tracer

Tracers are often used for studies of flow in various processes. A tracer is a minute amount of matter similar to the bulk material which is added to a flow system without affecting the bulk flow and the concentration of which is measurable. Obtaining information of the tracer flow by measurements provides information about bulk flow properties as illustrated in figure 2.1.1

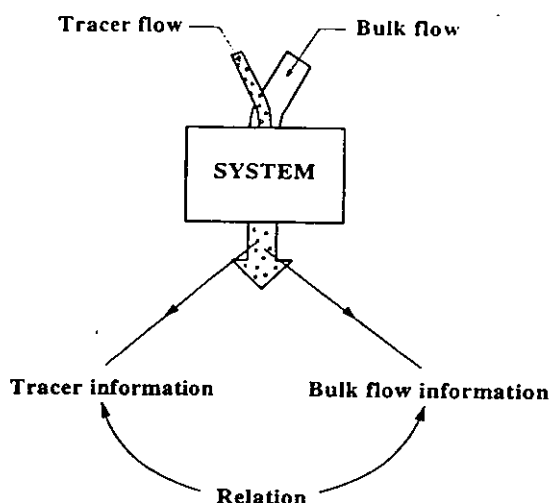


Figure 2.1.1 General principle of tracer methods.

Radioactive tracers show excellent properties as tracers since they are detectable in very low concentrations (i. e. high dilution) and with high specificity. Further γ -emitting radioactive tracers can be measured in situ, through pipe and vessel walls which enables e.g. studies of processes under high pressures, and processes involving a gaseous phase.

2.2 Continuous dilution method for flow measurements

The principle of the continuous dilution method is described in an ISO standard, /1/. The main application of said principle is measurements in open channels and partly filled pipes.

The tracer solution with a concentration of c is injected at a constant rate q into the flow to be measured. At a point downstream, where the tracer is completely mixed with the flow the concentration is measured to c_m . The flow at the injection site Q is thus calculated from a tracer balance (assuming steady state conditions and $q \ll Q$) as

$$(1) \quad Q = q \cdot c / c_m$$

The accuracy obtained by the single phase continuous dilution method is experienced to be $\pm 1\%$ or better, /2/.

2.3 Simultaneous measurement of three phases using three tracers

For the measurement of more than one flowing phase the same principle can be applied using individual tracers for each phase. Said tracers must be in a form that only distributes into one phase and remains there. Further they must show such differences in the emitting γ -radiation energy spectra that they can be simultaneously detected by on line γ -spectrometry. Preferred candidate tracers for gas, oil and water are listed in table 2.1

Table 2.1 Candidate tracers for water/oil/gas flow measurements.

Phase	Isotope	Half-life	γ radiation of interest (MeV)	Chemical form
Water	^{24}Na	15 hrs	1.37, 2.75	Carbonate salt
	^{140}La	40 hrs	0.33 - 2.54	EDTA-complex
Oil	^{82}Br	36 hrs.	0,55, 1.32	Bromobenzene
Gas	^{85}Kr	10.6 years	0.51	Noble gas

The tracers are injected simultaneously at a constant rate into the flow in the pressurised pipe, and the concentration is detected as series of instantaneous measurements taken downstream after complete mixing. The principle is illustrated in figure 2.3.1.

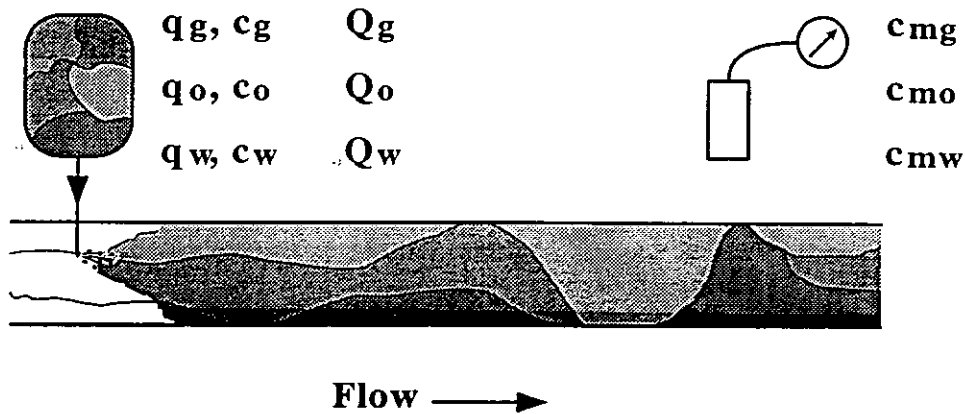


Figure 2.3.1 Principle of 3 phase flow measurements by the continuous dilution tracer method.

The flows at the injection position as functions of time are calculated according to the following equations which are derived correspondingly to equation (1):

$$(2) \quad Q_g(t) = q_g \cdot c_g / c_{mg}(t)$$

$$(3) \quad Q_o(t) = q_o \cdot c_o / c_{mo}(t)$$

$$(4) \quad Q_w(t) = q_w \cdot c_w / c_{mw}(t)$$

The average flow of a given phase is calculated from a number, n , of discrete measurements as:

$$(5) \quad \bar{Q}_p = \sum Q_p(t)/n$$

These basic equations are valid under certain assumptions about the flow, such as limited axial dispersion along the pipe in relation to the variations in flow rate during measurements. We assume that these conditions are fulfilled to a satisfactory degree.

3 DETERMINATION OF TRACER CONCENTRATIONS

In situ measurement of the concentration of radioactive tracers in the different phases requires that the phases are separated and arranged according to density difference over the measurement cross section in a horizontal pipe. At the measuring point the tracer method thus covers stratified flow, wavy flow, and slug flow, whereas bubble flow and annular flow can not be measured. The potential appearance of said flow regimes, however, can be observed from the current measurements.

3.1 Gammasspectrometric measurements with 2 detectors

In general, the measurements are performed with two spectral γ -detectors placed on top and bottom of the pipe respectively. The detectors are high sensitive 6x3" Sodium Iodide scintillation detectors with build-in or external multi channel spectrum analyser.

The measurement set-up is outlined in figure 3.1.1

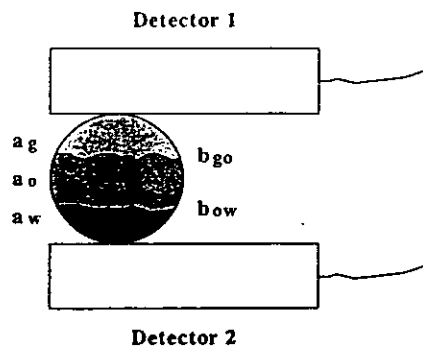


Figure 3.1.1: Detector set-up for tracer measurement in 3 phases.

In the case, where all 3 phases are present, the detector measurements reveal the amounts of tracers in each phase as seen over a unit length of the pipe by the detectors (a_g , a_o , and a_w) and the position of the boundaries between the phases (b_{go} and b_{ow}). The cross section area of each phase is calculated from the latter the inner radius (r) of the pipe using trigonometric formulas. From this the tracer concentrations (c_{mg} , c_{mo} , and c_{mw}) and hence the volume flows of the 3 phases are calculated.

The 3 cases of only two phases being present can be identified from the measurements and similar models for calculation of the concentration have been established. Also the 3 cases of

only one phase being present at a given time (slug flow) can be identified and the concentration calculation from the measurements in these 3 cases is simple.

3.2 Data generation from static laboratory experiments and model simulation

Measurements have been made in a laboratory set-up . The test pipe was made of plexiglass for visual inspection with the dimensions of \varnothing 110 mm x 500 mm. Steel plates were inserted between the pipe and the detectors to simulate the steel walls of real pipe. The test pipe could be filled with the 3 phases in any combination of amounts and tracer concentrations. The measurement program with the top and bottom detectors comprises a total of 24 combinations of the 5 key parameters a_g , a_o , a_w , b_{go} , and b_{ow} .

The variability in combinations of the key parameters is very large and the relations between the spectral radiation measurements with the top and bottom detectors and the 5 parameters is by no means simple. An optimal parameter estimation obviously calls for the use of advanced statistical data treatment which in turn requires a considerable amount of data. In order to generate the necessary amount of data modelling was used for simulating detector responses from a given physical geometry.

The model is a Monte Carlo Gamma Simulation model. In a specified, spatial arrangement of detectors, matter of a given density and composition and isotope sources, the MGS model computes the spectral response of said detectors. The MGS model was proven in various contexts including validation on data from the measuring program described above.

Figure 3.2.1 shows a simulation result for ^{82}Br in oil. The identity is sufficient for the purpose at present, but the MGS model is currently being improved.

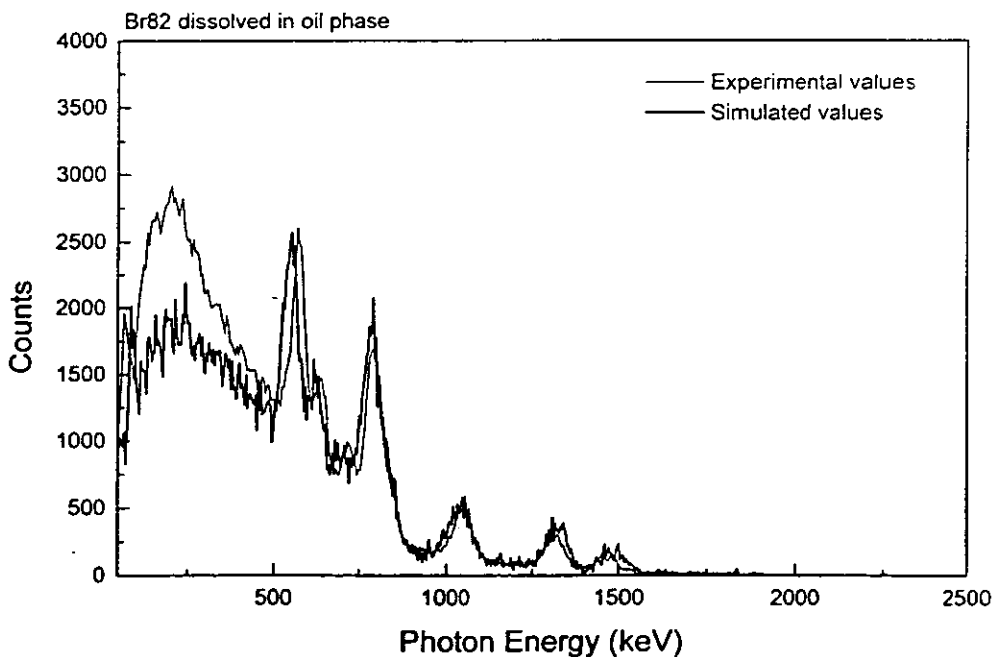


Figure 3.2.1 Measured and simulated γ -spectrum for ^{82}Br in oil.

3.3 Data transformation

Each measurement consists of two 1024 channel γ spectra (D_1 and D_2). The spectrum of ^{24}Na (water), ^{82}Br (oil), and ^{85}Kr (gas) is shown on the same diagram in figure 3.3.1., where the typical peaks of the different isotopes are seen. The measured spectra from the 3 tracers together will be a superimposition of such spectra upon each other with the relative intensity of contribution from each isotope depending on the amount of said isotope. Further the response depend on the distance from the isotope to the detector. The top detector will thus get relatively more response from the gas tracer than the bottom one, and vice versa for the water tracer.

To handle the estimation of the 5 key parameters it is necessary to use *data reduction operations* and to determine the optimal *transfer function* between input data and output parameters.

First D_1 and D_2 are reduced into a number (15) of properly selected windows giving the detector responses ($v_{11}, v_{12}, \dots, v_{1i}, \dots, v_{115}$) and ($v_{21}, v_{22}, \dots, v_{2i}, \dots, v_{215}$). The selection of windows is shown on figure 3.3.1.

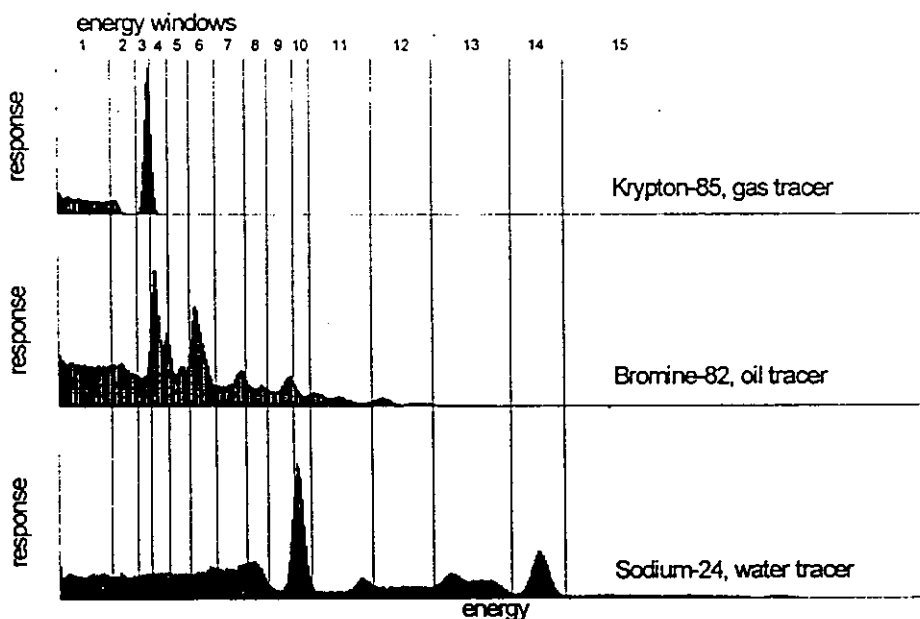


Figure 3.3.1: Spectra of isotope tracers and selection of observation windows.

The data are transformed into the data sets $s_i = v_{1i} + v_{2i}$ which is related to the amount of tracer and $r_i = \ln(v_{1i}/v_{2i})$ which relates to the tracer location.

For the given set-up of pipe and detectors a transfer function is determined for statistically optimal estimation of the 5 key parameter from the reduced data sets. The mathematical/statistical analysis is based on orthogonalisation of window response variance.

Measured data from the static test set-up and data generated by MGS simulation hereof are used for trial calculations. The presented data reduction operations and the determined data

transfer function on these data have shown that it is feasible to determine the 5 key parameters a_g , a_o , a_w , b_{go} and b_{ow} from measurements with γ -spectrometric detector on top and bottom of the flow media pipe.

The accuracy of the estimation method is illustrated in figure 3.3.2. This shows the error distribution for each parameter, the size of which has been normalised to 1.0. It also gives the relative standard deviations for the parameter estimates. It is seen that the best estimate is of the parameter a_w , representing the water tracer, whereas the gas/oil boundary, b_{go} is the most difficult to estimate.

Estimator error distribution for the five key parameters

gas tracer amount	oil tracer amount	water tracer amount	gas-oil boundary pos.	oil-water boundary
1.8 % RSD	1.6 % RSD	1.3 % RSD	5.9 % RSD	1.8 % RSD
largest error : 8.5 % (fs)	largest error : 6.7 % (fs)	largest error : 6.6 % (fs)	largest error : 32.5 % (fs)	largest error : 10.8 % (fs)

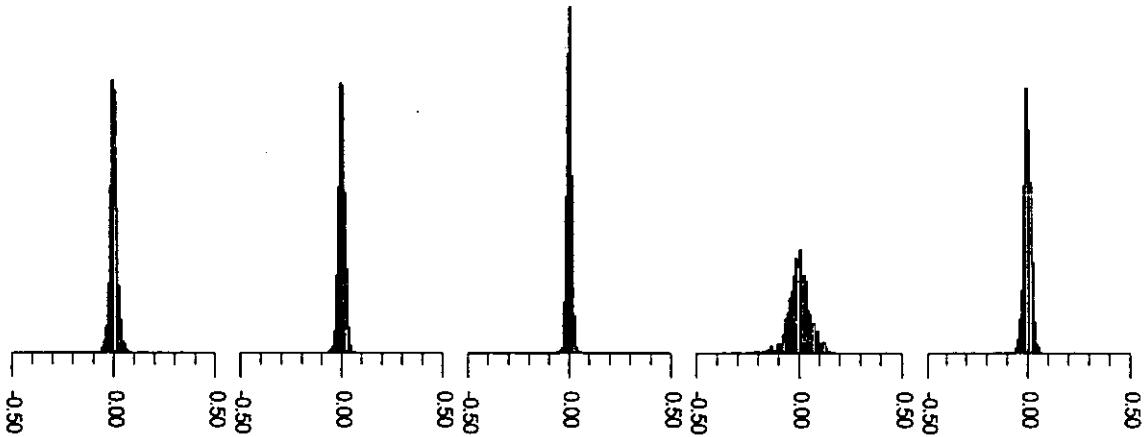


Figure 3.3.2: Error distribution and relative standard deviation for parameter estimates

Even though the estimation method may be refined these results clearly demonstrate that it is possible to determine the key parameter for flow calculation with promising accuracy by the methods proposed.

4 DESIGN OF A DYNAMIC FLOW TEST FACILITY FOR TRACER MEASUREMENTS

After having proved the principles of using 3 tracers for 3 components in a static test rig, a dynamic test facility has been designed. In this facility it will be possible to inject 3 tracers in a flowing liquid consisting of air, oil and water. By changing the relative amounts of the different components it will be possible to explore the phase diagram and assess the limits for the measurement principle. A sketch of the facility is shown in figure 4.1.

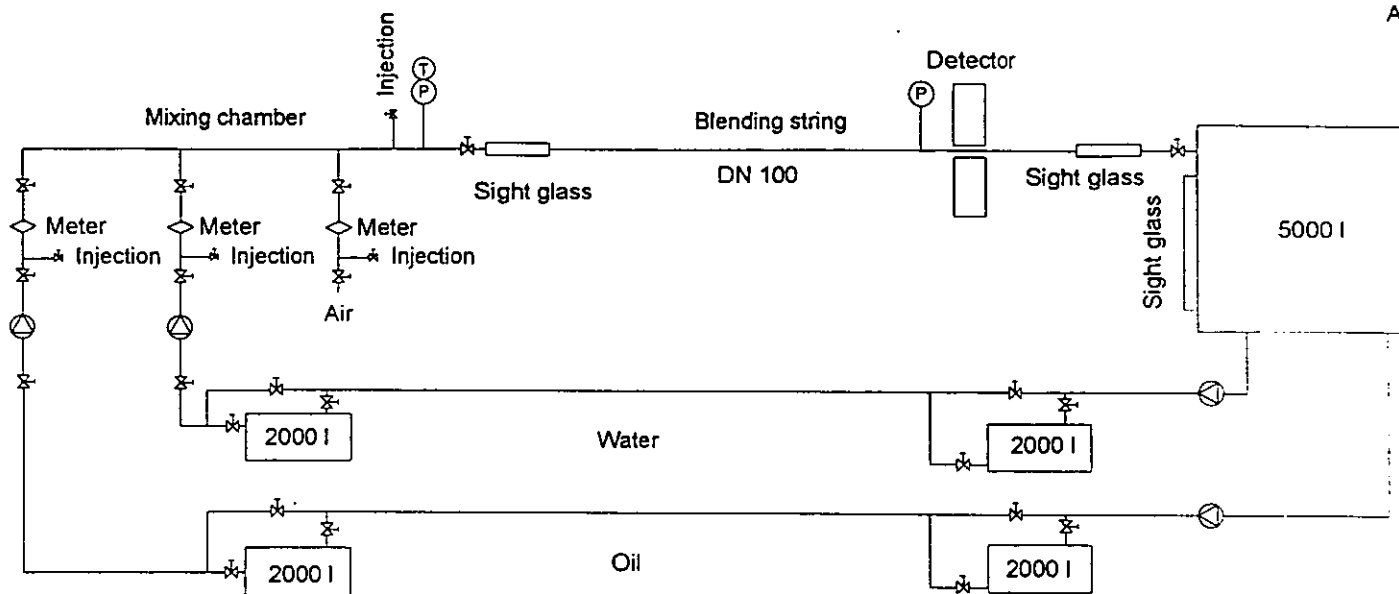


Figure 4.1: Dynamic test facility for 3 phase flow

The facility consists of five tanks, two each for oil and water and one tank for separation. For each liquid there is one tank for fresh fluid, and one tank for used fluid. In the last tanks, the tracer activity will decrease to insignificant level, i.e. a level which will not disturb the measurement, when the liquid is used again. The flow through the measurement string is controlled by variable frequency pumps. The air is supplied by a compressor. The test rig is prepared for recirculating flow, which can be used when we have gained experience with the test facility and with the measurement principle.

The tracers are injected after the mixing chamber, but it will possible to inject tracers in individual components. The detector is placed at the end of the blending string.

The flow rates of the individual components is measured by meters, which have been calibrated at the institutes laboratories.

5 IN-SITU MEASUREMENT SCENARIO

When validated in the dynamic test set-up the method should be implemented for in situ use.

Most of the required measurement equipment is already available as a result of the present project. Equipment for injection of tracers into pressurised pipes is constructed based on experience with existing equipment for injection of liquid and gas respectively.

The initial step in a calibration operation will be to examine the possibilities for *injection* and *detection* of tracers. An outline of the desired set-up is shown in figure 5.1.

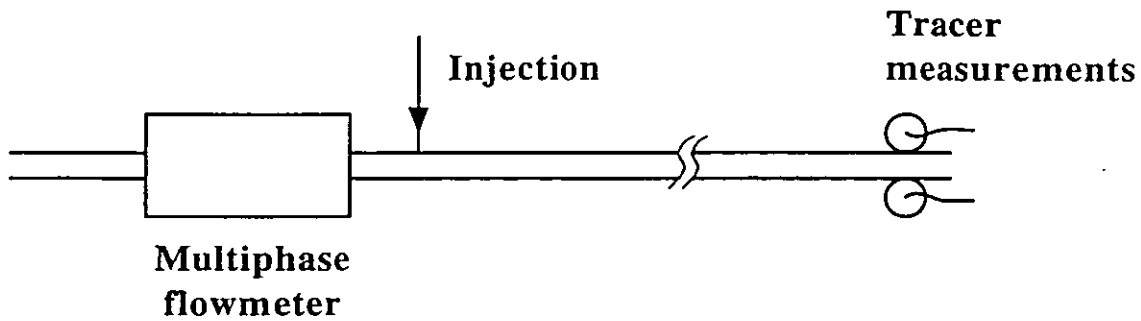


Figure 5.1: Set-up for in situ control and calibration

Since the method gives the flow at the injection position the injection should preferably be close to the multiphase flow meter to be calibrated. The use of radioactive tracers will disturb such multiphase flow meters using any nucleonic gauges, so injection downstream is preferred, but intermittent injection and meter reading is an alternative. It seems most feasible to inject from a platform being manned during the injection. In cases where the multiphase flowmeter is a sub sea device injection could be performed by the use of some form of ROV technology, possibly supplied with tracer through flexible pipes from a platform or a vessel.

The required distance to obtain sufficient mixing and to assure only minor gradients in the tracer concentration along the length of the pipe depends on the actual flow regimes in the pipe from the injection point downstream to the measuring point. When intensive mixing occurs the distance may be small, but if flow with long lasting slugs is dominant the optimal distance may be several kilometres.

At the detection position the flow should be in a horizontal pipe and in a flow regime where the phases are arranged according to their densities as mentioned earlier. Measurements should be performed on a platform or vessel providing power supply etc.

In order to utilise detector data as tracer concentrations for flow measurements it is necessary to establish the optimal data transfer function for each individual detector installation. The MGS model is run with actual pipe dimensions and materials and detector positions for generation of sufficient amount of measurement data from which the data transfer function is determined.

When the practical tasks are solved in accordance with considerations stated the method will be operational.

6 CONCLUSION

It has been showed by experiments in a static laboratory set-up and using model simulation and statistical parameter estimation, that it is possible to measure tracer concentrations in a 3 phase gas, oil, water system where the phases are arranged according to their densities with promising accuracies.

The experimental and computational tools developed have provided valuable experience for the design of a dynamic test rig and for the conduction experiments herein.

7 REFERENCES

- /1/ International Standard ISO555/3. Liquid flow measurements in open channels - Dilution methods for measurement of steady flow - Part 3: Constant rate injection method and integration method using radioactive tracers. 1982. 08.9
- /2/ IAEA, Guidebook on Radioisotope Tracers in Industry, Technical Report Series No. 316, Vienna ,1990

An Oil/Water/Gas Composition Meter based on Multiple Energy Gamma Ray Absorption (MEGRA) Measurement

A.M. Scheers, Shell International E & P - Research and Technical Services, Rijswijk

W. Letton, Daniel Industries, Inc, Houston

ABSTRACT

A class of multiphase flowmeters uses the principle of Dual Energy Gamma Ray Absorption (DEGRA) composition measurement to determine the individual water, oil and gas fractions. Under homogenous flow conditions the ultimate uncertainty in phase fractions achievable with this technique depends strongly on the choice of component hardware. The meter presented in this paper uses unique components optimised for water, oil and gas fraction measurement, yielding theoretical uncertainties of 2% in the fractions over a 1 second measurement period. Generally composition meters are sensitive to changes in production water salinity, causing significant systematic errors in the fraction and watercut measurements. A new measurement concept based on Multiple Energy Gamma Ray Absorption (MEGRA) which is insensitive to salinity variations is introduced. A multiphase flowmeter which employs the MEGRA concept does not require field calibration, a decisive advantage in subsea or marginal field developments.

1. INTRODUCTION

A multiphase flowmeter is a device, or a combination of devices, to measure the individual flow rates of water, oil and gas in a multiphase flow environment. The ultimate aim for multiphase flow meter technology is to replace the measurement function of the large, expensive, maintenance-intensive test separator. Multiphase metering should be considered as a means of providing measurements where conventional test separators would be either impractical or economically unattractive. The various measurement concepts used in multiphase meters have their specific areas of application; considerations such as flow rate, Gas Volume Fractions (GVF), watercut, flow regime and the uncertainties achievable under all prevailing conditions must be carefully considered (Ref. 1). In addition, operational aspects (e.g., calibration, use of radioactive sources, ease of installation) and costs (both capital and operating expenditures) should be given careful thought.

Most multiphase flowmeters consist of a total fluid (water, oil and gas) flow rate measurement combined with a composition measurement (Fig. 1). In homogeneous flow, these two measurements can be directly integrated resulting in individual water, oil and gas flow rates. In non-homogeneous flow, one needs either an advanced flow model, or some form of conditioning devices, such as a mixer or compact (in-line) separator upstream of the multiphase flowmeter.

Various types of multiphase composition meters are currently being developed. Most are based on either the measurement of electrical impedance or on gamma ray absorption. Use of gamma ray absorption has the advantage that it is able to cope with any oil-water ratio, in contrast to the impedance measurement. Also the non-intrusiveness of the method is an advantage.

2. COMPOSITION MEASUREMENT BASED ON DEGRA

As a further introduction, the basics of the Dual Energy Gamma Ray Absorption (DEGRA) measurement are explained here. The principle is based on the absorption of a narrow beam of γ - or X-rays of energies e_1 and e_2 . In a pipe, with inner diameter d , containing a water, oil and gas mixture with fractions α_w , α_o , α_g , the measured count rate $I_m(e)$ is :

$$I_m(e) = I_v(e) \cdot \exp\left[-\sum_{i=1}^3 \alpha_i \cdot \mu_i(e) \cdot d\right] \dots\dots\dots (1)$$

$I_v(e)$ is the count rate when the pipe is evacuated and μ_i represents the linear absorption coefficients for the water, oil and gas phases. For two energy levels, e_1 and e_2 , provided the linear absorption coefficients between water, oil and gas are sufficiently different, two independent equations are obtained. A third equation comes from the fact that the sum of the three fractions in a closed conduit should equal 1. A full set of linear equations is given below. R_w , R_o , R_g and R_m now represents the logarithm of the count rates for water, oil, gas and the mixture, respectively, at energies e_1 and e_2 .

The elements in the matrix are determined in a calibration process by filling the instrument with 100% water, 100% oil and 100% gas (air). Together with the measured count rates at the two energy levels from a multiphase mixture it is then possible to calculate the unknown phase fractions (Fig. 2).

$$\begin{bmatrix} R_w(e_1) & R_o(e_1) & R_g(e_1) \\ R_w(e_2) & R_o(e_2) & R_g(e_2) \\ 1 & 1 & 1 \end{bmatrix} \begin{bmatrix} \alpha_w \\ \alpha_o \\ \alpha_g \end{bmatrix} = \begin{bmatrix} R_m(e_1) \\ R_m(e_2) \\ 1 \end{bmatrix} \dots\dots\dots (2)$$

In Fig. 3 the above is graphically presented with the logarithm of the count rates of the two energy levels plotted along the axis. The corners of the triangle are the water, oil and gas calibrations, and any point inside this triangle represents a particular composition of water, oil and gas. Combining the composition measurement with a conventional venturi measurement (Fig. 4) results in a complete three phase flow measurement for homogeneous flow regimes.

3. HARDWARE SELECTION AND DESIGN

Three important considerations must be addressed in the selection of hardware. These are the available energy levels (i.e. selection of radioactive source), the detection system (e.g. scintillation counters, solid state detectors, etc.), and a suitable pressure barrier (window) material.

3.1. Energy selection

The emission and absorption of γ - and X-rays are statistical processes, described by a Poisson distribution, therefore the measured count rate has an inherent uncertainty. For single energy γ - or X-ray absorption techniques, the following criterion is generally accepted (see Ref. 2).

$$\mu \cdot d = \left(\frac{\mu}{\rho}\right) \cdot \rho \cdot d = 2 \dots\dots\dots (3)$$

Here μ is the linear absorption coefficient and $[\mu/\rho]$ is the mass absorption coefficient. Note that μ is temperature and pressure dependent, while $[\mu/\rho]$ is independent of both. For a dual energy γ - and X-ray absorption technique the criteria for the selection of the two energies and their relative intensities have also been developed. In Ref. 3 it is demonstrated that the selection of the low energy level has a large influence on the uncertainty of the phase fraction measurement. Similar to Eq. 3, the uncertainty depends on the fluid parameters and pipe diameter. For a water, oil and gas system, the low energy level should preferably be in the range of 10-30 keV. The selection of the high energy level is not so critical, provided it is higher than 40-50 keV. Based on the above, Americium-241 (Am-241) with emissions at 13.9, 17.8, 21.5, 26.3, and 59.5 keV is a suitable source. These energy selection criteria will not be much different for the MEGRA measurement, to be introduced below.

The main disadvantages of Am-241 is that it is an alpha radiator, and has a relatively long half-life. Alternatives to Am-241 are being considered. In Fig. 5, an example of an Am-241 spectrum measured with a Si solid state detector is presented.

3.2. Window material

Applying low-energy gamma rays in this manner calls for strong, radiation-transparent wall material. Metal pipes are not suitable. Carbon fibers are known to be extremely strong and are transparent to low-energy gamma rays. Held in place by an epoxy matrix, Carbon Fiber Reinforced Epoxy (CFRE) is thus an attractive window material. With an effective tensile strength of approximately 1800 to 2000 MPa, it is 4 to 5 times stronger than steel. A CFRE cylinder with an internal diameter of 44 mm and a wall thickness of 2 mm was placed in a steel housing for pressure testing. The steel housing also contained two holes (15 mm diameter) required for gamma ray transmission. This combination was pressure tested successfully up to 120 MPa (1200 bar). In the prototype composition meters, CFRE has been used as window material.

3.3. Detector selection

Two important characteristics were considered in the detector selection process :

3.3.1. Resolution

The resolution of semiconductor diodes used as solid state gamma ray detectors is much better than that of the more commonly used sodium iodide (NaI) scintillation detectors or of gas filled detectors. As an example, for a Silicon (Si) solid state detector which operates at a temperature of around 5 °C, the resolution can be on the order of 1.5-2 keV for the low energy region (14-26 keV). Detector resolution also depends on the detector area, i.e. a small area detector has a better resolution than a large area detector. Considering the Am-241 energy spectrum, with the 4 energy peaks in the 14-26 keV region and the relatively large difference in μ in that region, a high resolution detector is required for adequate peak separation. For the fully separated energy level of 59.5 keV, the resolution is less critical.

3.3.2. Efficiency

The efficiency of NaI scintillation crystals, almost 100% for the lower gamma energy levels, is significantly better than that of Si solid state detectors, since in the latter, interactions between the photons and the detector take place in the very thin barrier (300 μm - 1 mm) between the n- and the p-regions of the semiconductor. As an example, for a Si detector the efficiency is approximately 40% for the 18 keV energy level and on the order of only a few percent at 59.5 keV. In particular for the 59.5 keV peak, larger area detectors are needed to compensate for the poor efficiency and to obtain sufficiently high count rates.

3.4. Dual area solid state detector

The above considerations on resolution and efficiency resulted in the design of a "dual-area" solid state detector, consisting of one 14 mm² and one 100 mm² detector combined on a single chip. The small area detector, having a resolution of 1.7 keV, is used for the low gamma energy levels (14-26 keV). The large area detector, having a resolution of approximately 5 keV, is used for the higher gamma energy level (59.5 keV). These resolutions are for a detector temperature of 5 °C, which is achieved by means of a Peltier cooling element directly attached to the detector. The total power consumption required to achieve this temperature, with an ambient temperature of 40 °C and fluid temperature of 60 °C, is approximately 1 watt.

The gas spectra of the two detectors with the relevant count rates for the five energy levels of Am-241 are presented in Fig. 6. A drawback of the 100 mm² high-energy detector is that it contains a significant number of irrelevant low-energy counts. This has a negative impact on the "deadtime" of the counting electronics. By using a 100 μm -thick copper foil as a filter, this low energy radiation is almost completely absorbed with a only small effect on the 59.5 keV count rate. Fig. 7 presents a sketch of the combined 14/100 mm² detector, including the 100 μm thick copper filter and the Peltier cooling element. Fig. 8 shows the gas spectra of the 14 and 100 mm² detectors with the copper filter; the relevant count rates for the 5 energy levels are also presented. Thus, a solid state detector with both sufficient resolution for the low energies and sufficient efficiency for the high energy has been obtained.

3.5. Accuracy considerations

The uncertainty in the calculation of phase fractions is due to the statistical behaviour of the radioactive decay. It can be demonstrated that the absolute uncertainty in the oil fraction, when compared with those of water and gas, is always largest (Ref. 3). It is also obvious that the maximum absolute uncertainty in oil fraction occurs with the lowest count rate, e.g. with 100% water. In Fig. 9 this maximum absolute uncertainty in oil fraction is indicated as a function of the salinity and the fluid path over which the absorption takes place. The graph is

valid for a specific configuration, i.e. a 6,475 MBq (175 mCi) Am-241 source, the 14/100 mm² dual-area Si solid state detector of 300 µm thickness, 2 mm CFRE wall thickness and a relatively short counting time of only 1 second.

The fraction uncertainty is large for a small fluid path length, as there is insufficient contrast in the absorption between the oil and the water phases, but decreases as the fluid path is extended. However, beyond a certain fluid path the uncertainty again increases because increased absorption results in count rates which are too low. The salinity also has an effect on the optimum fluid path, since with increasing salinity the optimum fluid path is reduced. For a fluid path of 15-20 mm the uncertainty in the phase fractions is not greatly influenced by salinity, hence accurate fraction measurements can be made over the full range of 0-300 kg/m³ salt (NaCl) concentration.

3.6. Concentric Venturi

The DEGRA composition meter can be used as stand-alone device only or can be integrated with any total fluid meter (e.g. a venturi plus differential pressure device) to make up a full multiphase flowmeter. With a venturi applied to homogeneous flow, the total fluid volume flow rate (Q_{tot}) can be calculated if the differential pressure (Δp) over the venturi and density of the multiphase fluid mixture (ρ_m) are known.

$$Q_{tot} = C \cdot \sqrt{\frac{\Delta p}{\rho_m}} \dots\dots\dots (4)$$

C is a geometrical constant multiplied by the discharge coefficient. Using the measured phase fractions α_w , α_o , and α_g , the base densities ρ_w , ρ_o , and ρ_g , and the measured temperature and pressure, one can calculate the actual density of the multiphase fluid mixture, ρ_m . Subsequently, the actual total fluid volume flow rate can be calculated, and with α_w , α_o , and α_g the individual water, oil and gas actual volume flow rates can be determined.

For flow rates on the order of 100 to several 1000 m³/day, a venturi throat diameter (fluid path length) of 15-20 mm is highly impractical because of the large pressure drop. However, with the introduction of a concentric venturi it is possible to achieve a fluid absorption path length of 15-20 mm and at the same time almost any desired cross sectional area for the fluid flow. In Fig. 10 a schematic drawing of a concentric configuration for very high salinity concentration (saturated brine with a concentration of 300 kg/m³) is presented. The conical body in the centre of the pipe contains the radiation source. The effective cross sectional area of the concentric throat, with inner and outer diameters of 30 and 58 mm respectively, is equivalent to that of a normal venturi with a throat diameter of 50 mm.

3.7. Influence of fluid parameters

The 100% water reference count rates for the lower energies required in the DEGRA calibration are strongly dependent on the salinity of the production water, since salt has a high absorption coefficient compared to water. Systematic errors in the measured water, oil and gas fractions will occur if the salinity of the production water changes and the 100% water reference count rate is not corrected. In many potential multiphase metering applications, the salinity of the production water will indeed vary in time, and could be different for each well drilled in the same reservoir. In water injection reservoirs, for example, the salinity will vary between that of formation water and that of injection water. In Fig. 11 the production water salinity for the wells of a North Sea reservoir are shown as measured in January and June 1993. It not only shows that salinity is different for each well in the same reservoir, but also that in a 6 month period the salinity for some wells has changed by more than 10 kg/m³. Also horizontal and/or vertical gradients in formation water salinity across the reservoir may occur. Ref. 4 presents an example where such gradients can lead to salinity variations much larger than 10 kg/m³. In Fig. 12 the relative change in watercut ($\Delta \text{watercut}/\text{watercut}$) is indicated for a change in salinity of 10 kg/m³ from the calibration salinity. In this example, at a 50 kg/m³ salinity and a salinity change of 10 kg/m³ results in a ($\Delta \text{watercut}/\text{watercut}$) of 8%. At a watercut level of 50% this equals a 4% absolute error in watercut and an 8% relative error in net-oil production.

The curve in Fig. 12 is almost independent of the energy levels used. Multiphase meters using a Barium-133 source (30 and 360 keV) or a combination of Am-241 and Cesium-137 sources (60 keV and 660 keV) will suffer from the same errors in watercut due to a change in salinity. It should be noted that the problem of

salinity changes is not unique to the gamma ray absorption technique. Conductivity measurement techniques, often used in situations of water external emulsions, are also influenced by salinity changes (Ref. 5).

4. COMPOSITION MEASUREMENT BASED ON TEGRA

When two energy levels are used it is possible to calculate the three phase fractions in a mixture. When three energy levels are applied (TEGRA, or Triple Energy Gamma Ray Absorption), it is possible to calculate one additional parameter; in the case presented here, the parameter of interest is salinity. In the measured water, oil and gas calibration spectra (Fig. 5), it can be seen that 13.9, 21.5 and 26.3 keV energy levels are also available. The 26.3 keV level was chosen for the calculation.

4.1. Exact solution of TEGRA

It will be shown that the new set of equations is very sensitive to small measurement errors or to the statistical uncertainty in the measured count rates. The 4x4 matrix, similar to the 3x3 matrix of Eq. 2, is very poorly conditioned and small variations in the measured count rates will lead to large fluctuations in estimates of phase fractions and salinity. In a computer simulation, with $\alpha_w = \alpha_o = 0.15$, $\alpha_g = 0.70$, $S = 100 \text{ kg/m}^3$ and applying the Poisson-type of statistical fluctuations, the exact solution of the set of equations for each measurement shows enormous fluctuations in the calculated α_w , α_o , α_g and S . In Fig. 13 it is shown that the calculated fractions are even outside the region of 0 to 1, and salinity estimates vary from -600 to +600 kg/m^3 . Hence, solving the equations for each measurement (one calculation per second) will not result in an acceptable composition measurement.

4.2. Constant salinity approach

As indicated above, salinity typically changes either on a time scale of months (gradual change from formation water to injected water) or perhaps on a time scales of days (sudden injection water breakthrough). In the time span of a few hours the salinity can be assumed constant; an improved calculation scheme based on this assumption has been developed. After imposing this constraint to the algorithms, it is no longer possible to solve the set of 4 equations exactly, but instead a solution can be found which is optimal in a chi-square minimisation sense. The outcome of this minimisation process is a set of individual phase fractions for each measurement, and one salinity figure for all measurements. The previous simulation was repeated with this new algorithm and the results are presented in Fig. 14. The calculated phase fractions demonstrate acceptable variations, and the calculated salinity equals the input value.

The chi-square minimisation algorithm is not limited to 3 energy levels. When more energy levels are added to the algorithm, e.g., 13.9 and 21.5 keV, the minimum acquisition time is reduced and the accuracy of the composition measurement is further improved. Hence, a composition measurement based on Multiple Energy Gamma Ray Absorption (MEGRA) has been created.

4.3. Salt composition changes

The TEGRA or MEGRA algorithms cannot distinguish between salinity changes or salt composition changes. Heavier salt components, e.g. potassium or calcium based salts, have higher absorption coefficients than the more commonly occurring NaCl. However, a sensitivity analysis showed that salt composition changes affect only the calculated salinity, and that the errors in the calculated phase fractions are negligible - less than 1% absolute error in phase fraction for a worst case of 100% water with a salinity concentration of 100 kg/m^3 .

5. CALIBRATION FREE OPERATION USING MEGRA

The entire purpose of the DEGRA calibration is to determine the matrix elements of Eq. 2, i.e. to measure the reference count rates of (saline) water, oil and gas at two gamma energy levels. With TEGRA it is possible to measure the salinity concentration in-situ. The absorption coefficients of fresh water are well known (Ref. 6) so it is possible to calculate the reference saline water count rate from the empty-pipe count rate. A similar procedure can be followed for the oil reference count rates, for which the density and composition of the oil needs to be known. A sensitivity analysis shows that the errors in phase fractions resulting from density and composition changes are small. For example, a relatively large change of 10 kg/m^3 in oil density results in a maximum absolute error of approximately 1% in any phase fraction. Hence, all the reference rates can be

calculated from the empty-pipe count rates, assumed oil composition and density, and tabulated absorption coefficients. The measured spectra, the empty-pipe spectrum, and the mixture spectrum are each a linear combination of the peaks occurring in Am-241, fluorescence peaks for materials in the vicinity of the detector, sum peaks, Compton scattering and build-up contributions.

This approach of calibration free operation (Fig. 15) has been verified with a prototype meter, which was evaluated in the Shell test loop and subsequently transported to an oil field. In Fig. 16, the phase fractions from the meter as measured for a particular well are presented. These fractions have been calculated with on-site calibration, i.e. the DEGRA concept and filling the meter first with saline production water and then with oil. The average watercut in the period between 1600-4000 seconds was measured to be 78%.

All the measured spectra over the above period were then re-processed, but this time the MEGRA algorithm, the empty-pipe count rate from the earlier testloop evaluation, and the tabulated, known, absorption coefficients were used. The resulting phase fractions are presented in Fig. 17 and the average watercut estimate over the same period used above was 76%. It is concluded that calibration free composition is practically possible if correction of the various distorting effects on the measured spectra is under control.

6. AREAS OF APPLICATION

A composition meter which uses MEGRA without flow models is only applicable to homogeneous flows, i.e. when (1) there is no velocity difference between the individual phases, (2) the individual phases are homogeneous, and (3) there are no variations in composition during a measurement period (for the MEGRA, within the 1 second measurement time). Equation 2 contains the mean logarithm of the count rate, but the actual measurement gives the logarithm of the mean count rate; these two are not equal in the case of non-homogenous or varying compositions. In Fig. 18 a worst case situation of this phenomenon is schematically presented. Theoretically it can be demonstrated that in such a situation, or in any slug flow regime, the composition measurement always yields an under-reading of the watercut. This was further demonstrated in a testloop evaluation in which mixing intensity could be controlled (Fig. 19). The higher the mixing intensity, the better was the watercut measurement.

An overview of the various MEGRA applications in a multiphase flow measurement and classified by Gas Volume Fraction (GVF) is treated here.

6.1. Gassy liquid streams

Gas might be present in drainlines of separators because of excessive pressure loss causing gas breakout in the drainline or insufficient gas/liquid separation. Both phenomena result in fairly homogeneous "gassy liquid" streams (low GVF multiphase flows). Fig. 20 is an example which presents the watercut reading of a prototype MEGRA. The GVF of the mixture during these measurements was between 0 and 30%. This prototype MEGRA is currently undergoing a field evaluation on an offshore platform in the South China Sea.

6.2. Moderate Gas Volume Fraction streams

Naturally occurring flow streams with GVFs between 20% and 80% are ordinarily not homogeneous. Mixing of the multiphase flow is required upstream of the MEGRA to eliminate the velocity slip and reduce the variations in composition. This approach is already commercially available (Ref. 7-8).

6.3. High Gas Volume Fraction streams

At very high GVFs, i.e. GVFs higher than approximately 80%, it is difficult to achieve a slip-free and homogeneous mixture. Here the liquid and gas might be roughly separated using a small and simple separator followed by a measurement of the "gassy liquid" and "wet-gas" streams (Fig. 21). The "gassy liquid" stream can be measured with a MEGRA/venturi combination. This approach has been tested in the field recently; the well test package is commercially available.

7. FURTHER DEVELOPMENT OF MEGRA

In May of 1995 Shell awarded an exclusive License to Daniel Industries, Inc. to commercialize the MEGRA technology world-wide. As an initial step in the development of this product, Daniel designed and built several

prototype meters, the first of which was the unit currently located in the South China Sea and referenced above. This unit is also the one which produced the results shown in Fig. 20 from measurements made in the Shell multiphase flow loop.

In May of 1996, Daniel Industries, Inc. and Framo Engineering AS announced an agreement to cooperate as partners in the development, manufacture, and marketing of multiphase flow meters world-wide. Thus, once the MEGRA concept is proved through the deployment of prototype meters in various regions of the World, it will be integrated as the composition measurement of choice in the Daniel-Framo line of multiphase meters.

8. CONCLUSIONS

Accuracy considerations showed that the lower gamma energy levels of a composition meter based on DEGRA (TEGRA or MEGRA) should be in the range of 10-30 keV, and that the high energy level is not so critical provided it is above 40-50 keV. Am-241 proved to be a very attractive source from a measurement point of view.

The introduction of a unique dual-area solid state detector, with a small area detector providing good resolution for the various low energy levels (14-26 keV), and a large area detector with reduced resolution for the isolated high energy level (59.5 keV) of Am-241, is ideal for the MEGRA concept.

A sensitivity analysis for a combination of Am-241 and the dual-area solid state detector showed that with a fluid path length of 20 mm, the uncertainty of the measurement becomes almost independent of the salinity. Uncertainty in phase fractions are of the order of 2% if counting periods of 1 second are applied.

With a concentric configuration, having the Am-241 source in the centre of the pipe, the optimum 20 mm fluid path length can be selected without serious restriction in the fluid flow throughput.

Salinity changes, more than density and molecular composition changes, have a significant impact on the calculated phase fraction and watercut. With the introduction of a third energy level and an advanced calculation method, it is possible to calculate phase fractions and production water salinity with acceptable accuracy.

Calibration free composition measurement, which does not require field calibration with reference fluids, is feasible. For this only spectra for an empty-pipe, fresh water, and a "well defined" oil need be measured, and these only once. A subsequent analysis of the various background contributions will then result in instrument constants. All this can be done in the factory, and once installed in the field only a rough estimate of the salt composition and of the densities and molecular compositions of the oil and gas are required.

References

1. Wolff, C.J.M., "Required operating envelope of multi-phase flowmeters for oil well production measurement", presented at the North Sea Metering Workshop, Bergen, 26 Oct. 1993.
2. Garder, R.P. and Ely, L.E.; Radioisotope Measurement Applications in Engineering; pp. 282; Reinhold Publishing Corporation; New York (1967)
3. Santen, H. van, Kolar, Z.I. and Scheers, A.M.; "Photon energy selection for dual energy gamma and/or X-ray absorption composition measurements in oil, water and gas mixtures"; Nucl. Geophys Vol. 9, No. 3, pp 193-202 (1995)
4. McCoy, D.D., Warner H.R. and Fisher, T.E.; "Water salinity variations in the Ivishak and Sag River Reservoirs, Prudhoe Bay Field"; SPE 28577 (1984)
5. Slijkerman, W.F.J., Jamieson, A.W., Priddy, W.J., Okland, O. and Moestue, H.; "Oil companies needs in multiphase flow metering"; North Sea Flow Measurement Workshop; Lillehammer, Norway (23-26 October 1995)
6. Hubbell, J.H., "Photon cross sections, attenuation coefficients and energy absorption coefficients from 10 keV to 100 GeV", NSRDS-NBS 29, National Bureau of Standards (August 1969)
7. Torkildsen, B.H. and Olsen, A.B.; "Framo multiphase flowmeter prototype test"; Proceedings of the North Sea Flow Measurement Workshop; Glasgow (27-29 October 1992)
8. Olsen, A.B., Torkildsen, B.H.; "Framo subsea multiphase flowmeter"; Multiphase flowmeters and their subsea applications; London (14 April 1993)

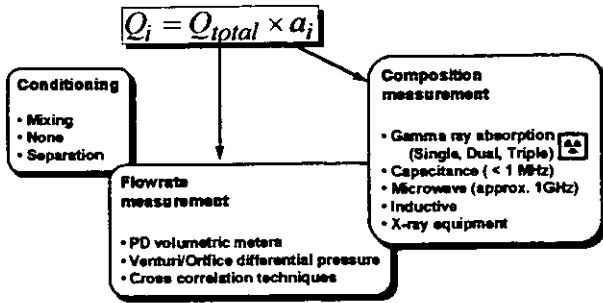


Fig. 1 - Building blocks of a multiphase flowmetering system. At higher Gas Volume Fractions, conditioning devices are required to reduce velocity slip between the gas/liquid phase or to remove the bulk of the gas. Alternatively advanced flow models might be used.

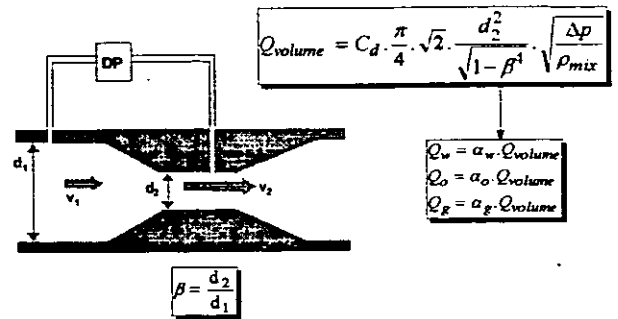


Fig. 4 - Venturi application in multiphase flow measurement. Density ρ_{mix} and the fractions α_i are measured with the gamma ray absorption technique.

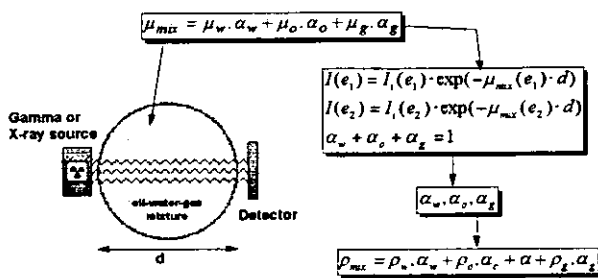


Fig. 2 - Principle of the Dual Energy Gamma Ray Absorption (DEGRA) technique.

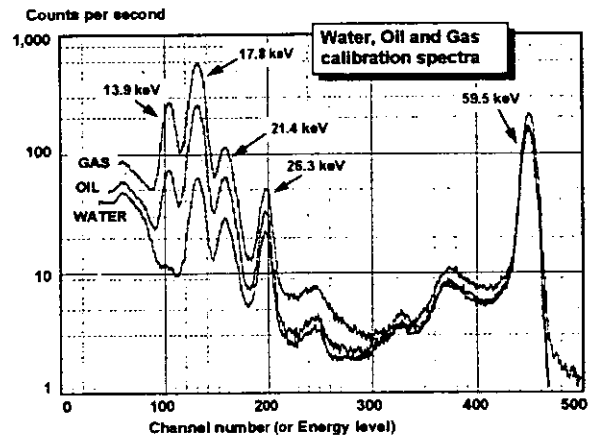


Fig. 5 - Water, oil and gas calibration spectra from a 6.475 GBq (175 mCi) Am-241 source as measured with a 14 mm² Si solid state detector cooled to 5°C.

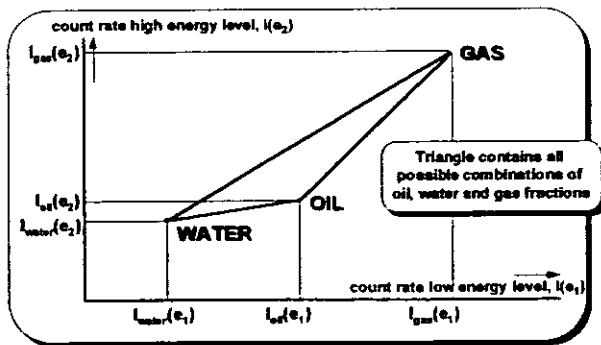


Fig. 3 - Graphical presentation of the DEGRA concept. The corner points of the triangle are the water, oil and gas calibration points.

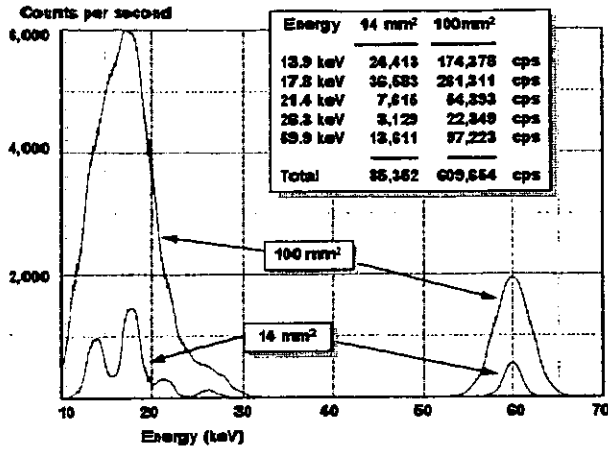


Fig. 6 - Gas spectra from two separate Si solid state detectors. The 14 mm² detector provides acceptable resolution and efficiency for the 14-26 keV energy levels. The 100 mm² is used to compensate for the poor efficiency at 59.5 keV.

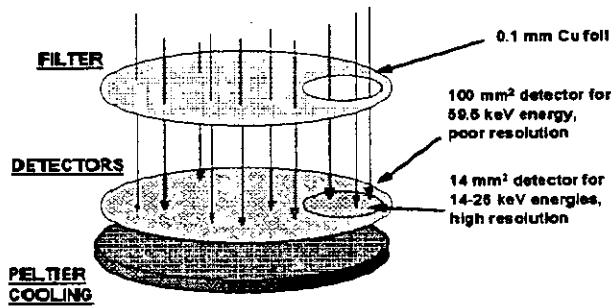


Fig. 7 - The "dual area Si solid state" detector. The 100 µm copper foil filters out the low energy gamma rays before they reach the 100 mm² detector. This large detector, having poor resolution, is dedicated to counting the 59.5 keV events.

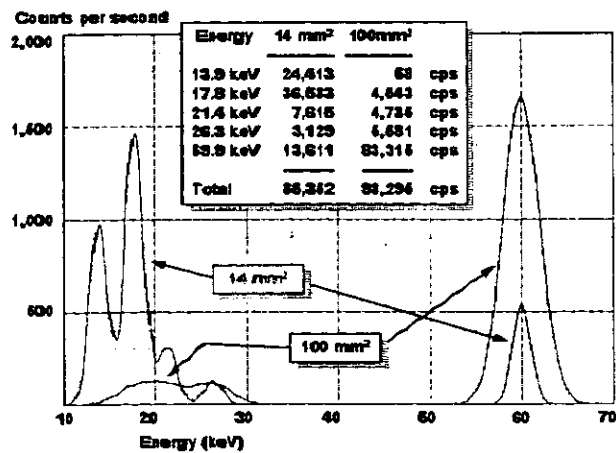


Fig. 8 - Gas spectra from the "dual area solid state" detector and the 100 µm copper filter. Low energy count rates on the 100 mm² detector have been reduced significantly with this filter.

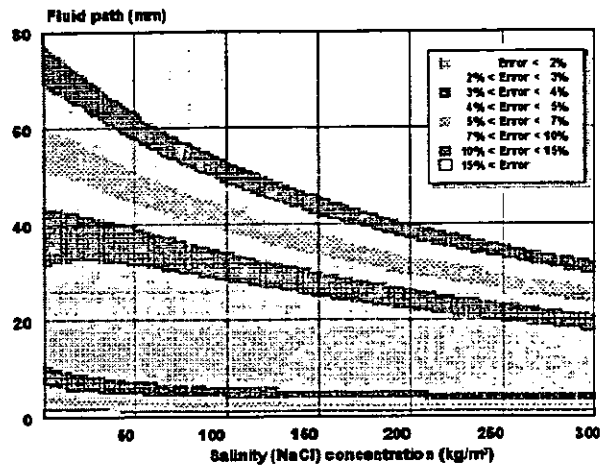


Fig. 9 - Uncertainty in the fraction calculation as a function of salinity and fluid path length. The plot is valid for a 6,475 MBq (175 mCi) Am-241 source, two 2 mm Carbon Fiber Reinforced Epoxy windows, and the 14/100 mm² "dual area solid state" detector shown in Fig. 7. Above plot for 100% water is a worst case situation (lowest count rate).

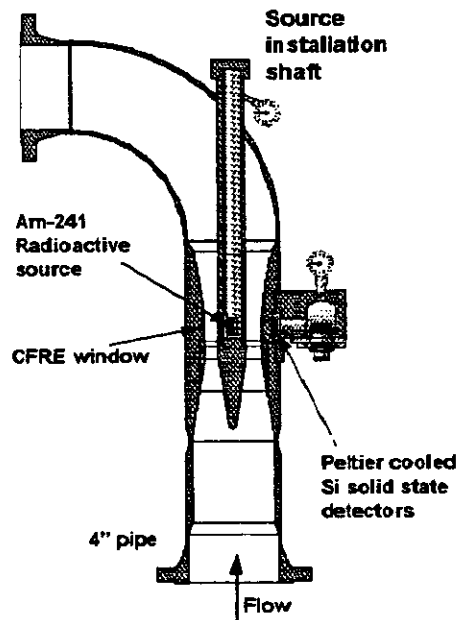


Fig. 10 - Schematic drawing of the concentric MEGRA. The source is installed in the centre of the pipe and a set of concentric Carbon Fiber Reinforced Epoxy cylinders are used as window material.

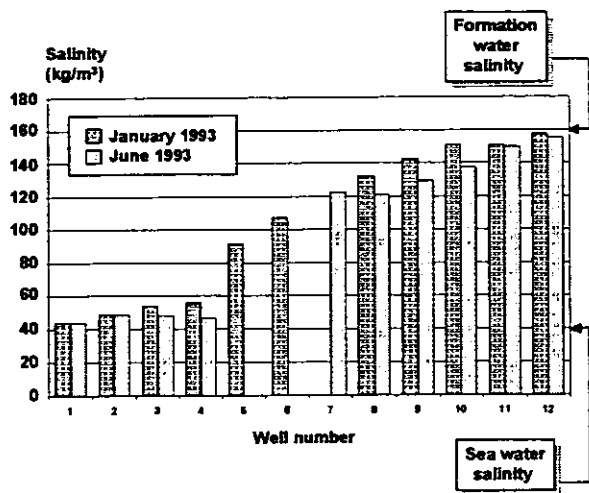


Fig. - 11 - The salinities of various wells from one North Sea field as measured in January and June 1993. The formation water salinity is 160 kg/m^3 while the sea water salinity is 35 kg/m^3 . The salinity measured changes gradually from that of the formation water to that of the sea water.

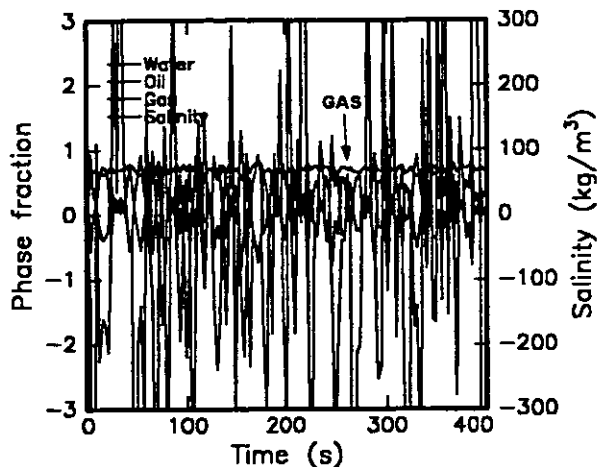


Fig. - 13 - Phase fractions and salinity obtained from the computer simulated count rates by directly solving the matrix equations. The left hand scale is valid for the phase fractions and the right hand for salinity. Input values are $\alpha_w=0.15$, $\alpha_o=0.15$, $\alpha_g=0.70$ and $S=100 \text{ kg/m}^3$. While the gas fraction calculation is acceptable, the oil and water fractions calculations and the salinity estimate are not acceptable.

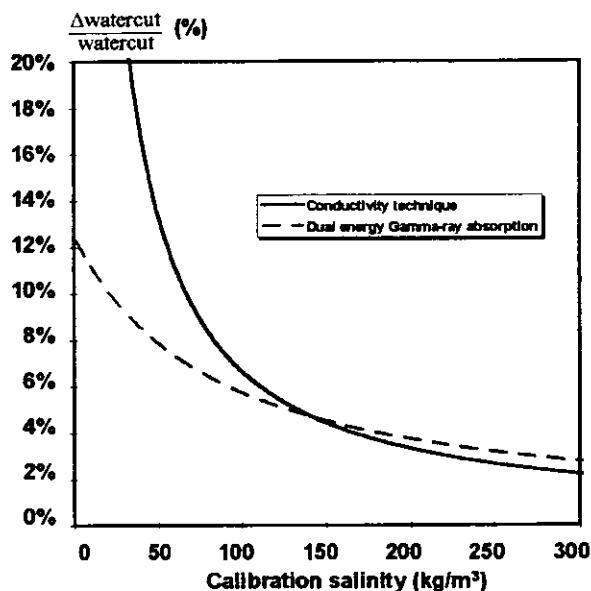


Fig. - 12 - The relative error in watercut as function of salinity for a change in salinity of 10 kg/m^3 .

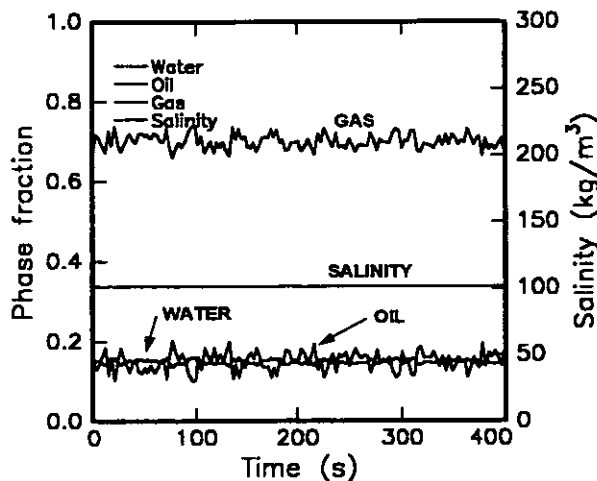


Fig. - 14 - Phase fractions and salinity obtained from the chi-square minimisation algorithm, where the same computer simulated count rates as in the previous figure were used as input. The left hand scale is valid for the phase fractions, that on the right for salinity. Input values are $\alpha_w=0.15$, $\alpha_o=0.15$, $\alpha_g=0.70$ and $S=100 \text{ kg/m}^3$. This new algorithm results in a statistically acceptable composition measurement and a proper estimation of the salinity.

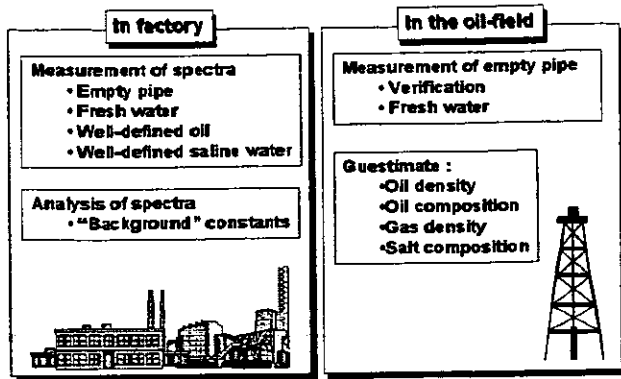


Fig. 15 - Principle of calibration free operation. No water, oil and gas calibration is required in the field.

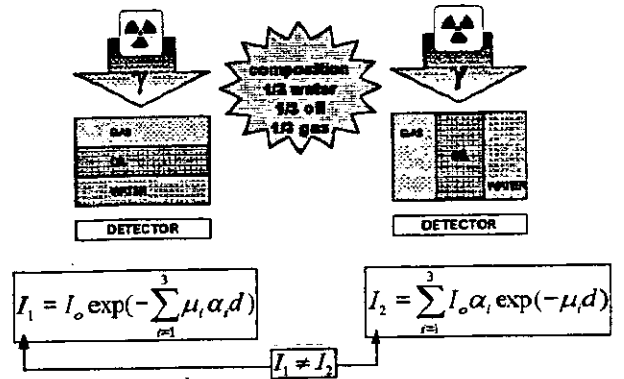


Fig. 18. - Count rates measured in these two situations are not equal, although the fractions in both are the same. If variations in time occur (second situation), the result is systematic underreading of the watercut.

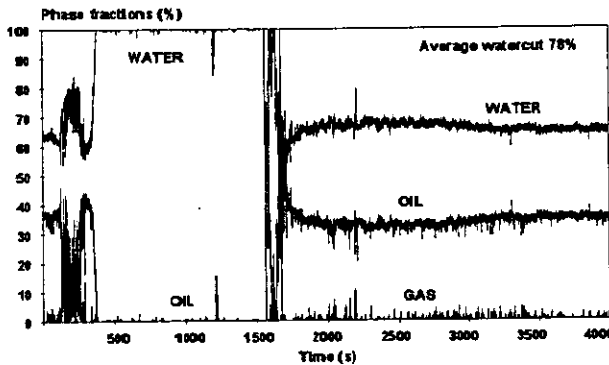


Fig. 16 - Fractions obtained using conventional calibration and the DEGRA calculation method. Saline water and oil reference count rates as measured in the oil field are used.

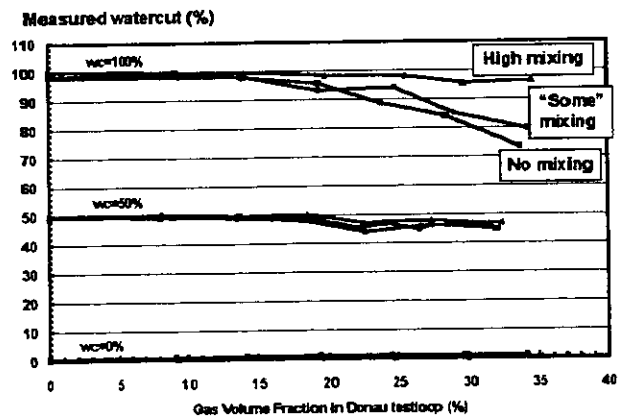


Fig. 19 - Watercut reading as a function of Gas Volume Fraction. Mixing is required above 20% GVF to avoid systematic errors in the composition measurement.

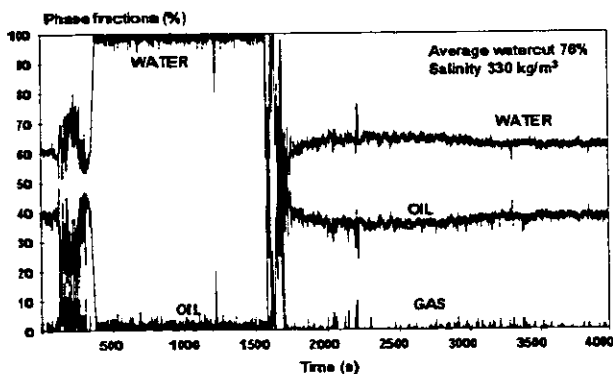


Fig. 17 - Fractions obtained using the calibration free concept plus the MEGRA algorithm. No reference spectra from the field are used, only spectra from the testloop evaluation.

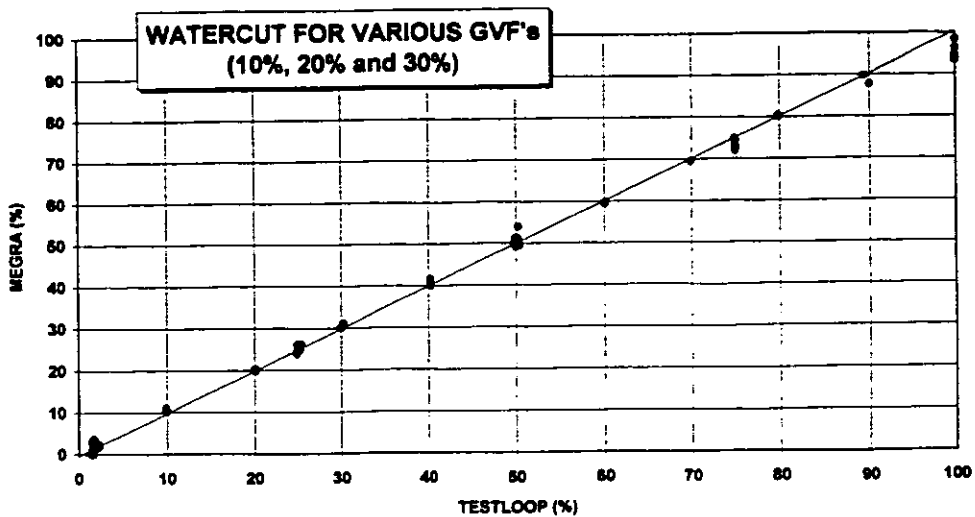


Fig. 20^a - Watercut reading of the Daniel prototype MEGRA versus the test loop reference measurement

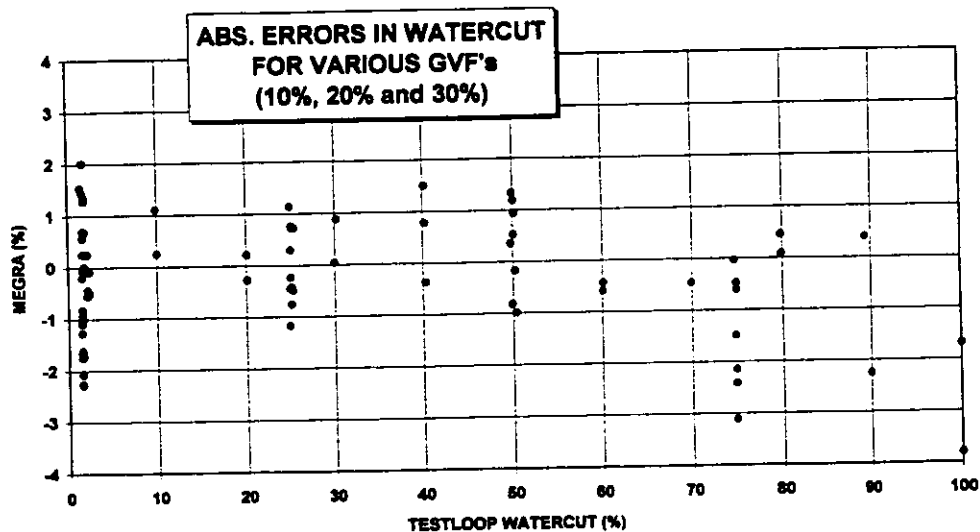


Fig. 20^b - Absolute error in watercut reading of the Daniel prototype MEGRA versus the reference measurement.

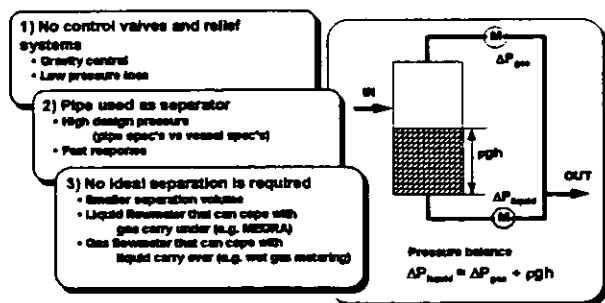


Fig. - 21 - A simple In-Line Conditioner (ILC) to remove the bulk of the gas from a high GVF multi-phase flow. MEGRA can be applied in the "gassy liquid" drainline, a "wet gas" meter in the gas line

Two-Phase Effects on Single-Phase Flowmeters

A.F. Skea, NEL

Summary

The effect of gas entrainment in oil on the performance of a range of single-phase flowmeters has been investigated experimentally using the national standard flow calibration facilities at NEL. The flowmeters tested were 4 inch positive displacement, venturi, helicoidal and flat-bladed turbine meters and a 2 inch U-tube and a 1.5 inch straight tube coriolis meters. The flowmeters were tested in oil flow with gas fractions up to 15% by volume.

The volume flowrate and gas fraction determine the flow regime. This affects the flowmeter response. At low flowrates (up to 20 l/s), slug flow was the dominant flow regime and most of the flowmeters estimated the total volume flowrate to within $\pm 10\%$. The higher flow rates produced either separated or mixed bubble flow regimes depending upon the gas fraction. At low gas fractions, the positive displacement and venturi flowmeters estimated the total flowrate to within $\pm 2\%$. Over 9% gas fraction, there was an improvement to the response from some of the flowmeters with increasing gas fractions. This was thought to be due to the flow regime becoming more homogeneous.

Introduction

A large range of measuring techniques exist for the determination of single-phase flowrates. Many single phase flowmeters have been developed which can measure liquid flowrates to an accuracy within $\pm 0.2\%$ over the operating range of the meter under design conditions. The uncertainty increases if a second phase or component is present.

Second-phase components emanate in single-phase flows from a variety of different sources including, leaking pump seals, the evolution of gases from volatile liquids at pressure losses (e.g. bends, expansion zones etc.), or from carry-over from liquid separators or hydrocyclones.

The aim of this work is to quantify the effect of second-phase fluid components on a range of single phase flowmeters and, as a consequence, identify which generic types of single-phase flowmeter are most suitable in these applications. The generic groups of flowmeters were turbine, helicoidal turbine, straight-tube and U-tube coriolis, venturi, vortex shedding and positive displacement.

The effect on the flowmeter performance of gas breakout and water-in-oil/oil-in-water carry over will be quantified to demonstrate meter effectiveness with two component flows. These tests will provide evidence of the suitability of a flowmeter for difficult, two-component applications. Comparisons will be made between generic type and size of flowmeter.

The conditions under which the flowmeters have been tested are as follows:

- a) Oil (viscosity = 10cSt) with gas fractions up to 15% by volume, simulating gas breakout or entrainment;
- b) Water with oil fractions up to 15% by volume;
- c) Oil (viscosity = 10cSt) with water fractions up to 15% by volume.

This paper presents some of the results from group a) above, oil with gas fractions up to 15% by volume.

Experimental

Measurements have been made on six single-phase flowmeters: 1.5 inch straight tube coriolis; 2 inch U-tube coriolis; 4 inch flat-bladed and helical turbine meters; 4 inch venturi and positive displacement flowmeters.

The meters were installed into the oil flowmeter calibration facilities at NEL in groups of three and a fourth flowmeter was used as a reference meter. A schematic of the experimental arrangement is shown in Figure 1. Velocite oil was used as the main fluid. The oil temperature was raised to 50°C to maintain a viscosity of 10cSt.

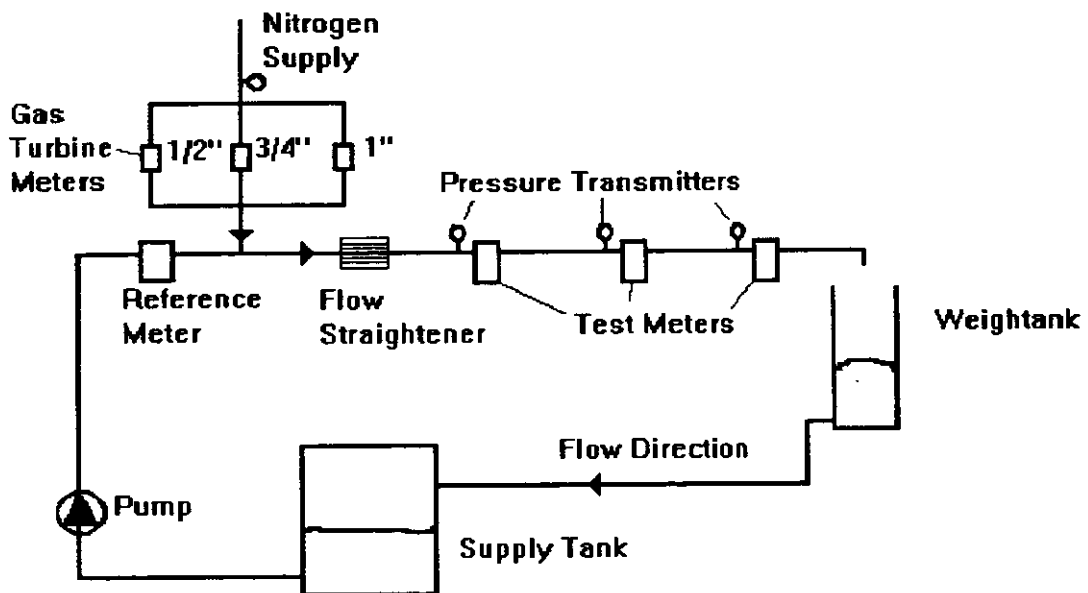


Figure 1 Schematic of the Experimental Set-up

The four meters were initially calibrated against a weight tank. The calibration resulted in a single-phase characteristic equation for each meter, expressing volumetric flowrate as a function of pulse frequency or current output. The tests with gas entrainment were performed using the reference meter to measure the oil flowrate.

Gas turbine meters were used to measure the gas flowrate. Nitrogen gas was injected downstream of the oil reference flowmeter and the nitrogen-oil mixture passed through a tube bundle flow conditioner before entering the test section. The two-phase flow was allowed to develop for 30 pipe diameters before entering each meter under test. The static pressure was measured at the gas turbine meter and at each of the test meters.

Tests were performed with gas fractions of 3%, 6%, 9%, 12% and 15% with oil flowrates from 4 to 50 l/s. The test meter output at each of these gas fractions was compared with the sum of the oil and gas reference meter outputs.

Discussion of Results

Figures 2 to 7 show the results of the gas in oil tests for the flat-bladed turbine meter, helicoidal turbine meter, positive displacement meter, venturi, straight tube and U-tube coriolis meters respectively.

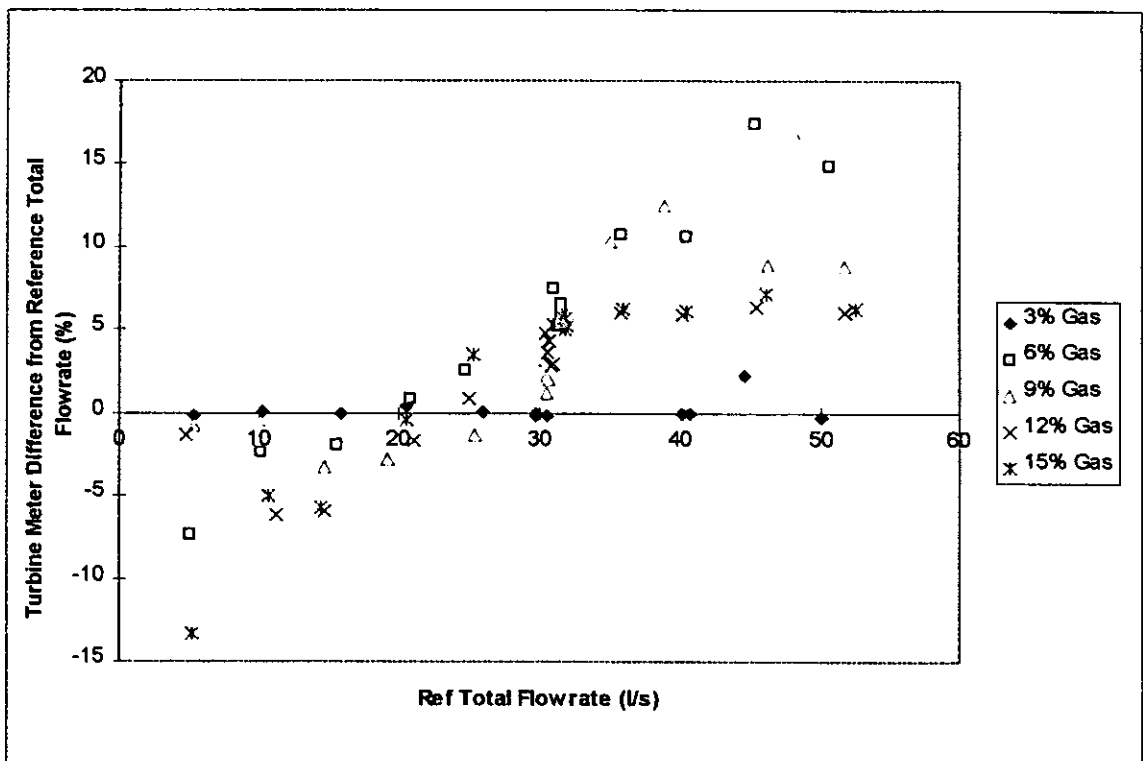


Figure 2 - 4" Flat-Bladed Turbine Meter / Gas in Oil

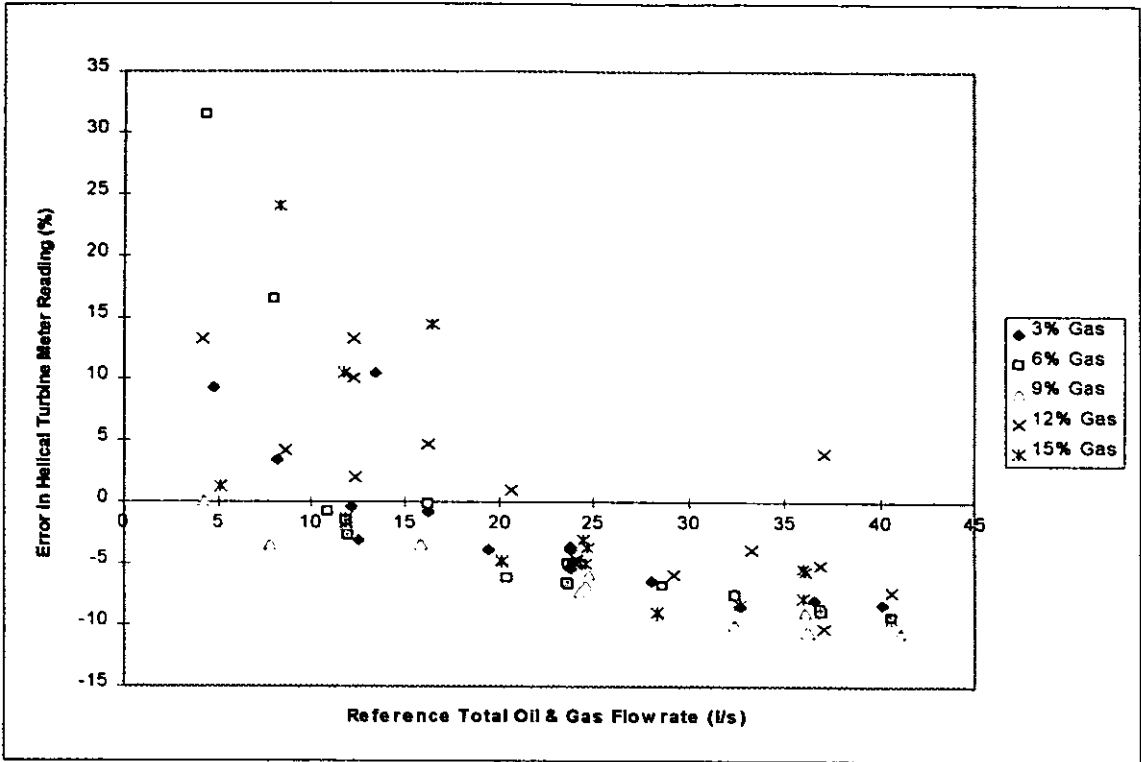


Figure 3 - 4" Helicoidal Turbine Meter / Gas in Oil

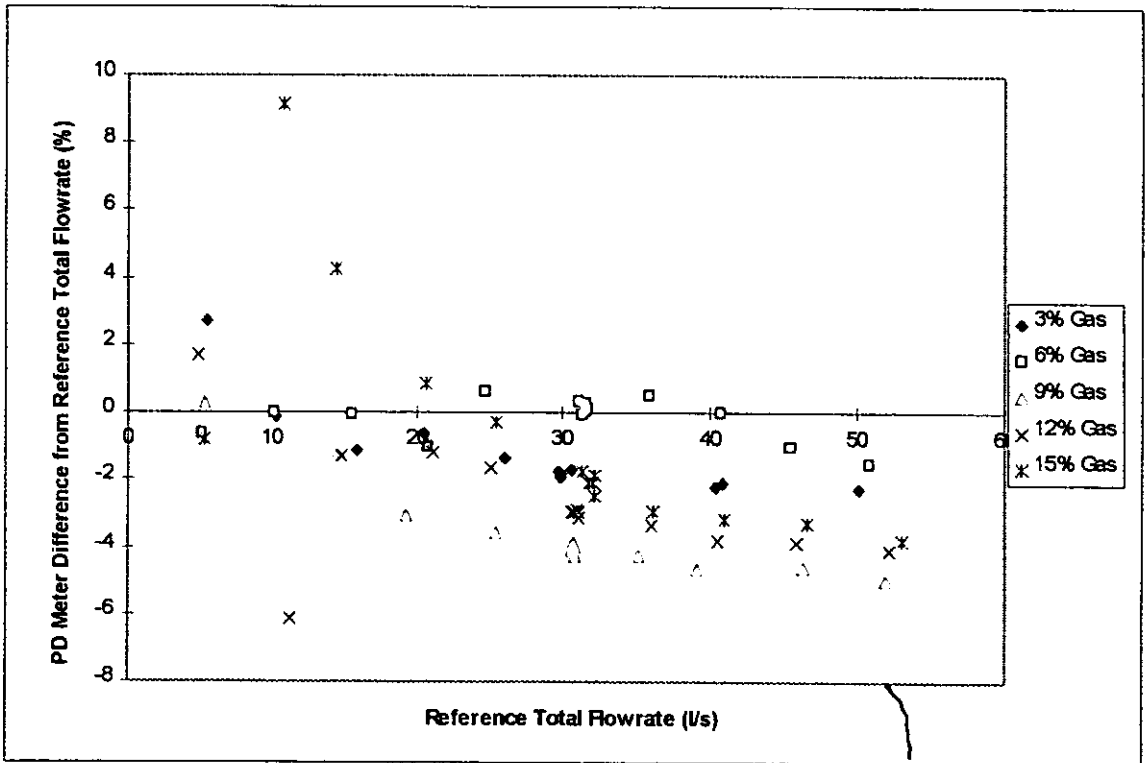


Figure 4 - 4" Positive Displacement / Gas in Oil

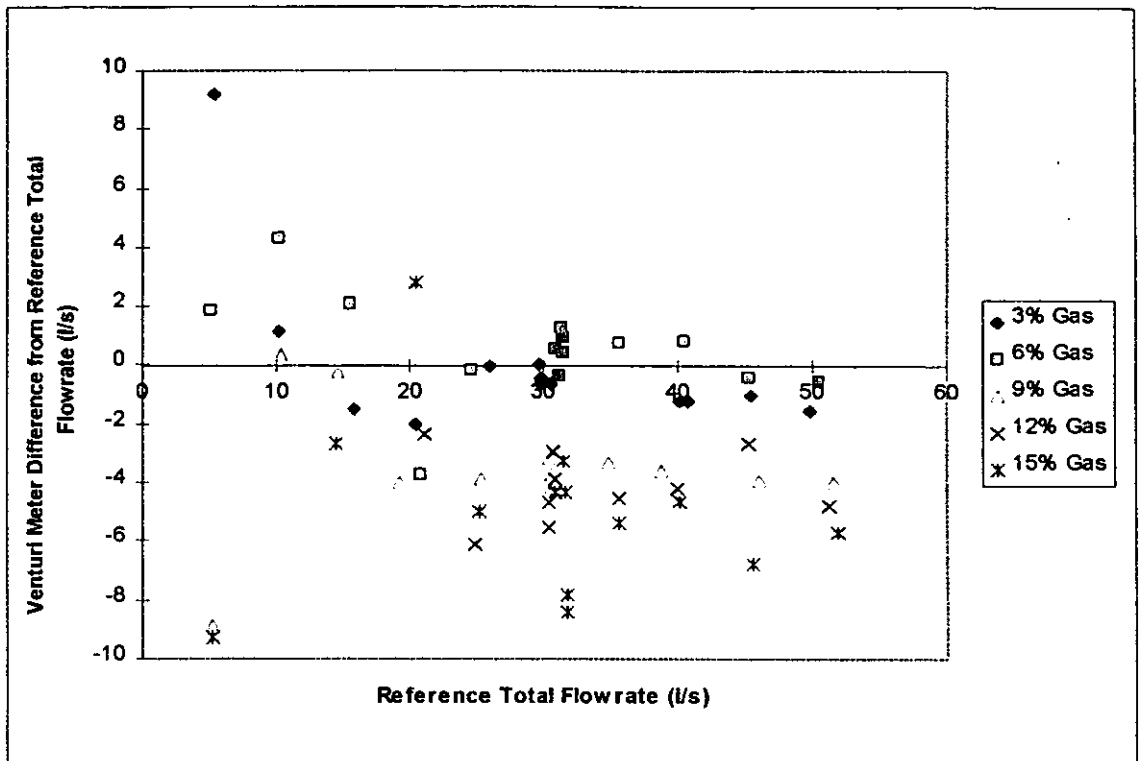


Figure 5 - 4" Venturi Meter / Gas in Oil

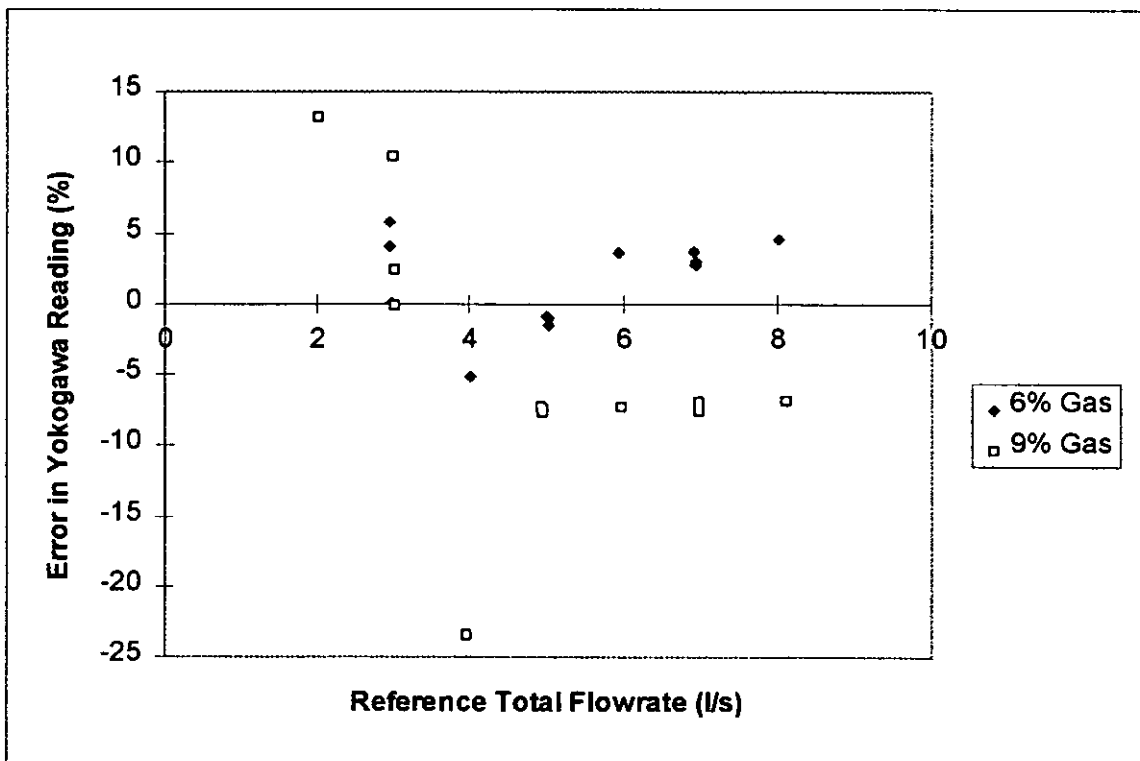


Figure 6 - 1.5" Straight Tube Coriolis Meter / Gas in Oil

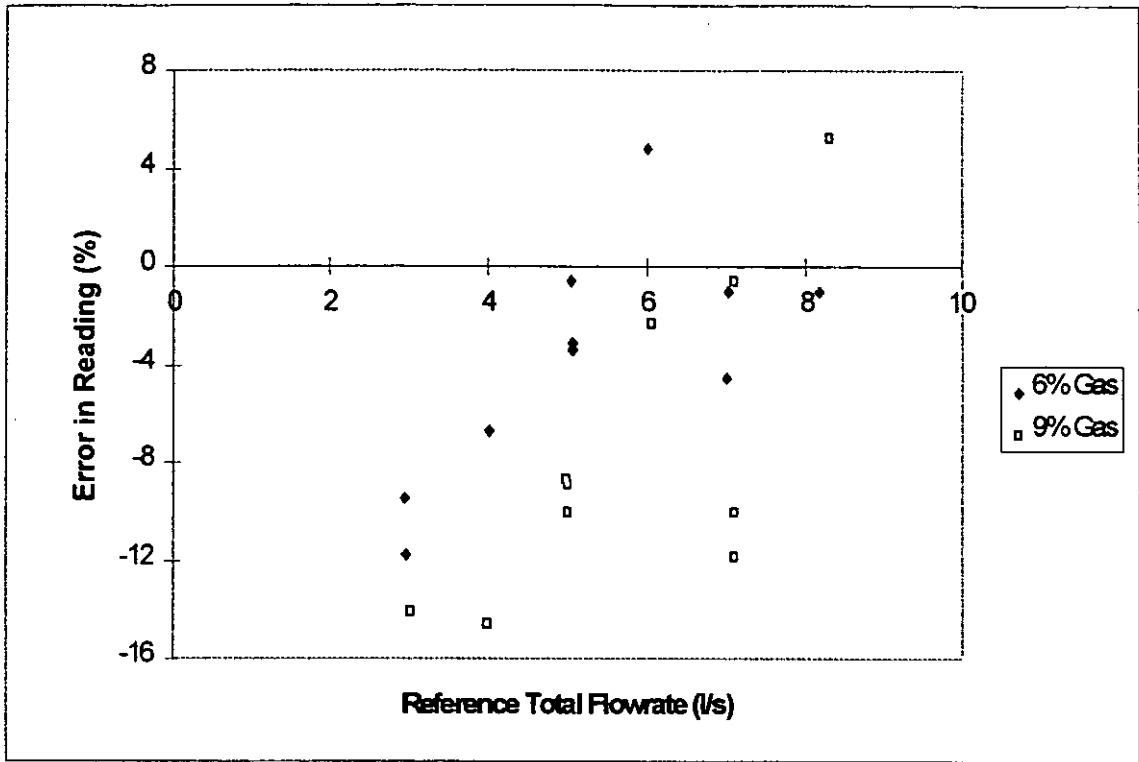


Figure 7 - 2" U-Tube Coriolis Meter / Gas in Oil

Flow visualisation of air in water (Mark et al 1989) and nitrogen in oil (Hall 1996) taken in 4 inch pipe have shown that at approximately 20 l/s there is a transition from slug flow to bubble flow. Figure 8 is adapted from data presented by Hall (1996) and shows the transition between the flow regimes. Some additional flow regimes are defined in Figure 9.

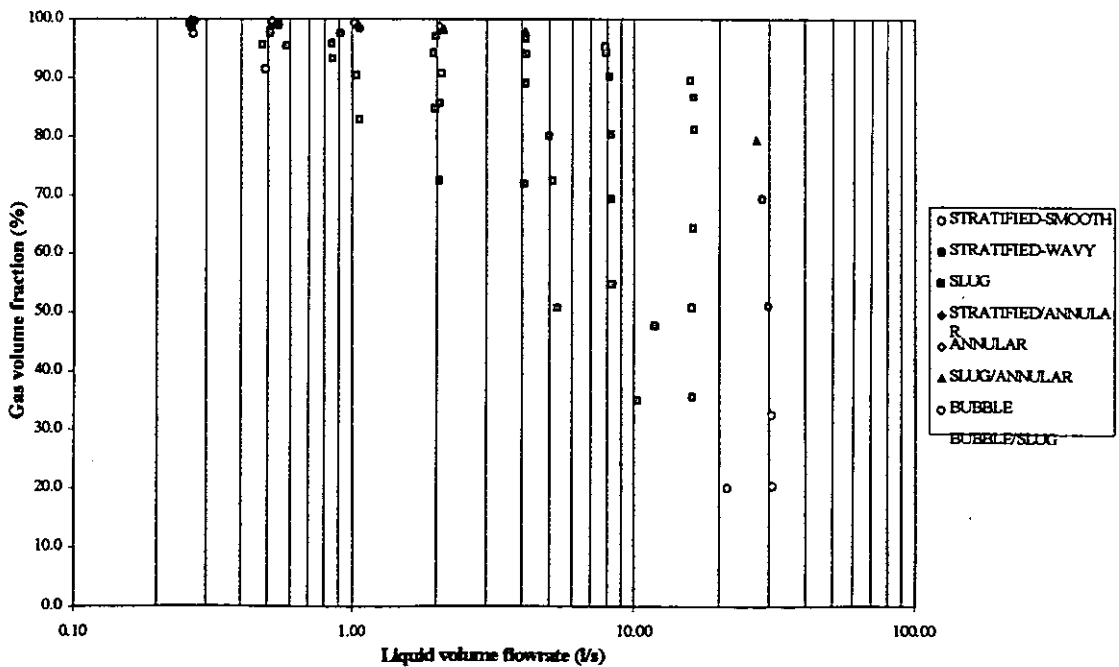


Figure 8 - Two-Phase Flow Patterns in 4" Test Section

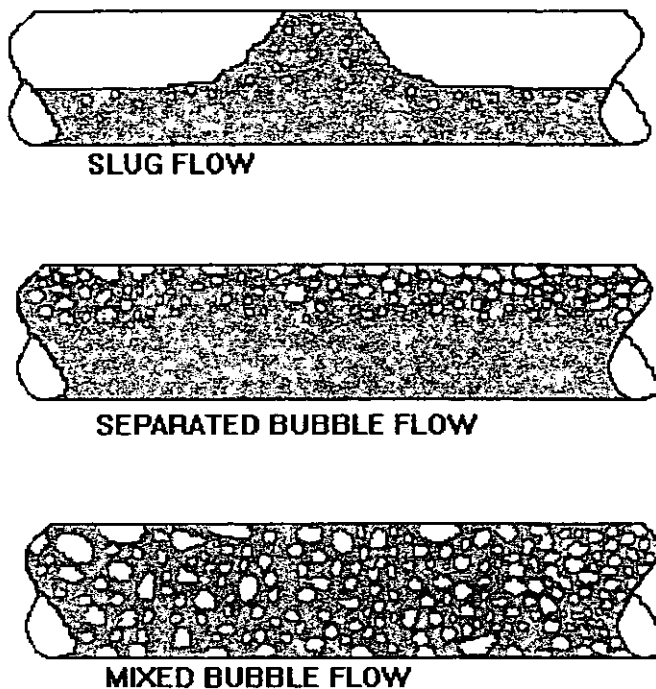


Figure 9 - Flow Regimes

The results presented in this paper from the 4 inch meters all show a transition at around 20 l/s. Additionally, there is a change in the trend of the results between gas fractions less than 9% and gas fractions greater than 9%. This may correspond to a change in the flow characteristic from separated bubble flow to mixed bubble flow.

The total volume flowrate and the gas void fraction each have an influence on the flow characteristics, these in turn have an effect on the flowmeter response. Each flowmeter responds in a different way depending upon its design.

The results from the flat-bladed turbine meter show that at flowrates less than 20 l/s the meter underestimates the total flow. This implies that during slug flow some of the gas is passing through the turbine meter blades without applying a driving torque. Over 30 l/s the turbine meter overestimated the total volumetric flowrate. Bubble flow is causing the blades to overspin.

These results show a marked difference from the measurements taken from the helicoidal turbine meter. Up to around 20 l/s the helicoidal turbine meter overestimates the total flowrate and above 20 l/s the meter underestimates the flowrate. The magnitude of the error is similar for the two turbine meters. Most of the points are within $\pm 10\%$ of the referenced total flow.

The results for the flat bladed turbine meter are in close agreement with previous experimental work performed by Mark et al (1989) on a flat bladed

turbine meter in water flow with up to 12.5% air injection. An overestimation of the total volumetric flowrate was observed at flowrates over 20 l/s. The greater the gas fraction the greater the overestimation, but only up to a gas fraction of 10%. Greater than 10% the overestimation is reduced. This was also observed in the results presented here except that the maximum overestimation observed by the turbine meter was at a gas fraction of 6%. A similar trend was observed from the results of the helicoidal turbine meter. The largest error at high flowrates was for a gas fraction of 9%, the magnitude of the error decreased as the gas fraction increase to 15%.

The improved performance with increasing gas fraction over 6% (or 9% for the helicoidal turbine meter), may be due to improved mixing of the gas in the oil as the flow regime changed from separated bubble to mixed bubble flow. At low gas fractions the gas bubbles travel along the pipe near to the upper surface, but as the gas fraction increases, the bubbles mix throughout all of the oil.

The positive displacement meter generally underestimated the total flowrate over the entire flow range and at all gas fractions. The magnitude of the error is less than for the other meters in the tests at high gas fractions. Most of the points are in the range of -4% to 1% from the reference total flowrate. Above 20 l/s the measurements became more stable and repeatable. The magnitude of the error also decreased as the gas fraction increased from 9% to 15%.

The repeatability of the measurements from the venturi meter also improved above 20 l/s. The error in the venturi meter measurements for 3% and 6% gas fractions was within $\pm 1\%$ of the reference total flowrate. For gas fractions greater than 6% the venturi meter underpredicts the total volumetric flowrate. The errors in these measurements are between -6% and -2% from the reference flowrate at flowrates greater than 20 l/s. The venturi meter underestimates the total volume flowrate because the density of the oil-gas mixture reduces with increasing gas fraction while the value for the density in the calculation remains constant. The performance of the venturi meter deteriorated with increased gas fraction.

The coriolis meters were both tested on a 2 inch line. The U-tube meter was 2 inch and the straight tube meter was 1.5 inch. Tests were performed on a 4 inch straight tube coriolis meter but, with the exception of the calibration results, no stable measurement could be obtained.

Coriolis meters are mass flowmeters and so it would be expected that the total volume flowrate would be underpredicted by an amount corresponding to the gas fraction. Measurements could only be obtained for gas fractions of 6% and 9%. The U-tube coriolis showed a certain amount of linearity for high flow rates and 9% gas fraction. There were no other reliable trends from these meters. The coriolis meters did not give any results for gas fractions greater than 9%.

Conclusions

Six single phase flow meters have been tested in two-phase flow. The main fluid component was velocite oil at 50°C and the second component was nitrogen. Tests were performed at 3%, 6%, 9%, 12% and 15% gas fractions. The flow regime changed with total volume flow rate and gas fraction. At volume flowrates less than 20 l/s there was slug flow and above 20 l/s the flow was either separated bubble or mixed bubble depending upon the gas fraction. Each of these flow characteristics had a different influence on the meter performance depending upon the meter design. The scale of the uncertainty in the meter response at these gas fractions has been quantified and the generic type of flowmeters most suitable for these flow conditions have been identified.

At low flowrates most of the meters tested estimated the total volume flowrate to within $\pm 10\%$. The venturi and positive displacement meters performed better than the other flowmeters at low gas fractions. They predicted the total volume flowrate to within $\pm 2\%$ for 3% and 6% gas fractions at flowrates greater than 20 l/s. At high gas fractions the positive displacement meter produced the lowest errors.

The repeatability of the measurements from the positive displacement and flat-bladed turbine meters improved for the higher flowrates with gas fractions greater than 9%. This may be due to the improved mixing of the oil and gas. The magnitude of the error decreased with increasing gas fractions over 9% for both of the turbine meters and for the positive displacement meter.

Different trends have been observed from each of the single-phase flowmeters with increasing total volume flowrate and with gas fraction. The performance of the flowmeters could be improved if correction factors were developed to represent the trends observed in these tests. Any improvements to the flowmeter estimations in two-phase flow first requires a knowledge of the flow characteristic in the pipe. Each flow characteristic requires separate modifications to be made to the single-phase characteristic equation for each meter to take the second component into consideration.

The flowmeters produced smoother curves that had good repeatability in the fully mixed bubble flow than in slug or separated bubble flow. Controlling the flow regime to a homogeneous flow over the flow range of the meters and at different gas fractions would provide the opportunity for the single-phase flowmeters to measure accurately the total volumetric flowrate. This would also require the use of another instrument, such as a gamma densitometer, to measure separately the gas fraction in the mixture.

Acknowledgement

The work described in this paper was carried out as part of the Flow Programme, under the sponsorship of the DTI's National Measurement System Policy Unit. The author would also like to thank ISA Controls, Endress & Hauser, Yokogawa and Rosemount for the loan of their flowmeters and their co-operation throughout this project.

References

MARK P A, SPROSTON J L, JOHNSTON M W. *Theoretical and Experimental Studies of Two-Phase Flows in Turbines Meters*, International Conference on Basic Principles and Industrial Applications of Multiphase Flow, 24-25 April 1990.

HALL A R W, *Flow Characteristics of Three-Phase Flows of Oil, Water and Gas*, International Conference of Flow Measurement, Flomeko '96, Beijing, China, 20-24 October 1996.

THREE PHASE METERING IN SUMATRA USING THE STARCUT METER: AN EXAMPLE OF A PERFECT FIT TO A SPECIALIZED NICHE

Jack Marrelli PhD, Texaco EPTD Humble Flow Facility, Humble, Texas

1. SUMMARY

Matching of multiphase meter (MPM) capabilities with field conditions has allowed exceptional performance in applications in Indonesia. Texaco's Starcut microwave sensor is unique in its ability to provide very accurate and stable WaterCut determination (<0.3% rms. error) at very high watercuts (>90%) even when some gas is present in the fluids and salinity is varying. Accuracy, stability and rapid transient response derives from slip stream sampling, small size, dual channel construction, bonded ceramic and steel components and heat exchange jacketing using production fluids. The system performs continual automatic calibration based on on-line estimates of fluid density and salinity. When combined with various options such as orifice meters STARCUT also provides accurate flow rate measurement (<1% rms. error). The above described production niche is not addressed by MPM manufacturers but is critically important to Texaco. In this niche most other MPMs are insufficiently accurate to provide useful well management data.

2. INTRODUCTION:

The name STARCUT refers to Texaco's patented microwave based oil, water and gas fraction measurement technology. This technology has proven to be very versatile and is incorporated into several multiphase metering contexts from full range gas volume fraction (GVF) cases to low and zero GVF applications. STARCUT is composed of microwave control and computational electronics and a dual channel microwave waveguide fluid sensor. The STARCUT sensor construction and operation is well documented in several reports, 1, 2. This fluid fraction sensor technology is unique in the industry in several ways, each of which contribute to its versatility, exceptional accuracy and long term stability.

The sensor is actually two identical sensors in one steel block. The sensors are microwave waveguides composed of ceramic bonded to steel fired at 1000 degrees Fahrenheit and coated with 3 mils of aluminum oxide. Geometry of the sensor is manufactured to .001 inch tolerance and is currently calibrated over 32 to 310 degrees Fahrenheit and pressure tested at 10,000 psi. These sensors are jacketed with a heat exchanger using the production fluids. During meter operation therefore both sensors are

at the same temperature but one contains a stationary reference fluid and the other receives a portion of the production flow from a 1/4 inch diameter main line slip stream. Microwaves at 10,000 megahertz are alternately passed completely through first the reference sensor and then the production sensor at up to several hundred times a second. Extreme sensitivity and high signal to noise ratio are achieved through continual differential measurement allowing common mode rejection of electronic noise, aging effects of electronics, transmission line effects and both effects of electronic and sensor temperature. Data collection from the sensor pair consists of temperature, microwave attenuation, microwave phase shift. These basic data are processed statistically using pattern recognition methods and are referenced to stored laboratory data consisting of tables of properties of pure oils, brines and gas as well as families of mixing curves, all as a function of temperature. These laboratory data combined with field data allow continual and on-line prediction of dry crude oil API gravity, pure field water salinity, gas fraction and finally WaterCut. At preset intervals of seconds to minutes, internal calibration is automatically reviewed relative to oil density, water salinity and gas fraction. Changes in fluid conditions immediately provokes automatic re-calibration. Fraction and density determinations are then used in overall MPM rate computations.

Total fluid rates are determined in a variety of ways depending on the application and the accuracy requirements. Many of our applications require higher accuracy than is possible using MPMs which take the entire flow stream through one sensor tube. We have developed two basic designs suited to our needs:

3. LOW GAS FRACTION DESIGN

The STARCUT Low Gas Three-Phase Meter is a design (<.15 GVF) which consists of the STARCUT sensor in parallel with an orifice plate flow meter. The orifice meter equation is continually updated using the fluid fraction data, API gravity and water salinity. This particular application was installed, tested, proven in the Minas oil field in central Sumatra. Figures 1, 2 and 3 present data used to prove the STARCUT application. The STARCUT Three Phase Meter is currently in portable use in Sumatran well testing operations.

4. ALL GAS FRACTION DESIGN

The STARCUT Full Range Multiphase Meter design recognizes that metering accuracy rises greatly when some fluid separation is allowed. Secondly we recognize that no separator performs a complete phase separation. Some gas always remains in the liquid legs of the separator. STARCUT gas insensitivity makes it the choice for accurate determination of WaterCut in this liquid portion of the MPM. We therefore have combined the STARCUT Low Gas Three-Phase Meter in series with a small, passive fluid conditioning device, the Gas Liquid Cylindrical Cyclone (GLCC) deliberately undersized to allow up to 0.15 GVF to pass out the liquid leg and emphasizing a dry gas stream. STARCUT, in parallel with an orifice meter in the liquid leg, is easily able to determine fluid fraction data. An orifice meter is also present in the gas leg to complete the design. The GLCC was design was aided with software provided by the University of Tulsa, Separation Technology Project. Meter testing is underway.

5. FIELD TESTING - AT LOW GVF

The STARCUT meter design for the Minas Application is of the Low Gas Three-Phase Meter design and is portable and operated from a truck battery. This STARCUT THREE PHASE METER has successfully passed accuracy and survival evaluation for portable use in the hilly, jungle environment of Minas well testing operations, Northern Area. Current and projected reservoir development in that area consists of 100s of wells whose production niche is characterized by low Gas Oil Ratio (GOR), very high temperatures, high WaterCut, variable and low salinity, multiple zone production, sand production and high flow rate ranges. During the test phase STARCUT was evaluated relative to separator data where facilities were available and by manual sampling. STARCUT demonstrated WaterCut measurement agreement with reference data with $\pm 0.3\%$, average deviation from reference, regardless of operating pressure and in the presence of up to 0.10 GVF estimated from empirically derived crude oil Pressure, Volume, Temperature (PVT) data, figure 1. Flow rate accuracy of 1% average deviation from reference, from 3000 to 16000 Barrels/day of produced fluid has also been demonstrated, figure 2. For a single well, 3D86, downstream pressure was varied over time to demonstrate WaterCut measurement stability at different GVF, figure 3 a. b. c. Figure 3c. indicates well head pressure set by closing downstream valves against the down hole ESP driven flow. Changes in well head pressure affect GVF negatively as seen in Figure 3a. Watercut of production fluids was monitored using STARCUT and separator testing (Tank Test). STARCUT watercut estimate, separator data indicate close agreement over the GVF indicated, figure 3b. Uncompensated reading of watercut demonstrate that without STARCUT gas detection and compensation the watercut errors would have been over 6% in that case.

This portable system replaces a portable coriolis-based WaterCut meter and gas orifice meter which required a perfectly functioning truck mounted two-phase separator. The physical principle of the STARCUT dual measurement microwave sensor is inherently more accurate than the density based coriolis method by a factor of 10 to 100 under the low GOR, high WaterCut Minas Northern area conditions.

STARCUT is licensed to Jiskoot AutoControl of England and distributed and supported in Southeast Asia by Matco Asia.

6. DISCUSSION

Full bore non-intrusive MPMs have not demonstrated sufficient accuracy's for high water low gas production well testing. Major improvements in MPM accuracy are possible using the STARCUT Microwave System in conjunction with various configurations using minimal and partial liquid gas separation. Drawbacks to partial separation are primarily related to footprint and weight however new concepts in separator design combined with STARCUT Gas insensitivity have allowed design of highly accurate portable compact MPMs with footprints of 3 feet by 5 feet and weighing less than 1200 pounds. Texaco EPTD engineers have filled a multiphase metering niche in which STARCUT has demonstrated high accuracy at low cost. Not only does the niche of high water, high temperature and low gas operations currently represent a significant portion of Texaco production in Indonesia, future trends for world wide oil production are also in the

direction of higher watercuts and lower gas fractions. Few, if any, other instruments are focused in this niche even though there is a critical need.

7. ACKNOWLEDGEMENTS

We wish to recognize the contributions of past and current members of the Texaco EPTD Multiphase Pumping and Metering Team and the staff of the EOR

Project for the Minas field for their exceptional effort in supporting the Starcut Three Phase Meter project.

8. REFERENCES

1. Marrelli, J.D. Hatton, G.J. Siddiqui, F. Pepin, L.L. 1992. Continuous Determination of Oil Pipeline Watercut, Salinity, and API Gravity Regardless of gas Fraction: The Microwave Watercut Monitor. Society of Petroleum Engineers, SPE International meeting on Petroleum Engineering, Beijing, China. SPE 22401.
2. Durrett, M.G. Hatton, G.J. Helms, D.A. Marrelli, J.D. 1989. Texaco Watercut Monitor - Microwave Based Technology. Indonesian Petroleum Association Proceedings, Eighteenth Annual Convention.

9. FIGURES

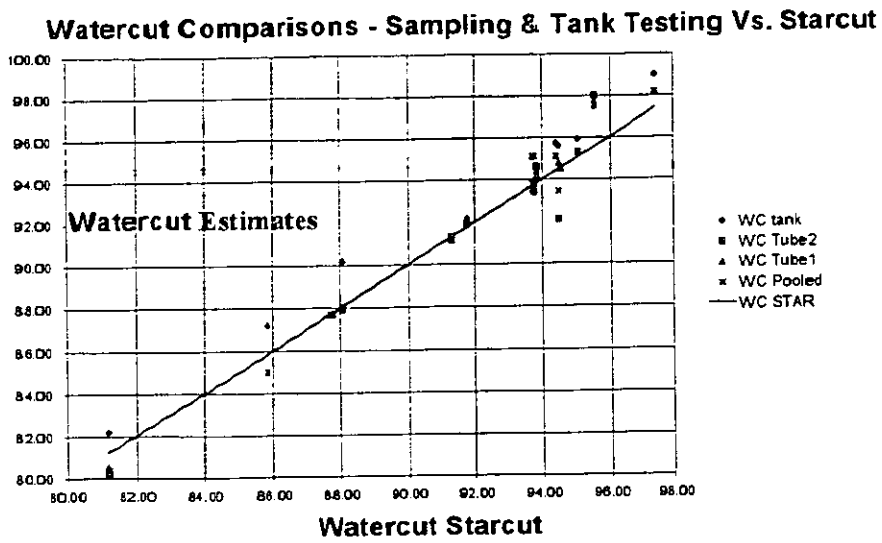


Figure 1 - Comparison of Watercut Obtained by Three Phase Separation, Sampling (Tube cuts) and Measurement by STARCUT

Total Liquid Flow Rate Comparison: Starcut Vs. Three Phase Separator Testing

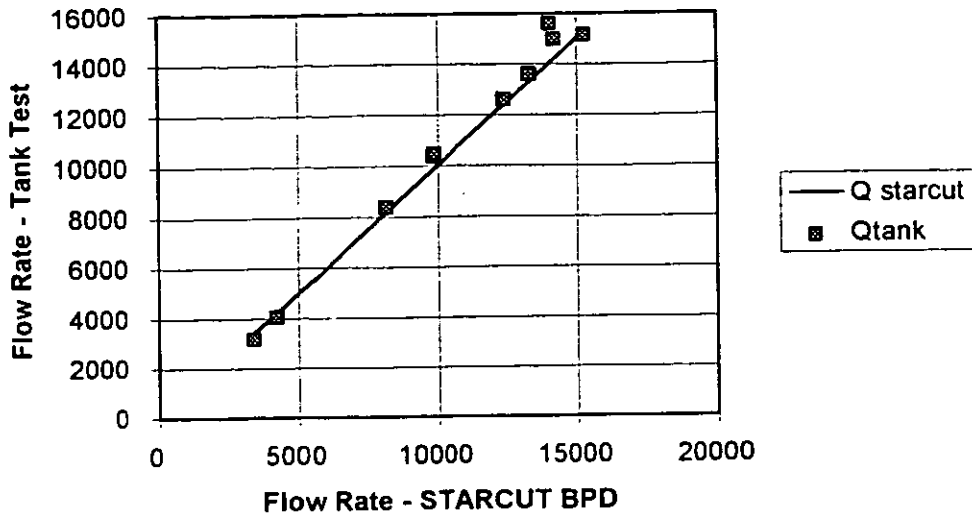


Figure 2: Total liquid flow rate as determined by STARCUT Meter versus three phase separator (Tank) results.

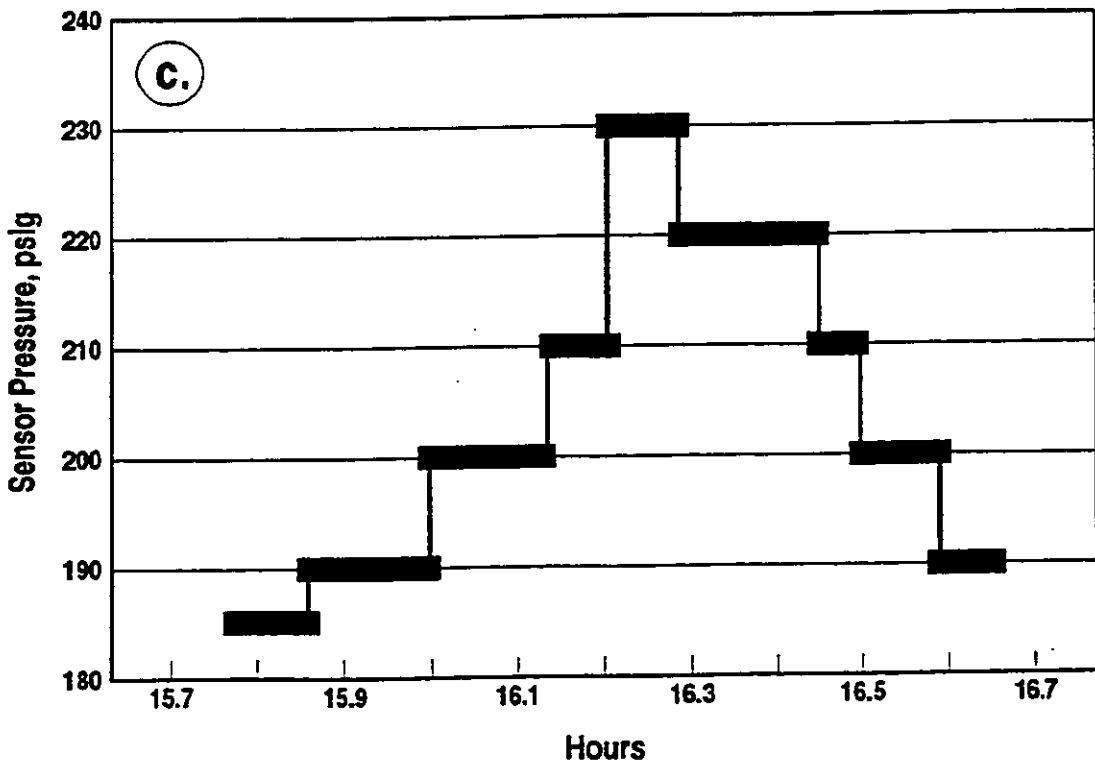
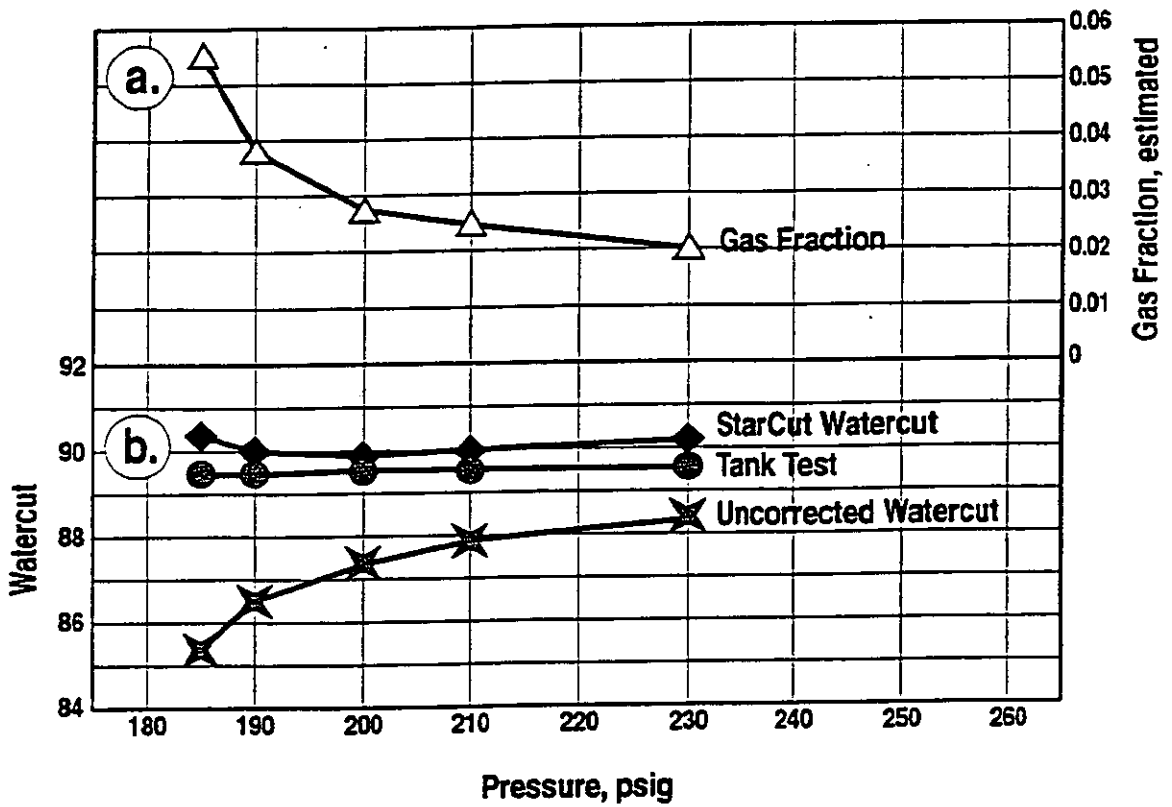


Figure 3 Demonstration of Starcut well test gas detection and compensation capability, well 3D-86

CURRENT STATUS OF DEVELOPMENT OF THE CSIRO GAMMA-RAY MULTIPHASE FLOW METER

by

G.J. Roach and J.S. Watt

CSIRO Division of Minerals
PMB 5. Menai, NSW 2234, Australia

SEPTEMBER 1996

CONFIDENTIAL UNTIL 28TH OCTOBER, 1996

Paper to be presented to The North Sea Flow Measurement Workshop
28-31 October 1996, Peebles, Scotland

CURRENT STATUS OF DEVELOPMENT OF THE CSIRO GAMMA-RAY MULTIPHASE FLOW METER

G.J. Roach and J.S. Watt

CSIRO Division of Minerals, PMB 5, Menai, NSW 2234, Australia

ABSTRACT

The CSIRO gamma-ray multiphase flow meter (MFM) determines the flow rates of oil, water and gas in pipelines from oil wells. The MFM consists of two specialised gamma-ray transmission gauges, and pressure and temperature sensors, which are mounted on a pipe carrying the full flow of the well stream, and processing electronics which are located in a control room.

The MFM was first demonstrated in three field trials in Australia. MFM and test separator flow rates were compared using least squares regression. The relative errors (r.m.s. difference/mean flow of component), averaged over all trials, were about 4% for liquids, 8% for oil, 5% for water, and 8% for gas. These include both MFM and separator errors. The MFM has been in routine use on the West Kingfish platform since November 1994.

The MFM was recently tested over a wide range of flow rates at Texaco's flow facility, Humble, Texas. CSIRO's analysis of the trial results shows that the MFM determined water cut to an r.m.s. error of 2.0%, with scatter about the line of best fit being 1.6%. By comparison of MFM and Texaco flow results, a slip correlation has been developed which led to, over the gas volume fraction (GVF) range 0 to 90%, relative errors of 6.6% for liquids, 6.2% for gas, 8.0% for oil, and 8.1% for water.

1. INTRODUCTION

CSIRO developed and field tested a gamma-ray multiphase flow meter (MFM) over the period 1989-1995 as part of a project sponsored by ERDC, Esso Australia Ltd., The Shell Company of Australia Ltd., WAPET, and Western Mining Corporation (WMC). The project was coordinated by the Australian Mineral Industries Research Association Ltd.

The field trials⁽¹⁻³⁾ undertaken during the sponsored project were on the Vicksburg offshore oil platform (1992), at the oil processing facilities on Thevenard Island (1993), and on the West Kingfish offshore oil platform (1994-95). These oil facilities are respectively operated by WMC, by WAPET and by Esso Australia. The first two facilities are on the North West Shelf, Western Australia, and the West Kingfish platform is in the Bass Strait off the Victorian coast.

In each trial, well streams were sequentially routed past the MFM which was mounted on a "test" pipeline joining the test manifold to the test separator. The bores of the test pipelines were 139.7 mm (Thevenard Island and West Kingfish platform) and 73.7 mm (Vicksburg platform). Pressures ranged from 640 to 2800 kPa, and fluid temperatures from 24 to 96°C.

The flow rates determined by the MFM and by the test separator were compared using least squares regression, and the relative errors (r.m.s. difference to mean component flow) calculated. The relative errors, averaged over all trials, were about 4% for liquids, 8% for oil, 5% for water, and 8% for gas. These include both MFM and separator errors.

This paper describes the gamma-ray MFM, the results of the eighteen week trial (1994-1995) and of the later routine use (1995-1996) of the MFM on the West Kingfish platform, and the recent trial at Texaco's Humble facility. Comments are then made on various aspects of the MFM based on CSIRO's experience in its use particularly in field trials.

2. THE GAMMA-RAY MFM

2.1 Principles

The MFM consists of two specialised gamma-ray transmission gauges, and pressure and temperature sensors, which are mounted on a pipe carrying the full flow of the well stream, and processing electronics which are located in a control room (Figure 1). The first gauge, a density gauge, measures the intensity of 662 keV gamma-rays (^{137}Cs) transmitted through the fluids in the pipeline. The second, a dual energy gamma-ray transmission (DUET) gauge, measures the transmitted intensities of 59.5 and 662 keV gamma-rays from ^{241}Am and ^{137}Cs .

All flow rates are calculated from separate determinations of water cut (WC) and flow rates of liquids and gas. Water cut is determined by dual energy gamma-ray transmission. The flow rates of liquids and gas are determined mainly from measurements of mass per unit area of liquids across a diameter of the pipeline by the density gauge; flow velocity from cross-correlation of the outputs of the two gamma-ray transmission gauges; and operating pressure and temperature in the pipeline. Gas volume fraction is calculated from the internal diameter (I.D.) of the pipe, the densities of oil and formation water at the line operating pressure and temperature, and the combined thickness of oil and water in the gamma-ray beam. In calculation of liquids and gas flow rates from these measurements, a correction is applied to make an allowance for slip between the liquid and gas phases. Oil and water flow are respectively determined by multiplying liquids flow by (1-WC) and by WC.

The DUET gauge determines the mass fractions of oil and water in the liquids. The basis of this determination is the difference in atomic number of the oil and the formation water. The intensity of the transmitted 59.5 keV gamma-rays depends both on the atomic number of the fluid constituents and the mass per unit area of the fluids in the gamma-ray beam. The intensity of the transmitted 662 keV gamma-rays depends on the mass per unit area of fluids in the gamma-ray beam. Water cut is determined by combining these two measurements and the densities of the oil and formation water at the pressure and temperature of the flowing stream of multiphase mixture.

2.2 Hardware and Software

Figure 1 shows a schematic of the MFM mounted on a vertical pipe, and Figure 2 the MFM mounted on a vertical section of pipe at Texaco's Humble flow facility. The DUET gauge is mounted onto a "ring" which is a squat steel cylindrical shell through which the multiphase

flow passes. This ring is bolted between two flanges of the pipe. The density gauge is mounted on a C-frame which is mounted on a saddle welded to the mainline pipe.

The DUET gauge requires low atomic number windows to ensure adequate transmission of the low energy (59.5 keV) gamma-rays. Thick windows of carbon fibre reinforced epoxy composite are incorporated into the DUET gauge ring. These have been designed to pass the American Petroleum Institute's "Fire Test for Soft-seated Quarter Turn Valves" (API Spec. 6FA). The inside surface of the carbon fibre epoxy window, exposed to the multiphase fluid, is shaped to match the curvature of the cylindrical inner walls of the ring, which has the same I.D. as that of the production pipeline.

The very narrow beam of gamma-rays emerging from the radioisotope source containers traverse a diameter of the pipeline. The transmitted gamma-rays are absorbed in the NaI crystal of the scintillation detector. For the DUET gauge, the intensities of the ^{241}Am and ^{137}Cs gamma-rays are separately determined using pulse height analysis. The scintillation detector, high voltage supply and preamplifier of each gauge are mounted in an approved flameproof container. The electrical signals from the preamplifier are carried via armoured cables, first to a flameproof junction box and from there to the processing electronics which are housed in a control room. Power is carried by the same armoured cable. The processing is undertaken by a fast nuclear counting system, and the outputs, in the form of counts per five millisecond time interval, are processed by an industrial 80486 DX computer. The computer outputs the flow rates, water cut, and various other parameters which are displayed in computer graphics. The MFM presents the flow rates of oil, water and gas as separate 4-20 mA signal outputs.

3. WEST KINGFISH PLATFORM

Esso Australia Ltd. operates, for the Esso/BHP Joint Venture, all the oil platforms and gas production facilities in the Bass Strait, Australia. The MFM trials were undertaken on the West Kingfish oil platform which lies 70 km from the coast in 80 m depth of water. There are about 20 wells in production on the platform. The densities of stabilised oil and formation water are respectively 0.802 and 1.023 g cm⁻³ at STP. The flows from each of the 20 production wells are measured by the test separator twice a month.

The MFM was mounted on a vertical upflow section (ID: 139.7 mm) of the test pipeline which carries the full flow of the multiphase mixture from the test manifold to the test separator. The length of straight vertical pipe upstream of the density gauge was 1500 mm (11 pipe bores).

3.1 Eighteen Week Trial

The eighteen week trial of the MFM on the West Kingfish platform was undertaken from November 1994 and March 1995. Prior to start of trial, all meters at the separator outputs were upgraded/replaced to ensure the best accuracy and reliability possible within operating constraints on the platform. Sand was cleared from the test separator. After installation of the MFM, the count rates for both gauges, and pressure and temperature, were sequentially measured with the pipe full of oil, formation water, and gas. These measurements are the

basis of the calibration of the MFM for the specific characteristics of the fluids from the oil field.

The MFM was calibrated by least squares regression of MFM and separator measurements obtained during the first (two week) round of well tests. The calibration, common to all well flows, was later found to be the same as that determined from the results of all well tests undertaken over the eighteen week trial.

The results of the trial are shown graphically in Figure 3, and the relative errors are detailed in Table 1. The MFM and separator results are obviously well correlated. The relative errors quoted are the combination of the errors both of the MFM and of the separator. Two sets of relative errors are given in Table 1. The first corresponds to all well measurements taken as separate data points, similar to those shown in Figure 3. The second corresponds to one data point for each well, each point being the average of all measurements on the same well over the eighteen week trial. The relative errors calculated using these averages for each well are considerably lower than those for all the well measurements treated separately.

3.2 Routine Use on Platform

Esso has continued to use the MFM on the WKF platform since the eighteen week trial under an arrangement with the CSIRO and involving CSIRO monitoring its operation via modem. The MFM has been in routine, 24 hours per day, operation. It soon became apparent that, for a good assessment of the MFM, CSIRO would also require a continuous record, over the one hour period of each well test, of the flows measured by the test separator output meters. This recording of separator flows was achieved in February 1996, with 30 second updates fed to the MFM computer.

The experience from the comparison of MFM and test separator flow determinations from March to the present date is that the MFM and separator determinations of liquids, water and gas flow rates generally agreed well, with accuracies for the MFM approximately the same as for the 18 week trial above.

4. TRIAL AT HUMBLE

The MFM was tested over a wide range of liquids and gas flow rates, gas volume fractions (GVFs), and water cuts, at Texaco's multiphase flow facility, Humble, Texas. CSIRO's analysis of the trial results, subsequent to the trial, has shown that the MFM determined water cut in all streams (GVFs: 6-98.4%) to an r.m.s. error of 2.0% over the range 0 to 100% water cut, and using least squares regression, to an r.m.s. difference of 1.6% (Figure 4). A slip correlation was developed by comparing the MFM and Texaco flow results. The MFM and Texaco liquids and gas flow rates were then compared using least squares regression. Over the gas volume fraction range 10-90%, the relative errors were 6.6% for liquids, 6.2% for gas, 8.0% for oil, and 8.1% for water.

The MFM slip correlation, determined from comparison of MFM and Texaco flow data, was applied to predict the flows at the West Kingfish platform. The liquids flows were determined to 15% (scatter about regression line: 5.4%), and the gas flows to 11%.

A calibration for liquids and gas flows, based on Australian field trial experience, was incorporated into the MFM for the trial at Humble. The Australian calibration was shown to determine liquids and gas flows at Humble to relative errors respectively of 13% and 15%, for mixtures with GVF's in the range 25 to 85%, and more in error over a wider range of GVF's. This is a reasonable agreement considering that the range of GVF's experienced in Australia was limited to 65 to 87%, and the Australian experience was based on light oils, compared with the medium density crude used at Texaco's facility.

5. DISCUSSION

Comments are now made on various aspects of the MFM based on CSIRO's experience in its use particularly in field trials.

5.1 Determination of water cut

The accurate determination of water cut is a feature of the gamma-ray MFM. The determination of water cut by the DUET gauge is independent of flow regime, continuous phase (oil or water), and emulsion, and sand and corrosion inhibitor at levels normally occurring in well streams. The offset and scatter in water cut determined during Humble trial were small, with offset of about 1.2% and scatter of 1.6%.

5.2 Reliability

The prototype MFM has proved to be reliable on the West Kingfish platform. The carbon fibre epoxy windows in DUET gauge ring have been demonstrated successful, with the windows showing no detectable wear over 22 months on-line. There have been two failures of the MFM equipment over the extended period of its operation on the platform: a hard disk crashed irretrievably within 2 weeks of installation, and a fan in the processor box failed after 7 months of operation (not entirely unrelated to the fact that a 12 volt rating fan was by mistake put on a 15 volt line). Both of these breakdowns occurred in the processing electronics in the control room, and none have occurred in the head units mounted on the pipeline.

One reason for the reliable operation of the MFM is that it is non-intrusive and does not depend on use of moving parts as with, say, turbine meters. The West Kingfish trial has demonstrated that the advanced prototype of the gamma-ray MFM is highly suited to unattended operation on offshore oil platforms.

5.3 Calibration

Ideally, MFMs should be configured based on knowledge of the properties of the well fluids, pressure and temperature, and the geometry of the pipeline, to have a universal equation covering all flow conditions. In practice, the MFM at its present stage of development requires calibration for liquids and gas against known flow rates to give the on-line calibration. We have extended the calibration over a range of flow rates and conditions based on the results of the Humble field trial and the Australian field trials, but further experience is required for some flow conditions not yet experienced.

The calibration for liquids and gas flow rates depends at present on deriving a correlation for slip based on MFM and separator measurements, as undertaken at Humble. Once the slip corresponding to a particular set of flow conditions has been determined, this calibration can be used in any future installation of the MFM for these flow conditions. The determination of oil and water flow rates simply depends on the liquids and water cut determinations.

The determination of water cut is now well understood, and calibration has now been simplified to making sequential measurements with the pipe filled with (static samples) oil, formation water and gas, and knowledge of the densities of oil and formation water, and the solubility of the gas in the fluids, as a function of pressure and temperature. The gamma-ray measurements required for calibration on static samples are normally undertaken on-line at the field site.

5.4 Operational advantages

The MFM has important operational advantages over the test separator/output meters system. The MFM is more reliable and requires far less operator support and time for determination of the well flows. The MFM operates continuously with operator intervention only being required to switch the appropriate stream through the pipe on which the MFM is mounted. Since the MFM can be mounted on the pipeline between the manifold and the production separator, there is no need for stabilisation of the well flow prior to the MFM measurement. With the test separator, each well must be stabilised prior to determination of flow rates because it operates at a different pressure to that of the production separator.

Operator intervention is required with the test separator when there is a considerable change in flow rates of oil or water or gas to ensure that the single phase output streams are routed to the appropriate output meter. For example, on the West Kingfish platform, the output oil and water streams are monitored by turbine meters, with both high and low flow meters on each stream. The gas flow output is metered by a high range orifice plate and a low range vortex meter. The one MFM on the West Kingfish platform measures all the component flow rates from all the wells fed to the platform; six single phase flow meters are required for use with the separator. The MFM has been shown to operate over a much wider range of flow rates of liquids, oil, water and gas than can be handled by the test separator and its output meters.

The MFM does not require regular maintenance such as removal of sand from the separator.

5.5 Engineering and other developments

The MFM can be adapted for use on a wide range of pipe diameters simply by adapting the design of DUET gauge ring or use of an appropriate diameter carbon fibre/epoxy spool piece. The DUET gauge with the ^{241}Am and ^{137}Cs radioisotope pair is suitable for use on pipelines with diameters between about 4 and 12 inches. For smaller diameters, use of ^{137}Cs (Ba K X-rays and 662 keV gamma-rays) would be appropriate.

The full limits of the MFM's operating envelope have not yet been determined. For example, there is little doubt that the GVF range can be extended considerably beyond the 10 to 90% GVF range which the authors have previously assumed were the limits to the operating envelope.

The simplicity and reliability of the MFM indicates its suitability for subsea development.

6. CONCLUSION

The gamma-ray MFM, successfully demonstrated in three Australian field trials and in long-term operation on the West Kingfish platform, is now suitable for routine use off-shore on platforms. CSIRO has recently gained considerable experience with the operation of the MFM over a wide range of flow rates, during the trial at Texaco's multiphase flow facility at Humble, Texas. This trial greatly extended the operating envelope over which the MFM has been successfully demonstrated.

7. ACKNOWLEDGMENTS

The authors wish thank a) the sponsors of the six year project (see Introduction) for their advice and unstinting support, and Mr. David Stribley for his role in coordinating the sponsored project b) Dr. E.R.Thomas, Exxon Production Research, and the Exxon company, for support of the trials at Texaco's Humble facility, c) Dr. Cliff Redus, and Dr. Jack Marrelli, and other Texaco staff, for their enthusiasm and great support during the trials at the Humble facility, and d) Mr. Tom Dermott of Esso Australia Ltd., and staff on the West Kingfish platform, for their encouragement and support relating to all aspects of work on West Kingfish platform.

8. REFERENCES

1. ROACH, G.J., WATT, J.S., ZASTAWNY, H.W., HARTLEY, P.E. and ELLIS, W.K. (1994). Multiphase flow meter for oil, water and gas in pipelines based on gamma-ray transmission techniques, *Nucl. Geophys.* **8** (3) 225-242.
2. ROACH G.J., WATT J.S., ZASTAWNY H.W., HARTLEY P.E. and ELLIS W.K. (1995). Field trial of a gamma-ray multiphase flow meter on Thevenard Island, *Nucl. Geophys.* **9** (1), 1-17.
3. HARTLEY, P.E., ROACH, G.J., STEWART, D., WATT J.S., ZASTAWNY, H.W. and ELLIS, W.K. (1995). Trial of a gamma-ray multiphase flow meter on the West Kingfish oil platform, *Nucl. Geophys.* **9** (6) 533-552.

Table 1. Relative errors for flows and water cut corresponding to the average, for each well, of the measurements over the eighteen weeks trial, and to each individual well treated separately.

Parameter measured	Relative error (%)	
	Mean for each well	All individual measurements
Liquids	2.8	3.9
Water Cut	2.4	3.3
Gas	6.3	7.6
Oil	5.1	7.9
Water	4.0	5.2

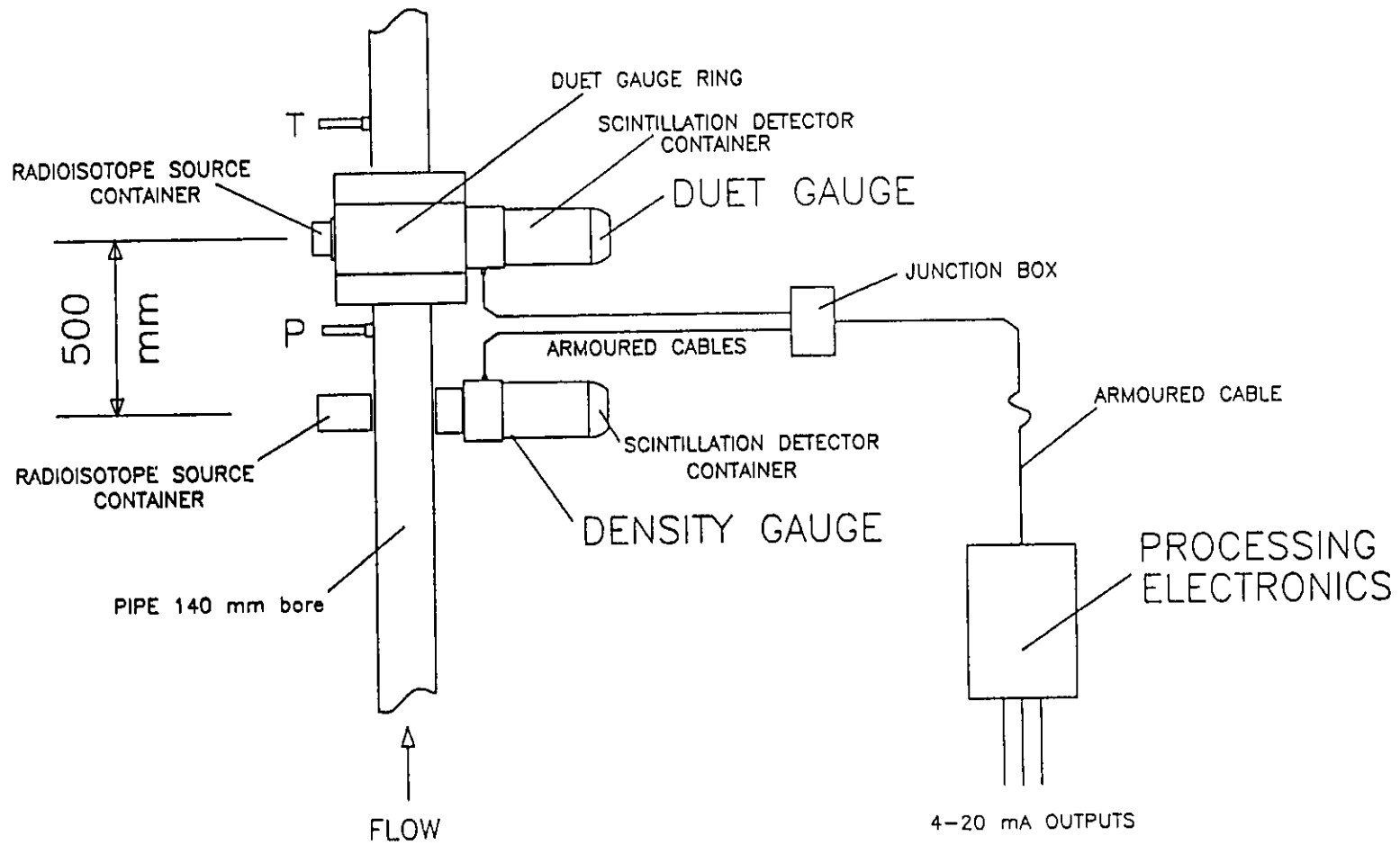


Figure 1. Schematic of the CSIRO MFM mounted on a six inch pipeline. P and T are pressure and temperature sensors.



Figure 2. Photograph of the CSIRO MFM mounted on a pipeline at the Humble facility.

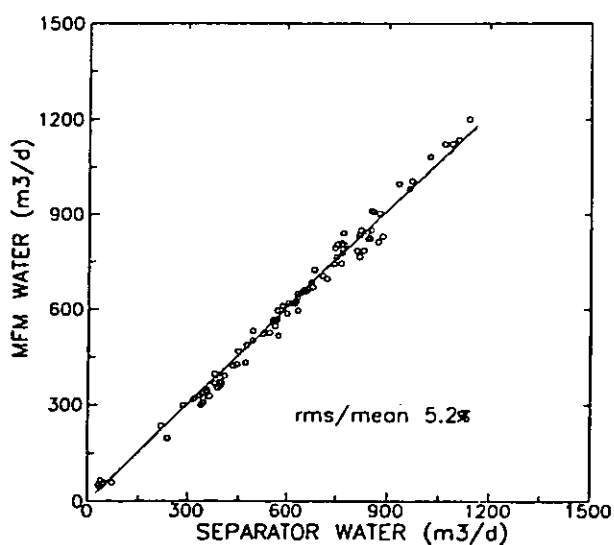
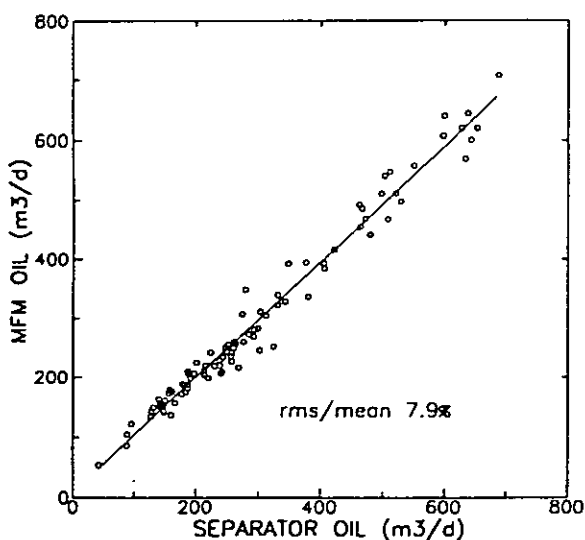
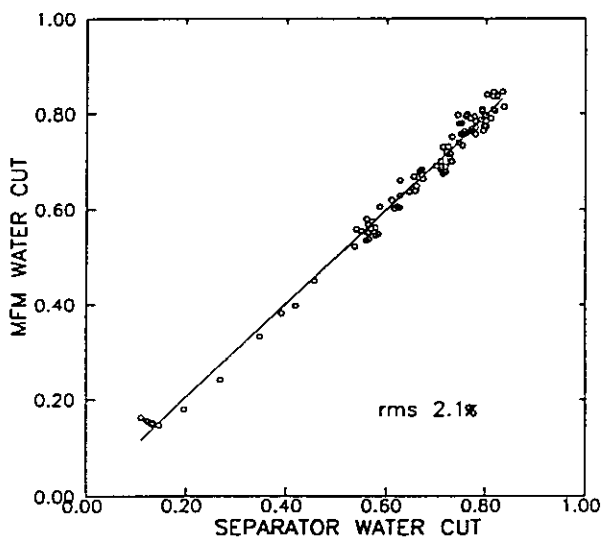
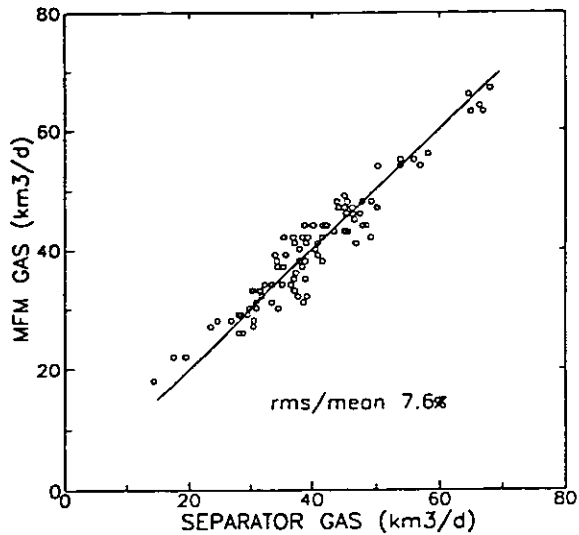
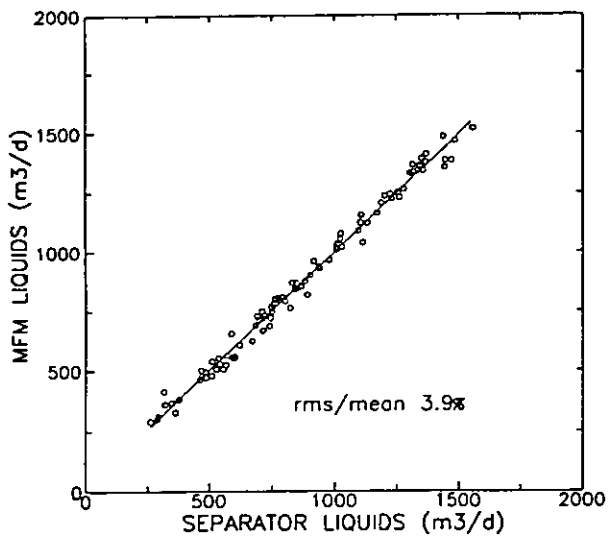


Figure 3. MFM and separator determinations of flow rates and water cut during the 18 week trial on the West Kingfish platform.

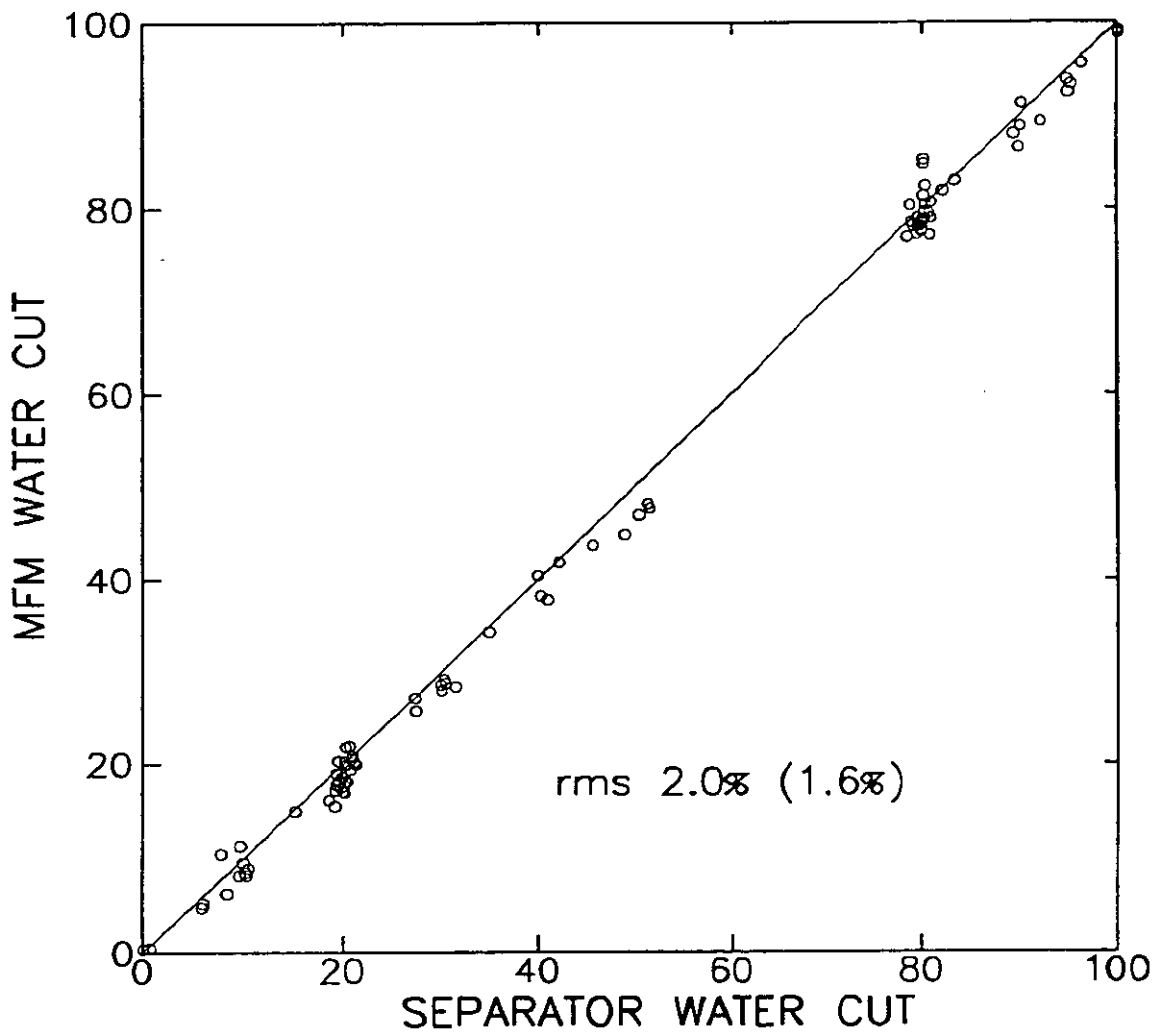


Figure 4. MFM and separator determinations of water cut at Texaco's Humble flow facility.

THE DENSITY OF RICH NATURAL GAS MIXTURES

James T. R. Watson
Jeffrey L. Savidge

NEL, East Kilbride, Glasgow, G75 0QU, UK.
Gas Research Institute, Chicago, Illinois, 60631, U.S.A.

Abstract

A major programme of work is being undertaken at NEL to establish reference-quality measurements of density for ten natural gas mixtures typical of those recovered from North Sea condensate fields. The measurements are being made using the UK's primary standard densitometer for gases over a range of pressures and temperatures commensurate with typical metering conditions. A description of the modified apparatus is presented together with preliminary findings for the first three mixtures.

This Joint Industry Project, being undertaken in collaboration with the Gas Research Institute and major oil and gas companies, will lead to a revision of the AGA8 equation allowing calculations to be made of the density of rich natural gas mixtures, at typical metering conditions, with a target uncertainty commensurate with fiscal-quality requirements.

1. INTRODUCTION

As a result of difficulties in the use of commercial densitometers for the metering of natural gas mixtures, many operators have opted to determine the density of the gas flows indirectly by gas chromatography. Density, in this instance, is derived from an equation of state and a knowledge of the temperature, pressure and composition of the gas. The equation of state most widely used with the gas chromatographic technique is the Detail Characterization Method or AGA8 equation developed by the American Gas Association^[1]. This equation is valid for lean natural gas mixtures over a wide range of conditions but its application to rich natural gases (some 60 % mole fraction of methane), as encountered in gas condensate fields, is untested.

In principle, the gas chromatographic technique for the determination of density should be as effective as that using fully calibrated and traceable densitometers. This assumes that a valid equation of state is employed for the gas mixture and that measurements of temperature, pressure and composition are made to a sufficiently high standard. However, indications are that for gases from condensate fields, at metering conditions of between 80 and 180 bar pressure and 40 to 80°C, differences of some 2.0 to 2.5% are regularly being observed between density values determined from the AGA8 equation and those monitored by gas densitometer.

There are a number of possible sources of error which could give rise to differences in density of this magnitude. The major causes were considered to be:-

- residual installation effects on the gas densitometer;
- errors in the analysis of composition possibly resulting from poor sampling techniques; and
- the suitability of the AGA8 equation for use with rich natural gas mixtures.

A Joint Industry Project (JIP) was established, in conjunction with the Gas Research Institute, a number of major oil and gas companies and two public bodies, to investigate the applicability of the AGA8 equation of state to rich natural gas mixtures. A major programme of work is now in progress at NEL to establish reference-quality measurements of density for ten natural gas mixtures typical of those recovered from North Sea condensate fields. The measurements are being made using the UK's primary standard densitometer for gases over a range of pressures and temperatures commensurate with typical metering conditions.

The principal objectives set by the JIP were to:-

- to determine the magnitude of the differences between the AGA8 equation of state and reference-quality density data produced for ten synthetic natural gas mixtures in the range $80 \geq p/\text{bar} \geq 180$ and $40 \geq t/^\circ\text{C} \geq 80$, which bracket current metering conditions; and
- to provide reference-quality density data for use in subsequent refinements to the AGA8 equation.

To prevent any loss of measurement accuracy in the near critical region and change of composition in the vicinity of the phase boundary it was agreed that the lower temperature of measurement for any specific system was a minimum of 10°C above the cricondenterm for the mixture.

2. DESIGN AND OPERATION OF THE FILLING CIRCUIT

The condensible nature of the rich natural gas mixtures required the use of an alternative filling circuit to that developed previously for the primary standard densitometer^[2]. Calculations showed that a significant source of measurement error could arise from small leaks of the test gas over prolonged periods of time from any part of the high-pressure circuit. Selective loss of the lighter components would lead to changes in the composition of the mixture and would, if not prevented, give rise to a significant systematic error of measurement. Circuit components with very low leakage rates were required to minimise this effect.

Though most of the existing pipework and valves might have proved suitable the leakage rate from one key component of the original pressure measurement circuit (a

hand-operated variable volume unit used to balance the pressure in the test and reference gas circuits) was known to be unsatisfactory. Despite modification, small but detectable leaks were still apparent from this component. A decision was taken to develop a new filling and pressure measurement circuit based on valves and fittings of the highest quality as used in the semiconductor industry. Although the valves have a working pressure limit of only 200 bar this was adequate for the planned series of measurements.

2.1 Minimisation of Loss of Component

As discussed any loss of component from the test mixtures during either the filling cycle or during the prolonged period of measurement would be selective and result in a change of composition of the test mixture. The problem of containment is exacerbated in this instance by the limited quantities of gas available. Great care was taken in the design of the loading facility to eliminate possible leakage sources and to prevent condensation from occurring in any part of the circuit.

A temperature-stabilised enclosure houses the new filling circuit, see Figure 1 for details. The enclosure is insulated and its temperature maintained at 55 °C by a heat exchange unit fed from a temperature-controlled circulation bath. The enclosure contains the sample gas cylinder, the compressor, all valves and most of the pipework.

Modifications were made to the compressor, a commercial, two-stage unit with a compression ratio of 40 to 1. The interstage cooler was removed to minimise the potential for phase changes resulting from rapid cooling, and of most of the original pipework replaced with low-leakage components. The compressor was also carefully adjusted to prevent stall at elevated pressures.

Diaphragm-sealed valves were utilised to eliminate the possibility of leakage past valve stems. Cajon VCR pipe fittings, suitable for both elevated pressure and high vacuum use, and welded joints, where possible, were used to minimise leakage from pipework and fittings.

The high-pressure line which leads from the filling circuit to the densitometer is trace heated and lagged. A resistance thermometer, placed in close thermal contact with the line, is used to monitor its temperature. The temperature of the line is maintained at 50.0 ± 0.1 °C by an electrical heater controlled by a three-term controller. Temperature fluctuations in the external components connected to the densitometer have an influence on the stability of the pressure and density of the test gas within the vessel. With moderately good temperature control the influence of these fluctuations can be reduced to acceptable levels by keeping the internal volume of the external circuit small compared to that of the densitometer. Here, the internal volume of the pipework, valves and transducer exposed to the test gas have been kept to some 4 ml, or about 1 % of the internal volume of the densitometer.

Prior to use the circuit was tested under vacuum and at pressure using both helium and nitrogen.

2.2 Pressure Measurement

Pressure measurements were made using a Parascientific transducer type 43K-101 which was supplied together with calibration certificate for use in the range 0-3000 psia at temperatures up to 125 °C. A 10 kg aluminium block was machined to house two such transducers together with two electric cartridge heaters and a platinum resistance thermometer. The block and the short length of pipework leading to the transducer were lagged with suitable insulation material. The temperature of this block is maintained at 50 ± 0.1 °C by a three-term proportional controller.

A digital display unit provides the necessary power supply to the transducer and undertakes the measurement of the time period for both the pressure and temperature elements. This display also gives a visual indication of the indicated pressure in bar. As the resolution of the display is limited to ± 0.01 bar it is not used for accurate measurement of pressure.

The pressure indicated by the transducer is a function of the period of oscillation of both the pressure and temperature components:-

$$p = p(\tau_p, \tau_T, a_1, \dots, a_{14}),$$

where τ_p and τ_T are the pressure and temperature periods, respectively, in μs , and a_1 to a_{14} are the calibration coefficients as determined by the supplier.

The calibration of the transducer was checked in situ against a Desgrange and Huot, metrology Class S2, gas-operated pressure balance together with a Druck digital pressure indicator for ambient pressure measurement. The uncertainty of the D&H balance is 0.005 % of indicated gauge pressure and that of the Druck is 0.015 % of ambient pressure. The circuit leading to the transducer was fitted with a small filter unit containing activated carbon to remove any traces of oil vapour which may be present in the nitrogen gas from the D&H balance. The checks on calibration were made at zero-pressure and at 10 bar intervals between 50 and 190 bar. The differences between the pressures calculated from the supplier's calibration equation and the known applied pressures are within a maximum of 14 mbar over the pressure range of the proposed measurements. Evidence from NIST (Boulder) and Imperial College suggested that the pressure component of calibration of this type of transducer remain constant over long periods of time, six months or more, but that the zero-pressure component, or offset, drifts more quickly with time. Software was developed to calculate the pressure at the transducer from its pressure and temperature periods. The software corrects the pressure calculated from the supplier's equation for the differences in pressure observed at calibration and for subsequent drifts in the zero-pressure offset. The results obtained to date suggest that the total uncertainty in the corrected pressure is within 7 mbar, or 0.01 % throughout the measurement range. This figure includes the uncertainty arising from the calculation of pressure heads in pipelines.

At the end of each set of isochoric measurements the pressure transducer is evacuated and the temperature and pressure period recorded. The zero-pressure offset is used to correct subsequent measurements of pressure. At the end of each series of

measurements on a mixture the calibration of the transducer is fully rechecked using the D&H and Druck pressure standards.

2.3 Density and Temperature Measurement

Density measurements were made using the primary standard densitometer, a dual-sinker magnetic-suspension densitometer, as described in reference 2. The only differences in equipment between the apparatus described and that used here relate to the use of the new filling circuit and the method of pressure measurement. The uncertainty in the measurement of pressure as assessed, from all observations made to date, is 0.01% of indicated pressure.

Temperature measurements were made using four standard 25 ohm platinum resistance thermometers as described in reference 2. The total uncertainty in measured temperature is 4 mK. The temperature in the main densitometer system can be set by computer controlled equipment to within a few milli-kelvin of any prescribed temperature in the interval -40 °C to 150 °C.

The total, or combined, uncertainty to be associated with each measurement of density at the specified temperature and pressure is given by the following expression:-

$$U_{\rho, \text{total}}^2 = U_{\rho}^2 + [(\partial\rho/\partial T)_p \cdot U_T]^2 + [(\partial\rho/\partial p)_T \cdot U_p]^2,$$

The measurement uncertainties in density, U_{ρ} , temperature, U_T , and pressure, U_p , were assessed for each individual measurement and take account of all factors excluding adsorption. The partial derivatives in the above expression were calculated at each point from the AGA8 equation of state. Using the above expression the combined uncertainty in density was calculated to be within 0.02% for each of the reported measurements.

2.4 Mixture Preparation and Handling

All of the gas mixtures were prepared for NEL by the National Institute for Standards and Technology (NIST) at Boulder, using their gravimetric standard. Each mixture was prepared by carefully weighing pre-determined quantities of the pure component gases into an evacuated and thoroughly degassed cylinder at 20 °C. The quantities of components added were such that the final filling pressure at this temperature was some 80 % of the dew-point pressure for the mixture. The filling pressures for the seven mixtures ranged from 22 to 35 bar at 20 °C. Since the quantity of gas contained in each 11 litre cylinder was limited, two cylinders of matching composition for each mixture were obtained.

Following shipment to NEL the gas cylinders were stored in a specially prepared room, fitted with gas sensors and an emergency evacuation system, and maintained at a temperature of around 55 °C (some 20 °C or more above the cricondentherms for the mixtures) for a minimum of three weeks prior to usage. The cylinders were turned on a regular basis during pre-treatment to ensure that any drop out of higher

hydrocarbons which might have taken place during shipment was completely reversed and that all components were in the gaseous phase.

2.5 Operating Procedure

Normally measurements of density would have been made on individual isotherms starting at the lowest pressure and steadily incrementing the pressure until the maximum test value had been reached. Because of the limited amount of gas contained in each sample cylinder and because of the possibility of selective loss of component from prolonged containment of the test gas in the compressor this procedure was rejected in favour of the following 'isochoric' method.

A planned measurement schedule for each mixture was prepared which conserved gas utilisation and minimised any loss of components through the gas compressor. A set of 48 state points for each mixture, uniformly distributed throughout the measurement range, were determined at eight prescribed temperatures using the AGA8 equation of state to model the mixture. The algorithm took no account of the small external volume of pipework linking the densitometer to the pressure transducer and the isolation valves or of the dilation of the densitometer and pipework with temperature and pressure. The first state point in each case corresponded to the highest pressure at the lowest temperature of measurement. Successive groups of state points corresponded to points on six 'isochores' spanning eight prescribed temperatures. Figure 2 shows the distribution, and the sequence, of measurement points for mixture 1. The filling and measurement sequence for each mixture was as follows:-

- (1) The densitometer and associated pipework were brought to working temperature, flushed several times with a small amount of test gas, then evacuated to a pressure of around 1 Pascal.
- (2) The densitometer was filled slowly with the test gas to the maximum working pressure at the lowest temperature of measurement.
- (3) The densitometer and pressure measurement system were isolated from the compressor and gas storage system.
- (4) Subsequent adjustments to the system pressure on the six 'isochores' were made by dropping the system temperature by 5 °C to the next predetermined measurement point.
- (5) On completion of measurements on an 'isochore the temperature was reset to the highest temperature for that isochore and the measurement of density repeated.
- (6) The system pressure was carefully reduced to the pressure corresponding to the first measurement point on the next isochore.

All pressure changes were made at the highest temperature of measurement for each isochore. A slow and controlled discharge was effected by returning the gas via a 3 m long capillary tube, maintained at around 54 °C, to the supply cylinder.

Density measurements at each of the 48 pre-determined state points for each mixture were made after full temperature and pressure stabilisation had been achieved. This normally took a period of 3 hours. The differences in density observed between the initial

and the repeat measurements on each isochore, made some days later, are consistent, when corrected to the same T and P, to within some 30 ppm. No observable changes in pressure were recorded between the first and repeat density measurement on each isochore.

3. RESULTS

3.1 Mixture Compositions

All gas mixtures have been prepared by the National Institute for Standards and Technology (NIST Boulder), using their gravimetric standard facility. The reported compositions of the mixtures used in this work are:-

Component	Composition/(% mole fraction)			
	Mixture 1A	Mixture 1B	Mixture 2B	Mixture 3A
methane	59.00282	59.00126	59.00555	58.98993
nitrogen	4.99504	5.00063	4.99786	5.01541
carbon dioxide	6.00502	5.99242	6.01770	5.97568
ethane	10.00080	9.99694	15.00506	18.01148
propane	14.01250	14.02653	9.99485	8.00367
n-butane	5.98382	5.98222	4.97898	3.29625
n-pentane	-	-	-	0.49186
n-hexane	-	-	-	0.21573
No. of components:	6	6	6	8
Molar mass / (kg/mol):	0.026171996	0.026171858	0.025327872	0.02490049
Cylinder Identity:	LL-10807	LL-10808	LL-10805	LL-10797

Each mixture was prepared by carefully weighing pre-determined quantities of the pure component gases into an evacuated and thoroughly degassed cylinder maintained at 20 °C. The purity of each of the component gases was verified by gas chromatography. The final filling pressure for each mixture was kept to 80% of the dew point pressure for the mixture at 20 °C. Filling pressures ranged from 22 to 35 bar.

3.2 The AGA8 Equation of State

The AGA8 equation was developed as a means of establishing accurate densities and compressibility factors for a range of natural gas mixtures and related hydrocarbon gases over a wide range of operational conditions. The coefficients of the equation were determined by regression to an extensive bank of experimental data for natural gas mixtures and for binary and higher order mixtures of hydrocarbons with nitrogen, carbon dioxide and other gases.

The uncertainties to be expected in density values calculated from AGA8 depend upon the composition of the natural gas and on both the temperature and pressure at the metering

conditions. The targeted uncertainties (at one standard deviation) for the AGA8 equation of state in terms of temperature and pressure are:-

Region	Temperature Range	Pressure Range	Uncertainty in Density
1	- 8 to 62°C	0 to 120 bar	0.1 %
2	- 60 to 120°C	0 to 170 bar	0.3 %
3	-130 to 200°C	0 to 700 bar	0.5 %
4	-130 to 200°C	0 to 1400 bar	1.0 %

The AGA8 equation is claimed to meet these expected or targeted uncertainties in density for gas mixtures having a normal range of compositions, see below, within Region 1 and in parts of Regions 2, 3, and 4. For the expanded range of compositions given in the following table the uncertainties in density are expected to be higher than those for the normal composition range, especially in Regions 2 to 4.

Component	Normal range		Expanded range	
	Lower Limit	Upper Limit	Lower Limit	Upper Limit
Methane	45	100	0	100
Nitrogen	0	50	0	100
Carbon dioxide	0	30	0	100
Ethane	0	10	0	100
Propane	0	4	0	12
Butanes	0	1	0	6
Pentanes	0	0.3	0	4
Hexanes plus	0	0.2	0	dew point

Details for seven inorganic compounds have been omitted from the above table. The temperatures and pressures at the metering conditions associated with the newer North Sea fields lie within Regions 1, 2 and 3 of the AGA8 equation. The composition of the natural gases extracted from these fields are, however, of much richer composition than those used in the development and testing of the AGA8 equation.

The measurements of density were compared with density values calculated from a software package based on the latest version of the AGA8 equation of state^[1]. The values of the constants and parameters of the equation used in the software implementation were adjusted in accordance with the errata issued in June 1993^[1]. The molar masses of the component gases were also replaced by the latest recommended values^[3].

All temperatures measured in the current programme of work are on the ITS-90 temperature scale^[4] whereas the AGA8 equation is based on the IPTS-68 scale^[5]. For the purpose of comparison, each of the measured values of temperature were converted to the IPTS-68 scale.

3.3. Comparison of Measurements with AGA8

Measurements on five gas mixtures have been completed. Outline details of the results for the first three mixtures are given here. Because of the commercial interest in the work only general trends can be given at this stage. Full details of the measurements and their comparison with the AGA8 equation may be published in the open literature at some future date.

For all of the reported measurements the total uncertainty in the measured value of density at the specified temperatures and pressures is within 0.02 %. The measured densities have been compared with values calculated from the AGA8 equation of state. The differences are defined in percentage terms as :

$$100 \cdot (\rho_{\text{meas}} - \rho_{\text{AGA8}}) / \rho_{\text{AGA8}}$$

Two forms of plot have been prepared; bubble plots , as described below; and a deviation plot showing the trend of the percentage differences for the various 'isochores' with density.

The bubble-plot diagram contains four main items:-

- a) a solid curve showing the calculated phase boundary for the mixture;
- (b) a dashed line showing the critical isochore for the mixture;
- (c) a series of circles centered at the pressure and temperature of each measurement of density. The diameters of the circles are proportional to the magnitude of the percentage differences at that point; and
- (d) a single circle in the top-left of the diagram showing the scale of the percentage differences. For commercial reasons this item is blanked out.

Plots showing the trend of the agreement between the measured and calculated densities are given in Figures 3 to 6. A similar comparison has been made for the BWRS equation of state. However, the agreement obtained between measured and calculated densities was almost an order of magnitude poorer than for the AGA8 equation. Comparisons with the NX19 and the Standing and Katz equations may be made at some future date.

3.4 Analysis of Results

From Figure 6 it can be seen that the AGA8 equation is in best overall agreement with the results for mixture 2A, followed fairly closely by those for mixture 3A. The differences for mixtures 1A and 1B, which have closely matched compositions, are considerably larger than for the other two mixtures. For all three mixtures the agreement improves both at low pressures and at high temperatures.

In the following table the compositions of the C₂ to C₆ components for the three mixtures are listed together with the limiting compositions of the same for both the normal and extended range of operation of the AGA8 equation, see section 3.2.

Component	Upper Limit of Normal Composition Range for AGA8 / %	Upper Limit of Extended Composition Range for AGA8 / %	Component Composition in Mixture/%		
			Mix. 1	Mix. 2A	Mix. 3A
Ethane	10	100	10	15	18
Propane	4	12	14 #	10	8
Butanes	1	6	6 #	5	3.3
Pentanes	0.3	4	-	-	0.5
Hexanes	0.2	dew point	-	-	0.22

From this table it should be noted that the composition of the C₂ to C₆ components of the mixtures, with one exception, all lie in the extended range of compositions. The propane content of mixture 1 lies beyond the limit of the extended range; the butane content of the same mixture is just within its limit for this range.

Of the differences observed those for mixture 1 are significantly larger than those for the other two mixtures. The best agreement between the results reported here and the AGA8 equation is for mixture 2A, followed by mixture 3A.

The higher hydrocarbon content of mixtures 2A and 3A are each within the extended composition limits of the AGA8 equation. Though good agreement is obtained with the data for both mixtures the predictive capability of the AGA8 equation is diminished by the presence of 0.5% pentane and 0.22% hexane in mixture 3A.

Mixture 1, however, exceeds the extended range composition limit for propane and is just within this limit for butane. It would therefore appear that the maximum differences between measured and calculated densities occur for those mixtures with component compositions above the extended range of compositions specified for the AGA8 equation.

4. CONCLUSIONS

The AGA8 equation of state^[1] gives a better representation of the data for these rich natural gas mixtures than had been expected at the outset of this work. Evidence to-date suggests that the maximum differences between measured and calculated densities occur for those mixtures with component compositions above, or possibly close to, the extended range of compositions specified for the AGA8 equation.

This result is not entirely unexpected and it is to the credit of the developers of the AGA8 equation that it performs as well as it does in the extended range of compositions.

The reference-quality density measured produced during the course of this JIP will allow refinements to be made to the parameters of the AGA8 equation which will:

- extend its normal compositional range; and
- improve its ability to determine accurately the density of a broad range of natural gas mixtures.

ACKNOWLEDGEMENTS

The authors are grateful to Amerada Hess Ltd., Amoco(UK) Exploration Co., Gas Research Institute, Lanarkshire Development Agency, Norsk Hydro AS, Phillips Petroleum Co.(UK) Ltd., Shell UK Exploration Ltd, Scottish Enterprise Operations, Statoil, and Texaco Britain Ltd for their technical participation in, and financial support of, this project and their permission to publish this paper.

REFERENCES

- (1) K.E. Starling and J.L. Savidge. *Compressibility Factors for Natural Gas and Other Related Hydrocarbon Gases*, Transmission Measurement Committee Report No. 8, American Gas Association, 2nd Edition, November, 1992. Also Errata No. 1, issued by the American Gas Association in June, 1993.
- (2) Watson, J. T. R., Ferguson, D. and Ryan, G. *National Standard Facilities for the Density of Liquids and Gases at Elevated Pressures*. Paper presented at Density Seminar held in James Watt Conference Centre, NEL, Glasgow, UK, on 24 October, 1994.
- (3) IUPAC Commission on Atomic Weights and Isotopic Abundances. *Atomic Weights of the Elements 1993*. J. Phys. Chem. Ref. Data, 1995, 24(4), 1561-1576.
- (4) Preston-Thomas, H. *The International Temperature Scale of 1990 (ITS-90)*. Metrologia, 1990, 27, 3-10.
- (5) Preston-Thomas, H. *The International Temperature Scale of 1968 - Amended Edition of 1975*. Metrologia, 1976, 12, 7-17.

Figure 1. Schematic Diagram of Modified Filling Circuit.

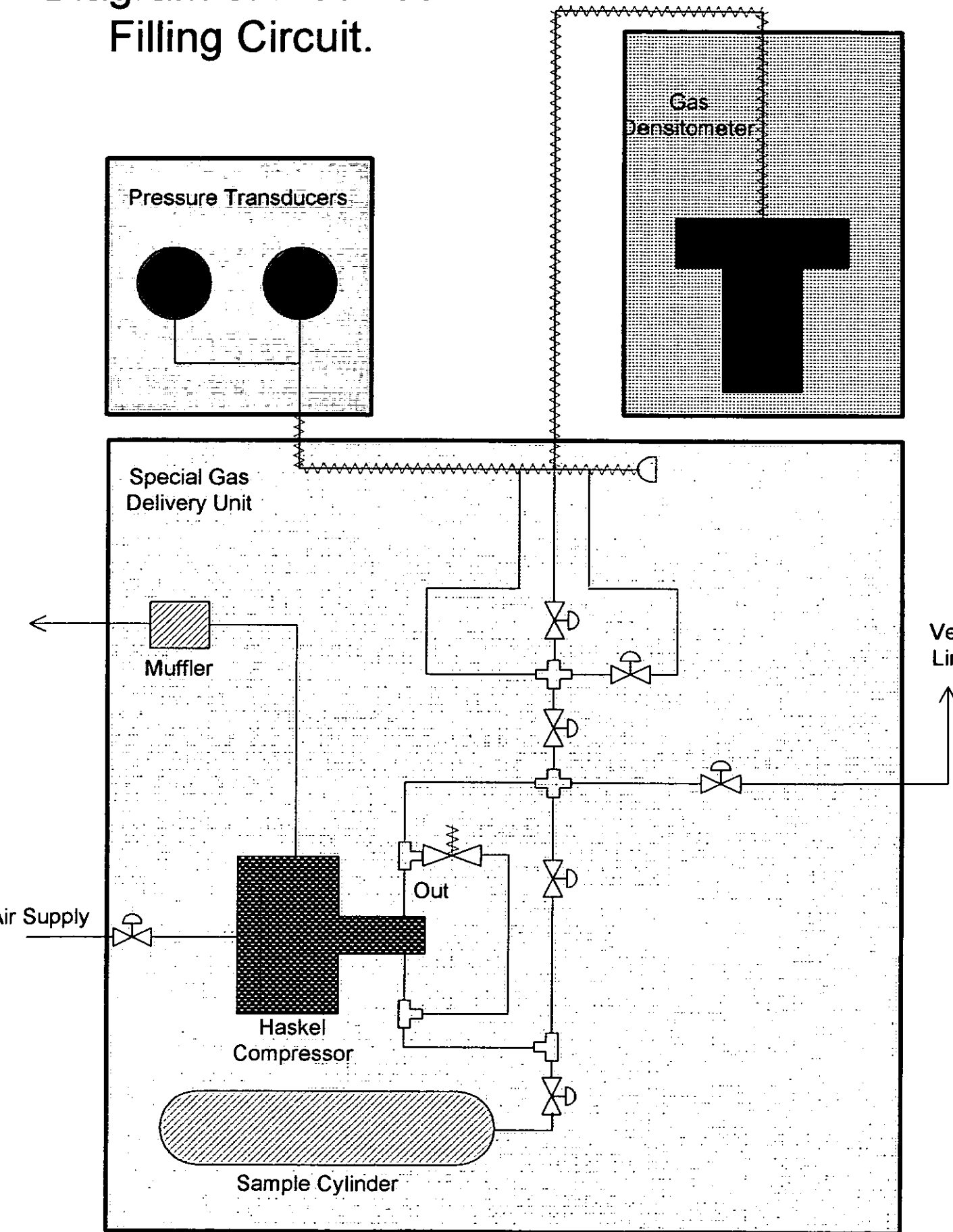
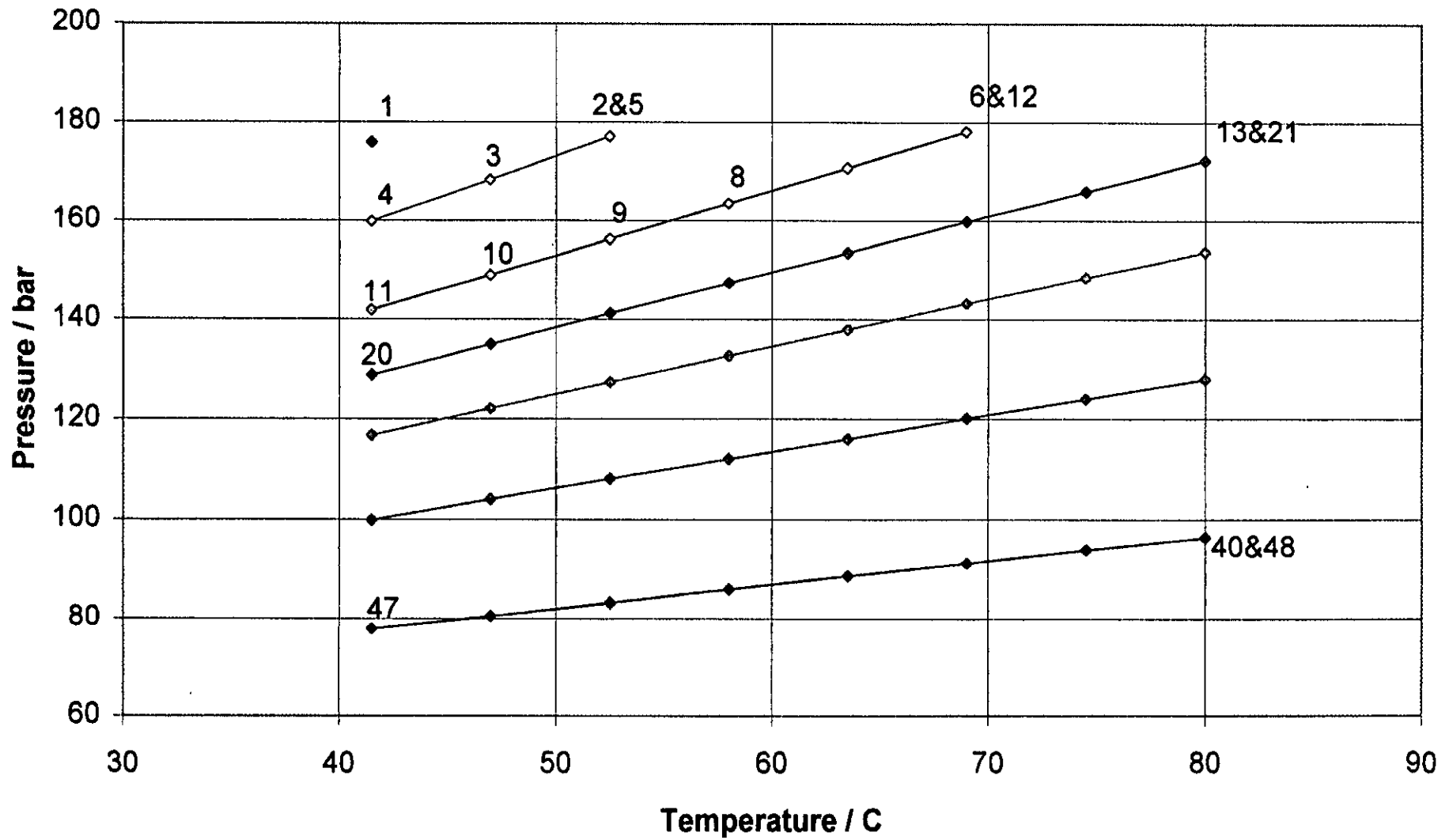


Figure 2. Sequence of Measurements for Mixture 1.



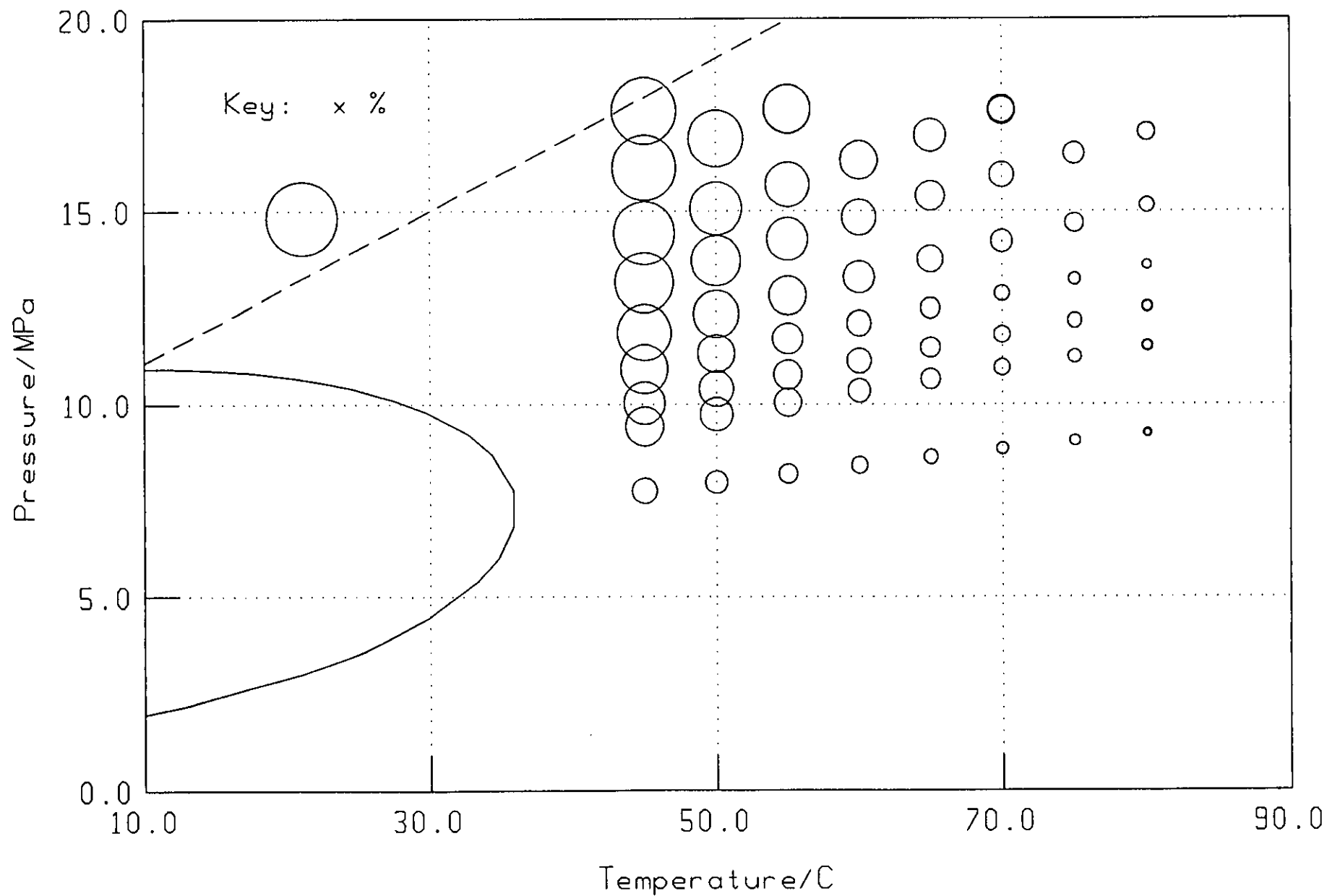


Fig.3 Comparison of density data for Mixture 1_ with the AGA8 eqn.

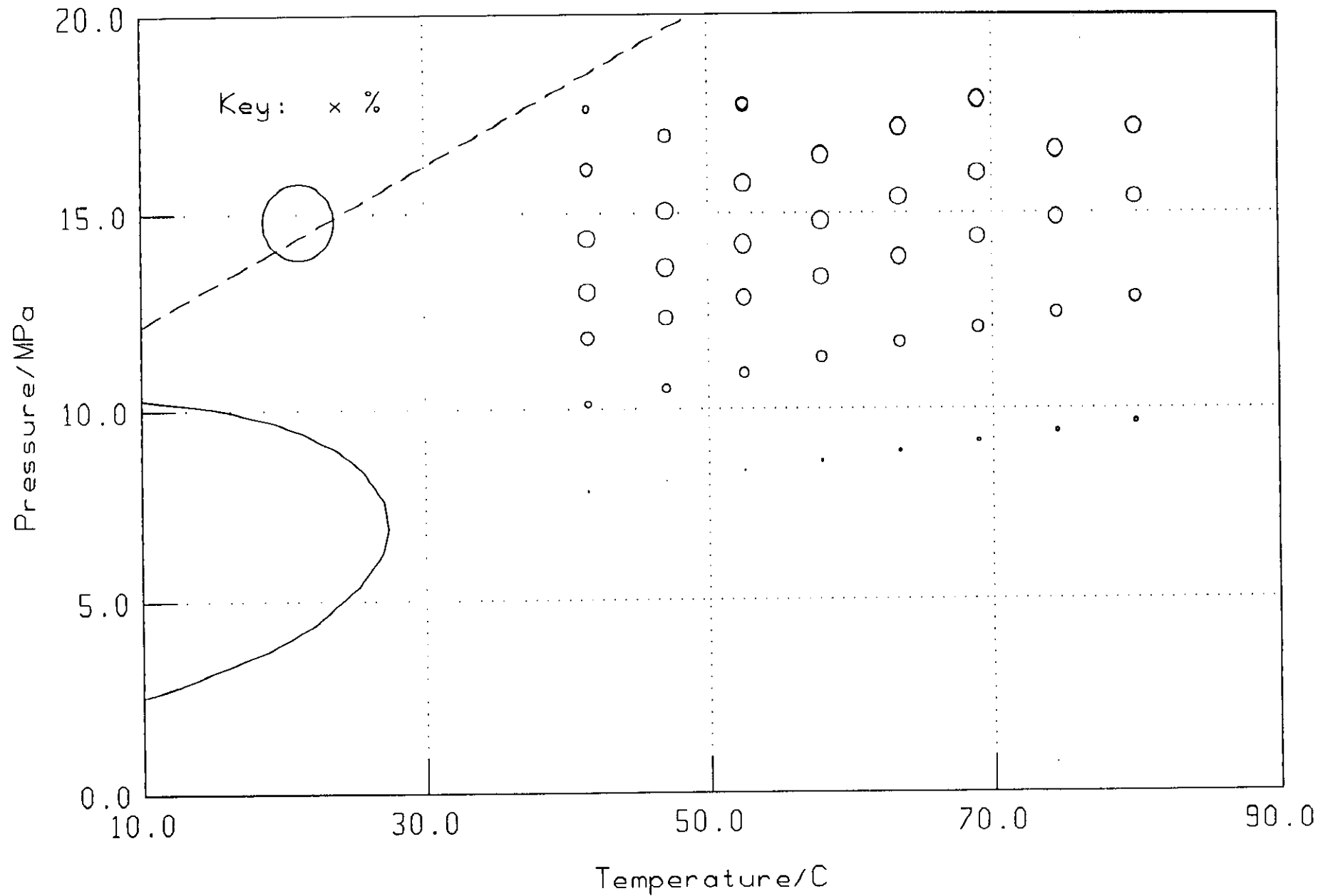


Fig.4 Comparison of density data for Mixture 2a with the AGA8 eqn.

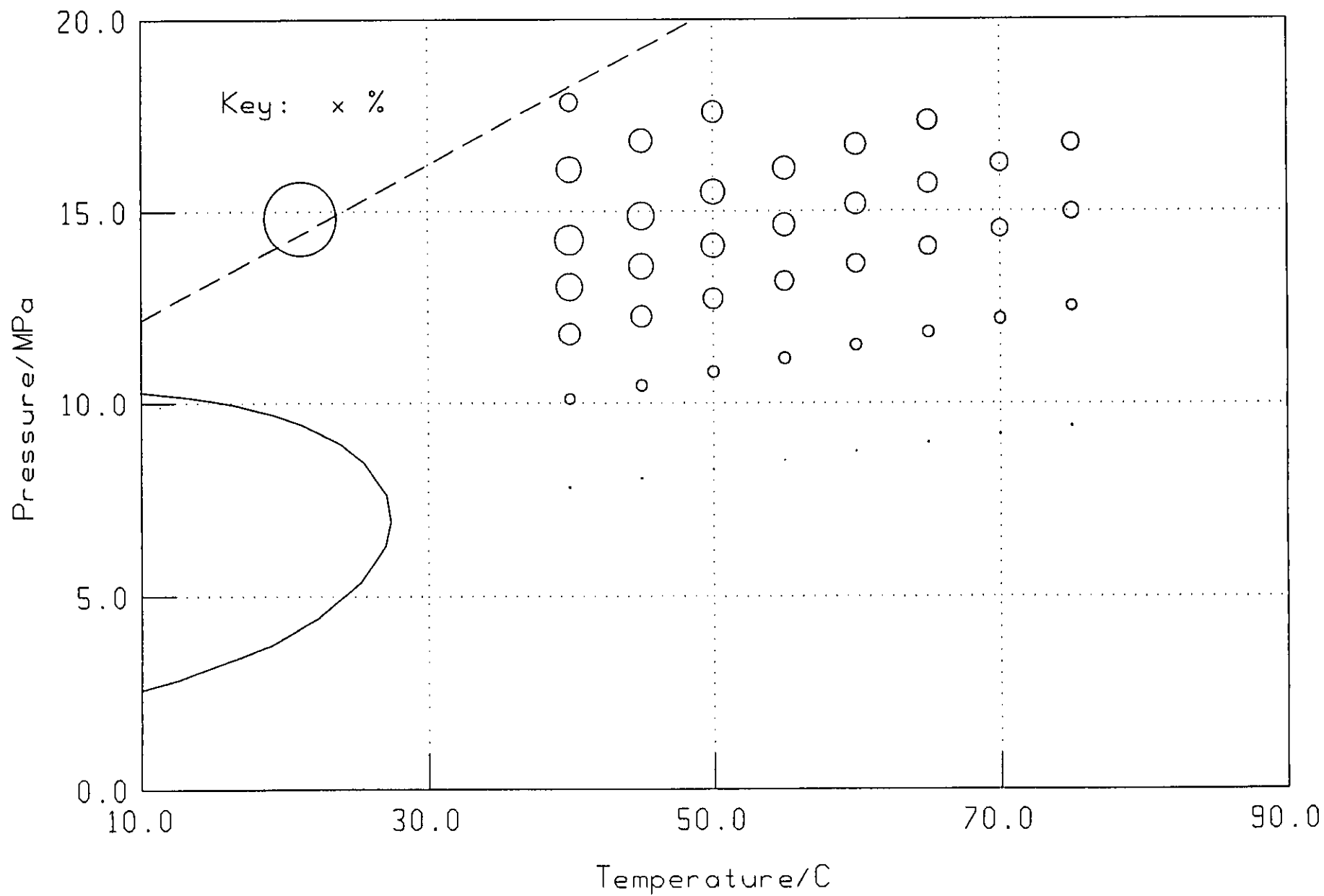


Fig.5 Comparison of density data for Mixture 3a with the AGA8 eqn.

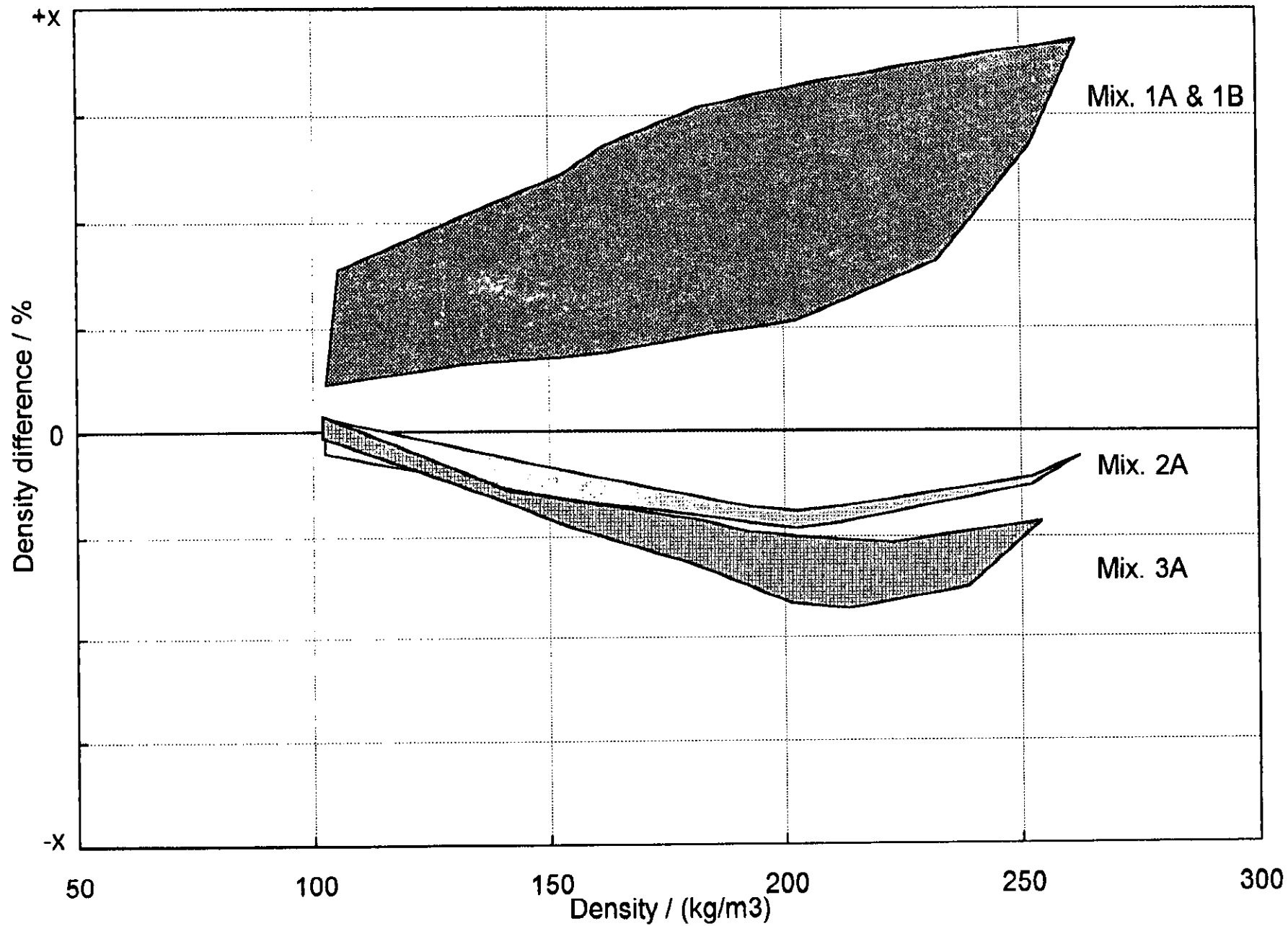


Fig. 6 Comparison of density data for Mixtures 1, 2A and 3A with the AGA8 eqn.

FLUIDIC PRESSURE PULSE TRANSMITTING FLOWMETERS FOR REMOTE OIL FLOW MEASUREMENT

H Wang, G H Priestman, S B M Beck and R F Boucher*

Department of Chemical and Process Engineering, University of Sheffield

*Present address: Principal and Vice-Chancellor, UMIST, Manchester

Summary

Details are given of the development of no-moving-part fluidic devices for the measurement of oil flow deep in the production string where the flow is single-phase. Two devices have been investigated which generate pressure pulses at a frequency proportional to the flowrate. The pulses are transmitted via the flowing two-phase mixture for detection downstream. A balance has been struck between pulse amplitude and pressure loss in the device so as to minimise any reduction of flow. One of the devices, the Blown Venturi flowmeter, is constructed from an oscillating Coanda Switch attached to a Variable Recovery Venturi. The other one is a Coanda Switched Vortex flowmeter, which is a hybrid device consisting of a Vortex Amplifier and an oscillating Coanda Switch. Optimisation of both flowmetering devices have been conducted and they show good performance over a wide operating range in the laboratory.

1. INTRODUCTION

In oil production, it is important to know how much oil is being supplied from each of the wells, for calculating royalty and working-interest payment, guiding daily production operation, and managing the reservoir. The bottom of these wells are usually several kilometres underground, and tend to be manifolded together to a surface station. As the crude oil approaches the surface, its pressure drops and the gas, which is kept in solution by high static pressure, comes out in bubbles. This can happen to such an extent that what is delivered to the surface is a foam. Conventional measuring devices are not suited to this situation, though some attempts have been made at two-phase flowmetering. Liu et al [1] and Millington et al [2] made this measurement with a separation method, and Baker and Hayes [3] and Fisher [4] tried to develop a metering system for the total mass flow of the multiphase medium.

An alternative approach is to measure the flow rate at the bottom of the well where the flow is still single-phase, though any such device must have high reliability and not reduce production rate. This paper describes development of such a meter which produces pressure pulses at the bottom of the well using a reliable no-moving-part fluidic device, with the frequency proportional to fluid flowrate. The pulses are transmitted through the fluid in the pipe to the surface, where they can be detected and recorded. To minimise any production loss, the mean pressure drop across the device must be kept small.

Pulse transmission of information is well established in oil drilling, where drilling mud is the fluid medium [5]. Measurement-while-drilling (MWD) techniques generate pulses, sent through the drilling mud to the drilling platform [6], and successful pulse reception after transmission over more than a kilometre is proven for single phase media. In oil production, the additional complication of two phase flow is present, with much greater attenuation beyond the bubble point. Experiments and computer modelling are therefore being conducted to determine suitable pulse amplitudes. Some compensation can be obtained, if needed, by locating the pulse detector on the sea bed rather than at the well-head.

Many studies have been done on the development of fluid oscillatory type flowmeters, which can be classified [7] as, fluidic oscillator, vortex-precession swirlmeter [8, 9] and vortex shedding flowmeter [10]. Fluidic oscillators, which include relaxation and feedback oscillators [11] work on the principle of the Coanda effect. The frequency of oscillation of the jet is a measurement of the flowrate. Although much work has been done on this type of flowmeter [12, 13, 14, 15, 16], none of the meters combine sufficient pressure pulse amplitude with the low overall pressure loss required in the proposed application.

Two fluidic flowmeter devices have been developed in this study. One, the Blown Venturi (BV) flowmeter, is constructed from an oscillating Coanda Switch attached to a Variable Recovery Venturi (VRV). The other one is a Coanda Switched Vortex (CSV) flowmeter, which is a hybrid device consisting of a Vortex Amplifier and an oscillating Coanda Switch. For both devices experiments have been conducted to optimise their geometry with respect to minimising total pressure drop, maximising pulse amplitude and ensuring a satisfactory relationship between pulse frequency and flowrate. Comparative data for the two devices should enable their relative merits to be assessed for use as oil flow measuring devices.

The downhole flowmeter produces pressure pulses which are transmitted by wave action to the well head. The analysis of the pulse transmission to ascertain if there is still sufficient signal at the surface to measure is clearly important. Because of the difficulty of experimentally modelling pressure pulse transmission in a vertical flow of crude oil-natural gas mixture, a computer programme called SUNAS [17] with Transmission Line Modelling [18] is being used to model pressure pulse transmission attenuation in vertical air-water bubble flow. The prediction can then be compared with experimental measurements being done with an air-water pipe rig. The air-water model can be adapted for vertical oil two-phase flow by use of a suitable attenuation coefficient. CFD modelling [19] using a time dependant boundary is also going to be used for modelling the air/water and oil/gas bubbly flow for comparison with both the predicted attenuation and the experimental measurements. This will be reported [20] in due course.

2. BLOWN VENTURI (BV) FLOWMETER

The Blown Venturi flowmeter (Fig.1) is constructed from an oscillating Coanda Switch attached to a Variable Recovery Venturi. The flow through the oscillating Coanda Switch acts as a small by-pass flow past the venturi. When there is no flow in control pipe "1", connected to the venturi throat, the overall pressure loss of the device, ΔP , is very low. When flow is introduced from control pipe "1" to the throat, it upsets the boundary layer and reduces the pressure recovery, increasing the pressure drop across the device. Introducing flow through control pipe "2" has little effect on ΔP . Using a control loop to connect together the control ports of the Coanda Switch causes the jet in the switch to alternate between control pipe 1 and 2 and so causes the VRV pressure drop to switch between a high and a low value. The device works as a flowmeter because the frequency of the oscillating Coanda switch is proportional to the flowrate going through it, so by measuring the frequency of the oscillations downstream, the flowrate can be measured.

Tests with low pressure air have been carried out [21] to optimise the design. Optimum performance was found to correspond to the following design:

- divergence angle, $\theta = 16^\circ$;
- venturi area ratio AR (outlet area/throat area) = 7.0;
- size ratio (venturi inlet area/Coanda supply nozzle area) = 122.

Based on these findings a brass device was designed for operation with water. Experimental work was done to study the effect of control loop geometry on the oscillation frequency, overall pressure drop and pulse amplitude.

Fig.2 shows the profile of the brass flowmeter. This device was constructed out of two pieces (body and lid) of brass. To measure the static performance a test arrangement was set up as shown in Fig.3. The outlet jet of the Coanda device was alternatively switched by introducing a control flow Q_{cL} or Q_{cH} , whilst the device outlet flow, Q_e , was held at a constant value. For example, to measure the low resistance state, valves H and L were closed, then valve L was briefly opened. In this way the jet from the Coanda supply nozzle was discharged through the control pipe "2" (Fig.1), the

jet remaining in this low resistance state due to the Coanda effect. Briefly opening valve H induced switching to the high resistance state. Measuring the pressure drop ($\Delta P = P_s - P_o$) of this device, at high and low resistance states, with different exit flows, allowed ΔP_{high} and ΔP_{low} to be measured.

For measuring static performance an important quantity is the Turndown Ratio N , given as

$$N = \sqrt{\frac{Eu_{high}}{Eu_{low}}} \quad (1)$$

where

$$Eu_{high} = \frac{\Delta P_{high}}{0.5 \rho V_o^2}, \quad \text{and} \quad Eu_{low} = \frac{\Delta P_{low}}{0.5 \rho V_o^2} \quad (2)$$

For constant flow, this turndown ratio simplifies to:

$$N = \sqrt{\frac{\Delta P_{high}}{\Delta P_{low}}} \quad (3)$$

where Eu is the Euler number for each resistance state, ρ is the fluid density, V_o is the average fluid velocity based on the flow in the outlet pipe for the meter. Since the flowmeter should constitute only a small part of whole system resistance, the condition maintained during switching should approximate to one of constant flow. Hence, with constant pressure upstream of the flowmeter, N gives an indication of the strength of the pressure pulse downstream of the device. Fig.4 shows the variation of turndown ratio with Reynolds number again based on the venturi outlet pipe. It can be seen that increasing flowrate gives an increase in turndown ratio, so the flowmeter operation is more effective at higher flowrates, although N does tend toward a constant value.

To obtain the operating performance of this flowmeter, a control loop was connected between the Coanda switch control ports to create an oscillating Coanda system. This control loop can be modelled as a fluid transmission line with zero mean flow and laminar oscillating flow. Tippetts et al [22] studied this oscillating Coanda switch as a flowmeter, and deduced a dimensionless control loop inductance as:

$$L' = 4l'n / (\pi d'^2) \quad (4)$$

where:

$$l' = l/d_n \quad \text{and} \quad d' = d/d_n \quad (5)$$

l and d are the length and diameter of the control loop, and n and d_n the aspect ratio and width of the Coanda supply nozzle respectively. L' is a factor required to be held the same if frequencies are to scale with size changes. Essentially it measures the ratio of the inductance of the pipe to that of the Coanda switch body.

Fig.5 shows the rig used to detect the pressure pulses generated by this device. The dynamic differential pressure pulses were captured by means of a differential pressure transducer (Druck®, PDCR 190-1436, ± 1 bar). The differential pressure pulse wave forms (Fig.6) were directly monitored by an oscilloscope and an electronic signal analyzer connected to the transducer. A personal computer equipped with a data acquisition board was also used to capture the differential pressure pulse signals from the transducer. 'GLOBAL LAB®' software was used, with a sample rate of 2000 Hz. For the meter operating with a control loop inductance, $L'=141$, differential pressure pulses are shown in Fig.6 for several flowrates. Pulse amplitude A (defined as $\Delta P_{max} - \Delta P_{min}$ from the oscillation data) and mean pressure drop ΔP , are important parameters for the flowmeter operating performance. Fig.6 shows an increase in both the pulse amplitude and frequency, f , with increasing flowrate. The important operational parameters, however, are frequency per unit volume f/Q and relative pulse amplitude A' ($=A/\Delta P$). Both of these criteria are found to be affected by the dimensions of the control loop. Fig.7 shows how f varied with Q for different control loop dimensions. For any fixed value L' , f is seen to increase linearly with Q . Increasing L' is seen to decrease f for a given flowrate. It can be seen from Fig.7 that Q increasing from 0.00027 to 0.00102 m^3/s corresponds to an oscillation frequency f , increasing from about 2.0 to 12.0 Hz for $L'=141$. The flowrate vs. frequency relationship is seen to be linear. A linear regression was applied to the data to give a fitted curve,

$$Q (\text{m}^3/\text{s}) = 7.41 \times 10^{-5} f (\text{Hz}) + 1.53 \times 10^{-4} \quad (6)$$

Thus the linear relationship between f and Q does not pass through the origin and the rate f/Q is not constant, although it tends toward a single value at high frequencies, when the intercept become less significant.

Fig.8 shows the effects of L' on the relative pulse amplitude A' , over the tested flow range. The largest pulses, relative to overall pressure drop, are seen to corresponds to $L' = 141$, which corresponded to $l = 0.6$ m and $d = 5$ mm in the device tested. Fig.9 shows the variation in meter pressure drop with flowrate, both for oscillation operation, and standby mode. Standby occurs with the control loop blocked so the device acts as a low resistance venturi. Thus having a means of blocking the control loop enables the meter to be de-activated, with an associated saving in pressure loss.

3. COANDA SWITCHED VORTEX (CSV) FLOWMETER

A Vortex Amplifier (VA) is attached to an oscillating Coanda switch to create a Coanda Switched Vortex (CSV) flowmeter (Fig.10). This device has two flow states, of high and low resistance respectively. The Coanda switch must be suitably matched to the VA such that one Coanda switch leg feeds all the flow to the VA tangential port, producing a vortex and leading to high resistance. The radially directed flow from the other Coanda outlet gives the low resistance mode (Fig.10). If an oscillating Coanda switch is employed, the flowmeter inlet flow will be alternatively switched to the two VA inlets, resulting in the production of a large pressure pulse.

The Coanda Switched Vortex was first introduced by Adams and Moor [23], and also studied by Tippetts [24]. The closest application of the Coanda Switched Vortex to that envisaged for remote flow measurement was the fluidic hydraulic ram [25] and the fluidic hammer for percussion drilling [18]. Both of these devices are, however, unsuited to flow measurement because of their high overall mean resistance and the significant flow interruptions, which would generally be unacceptable in an oil production string.

Fig.11 shows a traditional shape of VA. The flow through the radial port experiences a low resistance, since the flow has only to pass through a successive

sudden expansion into the VA chamber and the contraction at the exit of the device. The high resistance state occurs when the flow enters the tangential inlet port. The flow swirls inside the VA chamber producing a strong vortex exit flow which greatly increases the energy losses of the system through turbulent eddies. The effect of geometry on VA operation has been studied widely in the past [26, 27, 28, etc.]. Unfortunately, the traditional VAs such as in Fig.11 cannot easily be connected in series with a Coanda switch and positioned downhole inside an oil producer, because the two inlet connection pipes extend beyond the boundaries of the circular VA chamber. A new kind of 'in-line' VA (Fig.12) was needed to better fit the drill string. This VA is designed to have inlet ports opposite the exit port, such that all the pipes are parallel to the pipe housing. This requires that the flow turns through a 90° angle on entering the chamber. The in-line VA has a thin vortex chamber to achieve a high resistance and a total divergence 6° exit diffuser to help pressure recovery in the low resistance state. The inlet ports are directed by an internal guide, with high resistance flow directed around the periphery of the chamber.

Due to the geometrical restriction of the industry-standard producer pipe, the VA chamber had to be 125 mm (5 inches) diameter for the present study. To arrive at the optimum in-line VA size, some theoretical and experimental work was done [29] for matching the Coanda switch to the in-line VA. The best area ratio of the VA exit to the and Coanda switch supply nozzle was determined as 0.8, this giving a Coanda flowmeter maximum turndown ratio of 1.49. The exit diameter of the in-line VA was 24 mm and the VA inlet ports diameters were both 33 mm.

An experimental rig similar to Fig.5 was used to measure the meter performance with air. Different control loop designs (diameter from 20 to 40 mm, and length from 0.7 to 2.7 m) were used. Fig.13 shows the flowmeter calibration for different values of the dimensionless control loop inductance L' . It can be seen that flowrates from 0.004 to 0.024 m³/s corresponded to oscillation frequencies from 0.48 to 5.13 Hz for $L' = 206$. As with the venturi meter, the flowrate vs. frequency relationship was linear but did not pass through the origin, the fitted curve being:

$$Q \text{ (m}^3\text{/s)} = 4.39 \times 10^{-3} f \text{ (Hz)} + 1.84 \times 10^{-3} \quad (7)$$

Fig.13 also shows that the number of cycles per unit volume (f/Q) for $L' = 206$ again tends to a single value at high flows. Fig.14 shows that the relative pulse amplitude ($A/\Delta P$) changes with L' over the range of flowrates. $L'=206$ is seen to give best performance, corresponding to a control loop length of 2.5 m and diameter of 25 mm. Again, as with the venturi meter, blocking the control loop put the meter into a low pressure drop standby mode, as shown in Fig.15.

4. SELECTION OF FLOWMETERS FOR OIL FLOW MEASUREMENT

The choice between the venturi and CSV type meters for downhole oil flow measurement depends on the measurement requirements, flowmeter characteristics and flowmeter construction. The relative pressure pulse amplitudes generated are compared in Fig.16 for a range of Re , in each case for optimum L' . The Reynolds numbers, in each case is based on flow in the outlet pipe:

$$Re = \frac{V_o d_o}{\nu} \quad (8)$$

where d_o is the flowmeter outlet diameter and the average outlet flowmeter velocity $V_o = Q/A_o$, where Q is the volume flowrate and A_o the outlet cross sectional area, ν is the fluid kinematic viscosity. It is can be seen that the Coanda's relative pulse amplitude is greater than that for the venturi, particularly at lower Reynolds numbers. Thus for a given operating pressure drop, the Coanda meter would produces larger amplitude pulses.

In order to compare with performance of the venturi and Coanda flowmeters for a given application, the experimental data must be plotted in a dimensionless form, with the pipe flow specified as the reference velocity. The meters can be characterised by the relationship between Reynolds number Re (Eqn.8) and non-dimensional group representing frequency and pressure drop:

$$\text{Strouhal number} \quad Str = \frac{f d_o}{V_o} \quad (9)$$

$$\text{Euler number} \quad Eu = \frac{\Delta P}{0.5\rho V_o^2} \quad (10)$$

where f is the frequency of oscillation, V_o is the average outlet velocity, ΔP is the average pressure drop across the flowmeter and d_o is the outlet pipe diameter.

Fig.17 compares the characteristics for the two meter types. In all cases operation is more effective at the higher Reynolds numbers tested, the Strouhal numbers tending to a constant value and the Euler numbers reaching a minimum value. The venturi meter is seen to have a larger Eu, and so ΔP would be significantly lower than with the CSV. The venturi is seen to give a higher frequency signal than the CSV. The differences can be quantified with reference to a typical application.

Considering a 1000 m long oil production string of diameter 5.0 inches (0.125 m), volume oil flowrate 20,000 bbl/day (0.0368 m³/s), giving an average oil velocity in the producer of 3.0 m/s. At a saturated and gas freed oil bottom hole, the pressure is 200 bar, temperature is 200 °F, oil kinematic viscosity is 1×10^{-5} m²/s and oil density 757 kg/m³. The two flowmeters can be scaled from Fig.16 & 17 to give the performance as shown in Table 1.

Table 1 Using flowmeter in an oil production string

flowmeter	Re no.	Str no.	Eu no.	f (Hz)	A/ΔP	ΔP (bar)	A (bar)	ΔP _f * (bar)	ΔP _r [‡]
Venturi	37500	0.098	18	2.35	0.64	0.61	0.39	42.64	1.41
Coanda	37500	0.02	36	0.48	0.93	1.23	1.14	42.64	2.79

* means frictional pressure loss along the producer pipe

[‡] means % pressure loss in the whole length of producer $\{= \Delta P / (\Delta P + \Delta P_f) \times 100\}$

As expected the blown venturi gives higher frequencies and lower pressure drop, although in both cases the pressure loss is small compared to the pipe frictional loss. Signal transmission is also important and although Table 1 indicates that a venturi can be fitted into the pipe with lower pressure drop, the pulse amplitude will also be less. If the venturi was reduced in size so as to give the same pulse amplitude as the Coanda, the

venturi pressure drop would increase to 1.78 bar. Clearly the transmission of the pressure pulse through the pipe fluid is also important and is under consideration [20].

5. CONCLUSIONS

Two types of fluidic oscillatory flowmeter, the blown venturi and the Coanda switched valve, have been developed for downhole oil flowrate measurement. Design data and operating characteristics have been presented for each device. Pulse amplitude is expressed as a ratio relative to the average operating pressure drop, and pulse frequency increases linearly with the volumetric flowrate. The oscillator control loop inductance is shown to influence meter performance, with an optimum factor found for each device.

The use of non-dimensional groups to represent the characteristics enables the meter performance to be compared in a typical application. The blown venturi meter produces a higher pulse frequency and larger pressure drop, but the pulse amplitude is also lower, compared to the Coanda switched vortex meter.

References:

- 1 LIU K T, CANFIELD D R and CONLEY J T, application of a mass flowmeter for allocation measurement of crude oil production, SPE Production Engineering, November, 1988.
- 2 MILLINGTON B C and NEL EXECUTIVE AGENCY, a review of the uncertainties associated with the on-line measurement of oil/water/gas multiphase flow, 6th International Conference on Multi Phase Production, Cannes, France, pp.349-360, BHRA Group Conference Series Publication No.4, June, 1993.
- 3 BAKER R C and HAYES E R, multiphase measurement problems and techniques for crude oil production systems, Petroleum Review, pp.18-22, November, 1985.
- 4 FISHER C, development of a metering system for total mass flow and compositional measurements of multiphase/multicomponent flows such as oil/water/air mixtures, Flow Measurement Instrumentation, Vol.5, No.1, pp.31-42, 1994.
- 5 GEARTHART M, ZIEMER K A and KNIGHT O M, mud pulse MWD systems report, SPE (Society of Petroleum Engineers) paper no.10053, Richardson, Texas, 1983.
- 6 INGLIS T A, directional drilling, petroleum engineering and development studies, Vol.2, Graham & Trotman, London, 1987.
- 7 BOUCHER R F, a fluidic flowmeter for industrial and clinical applications, 4th Int. Fluidics Conf., paper B-12, pp.1-24, Varna, Bulgaria, 1972.
- 8 FURNESS R A, fluid flow measurement, Longman, London, 1989.
- 9 HAYWARD A T J, flowmeters, a basic guide and source-book for users, MacMillan, 1979.

-
- 10 YAMASAKI D, TAKAHASHI A and HONDA S, a new fluidic oscillator for flow measurement, proceedings of 2nd int. symposium on fluid control, measurement, mechanics and flow visualization (FLUCOME '88), Sheffield, 1988.
 - 11 BOUCHER R F and TIPPETTS J R, an investigation into the advantages of fluidics in fluid processing - Part 2, Aero. Res. Inst., Sweden, FFA TN., 1982.
 - 12 TIPPETTS J R, GOLDER J A and GRANT J A, improvements in fluid flow measurement, British Patent no. 1297154, Published 22 Nov. 1972
 - 13 GRANT J and TIPPETTS J R, improvements in or relating fluid flow meters, British Patent no. 1363762, Published 14 Aug. 1974
 - 14 GRANT J and COX A J, improvement in or relating to flowmeters', British Patent no.1453587, 1976.
 - 15 MAZHAROGLU C, low Reynolds number fluidic flowmetering, PhD Thesis, Sheffield University, 1988.
 - 16 BOUCHER R F, MAZHAROGLU C, CHURCHILL D and PARKINSON G J, a fluidic by-pass venturimeter, proceedings of 3rd triennial int. symposium on fluid control, measurement, and visualization (FLUCOME '91), San Francisco, USA, 1991.
 - 17 BECK, S B and BOUCHER R F, Sheffield university network analysis software (SUNAS), Dept. of Mech & Proc. Eng., University of Sheffield, 1993.
 - 18 BECK S M, HAIDER H and BOUCHER R F, transmission line modelling of simulated drill strings undergoing water-hammer, Journal of Mechanical Engineering Science, Proceedings of the Institution of Mechanical Engineers, Vol.209, No. C6, pp.419-427, 1995.
 - 19 FLUENT INC., fluent user's guide, Version 4.3, January, 1995.

-
- 20 WANG H, BECK S B M, PRIESTMAN G H and BOUCHER R F, simulation of pressure wave attenuation in a crude oil-natural gas mixture during crude oil extraction (in preparation).
 - 21 BOUCHER R F, BECK S B M and WANG H, a fluidic flowmetering device for remote measurement, *Journal of Process Mechanical Engineering, Proceedings of the Institution of Mechanical Engineers, Vol.210, No.E2, pp.93-100, 1996*
 - 22 TIPPETTS J R, NG H K and ROYLE J K, an oscillating bistable fluid amplifier for use as a flowmeter, *Journal of Fluid Control (Fluidics Quarterly), No.1, Vol.5, January, 1973.*
 - 23 ADAMS R B and MOORE C B, flow control apparatus, US patent no. 3267946, 23rd August, 1966.
 - 24 TIPPETTS J R, the characteristics and uses of unvented bistable fluid amplifiers, PhD Thesis, Dept. of Mechanical Engineering, Sheffield University, Sept., 1969.
 - 25 TIPPETTS J R, , the fluidic hydraulic ram and a conjectured pressure amplifier, *Fluidics Quarterly, Vol.6, Issue 2, pp.45-53, April, 1974.*
 - 26 LAWLEY T J and PRICE D C, design of vortex fluid amplifiers with asymmetrical flow fields, *Trans. ASME, Journal of Dynamic Systems, Measurement and Control, Vol.94, pp.82-84, 1972.*
 - 27 KING C F, some studies of vortex devices - vortex amplifier performance and behaviour, PhD Thesis, Dept. of Mechanical Engineering and Energy Studies, University College, Cardiff, UK, 1978.
 - 28 BECK S B M, DELIGIANNIS P and BOUCHER R F, a study of the geometrical effects of a vortex amplifier chamber on its performance, *proceedings of 4th Triennial Int. Symposium on Fluid Control, Fluid mechanics, and Visualisation (FLUCOME '94), pp.29-34, Toulouse, FRANCE, 1994*
 - 29 WANG H, BECK S B M, PRIESTMAN G H and BOUCHER R F, a Coanda switched vortex flowmeter (in preparation).

Figures:

Fig.1. Blown Venturi (BV) flowmeter

Fig.2. Profile of brass BV flowmeter

Fig.3. Measure static performance of BV flowmeter for water

Fig.4. Turndown ratio of BV flowmeter for water test

Fig.5. BV flowmeter water test

Fig.6. Pressure pulse waveforms

Fig.7. BV flowmeter calibration with dimensionless control loop inductance (L')

Fig.8. BV flowmeter optimising L' for relative pulse amplitude

Fig.9. Mean pressure drop of BV flowmeter

Fig.10. Coanda Switched Vortex (CSV) flowmeter

Fig.11. Traditional shape of Vortex Amplifier (VA)

Fig.12. Off-centred port in-lin VA

Fig.13. CSV flowmeter calibration with dimensionless control loop inductance (L')

Fig.14. CSV flowmeter optimising L' for relative pulse amplitude

Fig.15. Mean pressure drop of CSV flowmeter

Fig.16. Comparing the relative pulse amplitude of BV and CSV flowmeters

Fig.17. Overall dimensionless flowmeter calibration (referred to normalised diameter)

Fig.1. Blown Venturi (BV) flowmeter

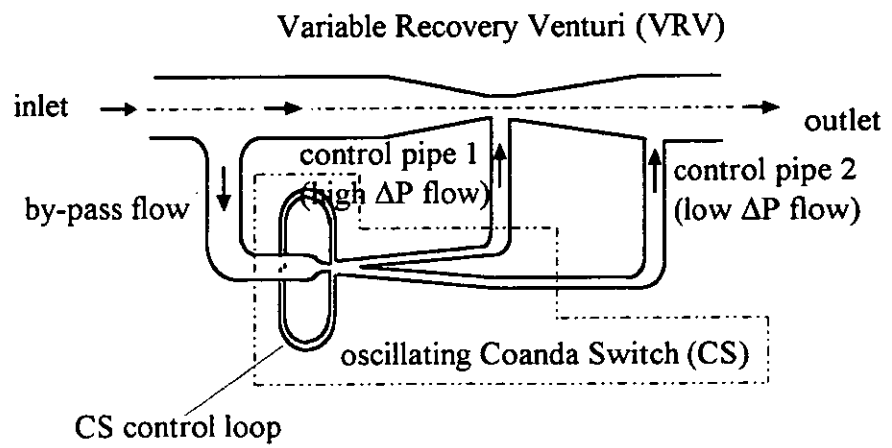


Fig.2. Profile of brass BV flowmeter

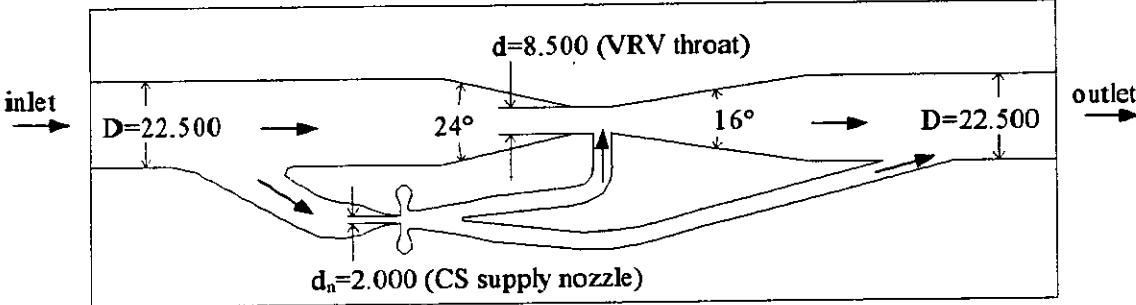


Fig.3. Measure static performance of BV flowmeter for water

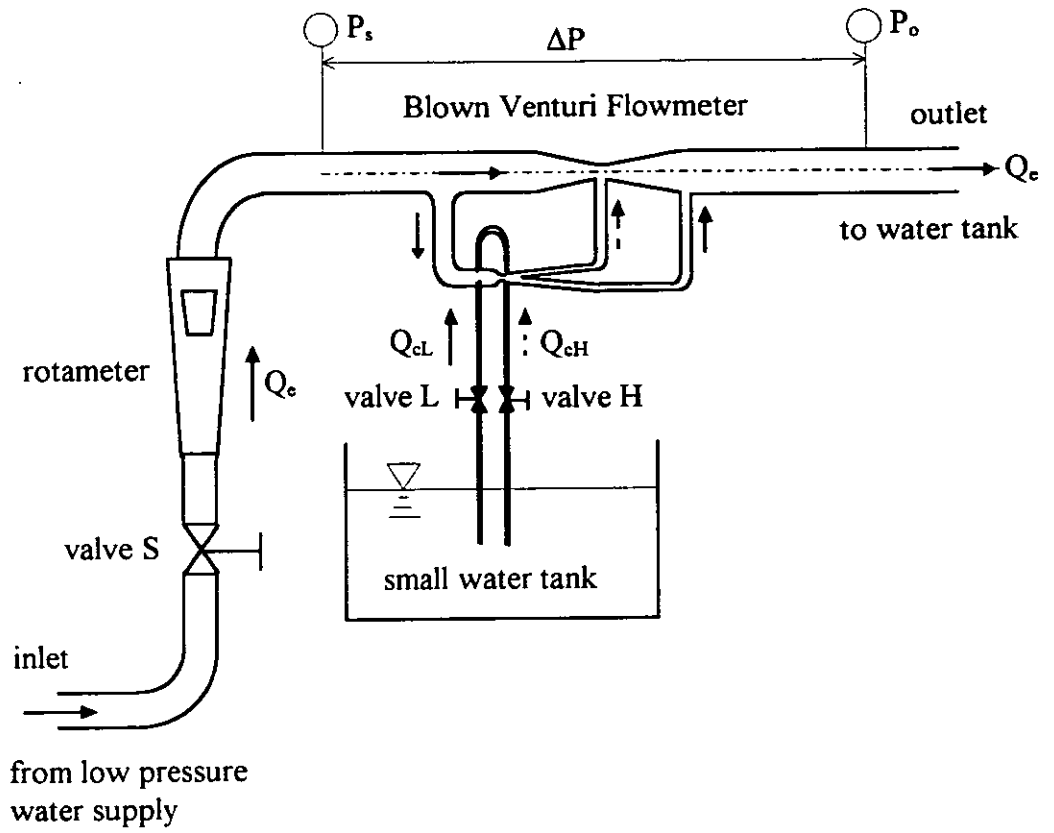


Fig 4. Turndown ratio of BV flowmeter for water test

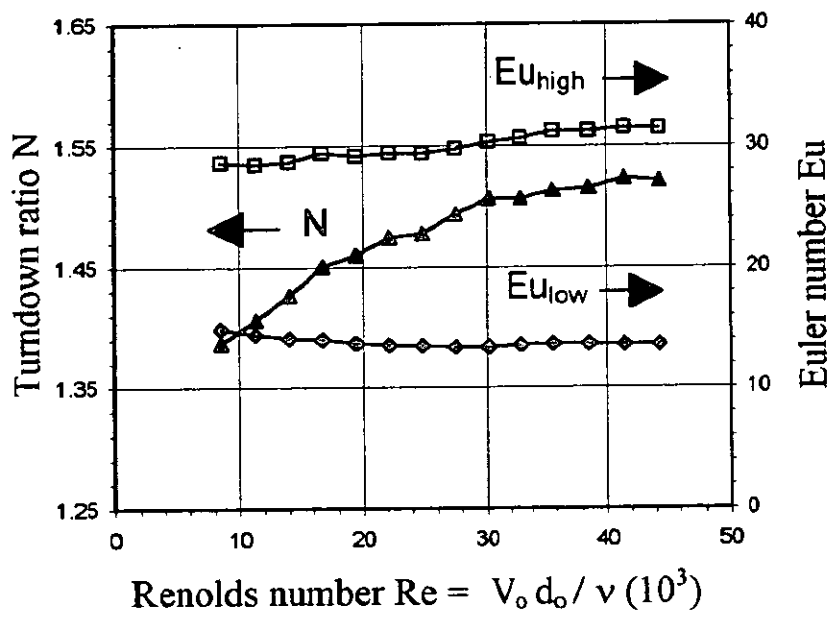


Fig.5. BV flowmeter water test

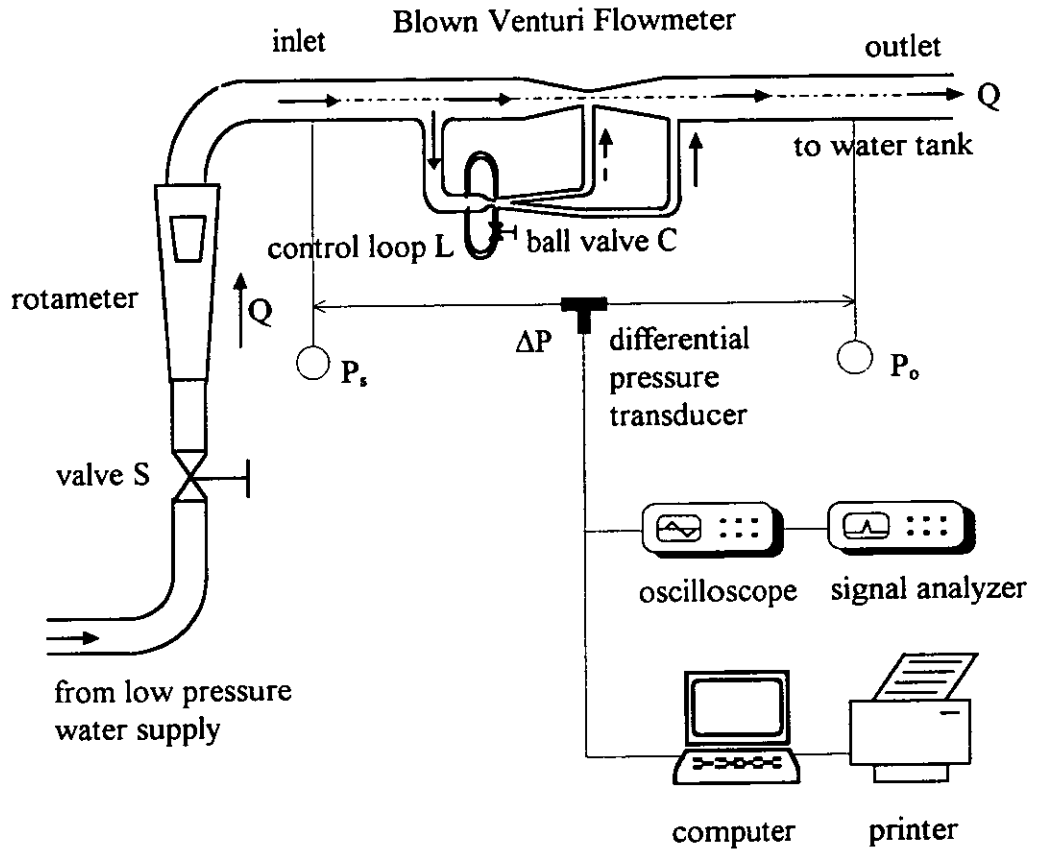


Fig.6. Pressure pulse waveforms

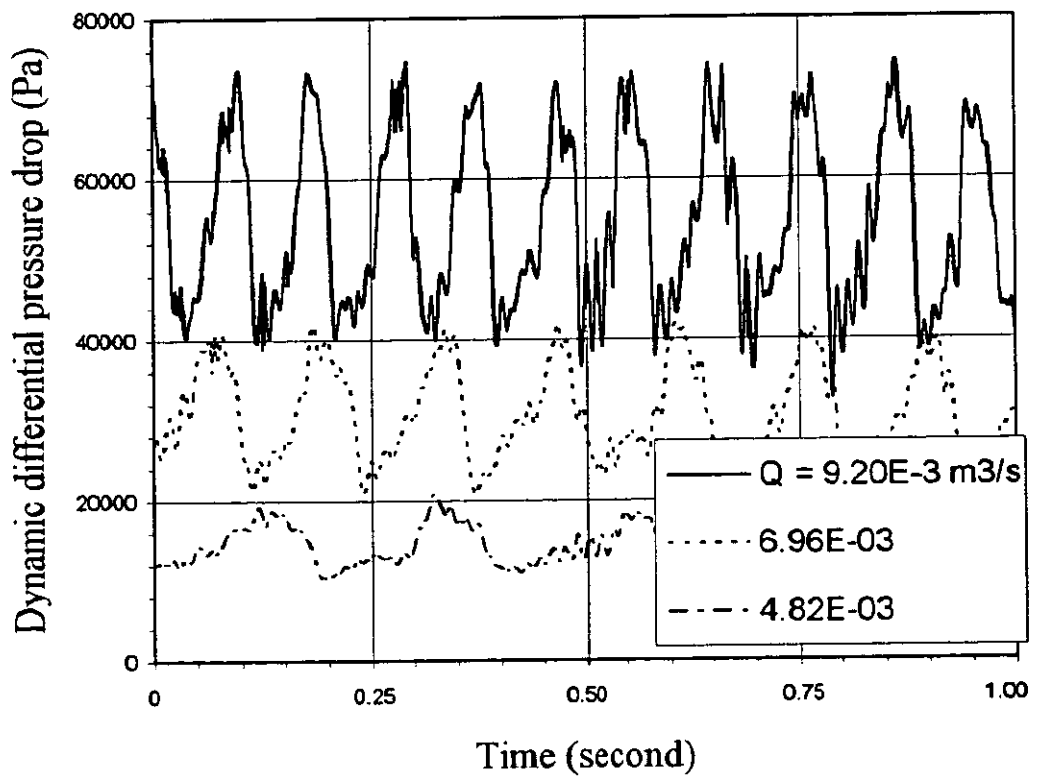


Fig.7. BV flowmeter calibration with dimensionless control loop inductance (L')

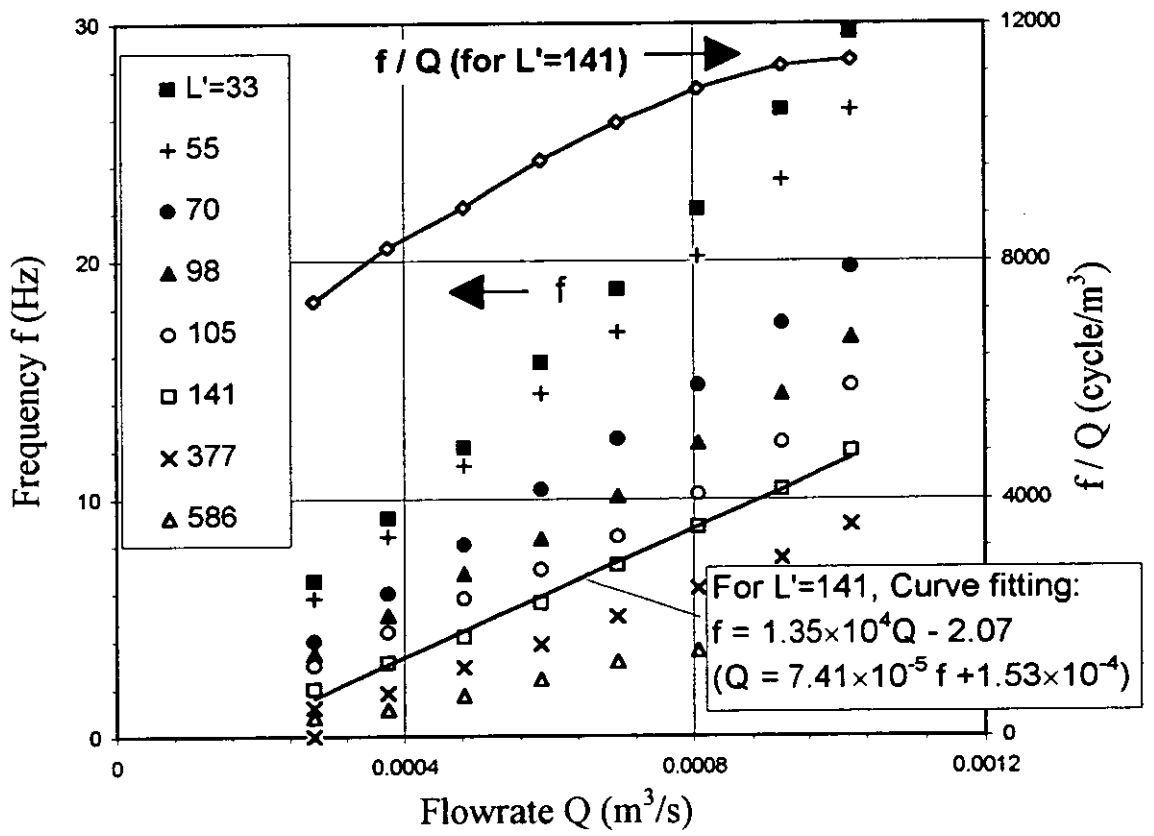


Fig. 8. BV flowmeter optimising L' for relative pulse amplitude

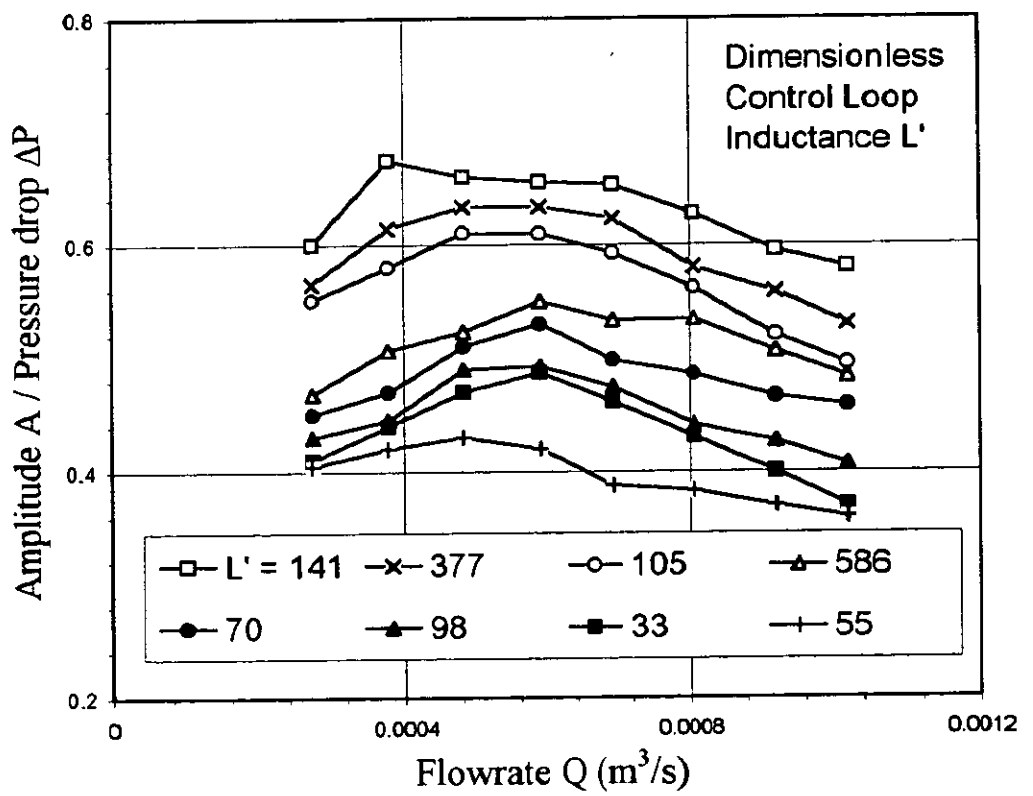


Fig.9. Mean pressure drop of BV flowmeter

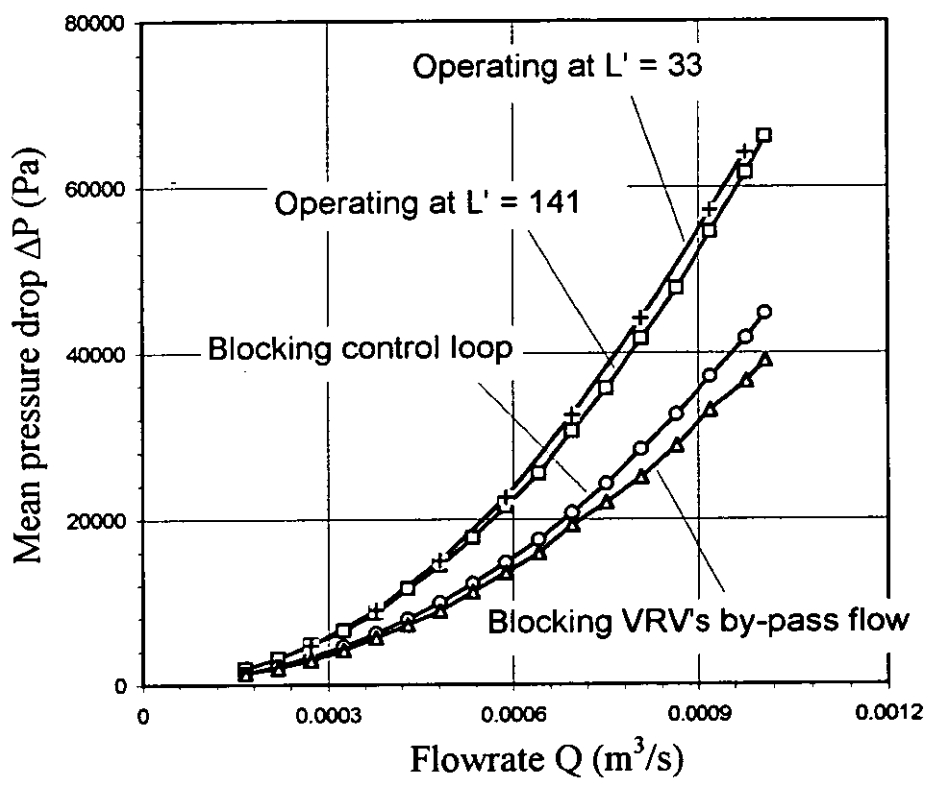


Fig. 10. Coanda Switched Vortex (CSV) flowmeter

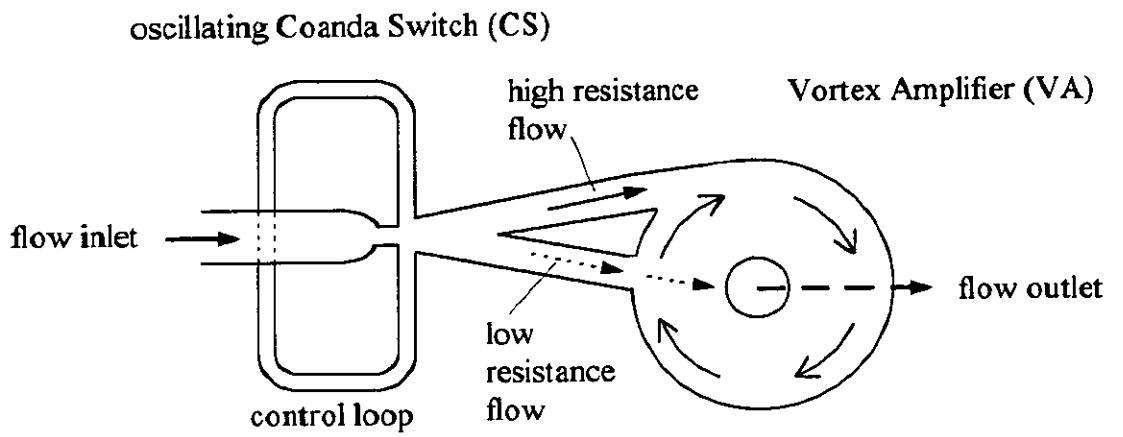


Fig.11. Traditional shape of Vortex Amplifier (VA)

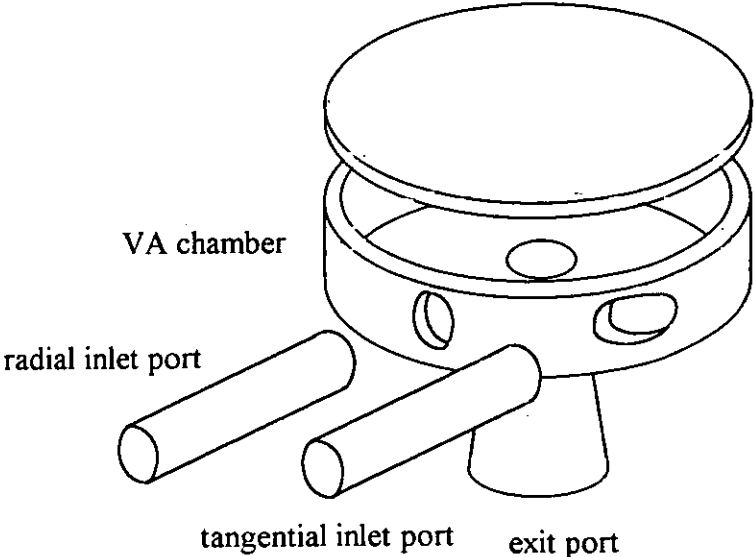


Fig. 12. Off-centred port in-line VA

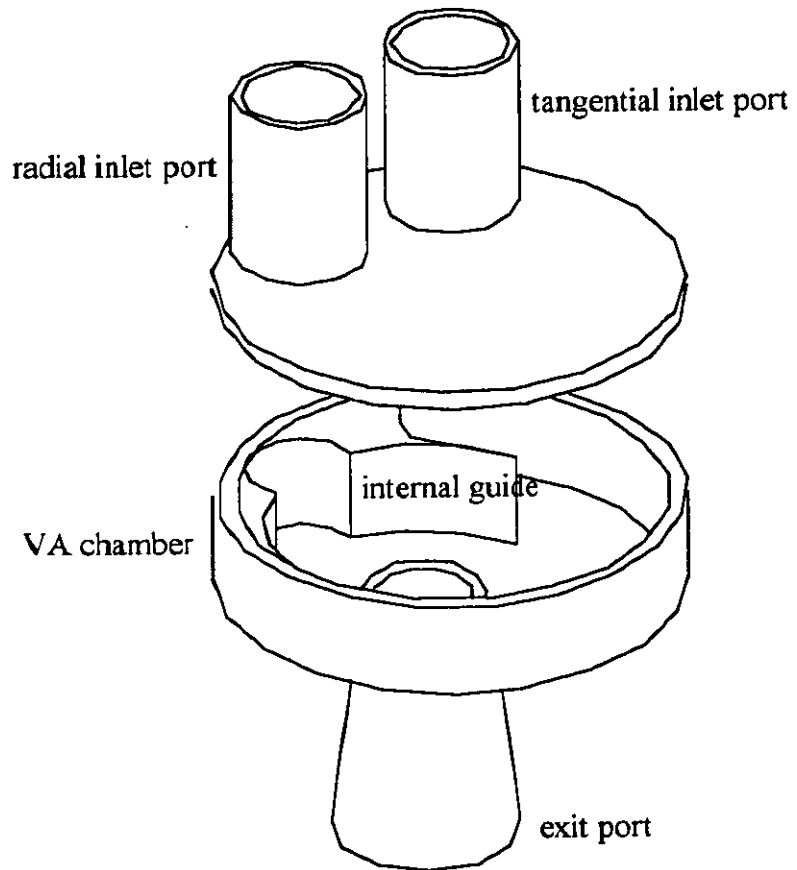


Fig. 13. CSV flowmeter calibration with dimensionless control loop inductance (L')

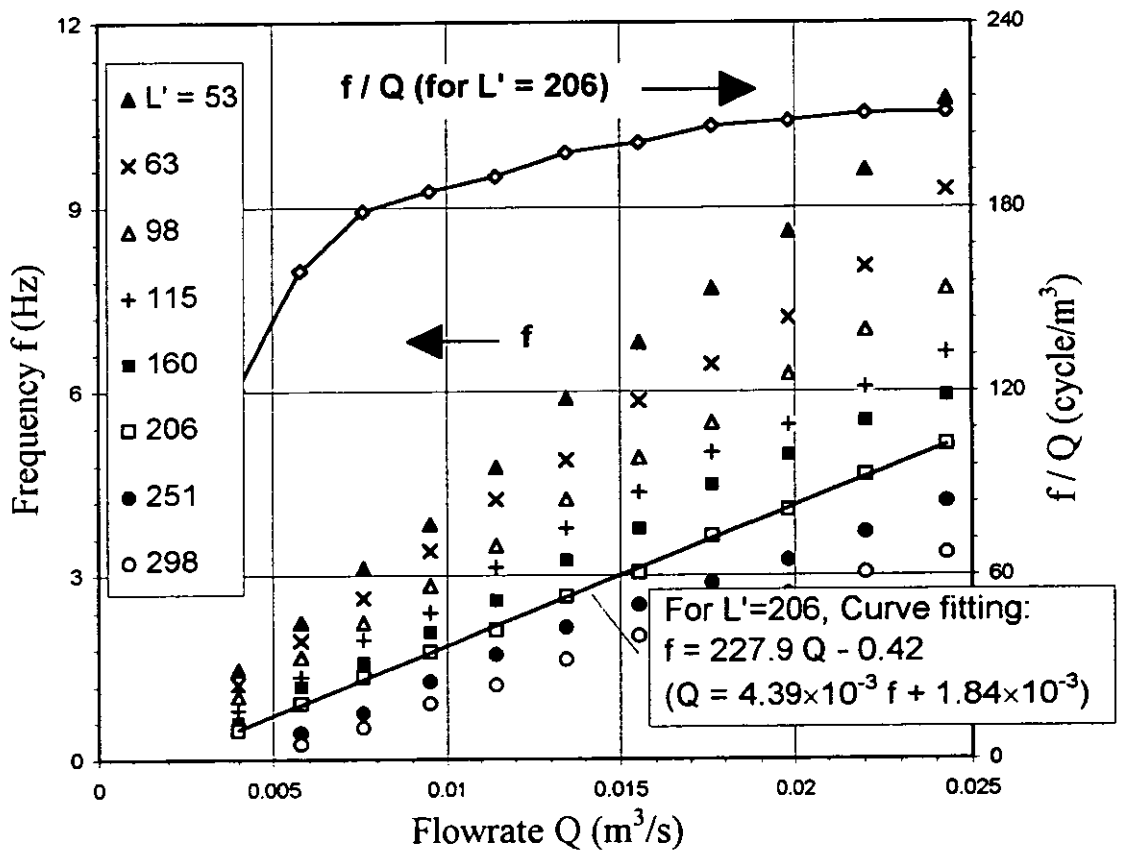


Fig.14. CSV flowmeter optimising L' for relative pulse amplitude

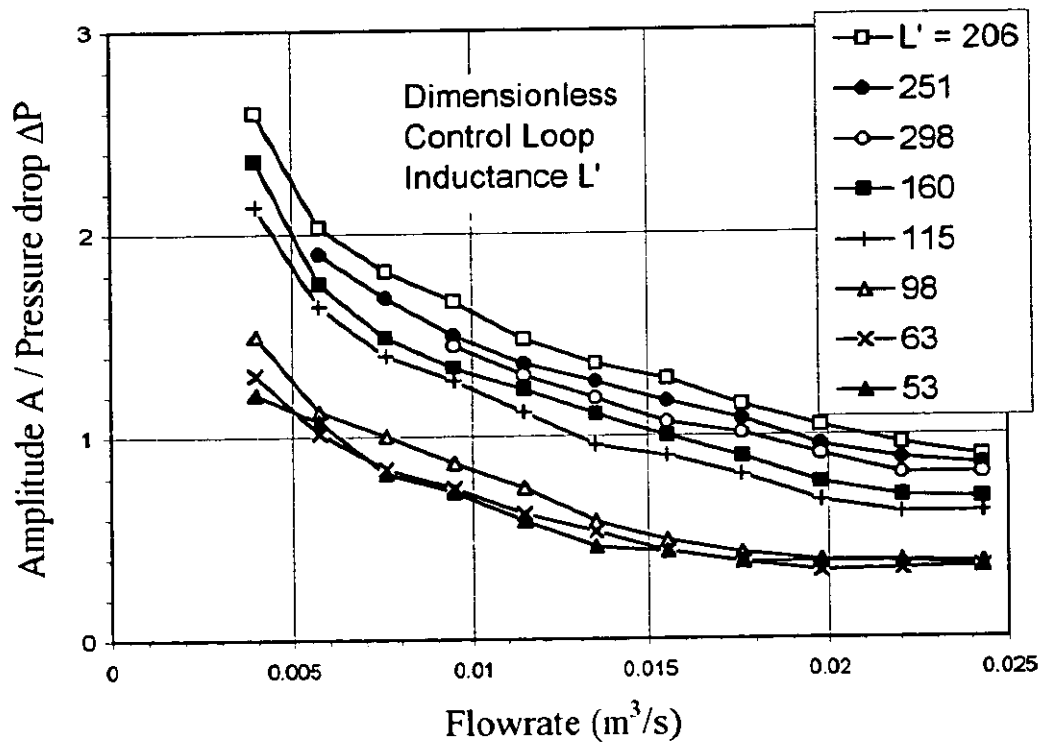


Fig.15. Mean pressure drop of CSV flowmeter

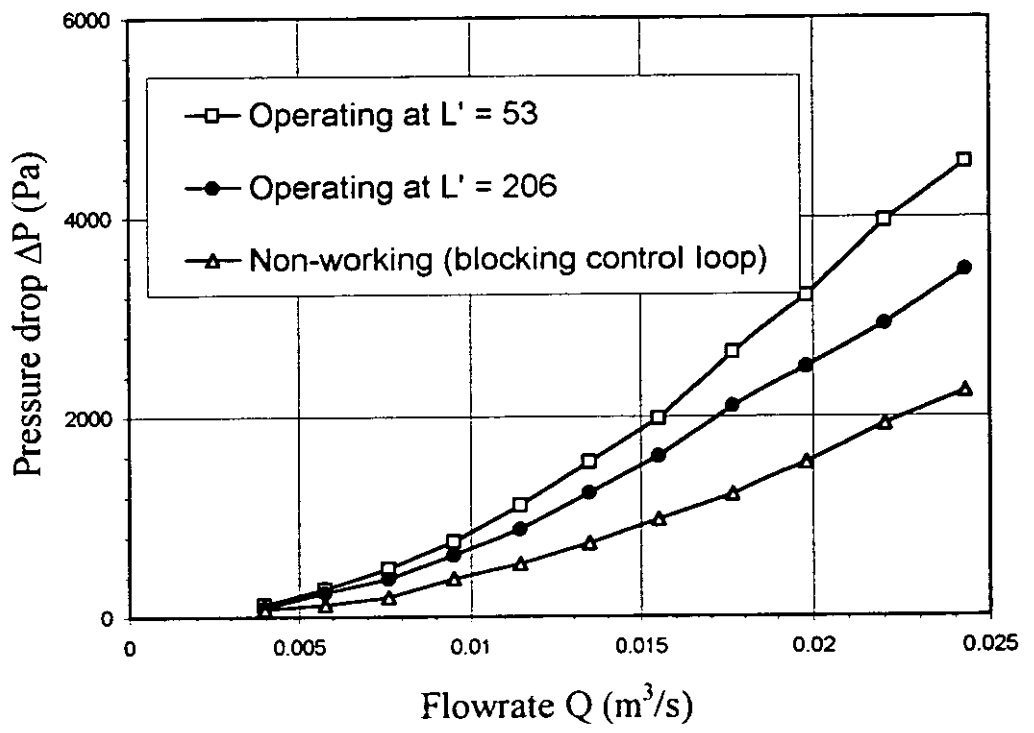


Fig.16. Comparing the relative pulse amplitude of BV and CSV flowmeters

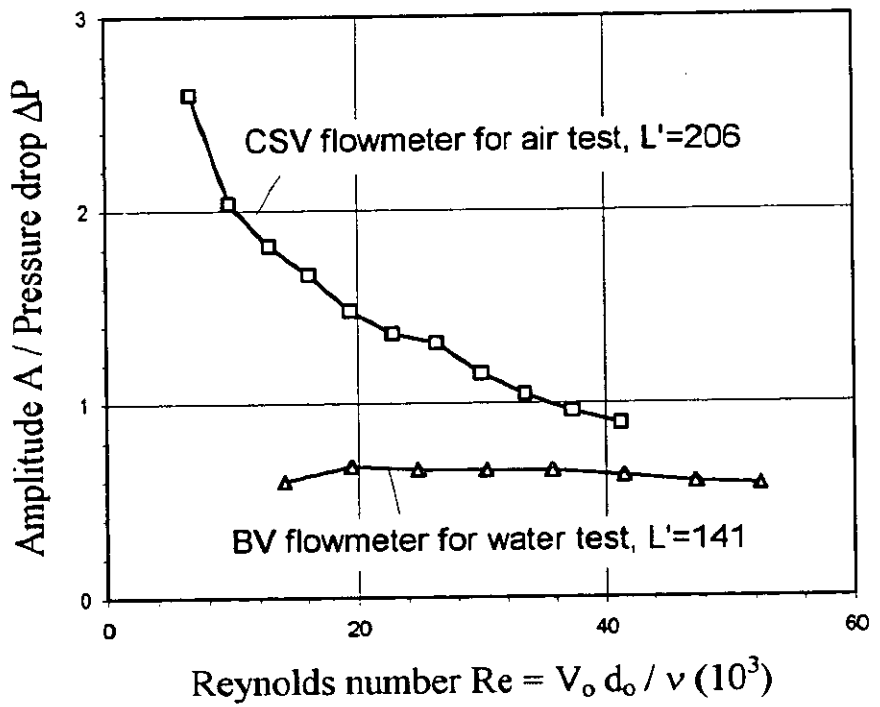
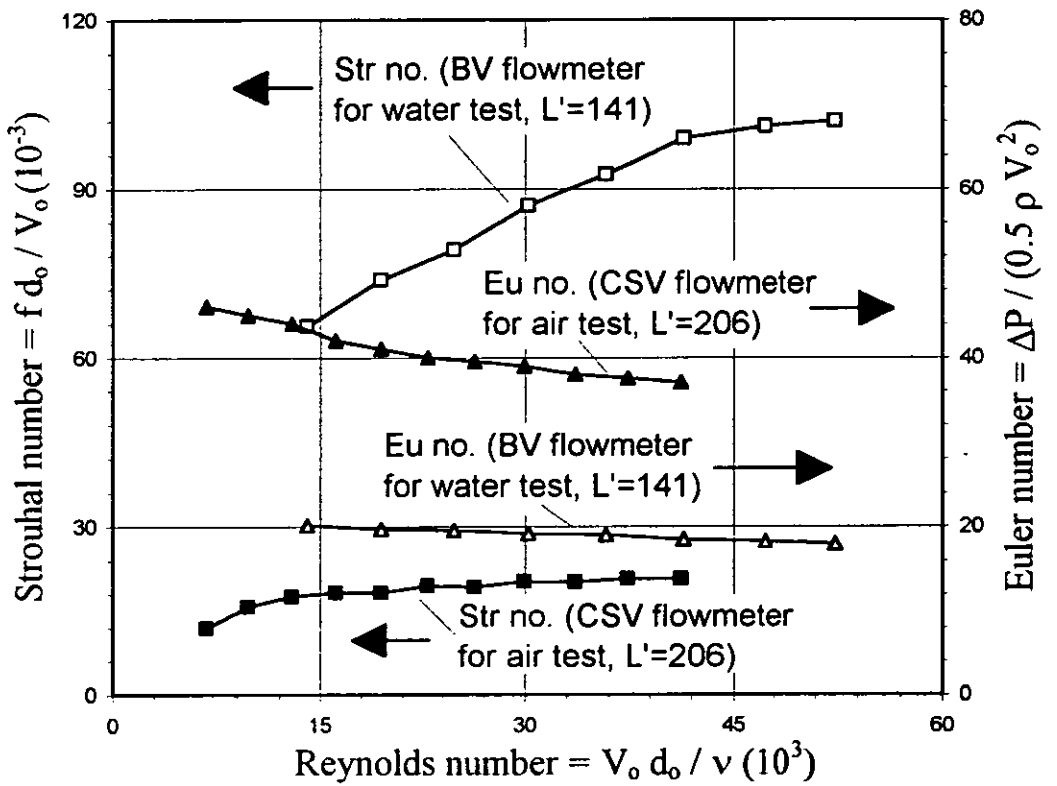


Fig.17. Overall dimensionless flowmeter calibration (refer to normalised diameter)



PAPER WITHDRAWN

C. J. FREITAS, South West Research Institute, USA

THE ORIFICE PLATE DISCHARGE COEFFICIENT EQUATION - THE EQUATION FOR ISO 5167-1

M J Reader-Harris and J A Sattary

National Engineering Laboratory, East Kilbride, Glasgow

S U M M A R Y

This report describes the final work undertaken to achieve the equation which is being balloted in ISO/TC 30/SC 2 for inclusion in ISO 5167-1. It is described as the Agreed Equation since it has the support of the ISO/TC 28 delegation. It includes a description of the work done to check that a change in the expansibility equation would not have a significant effect on discharge coefficient equations fitted to the database.

CONTENTS

	Page
NOTATION	2
1 INTRODUCTION	3
2 THE DATABASE	4
3 THE AGREED EQUATION	4
3.1 The Tapping Terms	4
3.2 The Small Pipe Diameter Term	5
3.3 The C_{∞} and Slope Terms	5
3.4 The Complete Equation	6
4 QUALITY OF FIT	7
5 COMPARISON BETWEEN EQUATIONS ON THE BASIS OF DEVIATIONS	7
6 THE EFFECT OF THE EXPANSIBILITY EQUATION	7
7 CONCLUSIONS	10
ACKNOWLEDGEMENTS	10
REFERENCES	10
LIST OF TABLES	12
LIST OF FIGURES	12

NOTATION

A	Function of orifice Reynolds number (see equation (3))
C	Orifice discharge coefficient
C_c	Orifice discharge coefficient using corner tapplings
C_s	Dependence of C_c on Reynolds number
C_∞	C_c for infinite Reynolds number for $D \geq 71.12$ mm (2.8 inch)
C_Σ	$C_\infty + C_s + \Delta C_D$
ΔC_D	Small pipe diameter term
ΔC_{down}	Downstream tapping term
ΔC_{up}	Upstream tapping term
D	Pipe diameter
d	Orifice diameter
L_1	Quotient of the distance of the upstream tapping from the upstream face of the plate and the pipe diameter
L_2'	Quotient of the distance of the downstream tapping from the downstream face of the plate and the pipe diameter
M_2'	Quotient of the distance of the downstream tapping from the downstream face of the plate and the dam height (as in equation (3))
Re_D	Pipe Reynolds number
s	Standard deviation of the data in the database about an equation
β	Diameter ratio
ε_1	Expansibility referred to upstream conditions

1 INTRODUCTION

Although the orifice plate is the recognized flowmeter for the measurement of natural gas and light hydrocarbon liquids, the orifice discharge coefficient equation in use in the international standard ISO 5167-1: 1991⁽¹⁾ is based on data collected more than 50 years ago. Moreover, for many years the United States and Europe have used different equations, a discrepancy with serious consequences for the oil and gas industry since many companies are multinational. Europe uses the Stolz Equation in ISO 5167-1: 1991 which was previously in ISO 5167: 1980. The United States used the Buckingham Equation⁽²⁾ until the Reader-Harris/Gallagher (RG) Equation (see Reference 3 and below) was adopted in 1990.

The Buckingham equation is based on the data collected by Beitler in the early 1930s at the Ohio State University Engineering Experimental Station⁽⁴⁾. Stolz⁽⁵⁾ used 303 points from the Ohio State University data together with a table of flow coefficients from ISO/R 541⁽⁶⁾. The ISO/R 541 table was established by the German VDI and is based on original data of Witte which are no longer available.

To resolve discrepancies between equations data on orifice plate discharge coefficients were collected in Europe and the United States over more than ten years in order to provide a new database from which an improved discharge coefficient equation could be obtained which would receive international acceptance.

In November 1988 a joint meeting of API (American Petroleum Institute) and EEC flow measurement experts in New Orleans accepted an equation derived by NEL⁽⁷⁾. At that time the database contained 11 346 points, collected in pipes whose diameters ranged from 50 to 250 mm (2 to 10 inch); 600 mm (24 inch) data were being collected but had not yet been included in the database. 600 mm data have since been collected in gas and in water and extend the database both in pipe diameter and in Reynolds number.

The data which were least well fitted by the equation presented at New Orleans were the 50 mm data, and following the meeting the American standard API 2530 was revised to include the Reader-Harris/Gallagher (RG) Equation based on the NEL equation accepted at New Orleans with an additional term proposed by Gallagher for pipes whose diameter lies below 71.12 mm (2.8 inch). Since there was no physical explanation for the additional term for small pipe diameter, additional data were collected in 50 mm pipe in water and oil and included in the database. Measurements by NEL of the edge radius of the plates used in European tests showed that orifices whose diameter is less than 50 mm tend to have edge radii outside those permitted by ISO 5167-1. An equation was therefore derived which included an additional term for small orifice diameter rather than one for small pipe diameter, and it was put forward in a report to EC BCR numbered PR14⁽⁸⁾. It is also described in papers at the North Sea Flow Measurement Workshop in 1992⁽⁹⁾ and in Flow Measurement and Instrumentation⁽¹⁰⁾.

However, neither this equation nor the attempt at compromise put forward at a meeting of ISO/TC 30 in Paris in 1993 were acceptable to the ISO/TC 28 delegation. It was considered by the ISO/TC 28 delegation that the PR14 Equation gave an insufficiently good fit to the data collected in 75 mm (3-inch) pipes, and their need was for an equation which was of the same form as the RG Equation in API MPMS 14.3: 1990⁽³⁾ for $Re_D \geq 4000$; only the

constants and exponents might be changed to give the best fit to the final database. Moreover, measurements by SwRI of the orifice edge radius for the orifice-plates used in 50 mm pipe were smaller than those made by NEL. Since one of the principal objectives of the last fourteen years of work was to obtain a common equation for use worldwide, an equation of the form of the RG Equation has been derived and is presented here. It is being balloted in ISO/TC 30/SC 2 for inclusion in ISO 5167-1. It is described here as the Agreed Equation since it has the support of the ISO/TC 28 Delegation. Given the definition that s is the standard deviation of the data in the database about an equation, the value of s for the Agreed Equation is very similar to the value of s for the PR14 Equation.

2 THE DATABASE

In addition to the database used for deriving the PR14 orifice plate discharge coefficient equation in 1992 an additional 146 points have been added: these are from SwRI, Texas⁽¹¹⁾; their inclusion makes essentially no difference to the final fitted equation.

3 THE AGREED EQUATION

As stated in the Introduction the Agreed Equation had to be of the same form as that of the RG Equation for $Re_D \geq 4000$ with only the constants and exponents changed.

3.1 The Tapping Terms

The form of the upstream and downstream tapping terms, ΔC_{up} and ΔC_{down} , in the RG equation (and also in the NEL equation for New Orleans described in Reference 7) is as follows:

$$\Delta C_{up} = (c_1 + c_2 e^{-f_1 L_1} - (c_1 + c_2) e^{-f_1 L_1}) (1 - c_3 A) \frac{\beta^4}{1 - \beta^4} \quad (1)$$

and

$$\Delta C_{down} = c_4 (M_2' - c_5 M_2'^{f_4}) (1 - c_6 A) \beta^{f_4} \quad (2)$$

where

$$A = \left(\frac{19000\beta}{Re_D} \right)^{0.8} \quad \text{and} \quad M_2' = \frac{2L_2'}{1 - \beta} \quad (3)$$

For high Reynolds numbers the tapping terms are identical in form to those obtained in deriving the PR14 Equation based on the enlarged database. Therefore, the coefficients c_1 , c_2 , c_4 , and c_5 and the exponents f_i ($i=1,4$), in the tapping terms for high Reynolds number are taken to be the same as those in the PR14 Equation⁽⁸⁻¹⁰⁾, except that it was found that the overall fit to the database was improved by making $c_2 = 0.08$ instead of 0.09. (The upstream tapping term for high Reynolds number is plotted in Figure 1 on the same basis as in References 8, 9 and 10.) Moreover, when the tapping terms for lower Reynolds numbers for the PR14 Equation were derived it was found that the dependence of the sum of the tapping

terms on Re_D for $Re_D \geq 4000$ could be expressed by making ΔC_{up} alone a function of Re_D . When determining the values of c_3 and c_6 to give the best fit of the form of the complete Agreed Equation to the database it was found that to permit a non-zero value of c_6 gives a negligible reduction in the standard deviation of the data about the equation. With $c_6 = 0$ the best-fit value of c_3 was 0.11. So that a good fit for the complete database (including data for $Re_D < 4000$) should still be obtained it is necessary to include an additional term in ΔC_{down} for $Re_D \leq 3700$ identical to that in the PR14 Equation. Therefore, the final tapping terms are given by

$$\Delta C_{up} = (0.043 + 0.080e^{-10L_1} - 0.123e^{-7L_1})(1 - 0.11A) \frac{\beta^4}{1 - \beta^4} \quad (4)$$

and

$$\Delta C_{down} = -0.031(M_2' - 0.8M_2'^{1.1})\{1 + 8 \max(\log_{10}(3700 / Re_D), 0.0)\}\beta^{1.3} \quad (5)$$

3.2 The Small Pipe Diameter Term

Instead of a small orifice diameter term the RG Equation uses a small pipe diameter term, ΔC_D , of the following form:

$$\Delta C_D = h_1(h_2 - \beta) \max(h_3 - D / 25.4, 0.0). \quad (D : \text{mm}) \quad (6)$$

The form of this term has no known physical basis (although the requirement for the term may be due to the edge radius of the orifice plates used in the 50 mm pipes), but the term gives a good fit to the database: C was larger in 50 mm pipes than in larger pipes even with corner and D and $D/2$ tapplings. Since there are essentially only discrete values of D in the database h_3 cannot be determined: following the RG Equation the value of h_3 was taken to be 2.8 inch (71.12 mm), 0.1 inch (2.54 mm) smaller than the internal diameter for 3-inch schedule 80 pipe. The quality of fit to the complete database improves as h_2 reduces to 0.75, the smallest value which ensures that this term does not become negative over the permissible range of use. If $(h_2 - \beta)$ were replaced by $\max(h_2 - \beta, 0)$ then the best fit is obtained with h_2 equal to 0.7, but the improvement in fit is very small and the equation significantly different from the RG Equation and also more complicated. With $h_2 = 0.75$ h_1 was determined by fitting the complete database and is equal to 0.011. Therefore, the small pipe diameter term is given by

$$\Delta C_D = 0.011(0.75 - \beta) \max(2.8 - D / 25.4, 0.0). \quad (D : \text{mm}) \quad (7)$$

3.3 The C_∞ and Slope Terms

The C_∞ and slope terms are of exactly the same form in the RG and in the PR14 Equations and so in the Agreed Equation are of the following form:

$$C_\infty + C_s = a_1 + a_2\beta^{m_1} + a_3\beta^{m_2} + b_1(10^6 \beta / Re_D)^{n_1} + (b_2 + b_3A)\beta^f \max\{(10^6 / Re_D)^{n_2}, g_1 - g_2(Re_D / 10^6)\} \quad (8)$$

The exponents used for the PR14 Equation were used for the final equation with the exception that m_1 was taken to be 2 since this value is used in the RG Equation and gives a better fit to the complete database. With m_1, m_2, l, n_1 and n_2 given by 2, 8, 3.5, 0.7 and 0.3, respectively, the tapping terms given in equations (4) and (5) and the small pipe diameter term given in equation (7) the optimum values of the constants in equation (8) were determined and the following equation obtained:

$$C_{\infty} + C_s = 0.5961 + 0.0261\beta^2 - 0.216\beta^8 + 0.000521(10^6\beta / Re_D)^{0.7} + (0.0188 + 0.0063A)\beta^{3.5} \max\{(10^6 / Re_D)^{0.3}, 22.7 - 4700(Re_D / 10^6)\}$$
 (9)

3.4 The Complete Equation

Therefore, the complete orifice plate discharge coefficient equation is as follows:

$$C = 0.5961 + 0.0261\beta^2 - 0.216\beta^8 + 0.000521(10^6\beta / Re_D)^{0.7} + (0.0188 + 0.0063A)\beta^{3.5} \max\{(10^6 / Re_D)^{0.3}, 22.7 - 4700(Re_D / 10^6)\} + (0.043 + 0.080e^{-10L_1} - 0.123e^{-7L_1})(1 - 0.11A) \frac{\beta^4}{1 - \beta^4} - 0.031(M_2' - 0.8M_2'^{1.1}) \{1 + 8 \max(\log_{10}(3700 / Re_D), 0.0)\} \beta^{1.3} + 0.011(0.75 - \beta) \max(2.8 - D / 25.4, 0.0). \quad (D : \text{mm})$$
 (10)

For $Re_D \geq 4000$ this equation can be written as follows:

For $D \geq 71.12$ mm (2.8 inch)

$$C = 0.5961 + 0.0261\beta^2 - 0.216\beta^8 + 0.000521(10^6\beta / Re_D)^{0.7} + (0.0188 + 0.0063A)\beta^{3.5}(10^6 / Re_D)^{0.3} + (0.043 + 0.080e^{-10L_1} - 0.123e^{-7L_1})(1 - 0.11A) \frac{\beta^4}{1 - \beta^4} - 0.031(M_2' - 0.8M_2'^{1.1})\beta^{1.3}.$$
 (11a)

Where $D < 71.12$ mm (2.8 inch) the following term should be added to equation (11a):

$$+0.011(0.75 - \beta) \left(2.8 - \frac{D}{25.4}\right). \quad (D : \text{mm})$$
 (11b)

Equation (11), comprising equation (11a) with the additional term (11b), is the Agreed Equation.

The notation of ISO 5167-1 has been used with the following additions:

$$A = \left(\frac{19000\beta}{Re_D} \right)^{0.8} \quad \text{and} \quad M_2' = \frac{2L_2'}{1-\beta}.$$

4 QUALITY OF FIT

The quality of the fit of equation (10) to the database is very good: the overall standard deviation of the data for $Re_D \geq 4000$ about the equation is 0.259 per cent; the mean deviations of the data about the equation as a function of β , D , Re_D and pair of tappings used and of pairs of these independent variables are both small and well-balanced.

The quality of fit is quantified in Tables 1 to 8. Table 1 gives a description of the meaning of the different lines in Tables 2 to 8. These tables give the deviations of the data in the database about the equation as a function of β , D , Re_D and pair of tappings used and certain combinations of these. The range of values of β corresponding to each nominal value of β is given in Table 2. The tappings described as Corner (GU) are tappings in the corners which were designed by Gasunie and are simpler to make than those in ISO 5167-1. They are described in Reference 12. The database used is the complete EEC/API database as described except that data with $Re_D < 4000$ were excluded in Tables 5 to 8.

5 COMPARISON BETWEEN EQUATIONS ON THE BASIS OF DEVIATIONS

A direct comparison between equation (11) and the RG and PR14 Equations for $Re_D \geq 4000$ is given here. To do this the data in Table 5 (and similar tables of deviations on the basis of D and β for the other equations) were analysed: the number of boxes (ranges of D and β) over which an equation gave a mean deviation greater than 0.1 per cent was counted and is given in Table 9; the number of boxes for which the mean deviation was greater than 0.2 per cent was also counted and is given in Table 9. A similar count was undertaken for Tables 6 - 8 and the results are also given in Table 9. These figures provide a measure of possible bias in an equation. The standard deviation of the data about each equation is also given as a measure of the quality of fit. The quality of fit for the Agreed Equation is similar to that of the PR14 Equation. They are both better than the RG Equation.

Since the Stolz Equation in ISO 5167-1: 1991 is applicable over a more limited range of values of Re_D and β than the three equations previously considered, the standard deviation and the number of boxes with mean deviations greater than 0.1 or 0.2 per cent are given in Table 10 for all four equations over the range of applicability of the Stolz ISO 5167-1: 1991 Equation. The need for an improved equation even over the limited range of Re_D and β is obvious.

6 THE EFFECT OF THE EXPANSIBILITY EQUATION

Since doubt has been expressed regarding the accuracy of the expansibility equation used for orifice plates in ISO 5167-1¹ (see Kinghorn⁽¹³⁾ and Seidl⁽¹⁴⁾) it has been suggested that the new discharge coefficient equation given in equation (10) and others based on the same database may have been significantly affected by errors in the discharge coefficient data

caused by errors in the expansibility, ε_1 , since the value of ε_1 given in Section 8.3.2.2 of ISO 5167-1: 1991 was used in the computation of discharge coefficient.

In order to test this theory, for each point of the database the value of discharge coefficient which would have been obtained if an alternative equation for ε_1 had been used was calculated and the equation refitted. If the value of discharge coefficient given in the database is termed C_f , based on the expansibility given by the equation in Section 8.3.2.2 of ISO 5167-1: 1991, $\varepsilon_{1,f}$, then C_N , the value of discharge coefficient based on an alternative value of expansibility, $\varepsilon_{1,N}$, is given by

$$C_N \varepsilon_{1,N} = C_f \varepsilon_{1,f}, \quad (12)$$

where

$$\varepsilon_{1,f} = 1 - (0.41 + 0.35\beta^4) \frac{\Delta p}{\kappa p_1}. \quad (13)$$

Where the value of $\varepsilon_{1,f}$ is given in the database it is possible to calculate κ using the values of β , Δp and p_1 and then to calculate $\varepsilon_{1,N}$. Where $\varepsilon_{1,f}$ is not given in the database it is necessary, in the first instance, to estimate what value of κ might have been used on the basis of other data; if it were shown to be the case that the discharge coefficient equation fitted to C_N differed significantly from that fitted to C_f it would be necessary to obtain better values for κ .

The only sets of gas data for which $\varepsilon_{1,f}$ was not provided in the database were those from SwRI and Ruhrgas. For SwRI the downstream expansion factor, Y_2 , (see Reference 3) was provided but not $\varepsilon_{1,f}$. So for SwRI and Ruhrgas values for κ of 1.41 and 1.32, respectively, were used: 1.41 is appropriate for nitrogen; 1.32 is a typical value for natural gas.

Three alternative equations for $\varepsilon_{1,N}$ were used: they were as follows:

$$\varepsilon_{1,N,1} = 1 - (0.35 + 0.38\beta^4) \frac{\Delta p}{\kappa p_1}, \quad (14)$$

$$\varepsilon_{1,N,2} = 1 - (0.352 + 0.433\beta^4) \frac{\Delta p}{\kappa p_1}, \quad (15)$$

and

$$\varepsilon_{1,N,3} = 1 - (0.357 + 0.557\beta^4) \frac{\Delta p}{\kappa p_1}. \quad (16)$$

$\varepsilon_{1,N,1}$ and $\varepsilon_{1,N,2}$ were taken from equations (9) (rounded as in the conclusions of the paper) and (10) of Kinghorn⁽¹³⁾ and $\varepsilon_{1,N,3}$ was taken from equation (8) (the recommended equation) of Seidl⁽¹⁴⁾.

Calculating $C_{N,i}$ on the basis of $\epsilon_{1,N,i}$ for $i=1,3$ and using the tapping terms given in equations (4) and (5), the sum of the C_∞ , C_s and ΔC_D terms, C_Σ , was refitted as follows:

$$C_\Sigma = C_\infty + C_s + \Delta C_D = a_1 + a_2\beta^2 + a_3\beta^8 + b_1(10^6\beta / Re_D)^{0.7} + (b_2 + b_3A)\beta^{3.5} \max\{(10^6 / Re_D)^{0.3}, 22.7 - 4700(Re_D / 10^6)\} + h(0.75 - \beta) \max(2.8 - D / 25.4, 0.0). \quad (D:\text{mm}) \quad (17)$$

In each case the standard deviation of the data in the database about the equation, s , the number of points which are shifted by more than 0.2 per cent, N_s , and the largest magnitude of shift, S_M , were calculated. The results were as follows:

$$C_{\Sigma,N,1} = 0.59590 + 0.02638\beta^2 - 0.21794\beta^8 + 0.0005288(10^6\beta / Re_D)^{0.7} + (0.01904 + 0.005864A)\beta^{3.5} \max\{(10^6 / Re_D)^{0.3}, 22.7 - 4700(Re_D / 10^6)\} + 0.01135(0.75 - \beta) \max(2.8 - D / 25.4, 0.0). \quad (D:\text{mm}) \quad (18)$$

$$s_{N,1} = 0.0016775; \quad N_{s,1} = 191; \quad S_{M,1} = 0.98 \text{ per cent.}$$

$$C_{\Sigma,N,2} = 0.59591 + 0.02645\beta^2 - 0.21778\beta^8 + 0.0005286(10^6\beta / Re_D)^{0.7} + (0.01895 + 0.005894A)\beta^{3.5} \max\{(10^6 / Re_D)^{0.3}, 22.7 - 4700(Re_D / 10^6)\} + 0.01133(0.75 - \beta) \max(2.8 - D / 25.4, 0.0). \quad (D:\text{mm}) \quad (19)$$

$$s_{N,2} = 0.0016768; \quad N_{s,2} = 177; \quad S_{M,2} = 0.85 \text{ per cent.}$$

$$C_{\Sigma,N,3} = 0.59592 + 0.02662\beta^2 - 0.21740\beta^8 + 0.0005281(10^6\beta / Re_D)^{0.7} + (0.01876 + 0.005965A)\beta^{3.5} \max\{(10^6 / Re_D)^{0.3}, 22.7 - 4700(Re_D / 10^6)\} + 0.01129(0.75 - \beta) \max(2.8 - D / 25.4, 0.0). \quad (D:\text{mm}) \quad (20)$$

$$s_{N,3} = 0.0016784; \quad N_{s,3} = 139; \quad S_{M,3} = 0.76 \text{ per cent.}$$

Since small differences between equations were being investigated the constants for C_Σ with the same number of decimal places as for $C_{\Sigma,N,i}$ are also required where $\epsilon_{1,I}$ was used:

$$C_{\Sigma,I} = 0.59615 + 0.02609\beta^2 - 0.21675\beta^8 + 0.0005216(10^6\beta / Re_D)^{0.7} + (0.01874 + 0.006071A)\beta^{3.5} \max\{(10^6 / Re_D)^{0.3}, 22.7 - 4700(Re_D / 10^6)\} + 0.01101(0.75 - \beta) \max(2.8 - D / 25.4, 0.0). \quad (D:\text{mm}) \quad (21)$$

$$s_I = 0.0016747.$$

The constants in equations (7) and (9) have been rounded and then rebalanced to ensure that there is no mean deviation between equation and database.

It can be seen that the differences in s and thus in overall quality of fit are very small but that $\epsilon_{1,j}$ gives the best result. Moreover the coefficients in equations (18) - (21) are very similar. The largest value of S_M for equations (18) - (20) occurs for equation (18); however, even in this case the largest magnitude of difference between the equation and equation (21) is 0.04 per cent for any values of β , D and Re_D except at the very lowest end of the Reynolds number range (below 4000). Therefore the choice of the expansibility equation has very little effect on the discharge coefficient equation and there is no problem in putting equation (11) in ISO 5167-1. However, the choice of expansibility equation has a significant effect both on some individual data points in the database and when it is used in the field, and it is important that the best equation is obtained.

7 CONCLUSIONS

The derivation of the Agreed discharge coefficient equation which is being balloted in ISO/TC 30/SC 2 for inclusion in ISO 5167-1 has been described; it has been shown that possible changes to the expansibility equation would have only a small effect on the discharge coefficient equation. Deviations of the data in the database from the Agreed equation have been tabulated and a comparison made with deviations from the PR14, RG and Stolz ISO 5167-1: 1991 equations.

ACKNOWLEDGEMENTS

The work described in this paper was carried out as part of the Flow Programme, under the sponsorship of the DTI's National Measurement System Policy Unit.

This paper is published by permission of the Director and General Manager, NEL.

REFERENCES

- 1 INTERNATIONAL ORGANIZATION FOR STANDARDIZATION. Measurement of fluid flow by means of pressure differential devices - Part 1: Orifice plates, nozzles and Venturi tubes inserted in circular cross-section conduits running full. ISO 5167-1. Geneva: International Organization for Standardization, 1991.
- 2 AMERICAN NATIONAL STANDARDS INSTITUTE. Orifice metering of natural gas. ANSI/API 2530-1975. New York: American National Standards Institute, 1975.
- 3 AMERICAN PETROLEUM INSTITUTE. Manual of Petroleum Measurement Standards, Chapter 14 - Natural Gas Fluids Measurement, Section 3 - Concentric, Square-Edged Orifice Meters, Part 1 - General Equations and Uncertainty Guidelines. MPMS Chapter 14, Section 3, Part 1, 3rd Edition. Washington DC: American Petroleum Institute, 1990.
- 4 BEITLER, S R. The flow of water through orifices. Bulletin 89. Columbus, Ohio: Ohio State University Engineering Experimental Station, 1935.

- 5 STOLZ, J. A universal equation for the calculation of discharge coefficients of orifice plates. In *Flow Measurement of Fluids*, H. H. Dijstelbergen and E. A. Spencer (eds), pp 519-534. North Holland Publishing Company, 1978.
- 6 INTERNATIONAL ORGANIZATION FOR STANDARDIZATION. *Measurement of fluid flow by means of orifice plates and nozzles*. ISO/R 541. Geneva: International Organisation for Standardisation, 1967.
- 7 READER-HARRIS, M. J. and SATTARY, J. A. The orifice plate discharge coefficient equation. *Flow Measurement and Instrumentation*, 1, 67-76, 1990.
- 8 READER-HARRIS, M. J., SATTARY, J. A. and SPEARMAN, E. P. The orifice plate discharge coefficient equation. Progress Report No PR14: EUEC/17 (EEC005). East Kilbride, Glasgow: National Engineering Laboratory Executive Agency, 1992.
- 9 READER-HARRIS, M. J., SATTARY, J. A., and SPEARMAN, E. P. The orifice plate discharge coefficient equation - further work. In *Proc. of North Sea Flow Measurement Workshop*, Peebles, ppr 1.1, Oct 1992. East Kilbride, Glasgow: National Engineering Laboratory Executive Agency.
- 10 READER-HARRIS, M. J., SATTARY, J. A., and SPEARMAN, E. P. The orifice plate discharge coefficient equation - further work. *Flow Measurement and Instrumentation*, Vol 6, pp 101-114, 1995.
- 11 MORROW, T. B. and PARK, J. T. Baseline conditions for orifice meter calibration. Report GRI-92/0097. Chicago, Illinois: Gas Research Institute, 1992 (as amended by Errata, 1993).
- 12 HOBBS, J. M., SATTARY, J. A. and MAXWELL, A. D. Experimental data for the determination of 250 mm orifice meter discharge coefficients under different installation conditions (European programme). Report EUR 10980. Brussels, Belgium: Commission of the European Communities, 1987.
- 13 KINGHORN, F. C. The expansibility correction for orifice plates: EEC data. In *Proc. Flow Measurement in the mid 80s*, Paper 5.2. East Kilbride, Glasgow: National Engineering Laboratory, 1986.
- 14 SEIDL, W. The orifice expansion correction for a 50mm line size at various diameter ratios. In *Proc. 3rd Int. Symp. on Fluid Flow Measurement*, San Antonio, Texas, 1995.

LIST OF TABLES

- 1 General information about the analysis of deviations in Tables 2 to 8
- 2 Residuals from Equation (10) as a function of β and D
- 3 Residuals from Equation (10) as a function of D and pair of tappings
- 4 Residuals from Equation (10) as a function of β and Re_D
- 5 Residuals from Equation (10) as a function of β and D ($Re_D \geq 4000$)
- 6 Residuals from Equation (10) as a function of β and Re_D ($Re_D \geq 4000$)
- 7 Residuals from Equation (10) as a function of D and Re_D ($Re_D \geq 4000$)
- 8 Residuals from Equation (10) as a function of β and pair of tappings ($Re_D \geq 4000$)
- 9 Analysis of deviations for the database ($Re_D \geq 4000$)
- 10 Analysis of deviations for the database over the range of the Stolz ISO 5167-1: 1991 Equation ($Re_D \geq 4000$).

LIST OF FIGURES

- 1 Upstream tapping term as a function of L_1 .

TABLE 1

GENERAL INFORMATION ABOUT THE ANALYSIS OF DEVIATIONS
IN TABLES 2 TO 8

For each cell, line 1 - Mean per cent error
line 2 - Per cent standard deviation
line 4 - Number of observations
line 5 - Per cent standard deviation about equation.

For the i^{th} point in a cell Per cent error, $P_i = \frac{(C_{im} - C_{ie})}{C_{im}} \times 100$,

where C_{im} is the measured discharge coefficient of the i th point, and

C_{ie} is the corresponding discharge coefficient from the equation.

Mean per cent error, $m = \frac{\sum_{i=1}^N P_i}{N}$,

where N is the number of points in the cell.

Per cent standard deviation = $\sqrt{\frac{\sum_{i=1}^N (P_i - m)^2}{N - 1}}$.

Per cent standard deviation about equation = $\sqrt{\frac{\sum_{i=1}^N P_i^2}{N}}$.

Statistics for the entire population appear in the bottom right hand cell.

TABLE 2

RESIDUALS FROM EQUATION (10) AS A FUNCTION OF β and D

D (mm)	50	75	100	150	250	600	Summary by β
β							
0.100 (0.0991 to 0.1028)	0.000 0.000 - 0 0.000	0.000 0.000 - 0 0.000	0.000 0.000 - 0 0.000	0.157 0.238 - 81 0.284	-0.004 0.269 - 79 0.268	0.000 0.000 - 0 0.000	0.078 0.265 - 160 0.276
0.200 (0.1982 to 0.2418)	0.012 0.467 - 507 0.467	-0.047 0.124 - 57 0.131	0.079 0.228 - 652 0.241	0.088 0.107 - 111 0.138	-0.170 0.187 - 714 0.253	0.028 0.239 - 394 0.240	-0.019 0.300 - 2435 0.300
0.375 (0.3620 to 0.3748)	0.073 0.296 - 444 0.304	-0.003 0.097 - 106 0.097	0.088 0.255 - 469 0.269	0.138 0.261 - 133 0.295	-0.106 0.159 - 439 0.191	0.037 0.113 - 591 0.119	0.031 0.225 - 2182 0.227
0.500 (0.4825 to 0.5003)	-0.030 0.296 - 398 0.297	0.138 0.054 - 69 0.148	0.135 0.190 - 300 0.233	0.098 0.103 - 109 0.142	0.033 0.164 - 392 0.168	-0.063 0.118 - 526 0.134	0.016 0.205 - 1794 0.205
0.570 (0.5427 to 0.5770)	-0.109 0.393 - 348 0.408	0.095 0.076 - 72 0.121	0.028 0.233 - 1008 0.235	0.009 0.143 - 136 0.143	0.074 0.260 - 1123 0.270	-0.090 0.117 - 567 0.148	0.009 0.255 - 3254 0.255
0.660 (0.6481 to 0.6646)	-0.088 0.305 - 498 0.318	0.101 0.100 - 64 0.142	-0.018 0.245 - 642 0.246	-0.097 0.204 - 92 0.225	0.050 0.197 - 823 0.204	-0.136 0.143 - 643 0.197	-0.038 0.233 - 2762 0.236
0.750 (0.7239 to 0.7509)	-0.051 0.342 - 866 0.345	0.092 0.106 - 101 0.140	0.120 0.322 - 1024 0.344	0.107 0.333 - 130 0.349	-0.024 0.321 - 1478 0.322	-0.251 0.338 - 336 0.421	-0.004 0.340 - 3935 0.340
Summary by D	-0.032 0.359 - 3061 0.361	0.062 0.113 - 469 0.129	0.067 0.264 - 4095 0.272	0.073 0.229 - 792 0.240	-0.013 0.262 - 5048 0.262	-0.073 0.199 - 3057 0.212	-0.002 0.274 - 16522 0.274

TABLE 3

RESIDUALS FROM EQUATION (10) AS A FUNCTION OF *D* AND
PAIR OF TAPPINGS

Tappings <i>D</i> (mm)	Corner (ISO)	Flange	<i>D</i> & <i>D</i> /2	Corner (GU)	Summary by <i>D</i>
50	0.008	-0.037	-0.063	0.000	-0.032
	0.411	0.314	0.393	0.000	0.359
	-	-	-	-	-
	728	1605	728	0	3061
	0.411	0.316	0.398	0.000	0.361
75	0.000	0.062	0.000	0.000	0.062
	0.000	0.113	0.000	0.000	0.113
	-	-	-	-	-
	0	469	0	0	469
	0.000	0.129	0.000	0.000	0.129
100	0.040	0.064	0.104	0.000	0.067
	0.224	0.257	0.313	0.000	0.264
	-	-	-	-	-
	1084	2078	933	0	4095
	0.228	0.265	0.330	0.000	0.272
150	0.000	0.073	0.000	0.000	0.073
	0.000	0.229	0.000	0.000	0.229
	-	-	-	-	-
	0	792	0	0	792
	0.000	0.240	0.000	0.000	0.240
250	0.026	-0.068	-0.009	0.044	-0.013
	0.249	0.212	0.280	0.320	0.262
	-	-	-	-	-
	1155	1841	1167	885	5048
	0.250	0.223	0.280	0.322	0.262
600	-0.156	0.003	-0.066	-0.097	-0.073
	0.199	0.160	0.200	0.209	0.199
	-	-	-	-	-
	828	876	1130	223	3057
	0.253	0.160	0.211	0.230	0.212
Summary by Tappings	-0.013	0.005	-0.009	0.016	-0.002
	0.283	0.248	0.301	0.306	0.274
	-	-	-	-	-
	3795	7661	3958	1108	16522
	0.283	0.249	0.301	0.306	0.274

TABLE 4

RESIDUALS FROM EQUATION (10) AS A FUNCTION OF β AND Re_D

Re_D β	10 to 4000	4000 to 10^4	10^4 to 10^5	10^5 to 10^6	10^6 to 10^7	10^7 to 10^8	Summary by β
0.100	0.095	0.108	0.037	0.000	0.000	0.000	0.078
	0.189	0.282	0.305	0.000	0.000	0.000	0.265
	-	-	-	-	-	-	-
	52	49	59	0	0	0	160
	0.211	0.299	0.305	0.000	0.000	0.000	0.276
0.200	-0.027	0.047	-0.050	-0.051	0.102	0.000	-0.019
	0.556	0.354	0.249	0.240	0.170	0.000	0.300
	-	-	-	-	-	-	-
	237	238	1190	454	316	0	2435
	0.556	0.357	0.254	0.245	0.198	0.000	0.300
0.375	0.376	0.125	0.008	-0.041	0.049	0.082	0.031
	0.509	0.322	0.175	0.157	0.084	0.083	0.225
	-	-	-	-	-	-	-
	125	133	748	711	325	140	2182
	0.631	0.344	0.175	0.162	0.097	0.116	0.227
0.500	-0.057	-0.093	0.034	0.071	-0.090	-0.057	0.016
	0.760	0.281	0.195	0.163	0.134	0.085	0.205
	-	-	-	-	-	-	-
	33	83	436	788	205	249	1794
	0.750	0.294	0.198	0.177	0.162	0.102	0.205
0.570	-0.546	-0.334	-0.040	0.002	0.083	0.028	0.009
	0.968	0.459	0.241	0.195	0.273	0.224	0.255
	-	-	-	-	-	-	-
	18	59	502	1430	782	463	3254
	1.087	0.564	0.244	0.195	0.285	0.226	0.255
0.660	-0.087	-0.325	-0.110	0.012	0.025	-0.100	-0.038
	0.116	0.522	0.307	0.203	0.193	0.177	0.233
	-	-	-	-	-	-	-
	5	35	466	1121	475	660	2762
	0.135	0.609	0.326	0.204	0.194	0.203	0.236
0.750	0.000	0.242	-0.073	0.038	-0.029	-0.053	-0.004
	0.000	0.514	0.404	0.303	0.315	0.355	0.340
	-	-	-	-	-	-	-
	0	78	615	1704	1062	476	3935
	0.000	0.565	0.410	0.305	0.316	0.359	0.340
Summary by Re_D	0.071	0.019	-0.038	0.013	0.024	-0.041	-0.002
	0.589	0.411	0.273	0.230	0.255	0.239	0.274
	-	-	-	-	-	-	-
	470	675	4016	6208	3165	1988	16522
	0.593	0.411	0.276	0.231	0.257	0.242	0.274

TABLE 5

RESIDUALS FROM EQUATION (10) AS A FUNCTION OF β and D ($Re_D \geq 4000$)

D (mm)	50	75	100	150	250	600	Summary by β
β							
0.100 (0.0991 to 0.1028)	0.000 0.000 - 0 0.000	0.000 0.000 - 0 0.000	0.000 0.000 - 0 0.000	0.267 0.277 - 29 0.381	-0.004 0.269 - 79 0.268	0.000 0.000 - 0 0.000	0.069 0.296 - 108 0.302
0.200 (0.1982 to 0.2418)	0.052 0.341 - 324 0.345	-0.047 0.124 - 57 0.131	0.079 0.232 - 626 0.244	0.095 0.079 - 83 0.123	-0.170 0.187 - 714 0.253	0.028 0.239 - 394 0.240	-0.018 0.258 - 2198 0.258
0.375 (0.3620 to 0.3748)	0.022 0.190 - 344 0.191	-0.003 0.097 - 106 0.097	0.061 0.200 - 455 0.209	0.081 0.175 - 122 0.192	-0.106 0.159 - 439 0.191	0.037 0.113 - 591 0.119	0.010 0.174 - 2057 0.174
0.500 (0.4825 to 0.5003)	-0.028 0.211 - 365 0.213	0.138 0.054 - 69 0.148	0.135 0.190 - 300 0.233	0.098 0.103 - 109 0.142	0.033 0.164 - 392 0.168	-0.063 0.118 - 526 0.134	0.017 0.179 - 1761 0.180
0.570 (0.5427 to 0.5770)	-0.086 0.322 - 330 0.333	0.095 0.076 - 72 0.121	0.028 0.233 - 1008 0.235	0.009 0.143 - 136 0.143	0.074 0.260 - 1123 0.270	-0.090 0.117 - 567 0.148	0.012 0.242 - 3236 0.243
0.660 (0.6481 to 0.6646)	-0.088 0.307 - 493 0.319	0.101 0.100 - 64 0.142	-0.018 0.245 - 642 0.246	-0.097 0.204 - 92 0.225	0.050 0.197 - 823 0.204	-0.136 0.143 - 643 0.197	-0.038 0.233 - 2757 0.236
0.750 (0.7239 to 0.7509)	-0.051 0.342 - 866 0.345	0.092 0.106 - 101 0.140	0.120 0.322 - 1024 0.344	0.107 0.333 - 130 0.349	-0.024 0.321 - 1478 0.322	-0.251 0.338 - 336 0.421	-0.004 0.340 - 3935 0.340
Summary by D	-0.037 0.305 - 2722 0.308	0.062 0.113 - 469 0.129	0.064 0.259 - 4055 0.267	0.061 0.217 - 701 0.225	-0.013 0.262 - 5048 0.262	-0.073 0.199 - 3057 0.212	-0.004 0.259 - 16052 0.259

TABLE 6

RESIDUALS FROM EQUATION (10) AS A FUNCTION OF β AND Re_D ($Re_D \geq 4000$)

Re_D β	10 to 4000	4000 to 10^4	10^4 to 10^5	10^5 to 10^6	10^6 to 10^7	10^7 to 10^8	Summary by β
0.100	0.000	0.108	0.037	0.000	0.000	0.000	0.069
	0.000	0.282	0.305	0.000	0.000	0.000	0.296
	-	-	-	-	-	-	-
	0	49	59	0	0	0	108
0.200	0.000	0.047	-0.050	-0.051	0.102	0.000	-0.018
	0.000	0.354	0.249	0.240	0.170	0.000	0.258
	-	-	-	-	-	-	-
	0	238	1190	454	316	0	2198
0.375	0.000	0.125	0.008	-0.041	0.049	0.082	0.010
	0.000	0.322	0.175	0.157	0.084	0.083	0.174
	-	-	-	-	-	-	-
	0	133	748	711	325	140	2057
0.500	0.000	-0.093	0.034	0.071	-0.090	-0.057	0.017
	0.000	0.281	0.195	0.163	0.134	0.085	0.179
	-	-	-	-	-	-	-
	0	83	436	788	205	249	1761
0.570	0.000	0.294	0.198	0.177	0.162	0.102	0.180
	0.000	-0.334	-0.040	0.002	0.083	0.028	0.012
	0.000	0.459	0.241	0.195	0.273	0.224	0.242
	-	-	-	-	-	-	-
0.660	0	59	502	1430	782	463	3236
	0.000	0.564	0.244	0.195	0.285	0.226	0.243
	0.000	-0.325	-0.110	0.012	0.025	-0.100	-0.038
	0.000	0.522	0.307	0.203	0.193	0.177	0.233
0.750	-	-	-	-	-	-	-
	0	35	466	1121	475	660	2757
	0.000	0.609	0.326	0.204	0.194	0.203	0.236
	0.000	0.242	-0.073	0.038	-0.029	-0.053	-0.004
Summary by Re_D	0.000	0.514	0.404	0.303	0.315	0.355	0.340
	-	-	-	-	-	-	-
	0	78	615	1704	1062	476	3935
	0.000	0.565	0.410	0.305	0.316	0.359	0.340
Summary by Re_D	0.000	0.019	-0.038	0.013	0.024	-0.041	-0.004
	0.000	0.411	0.273	0.230	0.255	0.239	0.259
	-	-	-	-	-	-	-
	0	675	4016	6208	3165	1988	16052
Summary by Re_D	0.000	0.411	0.276	0.231	0.257	0.242	0.259

TABLE 7

DEVIATIONS FROM EQUATION (10) AS A FUNCTION OF D AND Re_D ($Re_D \geq 4000$)

Re_D D (mm)	10 to 4000	4000 to 10^4	10^4 to 10^5	10^5 to 10^6	10^6 to 10^7	10^7 to 10^8	Summary by D
50	0.000	-0.031	-0.082	0.095	0.000	0.000	-0.037
	0.000	0.467	0.278	0.178	0.000	0.000	0.305
	-	-	-	-	-	-	-
	0	403	1749	570	0	0	2722
	0.000	0.467	0.289	0.202	0.000	0.000	0.308
75	0.000	-0.047	0.046	0.086	0.000	0.000	0.062
	0.000	0.137	0.119	0.097	0.000	0.000	0.113
	-	-	-	-	-	-	-
	0	22	209	238	0	0	469
	0.000	0.141	0.127	0.129	0.000	0.000	0.129
100	0.000	0.149	0.041	0.057	0.114	0.000	0.064
	0.000	0.252	0.271	0.259	0.228	0.000	0.259
	-	-	-	-	-	-	-
	0	134	1111	2276	534	0	4055
	0.000	0.292	0.274	0.265	0.255	0.000	0.267
150	0.000	0.225	0.149	-0.031	-0.119	0.000	0.061
	0.000	0.226	0.244	0.125	0.095	0.000	0.217
	-	-	-	-	-	-	-
	0	68	275	328	30	0	701
	0.000	0.317	0.286	0.129	0.151	0.000	0.225
250	0.000	-0.175	-0.153	-0.032	0.011	0.194	-0.013
	0.000	0.360	0.212	0.222	0.296	0.231	0.262
	-	-	-	-	-	-	-
	0	48	646	2348	1490	516	5048
	0.000	0.397	0.261	0.225	0.296	0.301	0.262
600	0.000	0.000	-0.323	-0.078	0.002	-0.123	-0.073
	0.000	0.000	0.336	0.194	0.196	0.179	0.199
	-	-	-	-	-	-	-
	0	0	26	448	1111	1472	3057
	0.000	0.000	0.461	0.209	0.196	0.218	0.212
Summary by Re_D	0.000	0.019	-0.038	0.013	0.024	-0.041	-0.004
	0.000	0.411	0.273	0.230	0.255	0.239	0.259
	-	-	-	-	-	-	-
	0	675	4016	6208	3165	1988	16052
	0.000	0.411	0.276	0.231	0.257	0.242	0.259

TABLE 8

DEVIATIONS FROM EQUATION (10) AS A FUNCTION OF β AND PAIR OF TAPPINGS
($Re_D \geq 4000$)

Tappings β	Corner (ISO)	Flange	$D\&D/2$	Corner (GU)	Summary by β
0.100	0.000	0.069	0.000	0.000	0.069
	0.000	0.296	0.000	0.000	0.296
	-	-	-	-	-
	0	108	0	0	108
0.200	0.000	0.302	0.000	0.000	0.302
	0.018	-0.034	-0.002	-0.098	-0.018
	0.274	0.233	0.272	0.259	0.258
	-	-	-	-	-
0.375	537	925	582	154	2198
	0.275	0.235	0.272	0.276	0.258
	-0.006	0.026	0.006	-0.072	0.010
	0.175	0.178	0.155	0.170	0.174
0.500	-	-	-	-	-
	382	1101	466	108	2057
	0.175	0.180	0.155	0.184	0.174
	0.012	0.020	0.029	-0.037	0.017
0.570	0.242	0.154	0.160	0.178	0.179
	-	-	-	-	-
	369	884	403	105	1761
	0.241	0.155	0.163	0.181	0.180
0.660	-0.002	-0.035	0.084	0.080	0.012
	0.231	0.197	0.274	0.314	0.242
	-	-	-	-	-
	794	1366	845	231	3236
0.750	0.231	0.200	0.286	0.323	0.243
	-0.068	-0.045	0.006	-0.040	-0.038
	0.231	0.215	0.256	0.244	-0.233
	-	-	-	-	-
Summary by Tappings	671	1200	690	196	2757
	0.241	0.220	0.256	0.246	0.236
	-0.026	0.060	-0.147	0.106	-0.004
	0.324	0.290	0.381	0.381	0.340
Summary by Tappings	-	-	-	-	-
	963	1765	893	314	3935
	0.325	0.296	0.408	0.395	0.340
	-0.017	0.004	-0.011	0.016	-0.004
Summary by Tappings	0.262	0.229	0.291	0.306	0.259
	-	-	-	-	-
	3716	7349	3879	1108	16052
	0.263	0.229	0.291	0.306	0.259

TABLE 9

ANALYSIS OF DEVIATIONS FOR THE DATABASE ($Re_D \geq 4000$)

	AGREED EQUATION (11)		PR14 EQUATION		RG EQUATION	
	N_1	N_2	N_1	N_2	N_1	N_2
$\beta \vee D$	10	2	14	2	18	6
$\beta \vee Re_D$	8	3	6	5	14	6
$D \vee Re_D$	10	2	7	2	12	2
$\beta \vee$ Tappings	2	0	2	0	6	1
TOTAL	30	7	29	9	50	15
s (per cent)	0.259		0.254		0.292	

TABLE 10

ANALYSIS OF DEVIATIONS FOR THE DATABASE OVER THE RANGE OF THE STOLZ ISO 5167-1:1991 EQUATION ($Re_D \geq 4000$)

	AGREED EQUATION (11)		PR14 EQUATION		RG EQUATION		STOLZ ISO 5167-1:1991 EQUATION	
	N_1	N_2	N_1	N_2	N_1	N_2	N_1	N_2
$\beta \vee D$	8	1	15	2	17	6	26	16
$\beta \vee Re_D$	4	0	3	1	10	4	16	12
$D \vee Re_D$	7	2	10	3	10	3	16	10
$\beta \vee$ Tappings	2	0	2	0	5	0	13	7
TOTAL	21	3	30	6	42	13	71	45
s (per cent)	0.245		0.247		0.277		0.390	

DEFINITIONS FOR TABLES 9 AND 10:

N_1 is the number of boxes with the mean deviation greater than 0.1 per cent.

N_2 is the number of boxes with the mean deviation greater than 0.2 per cent.

s is the standard deviation of the data in the database about the equation.

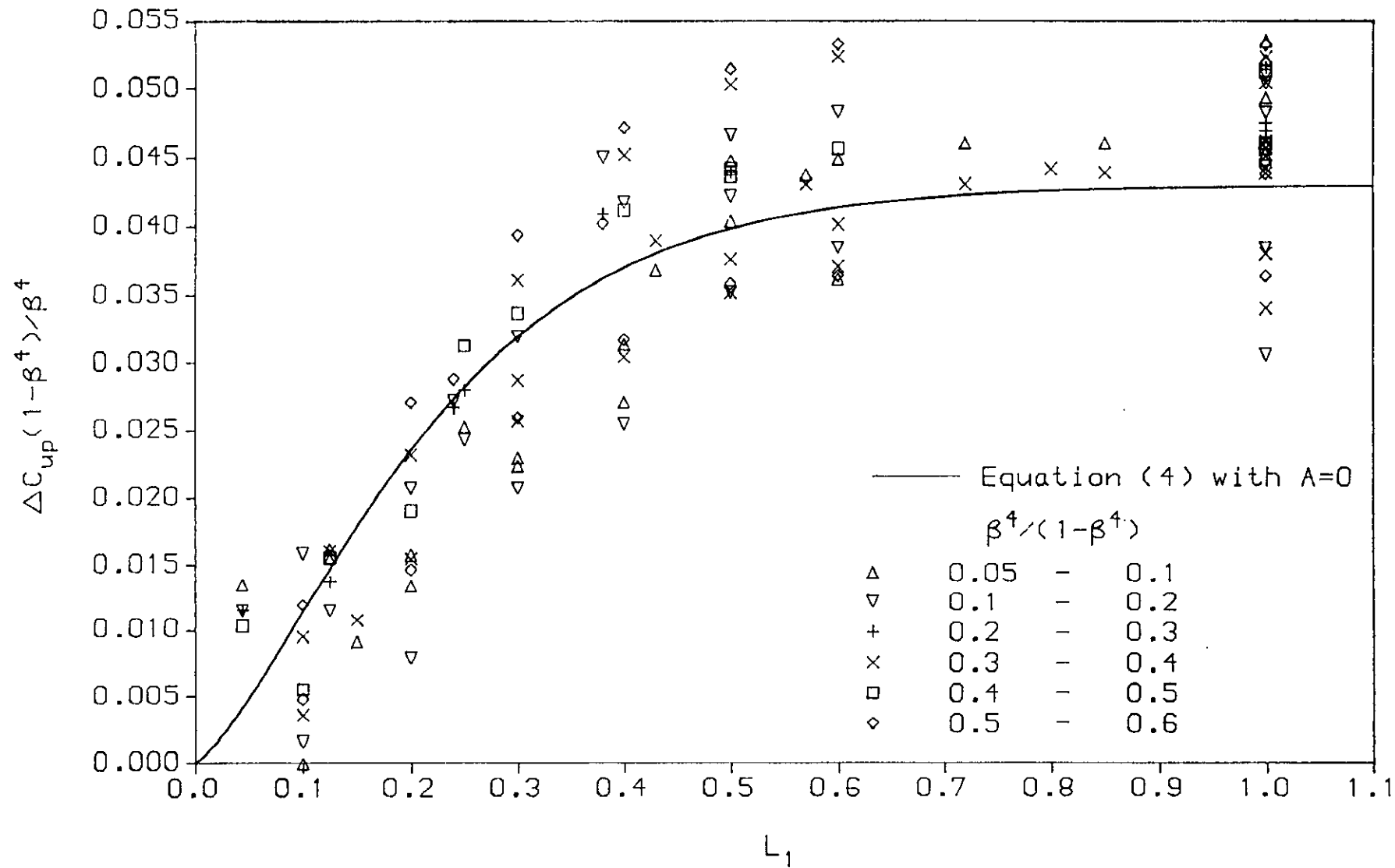


FIG 1 Upstream tapping term as a function of L_1

VERIFICATION OF METER PERFORMANCE AND WELL ALLOCATION
BY DATA ANALYSIS.

AUTHOR
FRANK KEMP
STATOIL

SUMMARY:

The Statfjord field is now past peak production. Sub-sea tie-in of satellite fields to the Statfjord C platform requires the use of well allocation by test separator for ownership allocation between fields.

The fiscal metering station is for oil transfer from platform storage to shuttle tanker.

The paper will show how, by data acquisition and analysis, the oil to storage flow measurement can be verified to fiscal standard, and well and field allocations can be verified to the standards specified by the Department of Trade and Industry (DTI) and the Norwegian Petroleum Directorate (NPD).

1. INTRODUCTION

Traditional fiscal flow measurement requirements are clearly specified and set stringent requirements for measurement uncertainty. These in turn set stringent requirements with regard to equipment, installation and the product to be measured.

With today's requirements for cheaper, faster, and simpler field developments, with use of existing infrastructure, we rarely have the luxury of a fiscal quality stream to be measured. This is reflected in the emphasis on multi-phase metering at this workshop.

DTI and NPD have also demonstrated their willingness to approve alternative field developments where measurement to fiscal standards is not economically justified by the cost of reducing the measurement uncertainty.

At the 1995 workshop Lewis Philp from the DTI included the following list of typical uncertainties by category in his presentation:

- | | | |
|--------------------------------|--------------|--------------|
| i) Fiscal: | 0.25% oil | 1.0% gas |
| ii) Allocation (continuous) | 0.5-1.0% oil | 2.0-3.0% gas |
| iii) Allocation (intermittent) | 5% oil | 5% gas |

These have been used as a guideline when evaluating performance on Statfjord.

2. THE STATFJORD FIELD DEVELOPMENT

The Statfjord field lies to the north of the Brend field and extends into the UK sector.

The UK share is currently 14.5% pending the results of the final redetermination. The metering system therefore has to meet the requirements of both the NPD and the DTI.

The field development consists of three concrete gravity basis production platforms. Each platform has separate crude oil storage capacity, offshore loading system, and fiscal metering stations for oil and gas export.

Production start was in November 1979 from Statfjord A and the field development was completed in 1985 when Statfjord C came on stream and gas export started. Plateau production rates of 700,000 barrels/day were maintained until 1992 when the Snorre field was tied in to Statfjord A at the end of the year. The current development was completed at the end of 1994 when the Statfjord Nord and Oest satellites were tied into the Statfjord C platform.

The Snorre field extends over two licences with the current split of 70.3/29.7 between the PL089 and PL057 groups.

The Statfjord Oest field also extends over two licences with the current split of 50/50 between PL089/PL037 groups. The Statfjord Nord field lies 100% within the PL037 license which is the norwegian license for the main Statfjord field.

The fiscaly metered export quantities of oil and gas must therefore be allocated between 4 fields, 7 license shares, and 15 participating companies where the majority have participating interests in more than one field.

3. THE METERING SYSTEM

The metering system shown in figure 1 represents the original configuration for all 3 platforms.

- i) Fiscal oil export metering station consisting of 5 turbine meters and a meter prover.
- ii) Oil inventory measurement by DP measurement of the oil/water interface in the storage cells.
- iii) Oil to storage metering by 2 turbine meters.
- iv) Gas export metering station consisting of orifice meters, samplers, and online gas chromatographs. (Statfjord B has an additional gas export metering station for UK gas export.
- v) Gas injection metering.
- vi) Fuel gas metering
(both fuel and injection gas are of export quality).
- vii) Flare gas metering.
- viii) Test seperator measurement of well streams for reservoir management.

The oil to storage meters used for daily production reporting are verified to fiscal standard on a monthly basis by comparing the metered inventory (opening inventory plus oil to storage minus oil export) to the DP measurement of inventory levels at the end of each day. The difference between the two inventory levels is plotted as shown in figure 2.

If the oil to storage meters are consistent with the fiscal meters the difference will fluctuate plus minus zero due to the uncertainty of the DP measurement.

As the output is metered to fiscal standard the slightest systematic variation in the metered input will accumulate as a difference between the two inventory figures.

An end of month adjustment is made to the monthly production figure to correct for the accumulated difference.

As there was no provision for online proving of the oil to storage meters the original procedure was to change out the meters at six month intervals for onshore proving. The meters are now only replaced when they no longer measure correctly.

The uncertainty of the method is +/- 2000 Sm³ which would seem to be high. For a daily production rate of 25000 Sm³ this would represent +/- 8%. However on a monthly basis, at the same production rate, the uncertainty is reduced to +/- 0.27% and the cumulative uncertainty is insignificant.

This means that a non-fiscal standard metering station can be used as the fiscal metering point for field allocation.

4. THE STATFJORD C METERING AND ALLOCATION SYSTEM

The development of the Nord and Oest satellite fields required an additional inlet separator for the satellite fields to provide sufficient processing capacity. Production reaches the platform through 4 flow lines from 4 subsea templates (2 for each field) with 4 well slots on each template. Fully developed each field will have 6 production wells with an additional 4 well template for water injection on each field.

The original metering and allocation concept was for a fiscal standard metering station on the oil and gas streams from the satellite inlet separator with proportional sampling in order to establish the total mass per component of hydrocarbons produced during the month. Proportional sampling was also added to the oil to storage metering station in order to establish the total mass per component of hydrocarbons processed on the platform (the gas composition is already available from the gas export metering station). No additional metering station was added to the oil and gas streams from the original inlet separator to establish the total hydrocarbons produced by the main field. This was calculated as the difference between the total processed hydrocarbons and the total satellite production on a mass per component basis. The C₆+ component oil recovery factor for the platform was then used to allocated this component to oil and gas produced from

each field. Light end components in the processed oil were then allocated to each field in proportion to the C6+ component

Finally the remaining mass per component was allocated as the gas stream for each field.

Allocation between the satellite fields is in proportion to the theoretical production per flowline established via the test separator. When a flowline is routed through the test separator this bypasses the new inlet separator metering station. The mass flow from the test separator therefore has to be added to the total mass from this metering station before the allocation can be made.

The disadvantages of this metering and allocation concept are obvious. No direct metering of oil production from any of the fields. No mass balance over the platform to enable verification of the meters. Dependency on the oil recovery factor being representative for all fields. Allocation by difference for the main field which therefore bears the total measurement and allocation uncertainty (plus or minus).

Some of the reasons for the choice are just as obvious.

First and foremost cost. Multiphase meters on the flowlines were proposed in addition to the new inlet separator metering station in order to allocate production between the satellite fields and reduce the requirement for well testing. The reduction in uncertainty did not justify the cost. A metering station on the original inlet separator was rejected for the same reason.

The allocation based on the new metering station, instead of well allocation for all 3 fields, was chosen because this concept was already approved and in operation for the tie-in of the Snorre field to Statfjord A. There, after two stages of separation and dehydration of the gas, the gas and live crude streams are fiscally measured on the Snorre platform before transfer to Statfjord A. (The oil stream is connected to the existing process trains upstream of the 2nd stage separator for two further stages of commingled separation upstream of the oil to storage meters. The gas stream enters a new gas separator for pressure reduction prior to entering the existing process trains together with the gas from the Statfjord A inlet separators).

For the well allocation alternative there were problems in reaching agreement as to the relative uncertainty of a well allocation where the satellite fields have two wells (flowlines) each and the main field has 22. On the one hand each well from the main field makes a smaller contribution to the overall uncertainty while on the other it is harder to pinpoint changes to individual wells due to increasing GOR or water cut. The shrinkage factor to be applied to the well test measurements in order to find the stock tank production rate was also a significant contributor to the overall uncertainty, and is still the most likely source of systematic error between the satellite fields.

The preliminary daily production figures after start up were based on the well allocation performed on the platform where the metered volume from the satellite metering station, with an average shrinkage factor for the two satellite field reservoirs applied, was used as the basis for calculating the daily production for the Nord and Oest fields while the oil to storage volume less the satellite volume was used for the main field well allocation.

In order to verify the shrinkage factors a comparison was made between the allocated and theoretical volumes.

The results for the first two months were as follows:

	TOTAL		SFC		SAT.		OEST		NORD	
	Diff.	vol.								
1	0.46	100	0.49	62	0.42	38	0.19	20	0.69	18
2	0.39	100	0.51	63	0.18	37	0.33	20	-0.01	17
cum2	0.42	100	0.50	62.5	0.30	37.5	0.27	20	0.34	17.5

Where: Diff. = Percentage variation between measured/allocated production.

Vol. = Percentage of total production volume for each stream.

Daily variations of +/- 5% or more between allocated and theoretical production for individual streams were registered. However, this can be expected under well testing, or after a production shut in when wells have to be beamed up to a stable production rate. The above table would however indicate that these variations even out over the monthly allocation period. The results also indicate the following:

- Total theoretical production has less than 0.5% variance from metered total production.
- Theoretical production from the satellites has less than 0.5% variance from metered satellite production (with shrinkage factor).
- No significant difference between the percentage variance for total platform or the individual fields.

- The shrinkage factors used for the individual reservoir fluids are correctly calculated and do not represent a source of systematic error for the allocation.

This may seem a rather small amount of data on which to base such sweeping conclusions, however two months data is the result of 60 daily allocations. For a monthly allocation it takes 5 years to collect a similar amount of data!

The result for months 3 and 4 were as follows:

	TOTAL		SFC		SAT		OEST		NORD	
	Diff.	vol.								
3	-1.98	100	-3.17	61	-0.10	39	-0.03	20	-0.17	19
4	-1.62	100	-2.54	61	0.19	39	-0.12	20	0.58	19
Cum2	-1.80	100	-2.85	61	0.03	39	-0.07	20	0.15	19
Cum4	-0.66	100	-1.55	63	0.17	37	0.10	20	0.25	17

At first glance the results would seem to be less promising than the first two months; however the larger difference between theoretical and allocated production is entirely due to water break through in some wells from the main field reservoir. This could be confirmed by the increase in water produced and by subsequent well tests. The variances for the satellite fields remain well within the required tolerances. In month 3 there was also water breakthrough in both of the satellite fields resulting in a difference of -5.61% between metered satellite production (with shrinkage factor) and theoretical satellite production.

When revised rates were applied after well testing the variance was reduced to -0.23%. As this could affect the field allocation between Oest and Nord a reallocation of the first 24 days in the month was carried out using the revised theoretical production rates after water breakthrough. It is the results from the reallocation which are shown in the table.

All other figures in the tables are based on the original data as collected. No effort has been made to improve the results by excluding unrepresentative data.

CONCLUSION:

Based on the result of the first two months one could conclude that a well allocation for all three fields, without an intermediate measurement of the satellite fields, would give a representative field allocation.

Subsequent results have shown that the volume metering of oil and water produced by the satellite fields has enabled us to provide an accurate allocation of the satellite fields despite increasing water production in the main field. Increasing GOR in the main field due to reproduction of injected gas would have also caused problems without the intermediate metering. On the other hand, increasing GOR on the main field, would have a significant effect on the oil recovery factor required for a mass allocation.

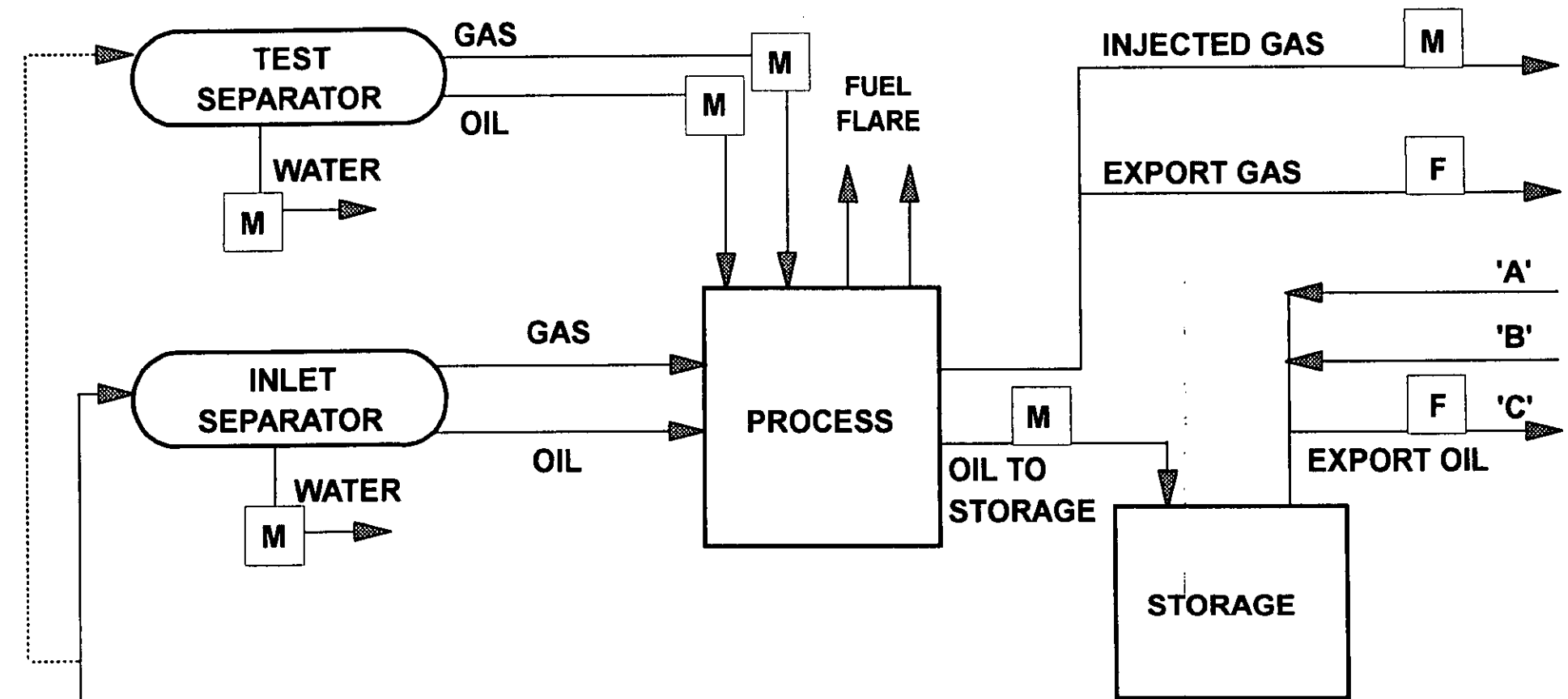
The overall conclusion is therefore:

Well allocation, based on theoretical production rates per flowline, of the Oest and Nord fields using the metered volume (with shrinkage factor) from the satellite metering station provides the most equitable allocation of production between the three fields.

The recommendation to the field owners was therefore to ammend the agreements accordingly to reflect the change from a mass to a volume based allocation for all fields.

STATFJORD PLATFORM

METERING AND SAMPLING



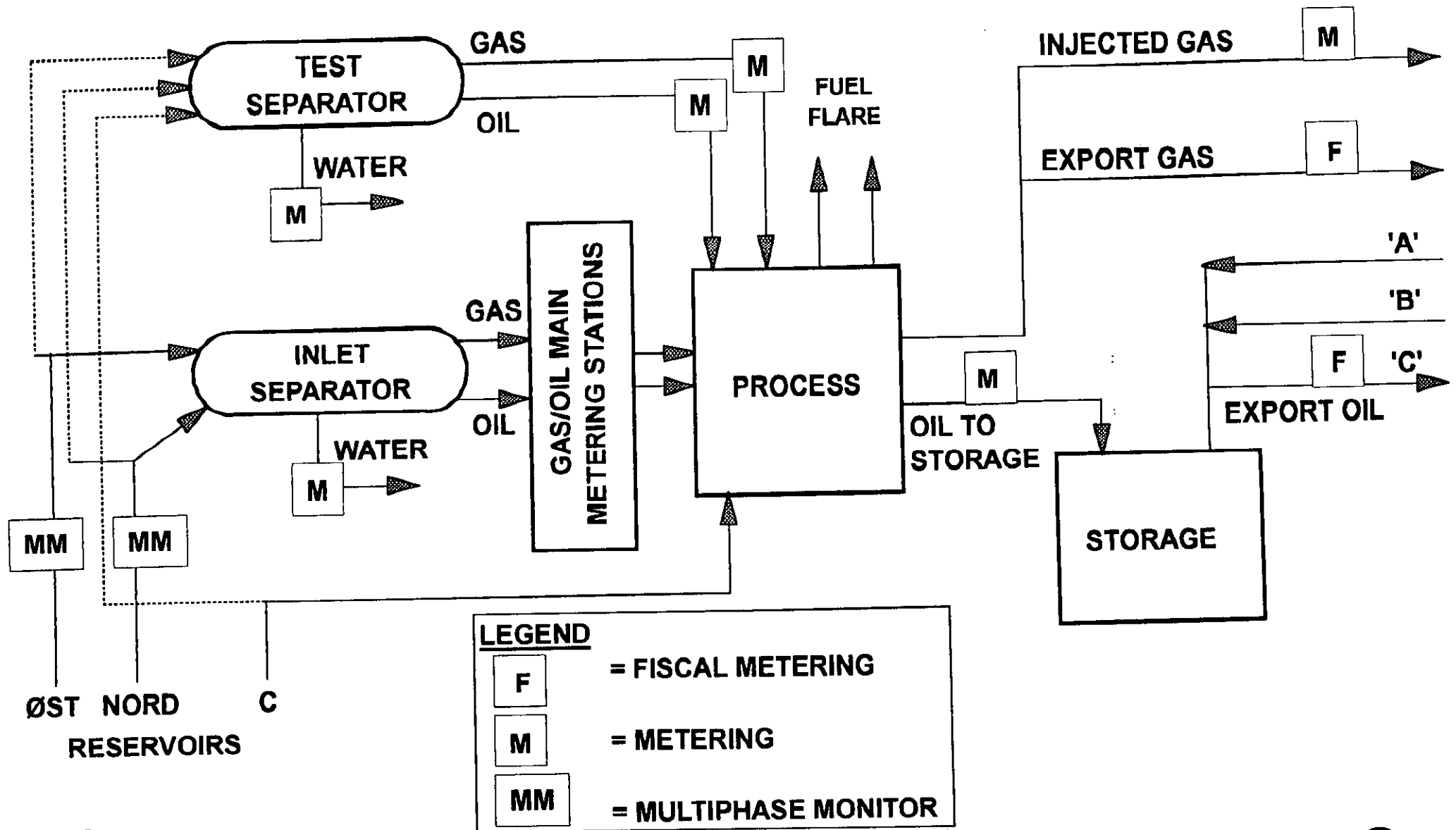
WELL STREAMS

LEGEND

- F** = FISCAL METERING
- M** = METERING

STATFJORD ØST/NORD TIE-IN STATFJORD 'C' PLATFORM

METERING AND SAMPLING



	total				statfjord C				satellites				oest				nord			
	prod.	diff.	diff.%	vol.%	prod.	diff.	diff.%	vol.%	prod.	diff.	diff.%	vol.%	prod.	diff.	diff.%	vol.%	prod.	diff.	diff.%	vol.%
nov.	1459789	6737	0,46	100	904728	4395	0,49	62,0	555048	2342	0,42	38,0	293488	543	0,19	32,4	261560	1799	0,69	17,9
dec.	1579789	6108	0,39	100	1002306	5085	0,51	63,4	577483	1023	0,18	36,6	320761	1085	0,34	32,0	256722	-35	-0,01	16,3
cum. 1	3039578	12845	0,42	100	1907034	9480	0,50	62,7	1132531	3365	0,30	37,3	614249	1628	0,27	32,2	518282	1764	0,34	17,1
jan.	1490001	-29436	-1,98	100	908891	-28853	-3,17	61,0	581110	-583	-0,10	39,0	300517	-93	-0,03	33,1	280593	-490	-0,17	18,8
feb.	1396842	-22602	-1,62	100	926326	-23497	-2,54	66,3	470516	895	0,19	33,7	261505	-317	-0,12	28,2	209011	1212	0,58	15,0
cum. 2	2886843	-52038	-1,80	100	1835217	-52350	-2,85	63,6	1051626	312	0,03	36,4	562022	-410	-0,07	30,6	489604	722	0,15	17,0
cum. 3	5926421	-39193	-0,66	100	3742251	-42870	-1,15	63,1	2184157	3677	0,17	36,9	1176271	1218	0,10	31,4	1007886	2486	0,25	17,0

NOVEMBER 1995					NOVEMBER 1995				
STATFJORD C + SATELLITES					STATFJORD C				
	ALLOK	TEOR	DIFF	DIFF		ALLOK	TEOR	DIFF	DIFF
DAY	SM3	SM3	SM3	%	DAY	SM3	SM3	SM3	%
2	39.490	39.377	113	0,29	2	25.672	25.835	-163	-0,63
3	52.074	52.416	-342	-0,66	3	34.372	33.406	966	2,81
4	49.093	49.267	-174	-0,35	4	31.399	31.308	91	0,29
5	50.804	50.031	773	1,52	5	31.852	30.970	882	2,77
6	51.138	51.458	-320	-0,63	6	29.783	30.175	-392	-1,32
7	51.789	50.762	1.027	1,98	7	30.865	30.275	590	1,91
8	48.840	48.588	252	0,52	8	30.795	30.399	396	1,29
9	50.469	49.917	552	1,09	9	34.303	33.706	597	1,74
10	51.453	51.320	133	0,26	10	32.789	33.009	-220	-0,67
11	50.524	50.496	28	0,06	11	30.819	31.287	-468	-1,52
12	48.263	49.208	-945	-1,96	12	27.590	28.690	-1.100	-3,99
13	52.058	50.771	1.287	2,47	13	33.244	32.419	825	2,48
14	51.211	50.227	984	1,92	14	32.332	31.913	419	1,30
15	52.078	51.391	687	1,32	15	31.611	31.209	402	1,27
16	51.522	51.588	-66	-0,13	16	30.683	31.061	-378	-1,23
17	52.048	51.889	159	0,31	17	31.300	31.364	-64	-0,20
18	51.159	50.821	338	0,66	18	30.461	30.302	159	0,52
19	52.080	52.128	-48	-0,09	19	31.420	31.687	-267	-0,85
20	52.041	52.077	-36	-0,07	20	31.417	31.686	-269	-0,86
21	51.851	51.728	123	0,24	21	31.273	31.401	-128	-0,41
22	47.835	48.537	-702	-1,47	22	33.677	33.462	215	0,64
23	51.175	50.496	679	1,33	23	30.834	30.213	621	2,01
24	52.039	51.550	489	0,94	24	31.787	31.508	279	0,88
25	49.356	50.310	-954	-1,93	25	30.144	30.890	-746	-2,47
26	52.027	51.155	872	1,68	26	33.351	32.438	913	2,74
27	52.017	51.297	720	1,38	27	31.556	31.256	300	0,95
28	42.359	43.596	-1.237	-2,92	28	27.076	27.560	-484	-1,79
29	51.661	50.091	1.570	3,04	29	31.464	30.437	1.027	3,26
30	51.322	50.547	775	1,51	30	30.859	30.467	392	1,27
	1.459.776	1.453.039	6.737	0,46		904.728	900.333	4.395	0,49

NOVEMBER 1995					NOVEMBER 1995					NOVEMBER 1995				
SATELLITES					ØST					NORD				
	ALLOK	TEOR	DIFF	DIFF		ALLOK	TEOR	DIFF	DIFF		ALLOK	TEOR	DIFF	DIFF
DAY	SM3	SM3	SM3	%	DAY	SM3	SM3	SM3	%	DAY	SM3	SM3	SM3	%
2	13.818	13.542	276	2.00	2	10.927	10.751	176	1,61	2	2.891	2.791	100	3,46
3	17.702	19.010	-1.308	-7,39	3	10.825	10.701	124	1,15	3	6.877	8.309	-1.432	-20,82
4	17.694	17.959	-265	-1,50	4	10.685	10.663	22	0,21	4	7.009	7.296	-287	-4,09
5	18.952	19.061	-109	-0,58	5	10.569	11.056	-487	-4,61	5	8.383	8.005	378	4,51
6	21.355	21.283	72	0,34	6	10.585	10.566	19	0,18	6	10.770	10.717	53	0,49
7	20.924	20.487	437	2,09	7	10.667	10.505	162	1,52	7	10.257	9.982	275	2,68
8	18.045	18.189	-144	-0,80	8	7.947	8.322	-375	-4,72	8	10.098	9.867	231	2,29
9	16.166	16.211	-45	-0,28	9	6.540	6.344	196	3,00	9	9.626	9.867	-241	-2,50
10	18.664	18.311	353	1,89	10	8.459	8.444	15	0,18	10	10.205	9.867	338	3,31
11	19.705	19.209	496	2,52	11	9.565	9.342	223	2,33	11	10.140	9.867	273	2,69
12	20.673	20.518	155	0,75	12	10.837	10.658	179	1,65	12	9.836	9.860	-24	-0,24
13	18.814	18.352	462	2,46	13	10.807	10.658	149	1,38	13	8.007	7.694	313	3,91
14	18.879	18.314	565	2,99	14	10.718	10.658	60	0,56	14	8.161	7.656	505	6,19
15	20.467	20.182	285	1,39	15	10.808	10.658	150	1,39	15	9.659	9.524	135	1,40
16	20.839	20.527	312	1,50	16	10.820	10.660	160	1,48	16	10.019	9.867	152	1,52
17	20.748	20.525	223	1,07	17	10.774	10.658	116	1,08	17	9.974	9.867	107	1,07
18	20.698	20.519	179	0,86	18	10.743	10.652	91	0,85	18	9.955	9.867	88	0,88
19	20.660	20.441	219	1,06	19	10.609	10.574	35	0,33	19	10.051	9.867	184	1,83
20	20.624	20.391	233	1,13	20	10.534	10.516	18	0,17	20	10.090	9.875	215	2,13
21	20.578	20.327	251	1,22	21	10.581	10.452	129	1,22	21	9.997	9.875	122	1,22
22	14.158	15.075	-917	-6,48	22	8.023	8.748	-725	-9,04	22	6.135	6.327	-192	-3,13
23	20.341	20.283	58	0,29	23	10.540	10.435	105	1,00	23	9.801	9.848	-47	-0,48
24	20.252	20.042	210	1,04	24	10.463	10.925	-462	-4,42	24	9.789	9.117	672	6,86
25	19.212	19.420	-208	-1,08	25	10.211	10.317	-106	-1,04	25	9.001	9.103	-102	-1,13
26	18.676	18.717	-41	-0,22	26	10.355	10.339	16	0,15	26	8.321	8.378	-57	-0,69
27	20.461	20.041	420	2,05	27	10.642	10.288	354	3,33	27	9.819	9.753	66	0,67
28	15.283	16.036	-753	-4,93	28	8.110	8.597	-487	-6,00	28	7.173	7.439	-266	-3,71
29	20.197	19.654	543	2,69	29	10.516	10.133	383	3,64	29	9.681	9.521	160	1,65
30	20.463	20.080	383	1,87	30	10.628	10.325	303	2,85	30	9.835	9.755	80	0,81
	555.048	552.706	2.342	0,42		293.488	292.945	543	0,19		261.560	259.761	1.799	0,69

DECEMBER 1995					DECEMBER 1995				
STATFJORD C + SATELLITES					STATFJORD C				
	ALLOK	TEOR	DIFF	DIFF		ALLOK	TEOR	DIFF	DIFF
DAY	SM3	SM3	SM3	%	DAY	SM3	SM3	SM3	%
1	38.714	37.297	1.417	3,66	1	18.162	17.235	927	5,10
2	52.114	50.572	1.542	2,96	2	31.461	30.492	969	3,08
3	51.692	50.973	719	1,39	3	31.090	30.861	229	0,74
4	52.187	51.174	1.013	1,94	4	31.639	31.039	600	1,90
5	52.358	51.717	641	1,22	5	31.912	31.602	310	0,97
6	51.914	51.835	79	0,15	6	31.535	31.720	-185	-0,59
7	51.137	50.402	735	1,44	7	30.744	30.279	465	1,51
8	51.880	51.800	80	0,15	8	31.536	31.677	-141	-0,45
9	51.897	51.690	207	0,40	9	31.530	31.572	-42	-0,13
10	51.876	51.774	102	0,20	10	31.587	31.656	-69	-0,22
11	51.980	52.292	-312	-0,60	11	31.923	32.140	-217	-0,68
12	51.550	52.429	-879	-1,71	12	34.310	34.247	63	0,18
13	40.562	40.670	-108	-0,27	13	21.023	20.854	169	0,80
14	48.890	48.332	558	1,14	14	28.698	28.185	513	1,79
15	52.250	52.290	-40	-0,08	15	32.978	32.727	251	0,76
16	52.065	51.932	133	0,26	16	32.939	32.704	235	0,71
17	52.068	52.149	-81	-0,16	17	31.815	31.800	15	0,05
18	52.275	52.369	-94	-0,18	18	32.758	32.795	-37	-0,11
19	52.647	52.516	131	0,25	19	36.281	35.326	955	2,63
20	51.658	50.901	757	1,47	20	35.413	34.817	596	1,68
21	52.748	51.953	795	1,51	21	36.517	35.872	645	1,77
22	52.159	51.666	493	0,95	22	35.946	35.592	354	0,98
23	50.823	49.567	1.256	2,47	23	34.629	33.493	1.136	3,28
24	51.609	51.505	104	0,20	24	35.436	35.424	12	0,03
25	52.597	52.647	-50	-0,10	25	36.428	36.563	-135	-0,37
26	52.252	52.002	250	0,48	26	36.095	35.905	190	0,53
27	50.841	51.904	-1.063	-2,09	27	35.464	35.990	-526	-1,48
28	51.216	52.061	-845	-1,65	28	33.795	34.465	-670	-1,98
29	50.316	51.592	-1.276	-2,54	29	32.998	33.996	-998	-3,02
30	51.311	51.267	44	0,09	30	34.086	33.882	204	0,60
31	52.203	52.403	-200	-0,38	31	31.578	32.311	-733	-2,32
	1.579.789	1.573.681	6.108	0,39		1.002.306	997.221	5.085	0,51

DECEMBER 1995					DECEMBER 1995					DECEMBER 1995				
SATELLITES					ØST					NORD				
DAY	ALLOK	TEOR	DIFF	DIFF	DAY	ALLOK	TEOR	DIFF	DIFF	DAY	ALLOK	TEOR	DIFF	DIFF
	SM3	SM3	SM3	%		SM3	SM3	SM3	%		SM3	SM3	SM3	%
1	20.552	20.062	490	2,38	1	10.619	10.325	294	2,77	1	9.933	9.737	196	1,97
2	20.653	20.080	573	2,77	2	10.619	10.325	294	2,77	2	10.034	9.755	279	2,78
3	20.602	20.112	490	2,38	3	10.577	10.325	252	2,38	3	10.025	9.787	238	2,37
4	20.548	20.135	413	2,01	4	10.537	10.325	212	2,01	4	10.011	9.810	201	2,01
5	20.446	20.115	331	1,62	5	10.495	10.325	170	1,62	5	9.951	9.790	161	1,62
6	20.379	20.115	264	1,30	6	10.461	10.325	136	1,30	6	9.918	9.790	128	1,29
7	20.393	20.123	270	1,32	7	10.464	10.325	139	1,33	7	9.929	9.798	131	1,32
8	20.344	20.123	221	1,09	8	10.438	10.325	113	1,08	8	9.906	9.798	108	1,09
9	20.367	20.118	249	1,22	9	10.455	10.328	127	1,21	9	9.912	9.790	122	1,23
10	20.289	20.118	171	0,84	10	10.416	10.328	88	0,84	10	9.873	9.790	83	0,84
11	20.057	20.152	-95	-0,47	11	10.381	10.354	27	0,26	11	9.676	9.798	-122	-1,26
12	17.240	18.182	-942	-5,46	12	7.801	8.384	-583	-7,47	12	9.439	9.798	-359	-3,80
13	19.539	19.816	-277	-1,42	13	9.886	10.026	-140	-1,42	13	9.653	9.790	-137	-1,42
14	20.192	20.147	45	0,22	14	10.361	10.349	12	0,12	14	9.831	9.798	33	0,34
15	19.272	19.563	-291	-1,51	15	9.410	9.773	-363	-3,86	15	9.862	9.790	72	0,73
16	19.126	19.228	-102	-0,53	16	9.292	9.430	-138	-1,49	16	9.834	9.798	36	0,37
17	20.253	20.349	-96	-0,47	17	10.619	10.559	60	0,57	17	9.634	9.790	-156	-1,62
18	19.517	19.574	-57	-0,29	18	10.676	10.543	133	1,25	18	8.841	9.031	-190	-2,15
19	16.366	17.190	-824	-5,03	19	10.654	10.543	111	1,04	19	5.712	6.647	-935	-16,37
20	16.245	16.084	161	0,99	20	10.648	10.543	105	0,99	20	5.597	5.541	56	1,00
21	16.231	16.081	150	0,92	21	10.638	10.540	98	0,92	21	5.593	5.541	52	0,93
22	16.213	16.074	139	0,86	22	10.631	10.540	91	0,86	22	5.582	5.534	48	0,86
23	16.194	16.074	120	0,74	23	10.619	10.540	79	0,74	23	5.575	5.534	41	0,74
24	16.173	16.081	92	0,57	24	10.600	10.540	60	0,57	24	5.573	5.541	32	0,57
25	16.169	16.084	85	0,53	25	10.599	10.543	56	0,53	25	5.570	5.541	29	0,52
26	16.157	16.097	60	0,37	26	10.590	10.540	50	0,47	26	5.567	5.557	10	0,18
27	15.377	15.914	-537	-3,49	27	10.302	10.540	-238	-2,31	27	5.075	5.374	-299	-5,89
28	17.421	17.596	-175	-1,00	28	10.582	10.540	42	0,40	28	6.839	7.056	-217	-3,17
29	17.318	17.596	-278	-1,61	29	10.374	10.540	-166	-1,60	29	6.944	7.056	-112	-1,61
30	17.225	17.385	-160	-0,93	30	10.432	10.540	-108	-1,04	30	6.793	6.845	-52	-0,77
31	20.625	20.092	533	2,58	31	10.585	10.540	45	0,43	31	10.040	9.552	488	4,86
	577.483	576.460	1.023	0,18		320.761	319.703	1.058	0,33		256.722	256.757	-35	-0,01

JANUARY 1996 REVISED					JANUARY 1996 REVISED				
STATFJORD C + SATELLITES					STATFJORD C				
	ALLOK	TEOR	DIFF	DIFF		ALLOK	TEOR	DIFF	DIFF
DAY	SM3	SM3	SM3	%	DAY	SM3	SM3	SM3	%
1	51.607	51.612	-5	-0,01	1	32.867	33.786	-919	-2,80
2	51.308	51.195	113	0,22	2	33.718	34.332	-614	-1,82
3	49.603	50.519	-916	-1,85	3	28.775	30.413	-1.638	-5,69
4	51.116	52.322	-1.206	-2,36	4	31.583	32.535	-952	-3,01
5	52.675	51.904	771	1,46	5	34.609	34.038	571	1,65
6	32.750	31.716	1.034	3,16	6	15.956	14.276	1.080	7,03
7	21.352	22.672	-1.320	-6,18	7	7.894	8.702	-808	-10,24
8	47.985	46.427	1.558	3,25	8	29.591	28.152	1.439	4,86
9	52.175	51.723	452	0,87	9	33.711	33.448	263	0,78
10	51.034	50.991	43	0,08	10	32.799	32.716	83	0,25
11	47.201	47.165	36	0,08	11	29.016	28.890	126	0,43
12	52.514	51.657	857	1,63	12	34.334	33.385	949	2,76
13	52.405	51.355	1.050	2,00	13	34.205	33.061	1.144	3,34
14	47.165	49.668	-2.503	-5,31	14	29.848	32.342	-2.494	-8,36
15	45.831	51.293	-5.462	-11,92	15	25.269	30.987	-5.718	-22,63
16	49.794	52.187	-2.393	-4,81	16	29.236	31.809	-2.573	-8,80
17	51.956	52.204	-248	-0,48	17	31.467	31.828	-361	-1,15
18	51.621	52.320	-699	-1,35	18	31.188	31.945	-757	-2,43
19	51.691	52.573	-882	-1,71	19	31.289	32.196	-907	-2,90
20	52.472	53.719	-1.247	-2,38	20	32.108	33.344	-1.236	-3,85
21	52.518	54.313	-1.795	-3,42	21	32.243	33.938	-1.695	-5,26
22	44.253	45.663	-1.410	-3,19	22	24.040	25.288	-1.248	-5,19
23	52.368	53.843	-1.475	-2,82	23	32.191	33.471	-1.280	-3,98
24	51.656	54.181	-2.525	-4,89	24	31.509	33.840	-2.331	-7,40
25	51.784	54.153	-2.369	-4,57	25	31.892	34.216	-2.324	-7,29
26	50.675	52.733	-2.058	-4,06	26	30.828	32.796	-1.968	-6,38
27	51.944	52.341	-397	-0,76	27	32.144	32.404	-260	-0,81
28	52.043	52.898	-855	-1,64	28	32.295	32.961	-666	-2,06
29	52.038	52.792	-754	-1,45	29	32.288	33.078	-790	-2,45
30	50.597	52.404	-1.807	-3,57	30	30.889	32.467	-1.578	-5,11
31	15.870	18.894	-3.024	-19,05	31	9.709	11.100	-1.391	-14,33
	1.490.001	1.519.437	-29.436	-1,98		908.891	937.744	-28.853	-3,17

JANUARY 1996 REVISED					JANUARY 1996 REVISED					JANUARY 1996 REVISED				
SATELLITES					ØST					NORD				
DAY	ALLOK SM3	TEOR SM3	DIFF SM3	DIFF %	DAY	ALLOK SM3	TEOR SM3	DIFF SM3	DIFF %	DAY	ALLOK SM3	TEOR SM3	DIFF SM3	DIFF %
1	18.740	17.826	914	4,88	1	10.502	9.991	511	4,87	1	8.238	7.835	403	4,89
2	17.590	16.863	727	4,13	2	10.419	9.991	428	4,11	2	7.171	6.872	299	4,17
3	20.828	20.106	722	3,47	3	10.348	9.991	357	3,45	3	10.480	10.115	365	3,48
4	19.533	19.787	-254	-1,30	4	9.861	9.991	-130	-1,32	4	9.672	9.796	-124	-1,28
5	18.066	17.866	200	1,11	5	10.102	9.991	111	1,10	5	7.964	7.875	89	1,12
6	17.394	17.440	-46	-0,26	6	9.555	9.582	-27	-0,28	6	7.839	7.858	-19	-0,24
7	13.458	13.970	-512	-3,80	7	7.698	7.992	-294	-3,82	7	5.760	5.978	-218	-3,78
8	18.394	18.275	119	0,65	8	10.052	9.988	64	0,64	8	8.342	8.287	55	0,66
9	18.464	18.275	189	1,02	9	10.090	9.988	102	1,01	9	8.374	8.287	87	1,04
10	18.235	18.275	-40	-0,22	10	9.966	9.988	-22	-0,22	10	8.269	8.287	-18	-0,22
11	18.185	18.275	-90	-0,49	11	9.937	9.988	-51	-0,51	11	8.248	8.287	-39	-0,47
12	18.180	18.272	-92	-0,51	12	9.947	9.998	-51	-0,51	12	8.233	8.274	-41	-0,50
13	18.200	18.294	-94	-0,52	13	9.955	10.007	-52	-0,52	13	8.245	8.287	-42	-0,51
14	17.317	17.326	-9	-0,05	14	10.000	10.007	-7	-0,07	14	7.317	7.319	-2	-0,03
15	20.562	20.306	256	1,25	15	10.132	10.007	125	1,23	15	10.430	10.299	131	1,26
16	20.558	20.378	180	0,88	16	10.094	10.007	87	0,86	16	10.464	10.371	93	0,89
17	20.489	20.376	113	0,55	17	10.059	10.005	54	0,54	17	10.430	10.371	59	0,57
18	20.433	20.375	58	0,28	18	10.031	10.004	27	0,27	18	10.402	10.371	31	0,30
19	20.402	20.377	25	0,12	19	10.015	10.004	11	0,11	19	10.387	10.373	14	0,13
20	20.364	20.375	-11	-0,05	20	9.997	10.004	-7	-0,07	20	10.367	10.371	-4	-0,04
21	20.275	20.375	-100	-0,49	21	9.953	10.004	-51	-0,51	21	10.322	10.371	-49	-0,47
22	20.213	20.375	-162	-0,80	22	9.923	10.004	-81	-0,82	22	10.290	10.371	-81	-0,79
23	20.177	20.372	-195	-0,97	23	9.903	10.001	-98	-0,99	23	10.274	10.371	-97	-0,94
24	20.147	20.341	-194	-0,96	24	9.903	10.000	-97	-0,98	24	10.244	10.341	-97	-0,95
25	19.892	19.937	-45	-0,23	25	9.971	10.000	-29	-0,29	25	9.921	9.937	-16	-0,16
26	19.847	19.937	-90	-0,45	26	9.955	10.000	-45	-0,45	26	9.892	9.937	-45	-0,45
27	19.800	19.937	-137	-0,69	27	9.931	10.000	-69	-0,69	27	9.869	9.937	-68	-0,69
28	19.748	19.937	-189	-0,96	28	9.905	10.000	-95	-0,96	28	9.843	9.937	-94	-0,95
29	19.750	19.714	36	0,18	29	9.820	9.777	43	0,44	29	9.930	9.937	-7	-0,07
30	19.708	19.937	-229	-1,16	30	9.885	10.000	-115	-1,16	30	9.823	9.937	-114	-1,16
31	6.161	7.794	-1.633	-26,51	31	2.608	3.300	-692	-26,53	31	3.553	4.494	-941	-26,48
	581.110	581.693	-583	-0,10		300.517	300.610	-93	-0,03		280.593	281.083	-490	-0,17

FEBRUARY 1996					FEBRUARY 1996				
STATFJORD C + SATELLITES					STATFJORD C				
DAY	ALLOK SM3	TEOR SM3	DIFF SM3	DIFF %	DAY	ALLOK SM3	TEOR SM3	DIFF SM3	DIFF %
1	2.070	1.968	102	4,93	1	2.070	1.968	102	4,93
2	40.566	41.141	-575	-1,42	2	35.541	35.374	167	0,47
3	50.667	50.505	162	0,32	3	30.793	31.805	-1.012	-3,29
4	51.808	50.640	1.168	2,25	4	32.044	31.458	586	1,83
5	49.671	50.669	-998	-2,01	5	31.867	32.870	-1.003	-3,15
6	51.966	52.075	-109	-0,21	6	34.297	34.305	-8	-0,02
7	50.413	51.373	-960	-1,90	7	32.815	33.603	-788	-2,40
8	51.576	51.808	-232	-0,45	8	34.001	34.038	-37	-0,11
9	51.201	51.776	-575	-1,12	9	34.416	35.209	-793	-2,30
10	51.547	51.727	-180	-0,35	10	34.047	34.410	-363	-1,07
11	50.820	51.745	-925	-1,82	11	32.503	33.910	-1.407	-4,33
12	49.161	50.857	-1.696	-3,45	12	29.873	31.800	-1.927	-6,45
13	50.080	52.796	-2.716	-5,42	13	30.906	33.766	-2.860	-9,25
14	52.901	53.175	-274	-0,52	14	33.698	34.140	-442	-1,31
15	51.683	53.042	-1.359	-2,63	15	34.240	35.094	-854	-2,49
16	50.481	51.096	-615	-1,22	16	34.441	35.249	-808	-2,35
17	39.844	39.888	-44	-0,11	17	23.750	24.025	-275	-1,16
18	49.934	51.106	-1.172	-2,35	18	33.570	34.646	-1.076	-3,21
19	50.805	51.952	-1.147	-2,26	19	34.568	35.637	-1.069	-3,09
20	50.571	51.983	-1.412	-2,79	20	34.356	35.673	-1.317	-3,83
21	50.747	51.900	-1.153	-2,27	21	34.493	35.709	-1.216	-3,53
22	49.168	53.247	-4.079	-8,30	22	32.828	36.862	-4.034	-12,29
23	49.915	51.366	-1.451	-2,91	23	33.608	34.981	-1.373	-4,09
24	51.893	50.814	1.079	2,08	24	35.598	34.429	1.169	3,28
25	50.122	49.890	232	0,46	25	33.848	33.505	343	1,01
26	51.069	51.019	50	0,10	26	34.790	34.632	158	0,45
27	50.851	50.836	15	0,03	27	34.571	34.449	122	0,35
28	49.434	49.122	312	0,63	28	33.166	32.735	431	1,30
29	49.878	49.928	-50	-0,10	29	33.628	33.541	87	0,26
	-4.000					-4.000			
	1.396.842	1.419.444	-22.602	-1,62		926.326	949.823	-23.497	-2,54

FEBRUARY 1996					FEBRUARY 1996					FEBRUARY 1996				
SATELLITES					ØST					NORD				
DAY	ALLOK	TEOR	DIFF	DIFF	DAY	ALLOK	TEOR	DIFF	DIFF	DAY	ALLOK	TEOR	DIFF	DIFF
	SM3	SM3	SM3	%		SM3	SM3	SM3	%		SM3	SM3	SM3	%
1	0	0	0	#DIV/0!	1	0	0	0	#DIV/0!	1	0	0	0	#DIV/0!
2	5.025	5.767	-742	-14,77	2	2.803	3.600	-797	-28,43	2	2.222	2.167	55	2,48
3	19.874	18.700	1.174	5,91	3	10.274	9.841	433	4,21	3	9.600	8.859	741	7,72
4	19.764	19.182	582	2,94	4	9.813	9.524	289	2,95	4	9.951	9.658	293	2,94
5	17.804	17.799	5	0,03	5	9.527	9.524	3	0,03	5	8.277	8.275	2	0,02
6	17.669	17.770	-101	-0,57	6	9.470	9.524	-54	-0,57	6	8.199	8.246	-47	-0,57
7	17.598	17.770	-172	-0,98	7	9.431	9.524	-93	-0,99	7	8.167	8.246	-79	-0,97
8	17.575	17.770	-195	-1,11	8	9.420	9.524	-104	-1,10	8	8.155	8.246	-91	-1,12
9	16.785	16.567	218	1,30	9	9.649	9.524	125	1,30	9	7.136	7.043	93	1,30
10	17.500	17.317	183	1,05	10	9.625	9.524	101	1,05	10	7.875	7.793	82	1,04
11	18.317	17.835	482	2,63	11	9.781	9.524	257	2,63	11	8.536	8.311	225	2,64
12	19.288	19.057	231	1,20	12	9.529	9.415	114	1,20	12	9.759	9.642	117	1,20
13	19.174	19.030	144	0,75	13	9.455	9.384	71	0,75	13	9.719	9.646	73	0,75
14	19.203	19.035	168	0,87	14	9.448	9.366	82	0,87	14	9.755	9.669	86	0,88
15	17.443	17.948	-505	-2,90	15	9.097	9.360	-263	-2,89	15	8.346	8.588	-242	-2,90
16	16.040	15.847	193	1,20	16	9.460	9.360	100	1,06	16	6.580	6.487	93	1,41
17	16.094	15.863	231	1,44	17	9.371	9.360	11	0,12	17	6.723	6.503	220	3,27
18	16.364	16.460	-96	-0,59	18	9.886	9.957	-71	-0,72	18	6.478	6.503	-25	-0,39
19	16.237	16.315	-78	-0,48	19	9.767	9.812	-45	-0,46	19	6.470	6.503	-33	-0,51
20	16.215	16.310	-95	-0,59	20	9.754	9.811	-57	-0,58	20	6.461	6.499	-38	-0,59
21	16.254	16.191	63	0,39	21	9.636	9.596	40	0,42	21	6.618	6.595	23	0,35
22	16.340	16.385	-45	-0,28	22	9.569	9.596	-27	-0,28	22	6.771	6.789	-18	-0,27
23	16.307	16.385	-78	-0,48	23	9.553	9.596	-43	-0,45	23	6.754	6.789	-35	-0,52
24	16.295	16.385	-90	-0,55	24	9.544	9.596	-52	-0,54	24	6.751	6.789	-38	-0,56
25	16.274	16.385	-111	-0,68	25	9.534	9.596	-62	-0,65	25	6.740	6.789	-49	-0,73
26	16.279	16.387	-108	-0,66	26	9.533	9.596	-63	-0,66	26	6.746	6.791	-45	-0,67
27	16.280	16.387	-107	-0,66	27	9.533	9.596	-63	-0,66	27	6.747	6.791	-44	-0,65
28	16.268	16.387	-119	-0,73	28	9.526	9.596	-70	-0,73	28	6.742	6.791	-49	-0,73
29	16.250	16.387	-137	-0,84	29	9.517	9.596	-79	-0,83	29	6.733	6.791	-58	-0,86
	470.516	469.621	895	0,19		261.505	261.822	-317	-0,12		209.011	207.799	1.212	0,58

COMPUTATION OF FLOW THROUGH BENDS

by

J A Sattary, M J Reader-Harris and L A Johnstone

NEL, East Kilbride, Glasgow

SUMMARY

Computations have been performed for flow through a single 90° swept bend and through two 90° swept bends, both in the same plane (S-configuration) and in perpendicular planes. Further computations were carried out in which the two bends were separated by a distance of 9D. The computational results show very good agreement with experimental data and give confidence in the ability of CFD to model flow in pipe bends accurately. Hence, a better understanding of the behaviour of flow downstream of bend installations has been obtained. The work reported in this paper shows that good installation design can eliminate some of the more severe flow conditions.

The S-bend with no separation between bends produces a very flat downstream velocity profile compared with those downstream of the single bend or the S-bend with 9D separation. The twisted S-bend with 9D separation between the bends does not produce swirl; this is confirmed by experimental data.

1 INTRODUCTION

This paper describes computational work undertaken by NEL within the Header Research Consortium project. The work has been supported by a Consortium consisting of Amerada Hess, Amoco, Daniel Industries, Gas Research Institute, Kvaerner H&G Offshore, N.V. Nederlandse Gasunie, Shell Expro and the UK Department of Trade and Industry. The overall aim of the project was to investigate the effectiveness of flow conditioners downstream of headers and bends, both as regards flow profiles and in terms of the performance of orifice meters; results of the experimental work were published in 1995¹.

Computational fluid dynamics (CFD) is a technique that is more frequently being used to predict flow profiles downstream of various pipe installations and their effect upon the performance of various types of flowmeter. The advantage of CFD over experimental measurements is that it gives profiles of all variables over the whole flow domain. This knowledge can be used to determine the effect of these profiles on various types of flowmeter.

Over the years many experimental measurements have been made of flow profiles downstream of various pipe installations, in particular downstream of single 90° swept bends and double bends. Hence, CFD results can be compared with experimental results to give confidence in the computational model. Profiles from any part of the domain can then

be used to obtain a better understanding of the behaviour of flow downstream of bend installations. This information is of importance to Standards. Also, good agreement between CFD and experiment in these configurations may make possible the use of CFD in the design of installations.

2 COMPUTATIONAL CODE

The commercially available CFD code FLUENT version 4.31² was run on a Silicon Graphics Indigo workstation. The standard k- ϵ turbulence model was used with the QUICK difference scheme. At the inlet a fully developed flow profile was specified with a mean velocity of 54 m/s and Reynolds number of approximately 8×10^5 . Details of the CFD code, boundary conditions and specifications are given in Appendix A.

3 GEOMETRY AND COMPUTATIONAL GRID

Each bend configuration was computed with a pipe diameter, D , of 0.254 m and a bend radius of $1.5D$.

A structured grid was used to divide the flow domain into cells. In order to increase the accuracy of the computed results it is necessary to maximise the number of cells used and to obtain an appropriate grid for a particular geometry. For comparison purposes the grids should be similar. Therefore, the grid in the axial direction is similar for all bend computations. Fig. 1 shows the node positions and bunching in the axial direction for the S-bend with $9D$ separation. It comprises: 14 cells for the $2D$ inlet, 20 cells on each bend, 40 cells for the $8D$ outlet pipe and 54 cells for the $9D$ of straight pipe between the bends. Two different cross-sectional grids were used in the computations; one for the S-bend and a different one for the twisted S-bend configurations; results were computed using both grids for the single 90° bend.

3.1 S-Bend (Fine Grid)

For the S-bend configurations the cross-sectional grid was 21×21 , as shown in Fig. 2. Since the geometry is symmetrical about the horizontal axis, it was only necessary to compute the flow in half of the pipe; thus this grid could be made fine in comparison with the twisted S-bend grid. With this type of grid a small hole is not computed in the centre of the pipe but it is assumed to have an insignificant effect on the results since its area is less than 0.01 per cent of the total cross-sectional area.

The bend geometries computed using this fine grid are: single 90° bend, S-bend with $0D$ separation and S-bend with $9D$ separation.

3.2 Twisted S-Bend (Coarse Grid)

For the twisted S-bend configurations computations were performed throughout the whole pipe using a cross-sectional grid of 21×21 (Fig. 3); thus this grid is much coarser than that for the S-bend configurations.

The bend geometries computed using this coarse grid are: single 90° bend, twisted S-bend with 0D separation and twisted S-bend with 9D separation.

4 COMPUTATIONAL RESULTS

The non-dimensional velocity magnitude, U , presented in this section is given by

$$U = \frac{(u^2 + v^2 + w^2)^{1/2}}{\bar{u}}$$

where u , v and w are the axial, tangential and radial velocity components respectively and \bar{u} is the mean axial velocity. Where transverse velocity vectors are presented the non-dimensional velocity magnitude, V , is the combination of the radial and tangential components only and is given by

$$V = \frac{(v^2 + w^2)^{1/2}}{\bar{u}}$$

4.1 Computational Results Using a Fine Grid

4.1.1 Single 90° bend

Fig. 4 shows a contour plot of the velocity magnitude for a slice on the horizontal plane (at the plane of symmetry). The maximum non-dimensional velocity magnitude, U_m , is 1.31 on the inside of the bend. The regions of minimum velocity are close to the outside of the bend and also near the inner wall less than 1D downstream of the bend.

(In the downstream straight pipe the region close to the pipe wall corresponding to the outer side of the nearest upstream bend is hereafter referred to as 'outer' and likewise the region corresponding to the inside of the nearest upstream bend is hereafter referred to as 'inner'. In the figures inner and outer are labelled as 'inside' and 'outside'.)

Fig. 5 shows contours of velocity magnitude for 8 cross-sectional slices downstream of the bend from 0D to 7D in approximately 1D increments. At 0D the maximum velocity has moved from the inside of the bend to close to the centreline. At 1D this maximum velocity has now been replaced by the minimum velocity and the maximum velocity is in the outer half of the pipe cross-section. At 3D and 4D this maximum velocity forms a crescent shape near the outer side of the slice. At 5D and 6D this maximum velocity decays and the crescent thins. At 7D the crescent has almost joined on the inner side of the slice and in the centre part of the slice the velocity profile is relatively flat and still less than the crescent velocity.

The velocity magnitude 4D downstream of the bend is shown in detail in Fig. 6. The maximum velocity is near the outer side of the slice where $U_m = 1.11$.

Fig. 7 shows transverse velocity vectors of the same slice 4D downstream of the bend. The shift of the maximum velocity from the inside of the bend to the outer side of the slice downstream causes flow along the axis of symmetry from the inner to the outer side of the

slice which in turn sets up two counter rotating vortices in the flow. The maximum non-dimensional velocity magnitude, V_m , is 0.22.

4.1.2 S-bend with no separation

Fig. 8 shows a contour plot of velocity magnitude for a slice at the plane of symmetry. As shown in Fig. 4, between 0D and 1D downstream of a single bend the velocity on the outer side of the bend is higher than that of a fully developed velocity profile. For the S-bend configuration with no separation between the bends this higher velocity enhances the velocity on the inner side of the second bend where $U_m = 1.44$. Conversely, the velocity on the outer side downstream of a single bend is lower than that of a fully developed flow profile and this acts to decrease the velocity even more on the outside of the bend.

Fig. 9 shows contours of velocity magnitude for 7 slices downstream of the second bend from 1D to 7D in approximately 1D increments. At 1D downstream of the second bend the crescent of maximum velocity is in the opposite direction to that observed downstream of the single 90° bend (Fig. 5); its back faces towards the inner side of the pipe where the minimum velocity is obtained. The profile 1D downstream is almost a mirror image of that at 4D downstream of the single bend (Fig. 6). Between 2D and 3D downstream the crescent disappears and at 4D the profile is very flat. Between 5D and 7D the area of minimum velocity on the outer side of the pipe appears to grow towards the centreline.

The velocity magnitude 4D downstream of the second bend is shown in detail in Fig. 10. It shows a very flat profile covering most of the pipe cross-section and $U_m = 1.03$.

Fig. 11 shows transverse velocity vectors of the same slice 4D downstream of the second bend. These are the combinations of the radial and tangential components of velocity. It is interesting to note that the velocity vectors along the axis of symmetry are in the opposite direction compared to those of the single bend (Fig. 7). Figs 7 and 11 are almost a mirror image of each other and $V_m = 0.16$, which is less than in the single bend case.

4.1.3 S-bend with 9D separation

Fig. 12 shows a contour plot of velocity magnitude for a slice at the plane of symmetry, for an S-bend with 9D separation between the bends. The velocity profile downstream of the first bend is the same as that downstream of the single bend. As with the S-bend with no separation the velocity magnitude on the inner side of the second bend is enhanced by the first bend. The maximum velocity is on the inner side of the second bend where $U_m = 1.39$, this is slightly lower than that of the S-bend with no separation.

Fig. 13 shows contours of velocity for 7 slices downstream of the second bend from 1D to 7D in approximately 1D increments. At 1D downstream of the second bend the crescent of maximum velocity is still in the opposite direction to that observed downstream of the single 90° bend (Fig. 5). The minimum velocity along the inner side is caused by the second bend and the lower velocity along the outer side is a result of the first bend. Between 2D and 6D downstream of the second bend this lower velocity along the outer side gradually decays. At 7D the crescent has spread and almost reversed.

The velocity magnitude 4D downstream of the second bend is shown in detail in Fig. 14. It shows a much flatter profile than that 4D downstream of the single bend (Fig. 6) but not as flat as 4D downstream of the S-bend with no separation (Fig. 10). On the inner side of the slice the minimum velocity covers a much larger area than it does downstream of the S-bend with no separation.

Fig. 15 shows transverse velocities of the same slice 4D downstream of the second bend. The velocity vectors along the axis of symmetry flow towards the centreline from both the inner side and outer side of the pipe wall. Instead of two there are four vortices of similar magnitude. The maximum velocity is towards the centre of the pipe where $V_m = 0.08$, half that for the S-bend with no separation at the same downstream distance.

4.2 Computational Results Using a Coarse Grid

4.2.1 Single 90° bend

The coarse grid shown in Fig 3 was also used to compute the single bend case to allow results for the two different grids to be compared for the same geometry. The results agree well and the velocity profiles look very similar to those with the fine grid (Figs 6 to 9).

4.2.2 Twisted S-bend with no separation

Fig. 16 shows a contour plot of velocity magnitude for a slice in the horizontal plane (the plane from the inner to the outer side of the pipe downstream of the second bend). The maximum velocity is on the inside of the second bend where $U_m = 1.35$ which is less than the value of U_m for the S-bend but more than that for the single bend.

Fig. 17 shows contours of velocity magnitude for 8 slices downstream of the second bend from 0D to 7D in approximately 1D increments. The profiles still retain the crescent shape but the region of minimum velocity progresses down the pipe in a clockwise direction (looking from bend to outlet).

The velocity magnitude at 4D downstream of the second bend is shown in detail in Fig. 18 and the corresponding transverse velocity vectors are shown in Fig. 19. Swirl dominates the profile and the position of the maximum velocity in Fig. 19 corresponds to the leading edge of the maximum velocity magnitude shown in Fig. 18.

4.2.3 Twisted S-bend with 9D separation

Fig. 20 shows a contour plot of velocity magnitude. The maximum velocity is in the same position as it is in the case of the twisted S-bend with no separation and of similar magnitude; $U_m = 1.34$.

Fig. 21 shows contours of velocity for 8 slices downstream of the second bend from 0D to 7D in approximately 1D increments. The area of minimum velocity along the length of the inner side and the area of maximum velocity along the outer side does not rotate as in the twisted S-bend with no separation case (Fig. 17). The profile does not change as rapidly from 1D to 7D as it does in the single bend case (Fig. 5).

The velocity magnitudes 4D downstream of the second bend are shown in detail in Fig. 22. Fig. 23 shows the combined radial and tangential components of the same slice 4D downstream of the second bend. This profile is not dominated by swirl; instead it has two counter-rotating vortices similar to the single bend case, although one vortex is more dominant and the profile is not symmetrical.

4.3 Comparison of Computational With Experimental Results

Figs 24 to 29 show comparisons of computational results using the fine grid given in Fig. 2 and the coarse grid given in Fig. 3, with experimental results in the plane of symmetry for the axial velocity at various distances downstream of the bend. The velocity profile data have been plotted non-dimensionally to allow comparison with experimental data. The inner wall is given by $r/R = -1$ and the outer wall is given by $r/R = +1$, where r is the radial distance from the pipe centreline and R is the pipe radius.

The $\frac{1}{8} D$ experimental data shown in Fig. 24 are LDV data for $D = 0.205\text{m}$ and $Re_D = 9 \times 10^5$ (Spearman³). The 4D experimental data shown in Fig. 25 are pitot traverse data obtained by NEL for the Header Research Consortium⁴: these data were obtained with $D = 0.254\text{ m}$ and $Re_D = 8 \times 10^5$. The 5D and 7D data shown in Figs 26 & 28 and in Figs 27 & 29 respectively are also LDV data obtained for $D = 0.1026\text{ m}$ and $Re_D \approx 5 \times 10^5$ (Spearman et al⁵).

Figs 24 to 27 show comparisons using both the fine and coarse grids for $\frac{1}{8} D$, 4D, 5D and 7D downstream of a single 90° bend. For the coarse grid, computations were performed using two different inlet profiles (for $n = 9.0$ and $n = 11.9$, where n is the exponent in the velocity profile power law equation, see Appendix A, equation A.7); in general the two different grids for $n = 9.0$ produced a much larger difference in the downstream velocity profiles than the difference in inlet profiles. The inlet velocity power law profile for $n = 9.0$ and the associated 5% limits specified in ISO 5167-1⁶ are also plotted for comparison.

The velocity profile for both the fine and coarse grid computations at $\frac{1}{8} D$ (Fig. 24) is much flatter than the experimental profile. For the fine grid the effect of the centreline hole is shown by the separation of the two points at $r/R = 0$. At 4D Fig. 25 shows very good agreement between experimental and computational data. At 5D Fig. 26 shows the experimental profile is now slightly flatter than the computational profile. Fig. 27 shows a marked decay in the peak of the experimental profile at 7D whereas the peak in the computational data, particularly using the fine grid, has only slightly decayed.

Figs 28 and 29 show comparisons using the coarse grid for 5D and 7D downstream of a twisted S-bend with no separation. It is more difficult to compare velocity profiles downstream of the twisted S-bend configuration because the profile across a single diameter changes more rapidly with downstream length owing to the corkscrew effect of the profile. At 5D (Fig. 28) the computational profile is flatter than the experimental profile and at 7D there is good agreement. For the same downstream length the profiles may agree better on a different diameter (ie for the comparison at 5D downstream (Fig 28) the computational profile on the diameter in the plane of symmetry agrees much better with

the profile of experimental data along the diameter of the perpendicular plane than it does with the experimental profile in the plane of symmetry).

For the twisted S-bend it is much better to compare the swirl angles with those of experimental data. The maximum swirl angle at 4D downstream of the twisted S-bend is 14.9° and is positioned near the wall at the position of the inside of the second bend (see Fig 19). The maximum swirl angle at 1D is 19.9° and is positioned near the wall halfway between the position of the inside of the first bend and the inside of the second bend. Mattingly and Yeh⁷ measured swirl angles for 1D, 5D and 11.7D downstream of a twisted S-bend and found swirl angles of 17° , 11° and 10° respectively; these data were means of two measurements taken at near wall positions on opposite sides of the pipe and are therefore expected to be slightly lower than the maximum. Mattingly and Yeh also measured swirl angles for a twisted S-bend with a 2.4D separation between the bends and found only 3.2° of swirl at 1D and 2.1° at 5D downstream of the second bend. For a twisted S-bend with a 5.3D separation they found only 2° of swirl at 1D and 1.3° at 5D downstream of the second bend. These experimental data confirm the findings for the computations of a twisted S-bend with 9D separation.

5 CONCLUSIONS

Computations have been performed for flow through a single 90° swept bend and through two 90° bends, both in the same plane (S-configuration) and in perpendicular planes. Further computations have been carried out in which the two bends are separated by a distance of 9D. For these configurations velocity profiles have been presented for a large part of the flow domain.

The computational results show good agreement with experimental data and give confidence in the ability of CFD to model flow in pipe bends accurately. Hence, a better understanding of the behaviour of flow downstream of bend installations has been obtained.

The S-bend with no separation between bends produces a very flat downstream velocity profile compared with those downstream of the single bend or the S-bend with 9D separation.

The twisted S-bend with 9D separation between the bends does not produce swirl; this is confirmed by experimental data.

Acknowledgements

This paper reports part of the work undertaken by NEL for the Header Research Consortium consisting of Amerada Hess, Amoco, Daniel Industries, Gas Research Institute, Kvaerner H&G Offshore, N.V. Nederlandse Gasunie, Shell Expro and the Department of Trade and Industry. The authors would like to thank the Header Research Consortium for their continued support and guidance.

This paper is published by permission of the Director and General Manager, NEL.

REFERENCES

- 1 READER-HARRIS, M. J., SATTARY, J. A. and WOODHEAD, E. The use of flow conditioners to improve flow measurement accuracy downstream of headers. Proceedings of the 3rd International Symposium on Fluid Flow Measurement. San Antonio, Texas, USA, March 1995.
- 2 FLUENT User's Guide. Version 4.3. January 1995. Fluent Europe Ltd., Holmwood House, Cortworth Rd, Sheffield, S11 9LP, UK.
- 3 SPEARMAN, E. P. Comprehensive LDV data on swirling and asymmetric flows through a conditioner/flowmeter package. NEL Report No 724. East Kilbride, Glasgow: National Engineering Laboratory, January 1992.
- 4 READER-HARRIS, M. J., WOODHEAD, E., SATTARY, J. A. and McEWEN, D. Flow conditions downstream of headers. HCP001 (223/94) Part 1. East Kilbride, Glasgow: National Engineering Laboratory, Sept 1995.
- 5 SPEARMAN, E. P., SATTARY, J. A., and READER-HARRIS, M. J. Comparison of velocity profiles downstream of perforated plate flow conditioners. Flomeko '94, Flow measurement in the mid-90s, 7th International conference on flow measurement, East Kilbride, Glasgow: National Engineering Laboratory, June 1994.
- 6 INTERNATIONAL ORGANIZATION FOR STANDARDIZATION. Measurement of fluid flow by means of orifice plates, nozzles and Venturi tubes inserted in circular cross-section conduits running full. ISO 5167-1, Geneva: International Organization for Standardization, 1991.
- 7 MATTINGLY, G. E., and YEH, T. T. Effects of pipe elbows and tube bundles on selected types of flowmeters. Flow Measurement and Instrumentation, Vol 2, pp 4-13, 1991.

APPENDIX A

NOTATION

C_1, C_2	Turbulence model coefficients	ϵ	Turbulence kinetic energy dissipation rate
C_μ	Turbulence model empirical constant	κ	von Karman's constant
E	Log law empirical constant	μ	Fluid viscosity
G_k	Generation term for k	μ_t	Turbulent viscosity
k	Turbulence kinetic energy	ρ	Fluid density
k_p	Turbulence kinetic energy at the near-wall grid point p	$\sigma_k, \sigma_\epsilon$	Turbulence model coefficients (Prandtl numbers)
n	Exponent in the velocity profile power law equation	τ	Wall shear stress.
R	Pipe radius		
Re_D	Reynolds number based on pipe diameter ($\rho \bar{u} D / \mu$)		
r	Radial distance from pipe centreline		
u	Local velocity		
u_{cl}	Centreline axial velocity		
u_p	Velocity at a point p near the wall		
u^+	Non-dimensional velocity = u/u^*		
u^*	Friction velocity = $(\tau/\rho)^{1/2}$		
\bar{u}	Mean velocity		
y_p	Distance from near-wall point p to the wall		
y^+	Non-dimensional distance from the pipe wall		

Details of the CFD code, the boundary conditions and specifications used for all computations are given below.

The k- ϵ turbulence model was used which has a turbulent viscosity given by

$$\mu_t = \rho C_\mu \frac{k^2}{\epsilon}, \quad (\text{A.1})$$

where $C_\mu = 0.09$, k is the turbulence kinetic energy, and ϵ is the turbulence kinetic energy dissipation rate. The differential transport equations for k and ϵ are:

$$\frac{\partial}{\partial t}(\rho k) + \frac{\partial}{\partial x_i}(\rho u_i k) = \frac{\partial}{\partial x_i} \left(\frac{\mu_t}{\sigma_k} \frac{\partial k}{\partial x_i} \right) + G_k - \rho \epsilon, \quad (\text{A.2})$$

$$\frac{\partial}{\partial t}(\rho \epsilon) + \frac{\partial}{\partial x_i}(\rho u_i \epsilon) = \frac{\partial}{\partial x_i} \left(\frac{\mu_t}{\sigma_\epsilon} \frac{\partial \epsilon}{\partial x_i} \right) + C_1 \frac{\epsilon}{k} G_k - C_2 \rho \frac{\epsilon^2}{k}, \quad (\text{A.3})$$

where G_k is the generation term for k and is given by the following formula:

$$G_k = \mu_t \left(\frac{\partial u_j}{\partial x_i} \right) \frac{\partial u_j}{\partial x_i}. \quad (\text{A.4})$$

The coefficients used are:

$$C_1 = 1.44, C_2 = 1.92, \sigma_k = 1.0 \text{ and } \sigma_\epsilon = 1.3.$$

The log-law of the wall can be used to compute the shear stress at the wall

$$\frac{u_p}{u^*} = u^+ = \frac{1}{\kappa} \ln(Ey^+) \quad (\text{A.5})$$

where u^* is the friction velocity, $(\tau/\rho)^{1/2}$, and

$$\kappa = 0.42 \text{ (von Karman's constant).}$$

Smooth pipewalls were assumed and for this case the roughness parameter, E , is 9.81.

The boundary conditions for k and ϵ are used to derive the following expression for y^+ , the non-dimensional distance from the pipe wall, given by

$$y^+ = \frac{\rho k_p^{1/2} C_\mu^{1/4} y_p}{\mu}, \quad (\text{A.6})$$

where y_p is the distance from the near-wall point p to the wall and k_p is the turbulence kinetic energy at that point.

At the inlet boundary a fully developed flow profile was specified using the following equations.

The axial velocity is represented by the empirical power law equation:

$$u = u_{cl}(1 - r/R)^{1/n} \quad (\text{A.7})$$

where $n = 9.0$ was used for the computations using the fine grid shown in Figs 4 to 15 and $n = 11.9$ for the computations using the coarse grid shown in Figs 16 to 23. In Figs 24 to 27 data computed with $n = 9.0$ and the coarse grid are also shown and the values of n are given for each set of computational data.

The turbulence kinetic energy is given by:

$$k = \frac{0.0121 + 0.0628 \left(\frac{r}{2R}\right)^{1.6}}{(2.95)^2} \bar{u}^2 \quad (\text{A.8})$$

and the turbulence kinetic energy dissipation rate is given by:

$$\varepsilon = \frac{9.277 \times 10^{-5}}{(R - r)} \bar{u}^3 \quad r/R > 0.686 \quad (\text{A.9})$$

$$\varepsilon = \frac{0.0026 + 0.274 \left(\frac{r}{2R}\right)^{2.9}}{51.34R} \bar{u}^3 \quad r/R \leq 0.686.$$

Equations (A.8) and (A.9) were derived from computations of flow in long straight pipes. The inlet radial velocity was zero and there was no swirl. At the outlet the default pressure boundary condition was specified. For the fine grid geometry a symmetry boundary was specified along the axis of symmetry and also for the centreline hole.

The QUICK (Quadratic Upstream Interpolation for Convection Kinematics) difference scheme was specified and the solution method used was SIMPLE (Semi-Implicit Method for Pressure-Linked Equations).

FLUENT was run until the normalised residuals were less than 10^{-4} .

The mean velocity, \bar{u} , was in each case set to 54.0 m/s giving $u_{cl} = 62.9$ m/s for $n = 9.0$ and $u_{cl} = 60.1$ m/s for $n = 11.9$. The density and viscosity were 1.1 kg/m^3 and $1.9 \times 10^{-5} \text{ kg m}^{-1} \text{ s}^{-1}$ respectively giving a Reynolds number, Re_D , of approximately 8×10^5 .

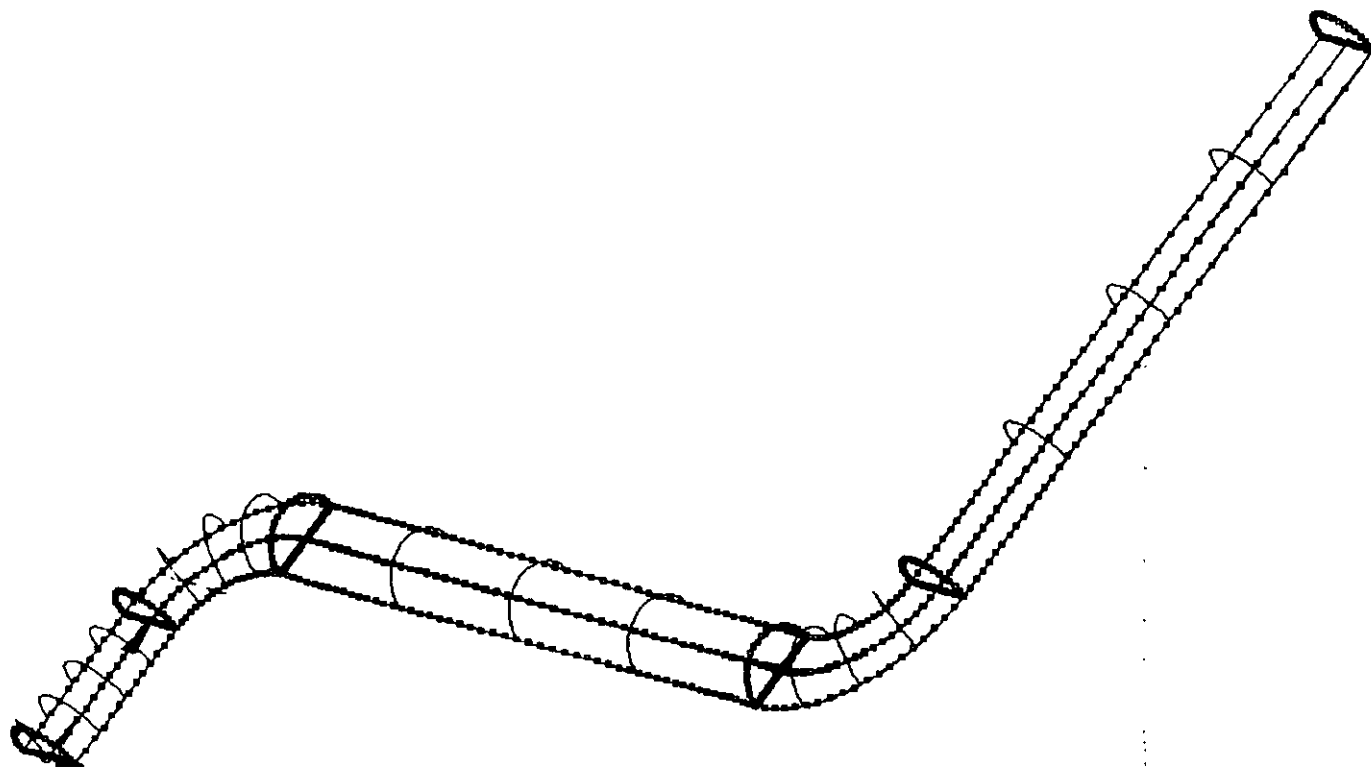


Fig. 1 Node Positions for the S-Bend with 9D Separation

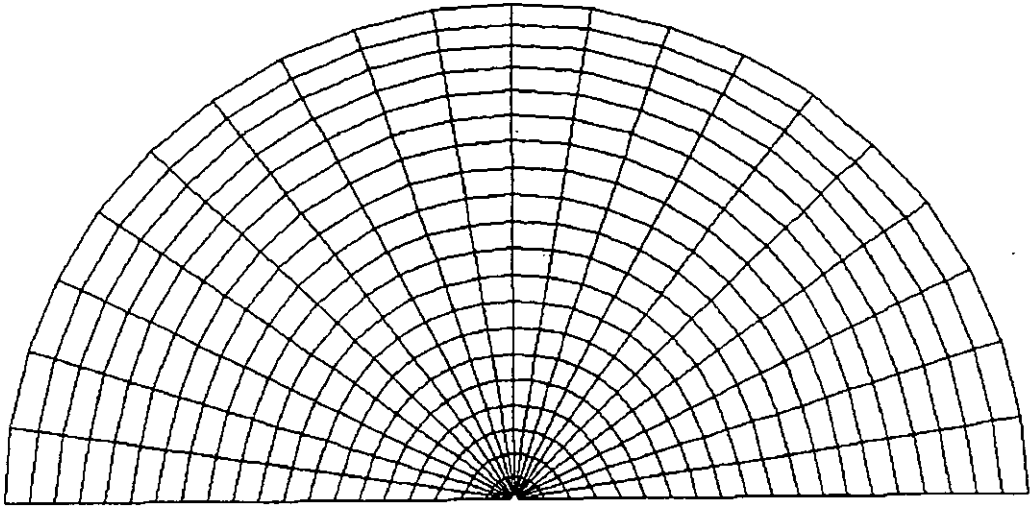


Fig. 2 S-Bend Cross-Sectional Grid (Fine Grid)

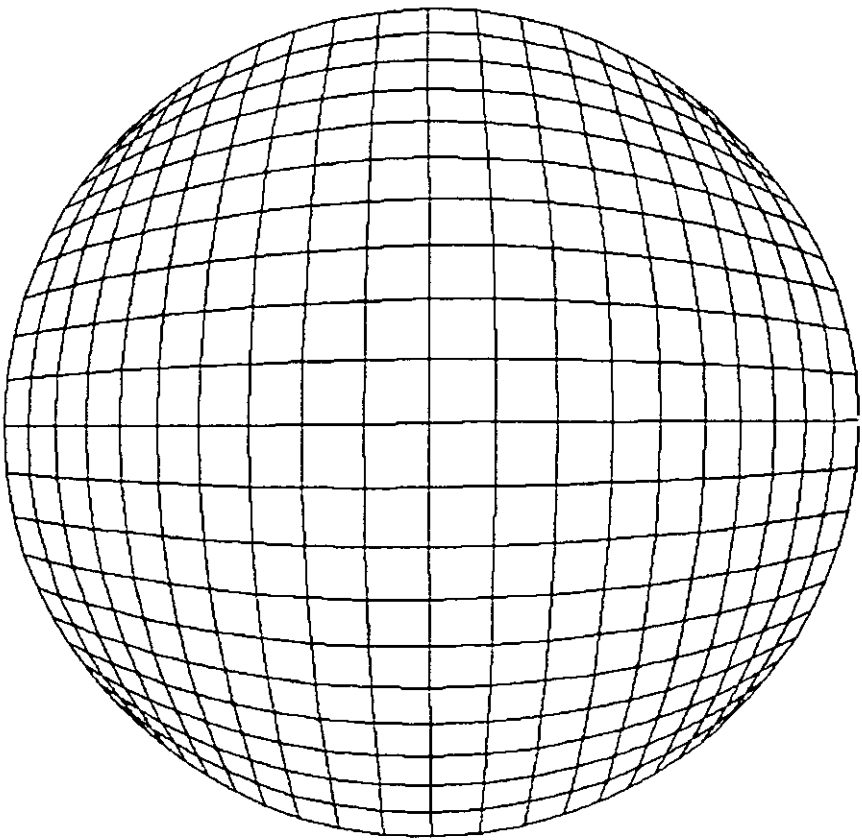
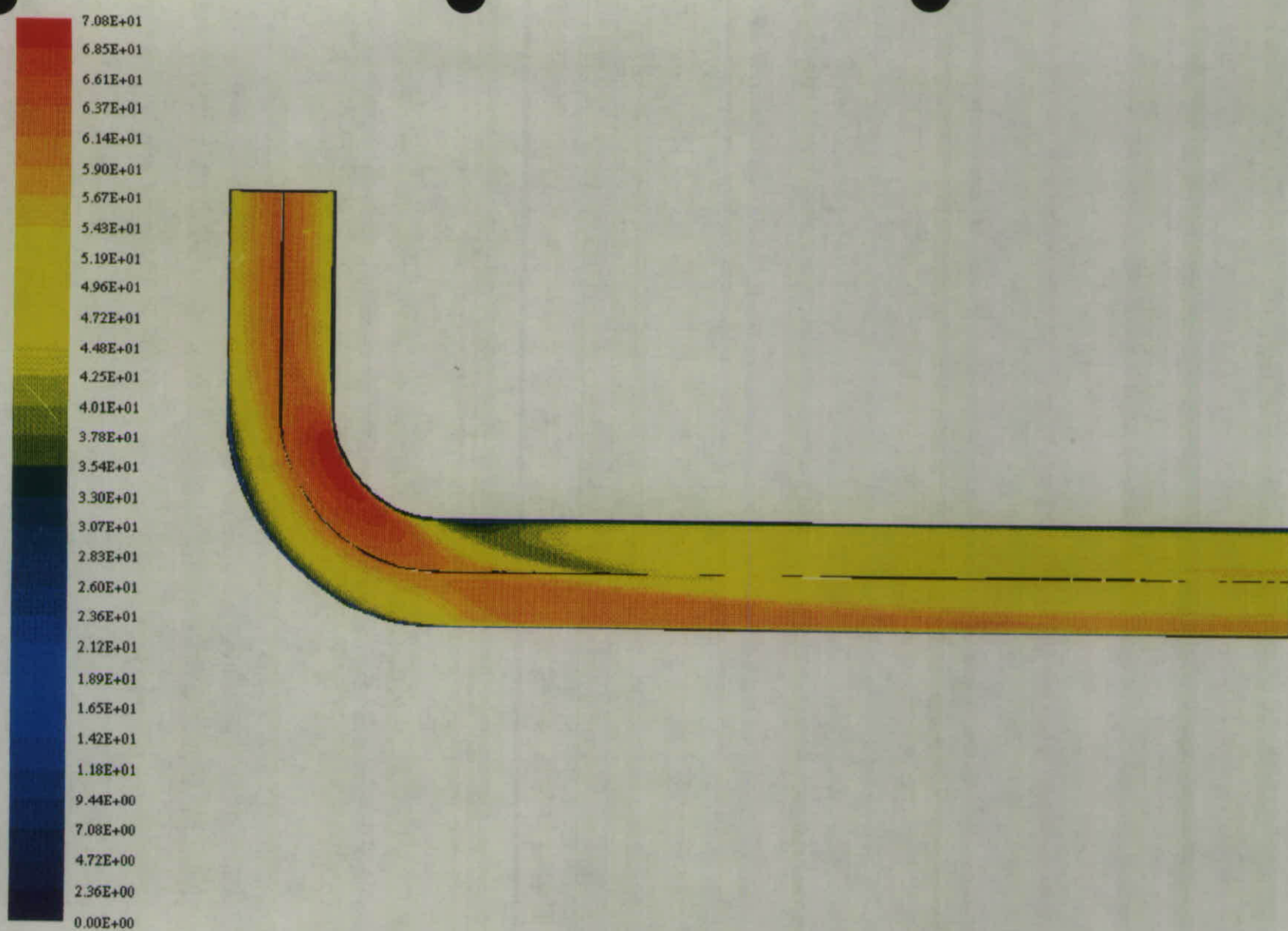


Fig. 3 Twisted S-Bend Cross-Sectional Grid (Coarse Grid)



NEL - Single 90 degree bend

Velocity Magnitude (M/S)

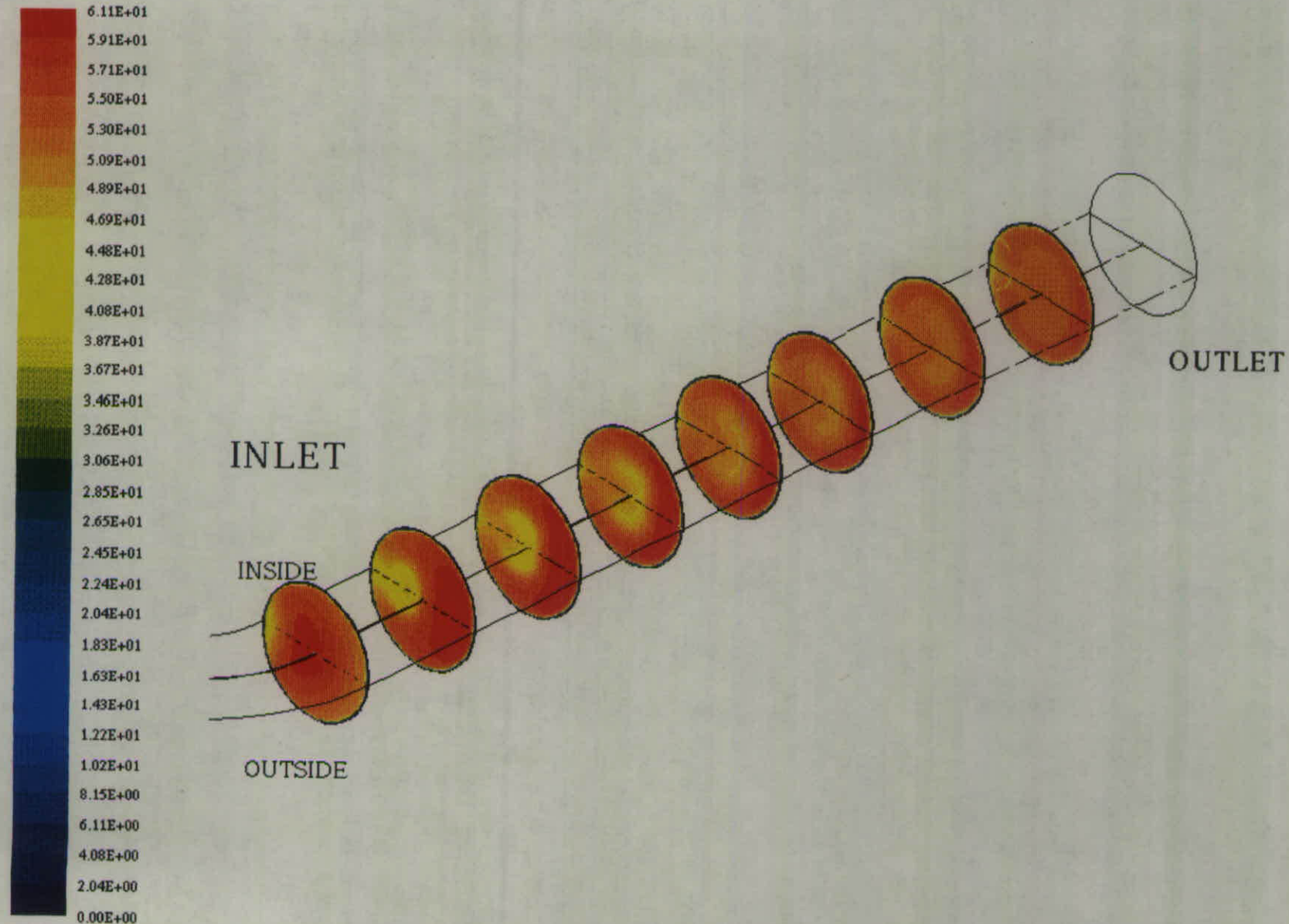
L max = 7.081E+01 L min = 0.000E+00



Fluent 4.31

Fluent Inc.

Fig. 4 Contours of Velocity Magnitude in the Plane of Symmetry for a Single Bend



NEL - Single 90 degree bend

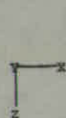
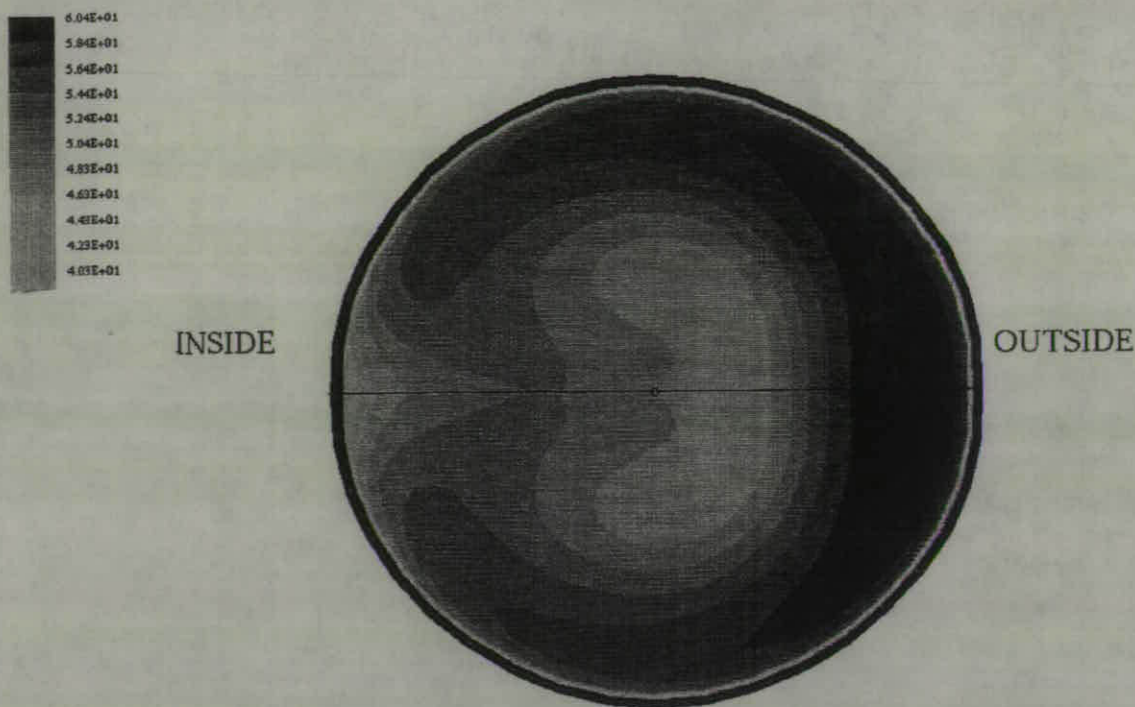
Velocity Magnitude (M/S)

L max = 6.113E+01 L min = 0.000E+00

Fluent 4.31

Fluent Inc.

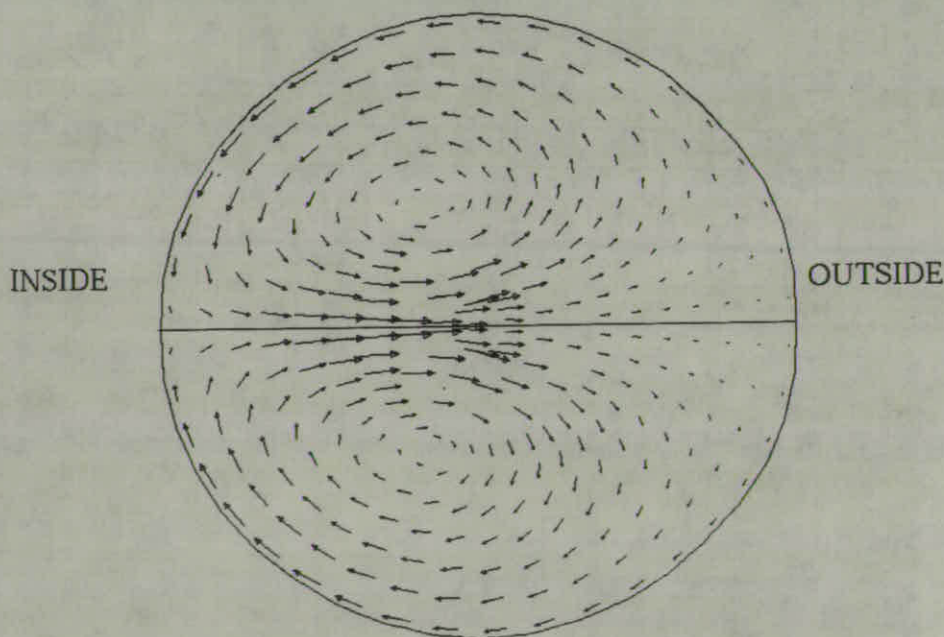
Fig. 5 Contours of Velocity Magnitude for Cross-sections Downstream of a Single Bend



NEL - Single 90 degree bend
 Velocity Magnitude (M/S)
 $L_{max} = 6.042E+01$ $L_{min} = 0.000E+00$

Fluent 4.31
 Fluent Inc.

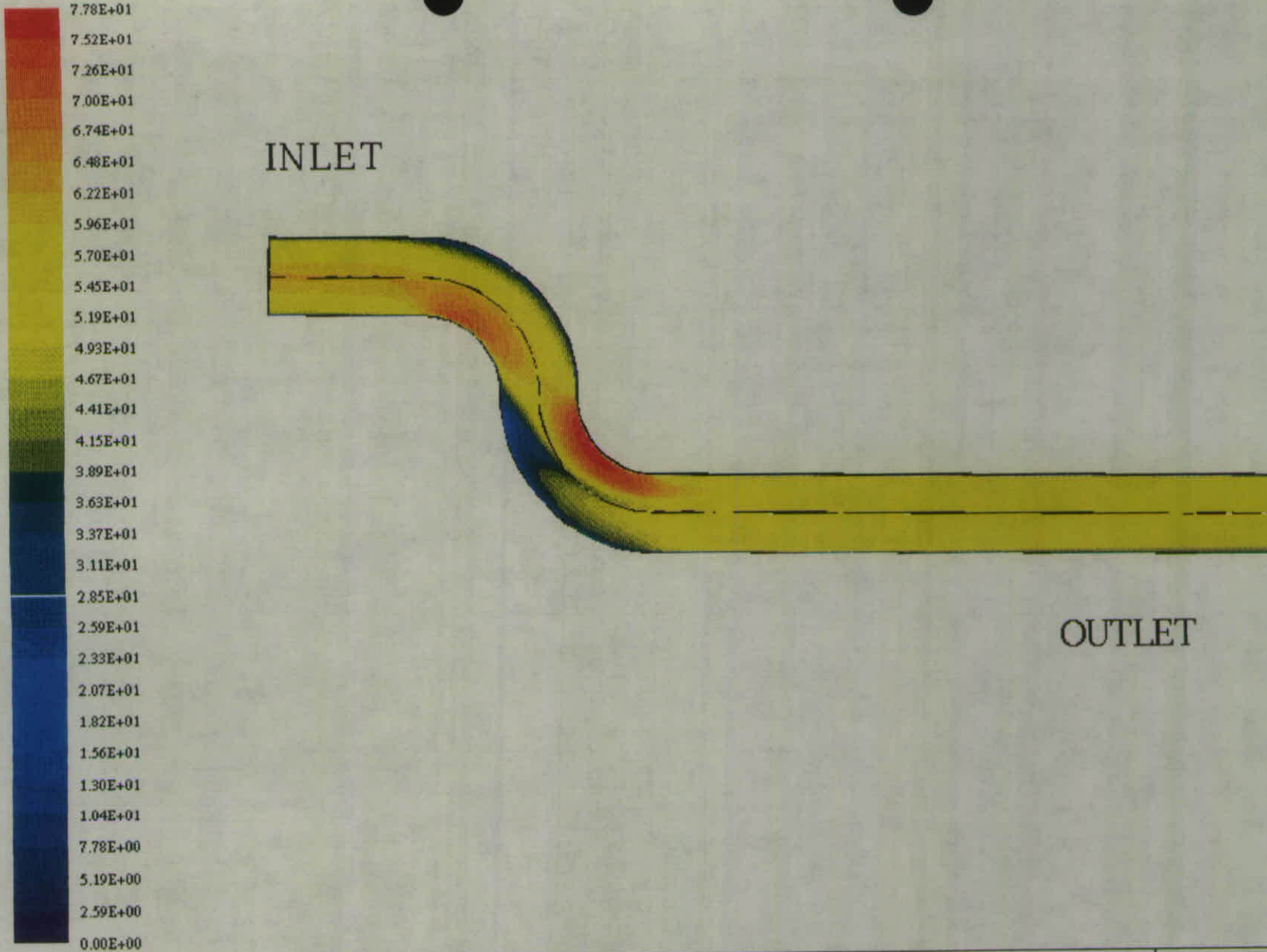
Fig. 6 Contours of Velocity Magnitude For a Cross-Section 4D Downstream of a Single Bend



NEL - Single 90 degree bend
 Velocity Vectors (M/S)

Sep 04 1995
 Fluent 4.31
 Fluent Inc.

Fig. 7 Velocity Vectors For a Cross-Section 4D Downstream of a Single Bend



NEL – S-bend with no separation

Velocity Magnitude (M/S)

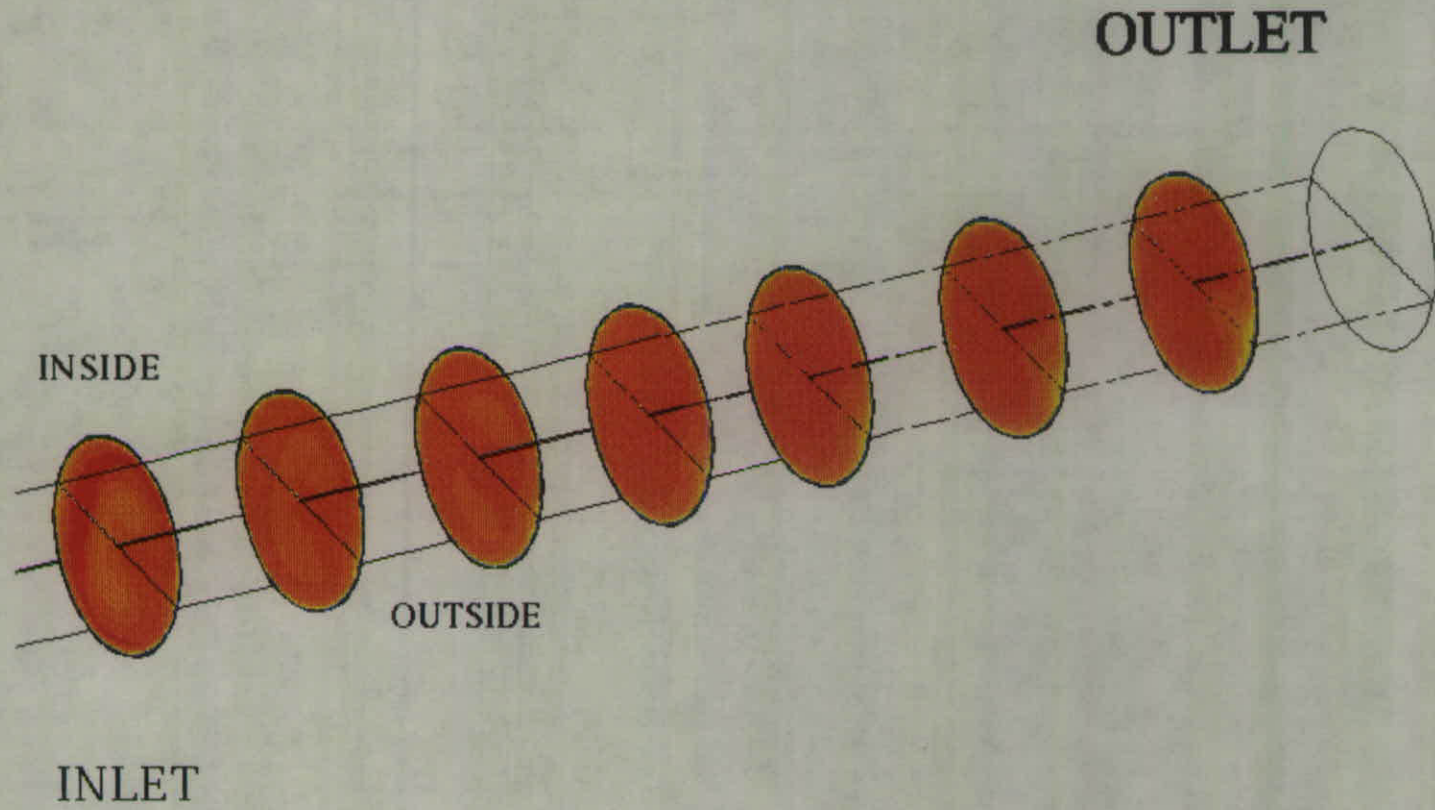
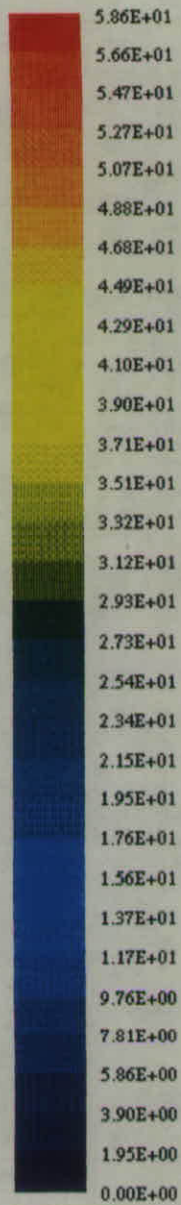
Lmax = 7.779E+01 Lmin = 0.000E+00



Fluent 4.31

Fluent Inc.

Fig. 8 Contours of Velocity Magnitude in the Plane of Symmetry for an S-Bend with no Separation



NEL – S-bend with no separation

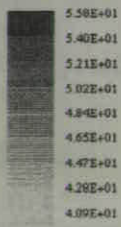
Velocity Magnitude (M/S)

Lmax = 5.856E+01 Lmin = 0.000E+00

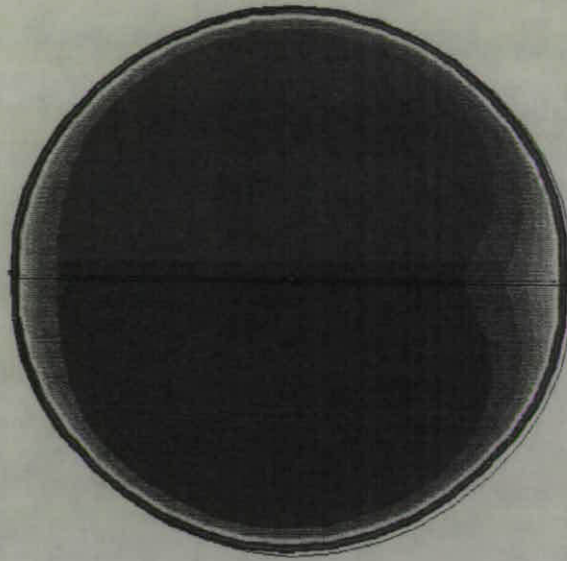
Fluent 4.31

Fluent Inc.

Fig. 9 Contours of Velocity Magnitude for Cross-sections Downstream of an S-Bend with no Separation



INSIDE



OUTSIDE

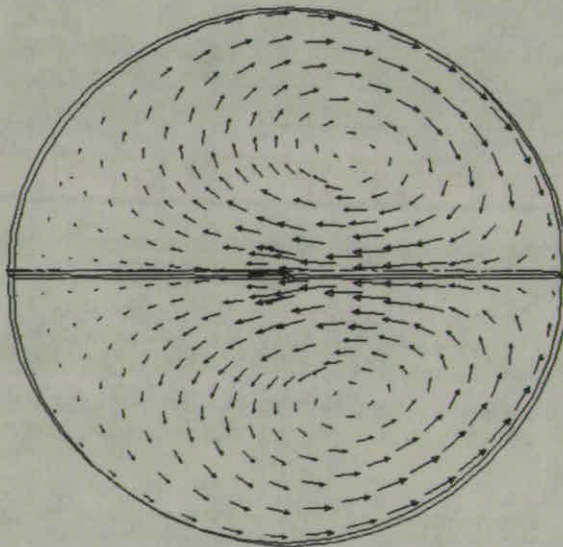


NEL - S-bend with no separation
Velocity Magnitude (M/S)
Lmax = 5.583E+01 Lmin = 0.000E+00

Fluent 4.31
Fluent Inc.

Fig. 10 Contours of Velocity Magnitude For a Cross-Section 4D Downstream of an S-Bend With No Separation

INSIDE

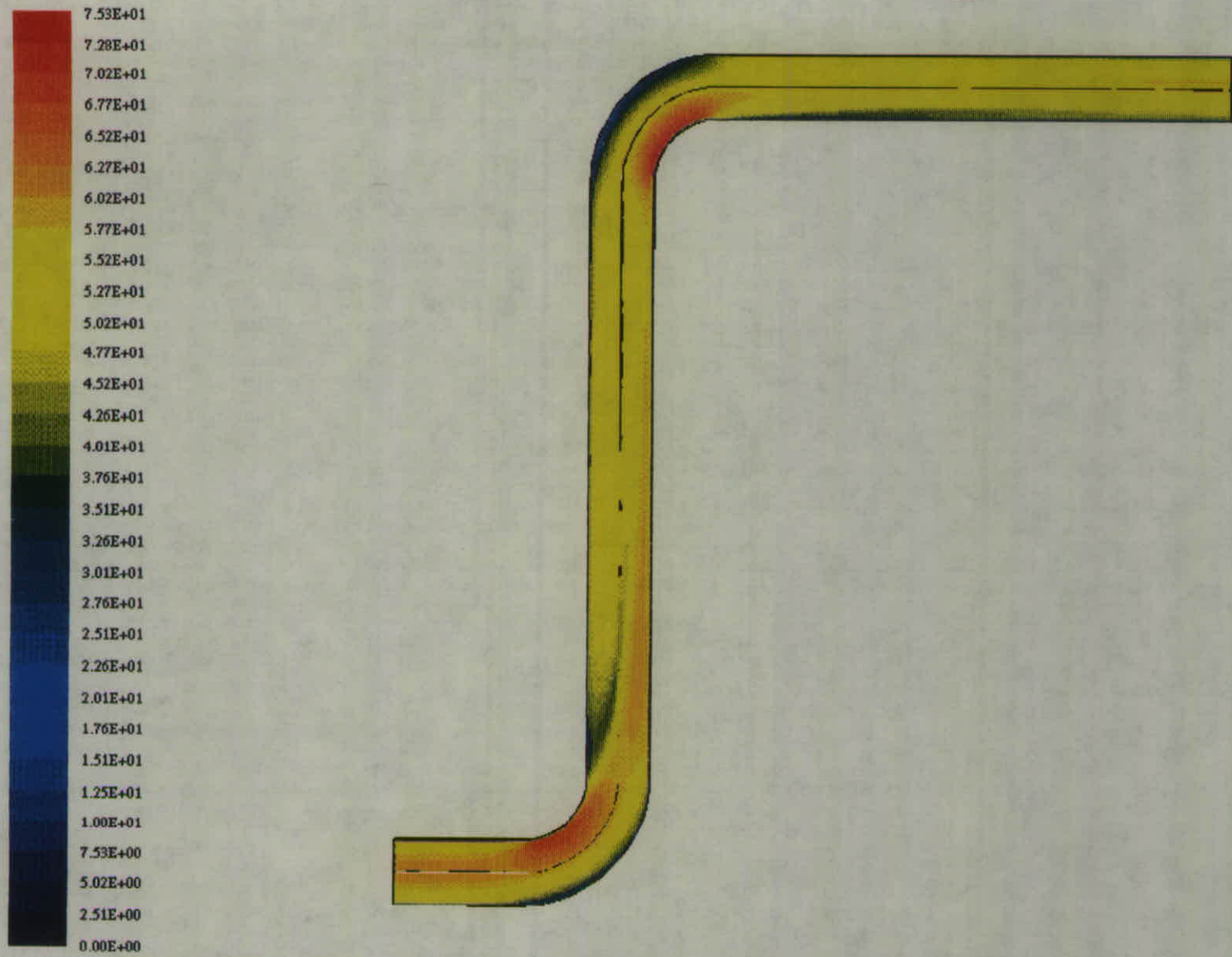


OUTSIDE

NEL - S-bend with no separation
Velocity Vectors (M/S)

Sep 05 1995
Fluent 4.31
Fluent Inc.

Fig. 11 Velocity Vectors For a Cross-Section 4D Downstream of an S-Bend With No Separation



NEL - S-bend with 9D separation

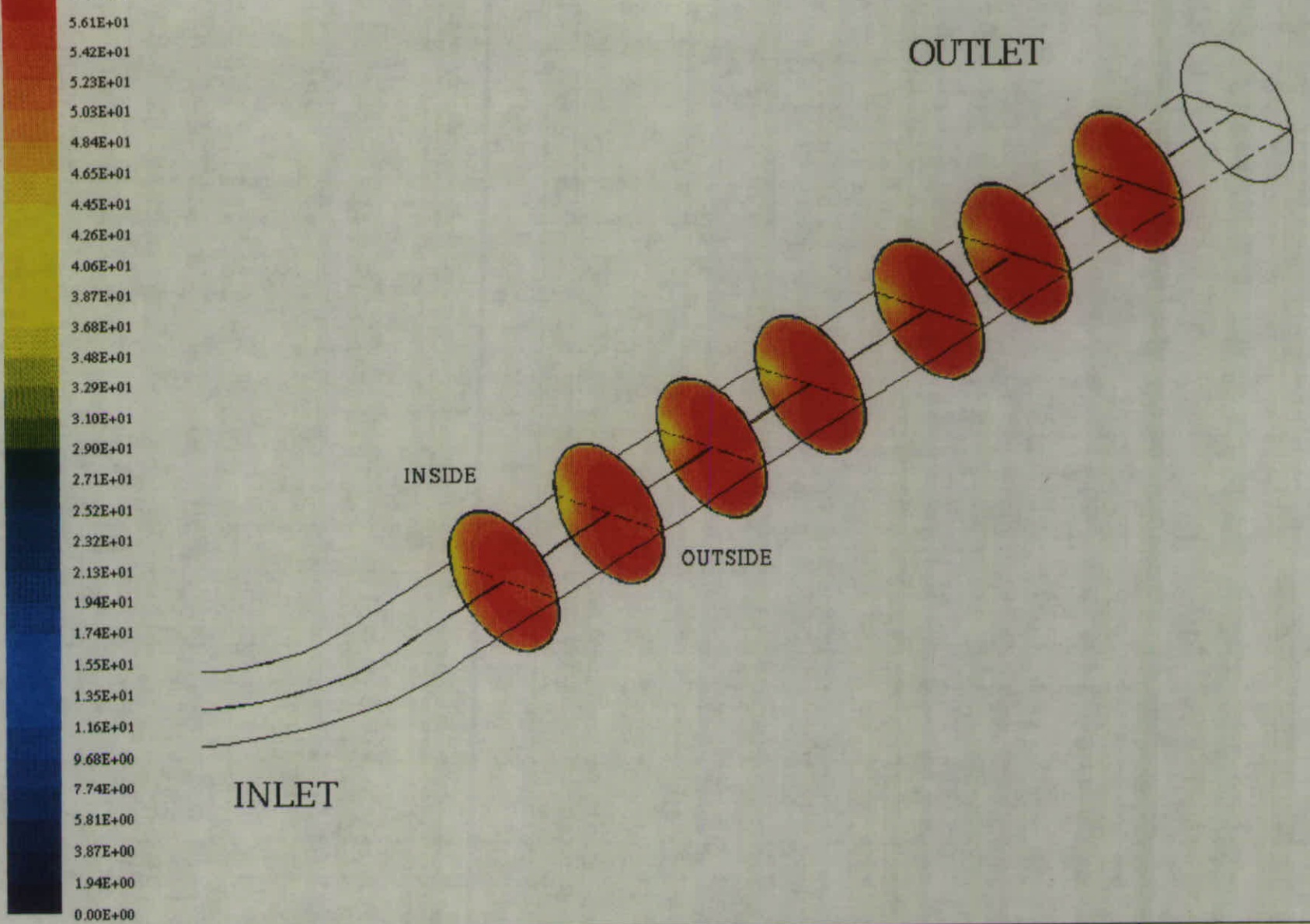
Velocity Magnitude (M/S)

Lmax = 7.526E+01 Lmin = 0.000E+00

Fluent 4.31

Fluent Inc.

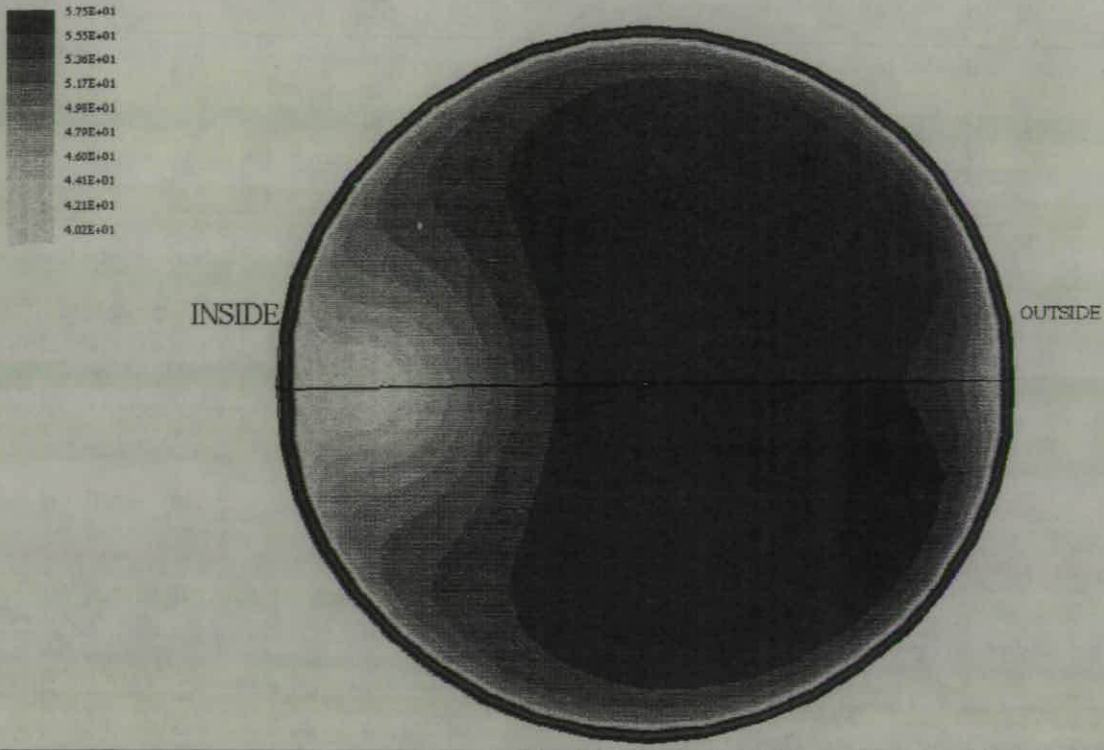
Fig. 12 Contours of Velocity Magnitude in the Plane of Symmetry for an S-Bend with 9D Separation



NEL - S-bend with 9D separation
Velocity Magnitude (M/S)
Lmax = 5.807E+01 Lmin = 0.000E+00

Fluent 4.31
Fluent Inc.

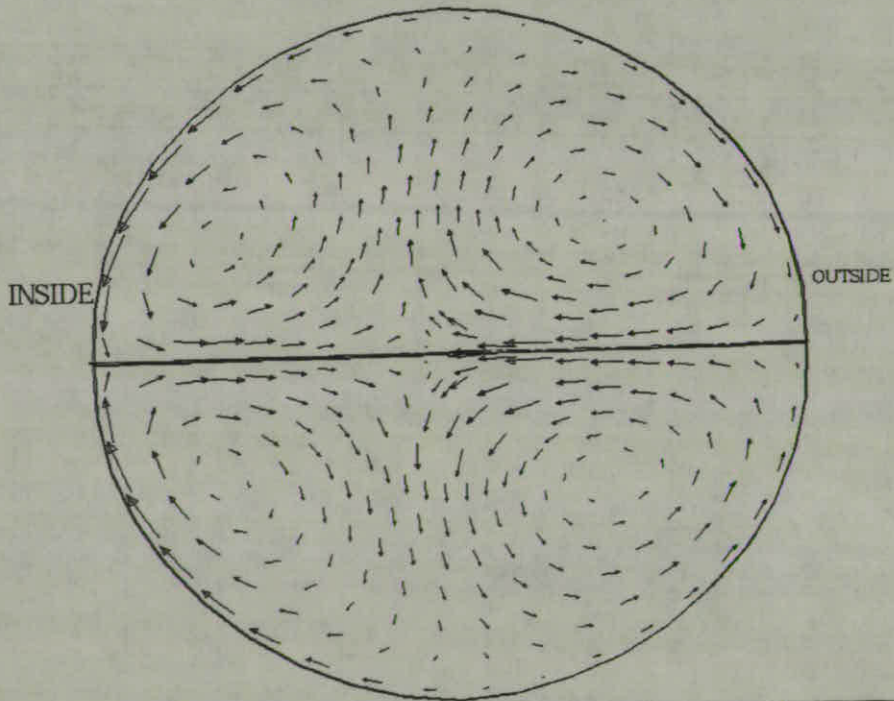
Fig. 13 Contours of Velocity Magnitude for Cross-sections Downstream of an S-Bend with 9D Separation



NEL - S-bend with 9D separation
Velocity Magnitude (M/S)
Lmax = 5.746E+01 Lmin = 0.000E+00

Fluent 4.31
Fluent Inc.

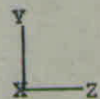
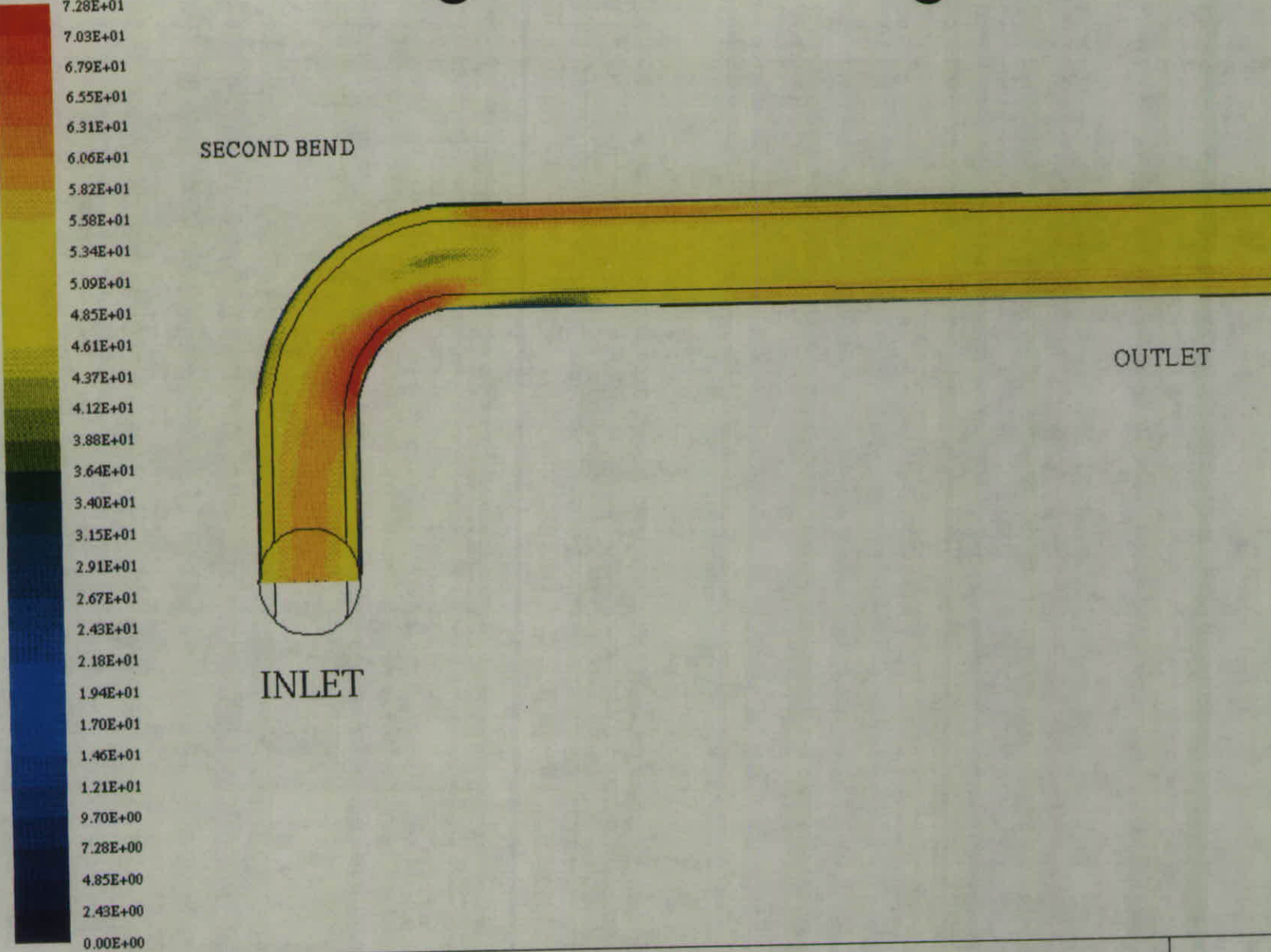
Fig. 14 Contours of Velocity Magnitude For a Cross-Section 4D Downstream of an S-Bend With 9D Separation



NEL - S-bend with 9D separation
Velocity Vectors (M/S)

Sep 04 1995
Fluent 4.31
Fluent Inc.

Fig. 15 Velocity Vectors For a Cross-Section 4D Downstream of an S-Bend With 9D Separation



NEL – Twisted S-bend with no separation

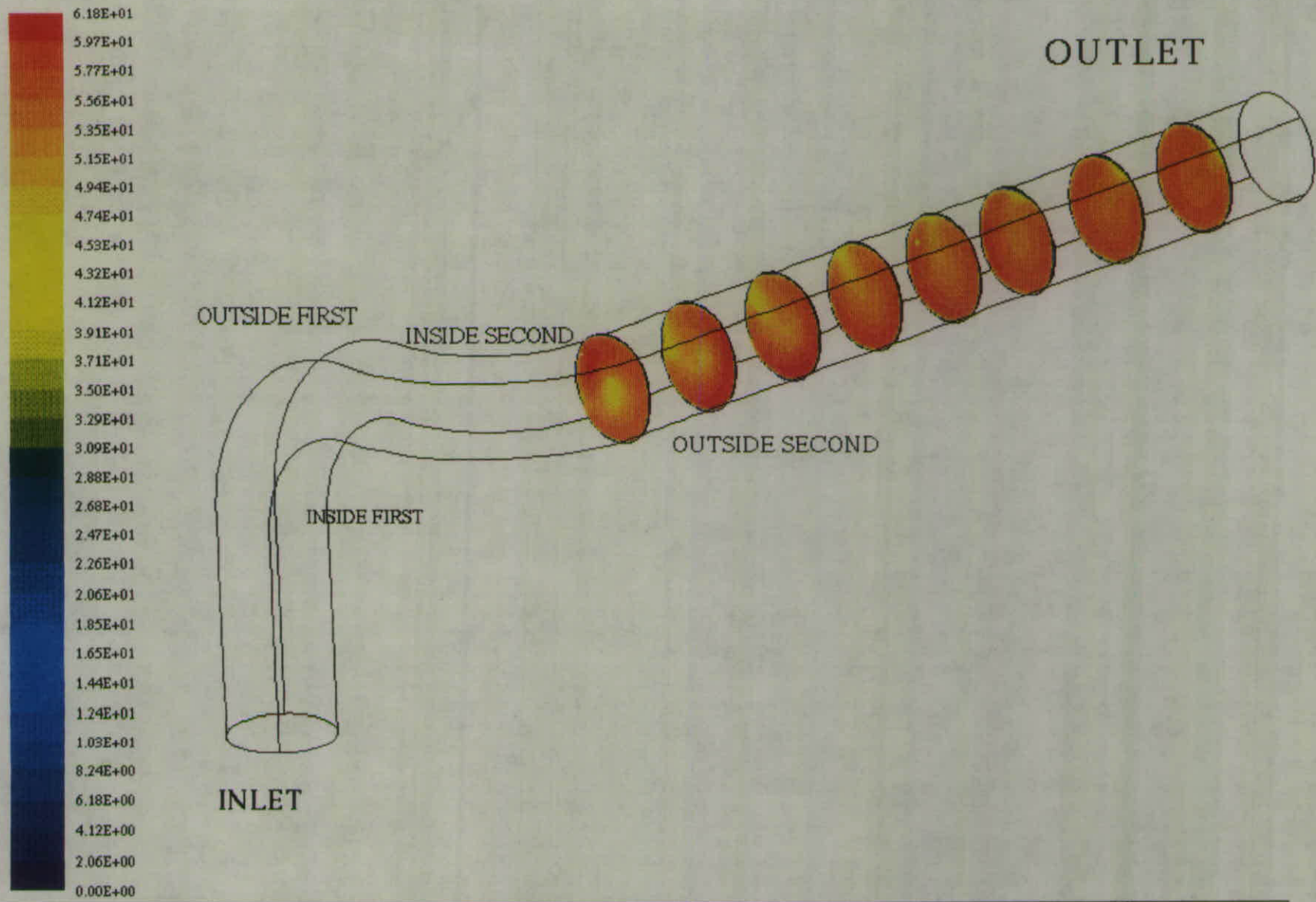
Velocity Magnitude (M/S)

$L_{max} = 7.275E+01$ $L_{min} = 0.000E+00$

Fluent 4.31

Fluent Inc.

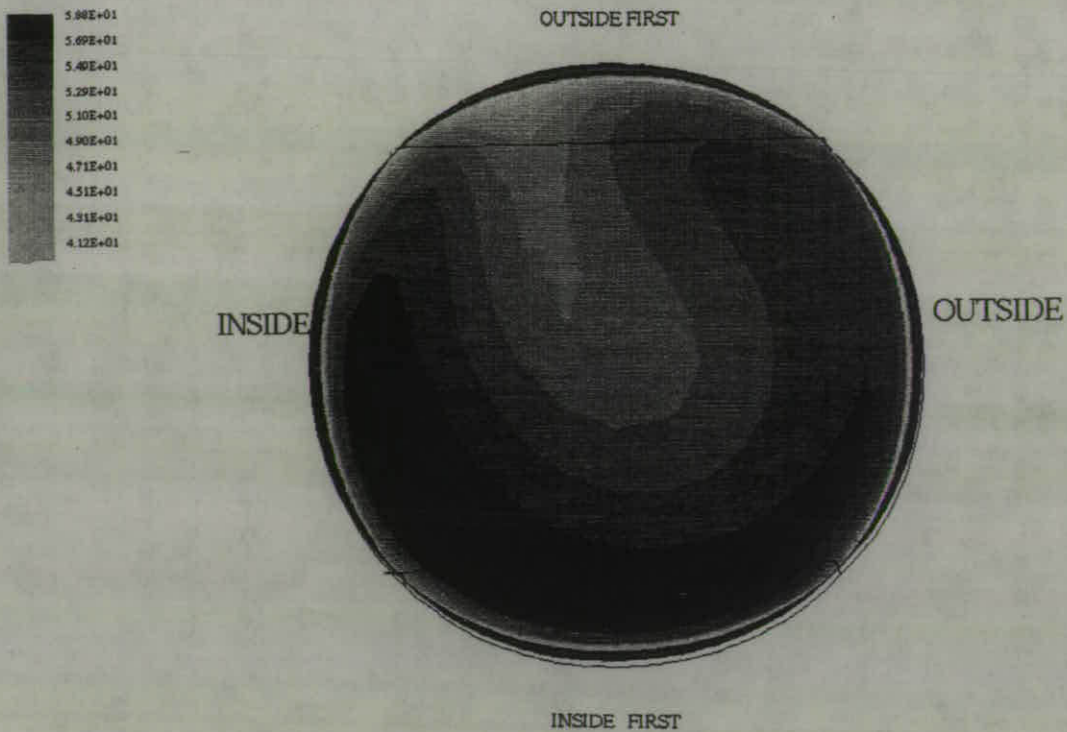
Fig. 16 Contours of Velocity Magnitude for a Twisted S-Bend in the Plane of Symmetry (With Respect to the Second Bend)



NEL - Twisted S-bend with no separation
Velocity Magnitude (M/S)
L max = 6.177E+01 L min = 0.000E+00

Fluent 4.31
Fluent Inc.

Fig. 17 Contours of Velocity Magnitude for Cross-sections Downstream of a Twisted S-Bend



NEL - Twisted S-bend with no separation

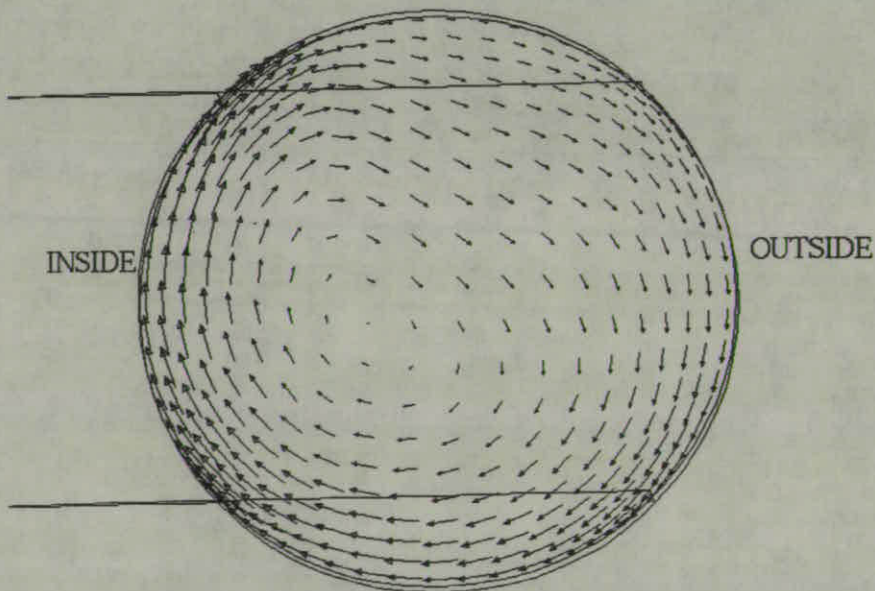
Velocity Magnitude (M/S)

Lmax = 5.881E+01 Lmin = 0.000E+00

Fluent 4.31

Fluent Inc.

Fig. 18 Contours of Velocity Magnitude For a Cross-Section 4D Downstream of a Twisted S-Bend



NEL - Twisted S-bend with no separation

Velocity Vectors (M/S)

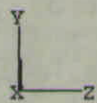
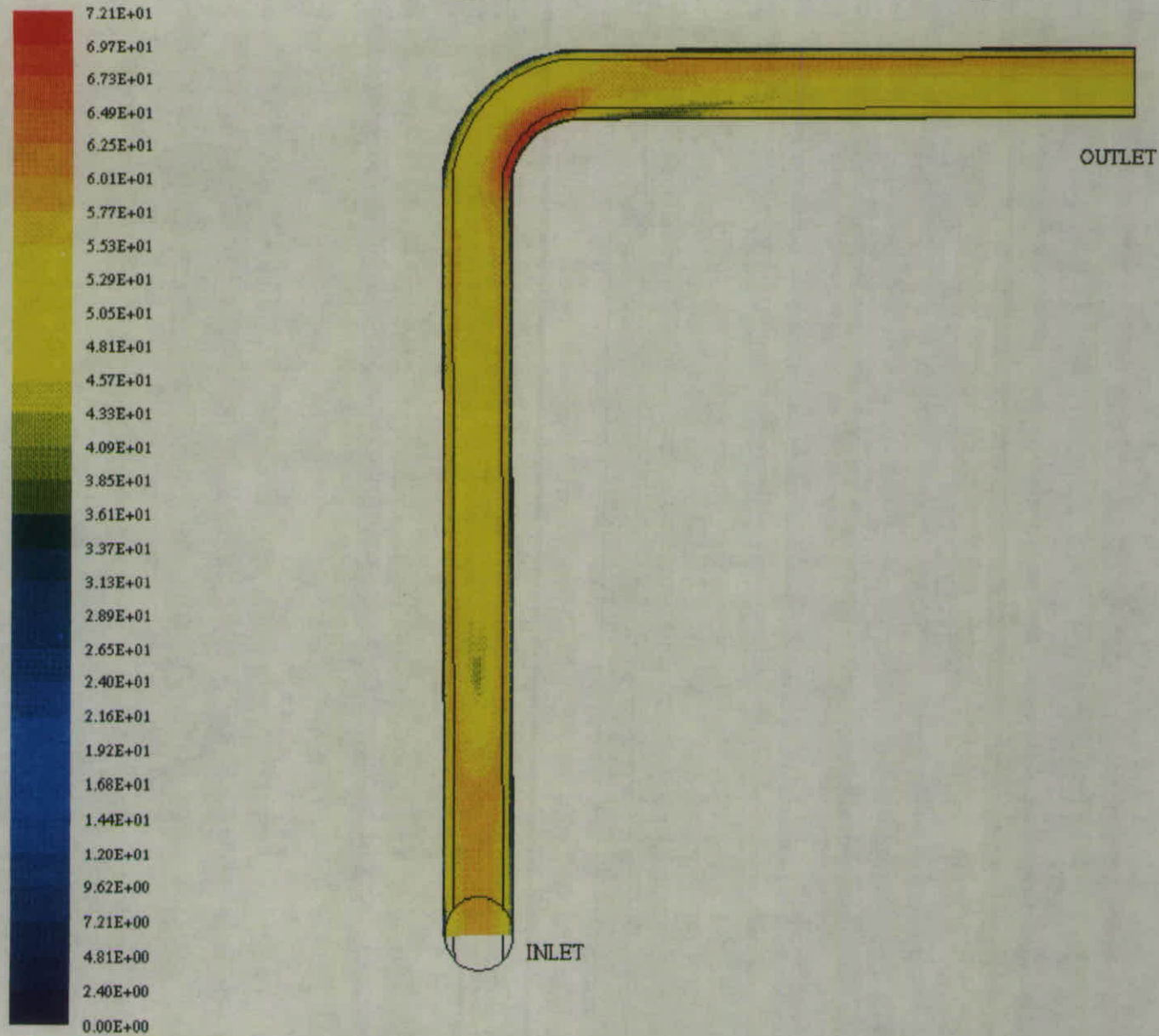
Lmax = 1.470E+01 Lmin = 4.320E-01

Sep 06 1995

Fluent 4.31

Fluent Inc.

Fig. 19 Velocity Vectors For a Cross-Section 4D Downstream of a Twisted S-Bend



NEL – Twisted S–bend with 9D separation

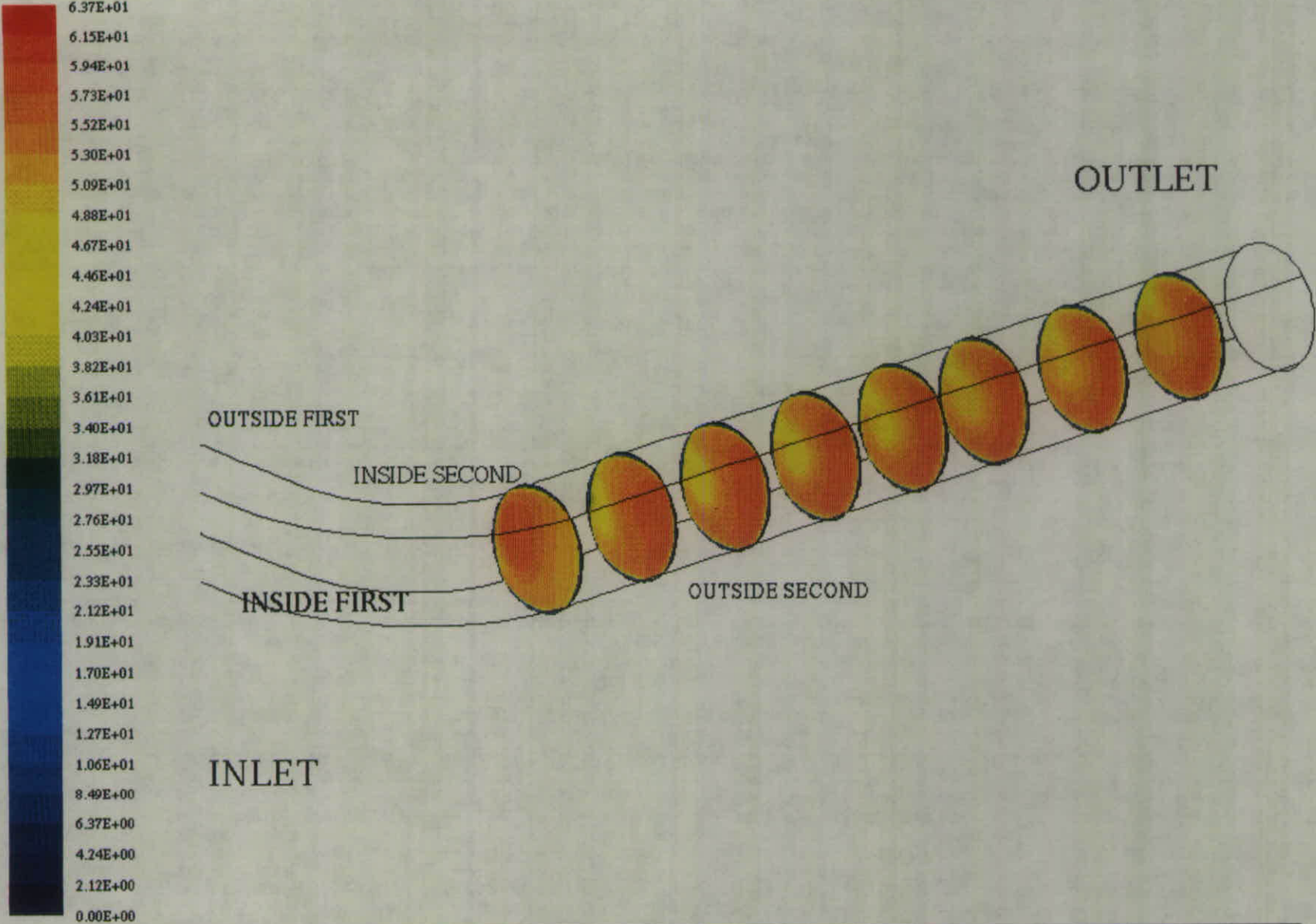
Velocity Magnitude (M/S)

Lmax = 7.215E+01 Lmin = 0.000E+00

Fluent 4.31

Fluent Inc.

Fig. 20 Contours of Velocity Magnitude for a Twisted S-Bend with 9D Separation in the Plane of Symmetry (With Respect to the Second Bend)



NEL – Twisted S-bend with 9D separation

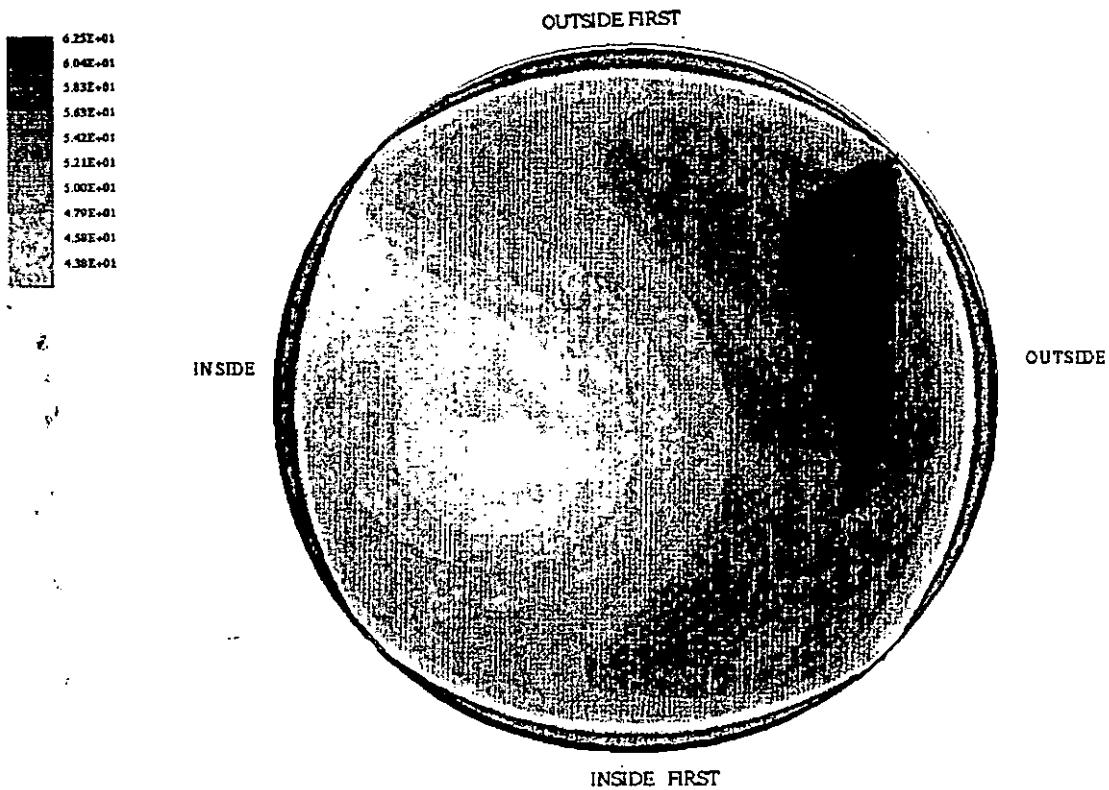
Velocity Magnitude (M/S)

Lmax = 6.366E+01 Lmin = 0.000E+00

Fluent 4.31

Fluent Inc.

Fig. 21 Contours of Velocity Magnitude for Cross-sections Downstream of a Twisted S-Bend with 9D Separation



NEL - Twisted S-bend with 9D separation

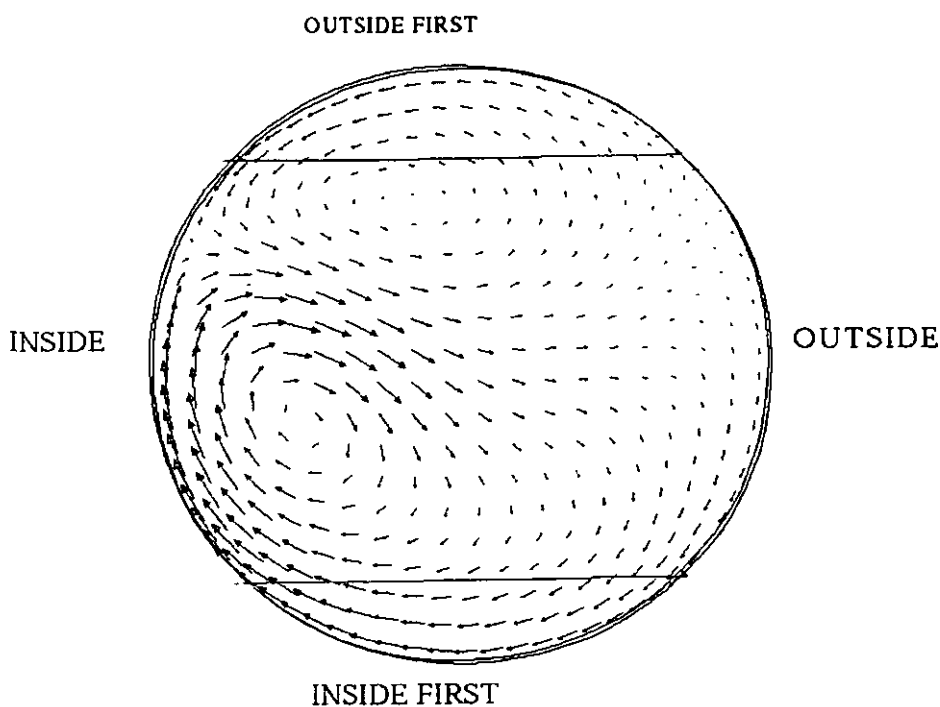
Velocity Magnitude (M/S)

Lmax - 6.252E+01 Lmin - 0.000E+00

Fluent 4.31

Fluent Inc.

Fig. 22 Contours of Velocity Magnitude For a Cross-Section 4D Downstream of a Twisted S-Bend With 9D Separation



NEL - Twisted S-bend with 9D separation

Velocity Vectors (M/S)

Lmax - 9.420E+00 Lmin - 5.965E-02

Sep 12 1996

Fluent 4.31

Fluent Inc.

Fig. 23 Velocity Vectors For a Cross-Section 4D Downstream of a Twisted S-Bend With 9D Separation

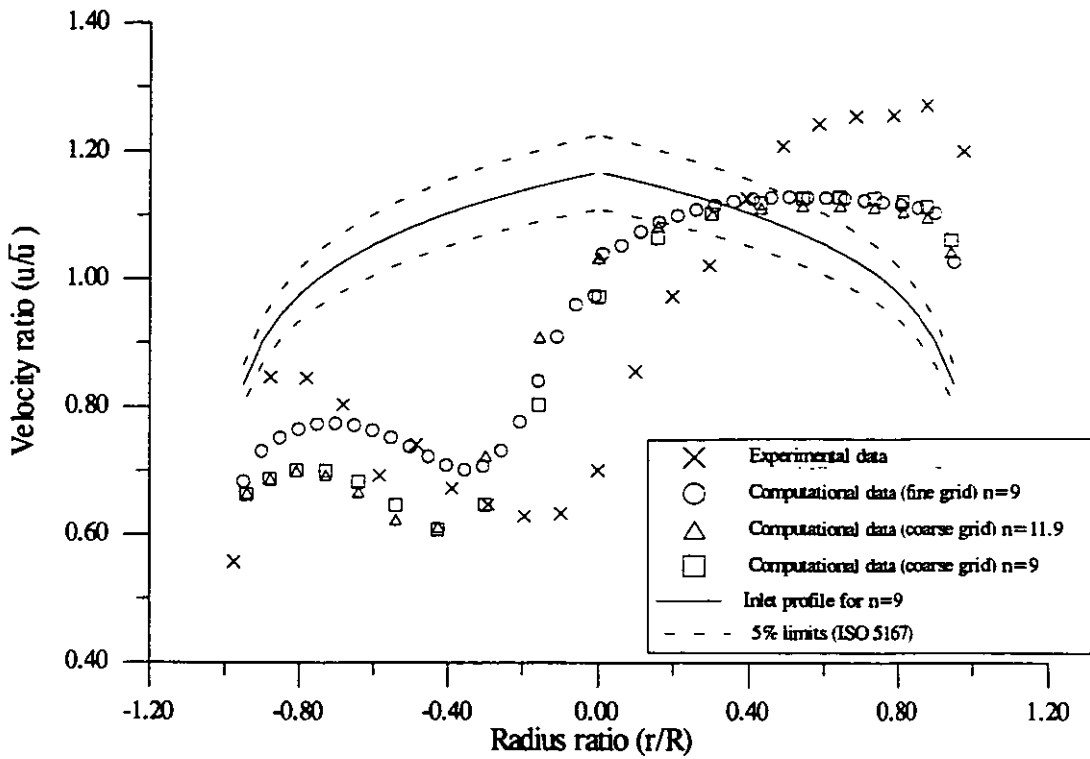


Fig. 24 Comparison of Experimental and Computational Axial Velocity Profiles 7/8D Downstream of a Single Bend on the Plane of Symmetry

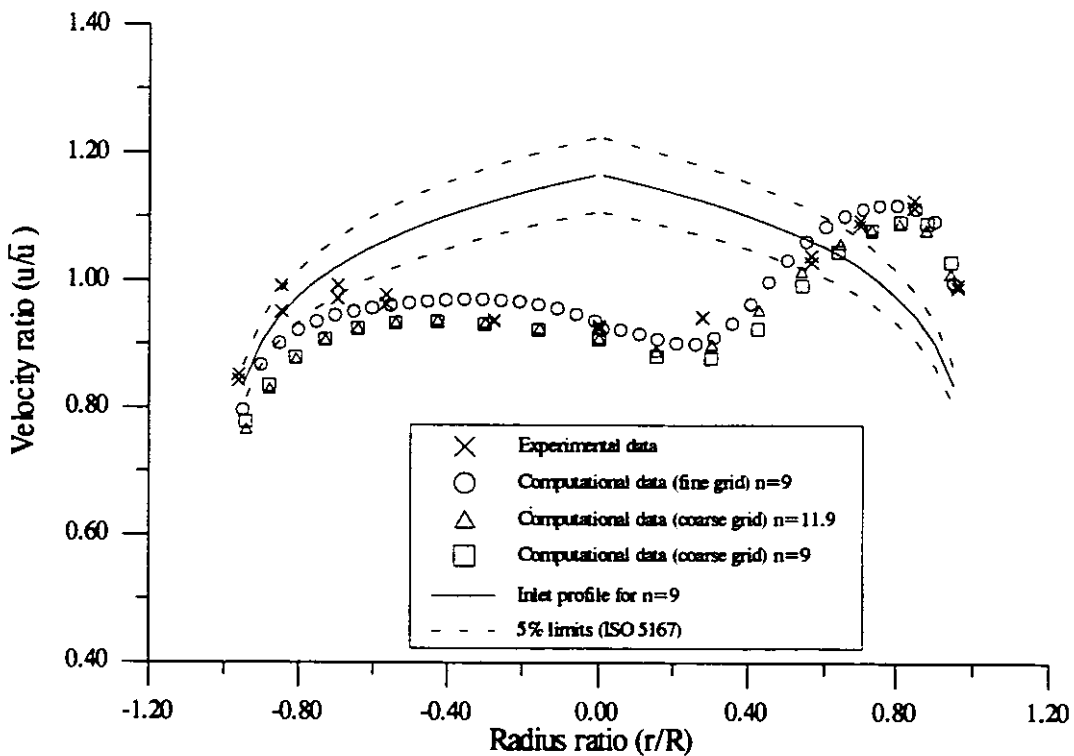


Fig. 25 Comparison of Experimental and Computational Axial Velocity Profiles 4D Downstream of a Single Bend on the Plane of Symmetry

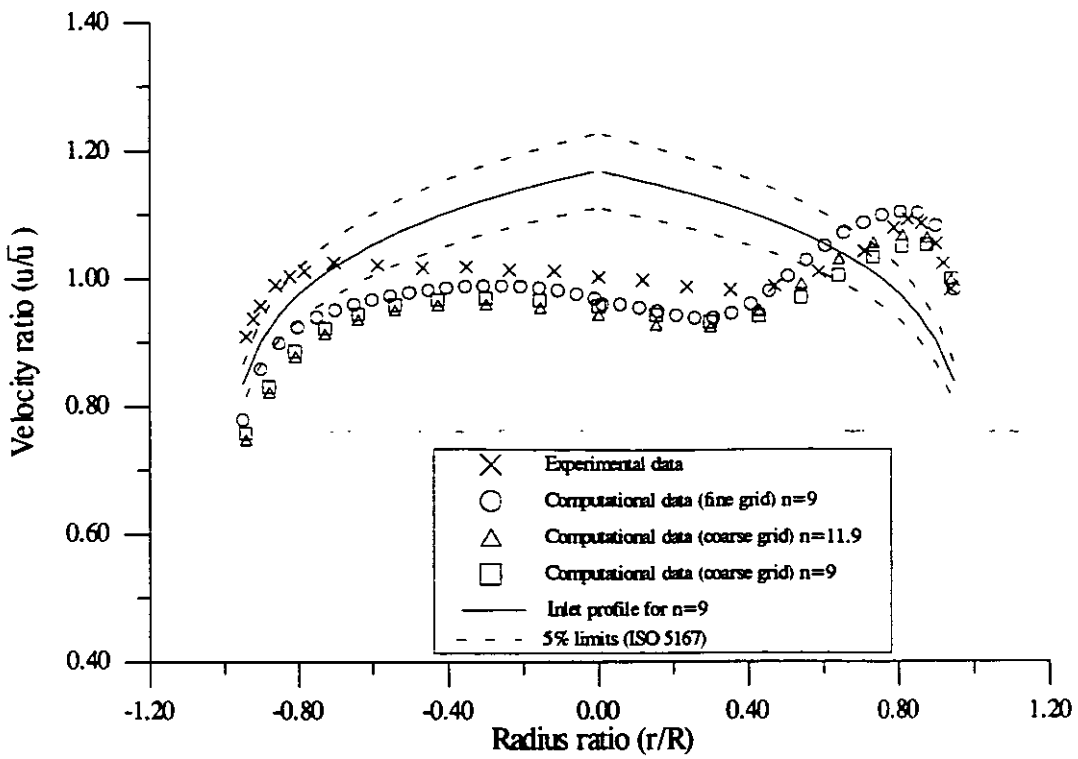


Fig. 26 Comparison of Experimental and Computational Axial Velocity Profiles 5D Downstream of a Single Bend on the Plane of Symmetry

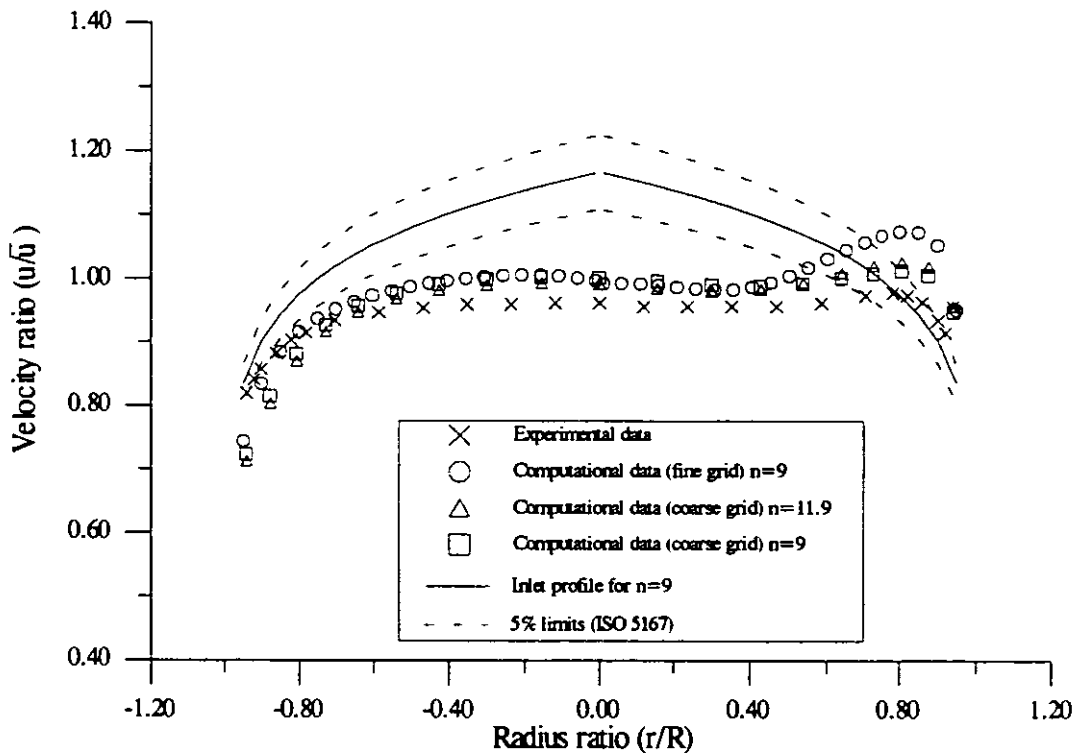


Fig. 27 Comparison of Experimental and Computational Axial Velocity Profiles 7D Downstream of a Single Bend on the Plane of Symmetry

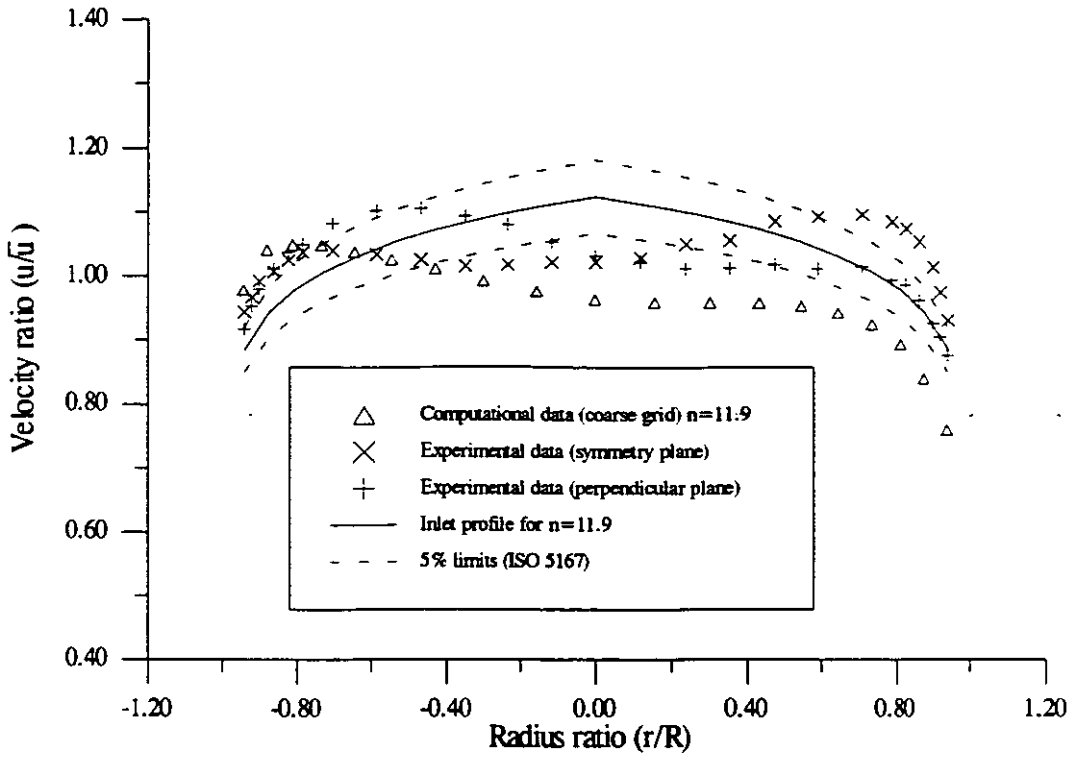


Fig. 28 Comparison of Experimental and Computational Axial Velocity Profiles 5D Downstream of a Twisted S-Bend on the Plane of Symmetry (With Respect to the Second Bend)

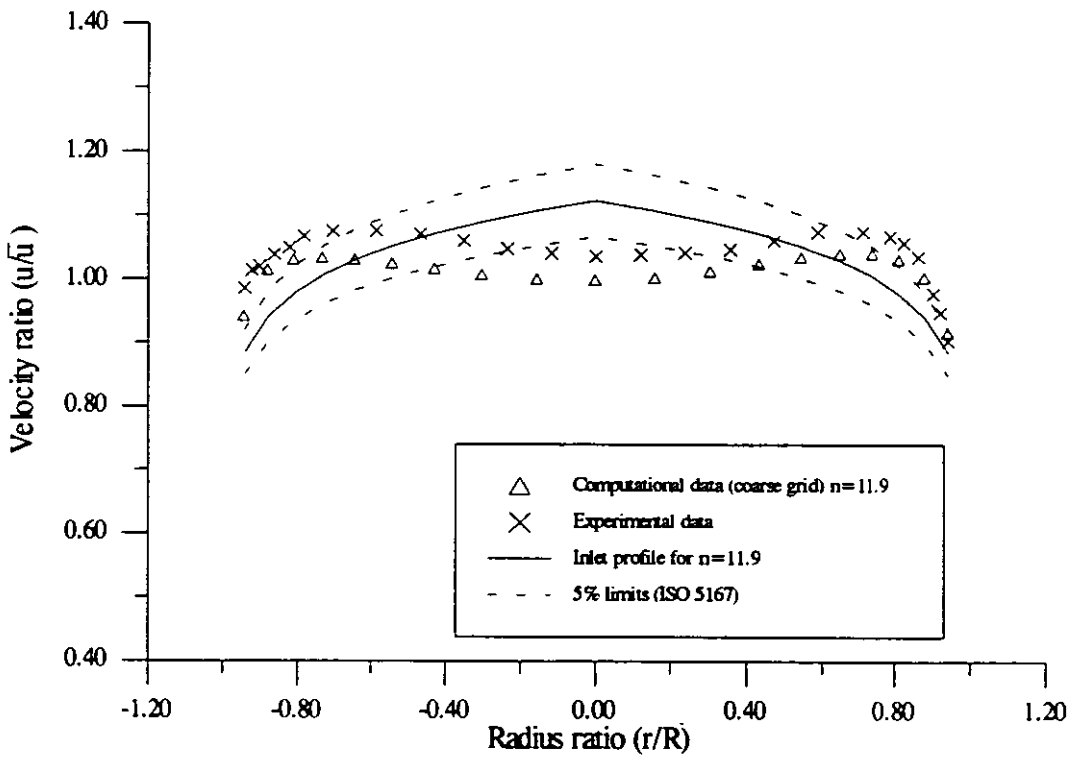


Fig. 29 Comparison of Experimental and Computational Axial Velocity Profiles 7D Downstream of a Twisted S-Bend on the Plane of Symmetry (With Respect to the Second Bend)

FOCUS DISCUSSION GROUP A

Recent Developments in Flow Measurement as it Relates to the Oil And Gas Industry.

A Cheshire, Fisher-Rosemount

RECENT DEVELOPMENTS IN FLOW MEASUREMENT AS IT RELATES TO THE OIL AND GAS INDUSTRY

Drew Cheshire
Fisher-Rosemount
Manager, International Flow Marketing

Abstract

In recent years developments in traditional flowmeter technology have substantially increased their functionality and performance, due in part to the wider acceptability and use of microprocessor based smart electronic transmitters. Similar developments have been taking place in other areas of instrumentation such as temperature measurement. The logical progression of such improvements is the consolidation of multiple process variables in a single transmitter package giving the user real-time compensated flow outputs, and access to the raw data for informational use. The emergence of this technology gives rise to a new generation of "head type Multivariable Flowmeters". Multivariable technology will, in the coming years, appear in other traditional flowmeters such as magnetic, vortex and ultrasonic. The implications to the user are significant cost savings and dramatic changes in the current control architecture. This paper includes an explanation of recent developments in multivariable flowmeters including calculated performance results for both liquid and gas, and recent advances in vortex flowmeters with practical experiences on their applications in the oil and gas industry.

Introduction

Differential pressure, or *head-class* metering is probably the most written about and best understood of all flow technologies, and historically is the most used; approximately half of all flow meters sold in the world today are differential pressure meters. The basic principle for measurement is Bernoulli's streamline energy equation. When the flow is contracted due to the insertion of a primary element such as an orifice plate or pitot tube, Kinetic energy increases resulting in a decrease in potential energy (static pressure). The pressure difference between the upstream (full pipe) section and the constriction at the primary element exhibits a square root relationship to the fluid velocity and can be written as:

$$q = K\sqrt{\frac{h}{d}} \quad (1)$$

Where: q = Flow rate
K = Meter constant
h = Differential pressure
d = density

Due to the square root relationship from equation (1), a transmitter with a 100:1 DP turndown is the same as a 10:1 flow turndown.

Mass Measurement

In measuring gasses, significant changes in actual volume can occur when operating conditions vary, resulting in significant uncertainties in the flow measurement. Pressure and temperature compensation has traditionally been the most commonly applied method of compensating for these uncertainties, this method assumed the compressibility factor was constant at operating conditions and often neglected compressibility effects as shown in the simplified equation: --

$$q_m = K_2 \sqrt{\frac{h P}{T}} \quad (2)$$

The use of microprocessor based flow computers significantly improves the accuracy of gas flow measurement; particularly natural gas where dynamic compensation is standard. Compensation is achieved through utilizing the inputs from a Differential Pressure, a Gauge Pressure and a Temperature transmitter. The flow computer can perform complex mathematical functions that relate to flowmeter output such as fluid density, flowmeter gas expansion coefficients and supercompressibility factors.

$$q_m = N C_d E Y_1 d^2 \sqrt{\rho h} \quad (3)$$

where: Q_m = Mass flow rate
 N = Units conversion factor
 C_d = Discharge coefficient
 E = Velocity of approach factor
 Y_1 = Gas expansion factor
 d = Orifice bore
 ρ = Fluid density
 h = Differential pressure

This method does, however, have a number of drawbacks including cost, high maintenance, cumulative errors of the transmitters, and programming requirements of the flow computer. Recent developments in ASIC technology has resulted in the emergence of a single Multivariable™ Mass Flow Transmitter which performs the same measurement and computing functions as the system previously described, but with greater accuracy and at a fraction of the total installed cost. Configuration is done through an Engineering Assistant software package containing all process information. With the advent of HART® digital communication users can now have access to a wide range of real-time process data.

Multivariable™ Transmitters

A Limiting factor to DP/orifice meter measurements has historically been the limitations on range (nominally 4:1). Test data from four Multivariable™ transmitters show that differential pressure does not significantly affect the flow data until 8:1 range down is achieved. Uncertainty is due largely to the geometry and installation of the orifice plate itself and properties of the gas or liquid such as viscosity and density. Indeed, the flow discharge coefficient proves to be the largest contributor to the overall uncertainty. To calculate flow uncertainties actual differential pressure data was used. The test results showed the average pressure uncertainty to be 0.04%. The temperature uncertainty was assumed to be 0.2%. The units tested had 62.2KPa of water URL (Upper Range Limit) differential pressure sensors, and 5515KPa URL pressure sensors. The sensors for each unit were trimmed at zero and URL prior to testing. Figure 1 shows the differential pressure range down results at 1378.95KPa static pressure along with the calculated flow uncertainty for the air flow example. The results for the water flow example were essentially the same.

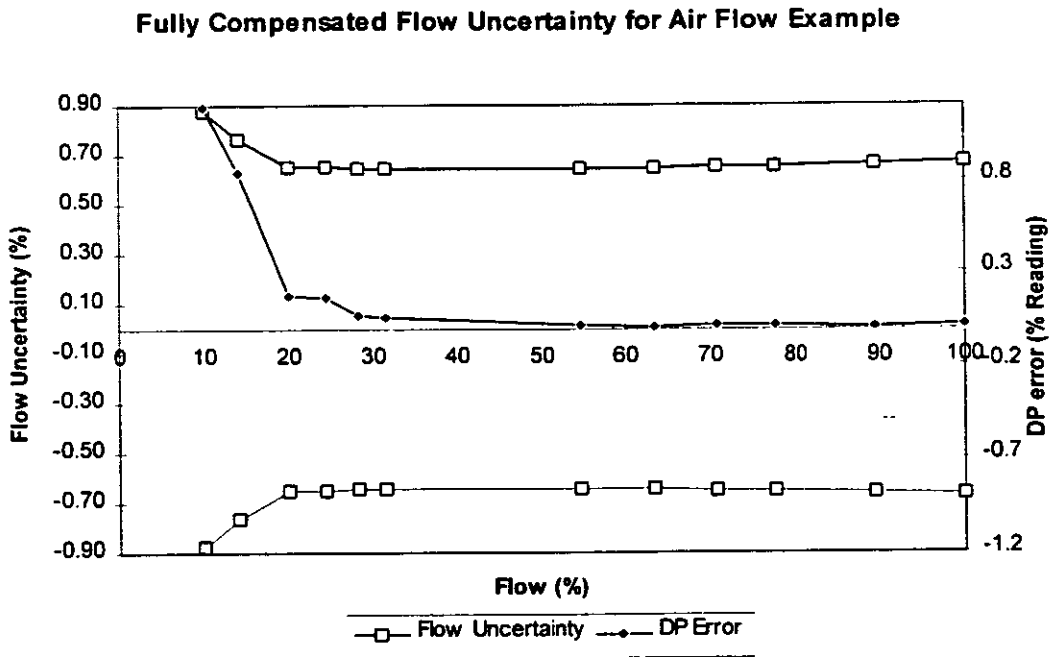


Figure 1. - DP Error and Flow Uncertainty vs. Flow Range

Table 1. shows a breakdown of the maximum flow uncertainty. This point occurred at 100:1 range down in differential pressure or 10:1 in flow.

Term	Uncertainty %	% Cont.
Cd	0.6	46.26
Y1	0.108	1.50
D	0.4	1.82
d	0.07	3.32
h	1.19	45.43
r	0.227	1.66
Total	0.88	100

Table 1.

Where Cd = Discharge coefficient
 Y1 = Gas expansion factor
 D = Meter tube diameter (inches)
 d = Orifice bore
 h = Differential pressure
 r = Fluid density

Even at high range downs, exceeding 8:1 rangedown in flow, the overall calculated flow uncertainty was less than 1% for all four transmitters.

Applications of Multivariable Transmitters in the Oil & Gas Industry

Heat management is an important area in which cost savings can be realized; one company in California, USA, reduced production costs from \$6.27/bbl in 1990 to \$4.86/bbl in 1994 due in large part to better heat management. Steam, gas and liquid measurement can be achieved through Multivariable pressure transmitters or Vortex meters with accuracy's of 1% or better.

The measurement of natural gas has very specific requirements as to how flow calculations are to be performed. In addition, many government agencies place strict audit trail requirements on the natural gas industry, creating the need for non-volatile logging of such parameters as process variables, flow rate calibration changes, orifice plate changes etc. Multivariable transmitters have undergone testing at the Colorado Engineering Experiment Station (CEESI). The results are summarized below.

The tests at CEESI were totalizing tests conducted with air as the flowing medium. A series of four tests were run on two transmitters using the CEESI gravimetric Primary A system as the reference. A 2 inch orifice meter run with a beta ratio of 0.2 was used across the tests. The two 3095FT transmitters were connected in parallel across the orifice meter to provide redundant data. The test conditions are tabulated in table 2.

Test Number	Static Pressure (KPa)	Differential Pressure (KPa)	Temperature Deg.C	Test Duration
1	2068.427	37.326	21	4 Hours
2	2068.427	37.326+/- 6221	21	4 Hours
3	2068.427	37.326	21	4 Hours

	+/- 344.738			
4	2068.427	37.326 varied to 0	21	4 Hours

Table 2.

During tests 2 & 3 the conditions were held at the respective levels for approximately one half hour. Changes in the flow conditions were made over approximately one minute. During test 4 the flow was shut off for several minutes at a time. Both transmitters were configured to calculate the compressibility factor using the Detail Characterization Method of A.G.A. Report No.8. Since the limits for the various constituent gases in this report allows for a gas composition which matches that of air, no correction was required to compare the results with those from CEESI's primary system. The results are tabulated in Table 3.

Test Number	CEESI Total Mass (Kg/m)	3095 FT #1 Total Mass (Kg/m)	3095 FT #2 Total Mass (Kg/m)	Deviation 3095 FT #1 (%)	Deviation 3095 FT #2 (%)	Deviation Between 3095 Fts (%)
1	4308.018	4276.463	4276.884	-0.732	-0.723	0.0098
2	4281.288	4255.906	4257.286	-0.593	-0.561	0.0324
3	4284.72	4255.603	4256.562	-0.680	-0.657	0.0255
4	2170.872	2156.550	2156.330	-0.861	-0.871	-0.0102

Table 3.

As can be seen from the above data, this Multivariable meter performs well within the requirements for the natural gas industry as a logging meter.

Vortex

Recent improvements in vortex shedder bar design and signal filtering has increased the acceptability of this technology in the industry. Historical problems such as susceptibility to vibration and process noise which had previously excluded it from many installations have been overcome, allowing the use of an accurate volumetric instrument which provides negligible pressure loss.

Resistance to vibration noise is achieved through mass-balancing of the shedder bar and sensor. An 8800 meter was tested under SAMA PMC 31.1-1980 Section 5.3 condition 3. from 5 to 2,000 Hz. The results are shown in Figure 2.

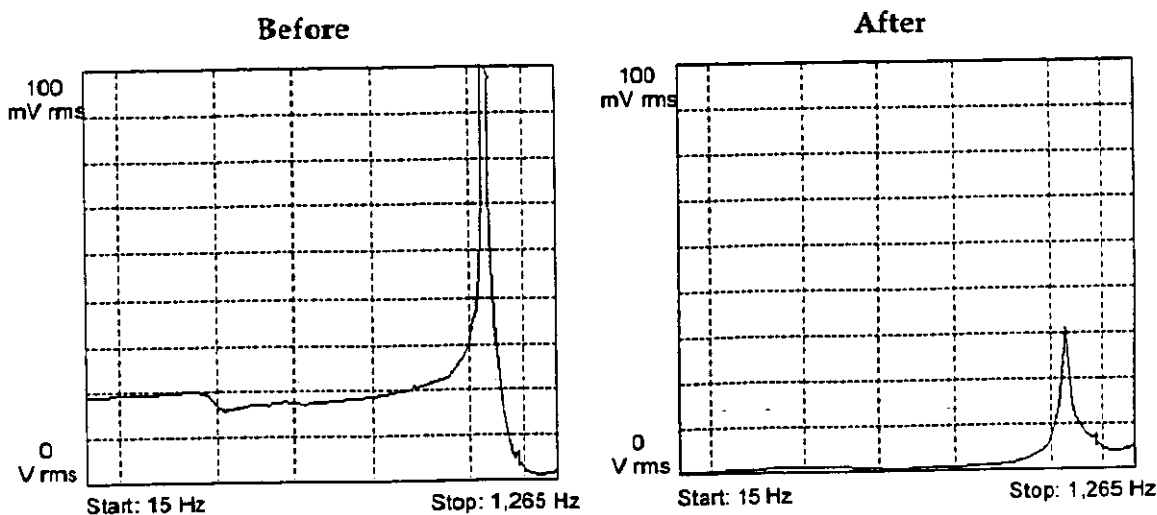


Figure 2.

Effects due to process noise are filtered out by means of Adaptive Digital Signal Processing (ADSP). At low flow rates, vortex signal amplitude is small and the signal to noise ratio can be adversely affected by the presence of both low and high frequency noise components. At higher flow rates the greater velocities result in higher amplitude signals, but those signals can be distorted by low frequency noise components. Signal to noise degradation is compounded by the potential amplitude swings presented by wide flow and density ranges. When density is constant, the flow range is approximately 25:1. This results in a significant amplitude range of 625:1. Density variation from atmospheric pressure air to liquids represents an 800:1 density range. This variation results in an even wider range of signal amplitudes. The wide dynamic range of the vortex signal coupled with the inherent potential for noise make the problem of accurate measurement a challenge.

The filtering scheme now available on the 8800 Vortex Transmitter reduces the effects of low and high noise components while enabling measurement of the vortex frequency throughout the wide dynamic range of the signal.

Conclusion

Companies are facing increasing pressures from competitors and shareholders to decrease costs and maximize profits. Transmitter technology is developing at a fast pace, more process information and control functions are being made available at the transmitter. Instrumentation which provides greater flexibility and multiple process variables in real-time enables the user to better understand and control the process. Increasing the efficiency of steam injected into the well is one such example.

References

a Paper

- 1 David E. Wiklund and Loren M. Engelstad Improving Flow Measurement By Real-time Flow Calculations In Transmitters Having Multiple Process Variables. p. 8, 9. 1995.
- 2 Bill O'Donnell Digital Filtering on the Rosemount Model 8800 Vortex Flow Transmitter. p 1,2 1994.
- 3 David E. Wiklund and Cindy Nelson. Multivariable Transmitters in Natural Gas Measurement p10,11. 1996.

b Book

- 1 Richard E. Miller. Flow Measurement Engineering Handbook, Second Edition, McGraw Hill, New York, 1989.
- 2 David W. Spitzer. Industrial Flow Measurement, Instrument Society of America, Charlotte. 1990.
- 3 International Petroleum Encyclopedia, Penwell Publishing Co. Tulsa, 1996
- 4 Bela G. Liptak, Kriszta Venczel Instrument Engineers' Handbook Chilton Book Co. 1982
- 5 American Gas Association, AGA Report No.3, Orifice Metering of Natural Gas and Other Related

FOCUS DISCUSSION GROUP B

MFI Multiphase Metering Verification at the Agip Trecate Test Loop.

**A Mazzoni, AGIP SPA
Arstein Bringsvor, Multi-Fluid International AS**

MFI MULTIPHASE METERING VERIFICATION AT THE AGIP TRECATE TEST LOOP

Agostino Mazzoni AGIP SPA, Italy and
Årstein Bringsvor Multi-Fluid International AS (MFI), Norway

SUMMARY

AGIP has during the last few years built a comprehensive test facility at their Trecate field near Milan in Italy, which is particularly suited for testing multiphase meters. As part of AGIP's long term strategy, the MFI MultiPhase Meter (LP) has been extensively tested at Trecate, during a period from December 1995 to April 1996. The result from the tests have shown the following performance of the MFI Meter:

- The relative error in the oil, gas and water flow rates are basically inside the 10% uncertainty band in the operative range.
- The accuracy of the meter, when applied to the wells in area TR2, is consistent with the well testing performed with the test separator.
- The MFI LP meter already installed in the Trecate field is used to perform the standard well testing.
- The MFI MultiPhase Meter is recommended for on-shore and offshore applications, and it can also be recommended for subsea applications.

1. INTRODUCTION

This paper describe the experience that AGIP and MFI gained during testing of the MFI MultiPhase Meter at the Trecate Test Loop in Italy. Results showing the performance of the MFI MultiPhase Meter in real field conditions, covering a wide range of flow rates, pressure and temperatures are presented. Instantaneous and endurance test results are included.

The first section describes the test loop configuration and the test procedures used to verify the multiphase metering. The reference measurements are also described in this section. In the second section the MFI MultiPhase Meter is described, and in the third section the main results of the tests are reported, with comparison between the reference measurements (flow rates) and the MFI measurements.

2. TEST CONFIGURATION

2.1 Loop Description

The Trecate test loop is very flexible, and allows for comprehensive testing of the MFI MultiPhase Meter, with a large variety of flowing conditions and flow regimes. Wells from two different areas of the field can be routed through the test section, and combined in a number of different ways. Oil, water and gas can be added to the natural well flows.

The loop can be configured in several ways, and this paper describes tests with flow through the MFI MultiPhase Meter in two ways:

- First through the test separator, with the possibility to add one or several wells directly, and then through the MFI MultiPhase Meter.
- First through the MFI MultiPhase Meter, and then through the test separator.

Both options are shown in Fig 2.

2.2 Reference Instrumentation

The MFI MultiPhase Meter could be fed directly from the wells and/or through the MultiPhase Metering Unit, skid 412, connected to the field test separator. The service company's well testing separator was used to verify the reference measurements, using positive displacements for the oil flow rates and orifice for the gas flow rates, respectively. The consistency of the oil flow rate measurements was very good and the specified error ($\pm 1\%$) on the reference meters can be considered correct. For the gas flow rate measurements, the consistency was quite good at high flow rates (actual flow rates $> 15\text{-}20\text{ m}^3/\text{h}$), but at low flow rates, it was less good. On the base of these results the errors on the gas flow rate measurement performed can be considered to be in the order of $\pm 5\%$.

The MultiPhase Metering Unit, skid 412, uses two turbine meters for the gas flow rates, two positive displacement meters for the oil flow rates, and two magnetic water flow meters for the water flow rates. The double set of flow meters are for low and high range.

The Water Injection Unit was also used to measure the injected water flow rate, and this unit, skid 410, uses two magnetic water flow meters.

2.3 Logging System

The measurements from the MFI MultiPhase Meter was presented by MFI's Graphical User Interface, and data logged to file. Reference measurements were logged by AGIP's DCS. Also, analog signals from the MFI MultiPhase Meter were available in the control room, but these signals are, at the moment, not connected to AGIP's DCS system.

2.4 Test Matrix

Max. gas void fraction (GVF):	81%
Max. water cut (WC):	45% (coincident with the transition to water continuous phase)
Mixture velocity range:	2 - 12 m/sec
Max. oil flow rate:	110 m ³ /h
Max. gas flow rate:	60 m ³ /h (actual conditions)
Water flow rate range:	2 - 45 m ³ /h
Pressure range:	50 - 70 bar
Temperature range:	30 - 90 °C
Flow regimes:	mixed and intermittent flow

3. MFI METER DESCRIPTION

The MFI Meter calculate continuously flow rates of oil, water and gas. Two measurements are performed: 1) composition and 2) velocity, which are combined to yield flow rates. Fig 1 shows a photo of the meter installed in the loop.

3.1 MFI Composition Meter

Instantaneous oil, water and gas fractions are measured by using 1) a commercial Cs 137 gamma densitometer for measuring mixture density and 2) a patented microwave measurement device for measuring mixture dielectric constant.

The micro wave sensor works by measuring a characteristic microwave frequency that is inversely proportional to the square root of the mixture dielectric constant. A change from 100% gas to 100% water can result in a change in the measured micro wave frequency from 100 to 1.

The MFI LP MultiPhase Meter used in this test is not able to measure the characteristic microwave frequency in a water continuous mixture, but the MFI FullRange MultiPhase Meter, already developed and tested, are able to do measurements in the whole range from 0% to 100% water.

3.2 Velocity Device

The system tested in Trecate was equipped with two devices to measure the flow velocity. The primary element for measuring the multiphase flow velocity is the MFI Cross (X) -Correlation meter. This device uses two identical microwave sensors (such as used in the composition sensor) separated by a known distance to measure the velocity at which the multiphase flow is moving through the pipe. The secondary element for measuring the flow velocity is a standard Venturi cell. This device was used very few times in the Trecate tests.

4. RESULTS

4.1 Two Phase Flow Test

These tests were performed using the wells TR2, TR20 and TR17 which arrive in the area where the multiphase meter is installed. Ordinary well testing and tests with additional oil and/or gas were performed. In this paper, only one test series will be

described: gas added to the flow of the well TR17. Two phase Flow Test refer to oil and gas.

The gas flow from the test separator was added to the flow of well TR17 through skid 412, see Fig 3 for configuration. Two of the gas flow rates were measured only with the turbine working in the low flow range, two with the high flow range turbine, and one gas flow rate were measured with both turbines. As seen in Fig 4, only one point has a relative error higher than 5%, all other points are inside $\pm 5\%$. Fig 5 describe the trend of the gas flow rates measured by the MFI MultiPhase Meter.

4.2 Three Phase Flow Test

These tests were performed adding water from the injection system of the loop to the flow coming directly from the wells. Several tests were performed, with water injected in the main flow just before the multiphase meter to create a homogenous mixture, and water injected far from the multiphase meter to see the effect of the water separation along the line upstream the meter. But in this paper, only the test with water added to well TR17 will be described.

In this series of tests, water was injected in the main flow of well TR17, and the reference water measurement used was the MultiPhase Metering Unit, skid 412. The water flow rate was increased step by step, as shown in the global transient of Fig 6. In Fig 7, the water trends are reported along with the oil and gas trends. It is possible to see from this figure, that the oil and gas flow rates are hardly affected by the changing of the water flow rates, as it should be. A detail of these trends, where the fluctuations are bigger, are reported in Fig 8.

Another test series done on the same well (TR17) but using the reference measurements on the Water Injection Unit, skid 410, were performed. Fig 9 shows the water flow rate errors, and as seen, all points are inside $\pm 5\%$. Fig 10 give the global trends of the flow rates measured by the meter (oil, water and gas) and of the reference water flow rates. Fig 11 reports only the water flow rate trends in the steady state periods.

5. CONCLUSIONS

- The Trecate test loop has proved to be very efficient for testing multiphase flow meters. It provides lots of flexibility, and covers a large variation in operating range.
- On the basis of the tests performed in Trecate, AGIP concludes that the MFI MultiPhase Meter can be used to perform standard well testing. The accuracy obtained with the meter is consistent with that which is obtained by a test separator.
- AGIP considers the MFI MultiPhase Meter ready for on-shore and offshore applications, and it is recommended also for subsea applications.

6. REFERENCES

- 1 A. MAZZONI MFI-LP MultiPhase Meter verification in the Trecate test loop
- 2 O. Økland Gullfaks B field test facility for multiphase meters
- 3 H. Berentsen/O. Økland Experience from water-in-oil monitors and multiphase meters
- 4 S. Gaisford/H.O. Hide A report of the field testing of the Multi-Fluid LP MultiPhase Meter
- 5 O. Økland/H. Berentsen Using the MFI MultiPhase Meter for well testing at Gullfaks B
- 6 O. Økland/H. Berentsen/J. Bruun-Olsen MultiPhase Meters, ready for field applications: Results from full scale qualification testing
- 7 S. Gaisford/J. Amdal/H. Berentsen Offshore multiphase meter nears acceptable accuracy level
- 8 M. Scruton Microwave technique solves metering problems
- 9 H.O. HIDE MFI MultiPhase Meter Development Field testing of industrial prototype
- 10 R. Sørhus/S. Gaisford MultiPhase Metering at Norne Field
- 11 Multi-Fluid MFI MultiPhase Meter, Brochure

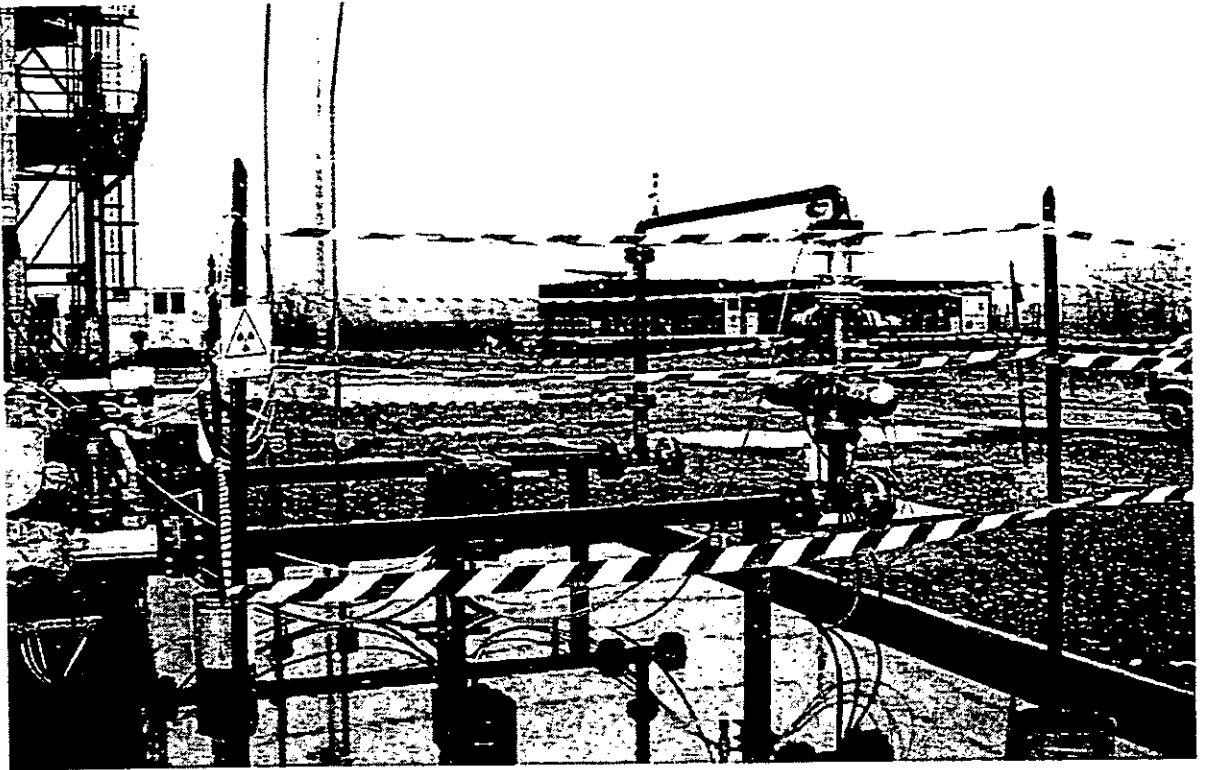
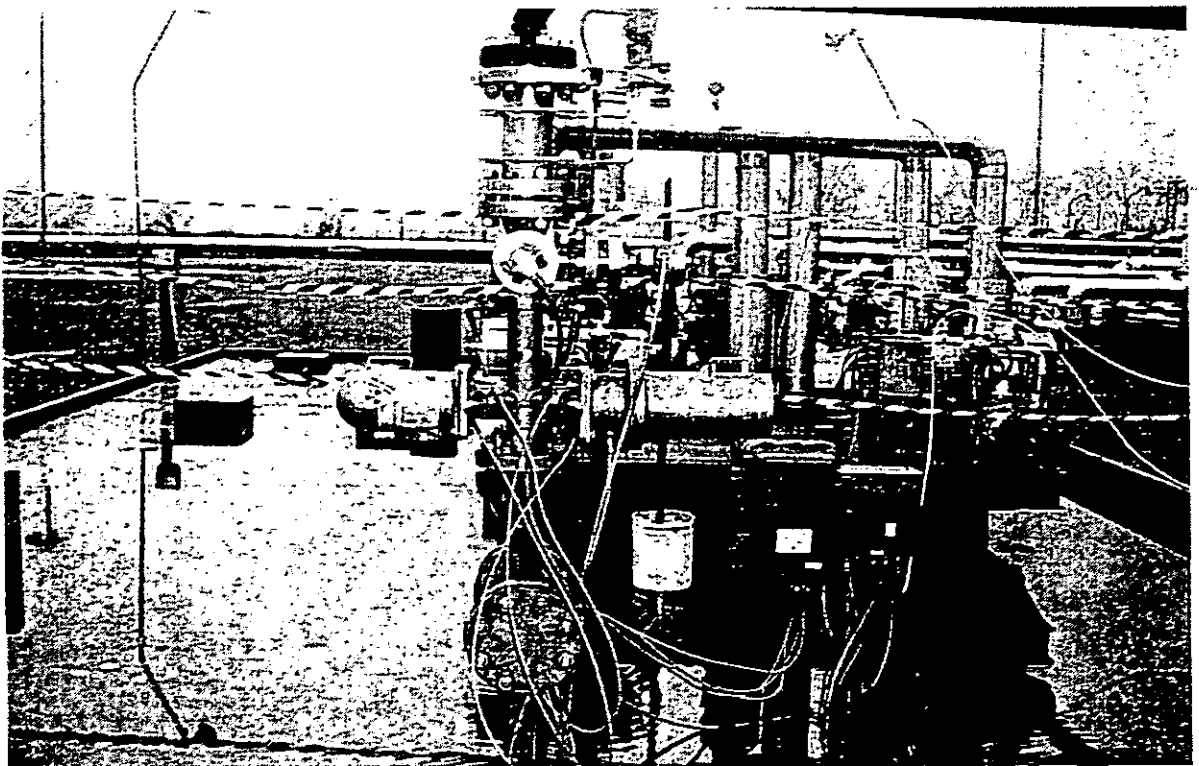


Fig. 1: MFI-LP multiphase meter installed in the Trecate Test Loop



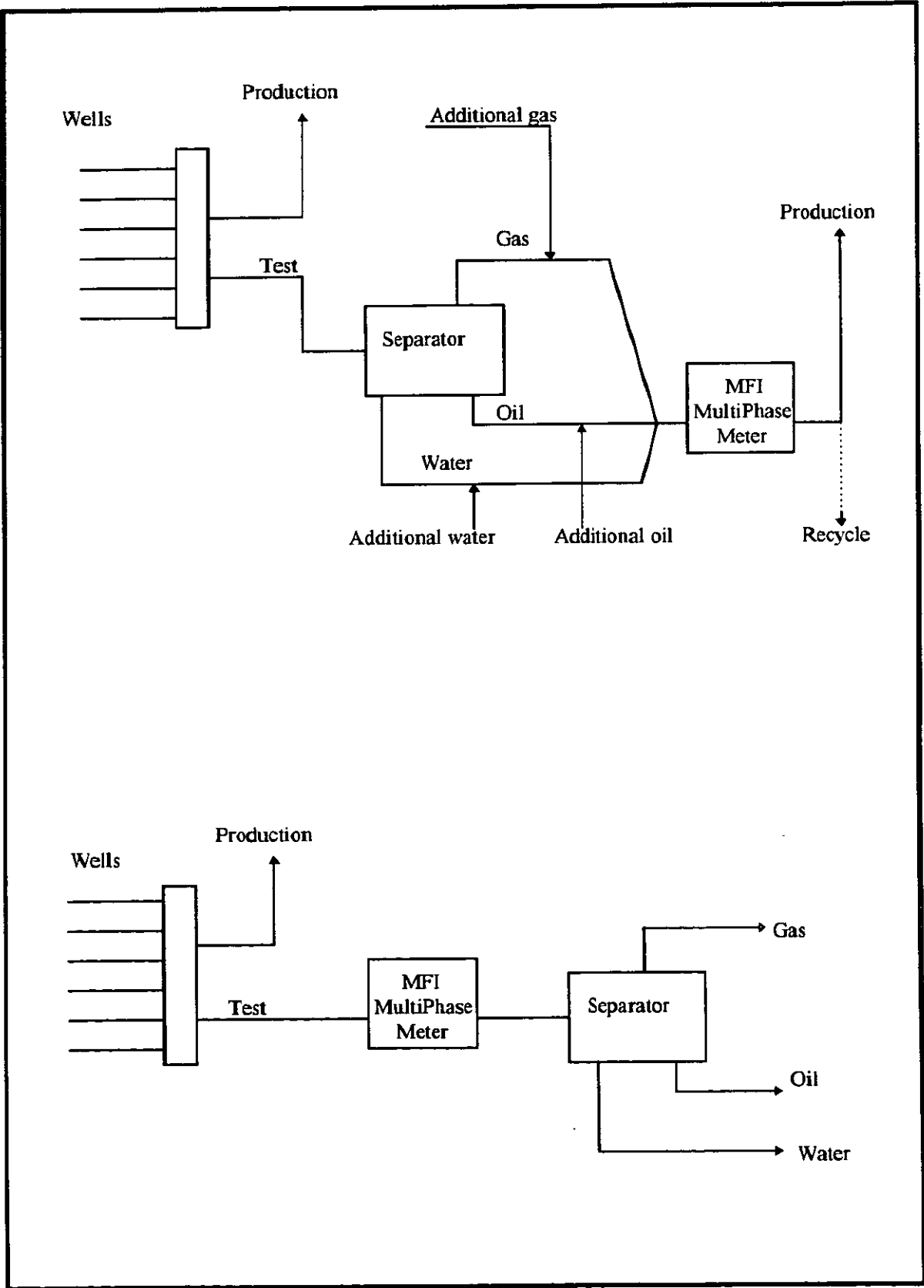


Fig. 2: Two different configurations of the loop.

Fig. 3 Trecate Test Loop over all flow diagram.

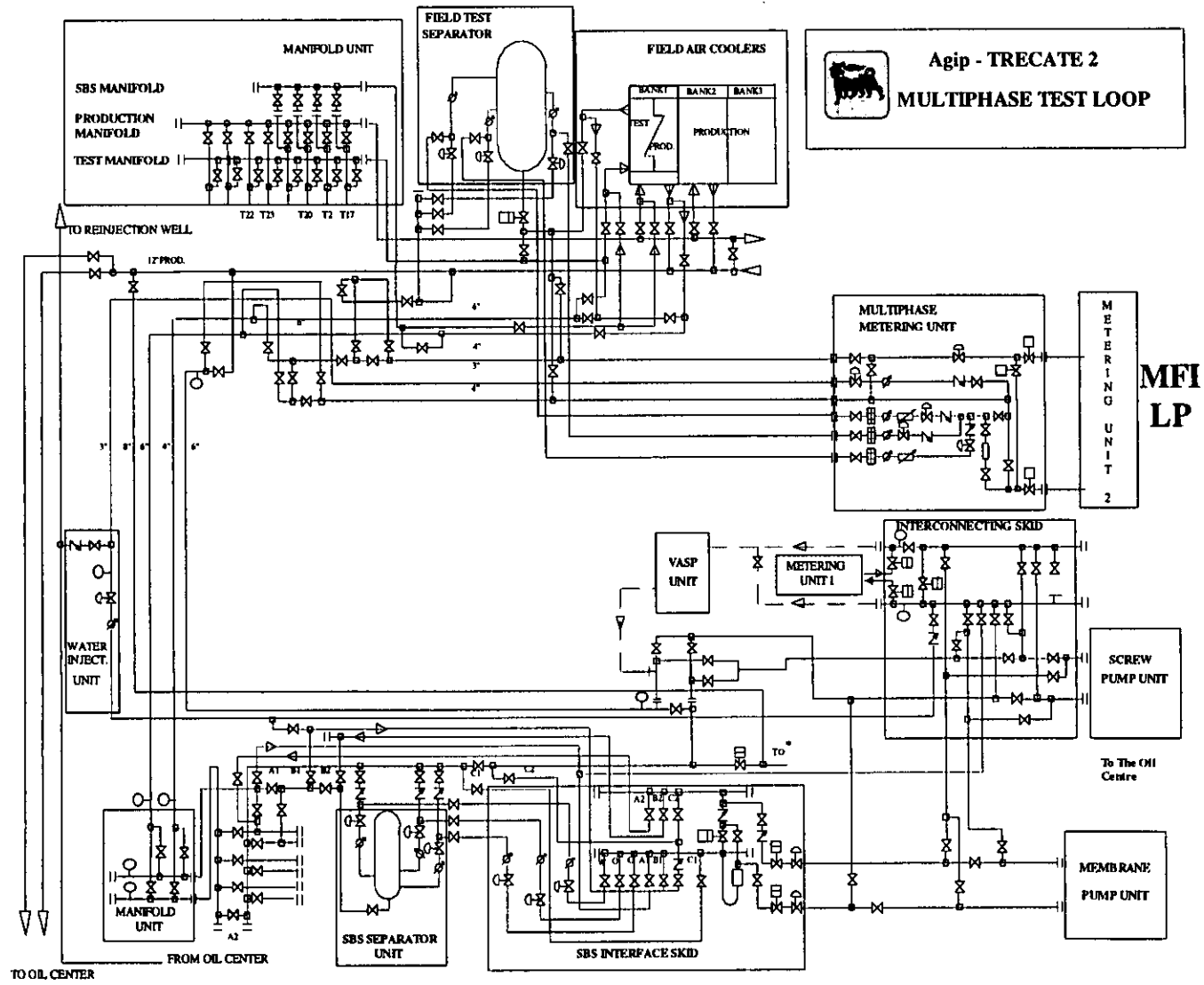


Fig.4: MFI-LP meter gas flow rate errors adding gas to the TR17 well

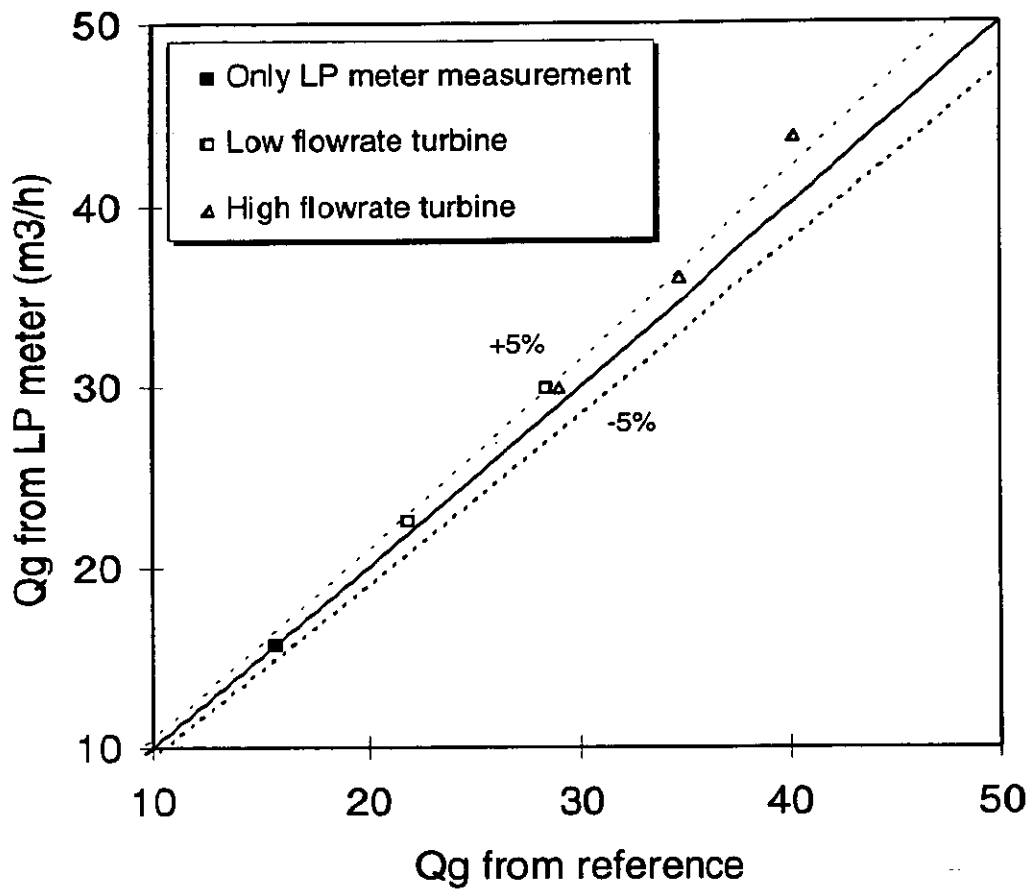


Fig. 5: Test with gas added to the TR17 well.

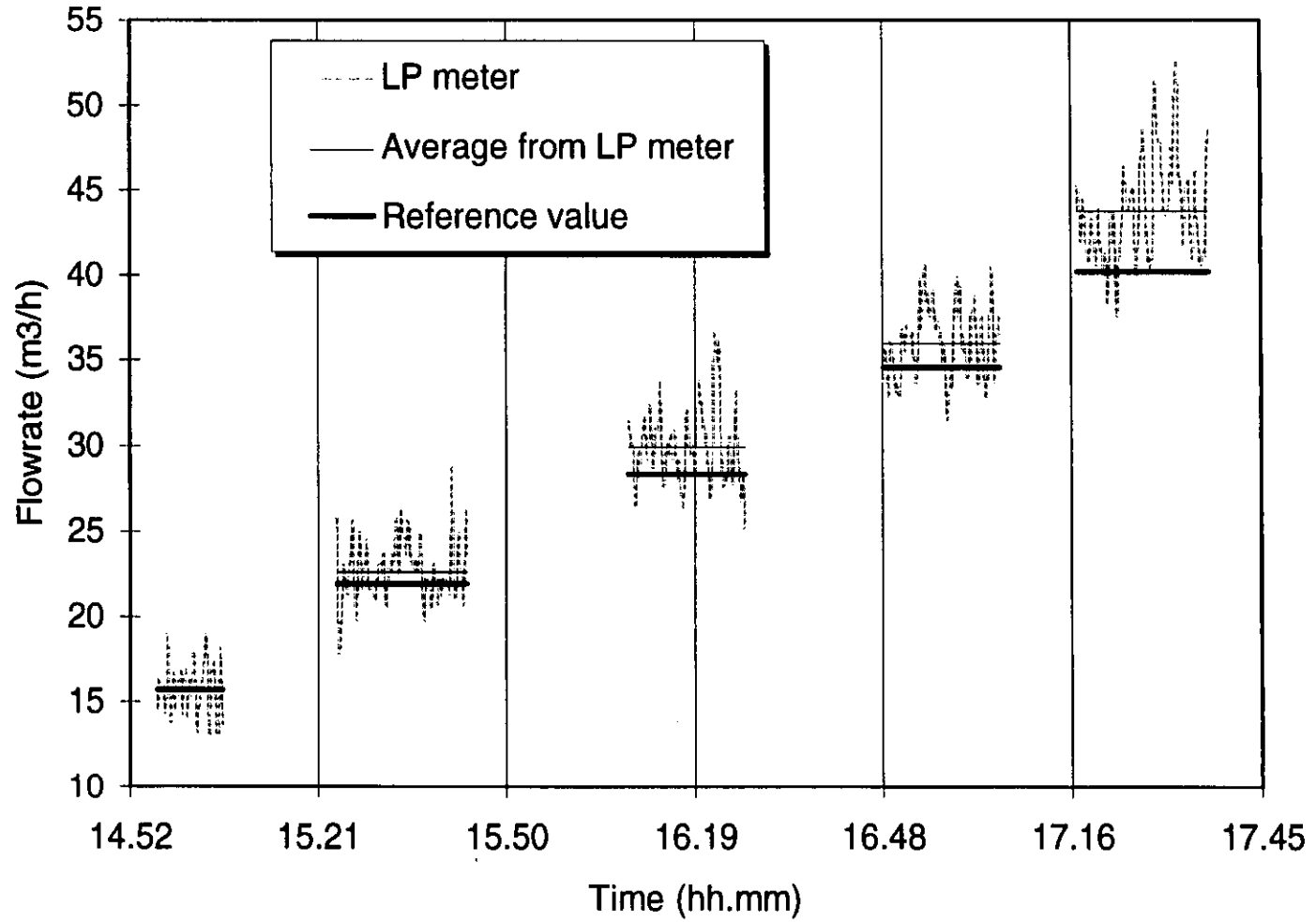


Fig. 6: MFI-LP meter water flowrate during the tests with mixed flow and water injected through the skid 412 using TR17.

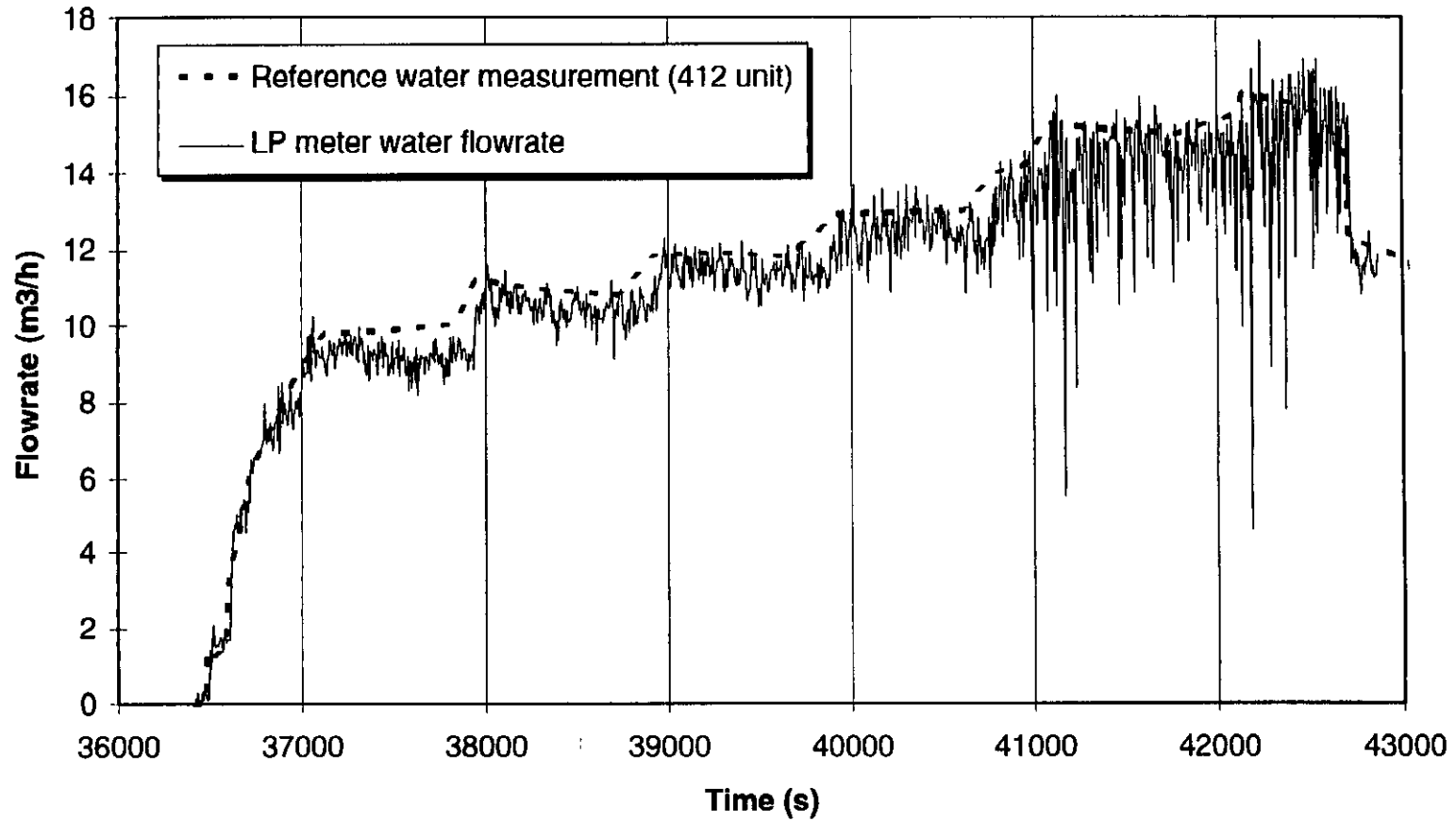


Fig. 7 MFI- LP meter flowrates during the tests with mixed flow and water injected through the skid 412 using TR17.

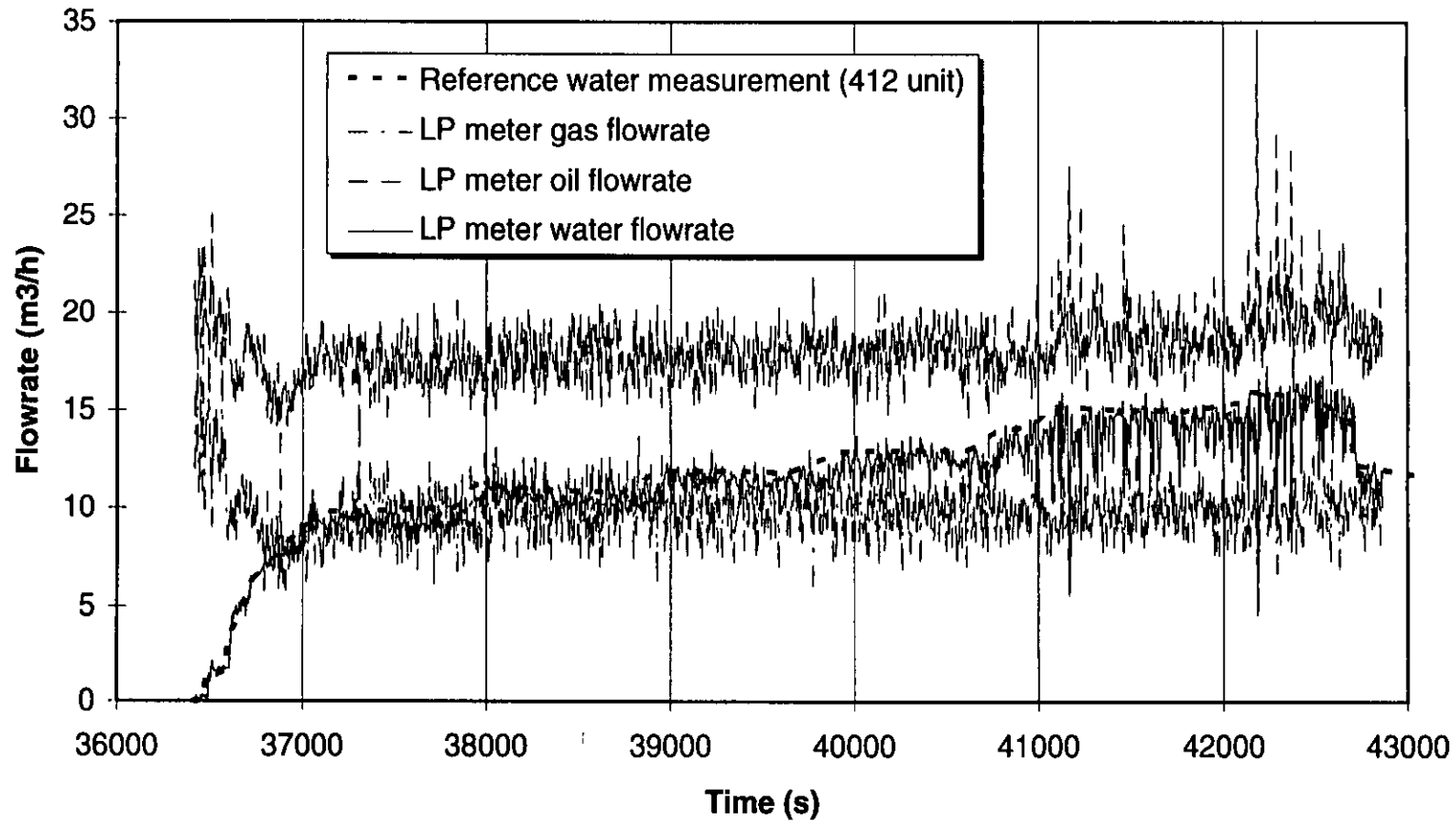


Fig. 8: MFI-LP meter flowrates during the tests 6-7 with mixed flow and water injected through the skid 412 using TR17.

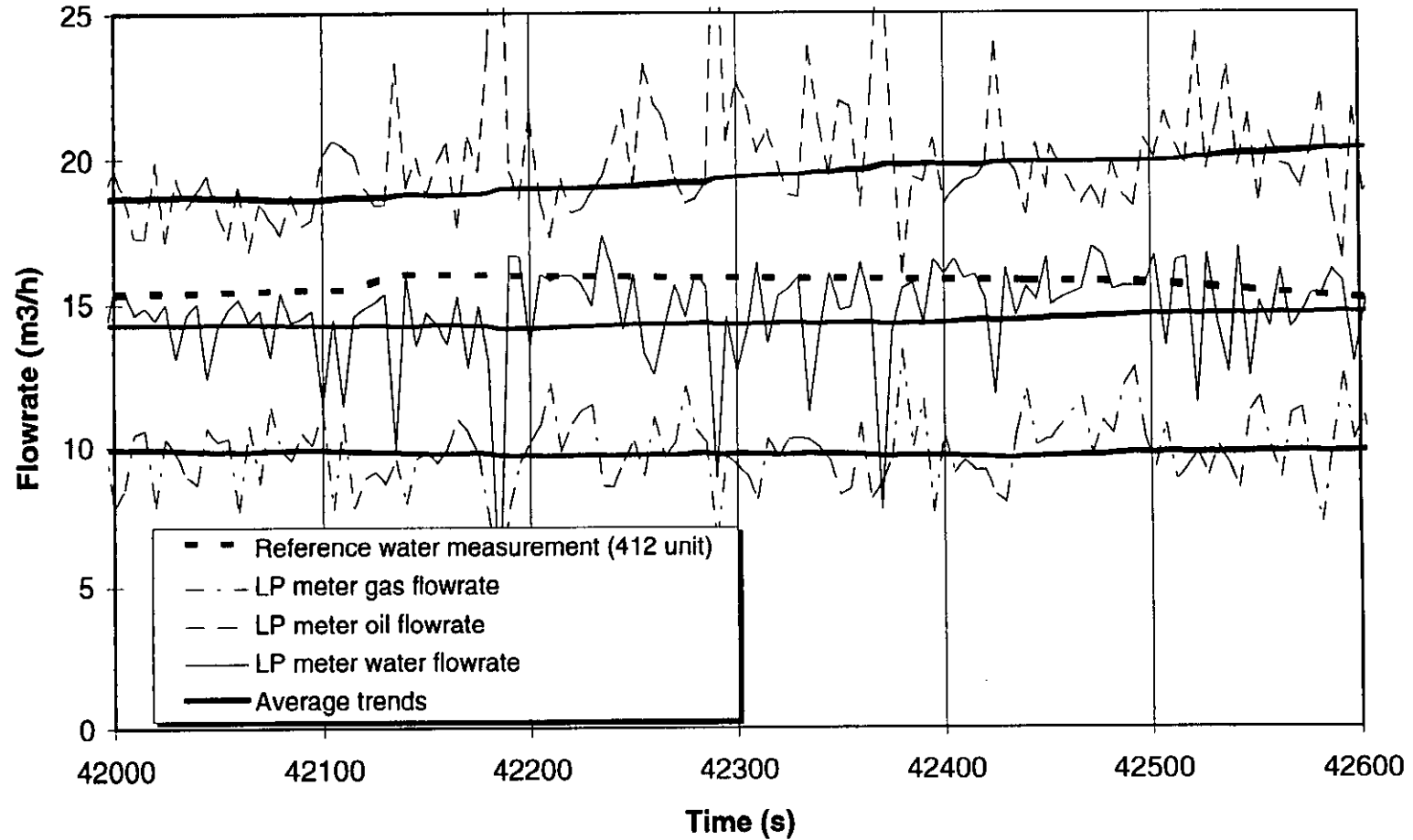


Fig. 9: MFI-LP meter water flowrate errors during the test with mixed flow and water injected from the skid 410 using TR17

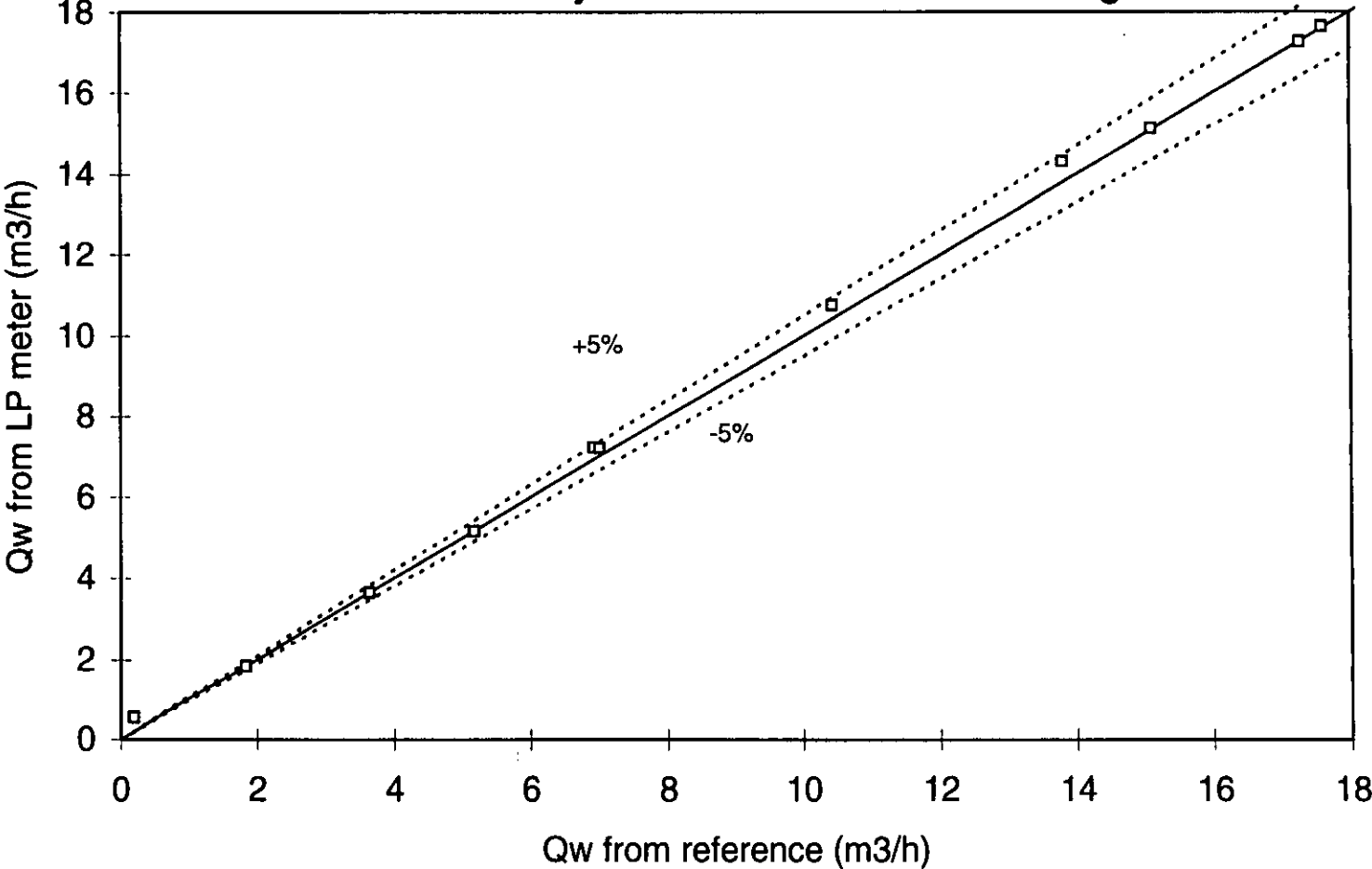


Fig. 10: MFI-LP meter flowrates during the tests with mixed flow and water injected from the skid 410 using TR17

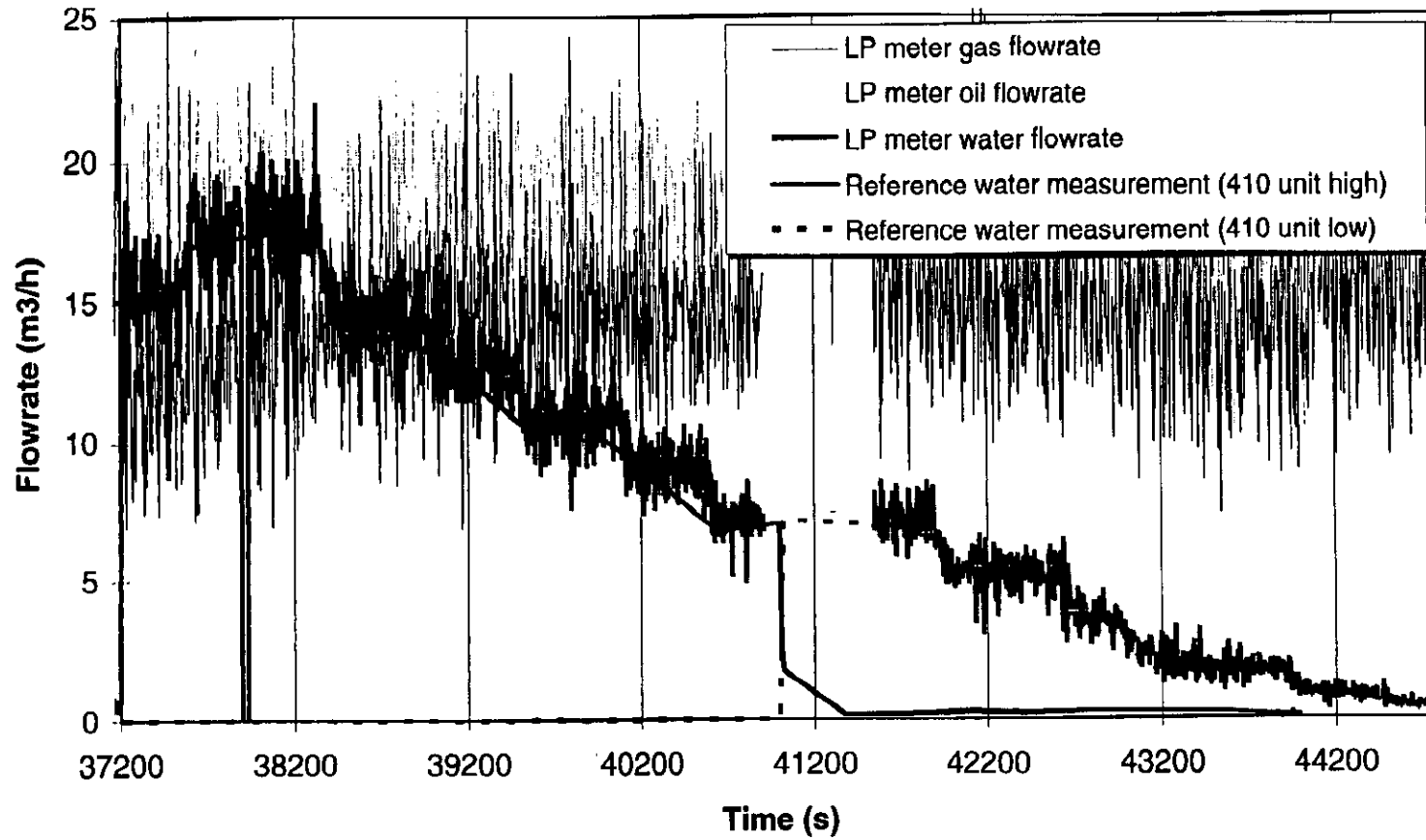
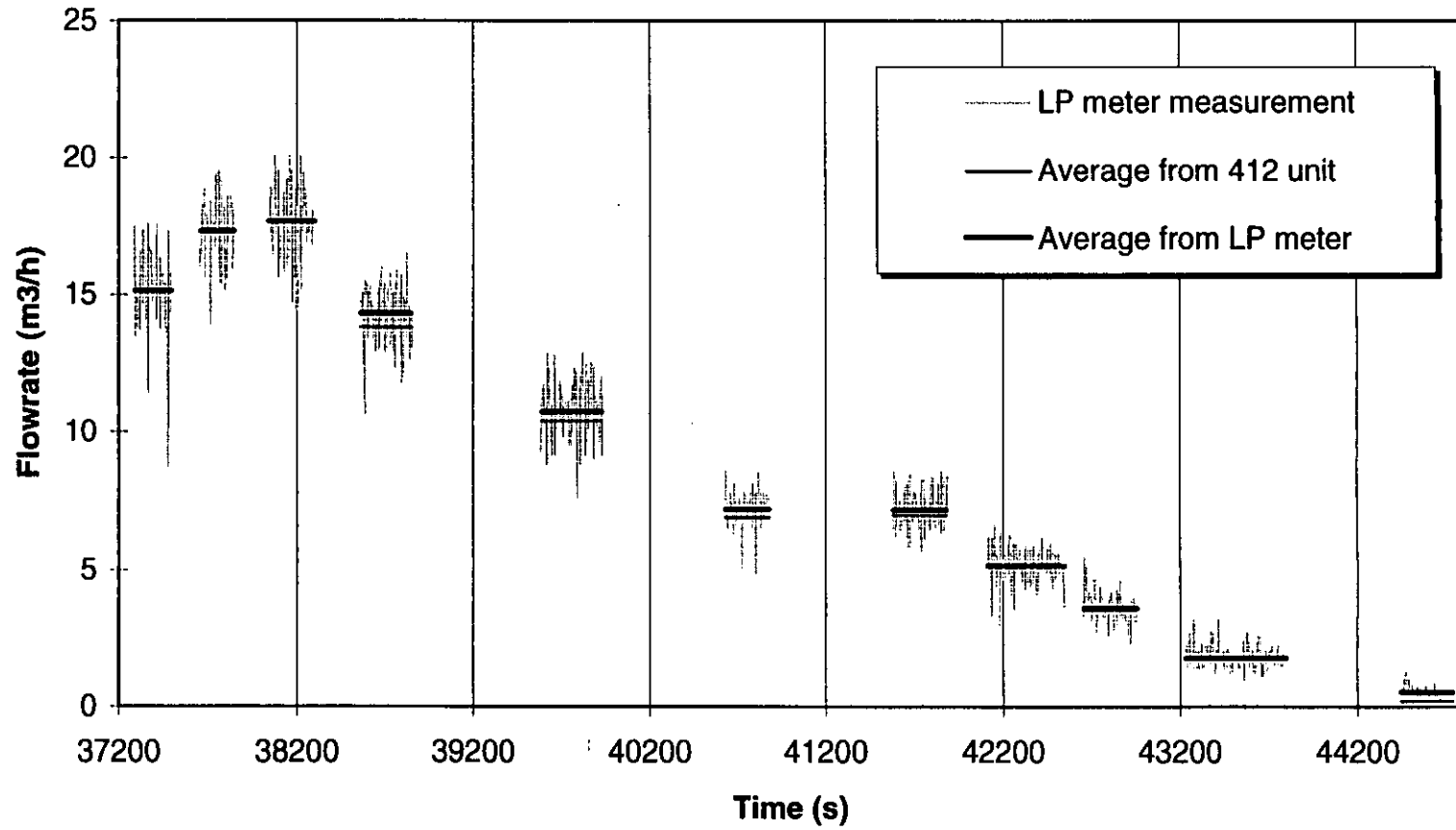


Fig. 11: MFI-LP meter water flowrate during the test with mixed flow and water injected from the skid 410 using TR17



FOCUS DISCUSSION GROUP C

The British Gas Metering Systems Group has Considerable Experience of Fiscal Gas Metering Systems throughout the North Sea and Overseas.

D Irvine, British Gas plc

A GAS BUYER'S GUIDE TO GAS METERING SYSTEMS

David Irvine

British Gas plc

Summary

This short discussion document is based on the experience of fiscal gas metering systems gained by the British Gas Metering Systems Group throughout the North Sea and overseas.

The paper looks at the ubiquitous orifice meter and discusses the important topics of alternative methods of density determination and energy measurement and considers the calibration and installation of differential pressure transducers.

There is a brief look at alternative meters, such as multi-path ultrasonic, turbine and energy meters, and their possible impact on the use of orifice meters.

The conclusion reached is that although much research has been carried out on primary devices and the effect of installation it is equally important for all components of a fiscal gas metering system to be installed, operated and maintained to the highest standards to ensure that the meter is unbiased with the minimum random uncertainty.

1.0 INTRODUCTION

The British Gas, Metering Systems Group was originally set up with two main objectives:

1 to provide technical support to the group negotiating Gas Purchase and Allocation Agreements and

2 to review and agree the proposals from gas suppliers for the fiscal metering systems associated with the Agreements.

The work of the Group developed to include preparation of the measurement provisions of the contracts, technical support during disputes, witnessing factory acceptance and commissioning tests, acceptance of the systems as being suitable for payment purposes and witnessing routine calibrations for British Gas and for outside companies.

This has given the Group over the past 13 years unprecedented access to well over 50 offshore and 15 onshore gas metering systems - all different from each other!

The daily average volume of gas put into the British Gas National Transmission System (NTS) is 300 - 325 million cubic metres with a maximum volume of gas on one day of over 388 million cubic metres (in February 1996).

At the time of writing all of this gas entering the NTS is measured by orifice plate meter and offshore most of the gas is exported and allocated through orifice meters.

Although all of this gas is measured through the same type of meter, using the same international standard for the primary device (the orifice fitting, tappings, orifice plate and a certain amount of the pipework) there are many differences between the meters.

It is with the secondary instrumentation that there is the most room for variation in equipment and design.

2.0 THE ORIFICE PLATE METERING SYSTEM

When installed strictly in accordance with the standard and using secondary instrumentation with known uncertainty the overall metering system uncertainty can be estimated.

Individual components may have or develop a bias and most gas contracts specify that all components of a metering system shall be checked regularly and where necessary shall be adjusted centrally and as accurately as

possible. It is also essential to use staff who understand the importance of operating and maintaining the equipment at the highest possible level.

Three different measurement parameters are considered in detail.

2.1 Density

Line density is required for most fiscal gas metering systems either as a part of the flow equation (orifice meters) or when the primary output of the meter is in actual volume units (turbine and ultrasonic meters).

Density may be determined by measurement or by calculation.

2.1.1 Measured density

The traditional instrument used for measuring density is the densitometer with the vibrating spool type being the most commonly used type in the UK.

Most densitometers are fitted into pockets inserted into the gas line. The instrument should be as close to the primary device as possible without affecting the measurement process. For orifice meters the distance should be 8 pipe diameters downstream of the orifice.

Although it is easy to calculate it is often not realised by the maintenance staff how critical it is for the gas in the densitometer to be at the same temperature as the gas in the flowing stream. For a typical terminal flowing at a pressure of 70 bar a one degree difference between the flowing stream temperature and that in the densitometer causes an error in density of approximately 0.6%. This equates to an error of 0.3% of flow.

The pressure in the densitometer should also be the same as that in the pipeline at the point to which the density is referenced. (The downstream tapping pressure in the case of an orifice meter using the pressure recovery method.)

Using the same example an error of 100 mbar produces an error in density of 0.17% or nearly 0.08% in flow.

What are the possible causes of these errors and how can they be avoided?

To ensure that the gas and densitometer are at the correct temperature the densitometer must be inserted in the line in a pocket which should contain a heat transfer medium such as paste or oil. All fittings and pipes must be thoroughly insulated or lagged ensuring that the lagging material is protected against the weather. Wet lagging does not insulate!

To ensure that the pressure of the gas in the densitometer is the same as at the reference point it is essential that only full bore valves are used (fully open) between the densitometer and reference point. Flow control and fine filtration must be on the other side of the densitometer .

Although it is another obvious point, vibrating cylinder densitometers do not function accurately if there is any deposit - liquid or solid - on the cylinder so care must be taken to ensure that the sample gas is dry and clean using suitable filtration if necessary.

Vibrating cylinder densitometers are usually calibrated with nitrogen and if the operating temperature and gas composition are specified a "user gas" certificate can be produced. The further away from the ideal conditions that the densitometer is operated then the higher the uncertainty. The manufacturer quotes an accuracy for a vibrating cylinder densitometer of $\pm 0.2\%$ of reading but this may not be achievable with some gas compositions.

2.1.2 Calculated density

It is becoming more common to calculate density for offshore applications from gas composition, determined by an on-line gas chromatograph, using an equation of state. My colleague, Malcolm Emms, presented a paper at the Workshop two years ago on the subject and he concluded that uncertainties of 0.38% and 0.55% are achievable using AGA8 1992 and GERG TM2 respectively when the gas composition is determined from a gas chromatograph and the gas contains water and methanol. He raised questions about the uncertainty in calculated density using an equation of state when the gas is near to a phase boundary.

Most gas chromatographs are set up to analyse the gas to C_{6+} . The proportion of these components vary with the separator conditions as well as longer term changes to the wellstream composition. It is possible with most modern flow computers to apportion the C_{6+} fraction of the gas reported by the gas chromatograph to the higher hydrocarbons. The proportions are determined from an off-line analysis of the process gas.

With 0.4% of C_{6+} in a typical natural gas stream, there can be variations in density of 0.3% depending on the proportions of the components set into the computer.

The installation of the gas chromatograph is critical to its correct operation. The gas entering the chromatograph, which should ideally be installed higher than the sample take-off point, must again be clean and dry. Sample lines should be as short as possible, lagged and heat traced and care must be taken with the pressure let-down system to ensure that liquid drop-out cannot occur.

2.2 Energy

Under sales gas Principal Agreements gas is bought and sold in energy units so the calorific value of the gas being metered is required to be measured. (Under an Allocation Agreement gas is usually allocated initially by component mass which is then converted to energy.)

Energy used to be measured by burning the gas in a calorimeter which was calibrated with methane and had a claimed uncertainty of $\pm 0.1\%$.

Heating value transmitters operating on the principle of stoichiometric combustion took over from calorimeters - the DTI approved one model for Gas Act applications - but they have been largely superseded and the majority of terminals now use on-line gas chromatographs.

The most common arrangement is for the gas chromatograph to determine gas composition up C_{6+} or, in some cases, C_{7+} and the comments in the previous section are applicable.

The modern gas chromatograph is a very effective and reliable piece of equipment provided that it has been set up correctly and is operated in accordance with the manufacturer's instructions. However, it is a comparator which compares the composition of two gases - the process gas and the calibration gas. If the composition of the calibration gas has not been accurately determined or is not appropriate for the process gas then errors can occur which will usually be in the form of a bias.

Calibration gas may be made up to a formula, approximating the process gas as closely as possible, or a sample of process gas which has been analysed in a laboratory and the laboratory should be accredited.

An evaluation of the suitability of the calibration gas for a particular application can be made and a range of process gas compositions for which it is suitable determined. However, if there are major changes to the processing of the gas then the process gas may fall outside the applicable range of the calibration gas and errors in the calculated calorific value (and calculated density) may occur.

As with calculated density, changes to the proportion of the components in C_{6+} or C_{7+} can cause errors in the calculated calorific value. These changes can also be caused by variations in the processing of the gas.

2.3 Differential pressure measurement

Two topics are covered on the subject of differential pressure (DP) transmitters.

2.3.1 Calibration

DP transmitters are now available with claimed uncertainties of better than 0.1% of span and they should be selected wherever possible.

The use of high and a low range DP transmitters is the most common arrangement. By way of illustration a turn-down of about 3.6:1 can be achieved using high and low DP transmitters with an uncertainty of $\pm 5\%$. The turn-down increases to just over 4:1 for a system using high and low transmitters with uncertainties of 0.25% and 0.35% respectively and to over 9:1 when 0.075% and 0.1% transmitters are used.

These high accuracy DP transmitters are still affected by pressure and temperature and like all DP transmitters they need recalibrating at regular interval. For optimum accuracy they should be calibrated in situ and at the line pressure at which they will be used. Most DP transmitters are affected by the way they are installed and it is impossible to be sure that calibrating a DP transmitter in a laboratory - even one on the same site as the metering station - and then installing it on the system does not introduce some additional uncertainty.

The question is, how should they be calibrated? The claimed uncertainty of the transmitters is now similar to most of the high static pressure calibration equipment available and even the National standard. One clue is given in the manufacturer's literature where the claimed accuracy includes "hysteresis, linearity and repeatability". This implies a transmitter with very good and stable metrological characteristics. For calibration onshore a high static calibrator should be used and for offshore the foot-print method is generally used.

Some work has been carried out on producing a transfer standard for calibrating DP transmitters offshore but this method is not currently available.

Whichever method is used the uncertainty of the test equipment must be combined with that of the transmitter when the system uncertainty is being calculated.

2.3.2 Installation

DP transmitters are affected by pulsations in the impulse lines so should be installed as close to the meter tapping points as possible. The impulse lines and transmitters should also be protected from the weather.

These two requirements are incompatible if a metering house is to be used in which to locate the DP transmitters (and other instruments) and where the equipment will be installed to calibrate the instruments.

One solution is to mount the transmitters directly on to the meter body and a manifold has recently been produced which makes for easy installation. The instruments can be installed in a small temperature controlled cabinet to provide weather and temperature protection. However, modern smart transmitters may be susceptible to rapid changes in temperature such as when the cabinet is opened for calibration due to the location of the temperature compensation device in the instrument. In addition protection is required for the calibration equipment (and the technician) during in situ calibration.

Another manufacturer has introduced a flow transmitter which incorporates DP, pressure and temperature in a single instrument which mounts directly on to the meter body and also includes a flow computer.

Neither of these two devices has been put into fiscal service in the UK, to my knowledge.

3.0 OTHER FISCAL GAS METERING DEVICES

With so much of the gas in the UK measured with orifice plate meters a strong financial case with demonstrable significant positive advantages needs to be made for using alternative measurement systems for new projects. An even stronger case needs to be made for changing out existing systems and replacing them with new meters such as turbine or ultrasonic meters where the costs of the change-out are considerable.

The outputs from the USM and the turbine meter are proportional to actual volume flow so secondary instrumentation is required to convert to standard volume, energy and mass flow.

There is a big advantage in using a meter that does not need calibrating on a flow rig. This is especially true offshore where the cost of transporting a meter for recalibration can be considerable.

Brief comments are made on three possible alternatives to the orifice plate meter

3.1 Multi-path ultrasonic meter

The theory of the "time of flight" ultrasonic meter (USM) is well known and multi-path devices were devised in the early 1980's. These meters have self diagnostics built in to the electronic circuits and swirl and velocity profile effects are largely eliminated by the use of a number of paths.

Modern digital circuits should eliminate the acoustic noise interference to which early analogue models were prone.

USM's have the same advantage as orifice plate meters. Because they rely on the metrology of the meter (path lengths and cross sectional area of the meter) and timing circuits (for timing the transit time of the ultrasonic signals) it should be possible, in time, to calibrate a meter in the factory without using a calibration rig. At present they are still considered to be novel devices and most purchasers require the meters to be calibrated on a flow rig. It is likely that some configurations of multi-path USM will always require calibration on a flow rig.

There are now two metering stations using multi-path ultrasonic meters USM's for fiscal duties in the UK.

There is, as yet, no International standard for USM's but a draft has been prepared by an ISO working group (ISO/TC 30/WG 20).

3.2 Turbine meter

Gas turbine meters have been around for a long time and are used extensively on the continent to measure large volumes of gas at high pressure.

Calibration on a flow rig is always required for fiscal measurement but at present there are no accredited natural gas high pressure calibration facilities in the UK.

There is an international standard for gas turbine meters, ISO 9951, which deals mainly with specifying the perturbation tests that a meter is required to pass for fiscal use.

3.3 Energy meter

As already stated, gas is bought and sold in energy units. One manufacturer is advertising an instrument which measures energy directly with a claimed repeatability of energy and volume flow-rate of $\pm 0.35\%$ of reading and an overall accuracy of $\pm 0.5\%$ depending on the accuracy of the reference gas and DP transmitters.

This is an interesting concept but there no reports available yet of any practical tests in the UK.

4.0 CONCLUSIONS

Fiscal gas metering systems have been around for many years and the associated technology has become more and more sophisticated. However, there are still fundamental issues which need to be addressed by the system designer, operator and maintenance engineer.

A gas metering system should be designed to carry out the job for which it is required. It should provide unbiased measurement within the uncertainty limits prescribed by regulation, contract or agreement. Different techniques may be required when trying to apply the same limits of uncertainty to a terminal metering system, measuring clean dry specification gas, as for an offshore allocation meter measuring gas at its dew point or even containing liquid droplets.

This paper has looked at several of the factors which may make a metering system acceptable or unacceptable.

High standard fiscal gas metering depends on three qualities -

- Quality of design
- Quality of components
- Quality of maintenance.

**LATE PAPER
FOR
FOCUS DISCUSSION GROUP C**

The British Gas Metering Systems Group has Considerable Experience of
Fiscal Gas Metering Systems throughout the North Sea and Overseas.
D Irvine, British Gas plc

**PLEASE ENSURE YOU PICK UP YOUR COPY FROM THE CONFERENCE
RECEPTION DESK.**

FOCUS DISCUSSION GROUP D

Practical Considerations Related to Multiphase Flowmetering of a Well Stream.

B H Torkildsen, Mr B V Hanssen, Framo Engineering AS

THE NORTH SEA FLOW MEASUREMENT WORKSHOP 1996
28th - 31st October 1996
Peebles Hotel Hydro, Scotland

PRACTICAL CONSIDERATIONS RELATED TO MULTIPHASE METERING OF A WELL STREAM

by Bernt Helge Torkildsen and Birger Velle Hanssen, FRAMO ENGINEERING AS

ABSTRACT

Multiphase Flow Meters have in recent years become a fully accepted tool for well testing, management and allocation metering. Metering of an unprocessed well stream does, however, involve conditions which are not straight forward to deal with, and which can not easily be simulated in a test laboratory. The FRAMO Multiphase Flow Meter concept has been designed particularly for such conditions, and its performance has been demonstrated in field installations on land, offshore and subsea.

This paper describes some of the design and operation particulars of the FRAMO Multiphase Flow Meter which make this flow meter concept suitable for the demanding task of accurate and reliable metering of an unprocessed well stream.

1. INTRODUCTION

The FRAMO Multiphase Flow Meter has for several years been marketed and sold to various commercial applications on land, offshore and subsea (Martin, Woiceshyn, Torkildsen, 1992 /2/ and Olsen, Hanssen 1994 /6/), and is today installed at several fields where it is used for well testing, management and allocation metering.

The FRAMO Multiphase Flow Meter has been received by the market as robust, simple and versatile, features which are of great importance to the environments where it is to be used. It has - as the only one in the market - been conceptually unchanged throughout all the development stages, a fact which has largely contributed to the relatively high degree of technical maturity even for this new technology.

Through several test installations, the FRAMO Multiphase Flow Meter has proved its capability to consistently measure multiphase flow, fully independent of upstream flow regimes, gas volume fractions and water in liquid ratios. The meter is also characterised by the extended use of standard off-the-shelf instrumentation, standard commercial programming tools and standard computers, all contributing to the robustness and high reliability of the concept.

Standardised methods and protocols have also been developed and verified for communication between the FRAMO flow computer and platform or process facility supervisory control systems as well as between the subsea version of the FRAMO Multiphase Flow Meter and all major subsea control systems.

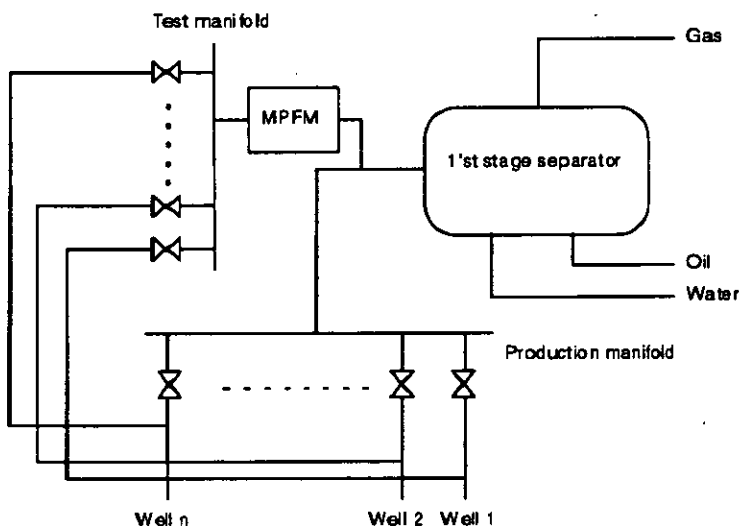


Figure 1: Typical application of the Framo Multiphase Flow Meter

2. THE FRAMO MULTIPHASE FLOW METER

The FRAMO Multiphase Flow Meter is designed for measuring the individual flow rates of oil, water and gas as well as the pressure and temperature of a well stream.

The meter consists of the following main elements:

- Static Flow Mixer for homogenisation of the multiphase flow
- Multi Energy Gamma Meter for measurement of the oil, water and gas fractions
- Venturi Meter for measurement of the total flow momentum flux

The Venturi Meter includes a standard differential pressure transmitter, a pressure transmitter and a temperature transmitter which together with the gamma detector are wired to a Data Acquisition Unit which transmits raw data and/or processed data to a PC based Flow Computer.

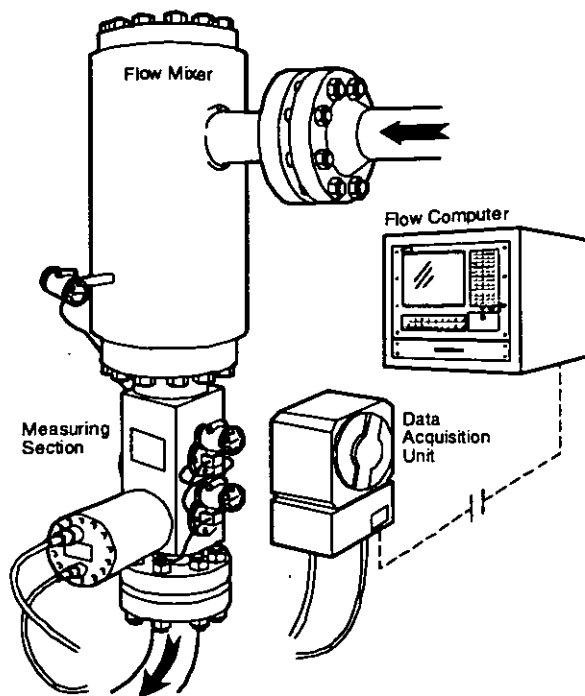


Figure 2: FRAMO Topside Multiphase Flow Meter

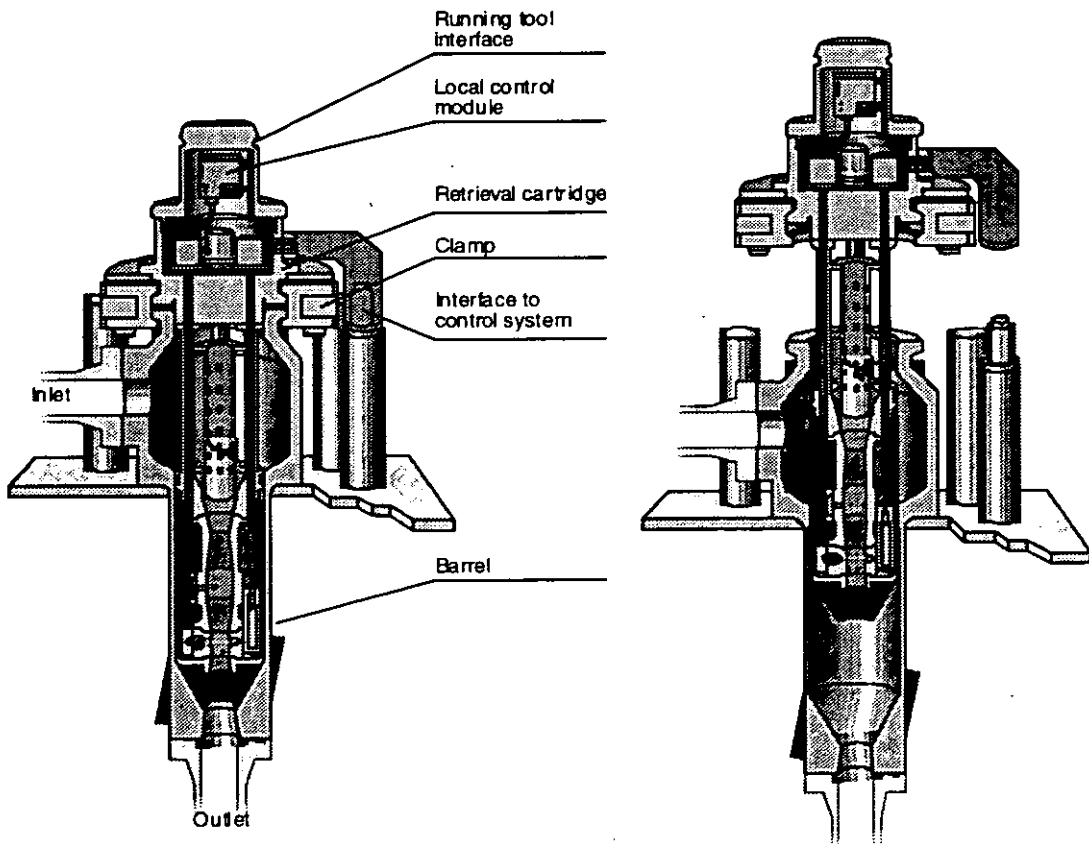


Figure 3: FRAMO Subsea Multiphase Flow Meter

3. WELL STREAM CONDITIONS

Characteristic for well streams is that fluid and flow parameters are continuously changing. In this section the different conditions which are encountered in a well stream will be addressed, and the relevant design and operating particulars of the FRAMO Multiphase Flow Meter will be described.

3.1 Multiphase flow regimes

Multiphase flow regimes are not only dependent on the individual phase flow rates or velocities, but also on pressure, temperature and fluid properties such as interfacial tension and densities as well as upstream pipe configuration. Consequently, reproducibility or the ability to measure with the same accuracy at changed inlet conditions is an essential feature of a multiphase flow meter.

Framo has therefore designed a multiphase flow meter based on flow mixing rather than flow modelling. An integrated static Flow Mixer of FRAMO design (patented) enables accurate and repeatable measurements independent of the upstream flow regime. Whether the multiphase flow regime is dispersed, separated or intermittent flows, or any combinations or transitions between these, the Flow Mixer provides homogeneous flow conditions to the downstream metering section allowing straight forward application of a Multi Energy Gamma Meter and a Venturi Meter.

3.2 Fluid composition

The fluid composition or fractions of oil, water and gas in the well stream will always change over time and large changes are normally encountered as a result of pressure decline and / or water breakthrough. The liquid phases will form various types of emulsions, and dependent on the actual water in liquid ratio, the liquid can be oil continuous, water continuous or even a combination of the two. At some conditions, even foaming occurs.

The Multi Energy Gamma Meter features the ability to measure all combinations of oil, water and gas fractions, including 0 - 100% water in liquid ratio independent of the liquid being oil continuous or water continuous (Rafa, Tomoda, Ridley 1989 /1/). This is possible since the Gamma Meter measurements are independent of electrical properties of the fluid. Whether the liquid is an oil external or water external emulsion, or the flow is foaming, has no effect on measurement accuracy, while such conditions can dramatically influence the performance of a separation based metering systems, including conventional test separator systems.

3.3 Turn-down in flow rate

Metering of an unprocessed well stream does normally involve measurements with large turn-down in flow rates. The venturi meter is ideally suitable for this application as the differential pressure across the venturi is proportional to the momentum flux of the total flow. The turn-down in total flow rate which can be achieved in a multiphase flow, is therefore 3 to 4 times larger than what can be achieved at single-phase conditions, since high flow velocity normally is associated with low multiphase density.

During life time of a well, flow rates may sometime change so much that even a venturi meter can not cover the required range. Very large turn-down is in some cases also required when a single multiphase flow meter is installed in a test manifold for several wells.

Framo has therefore developed and patented a venturi arrangement which allows in-line altering of the physical venturi size. The mechanical arrangement is simple and robust and can be remotely operated by means of hydraulic or electrical functions. This way it is possible to obtain a turn-down in total flow rate at multiphase conditions of more than 1000:1. It can easily be shown that from only two

different positions of the venturi arrangement, the turn-down ratio which can be achieved, is equal to the square of the turn-down ratio for a single venturi meter.

The physical venturi size can be altered when the multiphase flow meter is on-stream, and it can be done without affecting calibration of the meter. This allows continuous operation with one single meter on a range of flow rates or a range of different wells which otherwise would have required two or more meters. In remote area, offshore and particular subsea where changeout of a meter is critical, this option provides a large cost saving potential, both regarding investment and operating cost.

4. FLUID CHARACTERISATION

In order to make accurate and reliable measurements of both mass and volumetric flow rates, the Multiphase Flow Meter needs information about the oil and gas densities and the water salinity. However, since the composition measurement in the FRAMO Multiphase Flow Meter is based on gamma attenuation only, the sensitivity to varying salinity is relative low and far less than for those meters which primarily measure electrical fluid properties (Slijkerman W.F.J., Jamieson A.W., Priddy W.J., Økland O., Moestue H. 1995 /8/).

Information about the individual fluid phase properties is required for other purposes as well, such as converting the measured flow rates to stock tank conditions. The water salinity can also provide information to the reservoir engineer about the water source and possible scaling problems.

The FRAMO Multiphase Flow Meter can be utilised in several ways in order to obtain this information, and this will be discussed below.

4.1 Direct single-phase measurements

For some applications, the multiphase flow meter can relatively easily be filled with the fluid phase of interest at static conditions. This can be done simply by closing an upstream or downstream valve and let the fluid inside the multiphase flow meter settle. Alternatively if a test separator is available, any fluid phase can easily be back routed to the multiphase flow meter.

In these cases the FRAMO Multiphase Flow Meter can by itself measure the required fluid properties.

4.2 Multiphase sampling

The FRAMO Multiphase Flow Meter can also be used to take fluid samples by utilising the flow mixer arrangement. This sampling system provides an excellent basis for dedicated liquid and gas sampling which otherwise will be extremely difficult and unreliable due to the presence of multiphase flow regimes.

From the FRAMO Flow Mixer the liquid phases can be effectively drained for the low part of the compartment, and gas phases from the upper part. An arrangement and procedure for subsea sampling performed by an ROV have been developed and qualified.

4.3 Determination of water salinity by gamma spectrometry

The gamma meter, which is part of the FRAMO Multiphase Flow Meter, makes use of two distinct gamma energy levels in order to determine the oil, water and gas composition in the multiphase fluid flow. The gamma meter does, however, also measure attenuation of a third gamma energy level, and this measurement provides information about the water salinity.

Framo has developed and patented a unique method for on-line measurement of the water salinity in a multiphase stream, based on gamma spectrometry.

This measurement does not require any additional instrumentation, as it makes use of the same gamma spectre as is used for the composition measurement. The method provides an independent means of measuring the water salinity. This means that the measurement is not influenced by the other measurements of oil, water and gas nor by the density information required by the Multiphase Flow Meter.

The independent measurement of water salinity can therefore be made to automatically update the water property required by the Multiphase Flow Meter at any desired interval, and thereby ensure that maximum accuracy of the Multiphase Flow Meter is achieved.

5. CALIBRATION

The calibration of a multiphase flow meter is different from that of a single-phase flow meter. In a single-phase stream the flow parameters can be specified and controlled. Flowing calibration of a single-phase flow meter can therefor be performed in any appropriate flow laboratory with reference to a common standard, and the calibration will be valid as long as there are no changes in the meter itself. Accurate references for flow rates can easily be achieved since the changes in flow parameters between a reference and the meter are well understood.

None of these conditions are true for the calibration of a multiphase flow meter. In particular will flow parameters such as multiphase flow regimes not be known for the operator, and even if they were known, it would not be possible to reproduce or simulate the same conditions in a flow laboratory or in any other installation. No standards exist relevant for multiphase flow conditions, nor is it likely to be developed in the near future.

Even in-situ flowing calibration of a multiphase flow meter would have only very limited value, as fluid properties, composition and flow rates in a well stream normally are changing continuously and cause changes in the multiphase flow regime which are difficult or impossible to predict and which in general will invalidate a flowing calibration performed at other conditions.

Accurate references for flow rates are also very difficult to obtain as the thermodynamics governing the fluid phase and flow changes between a reference and the multiphase flow meter is complex and can not easily be modelled.

It is also for these reasons that Framo has developed a multiphase flow meter based on flow mixing rather than flow modelling, and which does not require any flowing calibration. The FRAMO Multiphase Flow Meter does only require individual static single-point calibration of the gamma detector and the venturi differential pressure transmitter.

This calibration is normally performed on air at atmospheric conditions prior to installation, however, it can as well be performed on any other fluid as long as its properties are known. This way a remotely operated multiphase flow meter, such as one subsea, can be calibrated simply on the fluid which may settle out inside the multiphase flow meter after closing of an upstream or downstream valve. Even without being properly calibrated, the gamma meter will identify whether the fluid is oil, water or gas, and the appropriate static single-point calibration can be performed.

6. CONCLUSIONS

The FRAMO Multiphase Flow Meter has been designed particularly for the severe and unpredictable flow conditions which are typical for unprocessed well streams. The meter which has been received by the market as robust, simple and versatile, consists of the following main elements:

- Static Flow Mixer
- Multi Energy Gamma Meter
- Venturi Meter

Through field installations on land, offshore and subsea the FRAMO Multiphase Flow Meter has proved its ability to cope with the extremes in:

- Multiphase flow regimes
- Fluid compositions
- Turn-down in flow rates

A mechanism for altering the venturi size is available for the FRAMO Multiphase Flow Meter.

The meter features methods for fluid characterisation including:

- Direct single-phase measurements
- Multiphase sampling
- Determination of water salinity by gamma spectrometry

Calibration of the FRAMO Multiphase Flow Meter is simple and involves only:

- Static single-point calibration of the gamma detector
- Static single-point calibration of the venturi differential pressure transmitter

ACKNOWLEDGEMENTS

The authors wish to thank the sponsors and parties that have been involved in the development of the FRAMO Multiphase Flow Meter; Statoil, Norsk Hydro, British Petroleum, Conoco, Elf, Shell, Saga and Institutt for Energiteknikk.

Also all the users have through their early commitment to the FRAMO Multiphase Flow Meters on a commercial basis, enabled Framo to continue the development of the product. Through a continued commitment to the technology and a good and open dialogue with the users, we are convinced that the product also in the future will continue to be refined.

REFERENCES

- /1/ Rafa K., Tomoda T., Ridley R. "Flow Loop and Field Testing of a Gamma Ray Compositional Meter". Energy-Sources Technology Conference and Exhibition, January 22-25, 1989, Houston Texas.
- /2/ Martin W., Woiceshyn G. E., Torkildsen B. H. "A Proven Oil-Water-Gas Flow Meter for Subsea". The 23rd Annual Offshore Technology Conference, May 6-9, 1991, Houston, Texas.
- /3/ Olsen A. B., Torkildsen B. H. "Subsea Multiphase Flowmeter System". Underwater Technology Conference, March 30 - April 1, 1992, Bergen, Norway.
- /4/ Torkildsen B. H., Olsen A. B. "Framo Multiphase Flow Meter Prototype Test". 10th North Sea Flow Measurement Workshop, October 26-29, 1992, Scotland.
- /5/ Olsen A. B., "Framo Subsea Multiphase Flow Meter System". Multiphase Meters and their Subsea Applications, April 13, 1993, London, UK.
- /6/ Olsen A. B., Hanssen B. V., "Framo Multiphase Flow Meter - Field testing experience from Statoil Gullfaks A and B platforms and Texaco Humble test facilities." 12th North Sea Flow Measurement Workshop, October 24-27, 1994, Scotland.
- /7/ Hanssen B.V., Torkildsen B.H., "Status of the Framo Subsea Multiphase Flow Meter", North Sea Flow Measurement Workshop, Lillehammer, October 1995.
- /8/ Slijkerman W.F.J., Jamieson A.W., Priddy W.J., Økland O., Moestue H. "Oil companies needs in multiphase flow metering", North Sea Flow Measurement Workshop, Lillehammer, October 1995.
- /9/ Hanssen B.V., Svaeren J.A. "Diverless subsea multiphase meter", Underwater Technology Conference, Bergen - March 1996.

FOCUS DISCUSSION GROUP E

Effect of Increasing Plate Thickness on the Metering Accuracy of an 8 Inch Orifice Meter Run.

U Karnik, Novacor Research & Technology Corporation

EFFECT OF INCREASING PLATE THICKNESS ON THE METERING ACCURACY OF AN 8 INCH ORIFICE METER.

U.Karnik
 NOVA Research & Technology Corporation
 2928-16th Street N.E.
 Calgary, Alberta, Canada
 T2E 7K7

ABSTRACT

The present study investigates the use of a thicker (0.25in.) orifice plate in a standard 8inch orifice meter run. In particular, the effect of retrofitting existing meter runs (*old fitting*) designed for 0.125in. thick plates as well as the performance of newly designed meter runs (*new fitting*) for 0.25in. plates is studied. For the 0.25in. thick plate, the effect of bevel angle and orifice edge thickness on metering accuracy is also evaluated.

Results obtained indicate that :

- a) 0.25in. thick orifice plates perform identically when used in old fittings or in new fittings. The use of 0.25in. thick orifice plates would not only increase the capacity of the meter run but also result in repeatable metering independent of β -ratio. For $0.3 \leq \beta \leq 0.6$, (i.e. for mass flow $> 3\text{kg/s}$), the average error is around 0.31% with a 2σ of $\pm 0.13\%$.
- b) in old fittings, for β -ratios ≥ 0.4 , there is no difference between the 0.25in. and the 0.125in. plates. For β -ratios < 0.4 , the 0.25in. thick plates would over-register by around 0.3%.
- c) bevel angle ($30^\circ \leq \alpha \leq 45^\circ$) and orifice bore edge thickness ($0.06\text{in.} \leq e \leq 0.16\text{in.}$), do not have a measurable effect on the metering accuracy in old or new fittings.
- d) plate thickness (0.125in. v/s 0.25in.) does not affect the performance of non-beveled plates in the old fitting.
- e) data indicates that for the 0.125in. thick plate, the difference between the beveled and non-beveled plates depends on the β -ratio and does not indicate a specific trend. In the case of the 0.25in. thick plates, the non-beveled plates tend to under-register in comparison to the beveled plates at β -ratios < 0.4 .

1.0 INTRODUCTION

It has been recognized in the past that the capacity of a orifice meter run could be increased by increasing the differential pressure to values beyond the allowed 50kPa (200in.). The issues to be recognized in adopting such a procedure are that

1. the plate should not deform permanently and
2. the plate should not undergo elastic deformation since this could lead to metering error.

The first issue can be easily addressed using available stress analysis expressions ^[1]. The orifice fitting is treated as a simply supported circular plate with a central hole. Results of this analysis are shown in Figure 1. The allowable differential pressure before permanent deformation is governed by the β -ratio and the ratio of the support diameter to the plate thickness (aspect ratio). If differential pressures of at least 200kPa are to be used for β -ratios ≥ 0.2 , then the aspect ratio of the plate should be around 40.

The second issue is also a function of the above two parameters ^{[2], [3], [4], [5], [6]}. Apart from this work, originating from the British Gas Engineering Research Station, other work on this subject matter has also been published ^{[7], [8], [9]}. The effect of plate deformation on metering error ^[2] is presented in Figures 2a,b,c & d. It is evident that if the metering errors due to plate deformation are to be minimized (<0.05%), then the aspect ratio should be less than 40. Experimental work performed on natural gas ^[10] at the NOVA gas dynamic Test Facility, confirmed the theoretical estimates shown in Figure 2 for aspect ratios of 32 (4in. meter run) and 80 (10in. meter run). Details of the theoretical estimates are also presented by ^[10].

On examining metering standards and existing 8in. meter runs in the NOVA system, it would not be possible to increase the capacity of these meter runs under the current specifications i.e. recommended plate thickness of 0.125in (an aspect ratio of 67.5). One approach to increase the capacity would be to use a thicker plate e.g. 0.25in. (an aspect ratio of 33.75). This results in the following issues that need to be addressed.

1. In the case of retrofitting existing meter runs with 0.25in. plates, one would be altering the location of the pressure taps. Standards stipulate that the flange taps should be located 1 inch from the upstream and downstream surface of the plate respectively. On using the thicker plate, the location of the taps from the respective surfaces would now be 0.9375in. The question to be answered is whether, this small shift in tap locations causes a significant

error in metering ? Further, can the R-G equation be modified to accommodate the new tap locations as part of the tap term ?

2. A corollary of the above issue is that if the upstream edge is the governing parameter for the flow structure, then the upstream edge will now be located 1.1875in. from the downstream tap instead of the 1.125in. as in the case of the 0.125in. thick plate. This change in the flow structure could alter the measured pressure drop and hence the measured flow rate.
3. If we buy into point #2, then consider the new fitting i.e. one manufactured for the 0.25in. thick plate with the appropriate location for the flange taps. In this case all specifications of the A.G.A. standard are met i.e. the plate thickness does not exceed the maximum value and the flange taps are appropriately placed. If the issue raised in point # 2 is now applied, the distance from the upstream edge to the downstream tap is now 1.25in. Would this further affect metering error adversely ?
4. The issues are further complicated by the fact that the orifice database on which the equation was generated apparently does not include any data from an 8in. meter run.

From NOVA's perspective, the need to increase meter capacity exists. This can be done quite easily for the 4in. and 6in. meter runs without any adverse effects on the measured flow. There exists a need to increase the capacity of 8in. meter runs. If NOVA is to request vendors to supply meter runs appropriately designed for the 0.25in. thick plate, it is important that we ensure that the performance of a retrofitted meter compares well with that of the new meter design.

Hence, the objectives of the project are follows :

- a) To evaluate the performance of old 8in. meter runs designed for 0.125in. thick plates.
- b) To examine the effect of retrofitting old 8in. meter runs with 0.25in. thick plates.
- c) To study the performance of the new 8in. meter run designed for 0.25in. thick plates.
- d) To study the effect of bevel angle and bore edge thickness on metering accuracy.

2.0 EXPERIMENTAL FACILITY

Experiments were performed in natural gas at NOVA's Gas Dynamic Test Facility at a line pressure which varied between 5000-6000kPa. A sketch of the test loop is shown in Figure 3. Following a straight section of around 39D, the flow was conditioned by means of a NOVA 50E flow conditioner. The orifice plate was located 30D downstream of the flow conditioner, ensuring a fully developed, symmetric velocity profile at the orifice plate. Past measurements with the NOVA 50E ^{[11], [12]} indicate that the profile is fully developed at 8D downstream of the flow conditioner with a 5D upstream mixing length. The orifice meter run was a standard Daniel orifice fitting. A thermowell was located 5.3D downstream of the orifice plate for the insertion of a RTD to measure the flow temperature.

The static pressure was measured by means of a Rosemount Smart static pressure transmitter and a Rosemount Smart temperature transmitter was used to power the RTD. The differential pressure across the orifice plate was measured by a Rosemount Smart differential pressure transmitter with a range from 0-200kPa. The static pressure transmitter was calibrated with an Ametek dead weight tester and its performance was monitored, at zero flow conditions, with another calibrated Smart transmitter located elsewhere in the loop. If the difference between the two transmitters exceeded by more than 0.1% (stated accuracy of the transmitter), the transmitters were re-calibrated.

The temperature RTD was calibrated with an Automatic Systems Laboratory (B125) dry block calibrator using a NIST traceable ERTCO-HART 850 high precision platinum RTD as a reference. Several checks performed during the course of the tests and the calibration was stable to within 0.05deg. C. The differential transmitter was calibrated at ambient conditions with an Ametek dead weight tester and was adjusted for the zero offset at line conditions. Calibration checks indicated that the drift in the slope was not more than 0.05%. The calibration curve was corrected for non-linear effects. Some typical calibration checks are presented in Table 1.

The set of orifice plates used in the present study were obtained from Daniel Industries and were manufactured to NOVA specifications, namely, a bevel angle of 37.5 degrees and a bore edge thickness of 0.06in among others. Other variations of orifice plates that were tested are tabulated in Table 2.

The flow rate from the orifice meter was compared to that from the sonic nozzle bank. Details of the uncertainty analysis and the traceability of the nozzle bank to the gravimetric

facility ^{[13], [14]} indicate that the uncertainty in mass flow is around 0.2%. The maximum flow rate capacity of the facility is currently around 14kg/s.

3.0 EXPERIMENTAL RESULTS

3.1 Beveled Plates

Results of testing beveled plates (0.125in. and 0.25in. thick), manufactured to A.G.A. and NOVA specifications (bevel angle =37.5deg. and bore edge thickness = 0.06in.), in an old fitting are shown in Figures 4a,b,c,d,e,& f. The data was taken such that, for any given β -ratio, the 0.125in. and the 0.25in. plate were tested on the same day thus improving the system repeatability. The first observation from these figures is that measurements taken at two tap locations 180 deg. apart show identical trends. This indicates that the velocity profile at the orifice plate is symmetric. Further, for $\beta \leq 0.6$, the metering error is within the $\pm 0.55\%$ band of the R-G equation.

The statistics presented in Table 3. (for $\Delta P > 20\text{kPa}$) may imply that the 0.25in. plate over-registers in comparison to the 0.125in. plate. However, on examining the figures and the 2σ levels of the data it can be concluded that, for $\beta \geq 0.4$, there is no difference between the performance of the two plates. For $\beta = 0.2$ and 0.3 , the thicker plate clearly seems to over-register in comparison to the thinner plate by about 0.3-0.4%. Using the R-G equation with the appropriate tap distances (0.9375in.) does not eliminate this difference.

In the past, the effect of plate thickness on orifice meter performance has been studied ^[15] in detail for a 6in. meter run. Although in their plate thickness tests the location of the taps with respect to the plate were constant (1inch) for all plates, some comparisons are made with the present results wherein the tap locations changed with plate thickness. The findings in the present study are similar to earlier findings ^[15]. For example, for plate thickness of 0.25in., they find that a $\beta = 0.3$ over registers a 0.125in. thick plate by around 0.3%. Further, for the larger β -ratios (0.5 and 0.7) no significant differences were measured as found in the present study.

It is also clear from Figures 4a. through 4f., that a 0.25inch thick plate performs identically when used in an old fitting and a new fitting.

3.2 Non-Beveled Plates

Results of testing the non-beveled plates in an old fitting, are presented in Figures 5a,b,c,d,e & f and tabulated in Table 4. For all β -ratios, there does not appear to be a significant or systematic difference between the performance of the 0.125in. and the 0.25in. thick plates. This is evident from the Figures as well as the statistics shown in Table 4. In the case of the non-beveled plates, previous findings ^[15] also indicate that there is no difference in the performance of a 0.25in. plate in comparison to the 0.125in. plate, for all β -ratios. Husain & Teyssandier ^[15] further state that for thickness upto 0.3in., within their system repeatability, there is no difference between the beveled and unbeveled plates. This is true in the present experiments for the 0.125in. plate as seen in Table 5a. where no definite trend seems to exist and the differences are comparable to the 2σ confidence levels. However, from Table 5b, it appears that the non-beveled plate under-registers in comparison to the beveled plates for a plate thickness of 0.25in. particularly at the lower β -ratios.

3.3 Effect of Bevel Angle and Bore Edge Thickness

This study was conducted for β -ratios of 0.2192 and 0.5952, so that two extreme, yet stable cases could be examined. Further, these tests have only been conducted with a 0.25in. thick plate because the effects are expected to become severe with increasing thickness. Specific details of the plates are provided in Table 2. Results of these tests are shown in Figures 6 & 7 and Table 6. Firstly, consider the data taken for the plates with $\alpha = 37.5\text{deg.}$ and $e=0.06\text{in.}$ Results of two plates are shown for each β -ratio. The two plates were ordered and tested almost 1 month apart. The data is very repeatable with deviations not greater than 0.1%. From Figures 6 & 7 and Table 6, it could be concluded that, for both orifice fittings, there is no effect of bevel angle and bore edge thickness, within the specifications provided by the standards. This is confirmed by the experiments of Husain & Teyssandier ^[15], except for $\beta=0.3$ where they measured a difference of around 0.4% between $\alpha=30\text{deg.}$ and 45deg.

4.0 ANALYSIS AND DISCUSSION

Various theories can be postulated to explain the performance of an orifice plate. Although more information is needed, the following attempts to propose some theories explaining some of the results that have been obtained in the present study. The performance of

the orifice plate, as reflected by the pressure drop measured across the plate, is influenced by the following parameters :

- (a) tap location with respect to the leading edge of the orifice plate
- (b) flow structure generated by the orifice plate
- (c) β -ratio

Consider the performance of the 0.125in. and 0.25in. beveled plates in the old fitting. It is possible that the smaller β -ratios result in a well defined jet and hence a region of pressure (tap location) sensitivity. If the location of the vena-contracta is determined by the leading edge, then for the smaller β -ratios, if a thicker plate is used, then the vena-contracta occurs closer to the plate. If the tap location is fixed, then the thicker plate sees a higher differential pressure. Thus, at smaller β -ratios the thicker plate over-registers in comparison to the thinner plate for a fixed tap location as indicated by the measurements. On the other hand a larger β -ratio could result in a rather large wake causing an insensitivity to tap location.

Why then does the 0.25in. plate not show tap sensitivity at lower β -ratios (i.e. in the old fitting and the new fitting) ? The answer possibly lies in the fact that the flow structure is similar i.e. "wake like" so that the pressure downstream is not sensitive to small changes in tap location. The same can be said with the 0.25in. thick plates used in the test of bevel angle and orifice edge bore edge thickness tests.

Consider the un-bevelled plates, the results indicate that there is no sensitivity to tap location i.e. a 0.125in. plate and a 0.25in. plate behave identically in the old fitting for all β -ratios as seen in Table 4. In the absence of a bevel, the knife-edge of the orifice plate is absent and this results in a "bluff body" like wake which camouflages any pressure sensitivity that may be associated with varying β -ratios.

There are some exceptions that do not conform to the above theories. For example, the 0.25in. thick plate with the edge thickness of 0.16in. Should its performance be similar to that of the 0.125in. and 0.25in. unbevelled plate ? This is not the case in the present experiments.

The fact remains that more than just the tap location is responsible for the performance exhibited by an orifice plate. Although, some ideas have been proposed, there are exceptions to the hypotheses. Further, studies involving the study of the structure of the flow just downstream of an orifice plate for various geometries using flow visualization or computational

techniques are warranted. These studies need to be supported with laboratory experiments where the relevant parameters involved can be artificially manipulated to isolate various effects.

In any event, comparing the performance of the plates (0.125in. and 0.25in.), using Figures 8a and 8b, one could recommend the retrofitting of existing meter runs with 0.25in. thick plates or using them in new fittings. In fact, this would not only increase the capacity but also improve the repeatability of the meter.

5.0 CONCLUSIONS

Based on the results obtained with older fittings designed for the 0.125in. plates the following can be concluded :

- a) 0.25in. thick orifice plates perform identically when used in existing fittings or in new fittings. The use of 0.25in. thick orifice plates would not only increase the capacity of the meter run but also result in repeatable metering independent of β -ratio. For $0.3 \leq \beta \leq 0.6$, (i.e. for mass flow $> 3\text{kg/s}$), the average error is around 0.32% with a 2σ of $\pm 0.16\%$.
- b) in existing fittings, for β -ratios ≥ 0.4 , there is no difference between the 0.25in. and the 0.125in. plates. For β -ratios < 0.4 , the 0.25in. thick plates would over-register by around 0.3%.
- c) bevel angle ($30^\circ \leq \alpha \leq 45^\circ$) and orifice bore edge thickness ($0.6\text{in.} \leq e \leq 0.16\text{in.}$), do not have a measurable effect on the metering accuracy in new or existing fittings.
- d) plate thickness (0.125in. v/s 0.25in.) does not affect the performance of non-beveled plates in the existing fitting.
- e) data indicates that for the 0.125in. thick plate, the difference between the beveled and non-beveled plates depends on the β -ratio and does not indicate a specific trend. In the case of the 0.25in. thick plates, the non-beveled plates tend to under-register in comparison to the beveled plates. The larger under-registration occurring at β -ratios < 0.4 .

6.0 ACKNOWLEDGMENT

The author would like to acknowledge the contributions of Shane Fry, John Geerligns, Russ Given and Dr. Wojciech Studzinski of NRTC; Blaine Sawchuk of NGTL; and the support of Fred Knoll of Daniel Industries.

7.0 REFERENCES

1. Marks Standard handbook for Mechanical Engineers, Mechanics of Materials, 9th edition, McGraw Hill. pg. 5-52.
2. Jepson, P. and Chipchase, R. 1975 "Effect of plate buckling on orifice meter accuracy", Journal Mechanical Engineering Science.
3. Norman, R., 1982, "A further investigation into the effect of orifice plate deformation on metering error". Report No. ERS R2554, British Gas Engineering Research Station.
4. Norman, R. , Rawat, M.S. and Jepson, P, 1983 "Buckling and eccentricity effects on orifice metering accuracy", International Gas Research Conference.
5. Norman, R. and Rawat, M.S 1983 "An experimental investigation into the flow measurement errors caused by elastic deformation of orifice plates", Re[port No. ERS R2713, British Engineering Research Station.
6. Norman, R. , Rawat, M.S. and Jepson, P, 1984 "An experimental investigation into the effects of plate eccentricity and elastic deformation on orifice meter accuracy". Presented at the International Conference on metering of natural gas and liquefied hydrocarbon gases.
7. Gorter, J. 1977 "Buckling of orifice plates and resulting errors in flow measurements by means of orifice meter runs", Flow Con 77, Proceedings of the Symposium "The Application of Measuring Techniques", Brighton.
8. Gorter, J. 1978 "Deformation of orifice plates, Theory and Practice, Flow Measurement of Fluids, Gromingen.
9. Mason, D., Wilson, M.P., and Birkhead, W.G. 1975 "Measurement error due to the bending of orifice plates". Presented at the ASME Annual Meeting, Houston.
10. Karnik, U. and Williamson, I 1992 "High Differential Orifice Metering" Reports to NGTL May, Sept. and Dec. 1992.
11. Karnik, U. et al. 1995 "Meter Prover Traceability", December report to NGTL.
12. Morrow, T. 1995 "Orifice meter installation effects in the GRI MRF". 3rd International Symposium on Fluid Flow Measurement, San Antonio, USA.
13. Williamson, I.D., Sawchuk, B.D. and Karnik, U. , 1995, "The NOVA Meter Prover", 3rd International Symposium on Fluid Flow Measurement, San Antonio, USA.
14. Karnik, U. 1995 "A Compact Orifice Meter/Flow Conditioner Package" 3rd International Symposium on Fluid Flow Measurement, San Antonio, USA.
15. Husain, Z. and Teyssandier, R. 1986 "The effects of plate thickness and bevel angle in a 150mm line size orifice meter" International Conference on Flow Measurement in the Mid-80's, NEL.

**Calibration of Differential Transmitter at Orifice Meter
First Calibrated on 27th September 1995.**

Date	Slope	% difference
27 Sept 1995	0.123225 counts/Pa	0.000%
27 Oct 1995	0.12317 counts/Pa	-0.045%
29 Nov. 1995	0.123164 counts/Pa	-0.050%

**Calibration Checks of Static Pressure Transmitter at Orifice Meter at zero flow.
Calibrated on 27th September 1995.**

Date	P _{noz} kPa	P _{orfs} kPa	max. diff. %
27 Sept. 1995	6257	6259	0.03%
17 Oct. 1995	5790	5787	0.05%
31 Oct. 1995	5255	5253	0.04%
06 Nov. 1995	6166	6165	0.02%
21 Nov. 1995	6031	6029	0.03%

**Calibration Checks of Temperature Transmitter at Orifice Meter with dry block.
Calibrated on 27th September 1995.**

Date	T _{ref} deg.C	T _{orfs} deg.C
07 Nov. 1995	14.69	14.69
	9.18	9.19
29 Nov. 1995	14.42	14.37
	8.42	8.42

Table 1. Typical performance of pressure and temperature transmitters.

β -Ratio	bevel angle α deg.	Plate thickness inches	Bore edge thickness inches
0.2193	37.5	0.125	0.06
	37.5	0.250	0.06
	37.5	0.250	0.16
	30.0	0.250	0.06
	30.0	0.250	0.16
	45.0	0.250	0.06
	45.0	0.250	0.16
0.3132	37.5	0.125	0.06
	37.5	0.250	0.06
0.4072	37.5	0.125	0.06
	37.5	0.250	0.06
0.5012	37.5	0.125	0.06
	37.5	0.250	0.06
0.5952	37.5	0.125	0.06
	37.5	0.250	0.06
	37.5	0.250	0.16
	30.0	0.250	0.06
	30.0	0.250	0.16
	45.0	0.250	0.06
	45.0	0.250	0.16
0.7205	37.5	0.125	0.06
	37.5	0.250	0.06

Table 2. Details of orifice plates used in the present study.

β -Ratio	Mean Error [%] with 2σ		Difference	New Fitting
	0.125inch	0.25inch		
0.2193	-0.29 \pm 0.18%	0.08 \pm 0.11%	-0.37%	0.11 \pm 0.13%
0.3132	0.09 \pm 0.07%	0.36 \pm 0.09%	-0.27%	0.36 \pm 0.13%
0.4072	0.13 \pm 0.15%	0.25 \pm 0.08%	-0.12%	0.28 \pm 0.11%
0.5012	0.17 \pm 0.08%	0.25 \pm 0.06%	-0.08%	0.23 \pm 0.16%
0.5952	0.34 \pm 0.15%	0.35 \pm 0.07%	-0.01%	0.36 \pm 0.08%
0.7205	0.69 \pm 0.28%	0.79 \pm 0.32%	-0.1%	0.60 \pm 0.02%

Table 3. Summary of results for beveled plates.

β -Ratio	Mean Error [%] with 2σ		Difference
	0.125inch	0.25inch	
0.2193	-0.10 \pm 0.17%	-0.18 \pm 0.15%	0.08%
0.3132	-0.045 \pm 0.09%	0.00 \pm 0.08%	-0.045%
0.4072	0.20 \pm 0.11%	0.09 \pm 0.01%	0.11%
0.5012	0.14 \pm 0.08%	0.15 \pm 0.05%	-0.01%
0.5952	0.11 \pm 0.21%	0.21 \pm 0.12%	-0.10%
0.7205	0.55 \pm 0.08%	0.57 \pm 0.05%	-0.02%

Table 4. Summary of results for non-beveled plates in old fitting

β -Ratio	Mean Error [%] with 2σ		Difference
	Beveled	Non-Beveled	Beveled minus Non Beveled
0.2193	-0.29±0.18%	-0.10±0.17%	-0.19%
0.3132	0.09±0.07%	-0.045±0.09%	0.14%
0.4072	0.13±0.15%	0.20±0.11%	-0.07%
0.5012	0.17±0.08%	0.14±0.08%	0.03%
0.5952	0.34±0.15%	0.11±0.21%	0.23%
0.7205	0.69±0.28%	0.55±0.08%	0.14%

Table 5a. Beveled v/s non-beveled for 0.125 in. thick plates.

β -Ratio	Mean Error [%] with 2σ		Difference
	Beveled	Non-Beveled	Beveled minus Non Beveled
0.2193	0.08±0.11%	-0.18±0.15%	0.26%
0.3132	0.36±0.09%	0.00±0.08%	0.36%
0.4072	0.25±0.08%	0.09±0.01%	0.16%
0.5012	0.25±0.06%	0.15±0.05%	0.10%
0.5952	0.35±0.07%	0.21±0.12%	0.14%
0.7205	0.79±0.32%	0.57±0.05%	0.22%

Table 5b. Beveled v/s non-beveled for 0.25 in. thick plates.

Bevel Angle (deg.)	orifice edge (in.)	Error $\pm 2\sigma$ (new Fitting)	Error $\pm 2\sigma$ (old Fitting)
45	0.06	0.35 \pm 0.08	0.41 \pm 0.17
37.5	0.06	0.36 \pm 0.08	0.37 \pm 0.11
30.0	0.06	0.39 \pm 0.08	0.48 \pm 0.11
		0.37%	0.42%
45	0.16	0.24 \pm 0.04	0.40 \pm 0.08
37.5	0.16	0.23 \pm 0.05	0.52 \pm 0.06
30.0	0.16	0.19 \pm 0.00	0.40 \pm 0.12
		0.22%	0.44%
0.0	0.25		0.21 \pm 0.12

Table 6a. Effect of bevel angle and orifice bore edge thickness (β -Ratio = 0.6) using a 0.25in. thick orifice plate.

Bevel Angle (deg.)	orifice edge (in.)	Error $\pm 2\sigma$ (new Fitting)	Error $\pm 2\sigma$ (old Fitting)
45	0.06	0.19 \pm 0.04	0.10 \pm 0.22
37.5	0.06	0.11 \pm 0.13	0.08 \pm 0.10
30.0	0.06	0.26 \pm 0.05	0.22 \pm 0.10
		0.20%	0.13%
45	0.16	0.02 \pm 0.12	0.10 \pm 0.11
37.5	0.16	0.12 \pm 0.09	0.10 \pm 0.13
30.0	0.16	-0.01 \pm 0.06	-0.02 \pm 0.09
		0.04%	0.06%
0.0	0.25		-0.18 \pm 0.15

Table 6b. Effect of bevel angle and orifice bore edge thickness (β -Ratio = 0.2) using a 0.25in. thick orifice plate.

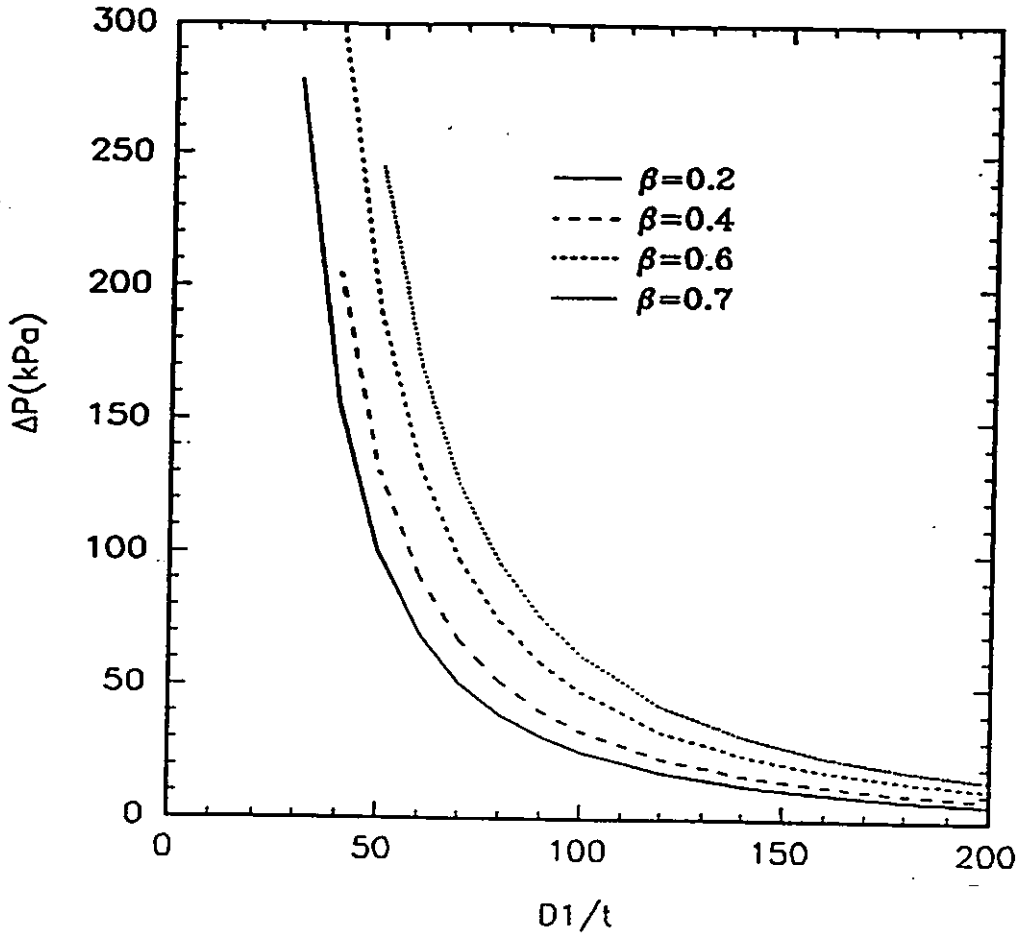
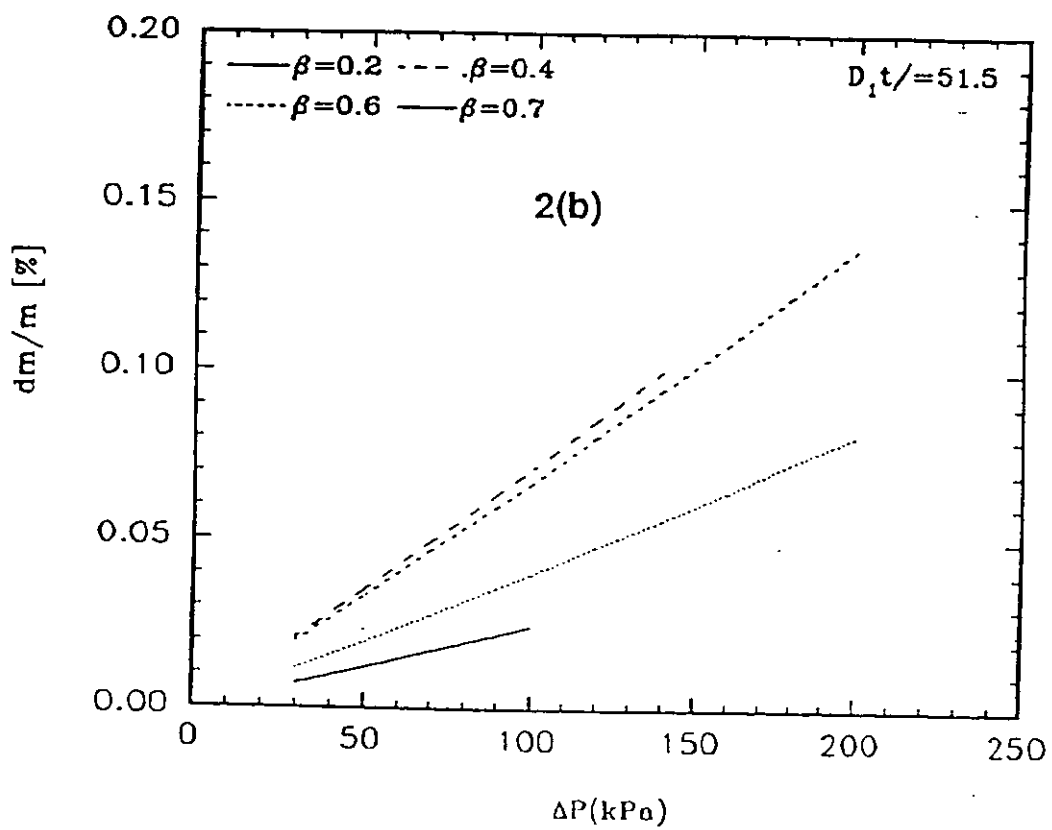
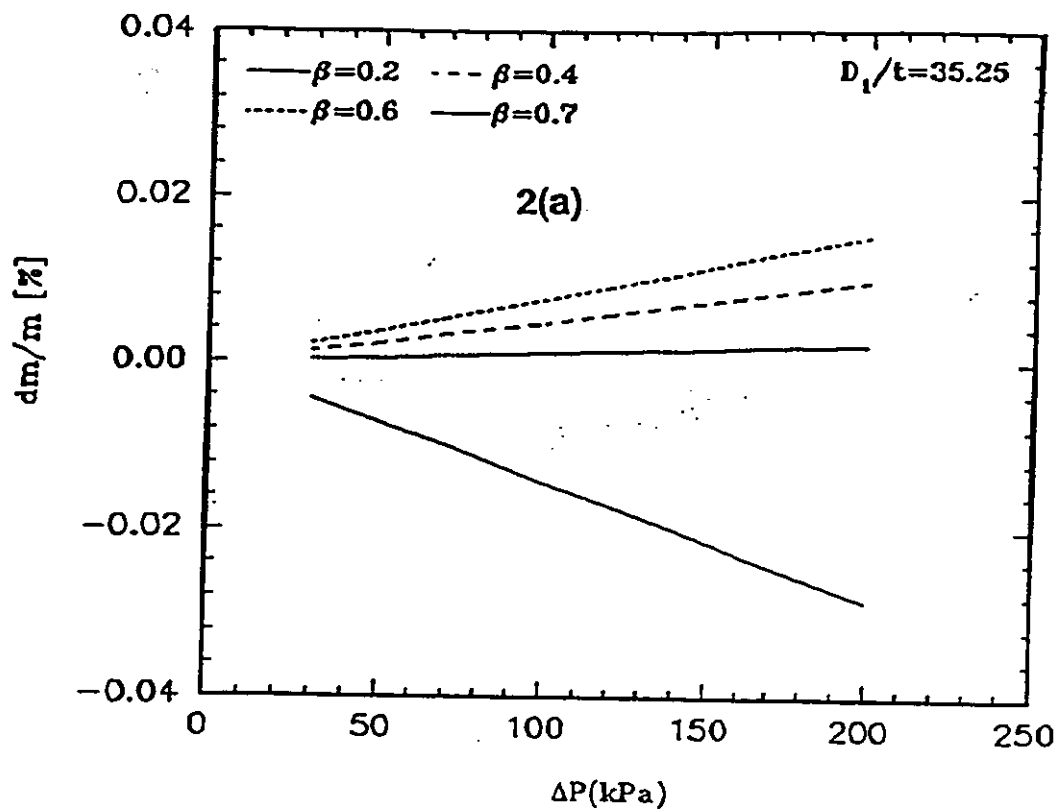


Figure 1. Allowable pressure difference across an orifice plate before yield.



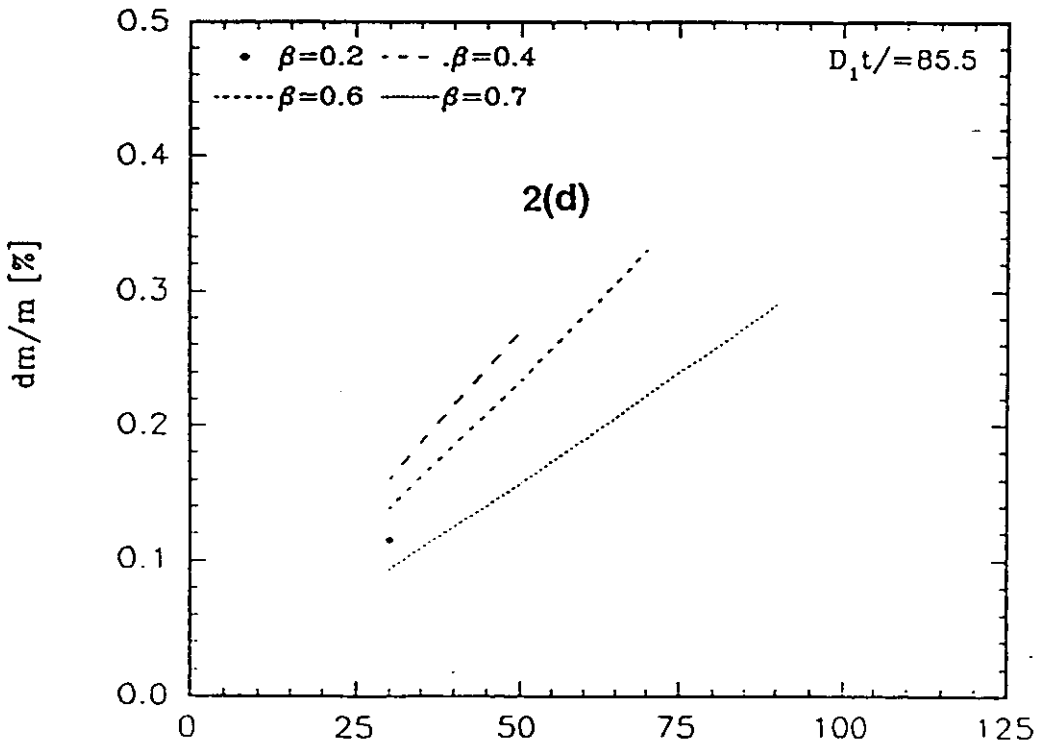
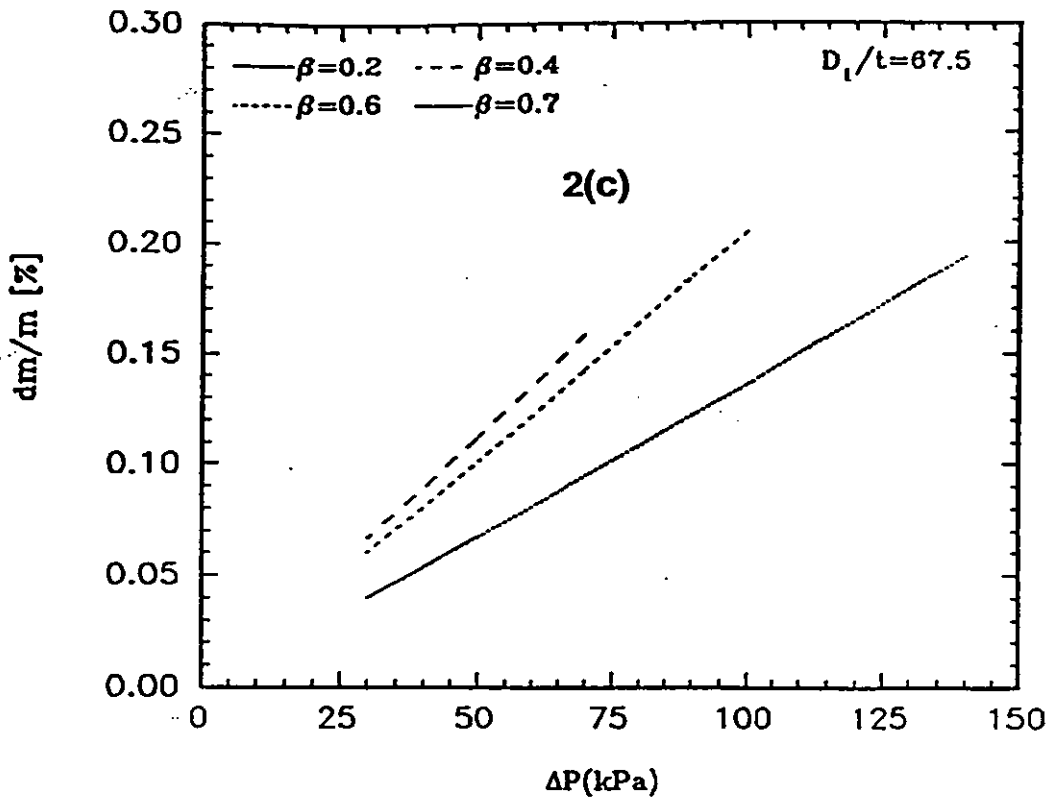
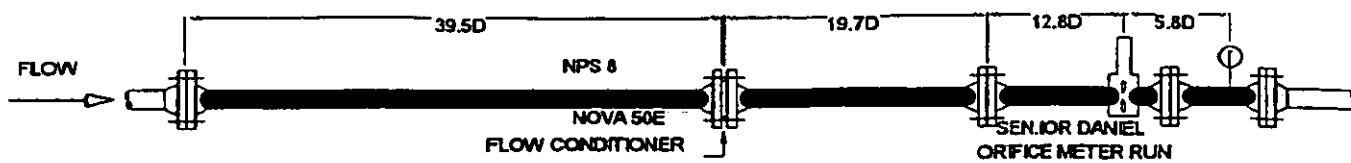


Figure 2. Total error in metering due to elastic deformation of an orifice plate.



DETAIL 'A'

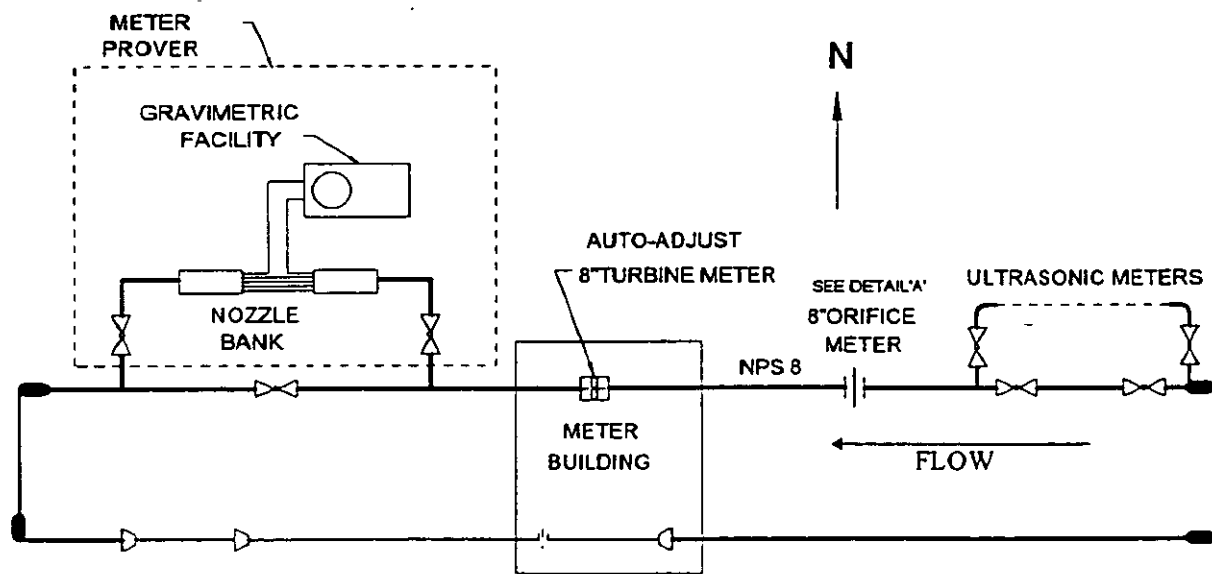


Figure 3. Schematic layout of the Test Facility

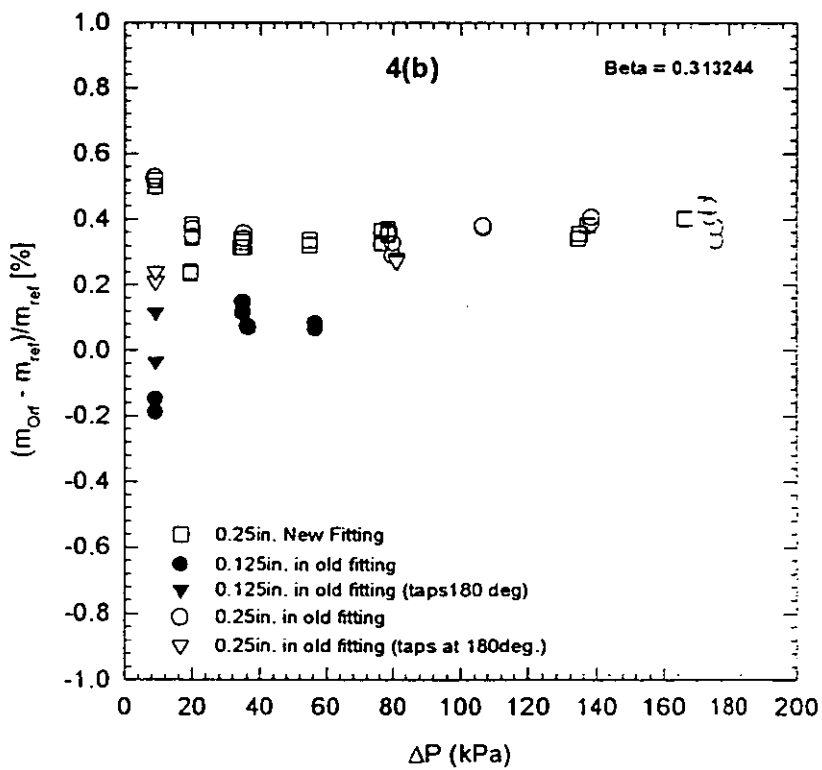
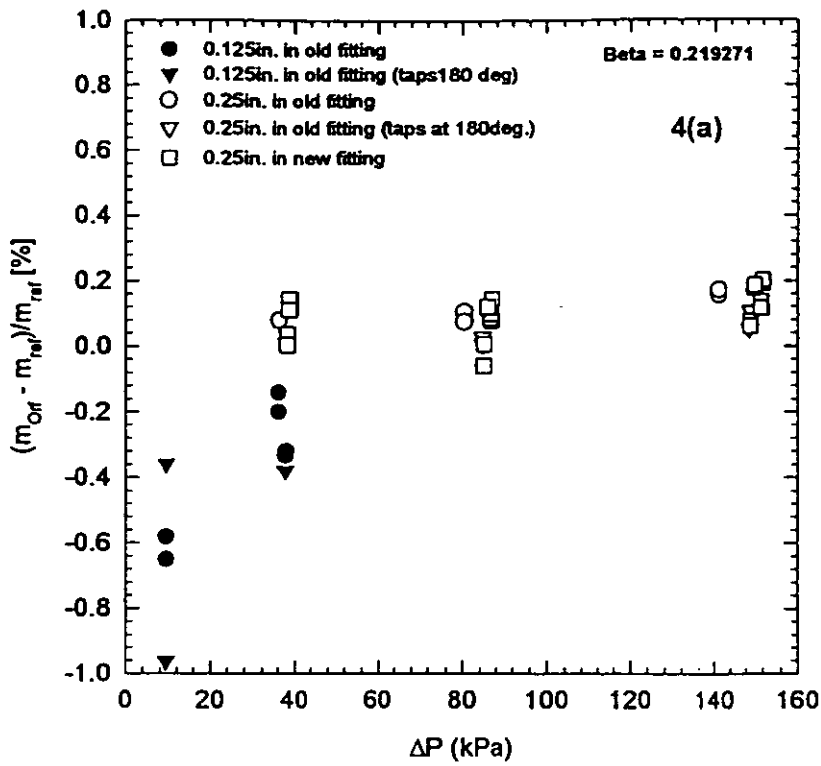


Figure 4a&b Comparison of performance of beveled orifice plates (a) $\beta=0.2193$
 (b) $\beta=0.3132$.

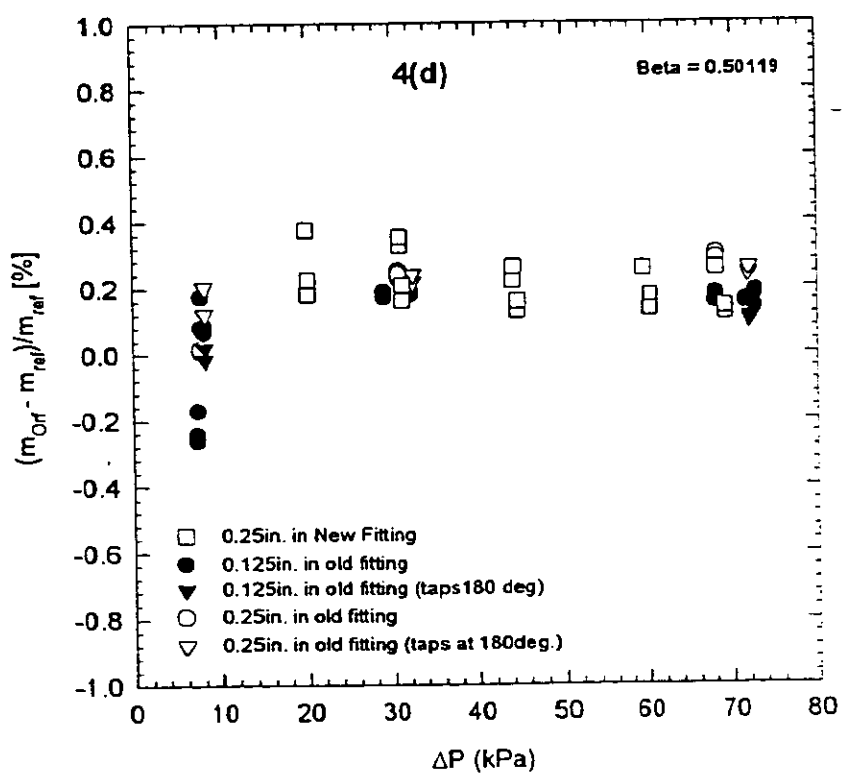
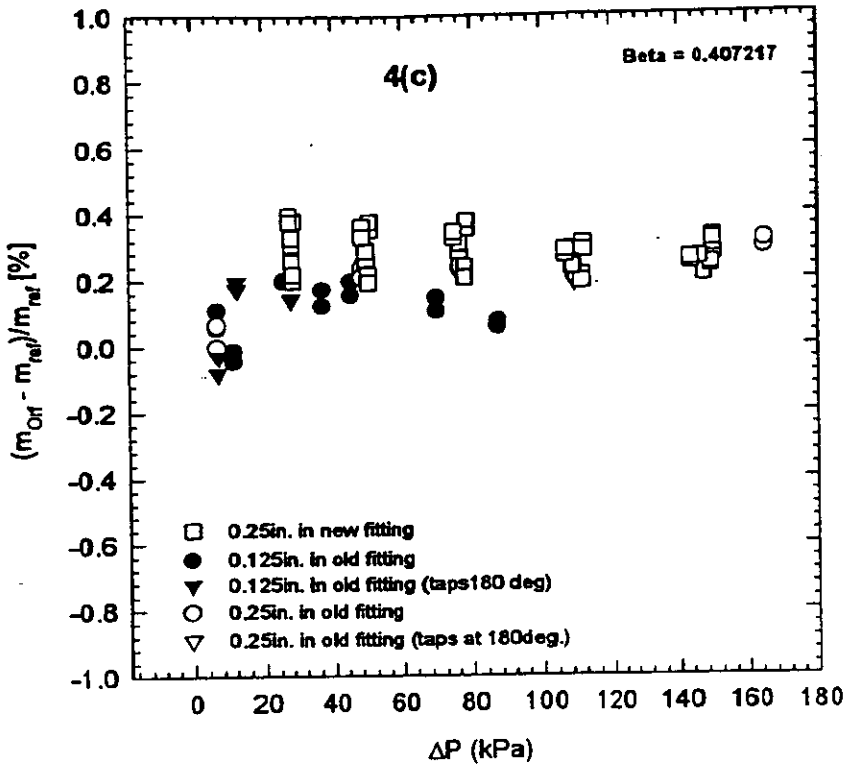


Figure 4c&d Comparison of performance of beveled orifice plates (c) $\beta=0.4072$ (d) $\beta=0.5012$.

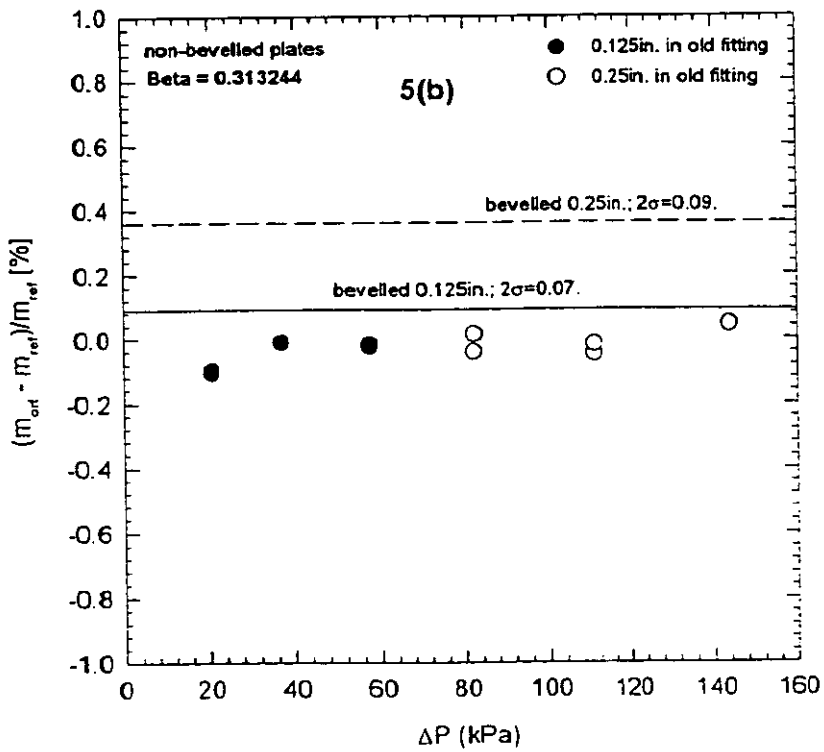
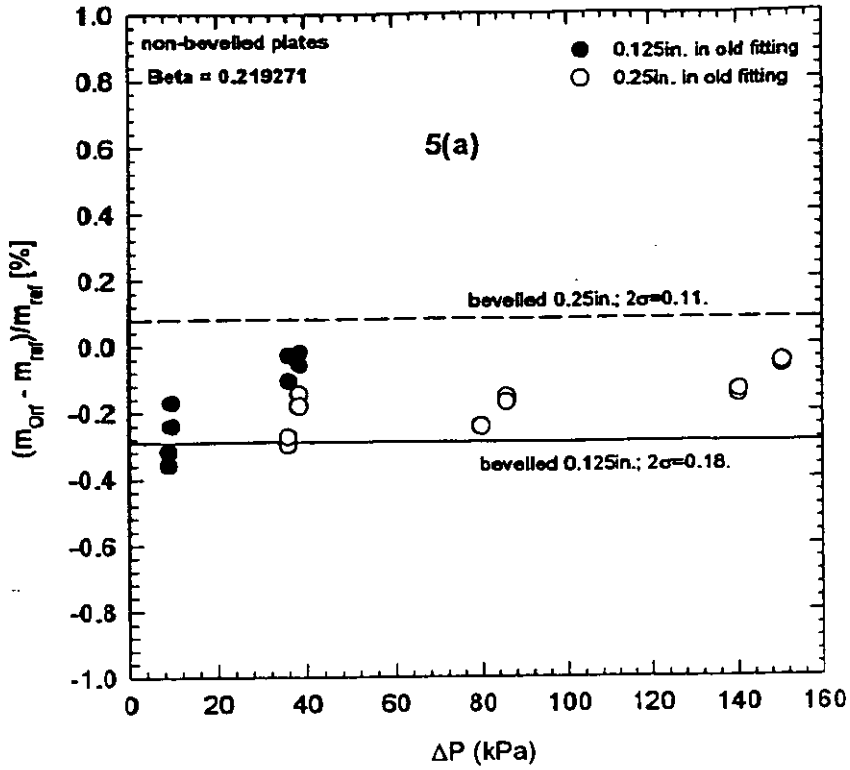


Figure 5a&b Comparison of performance of non-beveled orifice plates in old fitting (a) $\beta=0.2193$ (b) $\beta=0.3132$.

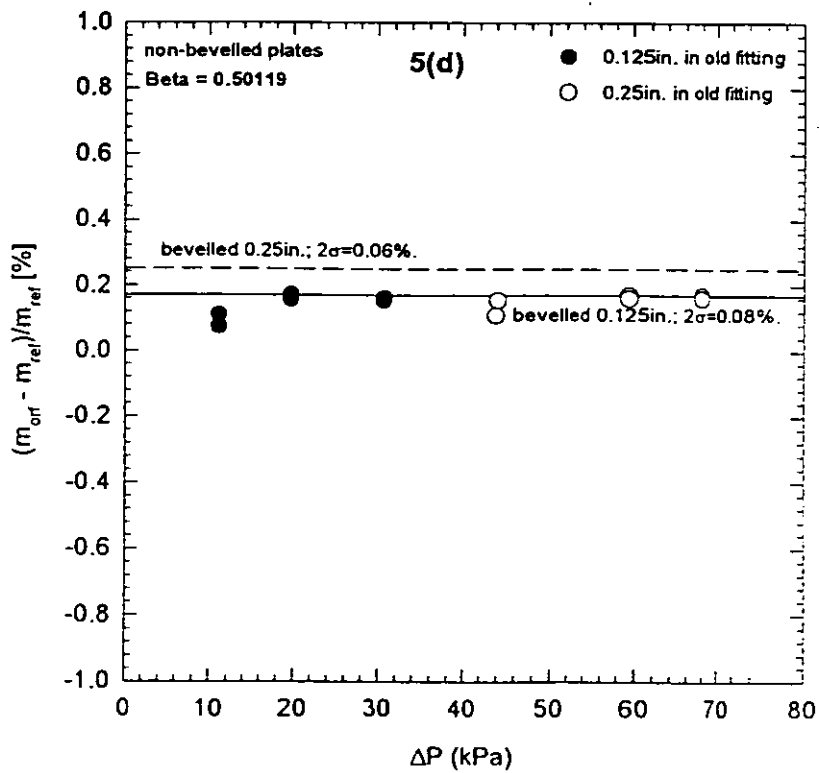
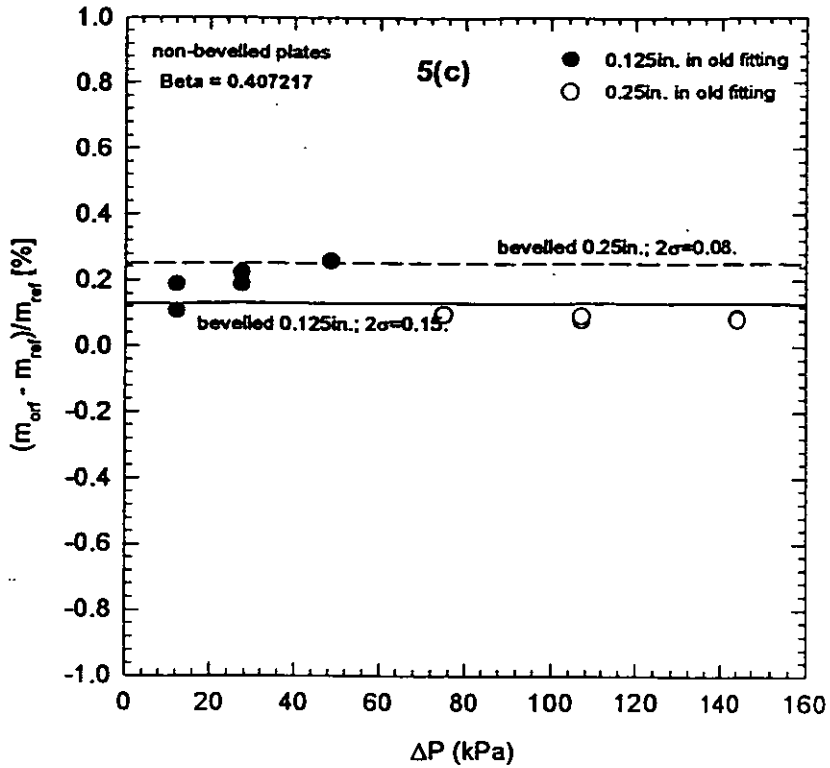


Figure 5c&d Comparison of performance of non-beveled orifice plates in old fitting (c) $\beta=0.4072$ (d) $\beta=0.5012$.

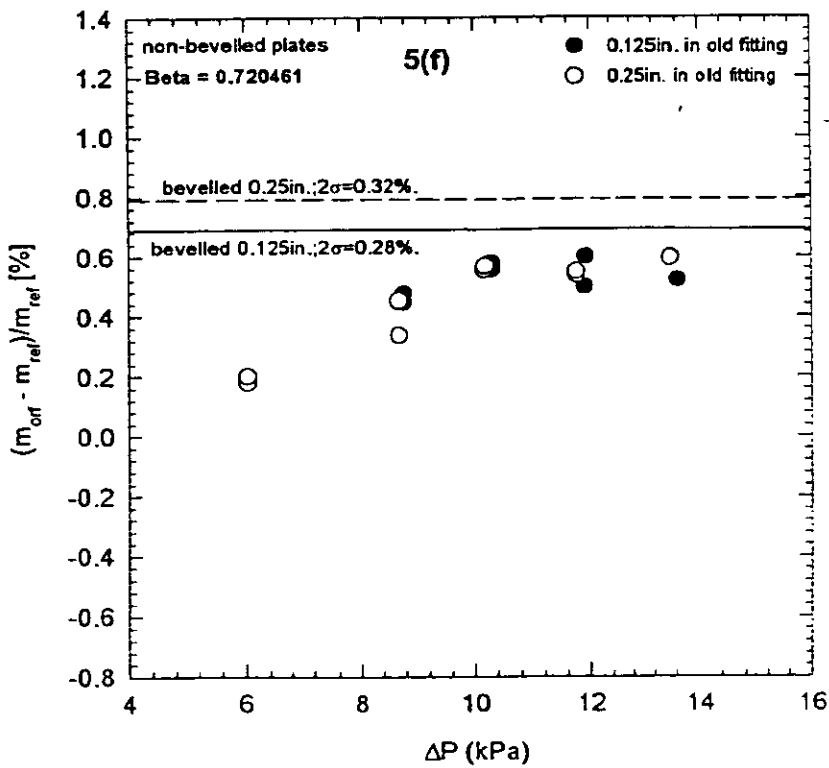
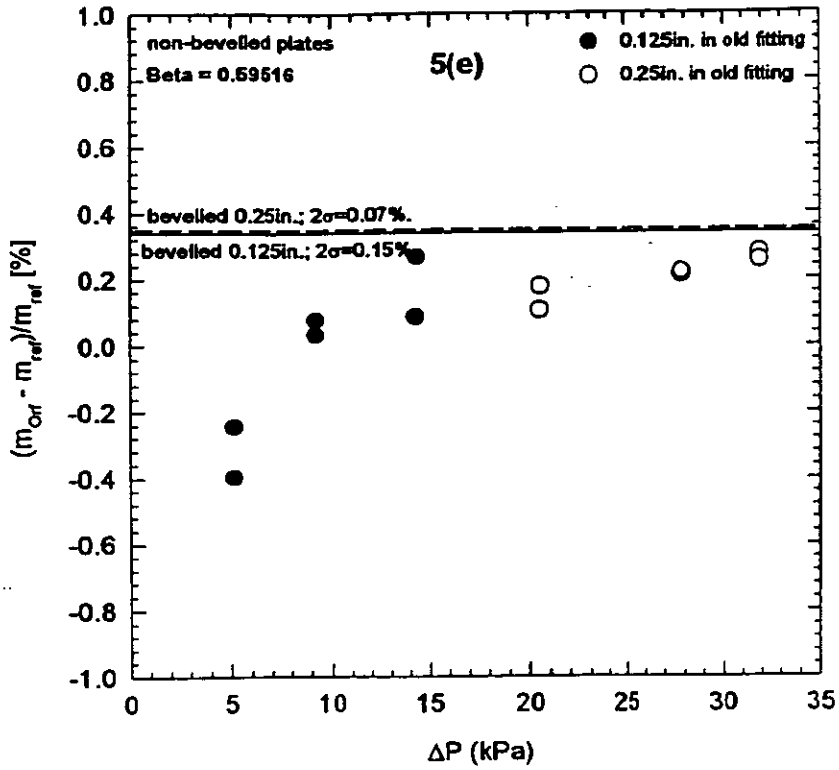


Figure 5e&f Comparison of performance of non-beveled orifice plates in old fitting (e) $\beta=0.5952$ (f) $\beta=0.7205$.

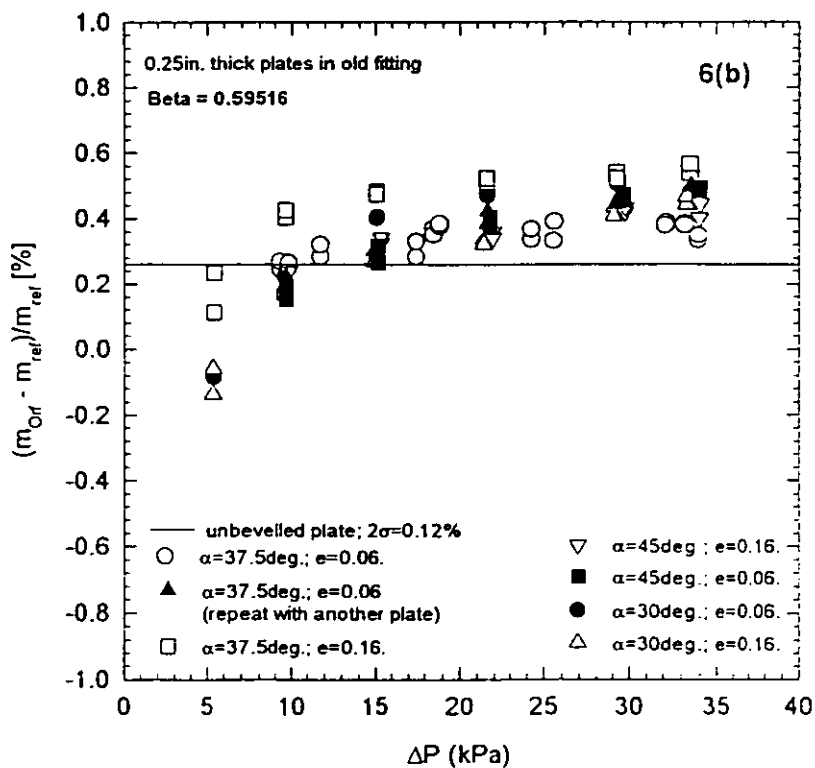
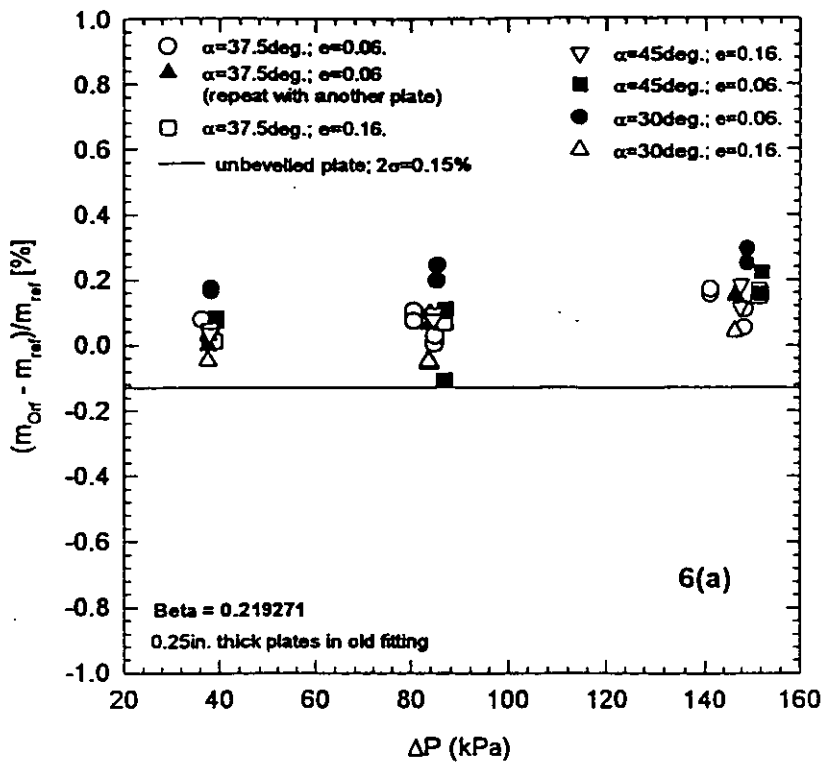


Figure 6. Effect of bevel angle and orifice bore edge thickness on meter performance; 0.25in. thick plates; (a) $\beta=0.2193$ (b) $\beta=0.5952$.

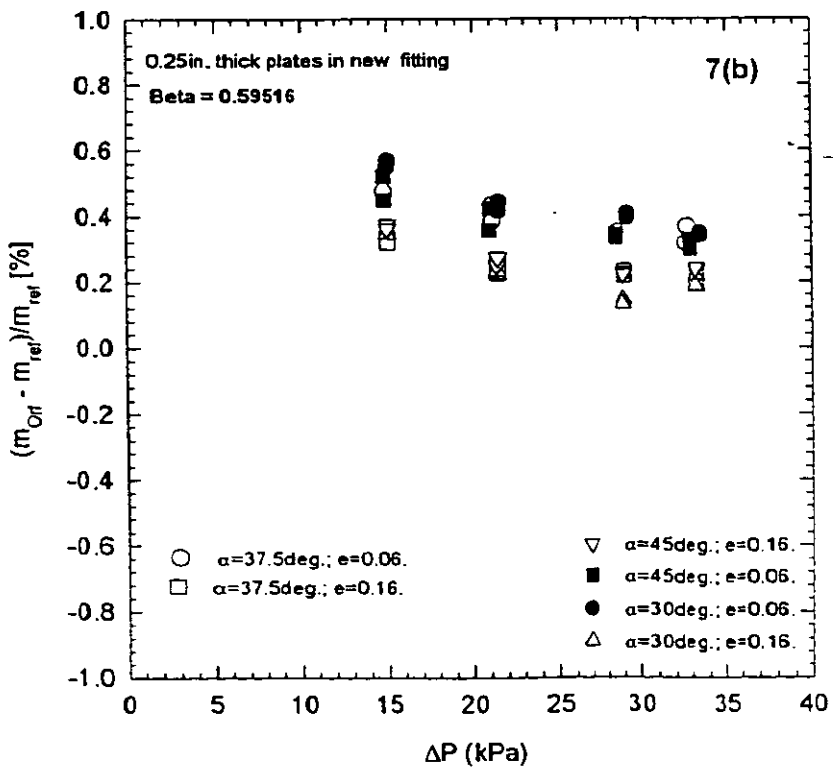
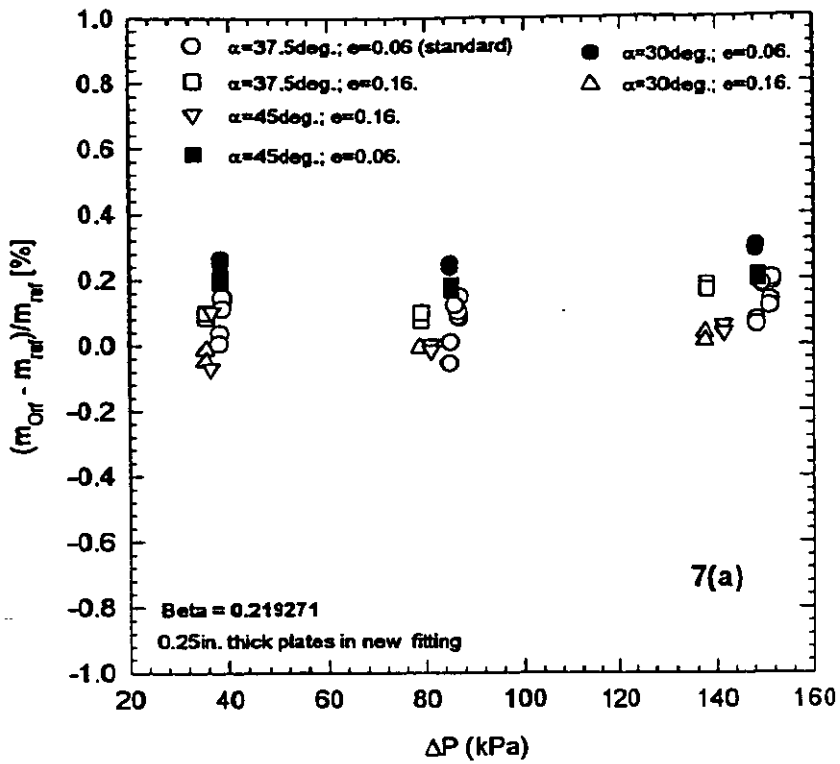


Figure 7. Effect of bevel angle and orifice bore edge thickness on new meter performance; 0.25in. thick plates; (a) $\beta=0.2193$ (b) $\beta=0.5952$.

FOCUS DISCUSSION GROUP F

The Realities of '1%' Gas Flow Measurement.

R Third, Rhomax

**LATE PAPER
FOR
FOCUS DISCUSSION GROUP F**

The Realities of '1%' Gas Flow Measurement
R Third, Rhomax

PLEASE ENSURE YOU PICK UP YOUR COPY FROM THE CONFERENCE
RECEPTION DESK.

FOCUS DISCUSSION GROUP G

The Role of an Oil / Gas Metering Auditor in Common Carriage Pipelines.

M Godfrey, Kelton Engineering Ltd

THE ROLE OF AN OIL/GAS METERING AUDITOR IN COMMON CARRIAGE PIPELINES

Mark Godfrey
Kelton Engineering Limited

SUMMARY

The objective of this paper is to cause discussion within the oil and gas industry concerning the need, role, responsibility and authority of a metering auditor/inspector within common carriage pipeline systems. The paper will examine the areas of Tick Box Audits, categorisation of non-compliant items, audit reporting, Auditors Independence, role responsibility, what happens when the audit is over and the report published, and the future and way ahead for measurement auditing.

1.0 INTRODUCTION

Annually, it is estimated that collectively in excess of £1 M is spent by UK pipeline operators and installation operators on measurement system auditing. Very often the auditor is appointed as an independent auditor from one of several specialist metering companies to carry out this service.

Whilst operators may believe that their audit criteria are necessarily specific to their pipeline, invariably we all play by the same technical rules eg ISO 5167, IP, DTI requirements etc. and most contractual conditions are similar. Therefore, there is a clear use for a common set of audit criteria for UK Continental Shelf operations and a standard reporting format.

Operators may be surprised to know that around 50-70% of auditing costs are spent in preparing the reports to the format required by a individual operator. In line with CRINE initiatives, this paper will focus on areas where commonality in auditing will result in more focused auditing activities, more concise and informative reports and give the industry cost reduction benefits.

2.0 TICKBOX AUDITS

Tick box audits is the term used here to describe the type of audit where the auditor is required to complete an audit report which has been preformatted by the pipeline operator. The auditor is then required to TICK or CROSS an item of the criteria either compliant or non-compliant as appropriate and to reference any comments that do not meet the criteria.

Key to any audit is a set of agreed audit criteria. In general the criteria used by most pipelines were developed and agreed some years ago. Many are in need of updating to reflect the way in which metering systems are actually operated and maintained. Some pipelines unfortunately, still need a set of criteria developed.

- 2.1 Many of the pipeline operators combine the audit criteria with the audit report. This means that the audit report can be some 50 pages long before any comments have been made. Are the people who read these reports at pipeline committee meetings really interested in the list of test equipment used, or do they need to have copies of the densitometer calibration certificates at a particular installation, especially when the auditor has already ticked a box to note the validity of all test equipment, certification etc.
- 2.2 Comments against a particular audit item must usually be made on the same page concerning the equipment to be inspected. Comments must then be carried forward to the front of the document together with their reference into a so called summary. All too often the summary can end up excessively long if the recommendations are also to be included in the summary. Would not a true summary simply state whether a metering system is, or is not fit for purpose ?
- 2.3 All too often, issues have to be reported in more than one section of the report.

As an example if a Relative Density (RD) analyser has been identified as having the wrong value of pure methane stated on the test gas certificate and used for its calibration, this has to be reported as follows:-

- i) Comment in the RD analyser section of the report,
- ii) The same comment in the Flow Computer section of the report, as this is also part of flow computer configuration,
- ii) The same comment in the section for Certification,
- iv) The same comment in the section for Calibration.

Therefore in the previous example, the same statement must be repeated at least 4 times to fully satisfy the operators reporting format.

- 2.4 Clearance of actions from previous audits are often required to be stated together with any actions taken by the installation operator. The auditor is often faced with a challenge on how to differentiate between comments from a previous audit that are still relevant and comments that are new or related to the previously reported item

All of the above can make a typical audit report some 60-80 pages in length. The question must be asked; is any one who reads these reports interested in what is compliant ? Surely the reader is only interested in what is non-compliant.

- 2.5 One way forward, would be for the audit report to take the form of an Exception Report only. Where an exception to the audit criteria has been found the auditor could reference the point to the operators criteria, but need only mention the exception once. The report length could be reduced to around 3 to 5 pages in length instead of > 50. Here there must be obvious advantages to both auditor, reader, platform and pipeline operator in terms of the quantity of data to be read, document storage, time spent writing and hence quicker delivery of audit report, (a continual issue between auditors and their clients).

There is also one further advantage in this reporting format. The reports are often not only used to report to the pipeline operator and all other pipeline participants, but are also used for reporting to field partners. There must be great advantage to field operator and field partner alike if a short form report is submitted where, only the clear issues are identified.

This process could be taken one step further. Currently, once all the pipeline metering station audits have been completed and the reports issued, a meeting of all pipeline participants is normally held and the findings of the relevant reports discussed. From these audit reports, an action or task list is made for each operator to action to ensure/maintain their system compliance. At this stage, there is therefore, an opportunity to cut out some of the paper work and for the auditor to issue his findings as an Issues and Action plan. An example of this is attached in Attachment 1.

Reporting only non-compliant items will save everyone time and effort.

3 CATEGORISATION OF NON-COMPLIANCE'S

The auditor is required to categorise all non-compliance's to a format agreed by all pipeline participants. There is great variation amongst all the various audit criteria with regard to this classification. It is believed that some of the categories used, were developed many years ago and were developed for political reasons rather than technical.

Two examples of the variation in non-compliance categories are shown below:-

Example 1

- Category 1** : A fundamental fault or deficiency which, in the auditor's opinion, causes a **major** (> 1%) measurement error.
- Category 2** : A fault or deficiency which, in the auditor's opinion, causes a **minor** (< 1%) measurement error.
- Category 3** : A deficiency in procedures, log books, etc. which has no effect on measurement integrity.
- Category 4** : Where some aspect of the metering station is less than satisfactory, but not in a way such that it would fall into categories 1 to 3. Such a deficiency could be rectified with little effort.

Example 2

- Category 1** : A fundamental fault identified during the audit visit.
- Category 2** : A fundamental fault which had occurred since the last audit but had been rectified before this audit.
- Category 3** : A minor problem with procedure's, log book's etc. which have no affect on measurement accuracy.

In *Example 1* above, the problems with this method of categorisation is that the 1% rule for significance will treat larger pipeline users differently to that of a small one. IE if 'Platform A' contributes 60% of a pipeline throughput and 'Platform B' contributes 10% of the same pipeline throughput, 'Operator A' can have much greater effect on the pipeline balance without penalty.

In *Example 2* above, when an operator is given a Category 1 finding, it simply means that this is a new finding, not a measure of its seriousness. Due to this, the auditor often receives phone calls and letters form the operator simply as a function of the issue being called Category 1 and often does not appreciate the actual categorisation the auditor is obliged to use for that particular pipeline.

A common set of categories for the classification of non-compliant items based on financial or allocation sensitivity/risk would help all concerned here.

4 WHAT IS THE ROLE OF THE AUDITOR ?

This may appear a straight forward question. However, the role of the auditor differs from pipeline to pipeline. Some pipelines have the auditor carry out the role of simply a witness to calibration activities. This would perhaps be better suited to Technician rather than an Engineer or Consultant. An auditor should be allowed to visit any area which he deems important or significant to maintaining and operating the metering system within the agreed standards. This should include production reporting, mismeasurement reporting, roles and responsibilities of key personnel of the facilities etc.

4.1 One area that is continually overlooked is the calibration of the prover on a liquid system. This is the single most important activity of a liquid system, yet it goes un-audited. Why ?

4.2 Other than actually verifying that the auditor was actually attending the audit, what purpose do the following example requirements of the auditor prove:-

- i) *"Obtain copies and append to the report of all test equipment certification"*
- ii) *"Obtain copies and append to the report all primary and secondary equipment certification".*

Statements like this are not uncommon audit requirements. Given that it is most unlikely that any readers of audit reports will examine equipment certificates and that several kilograms of paper is a nuisance to collate, transport and issue, why is this necessary ?

If you do not trust the auditor to carry out his job, what is he doing there in the first place ?

5.0 THE INDEPENDENCE OF THE AUDITOR

In order for the Auditor to carry out his remit, he should be completely independent of the operator of the facility being inspected. On pipelines where each platform operator is free to select their own auditor for the independent audit, the auditor should be selected on, amongst other criteria, the basis of independence.

5.1 Could the independence of an auditor can be compromised where an auditor or audit company is appointed by the pipeline operator to audit the whole pipeline system and that same company is engaged by a facility operator for other metering work ? The answer to this question has be yes as it must be concluded that complete independence is in doubt.

- 5.2 Whilst it is not suggested that any auditor is coerced to remove or dilute a comment that puts his company in a bad light, but it must be a difficult to put such a comment in writing in the first place for all to see. An analogy to support this could be:-

If your car keeps breaking down and you are concerned that the garage would not give an unbiased opinion as to the nature of the fault, would you take the car back to them or go to say the AA for an independent assessment, even though the garage has given an assurance that they would put their best man on the job ?

If it is an 'Independent Audit' that is required, then independence in the auditor should be sought.

6 WAYS AHEAD

The technology used in metering systems has changed over the years, however, the role of the auditor has remained relatively unchanged in that time.

- 6.1 Many operators these days employ the use of electronic systems to re-transmit all the metering data back to their offices onshore. At their finger tips they have available powerful data gathering, trending, alarming and as a result auditing facilities available. Comparative trending can be used to assess the performance of each piece of metering equipment without having to leave the office. If auditors were given access to this data, this would mean that a great deal of work traditionally carried offshore could be achieved onshore, (usually at less cost). This would leave the auditor free to concentrate on higher level issues whilst at the worksite and not waste time in somewhat trivial issues.
- 6.2 Log books are still currently hand written documents. If logbooks could be kept by electronic/computers means and made secure to the satisfaction of all concerned, this would further make the role of auditing easier and open for inspection at any time.

If auditors can be given access to the electronic data, the time spent offshore could be focused on more relevant issues.

7 CONCLUSIONS

The conclusions of this paper are:-

- i) Audit criteria should be produced that reflect the way in which modern measurement systems are operated and maintained.
- ii) Use non-compliance audit reporting to reduce costs to make life easier for all concerned with non-compliance categories that are meaningful and give focus to the issue.
- iii) Allow the auditor sufficient free scope in his audit to fully explore areas of concern.
- iv) Decide what 'Independence' of your auditor really means.
- v) And finally, a plea; Give the auditor adequate time at a facility to carry out his remit. Two days to witness the complete calibration of a three stream gas metering and sampling system including orifice plate inspection is not adequate.

ATTACHMENT 1

EXAMPLE AUDIT REPORT WHERE ONLY NON-COMPLIANCE'S ARE REPORTED

<***> PIPELINE SYSTEM
MEASUREMENT AUDIT REPORT
<Location>**

CLIENT REF : <----->

Prepared by: _____ **<AUDITOR>**

Revision: 1

Date: < >

1.1 EXECUTIVE SUMMARY

It is the opinion of the auditor that the oil/gas metering system at this location is/is not currently being maintained and operated to a satisfactory level and is/not fit for purpose.

2.0 NEW ISSUES AND ACTIONS

During this audit <X> new non-compliance's have been identified. Only <X> is considered as significant and is outlined below. All other new comments are of a minor nature.

All new and outstanding non-compliance's are detailed in section 3 of this report.

2.1 One new significant issue has been identified, Issue ref ABC 005.

At this meter station an internal inspection of the meter run revealed large quantities of sand in the meter run. This had built up to a level of around 15 mm in front of the orifice plate. This will be causing an under measurement of production through that particular meter run. Damage to the square edge of the orifice plate will also occur further causing under measurement.

The source of the contamination must be identified and contained. It is the recommendation of the auditor that no further production gas is passed through this meter station until it has been cleaned and the source of the contamination contained.

3.0 Category of Deficiencies

Faults, non-compliant items and omissions identified during an audit are categorised, in this report as follows:

- Category 1** A fundamental fault or deficiency which, in the auditor's opinion, causes a **major** (> 500 tonnes) measurement error.
- Category 2** A fault or deficiency which, in the auditor's opinion, causes a **minor** (< 500 tonnes) measurement error.
- Category 3** A deficiency in procedures, log books, etc. which has no effect on measurement integrity.
- Category 4** Where some aspect of the metering station is less than satisfactory, but not in a way such that it would fall into categories 1 to 3. Such a deficiency could be rectified with little effort.

ISSUES/COMMENTS AND ACTION PLAN

<Site> EXPORT METERING

<Date>

No	Significance	Issue/Comment	Management Comments/Action Plan	Target Date	Completion Date
1 Jan 96	3	The operator has revised its flow computer alarm limits as identified in point 4 of the Alpha report. All limits are satisfactory with the exception of the flow rate alarms. The low flow alarms have been set at the a value equivalent to the low flow cut-off value of 5%. A more realistic value would be the minimum flow rate that can be achieved through the meter run within the ±1.0% volume uncertainty limit.	Operator to implement comment	2Q96	
2 Jan 96	2	All densitometer pipe work has been replaced since the last inspection. Unfortunately, needle valves have been fitted in the return line to the orifice carrier. These should be full bore ball valves.	Needle valves have been replaced with full bore ball valves.	3Q96	Feb 96
3	1	At this meter station an internal inspection of the meter run 4 revealed large quantities of sand in the meter run. This had built up to a level of around 15 mm in front of the orifice plate. This will be causing an under measurement of production through this particular meter run. Damage to the square edge of the orifice plate has also occurred causing further under measurement. The source of the contamination must be identified and contained. It is the recommendation of the auditor that there is no further export via this meter station until it has been cleaned and the source of the contamination contained.	Operator to evaluate.	4Q96	

Differential Pressure Transfer Standard

The DPS4 Differential Pressure Transfer Standard has been developed in order to improve both productivity and accuracy of offshore calibrations.

The unit allows in-situ calibration, removes the need for atmospheric footprinting and dramatically reduces both manhours and transportation costs.

Peter H Dand, Sales & Marketing Director, Beamex, Leicester, England



The Beamex DPS4 System is a product created through European co-operation. The work carried out to research and develop the concept of the transfer standard was carried out by SIRA with the support of the National Measurement System Policy Unit of the DTI as a project within the flow programme.

The development contract was awarded on the basis that there was a need to improve both the productivity and the accuracy of offshore calibrations for DP (differential pressure) transmitters used for high pressure gas metering. This new calibration concept presents totally new innovative thinking. The DPS4 allows the calibration of differential pressure transmitters with low differential ranges under high static pressure.

Until today, differential pressure transmitters used in offshore environments have been removed from their location to be transported to an onshore based laboratory for calibration. The calibrations have been carried out by using twin post deadweight testers, after which the transmitters have been returned to the platform and installed to their process location.

The DPS4 allows high accuracy calibration of these differential pressure transmitters in-situ and therefore dramatically improves productivity. Also, as the calibration is carried out in the actual environment, errors caused by temperature changes and transportation are eliminated.

The prototype was developed by SIRA using three differential pressure sensor modules to measure differential pressure covering the range of 0 to 1000mbar at static pressures up to 200bar. The readings from each module are software corrected for ideal linearity and compensated for line pressure effects. All three compensated readings are compared by the software in order to identify any problems in the measurement system. In case the differences between the readings are accepted, the average differential pressure is displayed.

The three pressure sensor modules are extensively characterised and tested with optimum performance being achieved at four differential pressures (0, 200, 500 and 1000mbar) at each of five static pressures (0, 50, 100, 150, and 200bar). The sequence of differential pressure is applied three times, rising and falling.

In 1994 an agreement was signed between OY Beamex, Finland and SIRA, England to further develop the product and manufacture to production standards required by the offshore industry. As part of this agreement all of the production units during the first two years of manufacture will be characterised and tested in SIRA's NAMAS accredited laboratory.

The complete Beamex DPS4 System comprises:

Sensor Unit (*Intrinsic Safety Approved to EEx ia IIc T4*)

DPS4 Management Software

Interface Unit

The calibration data of the differential pressure transmitter under test is measured in the Sensor Unit and transmitted via the Interface Unit to the Laptop PC in the Control Room. The Interface Unit is designed to communicate with the DPS4 Sensor Unit and converts the digital signals to standard RS232 signals.

The lead between the Sensor and Interface Units may be up to 1000 metres long. Calibrations are normally carried out with the transmitter under test in-situ, but isolated from the process media. Pressure connection to the DPS4 Sensor Unit can either be made by compression, quick release couplings or via a conventional differential pressure transmitter manifold. Nitrogen gas or clean air is used for supply pressure generation.

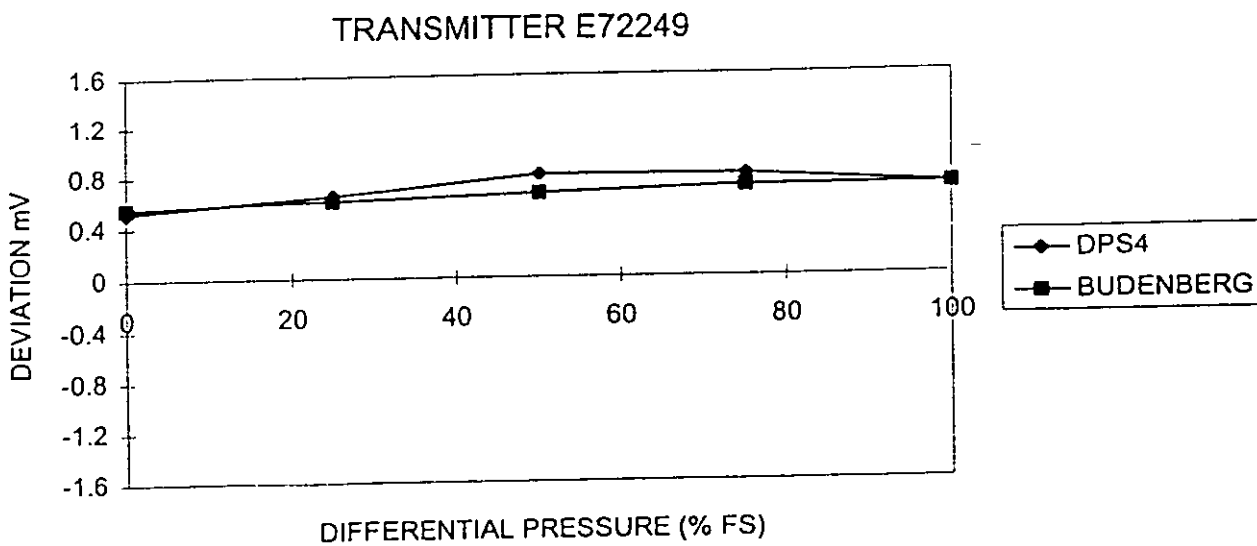
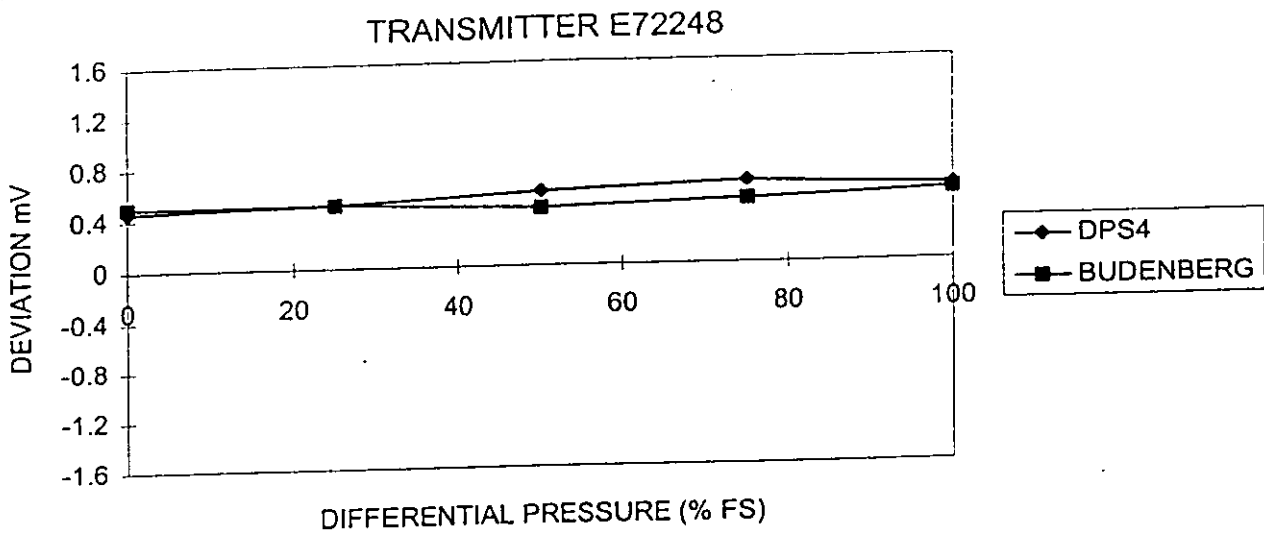
The performance specifications can be summarised as follows:-

Differential Pressure Ranges :	0/600, 0/1000 and 0/2000mbar
Static Pressure :	0 to 200bar
Static Pressure Effect :	± 0.0002 % reading/bar
Reference Accuracy :	± 0.3mbar
Stability (12 months) :	± 0.06 % reading
Vibration Effect :	$< \pm 0.03$mbar

The user-friendly Calibration Software package enables an operator to carry out a precision calibration in a matter of minutes, in-situ and with the minimum of training. The Calibration Software uses a simple graphical interface to control the instrument, implemented as a series of screens, each screen being dedicated to a particular function. The software may be controlled via a keyboard, via a mouse or trackerball, or any combination of the two.

Field trials were carried out at the Shell UK Exploration and Production gas terminal, Bacton, Norfolk, to demonstrate the performance of the DPS4 System when calibrating differential pressure transmitters used for gas flow metering. In order for it to gain acceptance, the DPS4 System must be capable of performing to a level equivalent to the current method, a twin post deadweight tester.

The medium and high range transmitters on the Phase One Fiscal Metering Stream were calibrated using the DPS4 System during the test period. The results obtained from each transmitter were compared with the previous calibration certificate using their Budenberg twin post deadweight tester, which is the current terminal calibration standard. Two transmitters were also calibrated immediately after a DPS4 calibration, using the deadweight tester, the results of which are shown below:-

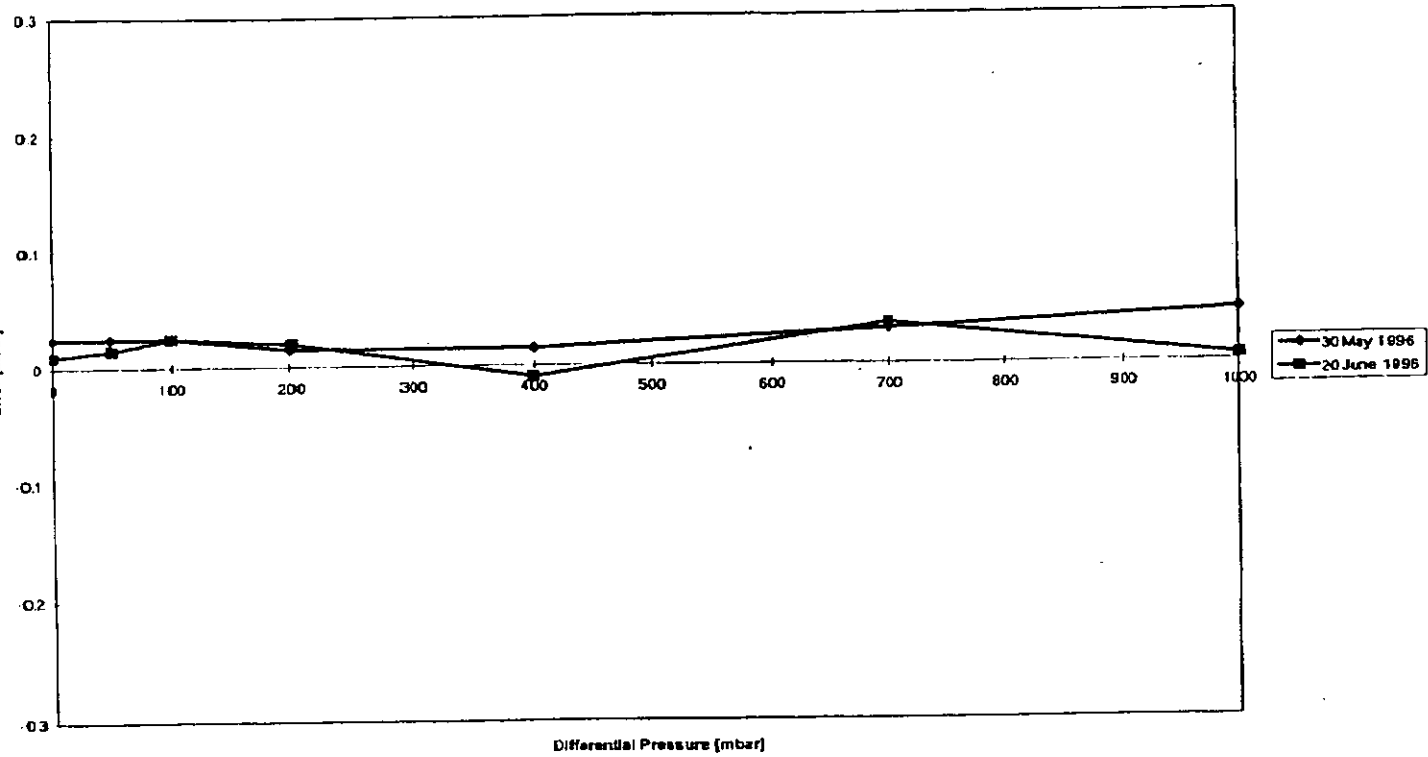


The results obtained during the trials confirmed that the performance of the DPS4 System is comparable with that of a twin post deadweight tester. The DPS4 calibration curves showed the same form as those generated some months earlier using the Budenberg twin post deadweight tester.

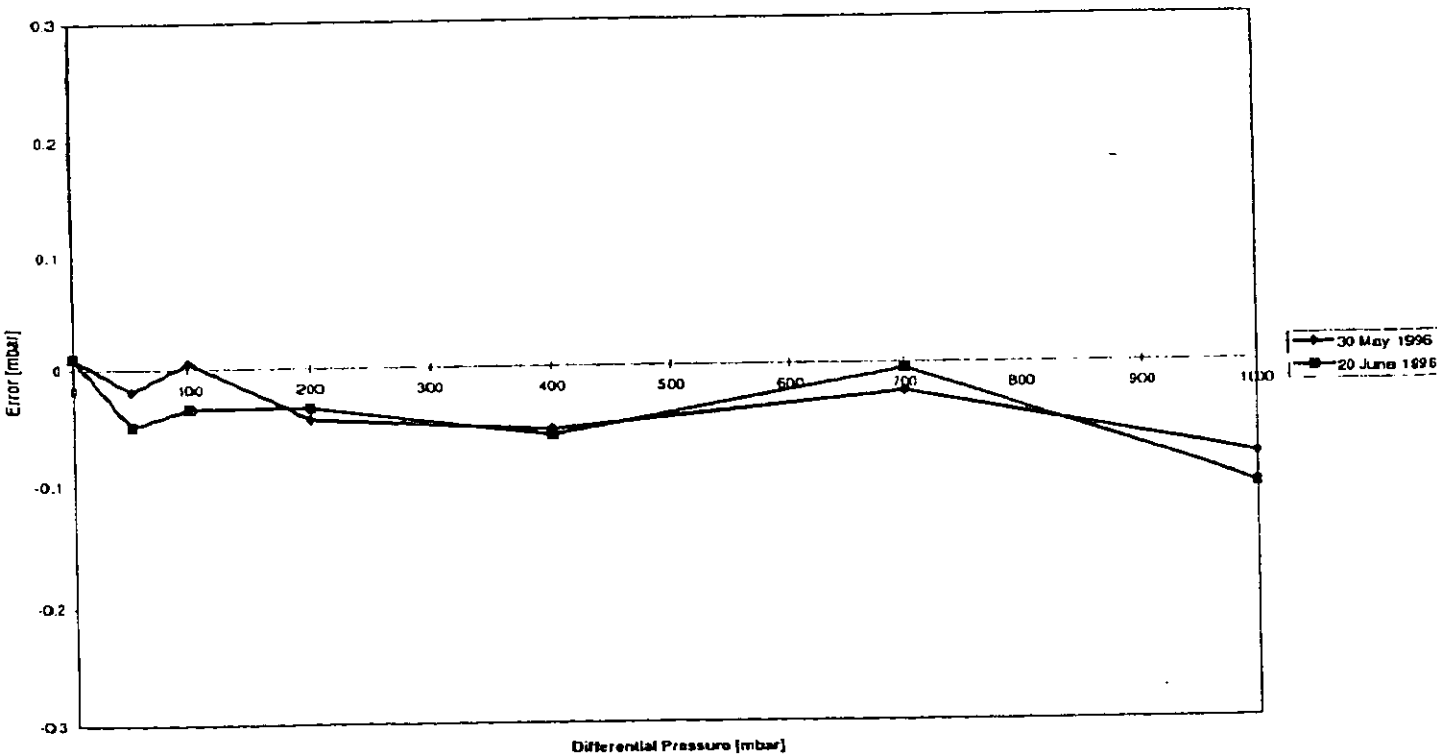
Back-to-back testing of the DPS4 with the Budenberg generated calibration curves of the same form and physical location, deviation between the two methods of less than 0.175mV (0.02% error) were apparent.

The DPS4 was calibrated by SIRA before and after the trials and the results obtained at 0 and 140bar line pressure are shown below:

DPS4 S/N 250 calibration data at atmospheric
(Calibrated by ST&C)



DPS4 S/N 250 calibration data at line pressure of 140 bar
(Calibrated by ST&C)



This product allows oil companies to confidently carry out calibrations on the platforms, hence eliminating current footprinting methods and providing in-situ calibrations at regular intervals thereby reducing transmitter down time and shipping costs.